Molecular Workstation Roadmap I:

Survey of Key Technologies Needed to Perform Positionally Controlled Diamondoid Mechanosynthesis using a Molecular Workstation

This document internally DECLASSIFIED in 2025

HISTORICAL NOTE: This document was **completed and privately circulated in 2009**. It was a part of **the first known effort to comprehensively describe one possible experimental technology development pathway that could directly lead to the first working nanofactory** capable of atomically precise manufacturing of products in macroscale quantities. The timescale for nanofactory development was originally estimated to require about 20 years of dedicated and intensive research effort. Elements of this initial proposal were later substantially simplified on the basis of subsequent research.

This document internally DECLASSIFIED in 2025

© 2009, 2025. Robert A. Freitas Jr. All Rights Reserved.

Cite as: Freitas RA Jr. Molecular Workstation Roadmap I: Survey of Key Technologies Needed to Perform Positionally Controlled Diamondoid Mechanosynthesis using a Molecular Workstation**.** IMM Report No. 59, 2009/2025; http://www.imm.org/Reports/rep059.pdf.

Table of Contents

1. Introduction to Atomically Precise UHV/Tip-Based Molecular Manufacturing .. 7

1.1 Diamondoid Mechanosynthesis (DMS) ... 10
1.2 Designing a Minimal Toolset for DMS ... 17
1.3 Building the First Mechanosynthetic Tools ... 25
1.4 Designing a Molecular Workstation that Uses the DMS Tools ... 25
1.5 General Description of the Molecular Workstation ... 26
1.6 Continuous Sensory Feedback Not Needed by the Workstation ... 31
1.7 Reliability of Workstation Operation ... 32

2. Basic Technology Background ... 36

2.1 Scanning Probe Microscope (SPM) Manipulation Technologies ... 36
2.1.1 Atomic Manipulations by STM ... 36
2.1.2 Atomic Manipulations by AFM ... 48
2.1.3 Challenges for Atomically Precise Tip Positioning in DMS ... 58
2.1.3.1 Mechanical Isolation ... 59
2.1.3.2 Jump to Contact ... 60
2.1.3.3 Noise in the Imaging Signal ... 62
2.1.3.4 Nonuniform Atomically Imprecise Tips ... 63
2.1.4 Classical vs. High-Stiffness FM-AFM ... 67
2.1.5 Dynamic Mode with Stiff Cantilevers and Small Amplitudes ... 73
2.1.6 qPlus Tuning Fork Tips ... 76
2.1.7 Typical SPM Topographic Raster Scanning Pattern ... 80

2.2 Basic Positioning Technologies ... 81
2.2.1 Piezoelectric and Piezoceramic Actuators ... 81
2.2.2 Voice Coil Actuators ... 83
2.2.3 Electrostatic Actuators ... 84
2.2.4 Aerostatic Actuators ... 85
2.2.5 Required Positional Accuracy in SPM-Based DMS Systems ... 89

2.3 Basic Positional Measurement Technologies ... 95
2.3.1 Metrological Optical Interferometry ... 96
2.3.1.1 Michelson Interferometry ... 96
2.3.1.2 Mach-Zehnder Interferometry ... 98
2.3.1.3 Fabry-Pérot Interferometry ... 99
2.3.1.3.1 Fabry-Pérot Etalons ... 100
2.3.1.3.2 Fabry-Pérot Interferometers ... 102
2.3.1.3.3 Fabry-Pérot Cavities ... 102
2.3.1.3.4 Fizeau and Gires-Tournois Interferometers ... 104
2.3.1.3.5 Fiber-Based Fabry-Pérot Interferometers ... 105
2.3.1.3.6 Pound-Drever-Hall Technique ... 107
2.3.1.4 Sagnac Interferometry ... 109
2.3.1.5 Heterodyne Interferometry ... 109
2.3.1.6 Homodyne Interferometry ... 113
2.3.1.7 Factors Affecting Optical Interferometry Accuracy ... 116
2.3.2 Combination Optical Source/Detector ... 118
2.3.3 Non-Optical Capacitive Sensors ... 119

2.3.4 Non-Optical Piezo Sensors 121
2.4 Tip-Based Nanofabrication (TBN) 121

3. Background on Atomic Force Microscope Systems 124

3.1 General Structure and Function of AFMs 124
3.1.1 Design Principles 125
3.1.1.1 General Requirements 126
3.1.1.2 Thermal Drift 126
3.1.1.3 Positioning Errors 127
3.1.2 Metrological Instruments 128
3.1.3 Commercial Instruments 133
3.2 Scanning Systems 134
3.2.1 Positioning Systems 135
3.2.2 Detection Systems 137
3.2.2.1 Survey of Detection Systems 137
3.2.2.2 Optical Detection Systems 142
3.2.2.3 Self-Sensing SPM Probes 142
3.2.2.4 Self-Actuated SPM Probes 144
3.2.2.5 Multiple SPM Probes and Probe Arrays 146
3.3 Cantilevers and Tips 148
3.3.1 Cantilever Beams 148
3.3.2 Cantilever Characterization 150
3.3.3 Tip Shape 151
3.3.4 Tip Characterizers 157
3.3.5 Tip Registration 162
3.4 Combination AFM Displacement Systems 164
3.4.1 AFM and X-ray Interferometry 165
3.4.2 AFM and CMM 166
3.4.3 Large-Range AFMs 167
3.5 Noise, Environmental Isolation, and Measurement Uncertainty 168

4. Key Enabling Technologies for the Molecular Workstation 172

4.1 Workspace Surfaces 172
4.1.1 Atomically Flat Surfaces 173
4.1.2 Feedstock Presentation Surface 177
4.1.3 Disposal Surface 180
4.1.4 DMS Fabrication Surface 181
4.1.5 Release Surface 181
4.1.6 Nanopart Gripper Tool 184
4.1.7 Rapid Surface Scanning 186
4.2 Atomically Sharp Tooltips 186
4.2.1 Survey of Ultrasharp SPM Tips 188
4.2.2 Plan A: Single-Atom Metallic SPM Tips 198
4.2.2.1 Fabrication and Availability 201
4.2.2.2 DMS Reaction Energetics Using Metal Tips 211
4.2.2.3 Bond Strength and Scission Forces with Metal Tips 217
4.2.2.4 Other Aspects of Using Single-Atom Metal Tips 222
4.2.3 Plan B: ALE-Coated Single-Atom SPM Tips 222

4.2.4 Plan C: Atomically-Precise Single-Atom Tooltips from PALE 224
4.2.5 Plan D: Graphene Dome Tips on Ir(111) Surface 231
4.2.6 Plan E: Atomically-Imprecise Tooltips 232

4.3 Tooltip Handles, Tool Chucks, and Toolrack 235

4.3.1 Tooltip Handles and MEMS-Based qPlus Toolheads 235
4.3.2 Tool Chucks 237
4.3.3 Tool Jigs 240
4.3.4 Toolrack 241

4.4 Tooltip Positional Registration 241

4.5 SPM Positioning Systems 243

4.5.1 Actuator Systems 243
4.5.2 Commercial Positioning Systems 247
4.5.3 SPM-Based Multi-Tip and Multi-DOF Systems 250

4.6 Metrological SPM Systems 260

4.6.1 High-Precision Large-Range SPM-Based Systems 260
4.6.1.1 Molecular Measuring Machine (M^3) at NIST (U.S.) 262
4.6.1.2 Large-Range Scanning Probe Microscope (LR-SPM) (Germany) 268
4.6.1.3 LORS and SAMM (Univ. N. Carolina, MIT) 276
4.6.1.4 NMi Nanopositioner (Netherlands) 279
4.6.1.5 3D Measuring Instrument (BNM-LNE, France) 281
4.6.1.6 NRC Metrological AFM (Canada) 282
4.6.1.7 Dual-Level Translation Stage (CEA, INM/CNAM, LIRIS, LNIO, France) 289
4.6.1.8 AFM Head for Nano-Measuring Machine (Tsinghua University, China) 289
4.6.1.9 6-DOF Laser Interferometry (Menq Group, Ohio State Univ.) 290
4.6.1.10 Parallel-Kinematics Nanopositioner (Univ. of Illinois) 291
4.6.1.11 LRM-AFM (Singapore) 292
4.6.1.12 DIU-AFM (Zhang group, Zhejiang University, China) 294
4.6.1.13 Magnetic Levitation Stage (Tsinghua University, China) 294
4.6.1.14 Nanorobotics Technologies (Univ. Nottingham, UK) 295
4.6.1.15 Directed Reconfigurable Nanomachines (Univ. Nottingham, UK) 297
4.6.1.16 Other Large-Range Systems 298
4.6.2 Combined Optical and X-ray Interferometry (COXI) Systems 300
4.6.2.1 The COXI System at NPL/PTB/IMGC (Europe) 303
4.6.2.2 Subsequent COXI Work at NPL (U.K.) and PTB (Germany) 313
4.6.2.3 Subsequent COXI Work at IMGC/INRIM (Italy) 319
4.6.2.4 EUROMET and the Nanotrace Project (Europe) 321
4.6.2.5 Atomic Displacement Metrology – COXI at NIST (U.S.) 325
4.6.2.6 2D COXI at KRISS/KAIST (South Korea) 326
4.6.2.7 XROI at NRLM/NMIJ (Japan) 331
4.6.2.8 Summary of COXI-Based Systems 332
4.6.3 Michelson Interferometry Systems 332
4.6.3.1 Lawall-Kessler Differential Optical Interferometry (NIST, U.S.) 332
4.6.3.2 Tunable-Laser Michelson Interferometer at NIST (U.S.) 341
4.6.3.3 Calibrated AFM at NIST (U.S.) 345
4.6.3.4 Multiple-Reflection Michelson Interferometer at INRIM (Italy) 347
4.6.3.5 Dual Optical Wavelength Interferometer (Czech Metrology Institute) 352
4.6.3.6 AFM with Three-Axis Laser Interferometer (Japan) 353
4.6.3.7 Crystal Reference Interferometry with SPM (Japan) 361
4.6.3.8 Dual-Wavelength Vernier Zooming Interferometer (China) 367
4.6.3.9 Super-Heterodyne Zooming Interferometer (Japan) 370
4.6.3.10 Positioning Control Method (Chassagne Group, France) 375
4.6.3.11 Laser Doppler Displacement Meter (Argonne Natl. Lab) 383

4.6.3.12 Heterodyne Displacement Measuring Interferometer (Univ. Florida) 387
4.6.3.13 Heterodyne Interferometer with Subatomic Periodic Nonlinearity (Wu et al. 1999) 390
4.6.3.14 Heidenhain Interferometer (Germany) 391
4.6.3.15 Phase Shifting Interferometry (PSI) 391
4.6.3.16 Other Michelson-Based Systems 395
4.6.3.17 Summary of Michelson-Based Systems 402
4.6.4 Fabry-Pérot (FP) Interferometry Systems 403
4.6.4.1 Atomic Displacement Metrology (ADM) Project at NIST (U.S.) 403
4.6.4.2 Tunable-Laser FP Interferometer at NIST (Lawall, U.S.) 407
4.6.4.3 Tunable-Laser FP Interferometer at NIST (Howard, U.S.) 413
4.6.4.4 Tunable-Laser FP using Optical Frequency Combs (Japan) 416
4.6.4.5 Fabry-Pérot 1D Metrology Platform (Haitjema group) 421
4.6.4.6 Combined Optical Interferometer (BUPE Project, S. Korea) 422
4.6.4.7 White-Light Interferometry (WLI) 425
4.6.4.8 Other Fabry-Pérot Interferometry Systems 438
4.6.4.9 Summary of Fabry-Pérot Interferometry Systems 440
4.6.5 Digitally Enhanced Heterodyne Interferometry (Shaddock, Australia) 440
4.6.6 Astronomical Metrological Interferometer Systems 445
4.6.6.1 Astrometry and Extrasolar Planet Detection 445
4.6.6.1.1 JPL/SIM Lite Astrometric Observatory 445
4.6.6.1.2 The Keck Interferometer 455
4.6.6.1.3 GAIA Astrometric Metrology Mission 458
4.6.6.1.4 Other Interferometric Astrometry Projects 460
4.6.6.2 Gravitational Wave Detection 461
4.6.6.2.1 Laser Interferometer Gravitational-Wave Observatory (LIGO) 461
4.6.6.2.2 Laser Interferometry Space Antenna (LISA) 463
4.6.7 Multimode Waveguide Interferometry (MWI) 465
4.6.8 Electron Interferometry 469
4.6.9 Non-Interferometric Backscatter Detection (Univ. of Colorado) 470
4.6.10 Other Metrology Approaches 480
4.6.11 Summary of Possible Workstation Metrology Systems 481
4.7 Environmental Isolation 484
4.7.1 Ultra-High Vacuum System 484
4.7.2 Temperature Regulation System 489
4.7.3 Vibration Isolation System 491
4.8 Ancillary Facilities 493
4.9 Control Software 493

5. Conclusions 495

Accompanying documents include:

Freitas RA Jr., Merkle RC. A Nanofactory Roadmap: Research Proposal for a Comprehensive Diamondoid Nanofactory Development Program. IMM Report No. 58, 2008/2025; http://www.imm.org/Reports/rep058.pdf.

and

Freitas RA Jr. Molecular Workstation Roadmap II: Survey of Single-Atom Tips (SATs) for Diamondoid Mechanosynthesis**.** IMM Report No. 60, 2010/2025; http://www.imm.org/Reports/rep060.pdf.

1. Introduction to Atomically Precise UHV/Tip-Based Molecular Manufacturing

The molecular workstation is a scanning probe microscopy (SPM) based system that will be used to perform atomically precise manufacturing – in particular, the fabrication of single instances of relatively small diamondoid nanostructures (i.e., up to 100-1000 atoms consisting mostly of the elements C, H, and Ge) on a flat bulk-prepared diamondoid fabrication surface using the techniques of diamondoid mechanosynthesis.

To accomplish this objective, we are following the proposed pathway to atomically precise manufacturing known as scanning probe diamondoid mechanosynthesis (DMS).[1] DMS employs scanning probe technology in combination with novel reactive tips to fabricate atomically-precise diamondoid components under positional control. This pathway has its roots in the 1986 book *Engines of Creation*, in which the manufacture of diamondoid parts was proposed as a long-term objective by Drexler,[2] and in the 1989 demonstration by Donald Eigler at IBM that individual atoms could be manipulated by a scanning tunneling microscope[3] (Figure 1-1). The proposed DMS-based pathway would skip intermediate technologies proposed by Drexler[4] – these begin with polymeric structures and solution-phase synthesis, though no specific methods for bridging the enormous gap between polymeric and diamondoid structures have ever been proposed[5] – and would instead move toward advanced DMS in a more direct way.

---

[1] Nanofactory Collaboration website, accessed February 2008; http://www.MolecularAssembler.com/Nanofactory.

[2] 700 K. Eric Drexler, Engines of Creation: The Coming Era of Nanotechnology, Anchor Press/Doubleday, New York, 1986.

[3] D.M. Eigler, E.K. Schweizer, "Positioning Single Atoms with a Scanning Tunnelling Microscope," Nature 344(5 April 1990):524-526; http://www.nature.com/nature/journal/v344/n6266/abs/344524a0.html (abstract).

[4] K. Eric Drexler, "Molecular engineering: an approach to the development of general capabilities for molecular manipulation," Proc. Natl. Acad. Sci. (USA) 78(September 1981):5275-5278. K. Eric Drexler, Nanosystems: Molecular Machinery, Manufacturing, and Computation, John Wiley & Sons, New York, 1992, Chapter 16. K. Eric Drexler, "Toward Integrated Nanosystems: Fundamental Issues in Design and Modeling," J. Comput. Theor. Nanosci. 3(February 2006):1-10.

[5] Hamid Ramezani, G. Ali Mansoori, Mohammad-Reza Saberi, "Diamondoids-DNA Nanoarchitecture: From Nanomodules Design to Self-Assembly," J. Comp. Theor. Nanosci. 4(February 2007):96-106.

Figure 1-1. IBM logo spelled out with 35 xenon atoms arranged on a nickel surface via scanning tunneling microscopy, using lateral manipulation of xenon atoms, in 1989.[6]

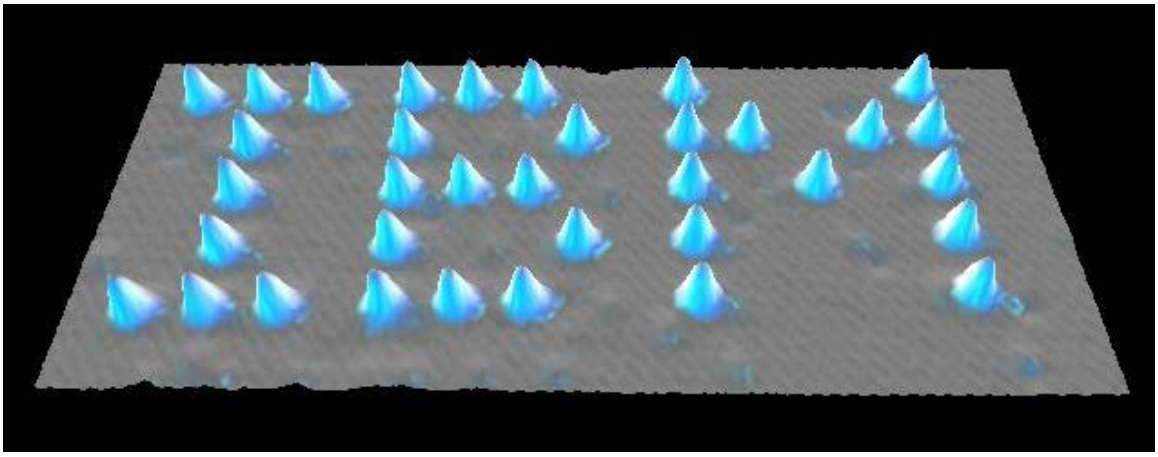

As noted in the 2007 Battelle-Foresight nanotechnology roadmap report:[7] "Perhaps the most important contribution of tip-based APM [Atomically Precise Manufacturing] will be to make the atomically precise components required for productive nanosystems....Iterating this process toward higher performance materials leads toward structures (for example, ceramics) that are denser and more stable than biopolymers. APM systems that build products of this sort are envisioned to use flexible tip-based processes, since **biomimetic approaches appear to have limited value in this area**. This anticipated convergence on tip-based inorganic systems suggests that **near-term, tip-based APM methods might be more directly developed in this direction**. The approaches of this kind also involve broadening the range of structures that can be built, leading to nanoscale structures that by themselves provide the central components necessary for APM." (emphasis added)

Although covalent-bonded self-assembly has been demonstrated,[8] complex atomically precise structures ranging from medical nanorobots to macroscale products also cannot be manufactured using the conventional techniques of self-assembly.[9] As noted in the final report[10] of the 2006

---

[6] D.M. Eigler, E.K. Schweizer, "Positioning Single Atoms with a Scanning Tunnelling Microscope," Nature 344(5 April 1990):524-526; http://www.nature.com/nature/journal/v344/n6266/abs/344524a0.html (abstract)

[7] Productive Nanosystems: A Technology Roadmap, Battelle Memorial Institute and Foresight Nanotech Institute, 2007; http://www.foresight.org/roadmaps/index.html.

[8] Leonhard Grill, Matthew Dyer, Leif Lafferentz, Mats Persson, Maike V. Peters, Stefan Hecht, "Nano-architectures by covalent assembly of molecular building blocks," Nature Nanotechnology 2(2007):687-691, http://dx.doi.org/10.1038/nnano.2007.346.

[9] N. Bowden, A. Terfort, J. Carbeck, G.M. Whitesides, "Self-assembly of mesoscale objects into ordered two-dimensional arrays," Science 276(1997)):233-235; A. Terfort, N. Bowden, G.M. Whitesides, "Three-

Congressionally-mandated review of the U.S. National Nanotechnology Initiative by the National Research Council (NRC) of the National Academies and the National Materials Advisory Board (NMAB): "For the manufacture of more sophisticated materials and devices, including complex objects produced in large quantities, it is unlikely that simple self-assembly processes will yield the desired results. The reason is that the probability of an error occurring at some point in the process will increase with the complexity of the system and the number of parts that must interoperate." Error detection and correction requires a minimum level of complexity that cannot easily be achieved via thermodynamically-driven self-assembly processes. Self-assembly is not conducive to rapid prototyping because small changes in the final product specification often require major changes in the self-assembly process, and small changes in the process or inputs can often produce large changes in the resulting product. Self-assembly usually produces relatively weak and compliant structures. Self-assembly also violates the principles of sound classical engineering design "because the functional requirements of components are very difficult to separate from each other....Changing one component often requires changing most of the other components also, resulting in a cascade of conflicting requirements that greatly restricts the search space of possible solutions, perhaps even making many sets of requirements unreachable."[11]

The opposite of self-assembly processes is positionally controlled processes, in which the positions and trajectories of all components of intermediate and final product objects are controlled at every moment during fabrication and assembly. For instance, positional control of laser-cooled individual atoms has been demonstrated using laser trapping,[12] and an atomic force microscope (AFM) has been used to manually operate a molecular rack-and-pinion system.[13]

---

dimensional self-assembly of millimetre-scale components," Nature 386(1997):162-164; T.L. Breen, J. Tien, S.R.J. Oliver, T. Hadzic, G.M. Whitesides, "Design and self-assembly of open, regular, 3D mesostructures," Science 284(1999):948-951; D.H. Gracias, J. Tien, T.L. Breen, C. Hsu, G.M. Whitesides, "Forming electrical networks in three dimensions by self-assembly," Science 289(2000):1170-1172; G.M. Whitesides. B. Grzybowski, Self-assembly at all scales," Science 295(2002):2418-2421; G.M. Whitesides, M. Boncheva, "Beyond molecules: Self-assembly of mesoscopic and macroscopic components," Proc. Natl. Acad. Sci. (USA) 99(2002):4769-4774; S. Griffith, D. Goldwater, J.M. Jacobson, "Self-replication from random parts," Nature 437(2005):636.

[10] Committee to Review the National Nanotechnology Initiative, National Materials Advisory Board (NMAB), National Research Council (NRC) (2006) A Matter of Size: Triennial Review of the National Nanotechnology Initiative. The National Academies Press, Washington DC; http://www.nap.edu/catalog/11752.html#toc.

[11] Tihamer Toth-Fejel, Modeling Kinematic Cellular Automata: Final Report, NASA Institute for Advanced Concepts, Phase I: CP-02-02, General Dynamics Advanced Information Systems Contract # P03-0984, 30 April 2004.

[12] Yevhen Miroshnychenko, Wolfgang Alt, Igor Dotsenko, Leonid Forster, Mkrtych Khudaverdyan, Dieter Meschede, Dominik Schrader, Arno Rauschenbeutel, "Quantum engineering: An atom-sorting machine," Nature 442(13 July 2006):151. See also: Frank Luerweg, "Quantum Computer: Laser tweezers sort atoms," PhysOrg.com, 12 July 2006; http://www.physorg.com/news71935118.html.

[13] Franco Chiaravalloti, Leo Gross, Karl-Heinz Rieder, Sladjana M. Stojkovic, André Gourdon, Christian Joachim, Francesca Moresco, "A rack-and-pinion device at the molecular scale," Nature Materials 6(2007):30-33; http://www.nature.com/nmat/journal/v6/n1/abs/nmat1802.html.

Positional processes should allow more complex products to be built with high quality and should enable rapid prototyping during product development. Positional assembly is the norm in conventional macroscale manufacturing (e.g., cars, appliances, houses) but is only recently[14] starting to be seriously investigated experimentally for nanoscale manufacturing. Of course, we already know that positional fabrication will work in the nanoscale realm. This is demonstrated in the biological world by ribosomes, which positionally assemble proteins in living cells by following a sequence of digitally encoded instructions (even though ribosomes themselves are self-assembled). Lacking this positional fabrication of proteins controlled by DNA-based software, large, complex, digitally-specified organisms would probably not be possible and biology as we know it would not exist.

The most important materials for positional assembly may be the rigid covalent or "diamondoid" solids, since these could potentially be used to build the most reliable and complex nanoscale machinery. Preliminary theoretical studies have suggested great promise for these materials in molecular manufacturing. The NMAB/NRC Review Committee recommended[15] that experimental work aimed at establishing the technical feasibility of positional molecular manufacturing should be pursued and supported: "Experimentation leading to demonstrations supplying ground truth for abstract models is appropriate to better characterize the potential for use of bottom-up or molecular manufacturing systems that utilize processes more complex than self-assembly." Making complex nanorobotic systems requires manufacturing techniques that can build a molecular structure by positional assembly.[16] This will involve picking and placing individual atoms, small molecules, or molecular parts one by one, moving them along controlled trajectories much like the robot arms that manufacture cars on automobile assembly lines. The procedure is then repeated over and over with all the different parts until the final product, such as a medical nanorobot, is fully assembled using a desktop nanofactory.

1.1 Diamondoid Mechanosynthesis (DMS)

Theorists believe that the most reliable and durable medical nanorobots will be built using diamondoid materials. What is diamondoid? First and foremost, diamondoid materials include pure diamond, the crystalline allotrope of carbon. Among other exceptional properties, diamond has extreme hardness, high thermal conductivity, low frictional coefficient, chemical inertness, a

---

[14] Nanofactory Collaboration website, accessed February 2008; http://www.MolecularAssembler.com/Nanofactory. T. Kenny, "Tip-Based Nanofabrication (TBN)," Defense Advanced Research Projects Agency (DARPA)/Microsystems Technology Office (MTO), Broad Agency Announcement BAA 07-59, July 2007; http://www.fbo.gov/spg/ODA/DARPA/CMO/BAA07-59/listing.html.

[15] Committee to Review the National Nanotechnology Initiative, National Materials Advisory Board (NMAB), National Research Council (NRC) (2006) A Matter of Size: Triennial Review of the National Nanotechnology Initiative. The National Academies Press, Washington DC; http://www.nap.edu/catalog/11752.html#toc.

[16] Robert A. Freitas Jr., "Current status of nanomedicine and medical nanorobotics," J. Comput. Theor. Nanosci. 2(2005):1-25; http://www.nanomedicine.com/Papers/NMRevMar05.pdf.

wide electronic bandgap, and is the strongest[17] and stiffest material presently known at ordinary pressures. Diamondoid materials also may include any stiff covalent solid that is similar to diamond in strength, chemical inertness, or other important material properties, and possesses a dense three-dimensional network of bonds. Examples of such materials are carbon nanotubes and fullerenes, several strong covalent ceramics such as silicon carbide, silicon nitride, and boron nitride, and a few very stiff ionic ceramics such as sapphire (monocrystalline aluminum oxide) that can be covalently bonded to pure covalent structures such as diamond. Of course, large pure crystals of diamond are brittle and easily fractured. The intricate molecular structure of a diamondoid nanofactory macroscale product will more closely resemble a complex composite material, not a brittle solid crystal. Such products, and the nanofactories that build them, should be extremely durable in normal use.

Mechanosynthesis, involving molecular positional fabrication, is the formation of covalent chemical bonds using precisely applied mechanical forces to build, for example, diamondoid structures. Mechanosynthesis employs chemical reactions driven by the mechanically precise placement of extremely reactive chemical species in an ultra-high vacuum environment. Chemical activation energy is supplied by mechanical force, not by heat.[18] Atomically precise fabrication involves holding feedstock atoms or molecules, and a growing nanoscale workpiece, in the proper relative positions and orientations with picoscale precision so that when they touch they will chemically bond in the desired manner. In this process, a mechanosynthetic tool is brought up to the surface of a workpiece. One or more transfer atoms are added to, or removed from, the workpiece by the tool. Then the tool is withdrawn and recharged. This process is repeated until the workpiece (e.g., a growing nanopart) is completely fabricated to molecular precision with each atom in exactly the right place. Note that the transfer atoms are under positional control at all times to prevent unwanted side reactions from occurring. Side reactions are also prevented using proper reaction design so that the reaction energetics help us avoid undesired pathological intermediate structures. Mechanosynthesis also may be automated via computer control, enabling programmable molecular positional fabrication.

The positional assembly of diamondoid structures, some almost atom by atom, using molecular feedstock has been examined theoretically[19] via computational models of diamond

---

[17] J.E. Field, "Chapter 9. Strength and Fracture Properties of Diamond," in J.E. Field, ed., The Properties of Diamond, Academic Press, New York, 1979, pp. 281-324; R.H. Telling, C.J. Pickard, M.C. Payne, J.E. Field, "Theoretical Strength and Cleavage of Diamond," Phys. Rev. Lett. 84(May 2000):5160-5163, http://www.tcm.phy.cam.ac.uk/~cjp20/publications/PRL84_5160.pdf.

[18] Martin Konôpka, Robert Turanský, Joachim Reichert, Harald Fuchs, Dominik Marx, Ivan Štich, "Mechanochemistry and Thermochemistry are Different: Stress-Induced Strengthening of Chemical Bonds," Phys. Rev. Lett. 100(19 March 2008):115503, http://link.aps.org/abstract/PRL/v100/e115503.

[19] Robert A. Freitas Jr., Ralph C. Merkle, "A Minimal Toolset for Positional Diamond Mechanosynthesis," J. Comput. Theor. Nanosci. 5(May 2008):760-861; http://www.molecularassembler.com/Papers/MinToolset.pdf. Jingping Peng, Robert A. Freitas Jr., Ralph C. Merkle, James R. Von Ehr, John N. Randall, George D. Skidmore, "Theoretical Analysis of Diamond Mechanosynthesis. Part III. Positional C_2 Deposition on Diamond C(110) Surface using Si/Ge/Sn-based Dimer Placement Tools," J. Comput. Theor. Nanosci. 3(February 2006):28-41; http://www.MolecularAssembler.com/Papers/JCTNPengFeb06.pdf. Berhane Temelso, C. David Sherrill, Ralph C. Merkle, Robert A. Freitas Jr., "High-level Ab Initio Studies of Hydrogen Abstraction from

mechanosynthesis (DMS). DMS is the controlled addition of individual carbon atoms, carbon dimers (C_2), single methyl (CH_3) or like groups to the growth surface of a diamond crystal lattice workpiece in a vacuum manufacturing environment. Covalent chemical bonds are formed one by one as the result of positionally constrained mechanical forces applied at the tip of a scanning probe microscope (SPM) apparatus. Programmed sequences of carbon dimer placement on growing diamond surfaces *in vacuo* appear feasible in theory,[20] as illustrated by the hypothetical DCB6Ge tooltip which is shown depositing two carbon atoms on a diamond surface in Figure 1-2.

Prototype Hydrocarbon Systems," J. Phys. Chem. A 110(28 September 2006):11160-11173; http://pubs.acs.org/cgi-bin/abstract.cgi/jpcafh/2006/110/i38/abs/jp061821e.html (abstract), http://www.MolecularAssembler.com/Papers/TemelsoHAbst.pdf (paper). Berhane Temelso, C. David Sherrill, Ralph C. Merkle, Robert A. Freitas Jr., "Ab Initio Thermochemistry of the Hydrogenation of Hydrocarbon Radicals Using Silicon, Germanium, Tin and Lead Substituted Methane and Isobutane," J. Phys. Chem. A 111(15 August 2007):8677-8688. http://pubs.acs.org/cgi-bin/abstract.cgi/jpcafh/asap/abs/jp071797k.html (abstract), http://www.MolecularAssembler.com/Papers/TemelsoHDon.pdf (paper). Ralph C. Merkle, Robert A. Freitas Jr., "Theoretical analysis of a carbon-carbon dimer placement tool for diamond mechanosynthesis," J. Nanosci. Nanotechnol. 3(August 2003):319-324; http://www.rfreitas.com/Nano/JNNDimerTool.pdf. See also: Ralph C. Merkle, Robert A. Freitas Jr., "Theoretical analysis of a carbon-carbon dimer placement tool for diamond mechanosynthesis," paper presented at the 10th Foresight Conference on Molecular Nanotechnology, October 2002; http://www.foresight.org/Conferences/MNT10/Abstracts/Merkle/index.html. Ralph C. Merkle, "A proposed 'metabolism' for a hydrocarbon assembler," Nanotechnology 8(1997):149-162; http://www.zyvex.com/nanotech/hydroCarbonMetabolism.html. K. Eric Drexler, Nanosystems: Molecular Machinery, Manufacturing, and Computation, John Wiley & Sons, New York, 1992, Chapter 8. David J. Mann, Jingping Peng, Robert A. Freitas Jr., Ralph C. Merkle, "Theoretical analysis of diamond mechanosynthesis. Part II. C_2 mediated growth of diamond C(110) surface via Si/Ge-triadamantane dimer placement tools," J. Comput. Theor. Nanosci. 1(March 2004):71-80; http://www.MolecularAssembler.com/JCTNMannMar04.pdf. Damian G. Allis, K. Eric Drexler, "Design and Analysis of a Molecular Tool for Carbon Transfer in Mechanosynthesis," J. Comput. Theor. Nanosci. 2(March 2005):45-55; http://e-drexler.com/d/05/00/DC10C-mechanosynthesis.pdf. Robert A. Freitas Jr., "A simple tool for positional diamond mechanosynthesis, and its method of manufacture," U.S. Provisional Patent Application No. 60/543,802, filed 11 February 2004; U.S. Patent Pending, 11 February 2005; http://www.MolecularAssembler.com/Papers/DMSToolbuildProvPat.htm. Robert A. Freitas Jr., Damian G. Allis, Ralph C. Merkle, "Horizontal Ge-Substituted Polymantane-Based C_2 Dimer Placement Tooltip Motifs for Diamond Mechanosynthesis," J. Comput. Theor. Nanosci. 4(May 2007):433-442; http://www.MolecularAssembler.com/Papers/DPTMotifs.pdf.

[20] Robert A. Freitas Jr., Ralph C. Merkle, "A Minimal Toolset for Positional Diamond Mechanosynthesis," J. Comput. Theor. Nanosci. 5(May 2008):760-861; http://www.molecularassembler.com/Papers/MinToolset.pdf. Jingping Peng, Robert A. Freitas Jr., Ralph C. Merkle, James R. Von Ehr, John N. Randall, George D. Skidmore, "Theoretical Analysis of Diamond Mechanosynthesis. Part III. Positional C_2 Deposition on Diamond C(110) Surface using Si/Ge/Sn-based Dimer Placement Tools," J. Comput. Theor. Nanosci. 3(February 2006):28-41; http://www.MolecularAssembler.com/Papers/JCTNPengFeb06.pdf.

Figure 1-2. DCB6Ge tooltip shown depositing two carbon atoms on a diamond surface.[21] (C = cyan, H = white, Ge = yellow)

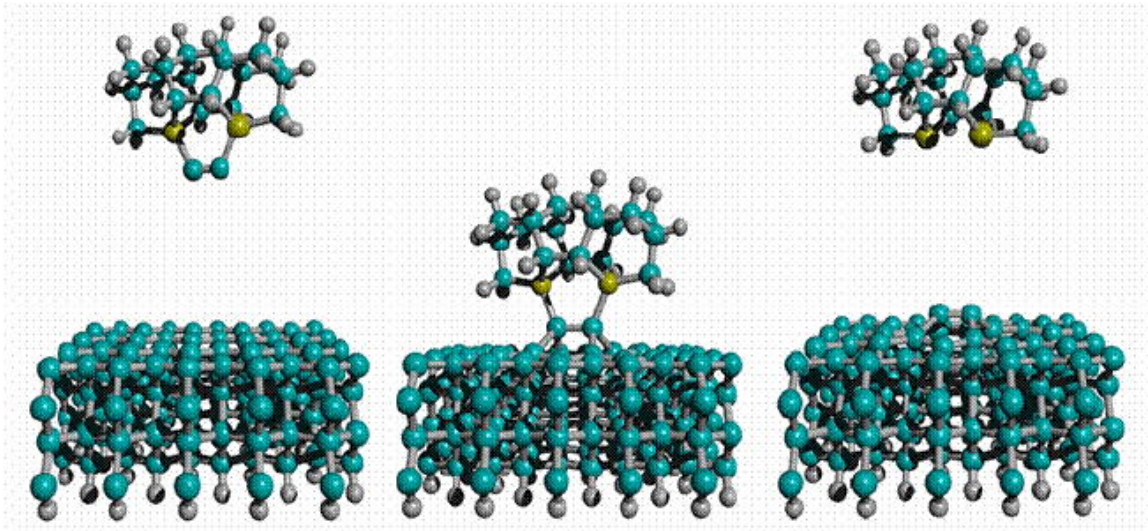

The first experimental proof that individual atoms could be manipulated was obtained by IBM scientists[22] in 1989 when they used a scanning tunneling microscope to precisely position 35 xenon atoms on a nickel surface to spell out the corporate logo "IBM" (Figure 1-1). However, this feat did not involve the formation of covalent chemical bonds. One important step toward the practical realization of DMS was achieved in 1999 by Ho and Lee,[23] who achieved the first site-repeatable site-specific covalent bonding operation of a two diatomic carbon-containing molecules (CO), one after the other, to the same atom of iron on a crystal surface, using an SPM. There have since been many other experimental demonstrations of single-molecule chemistry.[24]

---

[21] Nanofactory Collaboration website, accessed February 2008; http://www.MolecularAssembler.com/Nanofactory.

[22] D.M. Eigler, E.K. Schweizer, "Positioning Single Atoms with a Scanning Tunnelling Microscope," Nature 344(5 April 1990):524-526; http://www.nature.com/nature/journal/v344/n6266/abs/344524a0.html (abstract).

[23] Wilson Ho, Hyojune Lee, "Single bond formation and characterization with a scanning tunneling microscope," Science 286(26 November 1999):1719-1722; http://www.physics.uci.edu/~wilsonho/stm-iets.html.

[24] Saw-Wai Hla, Ludwig Bartels, Gerhard Meyer, Karl-Heinz Rieder, "Inducing All Steps of a Chemical Reaction with the Scanning Tunneling Microscope Tip: Towards Single Molecule Engineering," Phys. Rev. Lett. 85(September 2000):2777-2780; http://prola.aps.org/abstract/PRL/v85/i13/p2777_1 (abstract), http://www.phy.ohiou.edu/~hla/HLA2000-2.pdf (paper). B.C. Stipe, M.A. Rezaei, W. Ho, S. Gao, M. Persson, B.I. Lundqvist, "Single-Molecule Dissociation by Tunneling Electrons," Phys. Rev. Lett. 78(1997):4410-4413. J.R. Hahn, W. Ho, "Oxidation of a Single Carbon Monoxide Molecule Manipulated and Induced with a Scanning Tunneling Microscope," Phys. Rev. Lett. 87(28 September 2001):166102.

The first experimental demonstration of true mechanosynthesis, establishing covalent bonds using purely mechanical forces – albeit on silicon atoms, not carbon atoms – was reported in 2003 by Oyabu and colleagues[25] in the Custance group. In this landmark experiment, the researchers vertically manipulated single silicon atoms from the Si(111)-(7×7) surface, using a low-temperature near-contact atomic force microscope to demonstrate (1) removal of a selected silicon atom from its equilibrium position without perturbing the (7×7) unit cell and (2) the deposition of a single Si atom on a created vacancy, both via purely mechanical processes. They later repeated the same feat in 2004[26] with a Ge atom and again in 2008[27] with Sn, Pb and In atoms on a Si(111) surface (see Section 2.1.2 and Figure 2-11).

Following prior theoretical proposals[28] for experimental investigations, participants in the Nanofactory Collaboration[29] began planning work designed to achieve DMS with carbon and hydrogen atoms using an SPM apparatus (Section 1.3). (Both positionally controlled surface assembly of DNA-based structures using an AFM tip[30] and protein mechanosynthesis,[31] along

---

Jascha Repp, Gerhard Meyer, Sami Paavilainen, Fredrik E. Olsson, Mats Persson, "Imaging bond formation between a gold atom and pentacene on an insulating surface," Science 312(26 May 2006):1196-1199.

[25] Noriaki Oyabu, Oscar Custance, Insook Yi, Yasuhiro Sugawara, Seizo Morita, "Mechanical vertical manipulation of selected single atoms by soft nanoindentation using near contact atomic force microscopy," Phys. Rev. Lett. 90(2 May 2003):176102; http://link.aps.org/abstract/PRL/v90/e176102 (Abstract) http://focus.aps.org/story/v11/st19 (APS story)

[26] N. Oyabu, O. Custance, M. Abe, S. Moritabe, "Mechanical Vertical Manipulation of Single Atoms on the Ge(111)-c(2x8) Surface by Noncontact Atomic Force Microscopy," Abstracts of Seventh International Conference on non-contact Atomic Force Microscopy, Seattle, Washington, USA, 12-15 September, 2004, p. 34; http://www.engr.washington.edu/epp/afm/abstracts/15Oyabu2.pdf.

[27] Yoshiaki Sugimoto, Pablo Pou, Oscar Custance, Pavel Jelinek, Masayuki Abe, Ruben Perez, Seizo Morita, "Complex Patterning by Vertical Interchange Atom Manipulation Using Atomic Force Microscopy," Science 322(17 October 2008):413-417;
http://www.sciencemag.org/cgi/content/full/322/5900/413 (paper)
http://www.sciencemag.org/cgi/content/full/322/5900/413/DC1 (supplement).

[28] Robert A. Freitas Jr., Ralph C. Merkle, "A Minimal Toolset for Positional Diamond Mechanosynthesis," J. Comput. Theor. Nanosci. 5(May 2008):760-861;
http://www.molecularassembler.com/Papers/MinToolset.pdf. Robert A. Freitas Jr., "A simple tool for positional diamond mechanosynthesis, and its method of manufacture," U.S. Provisional Patent Application No. 60/543,802, filed 11 February 2004; U.S. Patent Pending, 11 February 2005;
http://www.MolecularAssembler.com/Papers/DMSToolbuildProvPat.htm.

[29] Nanofactory Collaboration website, accessed February 2008;
http://www.MolecularAssembler.com/Nanofactory.

[30] S.K. Kufer, E.M. Puchner, H. Gumpp, T. Liedl, H.E. Gaub, "Single-Molecule Cut-and-Paste Surface Assembly," Science 319(1 February 2008):594-596.

[31] T.P. Sullivan, M.L. Van Poll, P.Y. Dankers, W.T. Huck, "Forced Peptide Synthesis in Nanoscale Confinement under Elastomeric Stamps," Angew. Chem. Int. Ed. Engl. 43(13 August 2004):4190-4193.

with mechanically-augmented[32] and sonomechanically-augmented[33] organic chemical reaction rates, have already been demonstrated experimentally.)

There is a growing realization of the importance of tip-based methods in the field of nanoscale manufacturing. For example, in 2007 DARPA issued a Broad Agency Announcement (BAA) soliciting proposals on Tip-Based Nanofabrication to make nanowires, nanotubes, or quantum dots using functionalized scanning probe tips.[34] Also in 2007, Johannes et al.[35] reported using an AFM to draw patterns of local anodic oxidation on a silicon substrate, yielding 3D silicon dioxide structures with ~100 nm features in the shapes of circles, triangles, and stars (Figure 1-3). Note, however, that neither method specifies sufficient positional resolution to accomplish atomically precise manufacturing (Table 1-1). Similarly, in 2009 DARPA issued a solicitation notice[36] for innovative fundamental research proposals in the area of nanoelectromechanical systems (NEMS) and microelectromechanical systems (MEMS) devices and arrays enabled by emerging and maturing nano/micro technologies, seeking proposals for focus centers in technology areas including "***Single-Molecule Methods*:** Understanding fundamental issues associated with bottom-up construction of MEMS/NEMS structures and devices, surface functionalization, ***atom-by-atom engineering***, and self-replicating MEMS/NEMS."

---

[32] F. Kersey, W.C. Yount, S.L. Craig, "Single Molecule Force Spectroscopy of Bimolecular Reactions: System Homology in the Mechanical Activation of Ligand Substitution Reactions," J. Am. Chem. Soc. 128(2006):3886-3887, http://pubs.acs.org/cgi-bin/abstract.cgi/jacsat/2006/128/i12/abs/ja058516b.html; see also http://www.sciencemag.org/cgi/reprint/311/5767/1525c.pdf.

[33] C.R. Hickenboth, J.S. Moore, S.R. White, N.R. Sottos, J. Baudry, S.R. Wilson, "Biasing reaction pathways with mechanical force," Nature 446(22 March 2007):423-427.

[34] T. Kenny, "Tip-Based Nanofabrication (TBN)," Defense Advanced Research Projects Agency (DARPA)/Microsystems Technology Office (MTO), Broad Agency Announcement BAA 07-59, July 2007; http://www.fbo.gov/spg/ODA/DARPA/CMO/BAA07-59/listing.html.

[35] Matthew S. Johannes, Daniel G. Cole, Robert L. Clark, "Three-dimensional design and replication of silicon oxide nanostructures using an atomic force microscope," Nanotechnology 18(2007):345304.

[36] "N/MEMS S&T Fundamentals," Research Announcement, Microsystems Technology Office (MTO), DARPA-RA-09-42, 4 May 2009; https://www.fbo.gov/utils/view?id=663f38da098993f0e7b4f75f72faeeae.

Figure 1-3. Design and replication of select 3D nanostructures: (a) CAD design of desired features; (b)-(d) contact AFM height images of resulting structures. The sample structures are about 100 nm in feature size, using silicon oxide.[37]

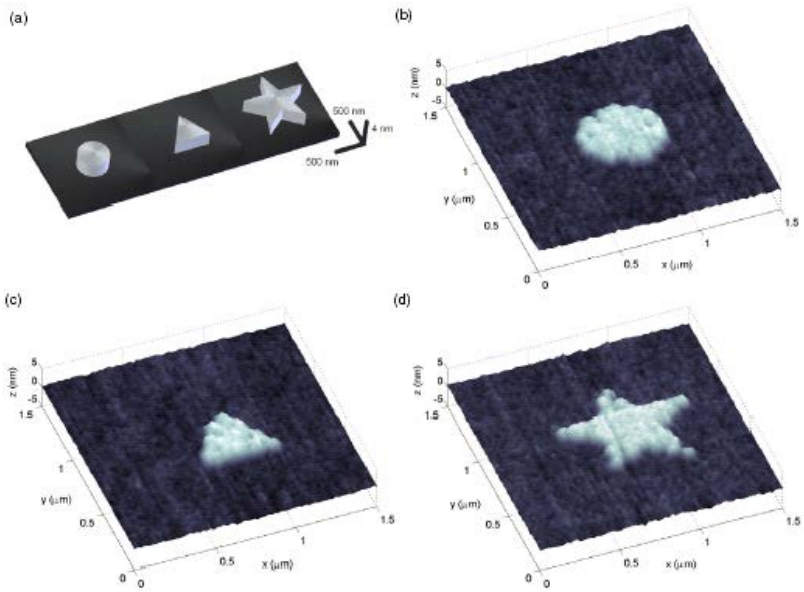

Table 1-1. Metrics in DARPA BAA for Tip-Based Nanomanufacturing[38]				
Metric	**Unit**	***Phase I***	***Phase II***	***Phase III***
Feature Position Control	nm	50	25	5
Feature Size Control	% of dimension	10%	3%	1%
Heterogeneity		2 values of one parameter	5 values of 2 parameters	Continuous control over 2 parameters
Feature Rate		1/min Single tip	5/min/tip 5-tip array	60/min/tip 30-tip array
Tip Shape Variation	% of dimension	Height < 10% Radius < 20% 100 operations	Height < 10% Radius < 20% 10^3 operations	Height < 10% Radius < 20% 10^6 operations
Tip Height Sensing	nm	20 nm	10 nm	2 nm

[37] 4 Matthew S. Johannes, Daniel G. Cole, Robert L. Clark, "Three-dimensional design and replication of silicon oxide nanostructures using an atomic force microscope," Nanotechnology 18(2007):345304.

[38] T. Kenny, "Tip-Based Nanofabrication (TBN)," Defense Advanced Research Projects Agency (DARPA)/Microsystems Technology Office (MTO), Broad Agency Announcement BAA 07-59, July 2007; http://www.fbo.gov/spg/ODA/DARPA/CMO/BAA07-59/listing.html.

Two-handed coordinated micromanipulation under the view of an SEM was demonstrated in 1993,[39] followed by the first microscale AFM in 1995.[40] In 1998, Zyvex demonstrated the first simultaneous coordinated operation of three independently controlled AFM tips within the same workspace at different orientations;[41] Zyvex's custom piezoelectric vacuum manipulator achieved positional resolutions comparable to SPMs along with the ability to manipulate objects along one rotational and three linear degrees of freedom with 0.1 nm spatial resolution, allowing the simultaneous coordinated operation of three independently controlled AFM tips within the same workspace, at different orientations. A successor 4-tip system was designed as early as 1999 and finally offered as a commercial product starting in 2003 (Figure 4-21). Recent work has proceeded to even more tooltips[42] and degrees of freedom (Section 4.5.3).

1.2 Designing a Minimal Toolset for DMS

It is already possible to synthesize bulk diamond today. In a process somewhat reminiscent of spray painting, layer after layer of diamond can be built up by holding a cloud of reactive hydrogen atoms and hydrocarbon molecules over a deposition surface. When these molecules bump into the surface they change it by adding, removing, or rearranging atoms. By carefully controlling the pressure, temperature, and the exact composition of the gas in this process – called chemical vapor deposition or CVD – conditions can be created that favor the growth of diamond on the surface. But randomly bombarding a surface with reactive molecules does not offer fine control over the growth process and lacks atomic-level positional control. To achieve molecularly precise fabrication, the first challenge is to make sure that all chemical reactions will occur at precisely specified places on the surface. A second problem is how to make the diamond surface reactive at the particular spots where we want to add another atom or molecule. A diamond surface is normally covered with a layer of hydrogen atoms. Without this layer, the raw diamond surface would be highly reactive because it would be studded with unused (or "dangling") bonds from the topmost plane of carbon atoms. While hydrogenation prevents unwanted reactions, it also renders the entire surface inert, making it difficult to add carbon (or anything else) to it.

---

[39] Hiroshi Morishita, Yotaro Hatamura, "Development of Ultra Micro Manipulator System Under Stereo SEM Observation," Proc. 1993 IEEE/RSJ Intl. Conf. on Intelligent Robots and Systems, 26-30 July 1993, Yokohama, Japan, Volume 3, pp. 1717-1721.

[40] Y. Xu, N.C. MacDonald, S.A Miller, "Integrated micro-scanning tunneling microscope," Appl. Phys. Lett. 67(1995):2305-2307.

[41] MinFeng Yu, Mark J. Dyer, George D. Skidmore, Henry W. Rohrs, Xue Kun Lu, Kevin D. Ausman, James Von Ehr, Rodney S. Ruoff, "3 dimensional manipulation of carbon nanotubes under a scanning electron microscope," 6th Foresight Nanotechnology Conference, November 1998; http://www.foresight.org/Conferences/MNT6/Papers/Yu/index.html. Robert F. Service, "AFMs wield parts for nanoconstruction," Science 282(27 November 1998):1620-1621.

[42] Jason J. Gorman, Yong-Sik Kim, András E. Vladár, Nicholas G. Dagalakis, "Design of an on-chip microscale nanoassembly system," Int. J. Nanomanufacturing 1(2007):710-721.

To overcome these problems, we're trying to use a set of molecular-scale tools that would, in a series of well-defined steps, prepare the surface and create hydrocarbon structures on a layer of diamond, atom by atom and molecule by molecule. A mechanosynthetic tool typically has two principal components – a chemically active tooltip and a chemically inert handle to which the tooltip is covalently bonded. The tooltip is the part of the tool where chemical reactions are forced to occur. The much larger handle structure is big enough to be grasped and positionally manipulated using an SPM or similar macroscale instrumentality. At least three types of basic mechanosynthetic tools (Figure 1-4) have already received considerable theoretical (and some experimental) study[43] and are likely among those required to build molecularly precise diamond via positional control:

Figure 1-4. Examples of three basic mechanosynthetic tooltypes that are required to build molecularly precise diamond via positional control (black = C atoms, yellow = Ge atoms, white = H atoms).[44]

(A) Hydrogen Abstraction Tool	(B) Hydrogen Donation Tool	(C) Carbon Dimer Placement Tool
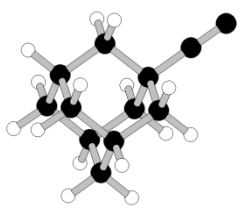	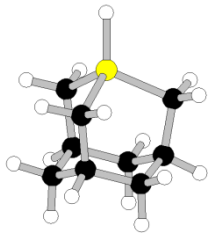	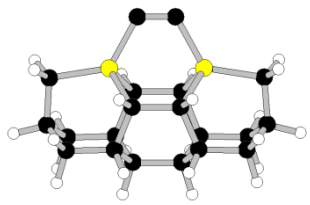

(1) **Hydrogen Abstraction Tools**. The first step in the process of mechanosynthetic fabrication of diamond might be to remove a hydrogen atom from each of two specific adjacent spots on the diamond surface, leaving behind two reactive dangling bonds. This could be done using a hydrogen abstraction tool[45] that has a high chemical affinity for hydrogen at one end but is elsewhere inert (Figure 1-4A). The tool's unreactive region serves as a handle or handle

---

[43] "Annotated Bibliography on Diamond Mechanosynthesis," Nanofactory Collaboration website, accessed February 2008; http://www.MolecularAssembler.com/Nanofactory/AnnBibDMS.htm.

[44] Robert A. Freitas Jr., Ralph C. Merkle, "A Minimal Toolset for Positional Diamond Mechanosynthesis," J. Comput. Theor. Nanosci. 5(May 2008):760-861; http://www.molecularassembler.com/Papers/MinToolset.pdf.

[45] Berhane Temelso, C. David Sherrill, Ralph C. Merkle, Robert A. Freitas Jr., "High-level Ab Initio Studies of Hydrogen Abstraction from Prototype Hydrocarbon Systems," J. Phys. Chem. A 110(28 September 2006):11160-11173; http://pubs.acs.org/cgi-bin/abstract.cgi/jpcafh/2006/110/i38/abs/jp061821e.html (abstract), http://www.MolecularAssembler.com/Papers/TemelsoHAbst.pdf (paper).

attachment point. The tool would be held by a molecular positional device, initially perhaps a scanning probe microscope tip but ultimately a molecular robotic arm, and moved directly over particular hydrogen atoms on the surface. One suitable molecule for a hydrogen abstraction tool is the acetylene or "ethynyl" radical, comprised of two carbon atoms triply bonded together. One carbon of the two serves as the handle connection, and would bond to a nanoscale positioning tool through a much larger handle structure perhaps consisting of a lattice of adamantane cages as shown in Figure 1-5. The other carbon of the two has a dangling bond where a hydrogen atom would normally be present in a molecule of ordinary acetylene (C_2H_2). The working environment around the tool would be inert (e.g., vacuum or a noble gas such as neon).

Figure 1-5. Recyclable DCB6Ge tooltip (carbon dimer placement tool) with "Xtip" crossbar handle motif (left),[46] which is then inverted and mounted on a massive diamond rod handle structure (right).

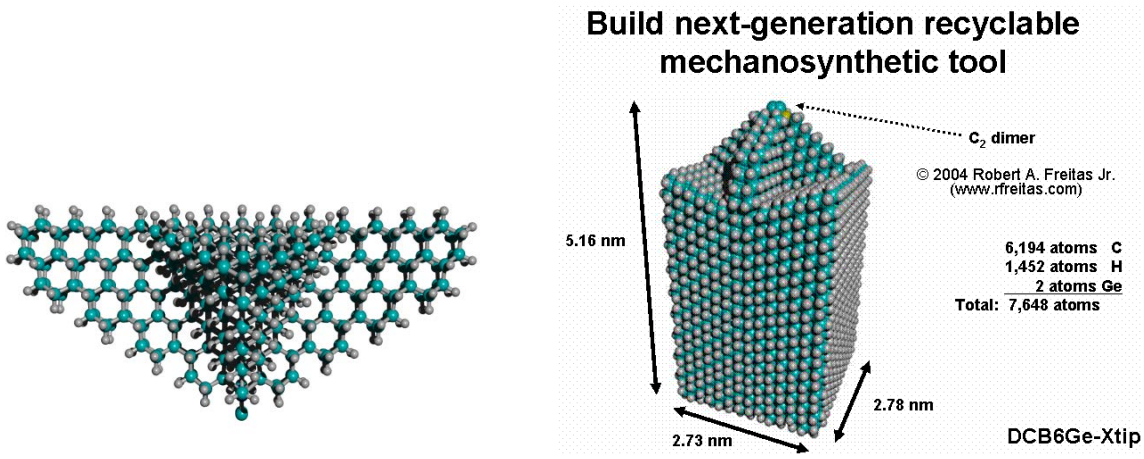

(2) **Hydrogen Donation Tools**. After a molecularly precise structure has been fabricated by a succession of hydrogen abstractions and carbon depositions, the fabricated structure must be passivated to prevent additional unplanned reactions. While the hydrogen abstraction tool is intended to make an inert structure reactive by creating a dangling bond, the hydrogen donation tool[47] does the opposite. It makes a reactive structure inert by terminating a dangling bond. Such

---

[46] Jingping Peng, Robert A. Freitas Jr., Ralph C. Merkle, James R. Von Ehr, John N. Randall, George D. Skidmore, "Theoretical Analysis of Diamond Mechanosynthesis. Part III. Positional C_2 Deposition on Diamond C(110) Surface using Si/Ge/Sn-based Dimer Placement Tools," J. Comput. Theor. Nanosci. 3(February 2006):28-41; http://www.MolecularAssembler.com/Papers/JCTNPengFeb06.pdf.

[47] Berhane Temelso, C. David Sherrill, Ralph C. Merkle, Robert A. Freitas Jr., "Ab Initio Thermochemistry of the Hydrogenation of Hydrocarbon Radicals Using Silicon, Germanium, Tin and Lead Substituted Methane and Isobutane," J. Phys. Chem. A 111(15 August 2007):8677-8688. http://pubs.acs.org/cgi-bin/abstract.cgi/jpcafh/asap/abs/jp071797k.html (abstract), http://www.MolecularAssembler.com/Papers/TemelsoHDon.pdf (paper).

a tool would be used to stabilize reactive surfaces and help prevent the surface atoms from rearranging in unexpected and undesired ways. The key requirement for a hydrogen donation tool is that it include a weakly attached hydrogen atom. Many molecules fit that description, but the bond between hydrogen and germanium is sufficiently weak so that a Ge-based hydrogen donation tool (Figure 1-4B) should be effective.

(3) **Carbon Placement Tools**. After the abstraction tool has created adjacent reactive spots by selectively removing hydrogen atoms from the diamond surface but before the surface is re-passivated by hydrogen, carbon placement tools may be used to deposit carbon atoms at the desired reactive surface sites. In this way a diamond structure would be built on the surface, molecule by molecule, according to plan. The first *complete* tool ever proposed for this carbon deposition function is the "DCB6Ge" dimer placement tool[48] – in this example, a carbon (C_2) dimer having two carbon atoms connected by a triple bond with each carbon in the dimer connected to a larger unreactive handle structure through two germanium atoms (Figure 1-4C). This dimer placement tool, also held by a molecular positional device, is brought close to the reactive spots along a particular trajectory, causing the two dangling surface bonds to react with the ends of the carbon dimer. The dimer placement tool would then withdraw, breaking the relatively weaker bonds between it and the C_2 dimer and transferring the carbon dimer from the tool to the surface, as illustrated in Figure 1-2. A positionally controlled carbon dimer could be bonded at many different sites on a growing diamondoid workpiece, in principle allowing the construction of a wide variety of useful nanopart shapes. As of 2009, the DCB6Ge dimer placement tool is the most intensively studied of any mechanosynthetic tooltip to date,[49] having

---

[48] Ralph C. Merkle, Robert A. Freitas Jr., "Theoretical analysis of a carbon-carbon dimer placement tool for diamond mechanosynthesis," J. Nanosci. Nanotechnol. 3(August 2003):319-324; http://www.rfreitas.com/Nano/JNNDimerTool.pdf. See also: Ralph C. Merkle, Robert A. Freitas Jr., "Theoretical analysis of a carbon-carbon dimer placement tool for diamond mechanosynthesis," paper presented at the 10th Foresight Conference on Molecular Nanotechnology, October 2002; http://www.foresight.org/Conferences/MNT10/Abstracts/Merkle/index.html.

[49] Robert A. Freitas Jr., Ralph C. Merkle, "A Minimal Toolset for Positional Diamond Mechanosynthesis," J. Comput. Theor. Nanosci. 5(May 2008):760-861; http://www.molecularassembler.com/Papers/MinToolset.pdf. Jingping Peng, Robert A. Freitas Jr., Ralph C. Merkle, James R. Von Ehr, John N. Randall, George D. Skidmore, "Theoretical Analysis of Diamond Mechanosynthesis. Part III. Positional C_2 Deposition on Diamond C(110) Surface using Si/Ge/Sn-based Dimer Placement Tools," J. Comput. Theor. Nanosci. 3(February 2006):28-41; http://www.MolecularAssembler.com/Papers/JCTNPengFeb06.pdf. Ralph C. Merkle, Robert A. Freitas Jr., "Theoretical analysis of a carbon-carbon dimer placement tool for diamond mechanosynthesis," J. Nanosci. Nanotechnol. 3(August 2003):319-324; http://www.rfreitas.com/Nano/JNNDimerTool.pdf. See also: Ralph C. Merkle, Robert A. Freitas Jr., "Theoretical analysis of a carbon-carbon dimer placement tool for diamond mechanosynthesis," paper presented at the 10th Foresight Conference on Molecular Nanotechnology, October 2002; http://www.foresight.org/Conferences/MNT10/Abstracts/Merkle/index.html. David J. Mann, Jingping Peng, Robert A. Freitas Jr., Ralph C. Merkle, "Theoretical analysis of diamond mechanosynthesis. Part II. C_2 mediated growth of diamond C(110) surface via Si/Ge-triadamantane dimer placement tools," J. Comput. Theor. Nanosci. 1(March 2004):71-80; http://www.MolecularAssembler.com/JCTNMannMar04.pdf. Robert A. Freitas Jr., "A simple tool for positional diamond mechanosynthesis, and its method of manufacture," U.S. Provisional Patent Application No. 60/543,802, filed 11 February 2004; U.S. Patent Pending, 11 February 2005; http://www.MolecularAssembler.com/Papers/DMSToolbuildProvPat.htm. Robert A. Freitas Jr., Damian

had more than 150,000 CPU-hours of computation invested thus far in its analysis, and it remains the only DMS tooltip motif that has been successfully simulated and validated for its intended function on a full 200-atom diamond surface model.[50] Other proposed dimer (and related carbon transfer) tooltip motifs[51] have received less extensive study but are also expected to perform well.

In 2007, Freitas and Merkle[52] completed a three-year project to computationally analyze a comprehensive set of DMS reactions and an associated minimal set of 9 tooltips (Figure 1-6) that could be used to build basic diamond, graphene (e.g., carbon nanotubes), and all of the tools themselves including all necessary tool recharging reactions. The research defined 65 DMS reaction sequences incorporating 328 reaction steps, with 354 pathological side reactions analyzed and with 1,321 unique individual DFT-based (Density Functional Theory) quantum chemistry reaction energies reported. (These mechanosynthetic reaction sequences range in length from 1-13 reaction steps (typically 4) with 0-10 possible pathological side reactions or rearrangements (typically 3) reported per reaction step.) One typical sequence – used to recharge a spent hydrogen abstraction tool – is Reaction Sequence RS5, illustrated in Figure 1-7. For the first time, this toolset provides clear developmental targets for a comprehensive near-term DMS implementation program.

G. Allis, Ralph C. Merkle, "Horizontal Ge-Substituted Polymantane-Based C_2 Dimer Placement Tooltip Motifs for Diamond Mechanosynthesis," J. Comput. Theor. Nanosci. 4(May 2007):433-442; http://www.MolecularAssembler.com/Papers/DPTMotifs.pdf.

[50] Jingping Peng, Robert A. Freitas Jr., Ralph C. Merkle, James R. Von Ehr, John N. Randall, George D. Skidmore, "Theoretical Analysis of Diamond Mechanosynthesis. Part III. Positional C_2 Deposition on Diamond C(110) Surface using Si/Ge/Sn-based Dimer Placement Tools," J. Comput. Theor. Nanosci. 3(February 2006):28-41; http://www.MolecularAssembler.com/Papers/JCTNPengFeb06.pdf.

[51] Robert A. Freitas Jr., Ralph C. Merkle, "A Minimal Toolset for Positional Diamond Mechanosynthesis," J. Comput. Theor. Nanosci. 5(May 2008):760-861; http://www.molecularassembler.com/Papers/MinToolset.pdf. Ralph C. Merkle, Robert A. Freitas Jr., "Theoretical analysis of a carbon-carbon dimer placement tool for diamond mechanosynthesis," J. Nanosci. Nanotechnol. 3(August 2003):319-324; http://www.rfreitas.com/Nano/JNNDimerTool.pdf. See also: Ralph C. Merkle, Robert A. Freitas Jr., "Theoretical analysis of a carbon-carbon dimer placement tool for diamond mechanosynthesis," paper presented at the 10th Foresight Conference on Molecular Nanotechnology, October 2002; http://www.foresight.org/Conferences/MNT10/Abstracts/Merkle/index.html. Ralph C. Merkle, "A proposed 'metabolism' for a hydrocarbon assembler," Nanotechnology 8(1997):149-162; http://www.zyvex.com/nanotech/hydroCarbonMetabolism.html. K. Eric Drexler, Nanosystems: Molecular Machinery, Manufacturing, and Computation, John Wiley & Sons, New York, 1992, Chapter 8. Damian G. Allis, K. Eric Drexler, "Design and Analysis of a Molecular Tool for Carbon Transfer in Mechanosynthesis," J. Comput. Theor. Nanosci. 2(March 2005):45-55; http://e-drexler.com/d/05/00/DC10C-mechanosynthesis.pdf. Robert A. Freitas Jr., Damian G. Allis, Ralph C. Merkle, "Horizontal Ge-Substituted Polymantane-Based C_2 Dimer Placement Tooltip Motifs for Diamond Mechanosynthesis," J. Comput. Theor. Nanosci. 4(May 2007):433-442; http://www.MolecularAssembler.com/Papers/DPTMotifs.pdf.

[52] Robert A. Freitas Jr., Ralph C. Merkle, "A Minimal Toolset for Positional Diamond Mechanosynthesis," J. Comput. Theor. Nanosci. 5(May 2008):760-861; http://www.molecularassembler.com/Papers/MinToolset.pdf.

Figure 1-6. A minimal toolset for diamond mechanosynthesis, including primary, auxiliary, and compound tools.[53] Only tooltips are shown. In an actual DMS toolhead, the tooltips would be mounted on a large diamond rod handle structure as shown in Figure 1-5.

(A) HAbst tool	(B) HDon tool	(C) HTrans tool	(D) DimerP tool
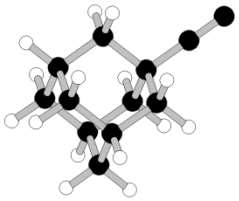	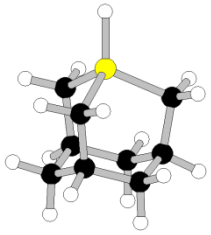	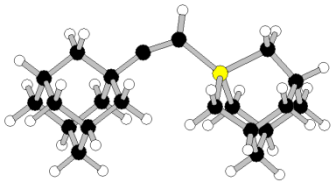	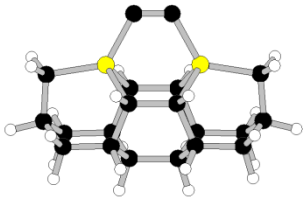

(E) AdamRad Handle	(F) GeRad Handle	(G) Methylene tool	(H) Germylmethylene tool	(I) Germylene tool
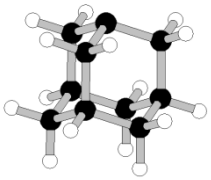	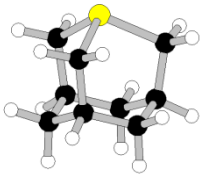	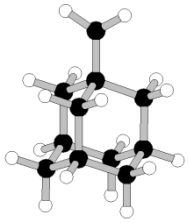	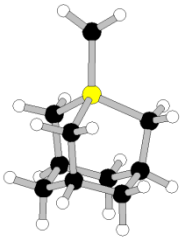	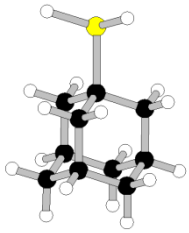

[53] Robert A. Freitas Jr., Ralph C. Merkle, "A Minimal Toolset for Positional Diamond Mechanosynthesis," J. Comput. Theor. Nanosci. 5(May 2008):760-861; http://www.molecularassembler.com/Papers/MinToolset.pdf.

Figure 1-7. Reaction Sequence RS5: Recharging the hydrogen abstraction tool.[54]

RS5: Recharge HAbst tool *and* recharge HDon tool from GeRad tool (Step 2) [full cage models illustrated]

Step 1	Step 2	Step 3

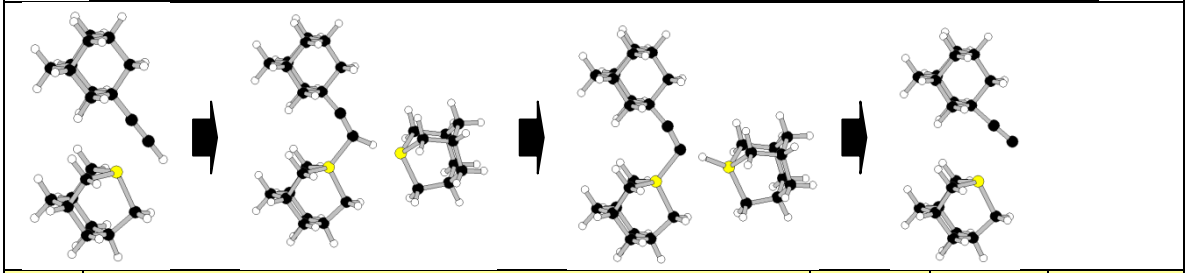

Step	Description of Reaction	Mult.	Ener. (eV)	Barr. (eV)
1	***Join GeRad tool to apical C atom of HAbstH tool***			
	R: HAbstH (ACC0A/28) + GeRad (ACC0A/25)	S+D		
	P: C15FCcis (ACC0A/53) **[≡ HTrans tool]**	D	**-0.43** [a]	
	T: Barrier map minimum from Tarasov (2009)[55]			**+0.10** [b]
	P: C15FCtrans (ACC0A/53)	D	-0.55	
	R: CH33Ge (ACC0A/13) + ClusterHAbH (ACC0A/16)	D+S		
	T: R1415Trans-QST3 (ACC1A/29)	D		**+0.27** [b]
1B1	H steal from HAbstH workpiece to GeRad tool			
	R: HAbstH (ACC0A/28) + GeRad (ACC0A/25)	S+D		
	P: HAbst (ACC0A/27) + HDon (ACC0A/26)	D+S	+2.19	
1D1	H migrates to radical site from adjacent CH in chain on HTrans			
	R: C15FCcis (ACC0A/53)	D		
	P: C15FCp2 (ACC0A/53)	D	-0.13	
	T: C15FCp2TS (ACC1A/53)	D		+1.66
1F6	H dissociates from -C●=CH- group on HTrans tool			
	R: S15cis (ACC0A/11)	D		
	P: S16Run0 (ACCCA/10) + H (ACC0A/1)	S+D	+2.68	
2	***Abstract apical H from HAbstH using GeRad tool***			
	R: S15cis (ACC0A/11) + GeRad (ACC0A/25)	D+D		
	P: S16Run0 (ACCCA/10) + HDon (ACC0A/26)	S	**-0.83** [cd]	
	R: S15trans (ACC0A/11) + GeRad (ACC0A/25)	D+D		
	P: S16Run0 (ACCCA/10) + HDon (ACC0A/26)	S	**-0.84** [c]	
2F6	H dissociates from GeRad handle of HDon tool			
	R: HDon (ACC0A/26)	S		
	P: GeRad (ACC0A/25) + H (ACC0A/1)	D+D	+3.51	
2H	Ge● radical bonds to C● adjacent to target CH group			

[54] Robert A. Freitas Jr., Ralph C. Merkle, "A Minimal Toolset for Positional Diamond Mechanosynthesis," J. Comput. Theor. Nanosci. 5(May 2008):760-861; http://www.molecularassembler.com/Papers/MinToolset.pdf.

[55] Denis Tarasov, Natalia Akberova, Ekaterina Izotova, Diana Alisheva, Maksim Astafiev, Robert A. Freitas Jr., "Optimal Tooltip Trajectories in a Hydrogen Abstraction Tool Recharge Reaction Sequence for Positionally Controlled Diamond Mechanosynthesis," J. Comput. Theor. Nanosci. 6(2009). In press.

	R: Cluster15cis (ACC1A/29) + CH33Ge (ACC0A/13)	D+D		
	P: Cluster28cis (ACC0A/42)	S	**-2.66** [e]	
2^1	***Abstract apical H from HAbstH using AdamRad tool***			
	R: S15cis (ACC0A/11) + AdamRad (ACC0A/25)	D+D		
	P: S16Run0 (ACCCA/10) + Adam (ACC0A/26)	S	**-1.43** [c]	
2^1F6	H dissociates from Adam bridgehead site			
	R: HDon (ACC0A/26)	S		
	P: GeRad (ACC0A/25) + H (ACC0A/1)	D+D	+4.12	
3	***Detach GeRad handle from workpiece***			
	R: C16FC-2 (ACC0A/52)	S		
	P: HAbst (ACC0A/27) + GeRad (ACC0A/25)	D+D	+4.81	
	Rotationally constrained:			
	R: S16Run10 (ACCCA/10) (CC-GeRad angle = 180°)	S		
	P: CH3CC (ACC0A/6) + GeH3 (ACC0A/4)	D+D	+4.83	
	R: S16Run0 (ACCCA/10) (CC-GeRad angle = 124°)	S		
	P: CH3CC (ACC0A/6) + GeH3 (ACC0A/4)	D+D	+3.62	
3C4	C≡C steal from workpiece by departing GeRad handle			
	R: C16FC-2 (ACC0A/52)	S		
	P: AdamRad (ACC0A/25) + GeRadCC (ACC0B/27)	D+D	**+5.06** [f]	

[a] This energy improves to -0.50 eV using an optimal tool approach trajectory as reported by Tarasov et al (2007).[56]

[b] The minimum barrier height improves to +0.10 eV using an optimal tool approach trajectory with full-cage positionally-constrained models producing only a ~0.3 Å deflection at the HAbstH tip prior to bonding, as reported by Tarasov et al (2009).[57]

[c] Deletion of apical H from S15cis (doublet) structure, followed by single point evaluation of the resulting structure either as singlet S16initS (ACC0S/10) or triplet S16initT (ACC1S/10), indicates singlet (C≡C) is significantly preferred (by -2.21 eV) to triplet (●C=C●).

[d] This energy may improve to -1.62 eV using constrained optimally-positioned full-cage models as reported by Tarasov et al (2009),[58] but our more conservative figure is used in the present paper pending a more detailed analysis of the HTrans tool in future work.

[e] This highly exoergic pathology is easily avoided by positional control because the H and C● are 2.07 Å apart, well in excess of the assumed 0.50 Å positional uncertainty.

[f] Even though the reaction energy for pathology 3C4 is only +0.25 eV above the main reaction, this dimer transfer pathology will not occur because C-C bonds (dimer to Adam handle) can withstand greater tensile loads (~5.53 nN) than C-Ge bonds (dimer to GeRad handle) can tolerate (~3.64 nN).

---

[56] Denis Tarasov, Natalia Akberova, Ekaterina Izotova, Diana Alisheva, Maksim Astafiev, Robert A. Freitas Jr., "Optimal Tooltip Trajectories in a Hydrogen Abstraction Tool Recharge Reaction Sequence for Positionally Controlled Diamond Mechanosynthesis," J. Comput. Theor. Nanosci. 6(2009). In press.

[57] Denis Tarasov, Natalia Akberova, Ekaterina Izotova, Diana Alisheva, Maksim Astafiev, Robert A. Freitas Jr., "Optimal Tooltip Trajectories in a Hydrogen Abstraction Tool Recharge Reaction Sequence for Positionally Controlled Diamond Mechanosynthesis," J. Comput. Theor. Nanosci. 6(2009). In press.

[58] Denis Tarasov, Natalia Akberova, Ekaterina Izotova, Diana Alisheva, Maksim Astafiev, Robert A. Freitas Jr., "Optimal Tooltip Trajectories in a Hydrogen Abstraction Tool Recharge Reaction Sequence for Positionally Controlled Diamond Mechanosynthesis," J. Comput. Theor. Nanosci. 6(2009). In press.

1.3 Building the First Mechanosynthetic Tools

The first practical proposal for building a DMS tool experimentally was published by Freitas in 2005 and was the subject of the first mechanosynthesis patent ever filed.[59] According to this proposal, the manufacture of a complete DCB6Ge positional carbon dimer placement tool would require four distinct steps: synthesizing a capped tooltip molecule, attaching it to a deposition surface, attaching a handle to it via CVD, then separating the tool from the deposition surface. The workability of the proposed process has already received valuable criticism from the scientific community and may be sufficiently viable to serve as a vital stepping-stone to more sophisticated DMS approaches.

An even simpler practical proposal for building DMS tools experimentally, also using only experimental methods available today, was published in 2008 by Freitas and Merkle as part of their minimal toolset work (Section 1.2).[60] Processes (currently under patent application) are identified for the experimental fabrication of a hydrogen abstraction tool, a hydrogen donation tool, two alternative carbon placement tools (the Methylene and Germylmethylene tooltips), and several germanium placement tools (the Germylene, Germylidyne, and DCB6GeGe tooltips), and these processes and tools are part of the second mechanosynthesis patent ever filed and the first to be filed by the Nanofactory Corporation.[61] Nanofactory Collaboration participants are currently undertaking direct experimental tests of these proposals that began in 2008 (Section 2.1.2).[62]

1.4 Designing a Molecular Workstation that Uses the DMS Tools

We want to use positionally controlled diamondoid mechanosynthesis to build diamondoid nanoparts and nanodevices. To do this, we need to design and build a picoscale-precision positioning system that can operate the tools we need to use, in a UHV manufacturing

---

[59] Robert A. Freitas Jr., "A simple tool for positional diamond mechanosynthesis, and its method of manufacture," U.S. Provisional Patent Application No. 60/543,802, filed 11 February 2004; U.S. Patent Pending, 11 February 2005; http://www.MolecularAssembler.com/Papers/DMSToolbuildProvPat.htm.

[60] Robert A. Freitas Jr., Ralph C. Merkle, "A Minimal Toolset for Positional Diamond Mechanosynthesis," J. Comput. Theor. Nanosci. 5(May 2008):760-861; http://www.molecularassembler.com/Papers/MinToolset.pdf.

[61] Robert A. Freitas Jr., Ralph C. Merkle, "Positional Diamond Mechanosynthesis: Toolset, Reactions, Uses and Products," U.S. Provisional Patent Application No. 60/970,658, filed 7 September 2007; U.S. Patent Pending, Application Number 12/204,642, filed 4 September 2008; http://appft1.uspto.gov/netacgi/nph-Parser?Sect1=PTO2&Sect2=HITOFF&u=%2Fnetahtml%2FPTO%2Fsearch-adv.html&r=1&f=G&l=50&d=PG01&p=1&S1=20090093659&OS=20090093659&RS=20090093659.

[62] "Nanofactory Collaboration Colleague Awarded $3M to Conduct First Diamond Mechanosynthesis Experiments," press release, Nanofactory Collaboration, 11 August 2008; http://www.molecularassembler.com/Nanofactory/Media/PressReleaseAug08.htm. Philip Moriarty, "Digital Matter?: Towards Mechanised Mechanosynthesis," EPSRC Fellowship Proposal, March 2008, 9 pp.

environment, towards the goal of creating a molecular workstation capable of performing basic diamondoid mechanosynthesis to build diamondoid nanoparts and nanodevices.

According to an OSTP 2004 Workshop on Nanoscale Metrology titled "Instrumentation and Metrology for Nanotechnology",[63] "Nanofabrication" is defined (p.3) as: "metrology to support **fabrication of device-like structures with features having dimensions as small as a single atom**; includes **manipulation and placement of individual atoms** and molecules, and external instrumentation to interact with structures and devices." In their Table 5.2 (p.69), a "Nanofabrication Grand Challenge" is listed as "Priority Topic 5.2", and reads as follows:

"High Accuracy 3D Positioning Over Large Volumes or Length Scales. **Vision and Goals**: The ability to accurately position (picometer scale) a nanoparticle or structure over large volumes (1 cm^3) or lengths is critical to the fabrication of nanostructures and devices. Accurate positioning will enable effective navigation to the nanofabricated structure. Technical Risk: High, Commercial Risk: High"

The present document provides a roadmap to the development of an entry-level molecular workstation. Chapter 2 provides basic background information on scanning probe microscopy, piezo manipulators, interferometry, and related technologies. Chapter 3 provides background on complete atomic force microscope scanning probe systems, and specific critical component technologies supporting the design of the molecular workstation are described in Chapter 4. This information must be analyzed and combined with the performance specifications of the workstation to develop a specific design that is suitable for construction, testing, and further development.

The following three Sections gives a brief overview of the proposed molecular workstation.

1.5 General Description of the Molecular Workstation

The key initial objective of the Nanofactory Corporation development program is to build a molecular workstation for diamondoid mechanosynthetic fabrication on a flat working surface. The workstation includes a 3-5 DOF (degrees of freedom) picopositioner system having one or two tips that is capable of performing diamondoid mechanosynthesis (DMS) (Section 1.1) on a bulk-prepared surface inside a vibration-isolated UHV workspace chamber, powered by electrical control signals that energize piezoelectric actuators to drive the positioning tips, with material feedstock provided on presentation surfaces accessible to the scanning probe tip-mounted tooltips. This system could create the basis for the world's first commercial diamondoid product fabrication workstation providing a limited capacity for positionally controlled diamondoid mechanosynthesis using a small set of mechanosynthetic tooltips that could be employed to fabricate small, simple, but atomically precise diamondoid nanostructures.

---

[63] "Instrumentation and Metrology for Nanotechnology," 2004 OSTP Workshop on Nanoscale Metrology, 188 pp; http://www.ostp.gov/galleries/NSTC%20Reports/NNI%20Instrumentation%20Metrology%20rpt%202004.pdf.

The molecular workstation is a scanning probe microscopy (SPM) based system for fabricating relatively small diamondoid nanostructures (i.e., up to 100-1000 atoms) on a flat bulk-prepared diamondoid fabrication surface using the techniques of diamondoid mechanosynthesis (Section 1.1). The final workstation scanning probe system (Figure 1-8) will employ 1-2 tips whose structure is either atomically precise or is characterized to atomic precision and whose operational envelopes include simultaneous and collisionless access both to the other tips and to the diamondoid fabrication surface and other adjacent workspace surfaces (e.g., perhaps two feedstock presentation surfaces and a hydrogen dump)[64] within an (up to) 100 micron x 100 micron area. Each tip may be capable of motion in all three Cartesian dimensions (XYZ) to a repeatable precision of 0.2-0.5 Å (20-50 pm) over 10-100 micron path lengths (as corrected for hysteresis effects). Each tip might also be capable of motion in up to two rotational directions (i.e., pitch and yaw) in perhaps ~1 degree angular increments, subject to the principle design constraint that such rotations must not destroy the precision of the motions in the three Cartesian directions. (Rotation stages with 5 μrad (0.0003 deg) rotational increments with 240 μrad (0.014 deg) of backlash are commercially available.[65]) The picopositioner probe system will be ensconced within a UHV chamber in a vibration-isolated environment and should be capable of operating at room temperature (~300 K) and at liquid nitrogen temperature (~80 K); operations at colder temperatures (e.g., LHe, near 4 K) are not currently envisioned but the utility or necessity of such operation should be analyzed further.

Figure 1-8. Schematic layout of the Molecular Workstation. (Scanning probe tip rack not shown)

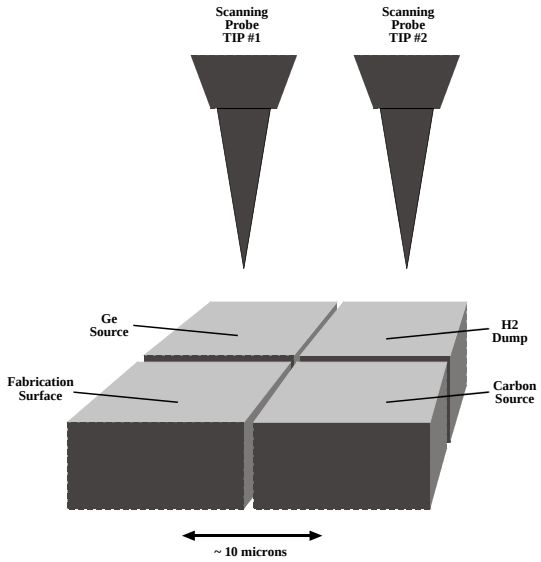

[64] Robert A. Freitas Jr., Ralph C. Merkle, "A Minimal Toolset for Positional Diamond Mechanosynthesis," J. Comput. Theor. Nanosci. 5(May 2008):760-861; http://www.molecularassembler.com/Papers/MinToolset.pdf.

[65] Physik Instrumente, "M-060 · M-061 · M-062, Series Rotation Stages with Worm Gear Drive," accessed January 2008, http://www.physikinstrumente.com/en/products/prdetail.php?sortnr=703100; see also http://www.physikinstrumente.com/en/pdf/M060_Datasheet.pdf.

To operate the molecular workstation, the workspace chamber containing the 3-5 DOF nanomanipulator system with repeatable 20-50 pm positioning accuracy over 1-100 micron round-trip excursions independently for all 1-2 tips (Section 2.2.5) is first pumped down to ultra-high vacuum (UHV) conditions (Section 4.7.1).

Next, four workspace surfaces are transferred into the UHV workspace chamber from an adjacent transfer chamber which has also been pumped down to UHV conditions, fully pre-degassing the four surfaces. The four workspace surfaces are:[66]

(1) a diamondoid fabrication surface, which in the initial setup might consist of a fully hydrogen-passivated diamond C(111), C(110) or C(100) surface depending upon the product nanostructures that are desired to be fabricated;

(2) a hydrogen dump consisting of a fully depassivated stable diamond C(110) surface (which will not reconstruct at any normal operating temperature) or C(100) surface (which reconstructs always in the same known manner, whether hydrogenated or not);

(3) a carbon source consisting of a depassivated germanium Ge(111) or Ge(100) surface that has been partially methylated (i.e., decorated with CH_3 groups) or has been deposited with a partial monolayer of C_2 dimers; and

(4) a germanium source consisting of a post-annealing depassivated and reconstructed Ge(111)-c(2x8) surface that has been partially germylated (i.e., decorated with GeH_3 groups).

The four workspace surfaces total at least 1-100 micron^2 of surface area and are transported on separate sample carriers inside the UHV workspace chamber to allow the surfaces to be positioned in close proximity – e.g., a "four-corners" juxtaposition of four squares (Figure 1-8). (Multiple juxtaposed samples is a widely-used technique, e.g., by Boland et al.[67] in low temperature tunneling spectroscopy where a diamond and a metal substrate are mounted side by side on an SPM sample holder.) The temperature of the sample carriers and their payload surfaces can be regulated as necessary for specific reactions – most importantly, for the storage and occasional retrieval of a GeH_3 feedstock molecule from the germanium source which may require one positionally controlled reaction step to be performed at ≤150 K to avoid unscheduled GeH_3 decomposition.[68] The passivated diamondoid fabrication surface can also serve as a source of hydrogen atoms and as a neutral test surface during one possible scheme for fabricating the GM tool.[69]

---

[66] Robert A. Freitas Jr., Ralph C. Merkle, "A Minimal Toolset for Positional Diamond Mechanosynthesis," J. Comput. Theor. Nanosci. 5(May 2008):760-861; http://www.molecularassembler.com/Papers/MinToolset.pdf.

[67] B. Naydenov, P. Ryan, L.C. Teague, John J. Boland, "Measuring the Force of Interaction between a Metallic Probe and a Single Molecule," Phys. Rev. Lett. 97(2006):098304.

[68] Robert A. Freitas Jr., Ralph C. Merkle, "A Minimal Toolset for Positional Diamond Mechanosynthesis," J. Comput. Theor. Nanosci. 5(May 2008):760-861; http://www.molecularassembler.com/Papers/MinToolset.pdf.

[69] Robert A. Freitas Jr., Ralph C. Merkle, "A Minimal Toolset for Positional Diamond Mechanosynthesis," J. Comput. Theor. Nanosci. 5(May 2008):760-861; http://www.molecularassembler.com/Papers/MinToolset.pdf.

The four workspace surfaces are juxtaposed, leveled flat and adjusted as close as possible to the same mutual altitude to ensure adequate vertical registration, then scanned and mapped: (1) to measure relative surface flatness and surface tilt, (2) to identify the regions of unbroken passivation and depassivation, and (3) to map the locations of all feedstock molecules. (AFMs can discriminate the chemical identity of individual atoms on a surface, even at room temperature.[70]) This procedure, which allows positional parameters for fabrication reaction sequences to be adjusted to actual local geometries, should be repeated every time the relative positions of workspace surfaces are disturbed. At least one of the workspace surfaces should include a metrological fiducial ledge structure at least a few atomic layers high to allow convenient tip alignment.

How long will it take to perform a scan of a presentation surface? We assume that feedstock molecules which are <0.5 nm in size lie an average of 10 nm apart on the presentation surface. The feedstock molecule surface density is therefore ~10,000 molecules/micron^2 (probably enough to build 2500-carbon-atom structures per micron^2 of feedstock presentation surface, assuming throwaway tooltips). According to Sinno,[71] a first demonstration[72] of a long scan using a metrological AFM was reported for a scan of 1 mm x 100 μm (10^5 micron^2) requiring a very long time consumption budget (12 hours), but with a resolution of only 100 nm. If resolution is reduced to 0.5 nm to ensure that all feedstock molecules are detected, then the 10^5 micron^2 scan will require (12 hours)(100 nm/0.5 nm) = 2400 hours, or 86 sec/micron^2. Thus the per-atom time budget for the molecular workstation need only be increased by roughly (86 sec/micron^2) / (2500-carbon-atoms/micron^2) ~ 0.03 sec/atom to accommodate the required presentation surface scan time overhead – a negligible burden when compared to the proposed 1-100 sec/atom time budget for the molecular workstation.

A set of macroscale SPM tips should be stored in a tool rack inside the main UHV chamber (Figure 1-8). The workstation must be able to replace its SPM tips under UHV conditions while the equipment is being operated and without breaking the vacuum seal. Once replaced, the precise location of the distal end of the new tip must be measured by comparison to a fiducial feature also present nearby within the workspace chamber. To prevent DMS radical tip poisoning, all chemically active tooltips which may be fabricated on the distal end of an SPM tip can be stored either in hydrogenated (unreactive) condition and then depassivated by H abstraction just prior to use, or possibly in tip-tip pairs that are easily pulled apart (e.g., GeRad-

---

[70] Yoshiaki Sugimoto, Pablo Pou, Masayuki Abe, Pavel Jelinek, Rubén Pérez, Seizo Morita, Óscar Custance, "Chemical identification of individual surface atoms by atomic force microscopy," Nature 446(1 March 2007):64-67. See also: David Shiga, "Microscope discerns atoms of different elements," NewScientist.com, 28 February 2007, http://www.newscientisttech.com/article/dn11272-microscope-discerns-atoms-of-different-elements.html.

[71] A. Sinno, P. Ruaux, L. Chassagne, S. Topçu, Y. Alayli, G. Lerondel, S. Blaize, A. Bruyant, P. Royer, "Enlarged atomic force microscopy scanning scope: Novel sample-holder device with millimeter range," Rev. Sci. Instrum. 78(2007):095107..

[72] G. Wilkening, L. Koenders, eds., Nanoscale Calibration Standards and Methods, Wiley-VCH, New York, 2005..

HAbst, GeRad-GeRad, GeRad-Meth, GeRad-AdamRad)[73] if the challenge of maintaining two-tooltip positional stability can be overcome. The compound HTrans tool should be assembled only when needed.

After mapping and sequence adjustment, the one or two 3-5 DOF manipulators in the workspace chamber are maneuvered and operated so as to effectuate the various reactions and reaction sequences previously described by Freitas and Merkle[74] to build a variety of simple diamond nanostructures on the diamondoid fabrication surface. The cycle of operation might include: grab a new SPM tip, measure tip position against the fiducial feature, transport the tip to the fabrication area on the fabrication surface, perform the DMS operation (perhaps in concert with 1-2 other tooltips), then withdraw the spent tip. In the most primitive system, SPM tips may be one-use throwaways, in which case the spent tip may be transported to a dump area (perhaps a section of tool rack). There the spent SPM tip is detached (e.g., by loosening mechanical fasters or sliding magnetic fasteners apart), after which the SPM tip holder is moved away and then attached to a new tip to begin the next cycle. In a less primitive system, the SPM tips will be rechargeable; in this scenario, the SPM tip holder later returns and regrasps the spent tip, then participates in a subsequent recharge cycle[75] following which the recharged tip may be returned to service.

To estimate workstation net productivity, we start by assuming (as detailed elsewhere) that ~6 mechanosynthetic operations per atom may typically be required to add each carbon atom to a growing diamond workpiece via DMS, or to add C and H atoms to a hydrogen-passivated diamond surface, including feedstock acquisition, tool operation, tool recharge, and toolrack exchange. We further assume that each operation requires a round-trip tip excursion of the maximum possible ~200 microns using interferometric counting increments of ~0.2 Å that are countable at a ~1 MHz rate, yielding a precision-trackable tip motion velocity of ~20 microns/sec. In this case the workstation can be operated at a rate of ~10 sec per round-trip tip excursion or ~10 sec/operation, yielding a gross productivity of 1 atom per ~60 sec taking ~6 operations required per atom. Assuming a 60% duty cycle for translational tip motions to allow various non-translational motions (e.g., tooltip changeouts) during 40% of the time, the net productivity of the macroscale workstation system is ~0.01 atom/sec (~0.01 Hz) for nanostructures fabricated on the diamondoid fabrication surface. This speed might be achieved under automated control but manually controlled workstation operations will undoubtedly go much slower.

---

[73] Robert A. Freitas Jr., Ralph C. Merkle, "A Minimal Toolset for Positional Diamond Mechanosynthesis," J. Comput. Theor. Nanosci. 5(May 2008):760-861; http://www.molecularassembler.com/Papers/MinToolset.pdf.

[74] Robert A. Freitas Jr., Ralph C. Merkle, "A Minimal Toolset for Positional Diamond Mechanosynthesis," J. Comput. Theor. Nanosci. 5(May 2008):760-861; http://www.molecularassembler.com/Papers/MinToolset.pdf.

[75] Robert A. Freitas Jr., Ralph C. Merkle, "A Minimal Toolset for Positional Diamond Mechanosynthesis," J. Comput. Theor. Nanosci. 5(May 2008):760-861; http://www.molecularassembler.com/Papers/MinToolset.pdf.

Note that in the first primitive experiment by Eigler and Schweizer[76] at IBM Almaden, an STM was used to drag 35 individual xenon atoms across a nickel surface to spell out the corporate logo "IBM" (Figure 1-1) in 22 hours of continuous manual effort,[77] giving an effective atom build rate of 0.00044 atom/sec – about 20-fold slower than the 0.01 atom/sec rate estimated for the workstation.

1.6 Continuous Sensory Feedback Not Needed by the Workstation

It has been observed that it may be difficult to separate successful trials from failures, and to elucidate the failure mechanisms of the failures, unless adequate sensor-based feedback can be employed at the tooltip during the fabrication of nanoscale parts. Unlike biological evolution, which proceeds by random variations in ensembles of organisms combined with deterministic reproduction/extinction as a selection process to achieve great complexity after billions of years (a set of mechanisms which Richard Dawkins has referred to as a "blind watchmaker"), deliberate design and positionally controlled fabrication of nanoscale mechanisms requires a means other than reproduction/extinction to winnow successes from failures in proceeding from simplicity to complexity. Similarly, macroscale factories are commonly constructed and operated by human engineers using continuous sensory feedback provided by eyes, ears, and hands.

While there are sensory advantages present at the macroscale compared to the limited sensorium available at the nanoscale (termed "sensory blight" by some critics),[78] proposals for positionally controlled nanoscale mechanosynthetic fabrication systems employ dead reckoning of tooltips combined with reliable reaction sequence design to ensure reliable results, hence a limited tooltip sensorium is no handicap. For example, reaction-by-reaction sensor-validated discrimination among the three possible outcomes of an attempted dimer placement – deposition at the correct location, deposition at the wrong location, and failure to place the dimer at all – is unnecessary because the proposal is to position the tooltip by dead reckoning, with the proper reaction assured by designing appropriate chemical energetics and relative bond strengths for the tooltip-surface interaction. In a macroscale factory, possible mechanical failure modes for each component mechanism are numerous (in part because macroscale components have poor quality control at the atomic scale), requiring significant sensory feedback to discriminate among them and diagnose the problem. In a nanoscale DMS workstation employing single-molecule tip-based chemical reactions, possible failure modes for each properly designed reaction are few (in part because nanoscale components can have excellent quality control at the atomic scale, being made of a small number of absolutely identical atoms), requiring minimal diagnostic sensory feedback to discriminate among them.

---

[76] D.M. Eigler, E.K. Schweizer, "Positioning Single Atoms with a Scanning Tunnelling Microscope," Nature 344(5 April 1990):524-526; http://www.nature.com/nature/journal/v344/n6266/abs/344524a0.html (abstract).

[77] Malcolm Ritter, "World's smallest moving job shifts just one atom at a time," Sacramento Bee, Thursday, 5 April 1990, p. A8.

[78] "New version of Productive Nanosystems film released," Nanodot, 28 March 2006; http://www.foresight.org/nanodot/?p=2188/Anonimouse5Apr06.htm#comment-8448.

If future experiments show that positional errors from dead reckoning may accumulate to unacceptable levels after some number of full-range tooltip motions, protocols for tooltip positional registration involving, e.g., in-theater fiducial markers,[79] scanning probe registration marks,[80] etc., can be re-executed as often as necessary to ensure continuous reliability of DMS reactions. Similar considerations apply to the positional assembly of small nanoparts. For closed-loop operation, encoders commercially available in 2009 already have ~nanometer precision.[81]

Regarding nonbiological methods for winnowing successes from failures, nanopart and nanofactory design evolution should occur deterministically and strictly under human control, using the conventional engineering paradigm of modeling, design, prototyping, testing, analysis, and redesign. In this case the limited sensorium is no handicap because, for example, prototype nanoparts and every one of their stable (or stabilizable) intermediate structures can be fabricated via dead reckoning using positionally controlled chemically active tooltips, then characterized by chemically inactive scanning probe tooltips or other technical means, with errors corrected or design changes sequentially implemented in the next prototyping iteration. Once mechanosynthetic tooltips and related positionally-controlled molecular tools are fabricated, the same technology will permit convenient prototyping, testing, and rework of failed designs.

1.7 Reliability of Workstation Operation

All manufacturing processes create defective product objects at some measurable rate. Molecular manufacturing processes will also have a measurable error rate. In each phase of the nanofactory development program, it is important to ensure that the manufacturing error rate will be low enough to satisfy the stated productivity requirements of that phase. Error can simultaneously accumulate from many sources and each major source must be accounted for in estimating the total likely error rate of a given sequence of manufacturing operations.

In Section 1.6, we asserted that reaction-by-reaction sensor-validated discrimination among possible outcomes of an attempted positionally-controlled mechanosynthetic reaction would be unnecessary for the workstation because the proposal is to position the tooltip by dead reckoning. Implicit to this assertion is the requirement that the picopositioning system (Section 1.5) must be designed with sufficient repeatable placement accuracy to ensure the required number of error-free round trip excursions of the positionally controlled DMS tooltip(s). For the workstation

---

[79] F.J. Rueb, L. Oberbeck, K.E.J. Goh, M.J. Butcher, E. Gauja, A.R. Hamilton, M.Y. Simmons, "The use of etched registration markers to make four-terminal electrical contacts to STM-patterned nanostructures," Nanotechnology 16(2005):2446-2449.

[80] A.W. Dunn, B.N. Cotier, A. Nogaret, P. Moriarty, P.H. Beton, S.P. Beaumont, "Molecular scale alignment strategies: An investigation of Ag adsorption on patterned fullerene layers," Appl. Phys.Lett. 71(17 November 1997):2937-2939.

[81] ACS Motion Control, "Nanometer Positioning & High Velocity," http://www.acs-tech80.com/Solutions/AdvancedFeatures/Nanometerpositioninghighvelocity/tabid/226/Default.aspx.

system, we have a target productivity rate of ~0.01 atom/sec with ~6 mechanosynthetic operations required for placement of each atom in the growing workpiece structure and a target workpiece size of up to 100-1000 atoms for each fabricated diamondoid nanostructure (Section 1.5). Building the largest 1000-atom structure thus requires ~6000 mechanosynthetic operations, so to avoid even a single misplacement error the picopositioner system must be capable of delivering a minimum of ~6000 error-free round trip excursions of the positionally controlled DMS tooltips. A highly reliable picopositioner system is clearly required, and additional steps for increasing positioning reliability are discussed at length in Section 4.6.

Another source of intrinsic manufacturing error arises from the reliability of the DMS reactions themselves. A proper reaction would be assured by designing appropriate chemical energetics and relative bond strengths for the tooltip-surface interaction. The DMS reaction sequences provisionally employed in this program proposal are based on the set of reactions described by Freitas and Merkle[82] in which net reaction exoergicities and energy barriers to accessible pathologies are no less than 0.40 eV (~64.1 zJ, ~9.2 kcal/mole).

As noted in that paper:[83] "Minimum acceptable reaction energies were guided by reaction reliability requirements. If the absolute value of an energy barrier or reaction exoergicity is E_{react}, then the Boltzmann population of the examined product structure may be approximated as $P_{react} \sim \exp(-E_{react}/k_B T)$ with $k_B = 1.381 \times 10^{-23}$ J/K and T = temperature in K. At T = 300 K, a reaction exoergicity of $E_{react} = 0.40$ eV gives $P_{react} = 2 \times 10^{-7}$ for the failed reaction, reliable enough for products requiring <~10^7 reaction steps for fabrication (e.g., products containing ~10^6 heavy atoms, assuming ~10 steps are required per heavy atom), at room temperature. At T = 80 K (LN_2 temperature), $E_{react} = 0.40$ eV gives $P_{react} = 5 \times 10^{-26}$ at 0.40 eV), indicating extreme reliability for fabricating products with very high atom counts at low temperature. Likewise, a barrier of $E_{react} = 0.40$ eV that blocks formation of an unwanted pathological structure along a second reaction pathway that competes with the desired more exoergic main reaction pathway gives $P_{react} = 2 \times 10^{-7}$ at T = 300 K for the unwanted structure, yielding similar reliability estimates as before. For these reasons, all proposed reactions have minimum energy barriers (blocking an undesired outcome) or relative exoergicities (favoring a desired outcome) of ~0.40 eV."

Table 1-2 gives the probability of misreaction at various relevant operating temperatures, assuming a defect energy threshold of 0.40 eV. At room temperature (~300 K) the misreaction probability per mechanosynthetic operation is 1.91×10^{-7}, conservatively assuming that all reactions have the minimum defect energy threshold of 0.40 eV (most have higher thresholds than this, hence are much less error prone), so the probability of finding a single erroneous atom placement in the largest 1000-atom workpiece after ~6000 mechanosynthetic operations is at most ~0.11%. If any workpiece having one or more erroneous atom placements is considered defective, then the room temperature DMS defect rate will be at most ~10^{-3} for 1000-atom

---

[82] Robert A. Freitas Jr., Ralph C. Merkle, "A Minimal Toolset for Positional Diamond Mechanosynthesis," J. Comput. Theor. Nanosci. 5(May 2008):760-861; http://www.molecularassembler.com/Papers/MinToolset.pdf.

[83] Robert A. Freitas Jr., Ralph C. Merkle, "A Minimal Toolset for Positional Diamond Mechanosynthesis," J. Comput. Theor. Nanosci. 5(May 2008):760-861; http://www.molecularassembler.com/Papers/MinToolset.pdf.

product objects and ~10^{-4} for 100-atom product objects fabricated using this set of DMS reactions, hence room temperature operation appears feasible. At near liquid nitrogen temperatures (~80 K), the DMS-related error rate using reaction sequences with a defect energy threshold of 0.40 eV falls to ~4 x 10^{-22} for a 1000-atom product object, completely negligible in this case.

Table 1-2. Probability of DMS Misreaction as a Function of Temperature, for Reactions Having Minimum Exoergicities and Minimum Barriers to Accessible Pathologies of 0.40 eV[84]

Operating Temperature (K)	Physical State of Feedstock Molecules	Probability of Misreaction (P_{react})
300	room temperature	1.91 x 10^{-7}
273.15	m.p. of water-ice	4.18 x 10^{-8}
194.65	dry ice (solid CO_2)	4.42 x 10^{-11}
185	C_2H_4 gas, GeH_4 gas	1.28 x 10^{-11}
184	C_2H_4 gas, GeH_4 liquid	1.11 x 10^{-11}
170	C_2H_4 gas, GeH_4 liquid	1.39 x 10^{-12}
169	C_2H_4 liquid, GeH_4 liquid	1.19 x 10^{-12}
118	C_2H_4 liquid, GeH_4 liquid	8.32 x 10^{-18}
109	C_2H_4 liquid, GeH_4 liquid	3.23 x 10^{-19}
104	C_2H_4/GeH_4 both solid	4.18 x 10^{-20}
80	C_2H_4/GeH_4 solid, near LN_2	6.41 x 10^{-26}
77.35	LN_2	8.79 x 10^{-27}
20	approaching liquid helium	1.69 x 10^{-101}

Another major source of error is radical poisoning by contaminants in an imperfect UHV environment. At a target productivity rate of ~0.01 atom/sec for the workstation system, the largest 1000-atom product object will require t_{fab} ~ 10^5 sec (~1 day) to fabricate. Assuming that a radical site susceptible to poisoning is exposed to the imperfect UHV environment for a fraction f_{vac} ~ 50% of the time, then the maximum tolerable UHV pressure that will permit one defect-free 1000-atom product object to be fabricated is:

$$P_{UHV} \leq (N_{encounters}\ T / n_{contam}\ A_{radical}\ f_{vac}\ t_{fab})\ (\pi\ MW_{kg} / 2\ k_B T\ N_A)^{1/2} \sim 10^{-12}\ \text{atm} \quad (4.2)$$

where n_{contam} = 7.34 x 10^{27} molecules-K/m^3-atm (= N_A/R_{gas}) for ideal gas (contaminant) molecules and T = 300 K, with the other quantities as defined in Section 4.7.1. If any workpiece having one or more erroneous atom placements is considered defective, then in a UHV environment maintained at ~10^{-16} atm (~10 million contaminant molecules present in a 5-liter UHV work volume; currently achievable experimentally, Section 4.7.1) the radical-poisoning defect rate at 300 K will be ~10^{-4} for 1000-atom product objects and ~10^{-5} for 100-atom product

[84] Robert A. Freitas Jr., Ralph C. Merkle, "A Minimal Toolset for Positional Diamond Mechanosynthesis," J. Comput. Theor. Nanosci. 5(May 2008):760-861; http://www.molecularassembler.com/Papers/MinToolset.pdf.

objects. If H_2 contaminant is determined not to be a serious radical poisoning risk or can be rigorously excluded from the workspace, then taking MW_{kg} = 0.014 kg/mole for N_2 raises the required P_{UHV} by a factor of ~2.6; conversely, operation at 80 K lowers the required P_{UHV} by a factor of ~2.

Other manufacturing errors are due to environmental conditions that have nothing to do with the operation of the workstation tooltips or the immediate vacuum workspace. For example, without impractical masses of shielding radiation induced errors cannot be avoided in small systems that are exposed to ordinary conditions found on the surface of the Earth. This sets a lower bound on error rates. Early studies[85] of radiation-induced enzyme inactivation found that ~1.06×10^{-17} J of absorbed radiation was required to produce one inactivating hit, yielding a failure condition of $\kappa_{fail} \sim 10^{15}$ hits/kg-rad. Conservatively assuming[86] a rather high value for background photonic and particulate radiation of $I_{rad} \sim 0.5$ rad/yr, the mean time τ_{rad} between radiation-disabling hits on a mostly-carbon 1000-atom diamondoid workpiece (or tooltip) of mass $m_{target} = 2 \times 10^{-23}$ kg is:

$$\tau_{rad} \sim (\kappa_{fail}\ m_{target}\ I_{rad})^{-1} \sim 10^{8} \text{ years,} \qquad (4.3)$$

conservatively assuming that one such hit will cause the workpiece or tooltip to fail with 100% certainty, a negligible error rate.

---

[85] G.R. Kepner, R.I. Macey, "Membrane enzyme systems: Molecular size determination from radiation inactivation," Biochim. Biophys. Acta 163(1968):188-203.

[86] K. Eric Drexler, Nanosystems: Molecular Machinery, Manufacturing, and Computation, John Wiley & Sons, New York, 1992, Section 6.6 "Radiation Damage," pp. 154-156.

2. Basic Technology Background

This section summarizes three of the basic key technologies required for the design of the molecular workstation, including scanning probe microscopy (SPM) manipulation technologies (Section 2.1), positioning technologies (Section 2.2), and positional measurement technologies (Section 2.3), and concludes with a brief discussion of tip-based nanofabrication (Section 2.4).

2.1 Scanning Probe Microscope (SPM) Manipulation Technologies

Scanning probe microscope (SPM)-based manipulation[87] involves two major technologies: scanning tunneling microscopy (STM) and atomic force microscopy (AFM). Both STM and AFM can be used for many areas of nanotechnology, including surface imaging, metrology, spectroscopy, and nanostructure patterning. Because the underlying principles and configuration of each technique are different, it is generally the case that STM can be controlled at higher resolutions with a lower scanning speed while AFM can have higher speeds but lower resolutions. Traditionally STM has been used to manipulate single atoms on electrically conductive surfaces with sizes at a subnanometer level, while AFM was normally used to manipulate nanoscale objects, including macromolecules and nanoparticles with sizes ranging between 10 and 100 nm. However, AFM is less restrictive than STM because AFM can be conducted in a normal room environment and can be used to image any kind of conducting or nonconducting material. More recently, AFM has undergone tremendous development and has evolved from a versatile imaging tool for atomic and molecular analyses to a major tool for the fabrication of nanoscale materials, components, and devices due to its low cost and unique atomic-level manipulation capability.

The following summary borrows liberally from excellent reviews by Tseng and Li[88] and Giessbl.[89]

2.1.1 Atomic Manipulations by STM

The first SPM was the STM invented in 1981 by Binnig et al.[90] STM uses a sharpened conducting tip with a bias voltage applied between the tip and the target sample. When the tip is

---

[87] Ampere A. Tseng, Zhuang Li, "Manipulations of Atoms and Molecules by Scanning Probe Microscopy," J. Nanosci. Nanotechnol. 7(2007):1-14.

[88] Ampere A. Tseng, Zhuang Li, "Manipulations of Atoms and Molecules by Scanning Probe Microscopy," J. Nanosci. Nanotechnol. 7(2007):1-14.

[89] Franz J. Giessibl, "Advances in atomic force microscopy," Rev. Mod. Phys. 75(2003):949-983.

[90] G. Binnig, H. Rohrer, C. Gerber, E. Weibel, "Surface Studies by Scanning Tunneling Microscopy," Phys. Rev. Lett. 49(1982):57-61.

within the atomic range (~1 nm) of the sample, electrons from the sample begin to tunnel through the gap to the tip or vice versa, depending on the sign of the bias voltage (Figure 2-1). The exponential dependence of the distance between the tip and target gives STM its remarkable sensitivity with sub-angstrom precision vertically and sub-nanometer resolution laterally. Two basic modes of operation, known as constant height and constant current modes are usually used for imaging. In the constant height mode, the tip travels in a horizontal plane above the sample. The induced tunneling current, which depends on topography and the electronic properties of the local surface, constitutes the STM image. In a constant current mode, the tip height is adjusted by feedback signals to keep the tunneling current constant during scanning, and the variation of the tip height represents the image.

In an operating STM, the tip approaches the sample surface until the set-point current is reached (at a given bias voltage). An adsorbed atom or molecule, which is hereinafter referred to as an adparticle, is held on the surface by chemical bonds with the surface atoms. In an imaging mode, the distance between the tip apex atom(s) and adparticle is far enough such that any forces between them are negligible as compared to the forces binding the adparticle with the surface, and the adparticle is not disturbed by the passage of the tip over it. However, if the tip-adparticle distance is gradually decreased, the tip-sample interaction changes from the conventional tunneling regime to the electronic-contact regime and then to the mechanical contact regime.[91]

Figure 2-1. <u>Left</u>: Schematic of controlling parameters between scanning probe microscope (STM) tip and an adparticle on a surface.[92] <u>Right</u>: Line profile (grid shows 20 pm vertical units) through an STM image of Si(111)-(7x7), running 5.5 nm in length, taken at 77 K using an Omicron LT STM-AFM system.[93]

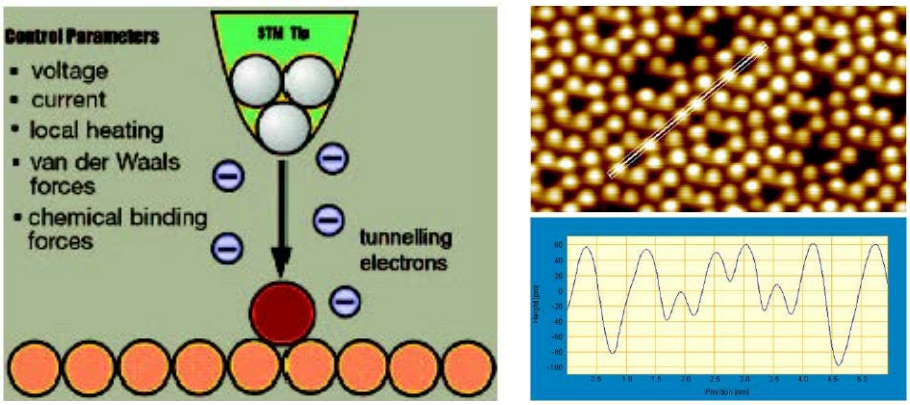

[91] S.N. Magonov, M.-H. Whangbo, Surface Analysis with STM and AFM, Wiley-VCH, New York, 1996. R. Wissendanger, Scanning Probe Microscopy and Spectroscopy Methods and Applications, Cambridge University Press, Cambridge, UK, 1998.

[92] Ampere A. Tseng, Zhuang Li, "Manipulations of Atoms and Molecules by Scanning Probe Microscopy," J. Nanosci. Nanotechnol. 7(2007):1-14.

[93] M. Bienias, S. Gao, K. Hasche, R. Seemann, K. Thiele, "A metrological scanning force microscope used for coating thickness and other topographical measurements," J. Appl. Phys. A 66(1998):837-842.

As summarized by Giessbl:[94] In an STM, "a sharp tip is mounted on a scanning device ("xyz scanner") which allows 3-dimensional positioning in x, y and z with subatomic precision. The tunneling tip is typically a wire that has been sharpened by chemical etching or mechanical grinding. W, Pt-Ir or pure Ir are often choosen as a tip material. A bias voltage V_t is applied to the sample and when the distance between tip and sample is in the range of several Angstroms, a tunneling current I_t flows between the tip and sample. This current is used as the feedback signal in a z-feedback loop. In the "topographic mode", images are created by scanning the tip in the xy-plane and recording the z-position required to keep I_t constant. In the "constant height mode", the probe is scanned rapidly such that the feedback cannot follow the atomic corrugations. The atoms are then apparent as modulations of I_t which are recorded as a function of x and y. The scanning is usually performed in a raster fashion with a fast scanning direction (sawtooth or sinusoidal signal) and a slow scanning direction (sawtooth signal). A computer controls the scanning of the surface in the xy plane while recording the z-position of the tip (topographic mode) or I_t (constant height mode). Thus, a three dimensional image $z(x, y, I_t \approx \text{constant})$ or $I_t(x, y, z \approx \text{constant})$ is created. When z is increased by one Angstrom, the current drops by an order of magnitude. This strong distance dependence is pivotal for the atomic resolution capability of the STM. Most of the tunneling current is carried by the atom that is closest to the sample ("front atom"). If the sample is very flat, this front atom remains the atom that is closest to the sample during scanning in x and y and even relatively blunt tips yield atomic resolution easily. In the AFM, the tunneling tip is replaced by a force-sensing cantilever. The tunneling tip can also be replaced by an optical near-field probe, a microthermometer etc., giving rise to a whole family of scanning probe microscopes."[95]

In the manipulation mode the STM tip is in close proximity to the surface such that the adparticle bonds to the tip as shown in Figure 2-2LMa. By varying the distance between the STM tip and the sample, a force may be exerted on the nanoparticle adsorbed on the surface. A controlled manipulation experiment can thus be performed by lowering the tip towards the target adparticle to enhance the tip-adparticle interaction to overcome the forces between the adparticle and the surface. By adjusting the tip position and reducing bias voltage, and/or increasing the tunneling current, it is possible to adjust the magnitude and direction of the force so that the tip can either push or drag an adparticle across a surface while the adparticle remains bound to the surface (Figure 2-2LMb). This process is known as lateral manipulation (LM), normally defined in terms of pulling, sliding or pushing, depending on the type of interaction that is used between the tip apex and adparticle (attractive for pulling and sliding and repulsive for pushing).[96] As shown in Figure 2-2VM, the adparticle can also be picked up by the tip and relocated to another position with the assistance of the electric fields from the STM tip to increase or reduce the tip-adparticle interaction. This process is called vertical manipulation (VM). At any point in the scan after

---

[94] Franz J. Giessibl, "Advances in atomic force microscopy," Rev. Mod. Phys. 75(2003):949-983.

[95] H.K. Wickramasinghe, "Scanned-Probe Microscopes," Sci. Am. (October 1989):74-81.

[96] L. Bartels, G. Meyer, K.-H. Rieder, "Basic Steps of Lateral Manipulation of Single Atoms and Diatomic Clusters with a Scanning Tunneling Microscope Tip," Phys. Rev. Lett. 79(1997):697-700.

such an operation, the tip can be retracted to the imaging distance by resetting the bias voltage and/or set point current to the imaging values, which thereby terminates the attractive interaction between the adparticle and the tip. These two manipulations require extremely fine control of the local interactions among the tip, adparticle, and surface. In general, it requires less force to move an adparticle along the surface by lateral manipulation than to pull it away from the surface using vertical manipulation. A schematic description of these interactions and the controlling parameters involved are also illustrated in Figure 2-1.

The first pioneering work demonstrating the ability of positioning single atoms on a metallic surface using lateral manipulation (Figure 2-2LM) was conducted in 1989 by Eigler and Schweizer[97] with an STM. An STM with a tungsten tip was used to arrange 35 Xe atoms in the shape of the company logo of "IBM" on a nickel surface (Figure 1-1). To accomplish this, a bias voltage was applied to weaken the adsorption of each atom to its nickel substrate, then each atom was dragged, one by one, to the desired locations at a speed of ~0.4 nm/sec to build a meaningful pattern.[98] Experiments are typically conducted using an STM at low temperatures under ultrahigh vacuum (UHV) ($<10^{-9}$ torr) conditions (Section 4.7.1). After careful cleaning of the sample surface, the construction of atomically precise structures can be achieved by a series of atom-by-atom relocations on the surface. The lateral manipulation is adopted and performed by moving the probe in a constant current mode. Given the close distance, the tip is almost in mechanical contact with the atom, and the proximity nature of the tip-atom interaction is the main driving force. The atom is left at the desired final location by retracting the tip to the original imaging height. For the IBM logo, it took 22 hours to make the entire structure or ~38 min/atom. The experiment had to be carried out at 4 K (i.e., liquid helium temperatures) because the arrangement would have been unstable at room temperature.

Many different geometrical configurations of atoms have been achieved and the clear interference effect of electron waves has been directly observed. For example, Figure 2-3 shows the image of two Chinese characters for "atom" made of iron atoms on a copper surface by D.M. Eigler and C.P. Lutz of IBM. As indicated by Crommie, Lutz, and Eigler,[99] the ripples around the characters are the standing wave patterns in the local density of states of the Cu(111) surface at low temperature. Libioulle et al.[100] and Foley et al.[101] provide reviews of more recent instrumentation developments of STMs for low temperature operations.

---

[97] D.M. Eigler, E.K. Schweizer, "Positioning Single Atoms with a Scanning Tunnelling Microscope," Nature 344(5 April 1990):524-526; http://www.nature.com/nature/journal/v344/n6266/abs/344524a0.html (abstract).

[98] Malcolm Ritter, "World's smallest moving job shifts just one atom at a time," Sacramento Bee, Thursday, 5 April 1990, p. A8.

[99] M.F. Crommie, C.P. Lutz, D.M. Eigler, "Confinement of electrons to quantum corrals on a metal surface," Science 262(8 October 1993):218-220.

[100] L. Libioulle, A. Radenovic, E. Bystrenova, G. Dietler, "Low noise current-to-voltage converter and vibration damping system for a low-temperature ultrahigh vacuum scanning tunneling microscope," Rev. Scientific Instrum. 74(2003):1016-1021.

Figure 2-2. Schematic of lateral manipulation (LM) at <u>left</u>, vertical manipulation (VM) at <u>right</u>. In <u>LM</u> (left), the adatom remains bound to the surface and is pushed or dragged by the STM tip as follows: (a) pulling where adatom discontinuously follows tip from one adsorption site to another due to attractive forces, (b) sliding where adatom is trapped under tip and follows its motion instantaneously and continuously, and (c) tip is retracted at desired place. In <u>VM</u> (right), the adatom is transferred from the surface to the STM tip and back to the surface as follows: (a) tip picking adatom from adsorption site and adatom dissociation occurring, (b) tip lifting adatom from surface and moving to desired place due to attractive forces, and (c) tip with adatom is loaded at desired site.

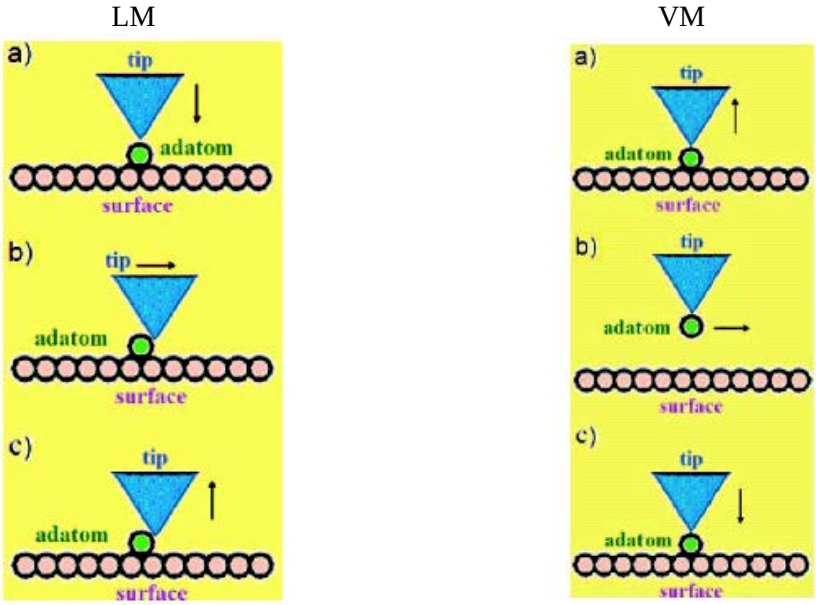

Figure 2-3. STM image of atomic manipulation of Fe atoms on Cu(111) surface in writing Chinese characters for "atom" by C.P. Lutz and D.M. Eigler,[102] to which the literal translation is something like "original child" (IBM Research, Almaden Research Center).

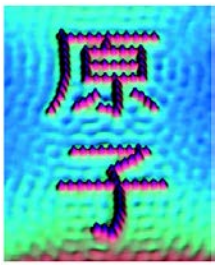

---

[101] E.T. Foley, N.L. Yoder, N.P. Guisinger, M.C. Hersam, "Cryogenic variable temperature ultra-high vacuum scanning tunneling microscope for single molecule studies on silicon surfaces," Rev. Scientific Instrum. 75(2004):5280-5287.

[102] M.F. Crommie, C.P. Lutz, D.M. Eigler, "Confinement of electrons to quantum corrals on a metal surface," Science 262(8 October 1993):218-220.

In vertical manipulation (Figure 2-2VM), involving picking an adatom from and releasing it back to the substrate surface, the direction of transferring atoms between the tip and the substrate surface is critical. Eigler, Lutz, and Rudge[103] found that the direction of transferring Xe atoms between the tip and the substrate surface is the same as that of the tunneling electrons, and that the corresponding atom transfer rate is a power-law function of the tunneling current (I). For the specific experiment conditions considered, the voltage (V) ranged from 18-180 mV with a tunneling junction such that V/I = 906 kΩ ±2%, giving a transfer rate that varied as $\sim I^{4.9\pm0.2}$. Lyo and Avouris[104] have also shown that voltage pulses can be used for vertical manipulation by extracting atoms from a Si(111) surface to the tunneling tip and then depositing them elsewhere using an opposite polarity pulse. They noted that the atom motion was in the same direction as the electron motion. Later, Shen et al.[105] also observed that the transfer of atomic H to Si surfaces at relatively low voltages is strongly power-law dependent. This reversible field (electron)-induced transfer of a single atom is also known as the Eigler switch.[106] This transfer phenomenon has been studied theoretically by many investigators.[107] The atom transfer in an Eigler switch can be viewed as a potential-barrier crossing problem between the potential wells formed by the interaction of the atom with the tip and the sample, respectively. The main mechanism behind the transfer is that the current excites the atom vibrationally in the double-well potential, sustained by the van der Waals attraction to surface and tip. The bond is broken by overcoming the potential barrier by gaining energy from the tunneling electrons. Also, the Xe atom dissipates energy to the surface phonons, so that the competition between the dissipation to surface phonons and the "heating" by inelastically tunneling electrons should be included in the mechanism. The theoretical predictions generally agree very well with the experimental findings, especially the bond-breaking rate being consistent with the power-law dependence transfer rate.

The electric-field driven vertical-manipulation mechanism has also been used by Salling and Lagally[108] to extract individual atoms from Si(100) surfaces to form nanometer scale rectangular

---

[103] D.M. Eigler, C.P. Lutz, W.E. Rudge, "An atomic switch realized with the scanning tunnelling microscope," Nature 352(15 August 1991):600-603.

[104] I.W. Lyo, P. Avouris, "Field-Induced Nanometer- to Atomic-Scale Manipulation of Silicon Surfaces with the STM," Science 253(12 July 1991):173-176.

[105] T.C. Shen, C. Wang, G.C. Abeln, J.R. Tucker, J.W. Lyding, P. Avouris, R.E. Walkup, " Atomic scale desorption through electronic and vibrational excitation mechanisms," Science 268(16 June 1995):1590-1592.

[106] M. Brandbyge, P. Hedegard, "Theory of the Eigler switch," Phys. Rev. Lett. 72(1994):2919-2922.

[107] M. Brandbyge, P. Hedegard, "Theory of the Eigler switch," Phys. Rev. Lett. 72(1994):2919-2922. S. Gao, M. Persson, B.I. Lundqvist, "Theory of atom transfer with a scanning tunneling microscope," Phys. Rev. B 55(1997):4825-4836. C.J. Chen, "A universal relation in NC-AFM, STM, and atom manipulation," Nanotechnology 16(March 2005):S27-S34.

[108] C.T. Salling, M.G. Lagally, "Fabrication of Atomic-Scale Structures on Si(001) Surfaces," Science 265(22 July 1994):502-506.

pits. Later, using multiple vertical manipulations, Salling et al.[109] wrote nanoscale trenches in Si(100) surfaces with a 2.4 nm resolution from Si films only three atomic layers thick. By studying the dynamics of a single cobalt (Co) atom, Stroscio and Celotta[110] concluded that, at low tunneling voltages (<5 meV), the transfer rate between sites is independent of tunneling voltage, current, and temperature. At higher voltages, the transfer rate exhibits a strong dependence on tunneling voltage, indicative of vibrational heating by inelastic electron scattering. Adatoms can be laterally manipulated from the surface sites, but can also be extracted or vertically manipulated from more strongly bound intrinsic sites to create atom-vacancy pair atoms. The differences between the forces involved in lateral and vertical manipulations have been analyzed by Pizzagalli and Baratoff.[111]

Normally, stable nanostructures consisting of adsorbed atoms can only be created at very low temperatures because the mobility of the adatom must be greatly reduced. The instrumental effects including piezo hysteresis and thermal drift can also be minimized at low temperatures. For example, the typical 24-hour lateral drift for adsorbed atoms can be less than a few Å for temperatures at a few K, which is a temperature achieved by cooling with liquid helium. Precision within a few Å is essential in single atom manipulation. However, it is possible to increase the working temperature (even up to room temperature) by using atoms embedded in the surface. For instance, Hasegawa and Avouris[112] have used the vertical manipulation via STM to observe the formation of standing wave patterns on Au(111) surfaces at room temperature. The oscillations are imaged from spectroscopic data or maps of $(dI/dV)(I/V)^{-1}$ where I and V are the bias current and voltage, respectively, and found near step edges and atomic defects from which the electrons scatter. The 2D standing wave patterns observed are consistent with the oscillations predicted by solving the classic eigenvalue problem in quantum mechanics for a particle in a hard-wall box.

Similar to atoms, single molecules, starting with small molecules, such as CO, can be manipulated with an STM tip by managing the tip-adsorbate interaction force, by regulating the induced electric field, or by applying tunneling electrons from the tip. In the early experiments, only one type of manipulation was applied; in more recent studies, multiple manipulations have been concurrently performed. The resulting chemical reactions on the molecules can be dissociation, diffusion, adsorption, and/or bond formation for creating molecule-based building blocks for patterning various nanostructures. Numerous experimental and theoretical studies have been reported to quantify these reactions. For example, Dujardin et al.[113] studied the

---

[109] C.T. Salling, I.I. Kravchenko, M.G. Lagally, "Atomic Manipulation for Patterning Ultrathin Films," J. Vac. Sci. Tech. B 13(1995):2828-2831.

[110] J.A. Stroscio, R.J. Celotta, "Controlling the Dynamics of a Single Atom in Lateral Atom Manipulation," Science 306(8 October 2004):242-247.

[111] L. Pizzagalli, A. Baratoff, "Theory of single atom manipulation with a scanning probe tip: Force signatures, constant-height, and constant-force scans," Phys. Rev. B 68(29 September 2003):115427.

[112] Y. Hasegawa, P. Avouris, "Direct observation of standing wave formation at surface steps using scanning tunneling spectroscopy," Phys. Rev. Lett. 71(1993):1071-1074.

[113] Y. Hasegawa, P. Avouris, "Direct observation of standing wave formation at surface steps using scanning tunneling spectroscopy," Phys. Rev. Lett. 71(1993):1071-1074. G. Dujardin, R.E. Walkup, P.

dissociation of individual $B_{10}H_{14}$ molecules from an Si(111) surface using low-energy tunneling electrons from the tip in a vacuum chamber at 10^{-8} torr. They found that the probability for the dissociation increases from 0.1 to 0.8 as the applied bias voltage increases from 4 V to 8 V with a current of 200 pA. Note that when electron energies higher than the work function of the tip (normally less than 3 eV) are applied to the molecule, the tip acts as an electron emission source and the field emission induces the dissociation.

Lateral Manipulation of Molecules. Stroscio and Eigler[114] and Zeppenfeld, Lutz, and Eigler[115] were the first group to study the lateral manipulation of CO molecules adsorbed on Pt(111) surfaces using cryogenic STM. CO molecules have also been laterally manipulated on various surfaces, including Cu(111) and Ag(110).[116] As shown in Figure 2-4, nanoscale millennial number "2000" is constructed with 47 CO-molecules regulated on a Cu(211) surface using lateral manipulation at 15 K.[117] At this temperature, the molecules can be sufficiently frozen so that a large number of them can be precisely moved to the desired location. Also the fabricated structure can remain stable for a relatively long time. During the lateral manipulation, CO molecules are usually pushed by the STM tip and moved discontinuously in front of the tip due to repulsive forces, while metal adatoms are usually dragged and slid. On close-packed surfaces like Cu(111), pushing is not very reliable because the molecules tend to move to the side of the tip and get lost. The successful creation of the nanostructure shown in Figure 2-4 can be attributed to the proper choice of the orientation of the surface. As shown, the parallel "valleys" (from the top to the bottom in Figure 2-4) of the Cu(211) surface can act as "railways" in which the CO adsorbed at the upper part of the intrinsic step edges can be pushed along the "railway" trails.

Avouris, "Single Molecule Dissociation by Electronic Excitation in the STM," Science 255(1992):1232-1235.

[114] Joseph A. Stroscio, D.M. Eigler, "Atomic and Molecular Manipulation with the Scanning Tunneling Microscope," Science 254(29 November 1991):1319-1326.

[115] P. Zeppenfeld, C.P. Lutz, D.M. Eigler, "Manipulating Atoms and Molecules With a Scanning Tunneling Microscope," Ultramicroscopy 42-44(1992):128-133.

[116] N. Lorente, H. Ueba, "CO dynamics induced by tunneling electrons: differences on Cu(110) and Ag(110)," Euro. Phys. J. D 35(August 2005):341-348.

[117] G. Meyer, J. Repp, S. Zophel, K.-F. Braun, S.W. Hla, S. Folsch, L. Bartels, F. Moresco, K.H. Rieder, "Controlled manipulation of atoms and small molecules with a low temperature scanning tunneling microscope," Single Molecule 1(2000):79-86.

Figure 2-4. Image of nanoscale millennial numbers "2000" are constructed with 47 CO molecules regulated on a Cu(211) surface using lateral manipulation at 15 K using STM.[118]

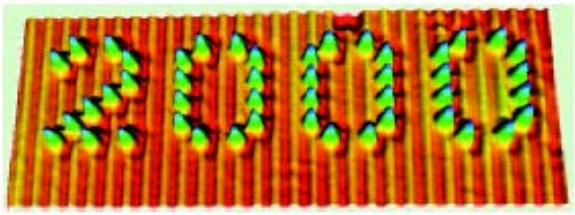

Jung et al.[119] applied lateral manipulation to bulky hydrocarbon molecules at room temperature. The hydrocarbons can maintain sufficiently strong interactions with the surface to prevent thermally activated diffusion at room temperature while still allowing controllable manipulation. Gimzewski and Joachim[120] have further demonstrated that the manipulation of single molecules at room temperature is also feasible by exploiting the strong interaction with the surface shown by macromolecules such as porphyrins. Furthermore, on the field of increasing the throughput and patterning speed, it is worth mentioning the Autonomous Atom Assembler (AAA) project of Stroscio et al.[121] in which they performed bottom-up fabrication of nanostructures by providing the STM with computer controlled capabilities of lateral displacements of atoms (Figure 2-5). Most manipulations are performed under the constant current mode, but the constant height modes have also been used for manipulation of complicated molecules.[122]

---

[118] G. Meyer, J. Repp, S. Zophel, K.-F. Braun, S.W. Hla, S. Folsch, L. Bartels, F. Moresco, K.H. Rieder, "Controlled manipulation of atoms and small molecules with a low temperature scanning tunneling microscope," Single Molecule 1(2000):79-86.

[119] T.A. Jung, R.R. Schlittler, J.K. Gimzewski, H. Tang, C. Joachim, "Controlled Room-Temperature Positioning of Individual Molecules: Molecular Flexure and Motion," Science 271(12 January 1996):181-184.

[120] J.K. Gimzewski, C. Joachim, "Nanoscale Science of Single Molecules Using Local Probes," Science 283(12 March 1999):1683-1688.

[121] J.A. Stroscio, E.W. Hudson, S.R. Blankenship, R.J. Celotta, A.P. Fein, "Nanostructure Science, Metrology, and Technology," Proc. SPIE 4608(2002):112-115.

[122] F. Moresco, G. Meyer, K.H. Rieder, H. Tang, A. Gourdon, C. Joachim, "Low temperature manipulation of big molecules in constant height mode," Appl. Phys. Lett. 78(2001):306-308.

Figure 2-5. NIST logo with cobalt atoms on a Cu surface produced in the NIST Nanoscale Physics Facility using the Autonomous Atom Assembler.[123] "The ripples in the background are due to electrons in the fluid-like layer at the copper surface bouncing off the cobalt atoms, much like the patterns produced when pebbles are dropped in a pond."

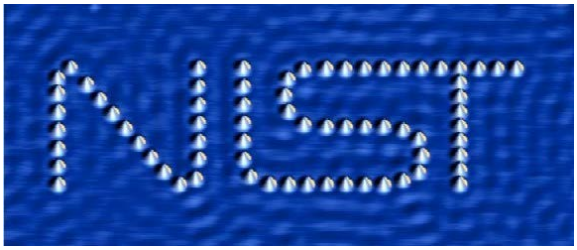

In molecular manipulation, an interesting phenomenon called "molecule cascades" has been demonstrated, that is similar to a row of toppling dominoes. Heinrich et al.[124] arranged CO molecules on Cu(111) at low temperature in staggered chains of dimers, where moving one molecule with the STM tip causes the subsequent motion or hopping of another, and so on. The hopping rate of CO molecules in cascades was found to be independent of temperature below 6 K and to exhibit a pronounced isotope effect, hallmarks of a quantum tunneling process. These molecule cascades could have many potential applications. For example, logic gates and other devices can be implemented by engineered arrangements of molecules at the intersections of cascades. Heinrich et al.[125] have shown that molecule cascades could be arranged into logic circuits such as onetime logic AND gates and two- and three-input sorters which incorporate logical AND and OR functions.

Vertical Manipulation of Molecules. In vertical manipulation, the molecular flipping during vertical transfer of CO molecules from a Cu surface to the tip has been studied by many investigators. As indicated by Ishi, Ohno and Viswanathan,[126] CO stands upright on metal surfaces with the carbon atom binding to the substrate. As the CO molecules have a similar absorption geometry to isolated Cu atoms adsorbed on a Cu surface, the CO molecule turns around when being transferred up to the tip. This additional degree of freedom associated with CO molecules makes the vertical manipulation of CO more complicated and less predicable than that of single atoms. To have a predicable or reliable vertical manipulation procedure, Bartels et

---

[123] "Autonomous Atom Assembly," NIST, July 2004; http://cnst.nist.gov/epg/Projects/STM/aaa_proj.html.

[124] J. Heinrich, C.P. Lutz, J.A. Gupta, D.M. Eigler, "Molecule Cascades," Science 298(15 November 2002):1381-1387.

[125] J. Heinrich, C.P. Lutz, J.A. Gupta, D.M. Eigler, "Molecule Cascades," Science 298(15 November 2002):1381-1387.

[126] S.-I. Ishi, Y. Ohno, B.Viswanathan, "An overview on the electronic and vibrational properties of adsorbed CO," Surf. Sci. 161(1985):349-372.

al.[127] found that the tunneling voltage must be slowly ramped to zero and the tip–CO distance should be simultaneously reduced to compensate the decrease in the current. In vertical manipulation, Bartels et al.[128] reported that the pickup of a single CO molecule can be applied for enhancing the ability of the STM tip. The sharpness of the STM tip can be greatly increased by deliberately transferring a molecule (or atom) to the normally etched tip apex. Thus, the image contrast can be improved. Additionally, the molecule (or atom) attached tip can have better chemical contrasts in molecular recognition imaging. For example, a CO-attached tip can distinguish between the adsorbed CO molecules and oxygen atoms relatively easily, which look very similar to the bare etched metal tip. Furthermore, the pickup step in vertical manipulation can be used as a material removal process for making various molecular structures such as nanotrenches, mentioned in the section on manipulation of single atoms. Also, the loading step in vertical manipulation can act like a material addition process. Theoretically, a three-dimensional molecular assembly can be built step by step using either material removal or material addition processes. The vertical manipulation is also capable in transporting the molecules (or atoms) across substrate obstacles, which should be difficult to perform by lateral manipulation.

In 1999, Ho and Lee[129] demonstrated the first repeatable site-specific mechanosynthetic covalent bonding operation of a diatomic carbon-containing molecule on a crystal surface, albeit electrically-mediated (Figure 2-6). These researchers used an STM tip to locate two carbon monoxide (CO) molecules and one iron (Fe) atom adsorbed on a silver surface in vacuum at 13 K. Next, they lowered the tip over one CO molecule and increased the voltage and current flow of the instrument to pick up the molecule; then they moved the tip-bound molecule over the surface-bound Fe atom and reversed the current flow, causing the CO molecule to covalently bond to the Fe atom, forming an iron carbonyl Fe(CO) molecule on the surface. Finally, the researchers repeated the procedure, returning to the exact site of the first Fe(CO) and adding a second CO molecule to the Fe(CO), forming a molecule of $Fe(CO)_2$, which in subsequent images of the surface appeared as a tiny "rabbit ears" structure, covalently bound to the silver surface.[130]

STM manipulation of atoms and molecules has been used to create various nanostructures, which can be *in situ* characterized and modified by using the tunneling electron current for rotations, diffusional jumps, vibrational excitations, desorption, dissociation. Rieder et al.[131] note that new

---

[127] L. Bartels, G. Meyer, K.-H. Rieder, "Controlled vertical manipulation of single CO molecules with the scanning tunneling microscope: A route to chemical contrast," Appl. Phys. Lett. 71(14 July 1997):213-216.

[128] L. Bartels, G. Meyer, K.-H. Rieder, "Controlled vertical manipulation of single CO molecules with the scanning tunneling microscope: A route to chemical contrast," Appl. Phys. Lett. 71(14 July 1997):213-216.

[129] Wilson Ho, Hyojune Lee, "Single bond formation and characterization with a scanning tunneling microscope," Science 286(26 November 1999):1719-1722; http://www.physics.uci.edu/~wilsonho/stm-iets.html.

[130] Wilson Ho, Hyojune Lee, "Single bond formation and characterization with a scanning tunneling microscope," Science 286(26 November 1999):1719-1722; http://www.physics.uci.edu/~wilsonho/stm-iets.html.

[131] K.-H. Rieder, G. Meyer, F. Moresco, K. Morgenstern, S.-W. Hla, J. Repp, M. Alemani, L. Grill, L. Gross, M. Mehlhorn, H. Gawronski, V. Simic-Milosevich, J. Henzl, K.F. Braun, S.Foelsch, L. Bartels,

opportunities for making molecular engines and switches become possible by tuning the voltage into the energy levels of specific vibrations or electronic levels. Iancu et al.[132] found that two conformations of isolated single TBrPP-Co molecules on a Cu(111) surface can be manipulated or switched without altering their chemical composition by applying +2.2 V voltage pulses from a STM tip at 4.6 K, allowing the molecule to be alternated as a molecular switch in a single molecular switching mechanism. Grill and Moresco[133] have presented several examples of molecular wire-electrode systems wherein single molecules are placed in contact in a controlled way. The associated electronic contact can be characterized using the additional contribution to the tunneling current, but also using the influence on the electronic states of the electrode and the molecule. Changed chemical structures of the molecule resulted in different shapes and dimensions of electrodes, creating a variety of contact configurations and molecular wire-electrode electronics.

Figure 2-6. STM is used by Ho and Lee[134] to vertically manipulate two CO molecules to build a V-shaped nanostructure on a single Fe atom embedded in a silver surface at low temperature.

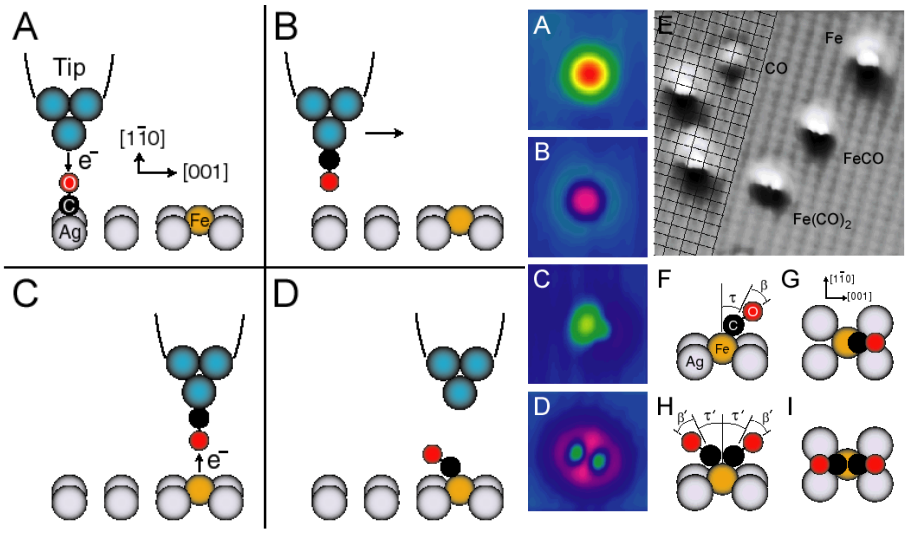

"Force Induced and Electron Stimulated STM Manipulations: Routes to Artificial Nanostructures as well as to Molecular Contacts, Engines, and Switches," J. Phys.: Conf. Series 19(2005):175-181.

[132] Violeta Iancu, Aparna Deshpande, Saw-Wai Hla, "Manipulating Kondo Temperature via Single Molecule Switching," Nano Lett. 6(2006):820-823.

[133] L. Grill, F. Moresco, "Contacting single molecules to metallic electrodes by scanning tunnelling microscope manipulation: model systems for molecular electronics," J. Phys.: Condens Matter 18(23 August 2006):S1887-S1908.

[134] Wilson Ho, Hyojune Lee, "Single bond formation and characterization with a scanning tunneling microscope," Science 286(26 November 1999):1719-1722; http://www.physics.uci.edu/~wilsonho/stm-iets.html.

2.1.2 Atomic Manipulations by AFM

Atomic Force Microscopy (AFM) has evolved from STM and operates by measuring attractive or repulsive forces between the tip and sample, which vary with the spacing between the two.[135] Since the tip is located at the free end of a cantilever, the attractive or repulsive forces cause the cantilever to deflect. Depending on the situation, forces that are measured in AFM include mechanical contact force, Van der Waals forces, capillary forces, chemical bonding, electrostatic forces, magnetic forces, Casimir forces, solvation forces etc. AFM has a much broader potential and range of applications over its predecessor STM because it can be used for imaging any conducting or non-conducting surface and be performed at room environment.[136]

Giessbl[137] notes that the spectacular spatial resolution and relative ease of obtaining atomic resolution by STM rests on three properties of the tunneling current:

(1) As a consequence of the strong distance dependence of the tunneling current, even with a relatively blunt tip the chance is high that a single atom protrudes far enough out of the tip such that it carries the main part of the tunneling current;

(2) Typical tunneling currents are in the nano-ampere range – measuring currents of this magnitude can be done with a very good signal to noise ratio even with a simple experimental setup; and

(3) Because the tunneling current is a monotonic function of the tip-sample distance, it is easy to establish a feedback loop which controls the distance such that the current is constant.

The AFM is similar to an STM except that the tunneling tip is replaced by a force sensor. Unlike the tunneling current, which has a very short range, the tip force that is sensed has long- and short-range contributions that can be classified by their range and strength. In vacuum DMS, there are short range chemical forces that operate over fractions of nm, and there are long-range van der Waals, electrostatic and magnetic forces that operate over distances of up to 100 nm.[138] Magnetic forces are not used in DMS, and there are no significant electrostatic forces when tip and sample/workpiece are not conductive and there is no charge present or electrostatic potential difference between them. This leaves van der Waals as the principal long-range force to be dealt with in vacuum DMS. In an atomically precise DMS tooltip-workpiece situation, the van der Waals force F_{vdw} between a vertically infinite conical tip of angle $\gamma \sim 60^o$ whose tip is positioned a distance z_o from a flat surface with Hamaker constant H ~ 340 zJ for diamond (tip + surface) can be approximated[139] by:

---

[135] Ampere A. Tseng, Zhuang Li, "Manipulations of Atoms and Molecules by Scanning Probe Microscopy," J. Nanosci. Nanotechnol. 7(2007):1-14.

[136] S.N. Magonov, M.-H. Whangbo, Surface Analysis with STM and AFM, Wiley-VCH, New York, 1996.

[137] Franz J. Giessibl, "Advances in atomic force microscopy," Rev. Mod. Phys. 75(2003):949-983.

[138] H.K. Wickramasinghe, "Scanned-Probe Microscopes," Sci. Am. (October 1989):74-81.

[139] Franz J. Giessibl, "Forces and frequency shifts in atomic-resolution dynamic-force microscopy," Phys. Rev. B 56(15 December 1997):16010-16015; http://dns.ntu-ccms.ntu.edu.tw/references/1Sorted-References/duplicated_references/PHYS_REV_B/Volume_56/PHYS_REV_B-56-16010-1997.pdf.

$$F_{vdw} = -H \tan^2(\gamma/2) / 6 z_o, \quad (2.1)$$

giving an attractive van der Waals force of F_{vdw} ~ -2 pN at 10 nm, -20 pN at z_o = 1 nm, and -100 pN at 0.2 nm (200 pm) which is the separation generally regarded as "in contact" in the literature. However, conventional AFM experimental setups might use an etched metal tip of radius 100 nm where a large number of tip atoms are simultaneously close to the flat workpiece surface, wherein F_{vdw} can reach 10,000 pN at z_o = 0.5 nm.[140] (Early experiments showed that both repulsive (W tip + Ag sample)[141] and attractive (Ir tip + Ir sample)[142] forces of the order of a few nN can act during STM operation.) "Because of their magnitude," notes Giessbl,[143] "van der Waals forces are a major disturbance in force microscopy."

In the first AFM, the deflection of the cantilever was measured with an STM – the backside of the cantilever was metalized, and a tunneling tip was brought close to it to measure the deflection.[144] Subsequent designs used optical (interferometer, beam-bounce)[145] or electrical methods (piezoresistive, piezoelectric)[146] for measuring the cantilever deflection. The deflection of silicon cantilevers is most commonly measured by optical detection through an interferometer or by bouncing a light beam of the cantilever and measuring its deflection ("beam bounce method"). Typically, "beam bounce" deflection is measured using a laser spot reflected from the top of the cantilever into an array of photodiodes as shown in Figure 2-7. Laser light from a solid state diode is reflected off the back of the cantilever and collected by a position sensitive detector (PSD) consisting of two closely spaced photodiodes whose output signal is collected by a differential amplifier. Angular displacement of cantilever results in one photodiode collecting a tiny bit more light than the other photodiode as the reflection spot moves slightly, producing an output signal (the difference between the photodiode signals normalized by their sum) which is proportional to the deflection of the cantilever. This scheme detects cantilever deflections <1Å (thermal noise limited). A long beam path (several cm) amplifies the changes in reflection beam angle, in much the same way that a long lever arm amplifies small displacements at one end.

---

[140] Franz J. Giessibl, "Advances in atomic force microscopy," Rev. Mod. Phys. 75(2003):949-983.

[141] U. Durig, J.K. Gimzewski, D. W. Pohl, "Experimental Observation of Forces Acting during Scanning Tunneling Microscopy," Phys. Rev. Lett. 57(1986):2403-2406.

[142] U. Durig, O. Zuger, D.W. Pohl, "Observation of Metallic Adhesion Using the Scanning Tunneling Microscope," Phys. Rev. Lett. 65(1990):349-352.

[143] Franz J. Giessibl, "Advances in atomic force microscopy," Rev. Mod. Phys. 75(2003):949-983.

[144] G. Binnig, C.F. Quate, Ch. Gerber, "Atomic Force Microscopy," Phys. Rev. Lett. 56(3 March 1986):930-933.

[145] L. Howald, Rasterkraftmikroskopie an Silizium und Ionenkristallen im Ultrahochvakuum, Ph.D. thesis, Universitat Basel, Switzerland, 1994.

[146] M. Tortonese, R.C. Barrett, C. Quate, "Atomic resolution with an atomic force microscope using piezoresistive detection," Appl. Phys. Lett. 62(1993):834-836.

Figure 2-7. Schematics of AFM apparatus illustrating the beam-bounce method.[147]

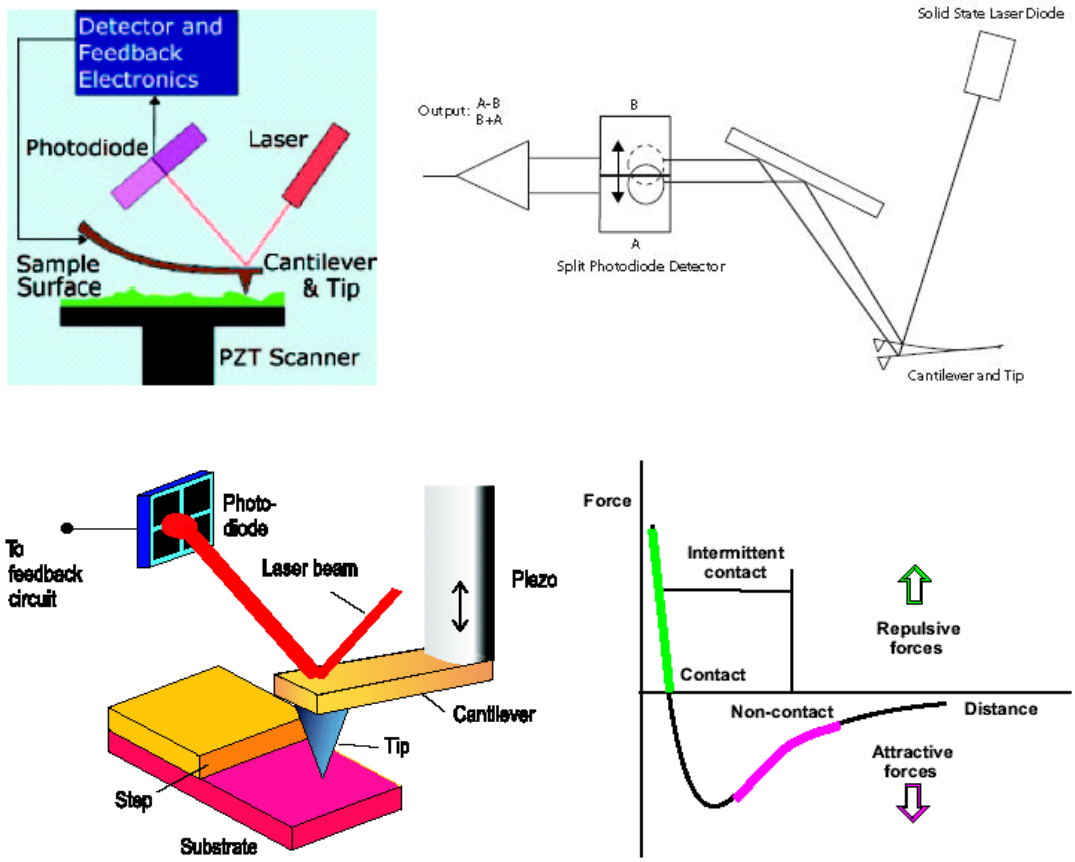

According to Chen,[148] a rectangular cantilever of width w, thickness t, length L, Young's modulus Y and density ρ has a spring constant:

$$k_{cantilver} = Ywt^3 / 4L^3 \tag{2.2}$$

and a fundamental eigenfrequency (natural resonant frequency) of:

$$f_0 = 0.162\ (t/L^2)\ (Y/\rho)^{1/2} \tag{2.3}$$

---

[147] Ampere A. Tseng, Zhuang Li, "Manipulations of Atoms and Molecules by Scanning Probe Microscopy," J. Nanosci. Nanotechnol. 7(2007):1-14. H.-U. Danzebrink, L. Koenders, G. Wilkening, A. Yacoot, H. Kunzmann, "Advances in Scanning Force Microscopy for Dimensional Metrology," CIRP Annals - Manufacturing Technology 55(2006):841-878.

[148] C.J. Chen, Introduction to Scanning Tunneling Microscopy, Oxford University Press, 1993.

Another key parameter of a cantilever is its "Q" value. In a resonant system in which the cantilever is vertically driven at some frequency f, the *Q* factor is a measurement of the effect of resistance to oscillation. It compares the frequency at which a system oscillates to the rate at which it dissipates its energy. A higher *Q* indicates a lower rate of energy dissipation relative to the oscillation frequency. Roughly speaking, a higher *Q* has less resistance to oscillation.

The deflection of a cantilever is subject to thermal drift and other noise factors.[149] This can be expressed in a plot of the deflection noise density versus frequency. A typical noise density is plotted in Figure 2-8, showing a 1/f dependence for low frequency that merges into a constant noise density ("white noise") above the "1/f corner frequency". This 1/f noise is also apparent in macroscopic force sensing devices, such as scales. Typically, scales have a reset or zero button, which allows the user to reset the effects of long-term drift. A change in temperature can also cause bending of the cantilever and a change in its eigenfrequency. Machining AFMs from materials with low thermal expansion coefficients like Invar or operation at low temperatures helps to minimize 1/f noise.

Figure 2-8. Noise spectrum of a typical cantilever deflection detector (schematic), characterized by 1/f noise for low frequencies and white noise for intermediate frequencies. For very high frequencies, the deflection noise density of typical cantilever deflection sensors goes up again ("blue noise", not shown here).[150]

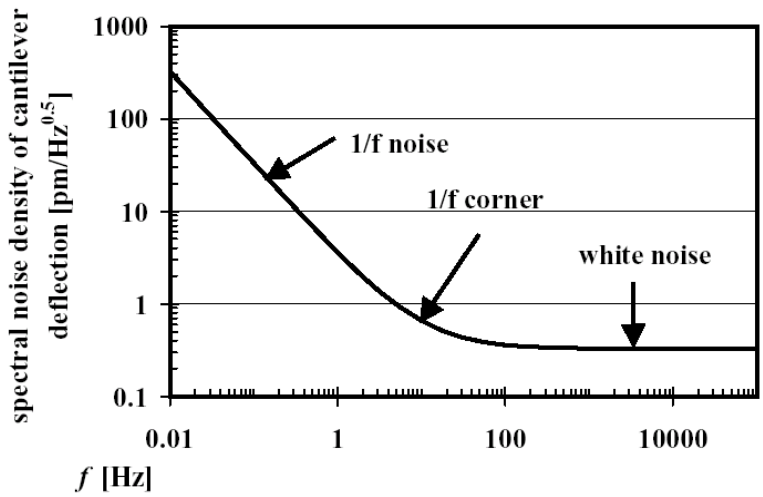

AFMs are generally operated in either of two modes,[151] contact or "static" mode and non-contact or "dynamic" mode, as follows.

---

[149] Franz J. Giessibl, "Advances in atomic force microscopy," Rev. Mod. Phys. 75(2003):949-983.

[150] Franz J. Giessibl, "Advances in atomic force microscopy," Rev. Mod. Phys. 75(2003):949-983.

[151] Franz J. Giessibl, "Advances in atomic force microscopy," Rev. Mod. Phys. 75(2003):949-983.

Contact / Static AFM. In static AFM, the force F_{ts} which acts between the tip and sample is used as the imaging signal. The physical interpretation of static AFM images is simple: the image is a map z(x, y, F_{ts} = constant). In the static mode of operation, the force translates into a deflection $q' = F_{ts}/k$ of the cantilever. Because the deflection of the cantilever should be significantly larger than the deformation of the tip and sample, restrictions on the useful range of k apply. Typically in the static mode, the cantilever should be much softer than the bonds between the bulk atoms in tip and sample. Interatomic force constants in solids are in a range from 10 N/m to about 100 N/m, though in biological samples they can be as small as 0.1 N/m. Thus, typical values for k in the static mode are 0.01-5 N/m. The eigenfrequency f_0 should be significantly higher than the desired detection bandwidth, i.e., if 10 lines per second are recorded during scan-imaging a width of, say, 100 atoms, f_0 should be at least 10 x 2 x 100 sec^{-1} = 2 kHz in order to prevent resonant excitation of the cantilever. Even though it has been demonstrated that atomic resolution is possible with static AFM,[152] the method can only be applied in certain cases. The magnitude of 1/f-noise can be reduced by low temperature operation[153] (minimizing thermal expansion) or by building the AFM of a material with a low thermal expansion coefficient such as Invar. Long-range attractive forces (van der Waals) can be cancelled by immersing tip and sample in a liquid[154] (obviously inconsistent with UHV operation) or by partly compensating the attractive force by pulling at the cantilever after a "jump-to-contact" has occurred.[155] Jarvis et al.[156] have introduced a method to cancel the long-range attractive force with an electromagnetic force applied to the cantilever.

Non-Contact / Dynamic AFM. In the dynamic operation modes, the cantilever is deliberately vibrated. The cantilever tip is made to vibrate near the sample surface with spacing on the order of a few nm or intermittently touching the surface at lowest deflection. The

---

[152] F.J. Giessibl, G. Binnig, "True atomic resolution on KBr with a low-temperature atomic force microscope in ultrahigh vacuum," Ultramicroscopy 42-44(1992):281-286. F. Ohnesorge, G. Binnig, "True Atomic Resolution by Atomic Force Microscopy Through Repulsive and Attractive Forces," Science 260(1993):1451-1456. T. Schimmel, T. Koch, J. Kuppers, M. Lux-Steiner, "True atomic resolution under ambient conditions obtained by atomc force microscopy in the contact mode," Appl. Phys. A 68(1999):399-402.

[153] F.J. Giessibl, "Theory for an electrostatic imaging mechanism allowing atomic resolution of ionic crystals by atomic force microscopy", Phys. Rev. B 45(1992):13815-13818.

[154] F. Ohnesorge, G. Binnig, "True Atomic Resolution by Atomic Force Microscopy Through Repulsive and Attractive Forces," Science 260(1993):1451-1456.

[155] F.J. Giessibl, G. Binnig, "True atomic resolution on KBr with a low-temperature atomic force microscope in ultrahigh vacuum," Ultramicroscopy 42-44(1992):281-286. F.J. Giessibl, "Theory for an electrostatic imaging mechanism allowing atomic resolution of ionic crystals by atomic force microscopy", Phys. Rev. B 45(1992):13815-13818. F.J. Giessibl, Rastertunnel- und Rasterkraftmikroskopie bei 4.2 K im Ultrahochvakuum, Ph.D. thesis, Ludwig-Maximilians-Universitat Munchen, Germany, 1991.

[156] S.P. Jarvis, H. Yamada, H. Tokumoto, J.B. Pethica, "Direct mechanical measurement of interatomic potentials", Nature 384(1996):247-249. S.P. Jarvis, H. Tokumoto, J.B. Pethica, "Measurement and Interpretation of Forces in the Atomic Force Microscope", Probe Microscopy 1(1997):65-79.

cantilever is mounted onto an actuator (e.g., piezoelectric) to allow an external excitation of an oscillation. There are two basic methods of dynamic operation: amplitude modulation (AM) and frequency modulation (FM) operation. In AM-AFM,[157] the actuator is driven by a fixed amplitude A_{drive} at a fixed frequency f_{drive} where f_{drive} is close to but different from f_0. When the tip approaches the sample, elastic and inelastic interactions cause a change in both the amplitude and the phase (relative to the driving signal) of the cantilever. These changes are used as the feedback signal. Typically the cantilever is oscillated at a frequency slightly above its resonance frequency where the amplitude of oscillation is perhaps a few nanometers (<10 nm). The van der Waals forces (strongest from 1-10 nm above the surface) or any other long range force which extends above the surface acts to decrease the resonance frequency of the cantilever. This decrease in resonance frequency, when combined with the feedback loop system, maintains a constant oscillation amplitude or frequency by adjusting the average tip-to-sample distance. Measuring the tip-to-sample distance at each (x,y) data point allows the scanning software to construct a topographic image of the sample surface.

The change in amplitude in AM mode does not occur instantaneously with a change in the tip-sample interaction, but on a timescale of $\tau_{AM} \approx 2Q/f_0$. With Q-factors reaching 100,000 in vacuum, the AM mode is very slow. Albrecht et al.[158] solved this problem by introducing the frequency modulation (FM) mode, where the change in the eigenfrequency occurs within a single oscillation cycle on a timescale of $\tau_{FM} \approx 1/f_0$. Both AM and FM modes were initially meant to be "non-contact" modes, i.e., the cantilever was far away from the surface and the net force between the front atom of the tip and the sample was clearly attractive. The AM mode was later used very successfully at a closer distance range in ambient conditions involving repulsive tip-sample interactions in "tapping mode"[159] and Erlandsson et al.[160] obtained atomic resolution on Si in vacuum with an etched tungsten cantilever operated in AM mode in 1996. Atomic resolution was also obtained using the FM mode in vacuum in 1995.[161] In non-contact or tapping mode operations, if the dynamic properties of the cantilever carrying the tip are measured then the specific AFM apparatus is often described as frequency modulation AFM (FM-AFM) or dynamic force microscopy (DFM). For atomic studies in vacuum the FM-mode is now the preferred AFM technique[162] – and it is usually assumed that frequency modulation is required for resolving

---

[157] Y. Martin, C.C. Williams, H.K. Wickramasinghe, "Atomic force microscope – force mapping and profiling on a sub 100-Å scale," J. Appl. Phys. 61(1987):4723-4729.

[158] T.R. Albrecht, P. Grutter, H.K. Horne, D. Rugar, "Frequency modulation detection using high-Q cantilevers for enhanced force microscope sensitivity," J. Appl. Phys. 69(1991):668-673.

[159] Q. Zhong, D. Innis, K. Kjoller, V.B. Elings, "Fractured polymer silica fiber surface studied by tapping mode atomic-force microscopy," Surface Science 290(1993):L688-L692.

[160] R. Erlandsson, L. Olsson, P. Martensson, "Inequivalent atoms and imaging mechanisms in ac-mode atomic-force microscopy of Si(111)7x7," Phys. Rev. B 54(1997):R8309-R8312.

[161] F.J. Giessibl, "Atomic Resolution of the Silicon (111)-(7x7) Surface by Atomic Force Microscopy," Science 267(1995):68-71.

[162] Franz J. Giessibl, "Advances in atomic force microscopy," Rev. Mod. Phys. 75(2003):949-983.

reactive surfaces, like Si(111) under UHV, where a chemical bond between a tip and a sample can be formed.[163]

Nano-manipulation by using AFM has wide applicability and has been demonstrated with various substrates and particles. Such manipulation is a versatile process, applicable to a wide range of environments (UHV, air and liquid) and using relatively simple sample preparation techniques.[164] As compared with STM, the AFM operation principle of manipulation is relatively simple. During scanning, the separation between the AFM tip and the adparticle is such that the lateral attractive van der Waals forces are sufficiently weak to avoid unintentional contact of the adparticle with the tip, as shown in Figure 2-9a. Using disabling the feedback loop and advancing the tip into contact with the particle (Figure 2-9b), the tip can move laterally to push the adparticle to a predetermined position on the surface. The force required for lateral pushing of atoms across surfaces by AFM can vary substantially – e.g., Ternes et al.[165] found that pushing a Co atom across a Pt(111) surface requires 210 pN, but only 17 pN across a Cu(111) surface.

Figure 2-9. Schematic of AFM tip positions in the imaging and manipulation modes: (a) in imaging mode, lateral attractive van der Waals forces are sufficiently weak to avoid contact between tip and adparticle, (b) in manipulation mode, tip is in contact with adparticle, which is pushed laterally.[166]

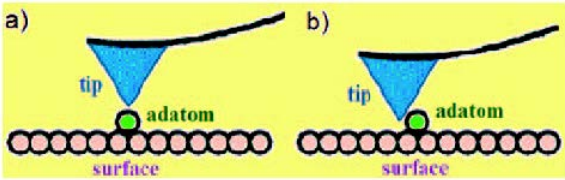

Morita and Sugawara[167] successfully extracted single atoms from a Si(111)-(7x7) surface in a controlled fashion with a force microscope. The Morita-Custance group[168] is believed to be the

---

[163] F.J. Giessibl, "Atomic Resolution of the Silicon (111)-(7x7) Surface by Atomic Force Microscopy," Science 267(1995):68-71.

[164] A.A.G. Requicha, "Nanoparticle Patterns," J. Nanoparticle Res. 1(1999):301.

[165] Markus Ternes, Christopher P. Lutz, Cyrus F. Hirjibehedin, Franz J. Giessibl, Andreas J. Heinrich, "The Force Needed to Move an Atom on a Surface," Science 319(22 February 2008):1066-1069.

[166] Ampere A. Tseng, Zhuang Li, "Manipulations of Atoms and Molecules by Scanning Probe Microscopy," J. Nanosci. Nanotechnol. 7(2007):1-14.

[167] S. Morita, Y. Sugawara, "Chapter 3"; in: S. Morita, R. Wiesendanger, E. Meyer, eds., Noncontact Atomic Force Microscopy, Springer Berlin Heidelberg New York, 2002, pp. 47-78.

[168] Noriaki Oyabu, Oscar Custance, Insook Yi, Yasuhiro Sugawara, Seizo Morita, "Mechanical vertical manipulation of selected single atoms by soft nanoindentation using near contact atomic force microscopy," Phys. Rev. Lett. 90(2 May 2003):176102; http://link.aps.org/abstract/PRL/v90/e176102 (Abstract) http://focus.aps.org/story/v11/st19 (APS story).

first group to use a cryogenic AFM near a contact mode to study the vertical manipulation of Si atoms on Si(111)-(7x7) surfaces, in 2003. The experiment was conducted at a temperature of 78 K under UHV (5 x 10^{11} torr). An n-doped Si cantilever with a spring constant of 48 N/m and 1st harmonic resonant frequency of 160 Hz was used. The corresponding quality (*Q*) factor for this cantilever system is 1.7 x 10^5. In manipulation, a soft nanoindentation was first performed by the tip to remove a selected Si atom from its equilibrium position at the surface without additional perturbation of the (7x7) unit cell. The short-range interaction force acting between the atom at the tip apex and closest adatom at surface activated the removing process. Unloading the manipulated atom is achieved by depositing it on a previously created vacancy at the surface. These manipulation processes are purely mechanical, since only short-range chemical interaction forces are involved and neither bias voltage nor voltage pulse is applied between probe and surface.

In 2005 the Custance group[169] extended their study to the lateral manipulation of a Ge adatom on Ge(111)-c(2x8) surfaces by frequency-modulation AFM. The study observed that the intrinsic adatoms of Ge(111) surfaces are suitable for lateral manipulation by the short-range interaction force acting between the outermost atoms of a tip and the atoms on the surface. Moreover, an atom inlay was conducted using an FM-AFM with a Si cantilever of 29.5 N/m spring constant under lateral manipulation of Sn adatoms at room temperature on a Ge(111)-c(2x8) surface and resulted in an embedded atom letter "Sn" as shown in Figure 2-10. The inlay was acquired with an oscillation amplitude of 15.7 nm, setting a frequency shift value of 4.6 Hz with respect to a free oscillation first-mechanical resonant frequency of 160,450 Hz under UHV environment.[170] They observed that during manipulation the adatoms possess only small amount of thermal energy and are stable for a relatively long period of time.

In 2006, Kawai and Kawakatsu[171] applied an AFM under the frequency-modulation mode to extend the lateral manipulation of Si adatoms on the Si(111)-(7x7) surface to room temperature under a UHV environment. Pushing and pulling steps were carried out with repulsive and attractive interaction forces between the cantilever tip and the adatom. A small amplitude of 0.4 nm was used to improve the detection sensitivity of the short-range interaction force gradient as well as to enhance the resolution of the manipulation. Enhanced detection sensitivity due to the small amplitude could also avoid accidental modifications of the surface during imaging. Since a stiff cantilever is necessary to realize a small amplitude operation, the 2nd flexural mode was used. In the pushing mode, the 2nd frequency and frequency shift were set to 1,701 kHz and 20 Hz, respectively, with a *Q* factor of 13,095, while the corresponding values used in the pulling mode are 1,697 kHz and 104 Hz, respectively, with a *Q* factor of 10,474. Kawai and Kawakatsu observed that small adatoms can not only be extracted and attached but also laterally manipulated

---

[169] N. Oyabu, Y. Sugimoto, M. Abe, O. Custance, S.Morita, "Lateral manipulation of single atoms at semiconductor surfaces using atomic force microscopy," Nanotechnology 16(2005):S112-S117.

[170] M. Sugimoto, S. Abe, N. Hirayama, N. Oyabu, O. Custance, S. Morita, "Atom inlays performed at room temperature using atomic force microscopy," Nat. Mater. 4(2005):156-159.

[171] S. Kawai, H. Kawakatsu, "Mechanical atom manipulation with small amplitude dynamic force microscopy," Appl. Phys. Lett. 89(2006):23113.

in and over the half unit cell with a repulsive interaction force. In the case of a tip condition that gave a strong image contrast, an adatom beside a vacancy could be pulled to the neighboring stable site with a strong attractive force.

Figure 2-10. AFM image (7.7 x 7.7 nm^2 image size) of atom inlaid letter "Sn" by rearranging Sn atoms on Ge(111)-c(2x8) surface at room temperature with cantilever oscillation amplitude of 15.7 nm, using Si cantilever of 29.5 N/m spring constant, setting frequency shift value of -4.6 Hz with respect to first-mechanical resonant frequency of 160 kHz.[172]

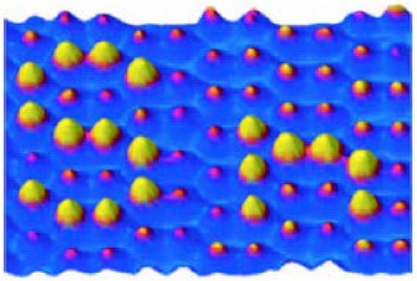

In 2006, Nishi et al.[173] used FM-AFM to investigate the atomic manipulation on an insulator surface, which normally is not suitable for STM manipulation. They adopted the soft nanoindentation approach, similar to that used by Oyabu et al.,[174] to manipulate atoms on a cleaved ionic crystalline KCl(100) surface in UHV at room temperature with limited success. Very often, more than one surface atom is vertically manipulated or dragged from the surface by nanoindentation, while in rare cases, single-atom manipulation is successfully performed. Lateral manipulation of a vacancy has occasionally succeeded on the KCl(100) surface. Nishi et al.[175] presumed that the lateral manipulation was induced by pulling. The difference between the covalent bonding of Si (Si–Si: 2.32 eV/bond) and the ionic bonding of KCl (K-Cl: 7.2 eV/ion pair) leads to the different results in the atom manipulation. They have introduced thermal drift compensation software to better approach the target atom.

---

[172] N. Oyabu, Y. Sugimoto, M. Abe, O. Custance, S.Morita, "Lateral manipulation of single atoms at semiconductor surfaces using atomic force microscopy," Nanotechnology 16(2005):S112-S117. M. Sugimoto, S. Abe, N. Hirayama, N. Oyabu, O. Custance, S. Morita, "Atom inlays performed at room temperature using atomic force microscopy," Nat. Mater. 4(2005):156-159.

[173] R. Nishi, D. Miyagawa, H. Etou, Y. Seino, Insook Yi, S. Morita, "NC-AFM study on atomic manipulation on ionic crystal surface by nanoindentation", Nanotechnology 17(2006):S142-S147.

[174] Noriaki Oyabu, Oscar Custance, Insook Yi, Yasuhiro Sugawara, Seizo Morita, "Mechanical vertical manipulation of selected single atoms by soft nanoindentation using near contact atomic force microscopy," Phys. Rev. Lett. 90(2 May 2003):176102; http://link.aps.org/abstract/PRL/v90/e176102 (Abstract) http://focus.aps.org/story/v11/st19 (APS story).

[175] R. Nishi, D. Miyagawa, H. Etou, Y. Seino, Insook Yi, S. Morita, "NC-AFM study on atomic manipulation on ionic crystal surface by nanoindentation", Nanotechnology 17(2006):S142-S147.

In 2008, the Custance group[176] reported purely mechanical-based covalent bond-making and bond-breaking (true vacuum-phase mechanosynthesis) involving atom by atom substitution of silicon (Si) atoms for tin (Sn) atoms in an Sn monolayer surface on a Si(111) surface via vertical manipulation (Figure 2-11). The group again used an AFM in dynamic mode using frequency modulation detection in FM-AFM. According to the abstract, the researchers were able to assemble 2D "complex atomic patterns at room temperature by the vertical interchange of atoms between the tip apex of an atomic force microscope and a semiconductor surface [via] manipulations...produced by exploring the repulsive part of the short-range chemical interaction between the closest tip-surface atoms." The group also demonstrated atomically precise exchange of lead (Pb) and indium (In) on Si(111) surface. This is the first report of a complex pattern being drawn on a 2D surface, literally atom by atom, purely via mechanical forces.

Figure 2-11. Complex atomic patterning by vertical interchange atom manipulation at room temperature, where Si atoms are substituted for Sn atoms, one at a time.[177]

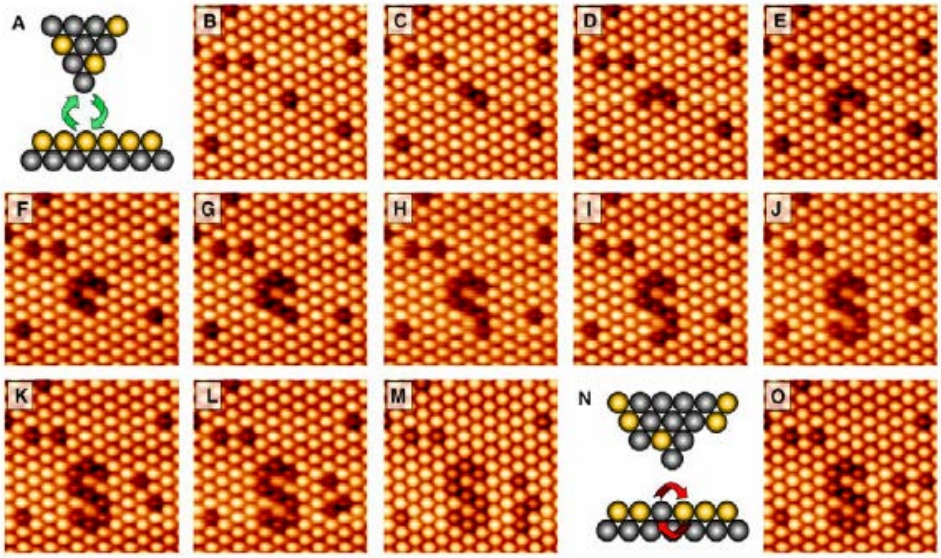

[176] Yoshiaki Sugimoto, Pablo Pou, Oscar Custance, Pavel Jelinek, Masayuki Abe, Ruben Perez, Seizo Morita, "Complex Patterning by Vertical Interchange Atom Manipulation Using Atomic Force Microscopy," Science 322(17 October 2008):413-417; http://www.sciencemag.org/cgi/content/full/322/5900/413 (paper) http://www.sciencemag.org/cgi/content/full/322/5900/413/DC1 (supplement).

[177] Yoshiaki Sugimoto, Pablo Pou, Oscar Custance, Pavel Jelinek, Masayuki Abe, Ruben Perez, Seizo Morita, "Complex Patterning by Vertical Interchange Atom Manipulation Using Atomic Force Microscopy," Science 322(17 October 2008):413-417; http://www.sciencemag.org/cgi/content/full/322/5900/413 (paper) http://www.sciencemag.org/cgi/content/full/322/5900/413/DC1 (supplement).

In 2008, the first attempt to perform diamond mechanosynthesis experimentally was initiated by Philip Moriarty at the University of Nottingham, UK.[178] The objective of this 5-year research effort is to fabricate an ethynyl-based hydrogen abstraction tool and then demonstrate its ability both to abstract individual hydrogen atoms from diamond surface and also to deposit C_2 dimers on a diamond surface, in a positionally controlled manner under UHV conditions, testing the theoretical predictions of Freitas and Merkle.[179] Oscar Custance [personal communication to P. Moriarty, 2008] has already tried to image the diamond surface to atomic resolution, but apparently without success as of late 2008.

2.1.3 Challenges for Atomically Precise Tip Positioning in DMS

DMS must be performed using an AFM-based apparatus, rather than STM, because diamond and diamondoid materials are generally nonconductive. We also restrict our efforts to purely mechanical synthesis operations requiring no externally imposed electrical fields or tunnel current flow, as distinguished from, for example, the experimental STM-based work of Ho and Lee[180] (electrically-mediated CO abstraction/donation), Hla et al.[181] (tunnel current-mediated synthesis of biphenyl from two iodobenzene molecules), or of Lyding et al.[182] and Basu et al.[183] (tunnel

---

[178] "Nanofactory Collaboration Colleague Awarded $3M to Conduct First Diamond Mechanosynthesis Experiments," press release, Nanofactory Collaboration, 11 August 2008; http://www.molecularassembler.com/Nanofactory/Media/PressReleaseAug08.htm.

[179] Robert A. Freitas Jr., Ralph C. Merkle, "A Minimal Toolset for Positional Diamond Mechanosynthesis," J. Comput. Theor. Nanosci. 5(May 2008):760-861; http://www.molecularassembler.com/Papers/MinToolset.pdf.

[180] Wilson Ho, Hyojune Lee, "Single bond formation and characterization with a scanning tunneling microscope," Science 286(26 November 1999):1719-1722; http://www.physics.uci.edu/~wilsonho/stm-iets.html.

[181] Saw-Wai Hla, Ludwig Bartels, Gerhard Meyer, Karl-Heinz Rieder, "Inducing All Steps of a Chemical Reaction with the Scanning Tunneling Microscope Tip: Towards Single Molecule Engineering," Phys. Rev. Lett. 85(September 2000):2777-2780; http://prola.aps.org/abstract/PRL/v85/i13/p2777_1 (abstract), http://www.phy.ohiou.edu/~hla/HLA2000-2.pdf (paper).

[182] J.W. Lyding, K. Hess, G.C. Abeln, D.S. Thompson, J.S. Moore, M.C. Hersam, E.T. Foley, J. Lee, Z. Chen, S.T. Hwang, H. Choi, P.H. Avouris, I.C. Kizilyalli, "UHV-STM nanofabrication and hydrogen/deuterium desorption from silicon surfaces: implications for CMOS technology," Appl. Surf. Sci. 130(1998):221-230. E.T. Foley, A.F. Kam, J.W. Lyding, P.H. Avouris, "Cryogenic UHV-STM study of hydrogen and deuterium desorption from Si(100)," Phys. Rev. Lett. 80(1998):1336-1339. M.C. Hersam, G.C. Abeln, J.W. Lyding, "An approach for efficiently locating and electrically contacting nanostructures fabricated via UHV-STM lithography on Si(100)," Microelectronic Engineering 47(June 1999):235-237.

[183] R. Basu, N.P. Guisinger, M.E. Greene, M.C. Hersam, "Room temperature nanofabrication of atomically registered heteromolecular organosilicon nanostructures using multistep feedback controlled lithography," Appl. Phys. Lett. 85(27 September 2004):2619-2621; http://scitation.aip.org/getabs/servlet/GetabsServlet?prog=normal&id=APPLAB000085000013002619000001.

current-mediated H abstraction), because external electric fields can induce nonlocal diffusion processes and many organic molecules (that might be present as feedstock or intermediates) are susceptible to unwanted electron-stimulated desorption.[184] For example, while defects in InP can be imaged by STMs[185] the required bias voltage causes the defects to move; using FM-AFM, a zero-bias operation is possible which allows study of these defects without moving them by the electric field.

To achieve atomically precise tip positioning for DMS, several key challenges must be overcome including mechanical isolation (Section 2.1.3.1), avoiding jump to contact (Section 2.1.3.2), avoiding noise in the imaging signal (Section 2.1.3.3), and avoiding nonuniform atomically imprecise tip structures (Section 2.1.3.4).

2.1.3.1 Mechanical Isolation

To achieve atomic resolution with an STM or AFM, a first necessary condition is that the mechanical vibrations between tip and sample are smaller than the atomic corrugations.[186] This condition is met by a microscope design emphasizing utmost stability and establishing proper vibration isolation. Thus, proper mechanical design and vibration isolation of the DMS apparatus are essential. Typical procedures range from mounting the vacuum system on air legs and adding a vibration insulation stage directly at the microscope, to complex systems up to pneumatically-isolated below-ground-level floors. The first STMs were insulated from external vibrations by levitation on superconducting magnets, but later STMs used much simpler systems for vibration insulation.[187]

Vibration isolation is a recognized engineering sub-specialty[188] and private companies[189] can be retained to design and construct systems having any degree of isolation required. Measures can

---

[184] R. Basu, N.P. Guisinger, M.E. Greene, M.C. Hersam, "Room temperature nanofabrication of atomically registered heteromolecular organosilicon nanostructures using multistep feedback controlled lithography," Appl. Phys. Lett. 85(27 September 2004):2619-2621; http://scitation.aip.org/getabs/servlet/GetabsServlet?prog=normal&id=APPLAB000085000013002619000001.

[185] Y. Sugawara, M. Ohta, H. Ueyama, S. Morita, "Defect Motion on an InP(110) Surface Observed with Noncontact Atomic Force Microscopy," Science 270(1995):1646-1648.

[186] Franz J. Giessibl, "Advances in atomic force microscopy," Rev. Mod. Phys. 75(2003):949-983.

[187] G. Binnig, Aus dem Nichts, 2nd edition, Piper, Munchen, Zurich, 1997.

[188] Hal Amick, Bea Sennewald, Norman C. Pardue, Clayton Teague, Brian Scace, "Analytical/Experimental Study of Vibration of a Room-Sized Airspring-Supported Slab," Noise Control Engineering Journal 46(March/April 1998):39-47. C.G. Gordon, "Generic Vibration Criteria for Vibration-Sensitive Equipment," International Society for Optical Engineering (SPIE) Conference on Current Developments in Vibration Control for Optomechanical Systems, Denver, Colorado, July 1999. Hal Amick, Michael Gendreau, Colin G. Gordon, "Facility Vibration Issues for Nanotechnology Research," Symposium on Nano Device Technology 2002, National Chiao-Tung University, Hsinchu, Taiwan, 2-3 May 2002. Colin Gordon & Associates (specialists in acoustic and vibration solutions),

be active or passive, can specify the maximum physical amplitude of vibrations to be allowed to pass, and can be targeted to specific ranges of vibrational frequencies that appear most problematic for the experiment or apparatus being studied.

2.1.3.2 Jump to Contact

One of the most serious challenges to static AFM-based mechanical DMS is to avoid "jump to contact" between tip and workpiece surface. Giessbl[190] notes that van der Waals forces in vacuum are always attractive, and if chemical bonding between tip and workpiece can occur the chemical forces are also attractive for distances greater than the equilibrium distance. Because the AFM tip is mounted on a spring (the cantilever), moving the tip toward the workpiece can cause a sudden "jump-to-contact" when the stiffness of the cantilever is smaller than a certain threshold value k_{ts}^{max}. This instability can be prevented in the quasistatic mode if the cantilever spring constant:

$$k \geq \max(- \partial^2 V_{ts} / \partial z^2) = k_{ts}^{max} \qquad (2.4)$$

where V_{ts} is the potential energy as a function of tip-surface separation distance z.[191] If the tip and surface are incapable of forming a chemical bond, then V_{ts} is just the van der Waals potential, or:

$$V_{ts} = z_o F_{vdw} = -H \tan^2(\gamma/2) / 6, \qquad (2.5)$$

hence $\partial^2 V_{ts} / \partial z^2 = H \tan^2(\gamma/2) / 3z^2$ and thus $k_{ts}^{max} = 1.0$ N/m at z = 0.2 nm (~contact).

If tip and surface can form a chemical bond, then we must add the Morse potential $V_{Morse} = D_e \{ (1 – \exp[-\beta(z - r_0)])^2 - 1\}$, where the Morse function scaling parameter $\beta = (k_s / 2D_e)^{1/2}$, D_e = standard experimental values for bond energy or potential well depth (= bond dissociation energy + zero point vibrational energy), r_0 = bond length, and k_s = bond stretching stiffness k_s. In this

---

http://www.colingordon.com/; HDR Architecture Inc., 1101 King Street, Suite 400, Alexandria, VA 22314; (703) 518-8552 office, (703) 518-8588 fax, http://hdrinc.com; see also http://physics.berkeley.edu/research/packard/related/Vibrations/Fwd%20RE%20low%20vibration%20building.txt.

[189] Colin Gordon & Associates (specialists in acoustic and vibration solutions), http://www.colingordon.com/; HDR Architecture Inc., 1101 King Street, Suite 400, Alexandria, VA 22314; (703) 518-8552 office, (703) 518-8588 fax, http://hdrinc.com; see also http://physics.berkeley.edu/research/packard/related/Vibrations/Fwd%20RE%20low%20vibration%20building.txt.

[190] Franz J. Giessibl, "Advances in atomic force microscopy," Rev. Mod. Phys. 75(2003):949-983.

[191] Burnham, N. and R. J. Colton, "Measuring the nanomechanical and surface forces of materials using an atomic force microscope," J. Vac. Sci. Technol. A 7(1989):2906-2913. G.M. McClelland, R. Erlandsson, S. Chiang, "Atomic force microscopy: general principles and a new implementation," Progress in Quantitative Non-destructive Evaluation 6B(1987):1307-1314. D. Tabor, R.H.S. Winterton, "The direct measurement of normal and retarded van der Waals forces," Proc. R. Soc. London A 312(1969):435-450.

case, $\partial^2 V_{Morse}/\partial z^2 = 2\, D_e\, \beta^2\, [2 \exp(2\beta(r_0 - z)) - \exp(\beta(r_0 - z))]$ whose maximum occurs at $z = r_0 + \beta^{-1} \ln(4)$ when the first derivative of $\partial^2 V_{Morse}/\partial z^2$ is set equal to zero. The values for $k_{ts}^{max} = \max(-\partial^2 V_{ts}/\partial z^2)$ are tabulated in Table 2-1, and indicate that $k \geq k_{ts}^{max}$ = 3-58 N/m to prevent single chemical bond formation between atoms of the elements C, Ge and H, and $k \geq k_{ts}^{max}$ = 120 N/m to prevent C=C double bond formation. (C=Ge double bonds are considerably weaker than C=C, hence would require much lower bond stiffness in order to resist their formation.) Hence a cantilever stiffness of k > 60 N/m should be sufficient to resist a jump-to-contact chemical bond formation, including both bond formation energy and van der Waals forces between tip and workpiece, or k > 121 N/m if C=C double bond formation is possible.

Table 2-1. Cantilever stiffness (spring constant) required to resist jump-to-contact event due to chemical bond formation for a particular bond (leftmost column).[192]

Bond Formed	**r_0 (Å)**	**D_e (eV)**	**k_s (N/m)**	**β^{-1} (m)**	**z (Å)**	**k_{ts}^{max} (N/m)**
C-H	1.113	4.19	460	5.40×10^{-11}	1.86	57.6
C-C	1.523	3.47	440	5.03×10^{-11}	2.20	54.8
C-Ge	1.950	2.44	270	5.38×10^{-11}	2.70	33.8
Ge-Ge	2.410	1.95	160	6.25×10^{-11}	4.99	2.5
C=C	1.340	7.53	960	5.01×10^{-11}	2.03	120.2

The jump-to-contact failure mode can also be avoided even for softer cantilevers by oscillating the cantilever at a large enough amplitude A[193] for dynamic AFM-based mechanical DMS such that:

$$kA \geq \max(-F_{ts}) = F_{ts}^{max} \quad (2.6)$$

and

$$(1/2)\, kA^2 \geq \Delta E_{ts}\, (Q/2\pi). \quad (2.7)$$

If hysteresis occurs in the $F_{ts}(z)$-relation, the energy ΔE_{ts} needs to be supplied to the cantilever for each oscillation cycle.[194] If this energy loss is large compared to the intrinsic energy loss of

---

[192] Donald F. McMillen, David M. Golden, "Hydrocarbon bond dissociation energies," Annu. Rev. Phys. Chem. 33(1982):493-532. HyperCube, Inc., HyperChem Computational Chemistry, Publication HC70-00-04-00, January 2002; MM2 (1991) parameter set (/runfiles/mmpstr.txt and /runfiles/mmpben.txt) contributed by Norman Allinger. M. Lesbre, P. Mazerolles, J. Stage, The Organic Compounds of Germanium, John Wiley & Sons, New York, 1971. C.D. Schaeffer, Jr., C.A. Strausser, M.W. Thomsen, Claude H. Yoder, "Table 6. Common Bond Energies and Bond Lengths," The Wired Chemist, A Collection of Chemistry Resources. Data for General, Inorganic, Organic, and Physical Chemistry, 1989; http://wulfenite.fandm.edu/Data%20/Table_6.html. J.A. Kerr, "Strengths of Chemical Bonds," in D.R. Lide, ed., CRC Handbook of Chemistry and Physics, 71st Edition, CRC Press, Boca Raton FL, 1990.

[193] Franz J. Giessibl, "Forces and frequency shifts in atomic-resolution dynamic-force microscopy," Phys. Rev. B 56(15 December 1997):16010-16015; http://dns.ntu-ccms.ntu.edu.tw/references/1Sorted-References/duplicated_references/PHYS_REV_B/Volume_56/PHYS_REV_B-56-16010-1997.pdf.

[194] Franz J. Giessibl, "Advances in atomic force microscopy," Rev. Mod. Phys. 75(2003):949-983.

the cantilever, amplitude control can become difficult. The validity of these two criteria is supported by an analysis of the values of k and A for many NC-AFM experiments with atomic resolution reported in table I of Giessbl.[195] Fulfilment of these stability criteria (Eqns. 2.6 and 2.7) thus requires either the use of large amplitudes, cantilevers with large spring constants, or both. Since the use of large amplitudes has critical disadvantages, this suggests that the use of very stiff cantilevers may be the optimal approach in both static and dynamic AFM-based mechanical DMS.

2.1.3.3 Noise in the Imaging Signal

In traditional SPM, the force between tip and sample is composed of short-range chemical forces and many long-range contributions including electrostatic, magnetic, and van-der-Waals forces in vacuum,[196] and in ambient conditions there may also be meniscus forces. Long-range electrostatic, magnetic and meniscus forces can be eliminated by equalizing the electrostatic potential between tip and sample, by using nonmagnetic tips, and by vacuum operation, but the long-range van-der-Waals forces cannot be switched off. For imaging by SPM with atomic resolution, it is desirable to filter out the long-range force contributions and only measure the force components which vary at the atomic scale. Another measurement difficulty arises because although forces can be measured by the deflection of a spring, measuring this deflection is not a trivial task and is subject to noise, especially at low frequencies (1/f noise; Figure 2-8).

In STM, the rapid decay of the tunneling current with distance naturally blocks contributions of tip atoms that are further distant to the sample, even for fairly blunt tips.

In static AFM, the imaging signal is the sum of long- and short-range forces. Use of this mixed-component signal for tip position feedback information provides poorer control than if the relevant component could be isolated to precisely control tip position. In static AFM, the imaging signal is given by the DC deflection of the cantilever. This deflection is subject to 1/f noise. To control tip position to atomic precision in static AFM, an independent absolute positional measurement system (i.e., dead reckoning with no direct feedback) such as COXI (Section 4.6.2) that does not depend on the imaging signal can be used.

In dynamic AFM, attenuation of the long-range contributions in the imaging signal can be achieved by proper choice of the cantilever's oscillation amplitude A. The low-frequency noise is discriminated if the eigenfrequency f_0 is larger than the 1/f corner frequency (in the flat valley of noise vs. 1/f where noise is lowest; see Figure 2-8). With a bandpass filter with a center frequency around f_0 only the white noise density is integrated across the bandwidth B of the bandpass filter.[197]

---

[195] Franz J. Giessibl, "Advances in atomic force microscopy," Rev. Mod. Phys. 75(2003):949-983.
[196] Franz J. Giessibl, "Advances in atomic force microscopy," Rev. Mod. Phys. 75(2003):949-983.
[197] Franz J. Giessibl, "Advances in atomic force microscopy," Rev. Mod. Phys. 75(2003):949-983.

A related issue is the monotonicity of the imaging signal in SPM.[198] For STMs, the tunneling current is a monotonic function of the tip-sample distance and increases sharply with decreasing distance. The magnitude of the tunneling current increases continuously as the tip-sample distance decreases, i.e. the tunneling current is a strictly monotonic decreasing function of the distance (Figure 2-12A). This property allows a simple implementation of a feedback loop: the tunneling current is fed into a logarithmic amplifier to produce an error signal that is linear with the tip-sample distance. In contrast, for AFMs the tip-sample force is not monotonic. In general, the force is attractive for large distances and upon decreasing the distance between tip and sample past a threshold distance, the force turns repulsive (Figure 2-12B).

Figure 2-12. (A) Tunneling current as a function of distance and relation between current noise δI_t and vertical noise δz (arbitrary units). (B) Plot of tunneling current I_t and force F_{ts} (typical values) as a function of distance z between center of front atom and plane defined by the centers of surface atom layer. From Giessibl.[199]

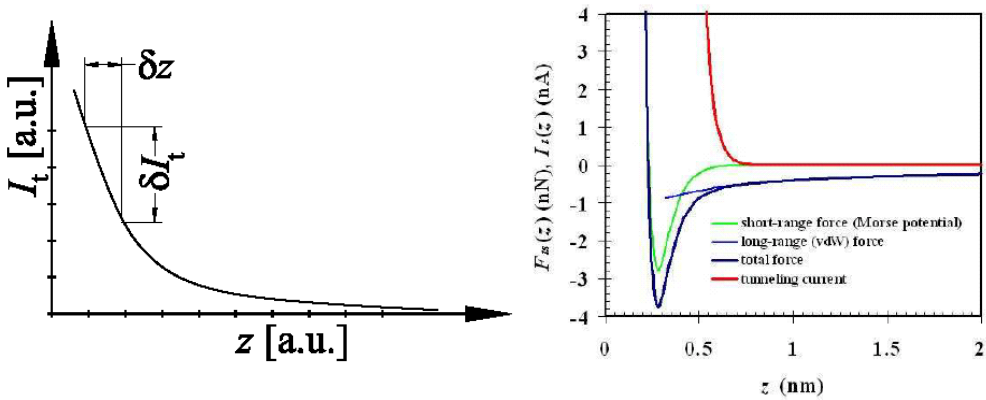

(A) (B)

Stable feedback using the imaging signal is only possible on a branch of the force curve where the curve is monotonic. Because the tunneling current is monotonic for the whole distance range and the tip-sample force is not monotonic, it is much easier to establish a z-distance feedback loop for STMs than for AFMs. Thus in both static and dynamic AFM, an independent absolute positional measurement system such as COXI (Section 4.6.2) that does not depend on the imaging signal (i.e., dead reckoning) can be used to achieve atomic precision in tip positioning.

2.1.3.4 Nonuniform Atomically Imprecise Tips

In the last 20 years there have been great strides in producing sharper and sharper SPM probe tips for use in atomic-scale scanning and related applications (see Table 4-1in Section 4.2.1). However, most of these tips are sub-optimal for "production" use in a DMS-based molecular

---

[198] Franz J. Giessibl, "Advances in atomic force microscopy," Rev. Mod. Phys. 75(2003):949-983.
[199] Franz J. Giessibl, "Advances in atomic force microscopy," Rev. Mod. Phys. 75(2003):949-983.

manufacturing system for two reasons: First, they are not atomically sharp, and second, their apex is not atomically precise (in fabrication *or* characterization) either at the start of use, or after significant use, in the lab.

Experimentalists pursuing ultrahigh vacuum (UHV) scanning probe microscopy frequently spend many (often fruitless) hours trying to coerce a commercially-obtained SPM probe into a structure that yields, retains, and accurately reproduces atomic resolution images, notes Philip Moriarty.[200] Collectively, vast numbers of researcher person-months in the scanning probe and nanoscience research communities are currently wasted in conditioning STM and AFM tips (during the scanning process) via voltage pulsing, field emission, high bandwidth scanning, high (or low) feedback loop gains, and other "tricks of the trade".[201] A number of techniques are used to form atomically sharp tips for state-of-the-art SPM imaging under UHV conditions but the acquisition of stable and high resolution images remains something of a "black art".[202] For example, following preparation of a probe using electrochemical etching, sometimes with subsequent heating to remove oxides and other contamination, it can still take many hours of a researcher's time to optimise the apex of the probe's structure. The operator in general adopts a poorly-defined approach to optimize the tip during scanning by altering various parameters such as voltage, current, scan speed, etc. This time-consuming procedure is required in order to modify the atomic scale/nanoscopic structure of the tip, as opposed to the microscale and macroscale modifications resulting from etching and annealing.[203] In some cases, experimentalists are forced to "gently crash the tip into the surface deliberately (i.e., turn the feedback loop off and push the tip a few nanometers towards the surface) to get a tip capable of atomic resolution".[204]

Figure 2-13a and Figure 2-13b show the dramatic changes in STM image quality that occur during an optimization process of this type.[205] The change from a very poorly resolved image, with no evidence of atomic-scale features, to the acquisition of high resolution data following a voltage or "height" (i.e., Δz) pulse will be familiar to practically every UHV scanning probe

---

[200] Philip Moriarty, Natalio Krasnogor, Richard Woolley, "Automated Optimisation of Scanning Probes: Accelerating Nanoscience," University of Nottingham, U.K., funding proposal, 2009. Philip Moriarty, personal communication to Robert A. Freitas Jr., 11 June 2009 and 26 June 2009.

[201] Philip Moriarty, Natalio Krasnogor, Richard Woolley, "Automated Optimisation of Scanning Probes: Accelerating Nanoscience," University of Nottingham, U.K., funding proposal, 2009.

[202] Peter Siepmann, Christopher P. Martin, Ioan Vancea, Philip J. Moriarty, Natalio Krasnogor, "A Genetic Algorithm Approach to Probing the Evolution of Self-Organized Nanostructured Systems," Nano Lett. 7(2007):1985-1990.

[203] Philip Moriarty, Natalio Krasnogor, Richard Woolley, "Automated Optimisation of Scanning Probes: Accelerating Nanoscience," University of Nottingham, U.K., funding proposal, 2009.

[204] Philip Moriarty, personal communication to Robert A. Freitas Jr., 11 June 2009 and 26 June 2009.

[205] Philip Moriarty, Natalio Krasnogor, Richard Woolley, "Automated Optimisation of Scanning Probes: Accelerating Nanoscience," University of Nottingham, U.K., funding proposal, 2009.

microscopist.[206] Figure 2-13c shows similar tip changes that occur during AFM imaging of Si(100) but, in this case, the changes are spontaneous (i.e., not induced by an operator-initiated change in scan parameters). In NC-AFM experiments (including those using the technique as well as those of others involving the more widely used cantilever approach) there can be many tip changes, due to strong surface-tip interactions and the associated dynamics of cantilever motion, before the tip settles down into a stable imaging mode. During this "settle" time, the operator needs to continually adjust the scan parameters (including the XY position of the tip) in order to ensure that, following a tip change, the highest quality image is obtained.[207]

Figure 2-13. Role of the tip structure in SPM imaging. (a) STM imaging of Si(100)-(2x1) where, prior to a voltage pulse (lower third of image), atomic resolution is not observed but defects in the dimer row structure are resolved. The image was acquired as the tip scanned from left to right and from the bottom to the top of the image in this case. (b) Examples of tip changes both induced by voltage pulsing and occurring spontaneously on Si(100)-(2x1). (c) Spontaneous tip changes during imaging of Si(100)-(2x1).[208]

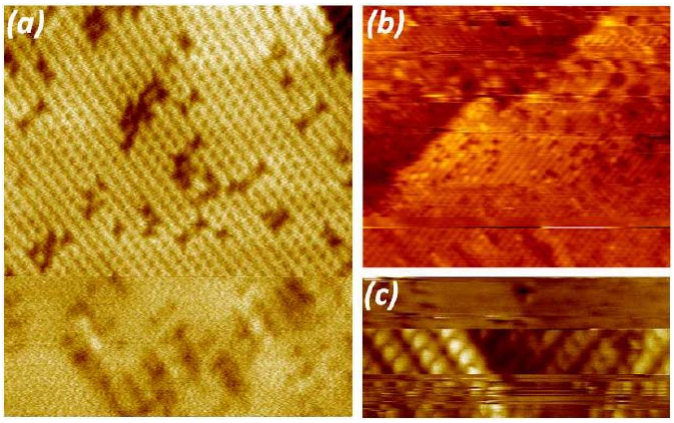

Nevertheless, some SPM tips have been produced that possess both atomic precision and a sub-nanometer radius of curvature (i.e., a few atomic diameters in width) at the apex, most notably various instances of three-atom (Figure 2-14A)[209] and single-atom (Figure 2-14B)[210] tungsten,

---

[206] Philip Moriarty, Natalio Krasnogor, Richard Woolley, "Automated Optimisation of Scanning Probes: Accelerating Nanoscience," University of Nottingham, U.K., funding proposal, 2009.

[207] Philip Moriarty, Natalio Krasnogor, Richard Woolley, "Automated Optimisation of Scanning Probes: Accelerating Nanoscience," University of Nottingham, U.K., funding proposal, 2009.

[208] Philip Moriarty, Natalio Krasnogor, Richard Woolley, "Automated Optimisation of Scanning Probes: Accelerating Nanoscience," University of Nottingham, U.K., funding proposal, 2009.

[209] Anne-Sophie Lucier, "Preparation and Characterization of Tungsten Tips Suitable for Molecular Electronics Studies," M.S. Thesis, Center for the Physics of Materials, Department of Physics, McGill University, Montreal, Quebec, Canada, February 2004; http://www.physics.mcgill.ca/~peter/theses/lucier.pdf. See also: Anne-Sophie Lucier, Henrik Mortensen,

Pd-coated tungsten,[211] and clean-facet iridium[212] tips (Section 4.2.2). Single-walled carbon nanotubes (SWCNTs) having near-atomic precision have been attached to SPM tips (Figure 2-14C)[213] and a diamond-like carbon (DLC) spike-probe tip with an asperity that is only a few carbon atoms wide at the tip is commercially available from NT-MDT (Figure 2-14D).[214] It is also possible that the PALE process currently being pursued by Zyvex could produce atomically precise tips, albeit in Si or Ge, not C (see further discussion in Section 4.2.4).

Yan Sun, and Peter Grütter, "Determination of the atomic structure of scanning probe microscopy tungsten tips by field ion microscopy," Phys. Rev. B 72, 235420 (2005).

[210] Moh'd Rezeq, Jason Pitters, Robert Wolkow, "Tungsten nanotip fabrication by spatially controlled field-assisted reaction with nitrogen," J. Chem. Phys. 124(28 May 2006):204716, http://www.aip.org/png/2006/264.htm (image), http://www.phys.ualberta.ca/~wolkow (movie) C.J. Chen, Introduction to Scanning Tunneling Microscopy, Oxford University Press, 1993. V.T. Binh, "In Situ Fabrication and Regeneration of Microtips for Scanning Tunnelling Microscopy," J. Microsc. 152(November 1988):355-361.

[211] T.-Y. Fu, L.C. Cheng, C.H. Nien, T.T. Tsong, "Method of creating a Pd-covered single-atom sharp W pyramidal tip: Mechanism and energetics of its formation," Phys. Rev. B 64(15 September 2001):113401; http://www.phys.sinica.edu.tw/~nano/publication/223.pdf. Theodore E. Madey, Kalman Pelhos, Qifei Wu, Robin Barnes, Ivan Ermanoski, Wenhua Chen, Jacek J. Kolodziej, John E. Rowe, "Nanoscale surface chemistry," Proc. Nat. Acad. Sci. USA 99(2002):6503-6508; http://www.physics.rutgers.edu/~wchen/Madey_page/Full_Publications/PDF/madey_PNAS_2002.pdf. H.S. Kuo, I.S. Hwang, T.-Y. Fu, J.Y. Wu, C.C. Chang, T.T. Tsong, "Preparation and characterization of single-atom tips," Nano Lett. 4(December 2004):2379-2382; http://aao.sinica.edu.tw/download/publication_e/Year2005/math04.pdf. T. Itagaki, E. Rokuta, H.-S. Kuo, K. Nomura, T. Ishikawa, B.-L. Cho, I.-S. Hwang, T.T. Tsong, C. Oshima, "Stabilities in field electron emissions from noble-metal covered W nano-tips: apex structure dependence," Surface and Interface Analysis 39(2006):299-303.

[212] Ivan Ermanoski, Kalman Pelhos, Wenhua Chen, Jamie S. Quinton, Theodore E. Madey, "Oxygen-induced nano-faceting of Ir(210)," Surf. Sci. 549(10 January 2004):1-23.

[213] J. Martinez, T.D. Yuzvinsky, A.M. Fennimore, A. Zettl, R. Garcia, C. Bustamante, "Length control and sharpening of atomic force microscope carbon nanotube tips assisted by an electron beam," Nanotechnology 16(2005):2493-2496; http://socrates.berkeley.edu/~tyuz/pub/nanotechnology16.pdf. attien V. Nguyen, Kuo-Jen Chao, Ramsey M.D. Stevens, Lance Delzeit, Alan Cassell, Jie Han, M. Meyyappan, "Carbon nanotube tip probes: stability and lateral resolution in scanning probe microscopy and application to surface science in semiconductors," Nanotechnology 12(September 2001):363-367; http://www.iop.org/EJ/abstract/0957-4484/12/3/326/. J.H. Hafner, C.L. Cheung, T.H. Oosterkamp, C.M. Lieber, "High-Yield Assembly of Individual Single-Walled Carbon Nanotube Tips for Scanning Probe Microscopies," J. Phys. Chem. B. 105(2001):743-746; http://cmliris.harvard.edu/publications/2000s/2001/jPCB105_743.pdf.

[214] NT-MDT (Molecular Devices and Tools for Nanotechnology, Moscow, Russia, http://www.ntmdt.com), "Super sharp Diamond_Like Carbon (DLC) tips," from their "SPM Probe and Accessories" catalog, 2008; http://www.ntmdt.com/download/accessories_catalog.pdf.

Figure 2-14. (A) Three-atom apex W(111) tip (<0.6 nm).[215] (B) FIM image of single-atom tip (~0.3 nm, inside centermost ring).[216] (C) SWCNT tip (0.5-1.4 nm).[217] (D) Super-sharp (<1 nm) diamond-like carbon (DLC) "asperity tip" from NT-MDT.[218]

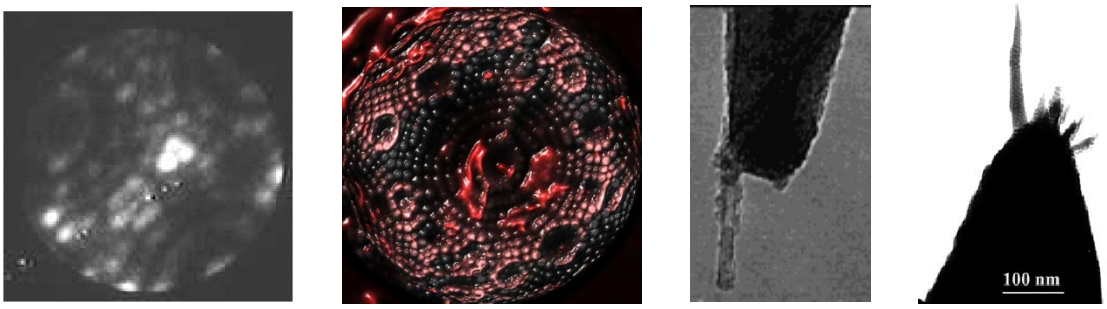

(A) **(B)** **(C)** **(D)**

2.1.4 Classical vs. High-Stiffness FM-AFM

In FM-AFM, a cantilever with eigenfrequency f_0 and spring constant k is subject to controlled positive feedback such that it oscillates with a constant amplitude A[219] as shown in Figure 2-15. The deflection signal first enters a bandpass filter. Then the signal splits in three branches: one branch is phase shifted, routed through an analog multiplier and fed back to the cantilever via an actuator; one branch is used to compute the actual oscillation amplitude, and this signal is used to

---

[215] Anne-Sophie Lucier, "Preparation and Characterization of Tungsten Tips Suitable for Molecular Electronics Studies," M.S. Thesis, Center for the Physics of Materials, Department of Physics, McGill University, Montreal, Quebec, Canada, February 2004; http://www.physics.mcgill.ca/~peter/theses/lucier.pdf. See also: Anne-Sophie Lucier, Henrik Mortensen, Yan Sun, and Peter Grütter, "Determination of the atomic structure of scanning probe microscopy tungsten tips by field ion microscopy," Phys. Rev. B 72, 235420 (2005).

[216] Moh'd Rezeq, Jason Pitters, Robert Wolkow, "Tungsten nanotip fabrication by spatially controlled field-assisted reaction with nitrogen," J. Chem. Phys. 124(28 May 2006):204716, http://www.aip.org/png/2006/264.htm (image), http://www.phys.ualberta.ca/~wolkow (movie).

[217] J.H. Hafner, C.L. Cheung, T.H. Oosterkamp, C.M. Lieber, "High-Yield Assembly of Individual Single-Walled Carbon Nanotube Tips for Scanning Probe Microscopies," J. Phys. Chem. B. 105(2001):743-746; http://cmliris.harvard.edu/publications/2000s/2001/jPCB105_743.pdf.

[218] NT-MDT (Molecular Devices and Tools for Nanotechnology, Moscow, Russia, http://www.ntmdt.com), "Super sharp Diamond_Like Carbon (DLC) tips," from their "SPM Probe and Accessories" catalog, 2008; http://www.ntmdt.com/download/accessories_catalog.pdf.

[219] T.R. Albrecht, P. Grutter, H.K. Horne, D. Rugar, "Frequency modulation detection using high-Q cantilevers for enhanced force microscope sensitivity," J. Appl. Phys. 69(1991):668-673. U. Durig, O. Zuger, A. Stalder, "Interaction force detection in scanning probe microscopy: Methods and applications," J. Appl. Phys. 72(1992):1788-1798.

calculate a gain input g for the analog multiplier; and the third branch is used to feed a frequency detector. The frequency f is determined by the eigenfrequency f_0 of the cantilever and the phase shift φ between the mechanical excitation generated at the actuator and the deflection of the cantilever. If $\varphi = \pi/2$, the loop oscillates at $f = f_0$. Forces between tip and sample cause a change in frequency of $f = f_0 + \Delta f$; measuring the frequency shift Δf allows the allows the tip-sample force gradient to be monitored and Δf is used as the imaging signal in FM-AFM. Figure 2-16 shows a typical frequency shift versus distance curve.[220] In the case of a closed feedback loop as shown in Figure 2-15, the driving frequency cannot be choosen freely but is determined by f_0 of the cantilever, the phase shift φ and the tip-sample forces. The purpose of the oscillator circuit is to provide controlled positive feedback (with a phase angle of $\varphi = \pi/2$) such that the cantilever oscillates at a constant amplitude.

Figure 2-15. (A) Block diagram of the frequency-modulation AFM feedback loop for constant amplitude control and frequency shift measurement. Three physical observables are available: frequency shift, damping signal and (average) tunneling current. (B) Schematic view of an oscillating cantilever at its upper and lower turnaround points. The minimum tip-sample distance is d and the amplitude is A. From Giessibl.[221]

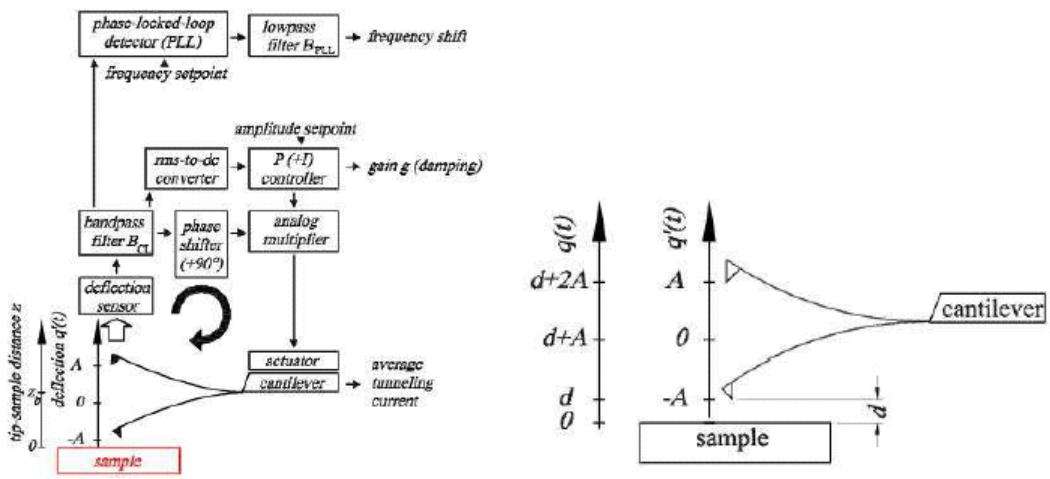

(A) (B)

---

[220] It is of practical importance to note that the minimum of the frequency shift versus distance curve shown in Figure 2-16 is a function of the lateral tip position. Directly over a sample atom, the minimum can be very deep. However, at other sample sites there may be small negative frequency shift. Imaging can only be performed with frequency shift setpoints which are reachable on every (x, y) position on the imaged sample area, otherwise a tip crash occurs; Franz J. Giessibl, "Advances in atomic force microscopy," Rev. Mod. Phys. 75(2003):949-983.

[221] Franz J. Giessibl, "Advances in atomic force microscopy," Rev. Mod. Phys. 75(2003):949-983.

FM-AFM was introduced in 1991 in magnetic force microscopy. In these experiments, Albrecht et al.[222] imaged a thin film CoPtCr magnetic recording disk with a cantilever with a spring constant k ≈ 10 N/m, eigenfrequency f_0 = 68 485Hz, amplitude A = 5 nm, a *Q* value of 40000 and a tip with a thin magnetic film coverage.[223] The noise level and imaging speed was enhanced significantly compared to amplitude modulation techniques. In 1993, the frequency modulation method was implemented in the prototype of a commercial STM/AFM for ultra-high vacuum.[224] Initial experiments on KCl yielded excellent resolution and soon after, the Si (111)-(7x7) surface was imaged with true atomic resolution for the first time by Giessibl.[225]

Figure 2-16. Schematic plot of frequency shift Δf as a function of tip-sample distance z. The noise in the tip-sample distance measurement is given by the noise of the frequency measurement Δf divided by the slope of the frequency shift curve. From Giessibl.[226]

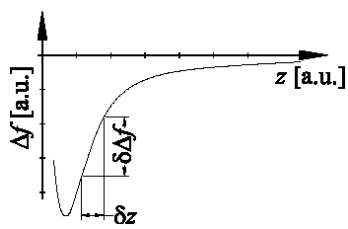

FM-AFM has five operating parameters:

(1) the spring constant of the cantilever, k;
(2) the eigenfrequency of the cantilever, f_0;
(3) the quality-value of the cantilever, *Q*;
(4) the oscillation amplitude, A; and
(5) the frequency shift of the cantilever, Δf.

The first three parameters are determined by the type of cantilever that is used, while the latter two parameters can be freely adjusted. The initial parameters which provided true atomic resolution (k = 17N/m, f_0 = 114 kHz, *Q* = 28000, A = 34 nm, Δf = -70Hz) were found empirically.[227] Surprisingly, the amplitude necessary for obtaining good results was very large

---

[222] T.R. Albrecht, P. Grutter, H.K. Horne, D. Rugar, "Frequency modulation detection using high-Q cantilevers for enhanced force microscope sensitivity," J. Appl. Phys. 69(1991):668-673.

[223] Franz J. Giessibl, "Advances in atomic force microscopy," Rev. Mod. Phys. 75(2003):949-983.

[224] F.J. Giessibl, B.M. Trafas, "Piezoresistive cantilevers utilized for scanning tunneling and scanning force microscope in ultrahigh vacuum," Rev. Sci. Instrum. 65(1994):1923-1929.

[225] F.J. Giessibl, "Atomic Resolution of the Silicon (111)-(7x7) Surface by Atomic Force Microscopy," Science 267(1995):68-71.

[226] Franz J. Giessibl, "Advances in atomic force microscopy," Rev. Mod. Phys. 75(2003):949-983.

[227] Franz J. Giessibl, "Advances in atomic force microscopy," Rev. Mod. Phys. 75(2003):949-983.

compared to atomic dimensions. The necessity of using large amplitudes for obtaining good results seemed counterintuitive because the tip of the cantilever spends only a small fraction of the time in each oscillation cycle in close vicinity to the sample, but it is now recognized that these large amplitudes were required to prevent jump-to-contact instability during the cantilever oscillation (Section 2.1.3.2). Apparently, the product of spring constant and amplitude, or kA (in Eqn. 2.6), must equal or exceed $F_{ts}^{max} \approx 100$ nN to provide a sufficiently strong withdrawing force;[228] an additional lower-threshold condition for A, given in Eqn. 2.7, is required for maintaining stable oscillation amplitudes. Atomic resolution on silicon and other samples was reproduced by other groups with similar operating parameters: $\Delta f \approx -100$ Hz, $k \approx 20$ N/m, $f_0 \approx 200$ kHz and $A \approx 10$ nm. Several commercial vendors now offer FM-AFMs that operate with these parameters.[229] The use of high-*Q* cantilevers with only a modest stiffness of $k \approx 20$ N/m oscillating with an amplitude of $A \approx 10$ nm has enabled many groups to routinely achieve atomic resolution by FM-AFM. This mode is used in many laboratories now and is commonly called the "classic" FM-AFM mode.

While the operating parameters of the classic FM-AFM mode provide good results routinely, it was not proven initially that these parameters yield optimal resolution. The search space for finding the optimal parameters was not completely open, because micromachined cantilevers were only available with a limited selection of spring constants. A theoretical study in 1999[230] showed that the optimal amplitudes are in the ~Å range, requiring spring constants on the order of a few hundred N/m, much stiffer than the spring constant typically found in commercially available cantilevers. This result has been verified experimentally by achieving unprecedented resolution with a cantilever with k = 1800 N/m and sub-nm oscillation amplitudes.[231]

For small amplitudes the frequency shift is very sensitive to short-range forces because short-range forces have a very strong force gradient, while for large amplitudes, long-range forces contribute heavily to the frequency shift. This dependence of the frequency shift on amplitude suggests that small amplitudes can increase sensitivity to short-range forces, which implies that when short-range interactions are to be probed, the amplitude should be in the range of the short-range forces. While amplitudes in the ~Å range have been elusive with conventional cantilevers because of the instability problem described in Section 2.1.3.2, stiff sensors such as the qPlus

---

[228] Franz J. Giessibl, "Advances in atomic force microscopy," Rev. Mod. Phys. 75(2003):949-983.

[229] Jeol, 2002, JEOL UHV STM AFM, JEOL Ltd., 1-2 Musashino 3-chome Akishima Tokyo, Japan; Omicron, 2002, Omicron UHV AFM/STM, Omicron Nanotechnology GmbH, Limburger Str. 75, D-65232 Taunusstein, Germany.

[230] F.J. Giessibl, H. Bielefeldt, S. Hembacher, J. Mannhart, "Calculation of the Optimal Imaging Parameters for Frequency Modulation Atomic Force Microscopy," Applied Surface Science 140(1999):352-357.

[231] F.J. Giessibl, S. Hembacher, H. Bielefeldt, J. Mannhart, "Subatomic Features on the Silicon(111)-(7x7) Surface Observed by Atomic Force Microscopy," Science 289(2000):422-425. F.J. Giessibl, H. Bielefeldt, S. Hembacher, J. Mannhart, "Imaging of atomic orbitals with the atomic force microscope - experiments and simulations," Annalen der Physik (Leipzig) 10(2001):887-910.

sensor shown in Figure 2-17 are well-suited for small-amplitude operation.[232] (Mechanical resonances in the actuator assembly are likely to occur at the high resonance frequencies of conventional cantilevers, but a self-oscillation technique for cantilevers[233] helps to avoid these resonances.) In 2001, Lantz et al.[234] used FM-AFM to perform mechanical spectroscopy over specific atomic sites on the silicon surface, with measured forces mainly caused by the interaction of two single atoms (one atom on the tip and one atom on the surface).

What is the optimal amplitude for minimal vertical noise in high-stiffness FM-AFM? Giessibl[235] considers a tip-sample interaction involving both chemical and van der Waals forces, given by a Morse potential with a depth of -2.15 eV, a decay length of $\kappa = 1.55$ Å^{-1} and an equilibrium distance of $\sigma = 2.35$ Å. The cantilever is assumed to be a qPlus sensor as shown in Figure 2-17 with k = 1800 N/m and noise density (cantilever thermal noise + detector deflection noise) $n_{q'}$ = 100 fm/√Hz, operated with a bandwidth B_{FM} = 100 Hz. Figure 2-18 shows the vertical noise as a function of amplitude for a fixed closest tip-sample distance of z_{min} = 4 Å. Minimum noise occurs for A ≈ 1.26 Å, whereas for A = 340 Å the noise is about one order of magnitude larger. For chemical forces, $A_{optimal}$ ≈ 1 Å. However, operating a conventional low-stiffness cantilever with amplitudes in the ~Å range close to a sample is impossible because of the jump-to-contact problem (Section 2.1.3.2). The cantilever spring constant k needs to be at least a few hundred N/m to enable operation with amplitudes in the ~Å range.[236]

Figure 2-18 also shows that noise is not significantly enhanced if the high-stiffness cantilever is operated with a slightly lower amplitude that spans the distance range of acceptable bond stretch – e.g., A = 0.3 Å (30 pm)[237] for a C-C bond of typical bondlength 1.54 Å with a maximum Morse stretch distance of 1.87 Å. This implies that such cantilevers should be operable in FM-AFM mode during bond-making and bond-breaking DMS operations, within the tensile tolerance of the affected chemical bonds. (If DMS tooltips are positioned via dead reckoning, they will not be scanned during DMS chemical bonding operations. Some scanning-mode operation may occur during periodic tip registration procedures, but this should constitute only a relatively small fraction of the total duty cycle of tip use, hence the limits on tip stiffness and the requirement for high eigenfrequency are not very restrictive in this case.) As of 2009, the typical amplitude used

---

[232] Franz J. Giessibl, "Advances in atomic force microscopy," Rev. Mod. Phys. 75(2003):949-983.

[233] F.J. Giessibl, M. Tortonese, "Self Oscillating Mode for Frequency Modulation Non-Contact Atomic Force Microscopy," Applied Physics Letters 70(1997):2529-2531.

[234] M. Lantz, H.J. Hug, R. Hoffmann, P. van Schendel, P. Kappenberger, S. Martin, A. Baratoff, H.-J. Guntherodt, "Quantitative Measurement of Short-Range Chemical Bonding Forces," Science 291(2001):2580-2583.

[235] Franz J. Giessibl, "Advances in atomic force microscopy," Rev. Mod. Phys. 75(2003):949-983.

[236] Franz J. Giessibl, "Advances in atomic force microscopy," Rev. Mod. Phys. 75(2003):949-983.

[237] Markus Ternes, Christopher P. Lutz, Cyrus F. Hirjibehedin, Franz J. Giessibl, Andreas J. Heinrich, "The Force Needed to Move an Atom on a Surface," Science 319(22 February 2008):1066-1069.

for imaging silicon atoms was A ~ 2.5 Å (250 pm) peak-to-peak and the record lowest amplitude achieved for commercial qPlus sensors was 70 pm peak-to-peak.[238]

Figure 2-17. <u>Left</u>: Micrograph of a qPlus sensor – a cantilever made from a quartz tuning fork. One of the prongs is fixed to a large substrate and a tip is mounted to the free prong. Because the fixed prong is attached to a heavy mass, the device is mechanically equivalent to a traditional cantilever. The dimensions of the free prong are: length 2400 µm, width 130 µm, thickness 214 µm.[239] <u>Right</u>: Schematic of electrodes and preamp.[240]

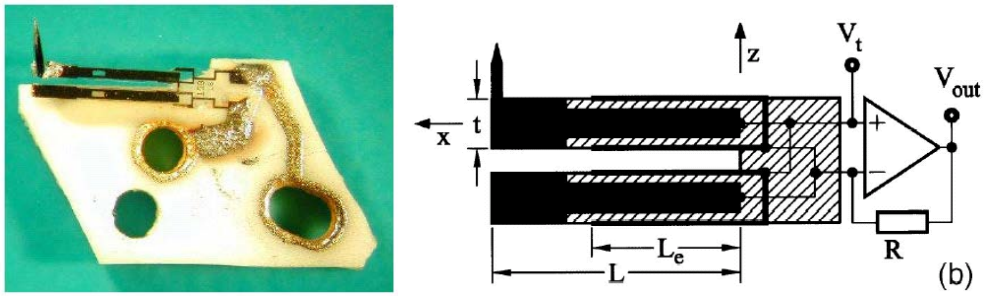

Figure 2-18. Vertical noise as a function of amplitude for the tip-sample potential (Morse type) described in the text. The amplitude value where minimal noise results (here $A_{optimal} \approx$ 1 Å) is approximately equal to the range of the tip-sample force. The absolute noise figure for this optimal amplitude is a function of bandwith, noise performance of the cantilever deflection sensor and temperature. From Giessibl.[241]

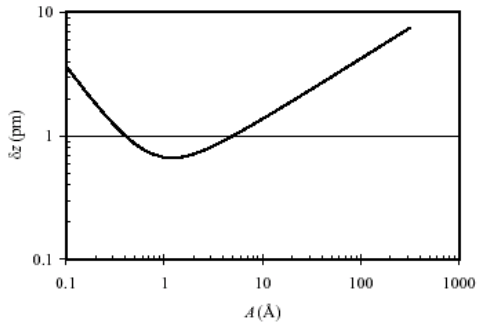

---

[238] Unpublished result achieved by Omicron in their applications lab; personal correspondence to Robert Freitas from Philip Moriarty, 10 June 2009.

[239] Franz J. Giessibl, "Advances in atomic force microscopy," Rev. Mod. Phys. 75(2003):949-983.

[240] Franz J. Giessibl, "Atomic resolution on Si(111)-(7x7) by noncontact atomic force microscopy with a force sensor based on a quartz tuning fork," Appl. Phys. Lett. 76(13 March 2000):1470; http://dns.ntu-ccms.ntu.edu.tw/references/APPL_PHYS_LETT-76-1470-2000.pdf.

[241] Franz J. Giessibl, "Advances in atomic force microscopy," Rev. Mod. Phys. 75(2003):949-983.

An alternative off-resonance technique with small amplitudes might also be employed. For small amplitudes the imaging signal is proportional to the force gradient and the weight of short-range forces is much larger than the weight of long-range forces.[242] This effect has been used in an off-resonance technique[243] in which a tungsten cantilever with $k \approx 300$ N/m is oscillated at a frequency far below its resonance frequency with an amplitude $A_0 \approx 0.5$ Å (50 pm). When the cantilever comes close to the sample, the oscillation amplitude changes according to:

$$A = A_0 / (1 + k_{ts}/k) \tag{2.8}$$

with a tip-sample stiffness k_{ts}. Using a stiff cantilever and the dynamic mode solves the AFM-related challenges of jump-to-contact instability (Section 2.1.3.2) and the 1/f-noise problem (Section 2.1.3.3). Conceptually, this small amplitude off-resonance technique is very attractive due to its simplicity in implementation and interpretation.

2.1.5 Dynamic Mode with Stiff Cantilevers and Small Amplitudes

Intuitively, the amplitudes that are used in classic FM-AFM are much too large: if a silicon atom was magnified to the size of an orange, the average distance of the cantilever used in classic non-contact AFM mode would amount to 15 meters. But it was always clear that greater sensitivity to short-range forces would be achieved with small amplitudes.

Notes Giessibl:[244] "In FM-AFM, it was finally shown that small amplitudes do work – however, only if extremely stiff cantilevers are used. After the theoretical proof of the benefits of using small amplitudes with stiff cantilevers,[245] we were trying to convince manufacturers of piezoresistive cantilevers to make devices with $k \approx 500$ N/m – without success. However, the theoretical findings gave us enough confidence to modify a quartz tuning fork to a quartz cantilever sensor with a stiffness of roughly 2 kN/m (qPlus sensor; Figure 2-17).[246] The first experiments were successful, yielding AFM images of silicon with excellent resolution. For the first time, clear features within the image of a single atom were observed (Figure 2-19A). The structure of these images was interpreted to originate from the orbitals of the tip atom, the first

---

[242] Franz J. Giessibl, "Advances in atomic force microscopy," Rev. Mod. Phys. 75(2003):949-983.

[243] P.M. Hoffmann, A. Oral, R.A. Grimble, H. Ozer, S. Jeffrey, J.B. Pethica, "Direct measurement of interatomic force gradients using an ultra-low-amplitude atomic force microscope," Proc. R. Soc. London A 457(2001):1161-1174.

[244] Franz J. Giessibl, "Advances in atomic force microscopy," Rev. Mod. Phys. 75(2003):949-983.

[245] F.J. Giessibl, H. Bielefeldt, S. Hembacher, J. Mannhart, "Calculation of the Optimal Imaging Parameters for Frequency Modulation Atomic Force Microscopy," Applied Surface Science 140(1999):352-357.

[246] F.J. Giessibl, "Vorrichtung zum beruhrungslosen Abtasten einer Oberflache und Verfahren dafur," Offenlegungsschrift German Patent Office DE 196 33 546, 1996. F.J. Giessibl, "High-Speed Force Sensor for Force Microscopy and Profilometry Utilizing a Quartz Tuning Fork", Applied Physics Letters 73(1998):3956-3958.

observation of charge structure within atoms in real space.[247] Figure 2-19A is an image of a single silicon adatom. Silicon adatoms display a single sp^3 dangling bond sticking out perpendicular from the surface. Thus, the image of this atom is expected to be spherically symmetric with respect to the vertical axis. We interpret the image as being caused by an overlap of two sp^3 dangling bonds from the tip with the single dangling bond from the surface.[248] On the subatomic level, the image is sensitive to the chemical identity and the structural surroundings of the front atom of the tip. First attempts to engineer tips with a known symmetry were underway by 2001.[249] Figure 2-19B is an image of a Si(111)-(7x7) surface imaged with a qPlus sensor with a (111) oriented Si tip with extremely small amplitudes (i.e., ~2.5 Å) and even positive frequency shifts, i.e., repulsive forces. The tip was found to be extremely stable compared to (001) oriented tips."

Notes Giessibl:[250] "The small amplitude technique with very stiff cantilevers allows to achieve tip-sample distances close to the bulk distances and obtains single-atom images with nontrivial internal structures (subatomic resolution) on silicon[251] and rare-earth metal atoms.[252] The enhanced resolution of short-range forces as a result of using small amplitudes was confirmed experimentally by Eguchi and Hasegawa.[253] The capacity of the stiff-cantilever-small-amplitude technique to image standard insulators with moderate short-range forces is shown in Figure 2-19C, where a KCl (001) surface is imaged with a qPlus sensor with a silicon tip."

---

[247] F.J. Giessibl, S. Hembacher, H. Bielefeldt, J. Mannhart, "Subatomic Features on the Silicon(111)-(7x7) Surface Observed by Atomic Force Microscopy," Science 289(2000):422-425.

[248] F.J. Giessibl, S. Hembacher, H. Bielefeldt, J. Mannhart, "Subatomic Features on the Silicon(111)-(7x7) Surface Observed by Atomic Force Microscopy," Science 289(2000):422-425. F.J. Giessibl, H. Bielefeldt, S. Hembacher, J. Mannhart, "Imaging of atomic orbitals with the atomic force microscope - experiments and simulations," Annalen der Physik (Leipzig) 10(2001):887-910.

[249] F.J. Giessibl, S. Hembacher, H. Bielefeldt, J. Mannhart, "Imaging Silicon with Crystallographically Oriented Tips by Atomic Force Microscopy," Applied Physics A 72(2001):15-17.

[250] Franz J. Giessibl, "Advances in atomic force microscopy," Rev. Mod. Phys. 75(2003):949-983.

[251] F.J. Giessibl, H. Bielefeldt, S. Hembacher, J. Mannhart, "Imaging of atomic orbitals with the atomic force microscope - experiments and simulations," Annalen der Physik (Leipzig) 10(2001):887-910.

[252] M. Herz, F.J. Giessibl, J. Mannhart, "Probing the Shape of Atoms in Real Space," unpublished. Cited in Giessibl (2003).

[253] T. Eguchi, Y. Hasegawa, "High Resolution Atomic Force Microscopic Imaging of the Si(111)(7x7) Surface: Contribution of Short-Range Force to the Images," Phys. Rev. Lett. 89(2002):266105.1-4.

Figure 2-19. <u>Left</u>: Image of a single adatom on Si(111)-(7x7). A $3sp^3$ state points towards the surface normal on the Si (111) surface, and the image of this atom should be symmetric with respect to the z-axis. Because images in AFM are a convolution of tip and sample states, and the sample state is well known in this case; the tip state is most likely to be two $3sp^3$ states originating in a single Si tip atom;[254] image size: 6.6 Å x 6.6 Å lateral, 1.4 Å vertical. <u>Center:</u> Image of a Si(111)-(7x7) surface imaged with a qPlus sensor; parameters: k = 1800 N/m, A = 2.5 Å, f_0 = 14772 Hz, Δf = +4 Hz, = 28 fN√m; image size: 40 Å lateral, 1.4 Å vertical.[255] <u>Right:</u> Image of a KCl(001) surface imaged with a qPlus sensor; parameters: k = 1800 N/m, A = 9 Å, f_0 = 14772 Hz, Δf = 4 Hz, = 13 fN√m; image size: 23.5 Å lateral, 0.3 Å (30 pm) vertical; contour lines are spaced vertically by ~3 pm.[256]

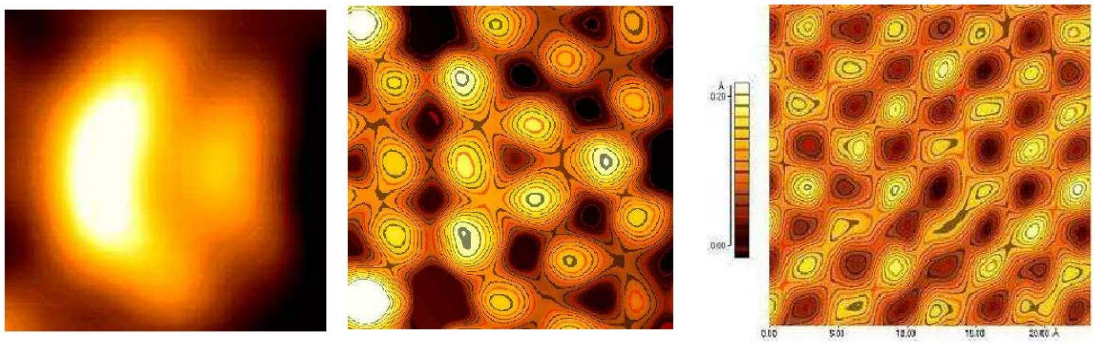

In sum, four techniques for atomic resolution AFM in vacuum are in use today: (1) the classic frequency modulation technique with large amplitudes (used by most experimenters) and soft cantilevers, (2) frequency modulation with small amplitudes and stiff cantilevers, (3) the off-resonance technique originated by the Pethica group, and (4) the amplitude modulation method. Among these, FM-AFM is an established experimental technique with applications in the surface science of insulators. AFM is still more complicated than STM and these complications appear to deter many scientists. Yet the possibilities of atomic resolution AFM are overwhelming, in particular:[257] "access to the very scaffolding of matter, the chemical bond....An exciting extension of this work would be possible if atoms could also be deposited with atomic precision by AFM, because the construction of, e.g., one dimensional conductors or semiconductors on insulating substrates would allow us to build electronic circuits consisting only of a few atoms."

---

[254] F.J. Giessibl, S. Hembacher, H. Bielefeldt, J. Mannhart, "Subatomic Features on the Silicon(111)-(7x7) Surface Observed by Atomic Force Microscopy," Science 289(2000):422-425.

[255] F.J. Giessibl, H. Bielefeldt, S. Hembacher, J. Mannhart, "Imaging of atomic orbitals with the atomic force microscope - experiments and simulations," Annalen der Physik (Leipzig) 10(2001):887-910.

[256] Franz J. Giessibl, "Advances in atomic force microscopy," Rev. Mod. Phys. 75(2003):949-983.

[257] Franz J. Giessibl, "Advances in atomic force microscopy," Rev. Mod. Phys. 75(2003):949-983.

2.1.6 qPlus Tuning Fork Tips

The qPlus sensor tip employed by Giessibl had a stiffness of 1800 N/m and used a tuning fork taken from a Swatch watch (Figure 2-20). Quartz oscillators (tuning forks) with spring constants ranging from 800 N/m to 10,000 N/m (depending on geometry) and resonance frequencies of 32 kHz to 100 kHz are commercially available and are ideally suited for this purpose.[258]

Figure 2-20. (A) Tuning fork from Swatch watch.[259] (B) "qPlus" sensor, comprising a quartz cantilever for ultra-high resolution atomic force microscopy.[260] (C) First experimental image (Si-7x7) showing internal atomic structures.[261] (D) qPlus sensor for lateral FM-AFM.[262] (E) qPlus tuning fork sensor inside AFM; approximate size of the view is 1.7 cm x 2.5 cm.[263] (F) qPlus tuning fork sensor; dimensions of the free prong are 2400 µm (length), 130 µm (width), 214 µm (thickness).[264]

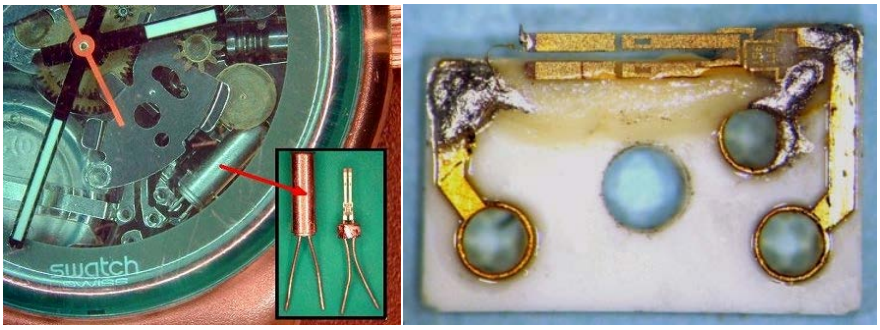

(A) (B)

---

[258] "Pushing QPlus Further: Smaller Amplitudes & Higher Frequencies," Omicron Newsletter 12(December 2008):2-4; http://omicron-nanotech.com/info/media/nlt_2008_2.pdf.

[259] qPlus Sensor; http://www.physik.uni-regensburg.de/forschung/giessibl/neu/research/qplus-sensor_e.phtml.

[260] qPlus Sensor; http://www.physik.uni-regensburg.de/forschung/giessibl/neu/research/qplus-sensor_e.phtml.

[261] qPlus Sensor; http://www.physik.uni-regensburg.de/forschung/giessibl/neu/research/qplus-sensor_e.phtml.

[262] http://www.physik.uni-regensburg.de/forschung/giessibl/fjg/imagegallery/afmaccessories/afmaccessories_d.shtml.

[263] "Taking the measure of atomic friction," 21 February 2008; http://www.rsc.org/chemistryworld/News/2008/February/21020802.asp.

[264] Franz J. Giessibl, "Advances in atomic force microscopy," Rev. Mod. Phys. 75(2003):949-983. Franz J. Giessibl, "Atomic resolution on Si(111)-(7x7) by noncontact atomic force microscopy with a force sensor based on a quartz tuning fork," Appl. Phys. Lett. 76(13 March 2000):1470; http://dns.ntu-ccms.ntu.edu.tw/references/APPL_PHYS_LETT-76-1470-2000.pdf.

Figure 2-20 (cont'd).

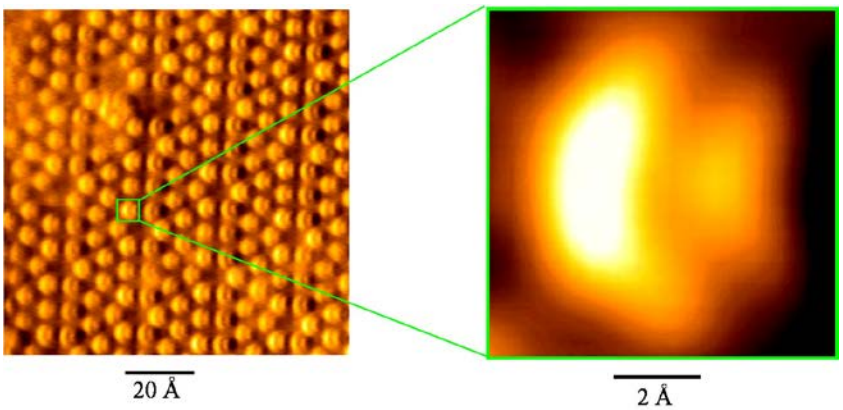

---------(C)---------

(D)

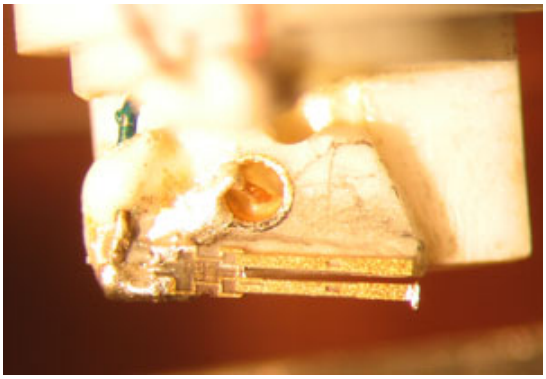

(E)

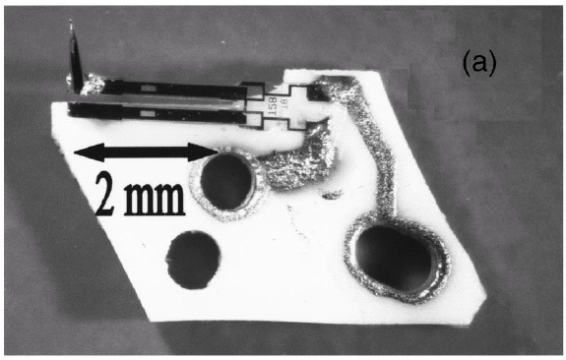

(F)

QPlus AFM technology was commercially established by Omicron in 2004. (QPlus sensors are available commercially from Omicron.) Key targets along the development have been: (i) high mechanical stability, (ii) optimal signal-to-noise ratio, and (iii) large detection bandwidth. Figure 2-21 shows the stability of qPlus FM-AFM measurements in Δf force feedback on Au(111) single crystal samples, revealing the herringbone reconstruction and atomic corrugations of only 2-4 pm.[265] 10 pm vertical resolution on NaCl using AFM/qPlus was reported in 2006.[266]

---

[265] "Pushing QPlus Further: Smaller Amplitudes & Higher Frequencies," Omicron Newsletter 12(December 2008):2-4; http://omicron-nanotech.com/info/media/nlt_2008_2.pdf.

[266] "QPlus Technology for Atomic-Resolution AFM on NaCl at 5K (Result of the month 11/2006)," Omicron Nanotechnology; http://www.omicron.de/index2.html?/results/qplus_atomi_resolution/index.html~Omicron.

Figure 2-21. <u>Above</u>: Imaging of rest atoms (raw data) of the Si(111)-7x7 surface with qPlus AFM in an Omicron VT at 50 K (top); line profile showing the height difference of the rest atoms (middle).[267] <u>Below</u>: Omicron qPlus AFM demonstrates ability to measure 2-4 pm atomic corrugations on Au(111) surface.[268]

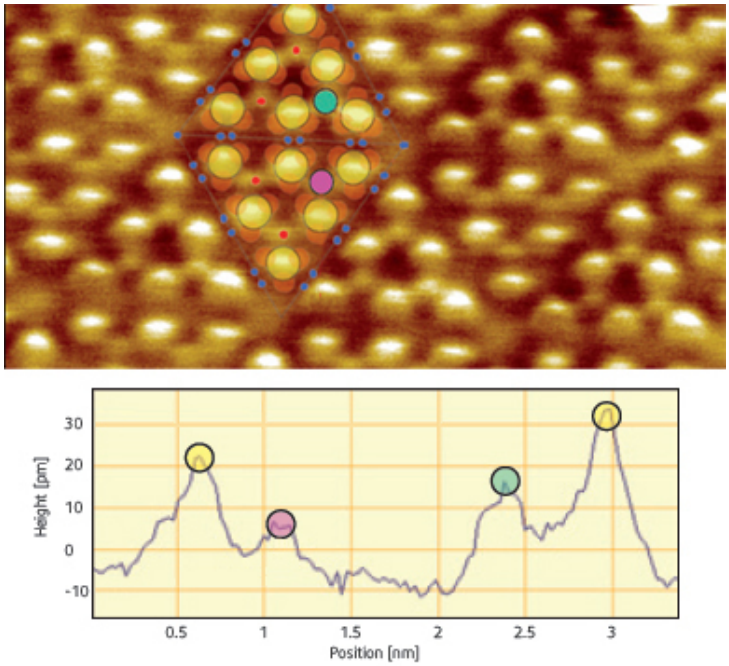

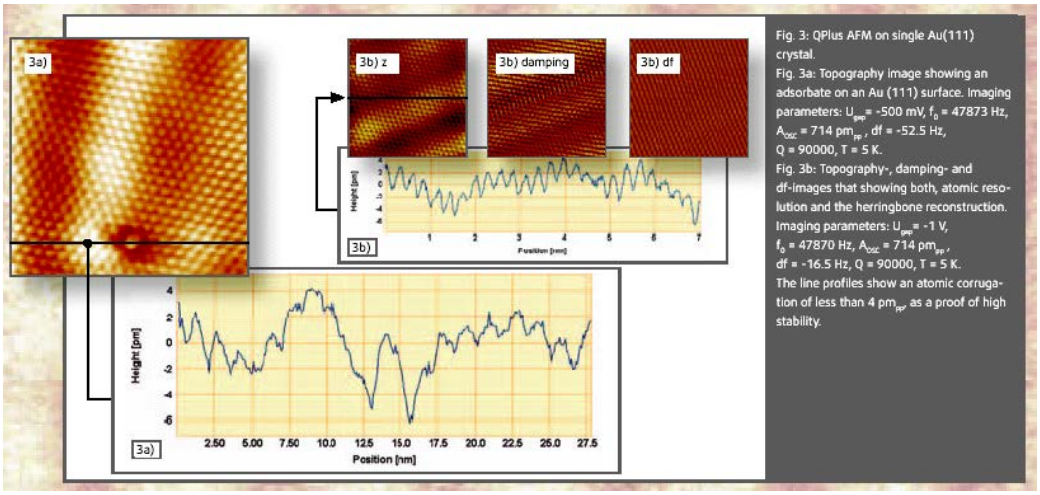

---

[267] Beam Deflection AFM with QPlus AFMCustomized (Result of the month 05/2009); http://www.omicron.de/rom/beam_deflection_afm_qplus/index.html#295.

[268] "Pushing QPlus Further: Smaller Amplitudes & Higher Frequencies," Omicron Newsletter 12(December 2008):2-4; http://omicron-nanotech.com/info/media/nlt_2008_2.pdf.

As of 2009, the construction of qPlus tips in AFM labs was still often done "by hand" to meet the unique requirements of the experiments being undertaken in the particular lab. Here is a description[269] of one such fabrication process:

"The steps we used to build up a qPlus sensor are the following. First, the tuning fork, which comes from a commercially available watch quartz,[270] is removed from its hermetically sealed canister. The sensors we have used have a fundamental resonance of 32,768 Hz. Then one prong of the tuning fork is affixed with Torr seal[271] to a Macor plate, which is fitted with wires for making connections to the two electrodes on the tuning fork. After the electrical connections are made to the tuning fork, a 10 mm long, 0.25 mm thick tungsten wire is glued with Torr seal at the very end of the free prong. The Torr seal is cured at 100 °C for 1 h. Then, the electrical contact between the tungsten wire and one of the tuning fork electrodes is made using silver epoxy,[272] which is cured at 150 °C for 1 h. The process of curing the vacuum compatible epoxies needed to make both the structural electrical contacts between the tungsten wire and the tuning fork preclude the option of etching a tungsten wire and then attaching it to the tuning fork. If an etched tip were generated then affixed to the tuning fork, the tip would oxidize rapidly in air at elevated temperatures rendering it less conductive and less sharp. This immediately prompted the investigation into etching a wire that has been attached to the tuning fork where the etching would be the last step before installation into the scanner assembly and evacuation of the system. We chose not to create a tip holder at the end of the tuning fork that would allow for ex situ etched tips to be used in order to minimize the mass load at the end of prong. The resonance frequency drops by as much as a factor of 2 with an etched wire attached directly and any additional material in the form of a tip holder would further decrease the fork resonance...."

Tuning forks are being used more frequently in UHV and low temperature environments due to the elimination of optical alignment requirements for FM-AFM imaging. In this technique, a cantilever beam is oscillated with constant amplitude A_0 at frequency f, where f depends on the eigenfrequency f_0 of the beam (determined by spring constant k and effective mass m*) and F_{ts}. An image can be created by scanning in the XY plane and keeping f constant by controlling Z.

---

[269] M. Kulawik, M. Nowicki, G. Thielsch, L. Cramer, H.-P. Rust, H.-J. Freund, T. P. Pearl, P. S. Weiss, "A double lamellae dropoff etching procedure for tungsten tips attached to tuning fork atomic force microscopy'scanning tunneling microscopy sensors," Rev. Sci. Instrum. 74(February 2003):1027-1030; http://www.fhi-berlin.mpg.de/cp/pubdl/348/367.pdf.

[270] Quartz 304-447, RS Components GmbH, Hessenring 13b, D-64546 Morfelden-Walldorf.

[271] Torr Seal Resin Sealant, Varian, Inc.

[272] H37-MP, Polytec GmbH, Polytec-Platz, D-76337 Waldbronn.

2.1.7 Typical SPM Topographic Raster Scanning Pattern

As noted by Marinello et al.,[273] SPMs can be considered as instruments scanning from the top with a probe moving over the surface. Therefore, the term "topography" is assumed to refer to the upper bound of the sample interface. Under such an assumption, undercut regions and/or hidden points are not considered to be part of the topography (Figure 2-22A).

The probe is scanned over the surface in a raster fashion, and the topography is reconstructed through a collection of parallel profiles. Normally, two main directions are used to describe the probe movement of SPMs: x, the so-called fast scan direction, parallel to the direction of a single traced profile, and y, the so-called slow scan direction, perpendicular to the first one. Each profile is normally scanned twice: once forward and once back. The two movements are normally indicated as "scan" or "trace" and "back-scan" or "retrace" (Figure 2-22B). The surface is eventually characterized by a matrix of points (usually referred to as pixels), called an "image". Positions i and j in the matrix correspond to physical positions x and y on the surface, respectively. The value stored in an (i, j) cell of the matrix is the vertical elevation z (Figure 2-22C). Topography maps then consist of data sets commonly reported in an orthonormal rectilinear Cartesian coordinate system, which is only ideally correct, since distortions occur during measurement.

Figure 2-22. SPM topography generation. <u>Top left:</u> The probe is scanned over the surface in a raster fashion; <u>Top right:</u> topographies are eventually achieved as a collection of profiles, each scanned twice, once forward and once back; and <u>Bottom left/right:</u> the scanned image is normally re-assembled as a data set stored as a rectangular matrix of points (pixels).[274]

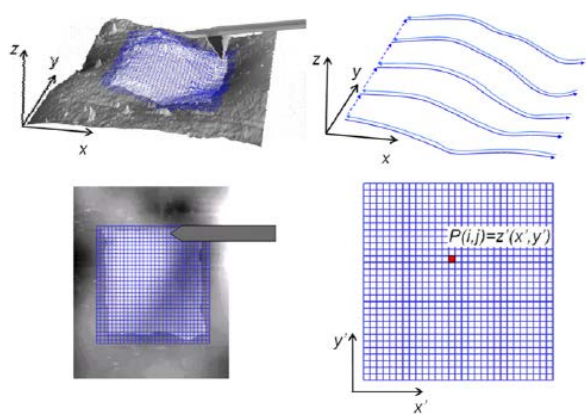

[273] F. Marinello, P. Bariani, S. Carmignato, E. Savio, "Geometrical modelling of scanning probe microscopes and characterization of errors," Meas. Sci. Technol. 20(2009):084013.

[274] F. Marinello, P. Bariani, S. Carmignato, E. Savio, "Geometrical modelling of scanning probe microscopes and characterization of errors," Meas. Sci. Technol. 20(2009):084013. F. Marinello, "Atomic force microscopy in nanometrology: modeling and enhancement of the instrument," PhD Dissertation, University of Padova and Technical University of Denmark, 2007; http://paduaresearch.cab.unipd.it/1295/01/PhD Thesis Marinello.pdf.

2.2 Basic Positioning Technologies

To make a high-accuracy picopositioner system, we first need an apparatus capable of performing a precise positioning displacement. The best-known are piezo, voice-coil and electrostatic actuators. The limits of some common positioning/actuation technologies are summarized in Table 2-2.

Table 2-2. Some limits to positioning and actuation (KAIST, 2003)[275]

Technology	Actuator Type	Max. Absolute Repeatability of Guideway	Max. Guideway Domain
Atmospheric pressure bearing	Electromagnetic actuator	10,000 pm	1 m
Electromagnetic bearing	Electromagnetic actuator	10,000 pm	1 m
Low friction polymer	Electromagnetic actuator	1000 pm	1 m
Dual guideway	Low friction polymer + elastic flexure	10 pm	1 m
Elastic flexure	Piezoelectric actuator	10 pm	1 cm

2.2.1 Piezoelectric and Piezoceramic Actuators

Piezoelectricity is the ability of some materials (notably crystals, e.g., quartz, and certain ceramics) to generate an electric potential in response to applied mechanical stress. This may take the form of a separation of electric charge across the crystal lattice. If the material is not short-circuited, the applied charge induces a voltage across the material. Piezoelectric materials also show the opposite effect, called converse piezoelectric effect, where the application of an electrical field creates mechanical deformation in the crystal. Thus piezos can be used either as both sensors and actuators.

AFM scanners are made from piezoelectric material, which expands and contracts proportionally to an applied voltage. Whether they elongate or contract depends upon the polarity of the voltage applied. The scanner is constructed by combining independently operated piezo electrodes for X, Y, and Z into a single tube, forming a scanner that can manipulate samples and probes with extreme precision in 3 dimensions (Figure 2-23). On the one hand, piezos make available the finest possible displacements, but on the other hand they also suffer from pronounced non-ideal behaviors such as drift, hysteresis, nonlinearity, creep and ageing, which are related to the polycrystalline nature of the piezo material.[276]

Piezo scanners are characterized by their sensitivity which is the ratio of piezo movement to piezo voltage, i.e., by how much the piezo material extends or contracts per applied volt. Because of

---

[275] "Billionth Precision Uncertainty Engineering (BUPE)," KAIST, Annual Report 2003, http://pem.kaist.ac.kr/bupe/.

[276] H.-U. Danzebrink, L. Koenders, G. Wilkening, A. Yacoot, H. Kunzmann, "Advances in Scanning Force Microscopy for Dimensional Metrology," CIRP Annals - Manufacturing Technology 55(2006):841-878.

differences in material or size, the sensitivity varies from scanner to scanner. Sensitivity varies non-linearly with respect to scan size. Piezo scanners exhibit more sensitivity at the end than at the beginning of a scan. This causes the forward and reverse scans to behave differently and display hysteresis between the two scan directions. This can be partially corrected by applying a non-linear voltage to the piezo electrodes to cause linear scanner movement and calibrating the scanner accordingly. The sensitivity of piezoelectric materials also decreases exponentially with time. This causes most of the change in sensitivity to occur in the initial stages of the scanner's life. Piezoelectric scanners are run for approximately 48 hours before they are shipped from the factory so that they are past the point where we can expect large changes in sensitivity. As the scanner ages, the sensitivity will change less with time and the scanner would seldom require recalibration.

Figure 2-23. Typical scanner piezo tube and X-Y-Z configurations.[277] AC signals applied to conductive areas of the tube crate piezo movement along the three major axes. Thus AC voltages applied to the different electrodes of the piezoelectric scanner produce a scanning raster motion in X and Y. Two segments of the piezoelectric crystal are shown for X and for Y.

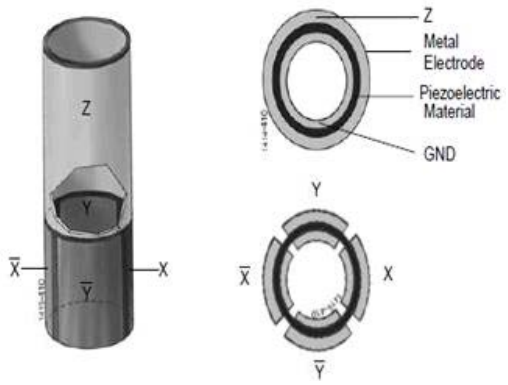

AFM images can also be affected by hysteresis of the piezoelectric material[278] and cross-talk between the (x,y,z) axes that may require software enhancement and filtering. Such filtering could "flatten" out real topographical features. However, newer AFM use real-time correction software (for example, feature-oriented scanning)[279] or closed-loop scanners which practically eliminate these problems. Some AFM also use separated orthogonal scanners (as opposed to a

---

[277] http://en.wikipedia.org/wiki/File:Piezoscanner.JPG.

[278] R.V. Lapshin, "Analytical model for the approximation of hysteresis loop and its application to the scanning tunneling microscope," Review of Scientific Instruments 66(1995):4718-4730.

[279] R.V. Lapshin, "Feature-oriented scanning methodology for probe microscopy and nanotechnology," Nanotechnology 15(2004):1135-1151. R.V. Lapshin, "Automatic drift elimination in probe microscope images based on techniques of counter-scanning and topography feature recognition," Measurement Science and Technology 18(2007):907-927.

single tube) which also serve to eliminate cross-talk problems. These properties, possible improvements and models have been discussed in a number of publications, and products have been improved substantially in recent years.[280] But for reliable measurements, the displacements generated by piezo elements still have to be measured by separate sensors, and controlled in closed loops – although the achievable resolution is degraded by extra electronic noise due to sensors and electronics for the closed-loop control.

The best piezo-based actuators can achieve 10-50 pm resolution (Table 2-3; Section 2.2.5), though subject to the many constraints noted above.

2.2.2 Voice Coil Actuators

Voice-coil actuation generally refers to any galvanometer-like mechanism that uses a solenoid to move an object back and forth within a magnetic field. One common high-precision application is the coil of wire that moves the read-write heads in a moving-head disk drive. In this application, a very lightweight coil of wires is mounted within a very strong magnetic field produced by rare earth permanent magnets. The voice coil linear actuator is the motor part of the servo system that positions the heads – an electric control signal drives the voice coil and the resulting force quickly and accurately positions the heads.

Voice coil actuators and motors generate force when subjected to an electrical current or magnetic field.[281] The coil within the motor is the only moving component and is usually attached to a moveable load with a device such as a voice coil valve. This design permits high-speed motion and accurate positioning. Voice coil motors are an effective alternative to electromechanical components such as servomotors. There are two basic types of voice coil products: linear and rotary. Linear voice coil actuators and linear voice coil motors provide precision linear motion over short distances. Rotary voice coil actuators and rotary voice coil motors provide precision circular motion over short angles. Both types of voice coil products are used in many types of control applications, from drive mechanisms in computers to robotic assembly lines.

The best commercially available linear voice-coil actuators typically exhibit positioning accuracy to 100-150 nm resolution.[282] Voice coil actuators have been employed as secondary actuators in nanopositioning systems to achieve ±1 nm stage positioning accuracy,[283] and to maintain 1.3 nm

---

[280] K. Dirscherl, Online correction of scanning probe microscopes with pixel accuracy, Ph.D. thesis, Technical University of Denmark (DTU), Lyngby, Denmark, 2000.

[281] http://motion-controls.globalspec.com/LearnMore/Motion_Controls/Motors/Voice_Coil_Motors.

[282] H2W Technologies, http://www.h2wtech.com/noncommdcactu.htm; "Voice Coil Stage from Equipment Solutions," 16 November 2006, http://www.ecnasiamag.com/article-11465-voicecoilstagefromequipsolution-Asia.html; "Introduction to VCS10 Voice Coil Stage," http://www.laserscanningsolutions.com/VoiceCoiltutorial.pdf.

[283] B.A. Awabdy, W.-C. Shih, D.M. Auslander, "Nanometer positioning of a linear motion stage under static loads," IEEE/ASME Transactions on Mechatronics 3(June 1998):113-119.

RMS stability in optical path length for the cryogenic optical delay line[284] for the planned DARWIN space interferometry mission (Section 4.6.6.1.4).

2.2.3 Electrostatic Actuators

Any electric charge creates around it an electric field, and any electric field applies a force to any charged particle. This principle, widely known since Maxwell's era, is used in the MEMS field in electrostatic actuators. Electrostatics is the most widely used force in the design of MEMS. In industry, it is used in microresonators, switches, micromirrors, accelerometers, etc. Almost every kind of microactuator has one or more electrostatic actuation based version. Electrostatic force depends largely on the size of the structures and the distance between electrodes, so electrostatic actuation has a large advantage when the electrode surface is large compared to the travel distance. But the equation of the force gives a dependancy to the square of the distance, so actuation voltage rises rapidly with distance – hence actuation voltages are often quite high, easily reaching tens or even hundreds of volts which are easy to get on a large device but not on very compact integrated systems. (Since the electric circuit is capacitive, the power consumption is very low regardless of voltage, so these actuators draw very little current.)

A widely used architecture for electrostatic actuation is a lateral translation of mobile parts, mostly achieved with comb-drive actuators (Figure 2-24). In this configuration, the force is equally and symmetrically applied on both side of the beams, and the mobile part moves in parallel to the beam direction. The total displacement is rather shorter than what is possible in straight actuation, but the force is constant, meaning an easier control of the displacement. This kind of system offers a very high precision level and a simpler electronic control. Systems like microaccelerometers make high use of comb-drives.

In a comb-drive, there is no pull-in effect unless a design error allows electrodes to touch. The displacement is linear, contrary to straight actuation, but the design is limited by the need to place electrodes beams opposite to each other. The designer must also take care to arrange the end stop to avoid contact between the mobile part and the fixed part, and to keep forces symmetric so that the direction of the displacement is kept linear.

---

[284] T.C. van den Dool, F. Kamphues, B.C. Braam, "The Development of a Cryogenic Optical Delay Line for DARWIN," Proc. International Conference on MEMS, NANO and Smart Systems, 24-27 July 2005, pp. 195-196; http://www.millhouse.nl/graphics/publications/The%20Development%20of%20a%20Cryogenic%20Optical%20Delay%20Line%20for%20DARWIN%20ICMENS%202005%20Banff%20paper.pdf.

Figure 2-24. Principle of comb-drive actuation: The comb is fixed and anchored to the substrate. The interdigitated array of tines is free to move in and out of the comb via joint flexure, except at the beam at far right where the back of the tine array is anchored to the substrate, so that the actuator can come back to its initial position thanks to the spring force of the compressed joint flexure.[285]

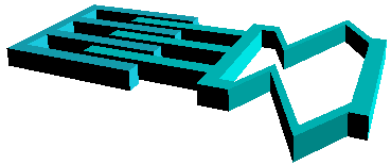

Electrostatic actuators, though generally employed in MEMS (micron-scale) constructions, can also achieve nanometer-scale actuation. For example, an electrostatic translational microstage based on the inchworm principal of actuation is capable of arbitrarily large translation distances with nanometer resolution, with user-adjustable actuation step size from **50-2000 nm**.[286] A trench isolation technology designed to improve MEMS fabrication was used to develop a low volume, large force (> 1 mN) electrostatic actuator for low-displacement applications requiring **nanometer resolution**.[287] A MEMS-based electrostatic actuator design is proposed for recording head fly height control below **10 nm** for magnetic hard drives.[288] And an electrostatic XYZ-actuator for an "atom chip" uses several comb drive structures for the XY-actuation allowing a translation of 17.5 μm with an accuracy in the sub-micron range and a parallel plate configuration for the Z-actuation with a maximum translation of 7 μm with an envisaged accuracy of a **few nanometers**.[289]

2.2.4 Aerostatic Actuators

It is a well-known principle in hydraulics that a pressure applied to a narrow cylinder of fluid in communication with a much larger-diameter cylinder of fluid will transmit the same pressure into

---

[285] MEMS World - Electrostatic actuators; http://matthieu.lagouge.free.fr/mems/electrostatic.html.

[286] M.V. Shutov, D.L. Howard, E.E. Sandoz, J.M. Sirota, R.L. Smith, S.D. Collins, "Electrostatic inchworm microsystem with long range translation," Sensors and Actuators A: Physical 114(1 September 2004):379-386.

[287] E. Sarajlic, E. Berenschot, G. Krijnen, M. Elwenspoek, "Versatile trench isolation technology for the fabrication of microactuators," Microelectronic Engineering 67-68(June 2003):430-437.

[288] Fang Chen, Huikai Xie, Gary K. Fedder, "A MEMS-Based Monolithic Electrostatic Microactuator for Ultra-Low Magnetic Disk Head Fly Height Control," IEEE Trans. on Magnetics 37(July 2001):1915-1918; http://www.ece.cmu.edu/~mems/pubs/pdfs/ieee/ieee_magnetics/0070_chen-2001.pdf.

[289] C.O. Gollasch, Z. Moktadir, M. Kraft, M. Trupke, S. Eriksson, E.A. Hinds, "A three-dimensional electrostatic actuator with a locking mechanism for microcavities on atom chips," J. Micromech. Microeng. 15(2005):S39-S46; http://eprints.ecs.soton.ac.uk/12405/1/jmmGollasch3DActuator.pdf.

the larger cylinder, with the fluid level in the small cylinder falling a great deal farther than the fluid level in the larger cylinder rises because the volume of transferred fluid spreads out over a much larger area. Interestingly, a similar concept has been applied by the Mizumoto group over the last decade[290] to develop an unusual aerostatic positioning system that is capable of generating displacements as small as **10 pm**.

Figure 2-25A shows the Active Inherent Restrictor (AIR) picometer positioning system. A ceramic machine table (size: 300 mm x 350 mm x 100 mm, mass: ~50 kg) of an ultraprecision machine tool[291] is guided by an aerostatic guideway in X direction (normal to the page). This X-table can also be positioned in Z direction (horizontal, cutting direction) by the AIR mechanism incorporated into the aerostatic guideway. A positioning instruction output from a microcomputer is converted into the supply voltage to the piezoelectric transducer (PZT) in the AIR. The X-table moves according to the deformation of the PZT. The table movement in the Z direction is detected by a fiberoptic sensor and fed back to the computer, completing a closed-

---

[290] H. Mizumoto, et al., "Active inherent restrictor for air-bearing spindle," Precision Engineering 19(1996):141-146. H. Mizumoto, M. Inoue, S. Arii, Y. Kami, M. Yabuya, "An Ultraprecision Machine Tool using Twist-roller Friction Drives and Active Control Aerostatic Guideways," Proceedings of 1st EUSPEN 1(1999):28-31. See also: H. Mizumoto, S. Inoue, S. Arii, Y. Kami, M. Yabuya, "An Ultraprecision Machine Tool with Active Control Aerostatic Guidewaya for Improving Quality of Machined Surface," Proceedings of the 9th International Conference on Production Engineering 1(1999):165-170; http://kaken.nii.ac.jp/ja/p/10555042/1999/3/ja. Hiroshi Mizumoto, Shiroh Arii, Makoto Yabuya, Yoshihiro Kami, "Picometer Positioning System Using Aerostatic Guideway As Motion-Reduction Mechanism," ASPE (2001); http://www.aspe.net/publications/Annual_2001/PDF/PAPERS/ACTUATE/1115.PDF. Hiroshi Mizumoto, Shiro Arii, Yoichi Tazoe, Yoshihiro Kami, "Picometer Positioning System for Ultraprecision Machine Tool," E35, 2004 JSPE Autumn Meeting. See also: Hiroshi Mizumoto, Yoshito Yabuta, Shiroh Arii, Tazoe Yoichi, Yoshihiro Kami, "A Picometer Positioning System using Active Aerostatic Guideway (precision positioning and control technology)," Proceedings of International Conference on Leading Edge Manufacturing in 21st century (LEM21), Vol. 2005, No.3 (20051018) pp. 1009-1014.. Hiroshi Mizumoto, Shiro Arii, Yoshito Yabuta, Yoichi Tazoe, "Tri-mode Picometer Positioning system for Ultraprecision Machine Tools," 2005 JSPE Spring Meeting. See also: Hiroshi Mizumoto, Yoichi Tazoe, "A Two-axis Tri-mode Picometer Positioning system," Journal of the Japan Society of Advanced Production Technology 23(2005):63-69; in Japanese. Hiroshi Mizumoto, Yoshito Yabuta, Shiro Arii, Makoto Yabuya, Yoichi Tazoe, "A Dual-mode Pico-positioning System using Active Aerostatic Coupling," International Journal of Precision Engineering and Manufacturing 8(2007):32-37. H. Mizumoto, S. Arii, Y. Yabuta, Y. Kami, Y. Tazoe, "Section 12-3. Active Aerostatic Bearings for Ultraprecision Applications," Proceedings of the 35th International MATADOR Conference (formerly The International Machine Tool Design and Research Conference), Srichand Hinduja, Kuang-Chao Fan eds., Springer, London, pp. 289-292. See also: Hiroshi Mizumoto, Makoto Yabuya, "Novel Positioning Devices for Ultraprecision Machine Tool," Key Engineering Materials 407-408(February 2009):81-84; http://www.scientific.net/KEM.407-408.81.

[291] H. Mizumoto, M. Inoue, S. Arii, Y. Kami, M. Yabuya, "An Ultraprecision Machine Tool using Twist-roller Friction Drives and Active Control Aerostatic Guideways," Proceedings of 1st EUSPEN 1(1999):28-31. See also: H. Mizumoto, S. Inoue, S. Arii, Y. Kami, M. Yabuya, "An Ultraprecision Machine Tool with Active Control Aerostatic Guidewaya for Improving Quality of Machined Surface," Proceedings of the 9th International Conference on Production Engineering 1(1999):165-170; http://kaken.nii.ac.jp/ja/p/10555042/1999/3/ja.

loop control system that allows the computer to output instructions for correcting the table's position.

Figure 2-25. (A) Ultraprecision positioning system using aerostatic guideway; (B) cross-section of assembled AIR unit; (C) motion reduction mechanism of AIR; (D) characteristic motion reduction by AIR.[292]

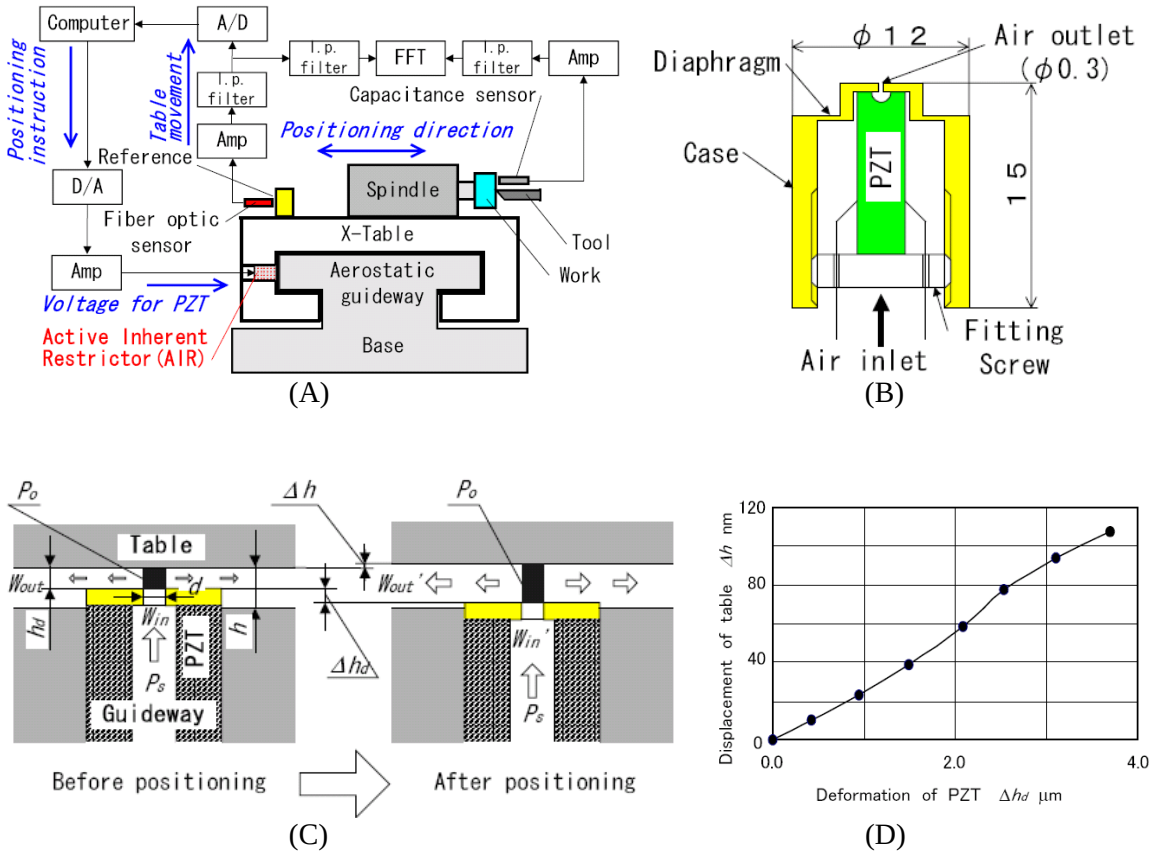

The assembled view of the AIR is shown in Figure 2-25B. The AIR unit consists of a piezoelectric transducer (PZT) and a diaphragm case that has an air outlet. The hole is small enough to function as an orifice when the transducer is embedded in the bearing surface. The positioning mechanism using the AIR is shown in Figure 2-25C. A table is supported by an aerostatic guideway with an inherent restrictor. Orifice area of the inherent restrictor formed on the bearing surface is $\pi d h_d$, where d is the diameter of the air outlet and h_d is the restriction gap that can be controlled by the PZT. When the length of the PZT decreases by Δh_d, the airflow rate and the pressure on the bearing surface increases, causing the air film thickness h to increase by Δh and the table to move upward. Owing to the aerostatic mechanism, the table displacement Δh

---

[292] Hiroshi Mizumoto, Shiroh Arii, Makoto Yabuya, Yoshihiro Kami, "Picometer Positioning System Using Aerostatic Guideway As Motion-Reduction Mechanism," ASPE (2001); http://www.aspe.net/publications/Annual_2001/PDF/PAPERS/ACTUATE/1115.PDF.

in the Z direction can be much less than the deformation of the transducer Δh_d. Figure 2-25D shows the experimental relationship between Δh_d and Δh: a full stroke of the piezoelectric transducer is 3.5 μm whereas the maximum **movement of the table is 110 nm**. Thus the aerostatic guideway with the AIR acts as a motion-reduction mechanism, with a motion reduction rate of about 30.

Figure 2-26 shows the results of static step positioning using various step widths (100pm, 50pm, 20pm and 10pm). In this test, steps of the same width were repeated five times in one direction, then five times in the reverse direction. A low-pass filter was used to decrease noise. Steps larger than 20 pm are clearly resolved. Steps of 10 pm are degraded by noise and not as clear as the others, but every step can be recognized. The positioning resolution of this system is therefore considered to be 10 pm.[293] Subsequent examination of several aerostatic-related control systems has confirmed that the positioning with sub-nanometer order of resolution can only be executed by active aerostatic bearings with the AIR, using an active restrictor of a bearing gap-feedback type.[294]

Figure 2-26. Picometer step positioning (step widths: 10pm, 20pm, 50pm, 100pm).[295]

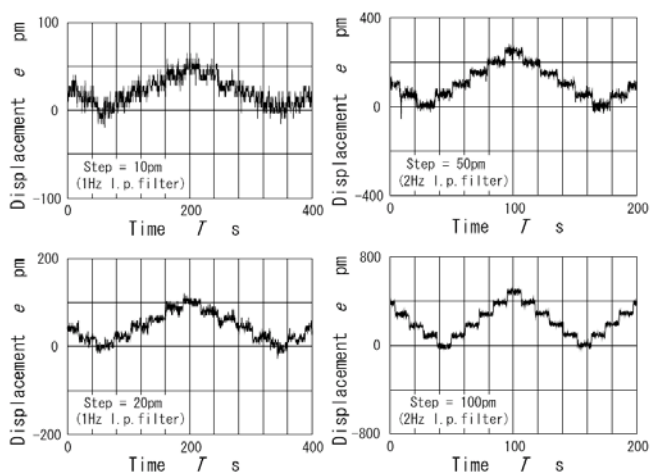

[293] Hiroshi Mizumoto, Shiroh Arii, Makoto Yabuya, Yoshihiro Kami, "Picometer Positioning System Using Aerostatic Guideway As Motion-Reduction Mechanism," ASPE (2001); http://www.aspe.net/publications/Annual_2001/PDF/PAPERS/ACTUATE/1115.PDF.

[294] H. Mizumoto, S. Arii, Y. Yabuta, Y. Kami, Y. Tazoe, "Section 12-3. Active Aerostatic Bearings for Ultraprecision Applications," Proceedings of the 35th International MATADOR Conference (formerly The International Machine Tool Design and Research Conference), Srichand Hinduja, Kuang-Chao Fan eds., Springer, London, pp. 289-292. See also: Hiroshi Mizumoto, Makoto Yabuya, "Novel Positioning Devices for Ultraprecision Machine Tool," Key Engineering Materials 407-408(February 2009):81-84; http://www.scientific.net/KEM.407-408.81.

[295] Hiroshi Mizumoto, Shiroh Arii, Makoto Yabuya, Yoshihiro Kami, "Picometer Positioning System Using Aerostatic Guideway As Motion-Reduction Mechanism," ASPE (2001); http://www.aspe.net/publications/Annual_2001/PDF/PAPERS/ACTUATE/1115.PDF.

2.2.5 Required Positional Accuracy in SPM-Based DMS Systems

What repeatable positional accuracy is actually required for reliable DMS work? Distances between neighboring competing radical sites are ~1.54 Å on C(110) for displacements across the dimer row, ~1.64 Å on C(100) for displacements in the cross-row direction, and ~2.50 Å on C(111) between neighboring surface sites. A tooltip which is mispositioned by more than half of the mean lateral distance between competing reactive sites (e.g., ~0.77 Å (77 pm) for C(110), ~0.82 Å (82 pm) for C(100), ~1.25 Å (125 pm) for C(111)) will be more likely to bond to the neighboring incorrect site than to the targeted correct site. (The presence of potentially abstractable passivating atoms ringing the perimeter of a depassivated target site, and other factors, greatly complicates this analysis.) Despite initial suggestions in *Nanosystems*[296] that positional placement accuracies on the order of one C-C bondlength (~1.54 Å, ~154 pm) might suffice for reliable DMS, subsequent more detailed studies and simulations have determined that reliable DMS operations such as hydrogen abstraction,[297] hydrogen donation,[298] and carbon dimer placement on the most positionally demanding C(110) diamond surface,[299] and reactions comprising the hydrogen abstraction tool recharge sequence,[300] will apparently all require better than one-third of a C-C bondlength of positional placement accuracy, typically 0.2-0.5 Å (20-50 pm). (Changing SPM tip height (tip-surface distance) by just 10 pm can cause a laterally

---

[296] K. Eric Drexler, Nanosystems: Molecular Machinery, Manufacturing, and Computation, John Wiley & Sons, New York, 1992, Chapter 16.

[297] Berhane Temelso, C. David Sherrill, Ralph C. Merkle, Robert A. Freitas Jr., "High-level Ab Initio Studies of Hydrogen Abstraction from Prototype Hydrocarbon Systems," J. Phys. Chem. A 110(28 September 2006):11160-11173; http://pubs.acs.org/cgi-bin/abstract.cgi/jpcafh/2006/110/i38/abs/jp061821e.html (abstract), http://www.MolecularAssembler.com/Papers/TemelsoHAbst.pdf (paper).

[298] Berhane Temelso, C. David Sherrill, Ralph C. Merkle, Robert A. Freitas Jr., "Ab Initio Thermochemistry of the Hydrogenation of Hydrocarbon Radicals Using Silicon, Germanium, Tin and Lead Substituted Methane and Isobutane," J. Phys. Chem. A 111(15 August 2007):8677-8688. http://pubs.acs.org/cgi-bin/abstract.cgi/jpcafh/asap/abs/jp071797k.html (abstract), http://www.MolecularAssembler.com/Papers/TemelsoHDon.pdf (paper).

[299] Jingping Peng, Robert A. Freitas Jr., Ralph C. Merkle, James R. Von Ehr, John N. Randall, George D. Skidmore, "Theoretical Analysis of Diamond Mechanosynthesis. Part III. Positional C_2 Deposition on Diamond C(110) Surface using Si/Ge/Sn-based Dimer Placement Tools," J. Comput. Theor. Nanosci. 3(February 2006):28-41; http://www.MolecularAssembler.com/Papers/JCTNPengFeb06.pdf. Denis Tarasov, Natalia Akberova, Ekaterina Izotova, Diana Alisheva, Maksim Astafiev, Robert A. Freitas Jr., "Optimal Tooltip Trajectories in a Hydrogen Abstraction Tool Recharge Reaction Sequence for Positionally Controlled Diamond Mechanosynthesis," J. Comput. Theor. Nanosci. 6(2009). In press. Jingping Peng, Robert A. Freitas Jr., Ralph C. Merkle, "Theoretical Analysis of Diamond Mechanosynthesis. Part I. Stability of C_2 Mediated Growth of Nanocrystalline Diamond C(110) Surface," J. Comput. Theor. Nanosci. 1(March 2004):62-70; http://www.MolecularAssembler.com/JCTNPengMar04.pdf.

[300] Denis Tarasov, Natalia Akberova, Ekaterina Izotova, Diana Alisheva, Maksim Astafiev, Robert A. Freitas Jr., "Optimal Tooltip Trajectories in a Hydrogen Abstraction Tool Recharge Reaction Sequence for Positionally Controlled Diamond Mechanosynthesis," J. Comput. Theor. Nanosci. 6(2009). In press.

manipulated adatom to switch between fcc and hcp sites.[301]) The general requirement for 20-50 picometer repeatable positional accuracy in SPM-based systems appears to be at or very near the current state of the art (e.g., see Figure 2-27) – both for positioning resolution and for positioning repeatability.

Figure 2-27. Left: Image of the Physik Instrumente PicoCube P-363 XYZ Nanopositioner[302] and E-536 Controller,[303] which can provide 0.5 Å (50 pm) positioning accuracy with 5 A (500 pm) repeatability across a 1 micron round-trip pathway. Right: Image of the Queensgate NPS-XYZ-100A/15A XYZ Nanopositioner,[304] which can provide 2.5 Å (250 pm) positioning accuracy with 1 Å (100 pm) repeatability across a 1 micron round-trip pathway. Both are capacitive positioning systems.

[301] J.A. Stroscio, R.J. Celotta, "Controlling the Dynamics of a Single Atom in Lateral Atom Manipulation," Science 306(8 October 2004):242-247..

[302] Physik Instrumente, "PicoCube™ Ultra-Fast, XY and XYZ NanoPositioning and Scanning Stages," accessed January 2008, http://www.pionline.it/html/schede/PicoCube.pdf; see also http://www.physikinstrumente.de/pdf/P363_Datasheet.pdf.

[303] "E-536 PicoCube® Piezo Controller," accessed January 2008; http://www.physikinstrumente.com/en/products/prdetail.php?sortnr=602950. See also: "XYZ-Piezo-Scanner for AFM Provides 25 Picometers Resolution," 4 June 2007; http://www.lambdaphoto.co.uk/press_releases/200642.

[304] Queensgate Instruments Ltd., "NPS-XYZ-100A/15A Technical Specification," accessed June 2004, http://www.nanopositioning.co.uk/products/NanoMechanisms/NPS-XYZ-100A-15A/specification.aspx; model NPS-XYZ-100A/15H has the same parameters, http://www.nanopositioning.co.uk/products/NanoMechanisms/NPS-XYZ-100A-15H/specification.aspx; Queensgate Instruments Ltd., "NPS-XYZ-100A/15A Technical Specification," accessed January 2008, http://www.nanopositioning.co.uk/catalogue/line.aspx?lne_id=6dfca5f5-4a3c-49cb-afaa-ae4b4acb558a.

Table 2-3 reports the results of a 2004 survey of commercially available high-precision positioning components or systems. The "repeatability" columns report the positional hysteresis or linearity for each system, assuming a 1 micron round-trip excursion with a return to the original position. The survey, now 5 years old, showed that as of 2004 at least three commercial positioning systems already possessed 0.5 Å (50 pm) step accuracy though only with 5-10 Å (500-1000 pm) repeatability across 0.4 micron paths in closed-loop mode; one positioning system had 1 Å (100 pm) repeatability over a 1-micron round trip path but did not simultaneously possess high step accuracy.

Research systems have approached or exceeded the required minimum DMS performance levels in related areas. For example, in imaging, isolated SPM-based positioning systems have achieved high-resolution imaging scans – one demonstrated by a German group at Augsburg University[305] showing features of 0.77 Å (77 pm) and another by an ORNL group[306] showing 0.6 Å (60 pm) features. A UCSB team[307] has reported the record-breaking detection of ~0.023 pm deflections in a 250-nm-wide beam of GaAs at a temperature of 3 millikelvins. FEI Company's Titan 80-300 High-Resolution Scanning-Transmission Electron Microscope (HR-STEM) can image diamond C(110) surface at 0.9 Å (90 pm) resolution and germanium Ge(112) surface at 0.81 Å (81 pm) resolution,[308] and the TEAM 0.5 transmission electron achromatic microscope (the world's most powerful transmission electron microscope can produce images with ~0.5 Å (50 pm) resolution.[309] In metrology, Chassagne's group in France has designed a positioning control system with repeatable 0.53 Å (53 pm) precision over 1 micron of travel[310] and another control system with repeatable 5 Å (500 pm) precision over 5 mm of travel.[311] A NIST group[312] reported

---

[305] Stefan Hembacher, Franz J. Giessibl, Jochen Mannhart, "Force Microscopy with Light-Atom Probes," Science 305(16 July 2004):380-383. See also: Belle Dumé, "Microscopy Moves to the Picoscale," PhysicsWeb.org, 10 June 2004; http://physicsweb.org/article/news/8/6/6.

[306] P.D. Nellist, M.F. Chisholm, N. Dellby, O.L. Krivanek, M.F. Murfitt, Z.S. Szilagyi, A.R. Lupini, A. Borisevich, W.H. Sides, Jr., S.J. Pennycook, "Direct Sub-Angstrom Imaging of a Crystal Lattice," Science 305(17 September 2004):1741. See also: "ORNL Microscope Pushes Back Barrier of 'How Small'," 19 September 2004; http://www.nanotechnology.com/news/?id=5025.

[307] Robert G. Knobel, Andrew N. Cleland, "Nanometer-scale displacement sensing using a Single-Electron Transistor," Nature 424(17 July 2003):291-293. See also: Jyllian Kemsley, "Device Measures Femtometers: Nanoscale sensor couples transistor with crystal to approach quantum limit," Chemical & Engineering News 81(21 July 2003):6; http://pubs.acs.org/cen/topstory/8129/8129notw5.html.

[308] FEI Company, "Titan™ 80-300," accessed January 2008; http://www.feicompany.com/Portals/_default/PDFs/content/2007_10_TitanFamily_pb.pdf.

[309] "0.5 Angstrom transmission electron microscope," 22 January 2008; http://nextbigfuture.com/2008/01/05-angstrom-transmission-electron.html.

[310] Luc Chassagne, Suat Topcu, Yasser Alayli, Patrick Juncar, "Highly accurate positioning control method for piezoelectric actuators based on phase-shifting optoelectronics," Meas. Sci. Technol. 16(2005):1771-1777.

[311] L. Chassagne, M. Wakim, S. Xu, S. Topçu, P. Ruaux, P. Juncar, Y. Alayli, "A 2D nano-positioning system with sub-nanometric repeatability over the millimetre displacement range," Meas. Sci. Technol. 18(2007):3267-3272; http://www.iop.org/EJ/abstract/0957-0233/18/11/001.

operating a vacuum chamber-based laser-based device able to measure 25 millimeter distances to 0.1 Å (10 pm) accuracy in 2005. In 2006 Robert Celotta (also of NIST) reported[313] the ability to stabilize an STM to 0.002 Å (0.2 pm).

Table 2-3. Experimentally Attainable Positioning Precision for Commercially Available Systems that were Available in 2004 (1 Å = 100 pm)

Nanopositioning System Manufacturer	**Nanopositioning Model**	**Resolution (Å)**			**Repeatability* (Å)**		
		X	Y	Z	X	Y	Z
Veeco	Dimension 3100[314]	60	60	0.5 [a]	100 [b]	100 [b]	*n/a*
Zyvex Corp.	S-100 Nanomanipulator[315]	50	50	50	*n/a*	*n/a*	*n/a*
Klocke Nanotechnik	XYZ-Manipulator[316]	100	100	100	*n/a*	*n/a*	*n/a*
	NMT-Modules[317]	20	20	20	*n/a*	*n/a*	*n/a*
	Nanomanipulator[318]	10	10	–	10 [c]	10 [c]	–
Danish MicroEngineer.	95-200 AFM Scanner[319]	10	10	5	*n/a*	*n/a*	50 [d]

[312] J.R. Lawall, "Fabry-Perot metrology for displacements up to 50 mm," J. Optical Soc. Amer. A 22(December 2005):2786-2798; http://www.opticsinfobase.org/abstract.cfm?URI=josaa-22-12-2786 . See also: "Physicists measure 'long' distances with picometer accuracy," 2 December 2005; http://www.physorg.com/news8668.html.

[313] Robert Celotta, "Enabling Nanotechnology: An Introduction to NIST's New Center for Nanoscale Science & Technology," presentation at the SME Conference: "The Next Industrial Revolution: Nanotechnology & Manufacturing," Oak Ridge, TN, 24 August 2006; http://www.sme.org/cgi-bin/get-evdoc.pl?&&001640&000007&020104&&SME&.

[314] Veeco, "Dimension 3100 Datasheet," accessed June 2004, http://www.veeco.com/html/datasheet_d3100.asp.

[315] Zyvex Corp., "S100 Nanomanipulator Specifications," accessed June 2004, http://www.zyvex.com/Products/S100_Spec.html; "Zyvex's S100 Nanomanipulator System," accessed June 2004, http://www.zyvex.com/Products/S100_Faq.html.

[316] Klocke Nanotechnik, "XYZ – Manipulator: Orthogonal Movement with High Resolution," accessed June 2004, http://www.nanomotor.de/n_xyz_manipulator.htm.

[317] Klocke Nanotechnik, "SEM-Manipulators: Comparison of Different Systems," accessed June 2004, http://www.nanomotor.de/pdf/Compare_e_lo.pdf; "The Nanomanipulator: A Universal Tool With One Nanometer Resolution," accessed June 2004; http://www.nanomotor.de/pdf/nanoman_e_lo.PDF.

[318] Klocke Nanotechnik, "Manipulators: Univeral Tools with 1 Nanometer Resolution," June 2004, http://www.nanomotor.de/p_nanomanipulator.htm; "Processing Material in Electron Microscopes: Nanomanipulation With Several D.O.F.," accessed June 2004, http://www.nanomotor.de/aa_processing.htm.

Asylum Research	MFP-3D™ AFM[320]	6	6	3	50 [e]	50 [e]	20 [f]
Attocube Systems	ANSxyz100 XYZ-scanner[321]	~5	~5	~5	500 [s]	500 [s]	500 [s]
PiezoMax/nPoint	XY40Z25 3-axis stage[322]	3	3	2	2 [g]	2 [g]	2 [g]
Mad City Labs	Nano-F100 positioner[323]	2	–	–	*n/a*	–	–
	Nano-M350 XYZ positioner[324]	1	1	0.5	*n/a*	*n/a*	*n/a*
	Nano-T Series XYZ positioner[325]	2	2	0.4	*n/a*	*n/a*	*n/a*
Pacific Nanotechnology	Nano-R[326]	1	1	1	20 [h]	20 [h]	*n/a*
	Nano-I[327]	2	2	2	20 [h]	20 [h]	*n/a*
Concern Nanoindustry	Base system[328]	1	1	–	*n/a*	*n/a*	–
Queensgate Instruments	NPS-X-15A, 1-axis[329]	0.5 [i]	–	–	1 [j]	–	–
	NPS-XY-100A, 2-axis[330]	1 [k]	1 [k]	–	0.5 [j]	0.5 [j]	–

[319] Danish Micro Engineering (DME), "DME AFM scanners: Technical specifications for 95-200 AFM scanner,' accessed June 2004, http://www.dme-spm.dk/Products/AFMScanner.htm.

[320] Asylum Research, "MFP-3D™ Atomic Force Microscope: Power and Flexibility in One Complete System," accessed June 2004, http://www.asylumresearch.com/Products/Mfp3D/Mfp3D.pdf.

[321] Attocube Systems, "ANSxyz100 large range xyz-scanner," accessed January 2008, http://attocube.com/nanoPOSITIONING/ANSxyz100/Specifications_ANSxyz100.pdf.

[322] PiezoMax/nPoint, "Specification Table: XY40Z25 3-axis stage," accessed June 2004, http://www.piezomax.com/dnld/spec/spec-XY40Z25_3715109.pdf.

[323] Mad City Labs, Inc., "Nano-F Series," accessed January 2008, http://www.madcitylabs.com/nanofseries.html.

[324] Mad City Labs, Inc., "Nano-M350," accessed January 2008, http://www.madcitylabs.com/nanom350.html.

[325] Mad City Labs, Inc., "Nano-T Series," accessed January 2008, http://www.madcitylabs.com/nanotseries.html.

[326] Pacific Nanotechnology, Inc., "The Nano-R™ Atomic Force Microscope," accessed June 2004, http://pacificnanotech.com/nano-r-afm_nano-r-specifications.html.

[327] Pacific Nanotechnology, Inc., "The Nano-I™ Atomic Force Microscope," accessed June 2004, http://pacificnanotech.com/nano-i-afm_nano-i-specifications.html.

[328] Concern Nanoindustry, "Nanotechnological System," accessed June 2004, http://www.nanotech.ru/cn/e/tech6.php.

[329] Queensgate Instruments Ltd., "NPS-X-30A Technical Specification," accessed June 2004, http://www.nanopositioning.co.uk/products/NanoMechanisms/NPS-X-30A/specification.aspx; Queensgate Instruments Ltd., "Nano Mechanisms-NPS-X-15A Technical Datasheet," accessed January 2008, http://www.nanopositioning.co.uk/catalogue/line.aspx?lne_id=1b7c9a8d-6bca-4003-a880-ceabbc029c17.

	NPS-XYZ-100A/15A[331]	2.5 [l]	2.5 [l]	0.5 [m]	1 [j]	1 [j]	1 [j]
Physik Instrumente (PI)	PicoCube P-363 XYZ[332]	0.5 [n]	0.5 [n]	0.5 [n]	10 [o]	10 [o]	20 [o]
	PicoCube P-363 XY[333]	0.5 [n]	0.5 [n]	–	5 [o]	5 [o]	–
	P.C. P-363 + E-536 Controller[334]	0.25 [n]	0.25 [n]	–	5 [o]	5 [o]	–
	Capacitive Position Sensors[335]	0.1	–	–	0.3 [p]	–	–
	N-310 NEXACT® PiezoWalk[336]	0.25	–	–	0.25 [c]	–	–
NanoWave	NW SPPE[337]	0.13 [q]	–	–	10 [r]	–	–
Minimum needed to achieve controlled DMS:		***0.5***	***0.5***	***0.5***	***0.5***	***0.5***	***0.5***

---

[330] Queensgate Instruments Ltd., "NPS-XY-100B Technical Specification," accessed June 2004, http://www.nanopositioning.co.uk/products/NanoMechanisms/NPS-XY-100B/specification.aspx; Queensgate Instruments Ltd., "NPS-XY-100A Technical Datasheet," accessed January 2008, http://www.nanopositioning.co.uk/catalogue/line.aspx?lne_id=400ed857-5446-4fb9-a622-c91483b290ab.

[331] Queensgate Instruments Ltd., "NPS-XYZ-100A/15A Technical Specification," accessed June 2004, http://www.nanopositioning.co.uk/products/NanoMechanisms/NPS-XYZ-100A-15A/specification.aspx; model NPS-XYZ-100A/15H has the same parameters, http://www.nanopositioning.co.uk/products/NanoMechanisms/NPS-XYZ-100A-15H/specification.aspx; Queensgate Instruments Ltd., "NPS-XYZ-100A/15A Technical Specification," accessed January 2008, http://www.nanopositioning.co.uk/catalogue/line.aspx?lne_id=6dfca5f5-4a3c-49cb-afaa-ae4b4acb558a.

[332] Physik Instrumente, "PicoCube™ Ultra-Fast, XY and XYZ NanoPositioning and Scanning Stages," accessed January 2008, http://www.pionline.it/html/schede/PicoCube.pdf; see also http://www.physikinstrumente.de/pdf/P363_Datasheet.pdf.

[333] Physik Instrumente, "PicoCube™ Ultra-Fast, XY and XYZ NanoPositioning and Scanning Stages," accessed January 2008, http://www.pionline.it/html/schede/PicoCube.pdf; see also http://www.physikinstrumente.de/pdf/P363_Datasheet.pdf.

[334] "E-536 PicoCube® Piezo Controller," accessed January 2008; http://www.physikinstrumente.com/en/products/prdetail.php?sortnr=602950. See also: "XYZ-Piezo-Scanner for AFM Provides 25 Picometers Resolution," 4 June 2007; http://www.lambdaphoto.co.uk/press_releases/200642.

[335] Physik Instrumente, "Capacitive Position Sensors / Controllers, Featuring Sub-Nanometer Resolution," accessed January 2008, http://nanotechweb.org/buyers/index.cfm?action=viewcomp&id=698.

[336] Physik Instrumente, "N-310 Compact NEXACT® OEM Piezo Stepping Drives with Long Travel Ranges," accessed January 2008, http://www.physikinstrumente.com/en/pdf/N310_Datasheet.pdf.

[337] Physik Instrumente, "Characteristics of Capacitive Position Sensors: Stability and Linearity of PI Capacitive Position Sensors," accessed June 2004, http://www.physikinstrumente.de/products/prdetail.php?secid=5-6. NanoWave, Inc., "NanoWave Inc. Breakthrough – Attains Picometer-Resolution Position Measurement System for True NanoScale Manufacturing," June 2003 Press Release, accessed June 2004, http://www.nanowave.com/news_FAQs/news_PR_02.html.

* positional hysteresis or linearity, assuming 1 µm round-trip excursion with return to original position
Open loop control = dead reckoning with no sensory feedback; closed loop control = motion guided by sensory feedback

[a] "RMS Z-noise, in appropriate environment"
[b] "XY nonlinearity 1%"
[c] "with no backlash"
[d] "Z-linearization: 0.5% on full-scale scan"
[e] "sensor nonlinearity 0.5% full travel, closed-loop all 3 axes"
[f] "sensor nonlinearity 0.2% full travel, closed-loop all 3 axes"
[g] "typical linearity and hysteresis 0.02% at slew rate of 8 mm/sec"
[h] "scan linearity 1%"
[i] "position noise (1 sigma) at slowest slew rate of 1.0 mm/sec"
[j] typical linearity error is 0.005%-0.01%, "percent error over the full range of motion"; 0.01% hysteresis error peak-to-peak, "hysteresis specification for a displacement of less than 1 µm amplitude is 0.1 nm"
[k] "position noise (1 sigma) at slowest slew rate of 0.5 mm/sec"
[l] "position noise (1 sigma) at slowest slew rate of 0.5 mm/sec"
[m] "position noise (1 sigma) at slowest slew rate of 0.5 mm/sec"
[n] "open-loop resolution"
[o] "typical closed loop P-363 repeatability" (across 0.4 µm of travel)
[p] "When used with PI digital controllers (which use 4th order polynomial linearization techniques), positioning linearity up to 0.003% is achievable"[338]
[q] "NanoWave Scanning Probe Position Encoder demonstrated approximately 13 picometers resolution"
[r] "precision/repeatability"
[s] linearity "typically 5-10%"

We conclude that the components needed to construct a reliable 20-50 pm 1-tip 3-DOF (degrees of freedom) picomanipulator are likely already in existence, but that to build such a system will require sufficient dedicated resources and a well-focused development effort.

2.3 Basic Positional Measurement Technologies

To make a high-accuracy picopositioner system, we also need an apparatus for measuring displacement to very high precision (Table 2-4 and Table 3-3). The principal techniques are optical methods, including interferometry (Section 2.3.1) and combination source/detectors (Section 2.3.2), and nonoptical methods, including capacitive sensors (Section 2.3.3) and piezo sensors (Section 2.3.4). The beam-bounce technique has previously been described in connection with the measurement of AFM cantilever deflection (Section 2.1.2; Figure 2-7).

[338] NanoWave, Inc., "Technology/capabilities," accessed June 2004, http://www.nanowave.com/technology_applications/tech_cap.html.

Table 2-4. Some limits to displacement measurement (KAIST, 2003)[339]		
Technology	**Max. Attainable measuring resolution**	**Max. Attainable Measuring Range**
Optical scale	1000 pm	≃0.3m
Scanning tunneling microscope	100 pm	<1mm
Capacitance displacement sensor	100 pm	~3 mm
Heterodyne laser interferometer	100 pm	≥1m
X-ray interferometer	10 pm	~3 mm
Fabry-Pérot laser interferometer	1 pm	<1mm

2.3.1 Metrological Optical Interferometry

An interferometer is an optical device that utilizes the phenomenon of interference. Typically, it starts with some input beam, splits it into two separate beams with some kind of beam splitter (a partially transmissive or "half-silvered" mirror), possibly exposes some of these beams to some external influences (e.g. some length changes or refractive index changes in a transparent medium), and recombines the beams on another beam splitter. The power or the spatial shape of the resulting beam can then be used for a measurement.[340]

Optical interferometry combines two or more light waves in an optical instrument in such a way that interference occurs between them. Interferometers can use white light sources or monochromatic light from atomic sources. Laser "metrology" (the science of measurement) is the technique of choice for the precision measurement of displacement. Here we concentrate on the principle types of optical interferometry most relevant to atomic force microscopy, including Michelson interferometry (Section 2.3.1.1), Mach-Zehnder interferometry (Section 2.3.1.2), Fabry-Pérot interferometry (Section 2.3.1.3), Sagnac interferometry (Section 2.3.1.4), and two basic approaches to optical interferometry known as heterodyne detection (Section 2.3.1.5) and homodyne detection (Section 2.3.1.6). Several factors that affect the accuracy of optical interferometry are briefly summarized in Section 2.3.1.7.

2.3.1.1 Michelson Interferometry

The Michelson interferometer is the most common configuration for optical interferometry and was invented by Albert Abraham Michelson. An interference pattern is produced by splitting a beam of light into two paths (Figure 2-28A), bouncing the beams back and recombining them (Figure 2-28B). The different paths may be of different lengths or be composed of different materials to create alternating interference fringes on a back detector.

---

[339] "Billionth Precision Uncertainty Engineering (BUPE)," KAIST, Annual Report 2003, http://pem.kaist.ac.kr/bupe/.

[340] Encyclopedia of Laser Physics and Technology; http://www.rp-photonics.com/interferometers.html.

Figure 2-28. (A) Michelson interferometer for use on an optical table. (B) The light path through a Michelson interferometer. (C) With mirrors at one separation (above), the peaks of coherent light waves coincide, causing constructive interference and creating a bright fringe; if one mirror is displaced by a half-wavelength (below), one light wave's peaks will coincide with the other wave's valleys, causing destructive interference and creating a dark fringe. (D) Mirror (above) and corner- or retro-reflector (below) versions.[341]

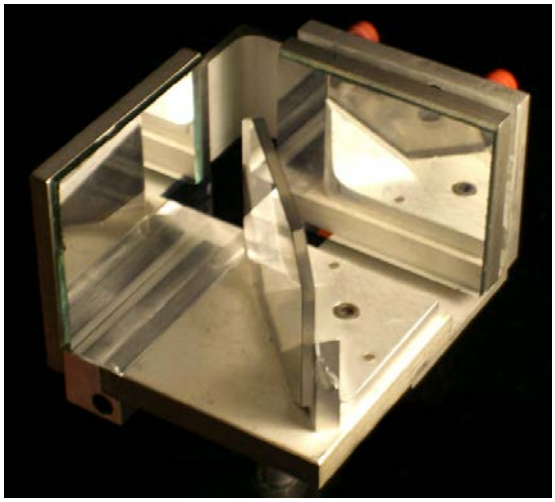

(A)

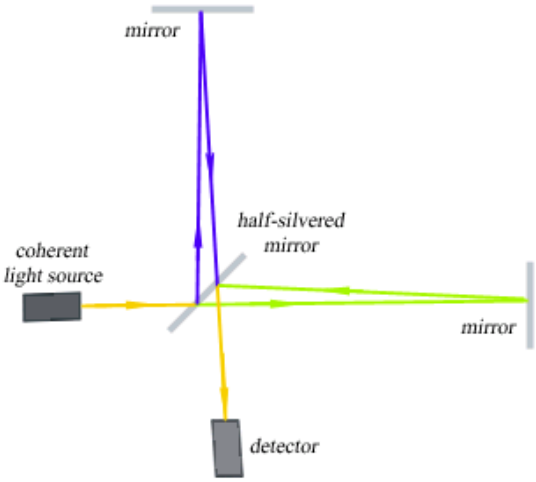

(B)

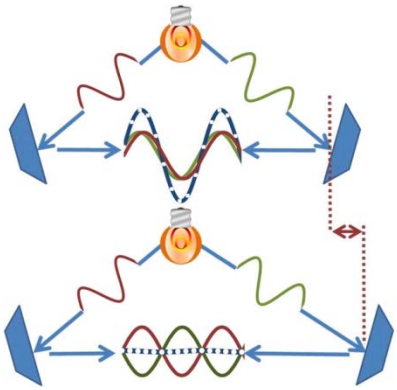

(C)

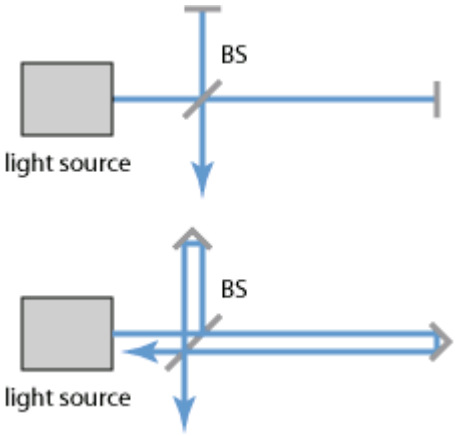

(D)

There are two paths from the (light) source to the detector. One reflects off the semi-transparent mirror, goes to the top mirror and then reflects back, goes through the semi-transparent mirror, to the detector. The other first goes through the semi-transparent mirror, to the mirror on the right, reflects back to the semi-transparent mirror, then reflects from the semi-transparent mirror into

---

[341] Encyclopedia of Laser Physics and Technology; http://www.rp-photonics.com/interferometers.html.

the detector. If these two paths differ by a whole number (including 0) of wavelengths, there is constructive interference and a strong signal at the detector; if they differ by a whole number and a half wavelengths (e.g., 0.5, 1.5, 2.5 ...) there is destructive interference and a weak signal (Figure 2-28C). This allows mirror displacement to be measured to an accuracy of half a wavelength of light, typically ~250 nm or so – because moving a mirror by 1/2 wavelength increases the pathlength of that beam by one full wavelength, advancing the interference pattern by one fringe.

A Michelson interferometer uses a single beam splitter for separating and recombining the beams. If the two mirrors are aligned for exact perpendicular incidence (Figure 2-28D(upper)), only one output is accessible, and the light of the other output goes back to the light source. If that optical feedback is unwanted (as is often the case with a laser, which might be destabilized), and/or access to the second output is required, the recombination of beams can occur at a somewhat different location on the beam splitter. One possibility is to use retro-reflectors, as shown in Figure 2-28D(lower); this also has the advantage that the interferometer is fairly insensitive to slight misalignment of the retroreflectors. Alternatively, simple mirrors at slightly non-normal incidence can be used.

There are many variations of the Michelson interferometer. For example, a Twyman-Green interferometer is essentially a Michelson interferometer illuminated with a monochromatic point source. It is used for characterizing optical elements.[342]

2.3.1.2 Mach-Zehnder Interferometry

The Mach-Zehnder interferometer (named after physicists Ludwig Mach, son of Ernst Mach, and Ludwig Zehnder) is a device used to determine the phase shift caused by a small sample which is placed in the path of one of two collimated beams (thus having plane wavefronts) from a coherent light source. In contrast to the Michelson interferometer, there are two output ports.

Figure 2-29. Mach-Zehnder interferometer[343]

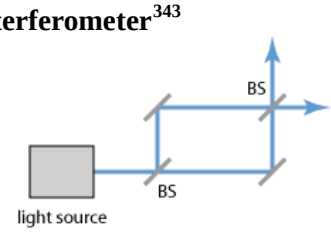

As shown in Figure 2-29, the Mach-Zehnder interferometer uses two separate beam splitters (BS) to split and recombine the beams, and has two outputs, which can, e.g., be sent to photodetectors. The optical path lengths in the two arms may be nearly identical (as in the figure), or may be

[342] Encyclopedia of Laser Physics and Technology; http://www.rp-photonics.com/interferometers.html.

[343] Encyclopedia of Laser Physics and Technology; http://www.rp-photonics.com/interferometers.html.

different (e.g., with an extra delay line). The distribution of optical powers at the two outputs depends on the precise difference in optical arm lengths and on the wavelength (optical frequency).[344]

If the Mach-Zehnder interferometer is well aligned, the path length difference can be adjusted (e.g., by slightly moving one of the mirrors) so that for a particular optical frequency the total power goes into one of the outputs. For misaligned beams (e.g., with one mirror being slightly tilted), there will be some fringe patterns in both outputs, and variations of the path length difference affect mainly the shapes of these interference patterns, whereas the distribution of total powers on the outputs may not change very much.[345] An additional source of error can be the slight difference in thickness of commercially available high-quality beam splitters, which are often matched to a tolerance of only ~100 µm of optical path length (OPL) and can vary significantly from one piece to the next.[346]

2.3.1.3 Fabry-Pérot Interferometry

A Fabry-Pérot (FP) interferometer (Figure 2-30) consists of two parallel mirrors, allowing for multiple round trips of light. (A monolithic version of this can be a glass plate with reflective coatings on both sides.) For high mirror reflectivities, such a device can have very sharp resonances (a high "finesse"), i.e., exhibit a high transmission only for optical frequencies which closely match certain values.

Figure 2-30. Fabry-Pérot interferometer[347]

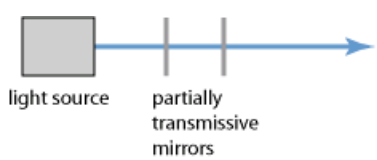

---

[344] Encyclopedia of Laser Physics and Technology; http://www.rp-photonics.com/interferometers.html.
[345] Encyclopedia of Laser Physics and Technology; http://www.rp-photonics.com/interferometers.html.

[346] White light interferometers (**Section 4.6.4.7**) typically require a much closer control of the OPL, ranging from 0.1-10µm depending on the application. Some commercial cube beamsplitters optimized for equal OPL are available, but achieving 0.1 µm accuracy is often prohibitively expensive and difficult to accomplish,[*] though easier methods have now been demonstrated to match beamsplitters to less than 100 nm of on-axis optical path length variations that could be further improved to less than 30 nm. Peter D. Koudelka, James H. Burge, "Fabrication of Cube Beamsplitters for White Light Interferometry," in: Roland Geyl, David Rimmer, Lingli Wang, eds., Optical Fabrication, Testing, and Metrology, Proceedings SPIE 5252(2004):17-25.
[*] J. Schwider Pförner, "3-λ Metrology," in: K. Creath, J. Schmidt, eds., Interferometry XI: Techniques and Analysis, Proceedings SPIE 4777 (2002).

[347] Encyclopedia of Laser Physics and Technology; http://www.rp-photonics.com/interferometers.html.

Based on these sharp features, distances (or changes of distances) can be measured with a resolution far better than the wavelength. Similarly, resonance frequencies can be defined very precisely.

2.3.1.3.1 Fabry-Pérot Etalons

In optics, a Fabry-Pérot etalon or interferometer is typically made of a transparent plate with two reflecting surfaces (Figure 2-31A), or two parallel highly reflecting mirrors (Figure 2-32). These devices are named after Charles Fabry and Alfred Perot; "etalon" is from the French étalon, meaning "measuring gauge" or "standard". Technically, the transparent plate is called an "etalon" and the parallel mirror configuration is called an "interferometer", though the terminology is often used inconsistently.

The varying transmission function of a Fabry-Pérot etalon is caused by interference between the multiple reflections of light between the two reflecting surfaces.[348] The transmission spectrum as a function of wavelength exhibits peaks of large transmission corresponding to resonances of the etalon. Constructive interference occurs if the transmitted beams are in phase, and this corresponds to a high-transmission peak of the etalon (Figure 2-31B). If the transmitted beams are out-of-phase, destructive interference occurs and this corresponds to a transmission minimum. Whether the multiply-reflected beams are in-phase or not depends on the wavelength (λ) of the light (in vacuum), the angle the light travels through the etalon (θ), the thickness of the etalon (l) and the refractive index of the material between the reflecting surfaces (n). The wavelength separation between adjacent transmission peaks is called the free spectral range (FSR) of the etalon, $\Delta\lambda$; the FSR is related to the full-width half-maximum (FWHM), $\delta\lambda$, of any one transmission band by a quantity known as the *finesse*: $F = \Delta\lambda / \delta\lambda$. Etalons with high finesse show sharper transmission peaks with lower minimum transmission coefficients (Figure 2-31C); for interferometers, very high finesse factors require highly reflective mirrors (Figure 2-31D). Due to the angle dependence of the transmission, the peaks can also be shifted by rotating the etalon with respect to the beam.

---

[348] http://en.wikipedia.org/wiki/Fabry-P%C3%A9rot_interferometer.

Figure 2-31. (A) A Fabry-Pérot etalon: light enters the etalon and undergoes multiple internal reflections.[349] (B) Interference fringes for transmitted light, showing fine structure, from a Fabry-Pérot etalon, using a cooled deuterium lamp source emitting at one particular wavelength.[350] (C) Transmission of an etalon as a function of wavelength and coefficient of finesse (*F*): a high-finesse etalon (red line) shows sharper peaks and lower transmission minima than a low-finesse etalon (blue).[351] (D) Finesse as a function of reflectivity: very high finesse factors require highly reflective mirrors.[352]

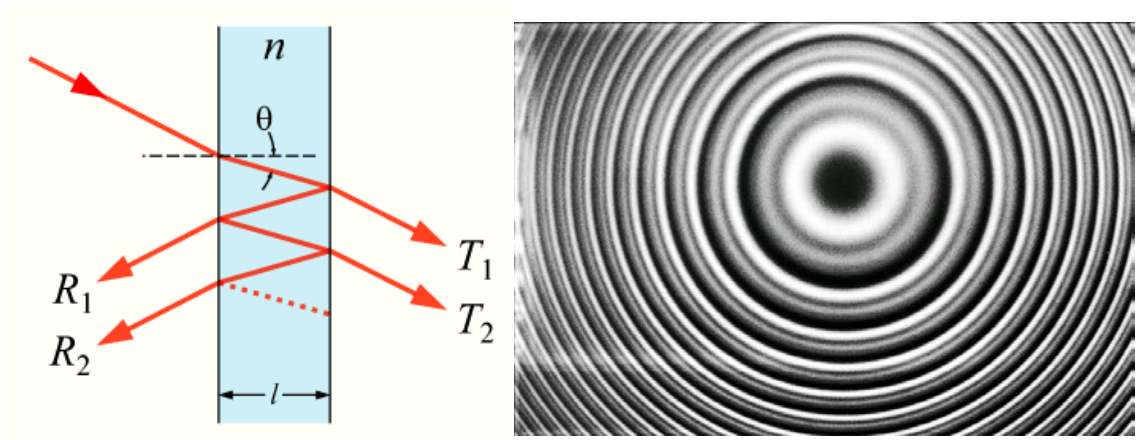

(A) **(B)**

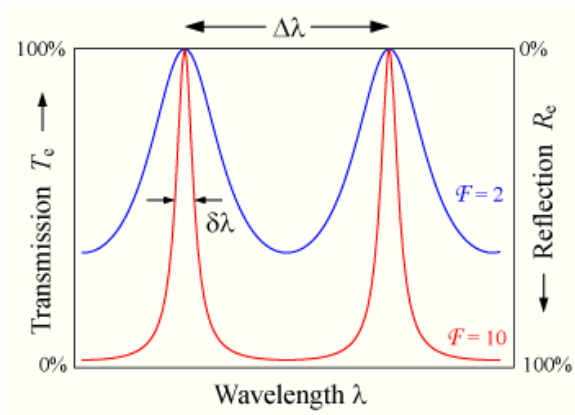

(C)

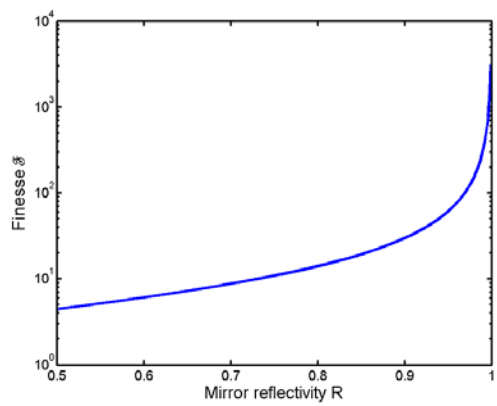

(D)

Etalons are used to construct single-mode lasers. Without an etalon, a laser will generally produce light over a wavelength range corresponding to a number of cavity modes, which are similar to Fabry-Pérot modes (Figure 2-32B/C; Section 2.3.1.3.3). Inserting an etalon into the

---

349 http://en.wikipedia.org/wiki/File:Etalon-1.png.
350 http://en.wikipedia.org/wiki/File:Fabry_Perot_Etalon_Rings_Fringes.png.
351 http://en.wikipedia.org/wiki/File:Etalon-2.png.
352 http://en.wikipedia.org/wiki/File:Etalon-finesse-vs-reflectivity-2.png.

laser cavity, with well-chosen finesse and free-spectral range, can suppress all cavity modes except for one, thus changing the operation of the laser from multi-mode to single-mode.

2.3.1.3.2 Fabry-Pérot Interferometers

A Fabry-Pérot interferometer[353] differs from a Fabry-Pérot etalon in the fact that the distance *l* between the mirrored plates can be tuned in order to change the wavelengths at which transmission peaks occur in the interferometer. If one plate is fixed, the displacement of the other plate can be precisely measured by monitoring the fringe count as the interference pattern moves. The resonance effect of the Fabry-Pérot interferometer is identical to that used in a dichroic filter. (Dichroic filters are very thin sequential arrays of Fabry-Pérot interferometers and are characterized and designed using the same mathematics.)

2.3.1.3.3 Fabry-Pérot Cavities

Laser resonators are often described as Fabry-Pérot resonators, although for many types of laser the reflectivity of one mirror is close to 100%, making it more similar to a Gires-Tournois interferometer. (A **Gires-Tournois etalon** is a transparent plate with two reflecting surfaces, one of which has very high reflectivity. Due to multiple-beam interference, light incident on the lower-reflectivity surface of a Gires-Tournois etalon is almost completely reflected but has a phase shift that depends strongly on the wavelength of the light.)

The Fabry-Pérot resonator is also called a Fabry-Pérot cavity in some applications. For example, in gravitational wave detection a Fabry-Pérot cavity is used to store photons for almost a millisecond while they bounce up and down between the mirrors. This increases the time a gravitational wave can interact with the light, which results in a better sensitivity at low frequencies. This principle is used by detectors such as LIGO and Virgo, which consist of a Michelson interferometer with a Fabry-Pérot cavity with a length of several kilometers in both arms.

There are many different optical resonator types. The most common types of optical cavities consist of two facing plane (flat) or spherical mirrors. The simplest of these is the plane-parallel or Fabry-Pérot cavity, consisting of two opposing flat mirrors (Figure 2-32A). While simple, this arrangement is rarely used in large-scale lasers due the difficulty of alignment; the mirrors must be aligned parallel within a few seconds of arc, or "walkoff" of the intracavity beam will result in it spilling out of the sides of the cavity. However, this problem is much reduced for very short cavities with a small mirror separation distance ($L < 1$ cm). Plane-parallel resonators are therefore commonly used in microchip and microcavity lasers and semiconductor lasers. (Semiconductor diode lasers sometimes use a true Fabry-Pérot geometry due to the difficulty of coating the end facets of the chip.) In these cases, rather than using separate mirrors, a reflective optical coating may be directly applied to the laser medium itself. The plane-parallel resonator is also the basis of the Fabry-Pérot interferometer.

---

[353] G. Hernandez, Fabry-Pérot Interferometers, Cambridge University Press, Cambridge, 1986..

Figure 2-32. (A) Types of two-mirror optical cavities, with mirrors of various curvatures, showing the radiation pattern inside each cavity.[354] (B) The first six longitudinal modes of a plane-parallel Fabry-Pérot cavity.[355] (C) Cylindrical transverse mode patterns of a plane-parallel Fabry-Pérot cavity.[356]

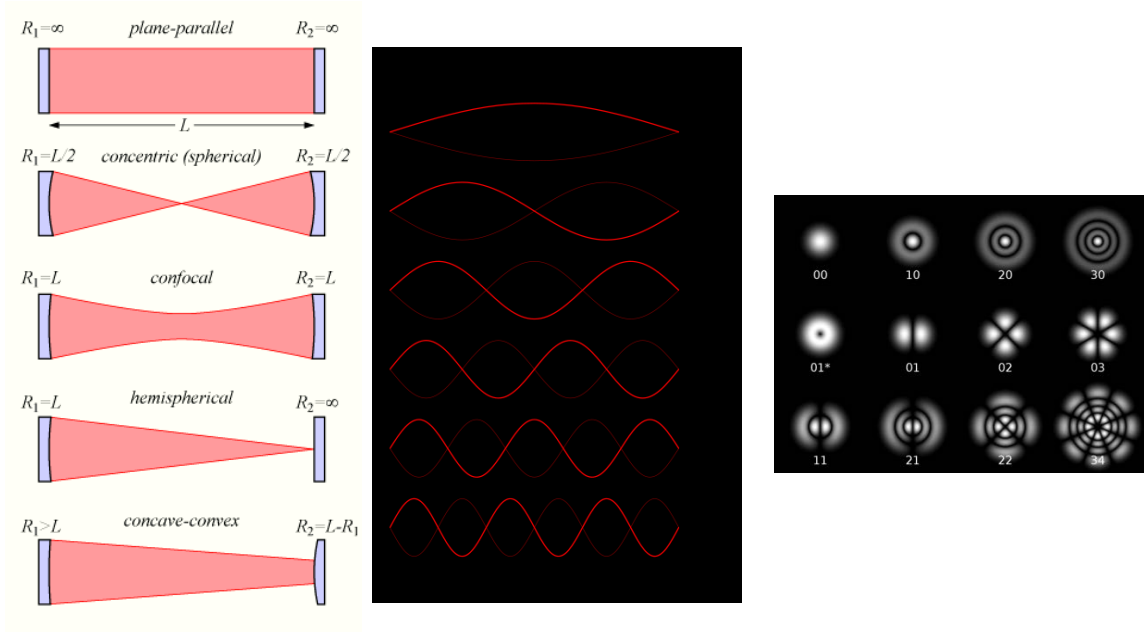

(A) **(B)** **(C)**

Fabry-Pérot cavities exhibit multiple resonator modes. Light confined in a resonator will reflect multiple times from the mirrors, and due to the effects of interference, only certain patterns and frequencies of radiation will be sustained by the resonator, with the others being suppressed by destructive interference. In general, radiation patterns which are reproduced on every round-trip of the light through the resonator are the most stable, and these are the eigenmodes, known as the *modes*, of the resonator. Resonator modes can be divided into two types: longitudinal modes (Figure 2-32B), which differ in frequency from each other; and transverse modes (Figure 2-32C), which may differ in both frequency and the intensity pattern of the light. (The basic or "00" fundamental transverse mode of a resonator is called a "Gaussian beam".)

In AFM, displacement detectors can use a fiber-optic interferometer where the cleaved end of a single-mode optical fiber and the cantilever act as a Fabry-Pérot interferometer. These setups have been in use for more than 2 decades[357] and are available in commercial AFM systems.[358]

---

[354] http://en.wikipedia.org/wiki/File:Optical-cavity1.png.
[355] http://en.wikipedia.org/wiki/File:Longitudinal_mode_v2.svg.
[356] http://en.wikipedia.org/wiki/File:Laguerre-gaussian.png.

[357] D. Rugar, H.J. Mamin, R. Erlandsson, J.E. Stern, B.D. Terris, "Force microscope using a fiberoptic displacement sensor," Rev. Sci. Instrum. 59(1988):2337-2340. P.J. Mulhern, T. Hubbert, C.S. Arnold, B.L. Blackford, M.H. Jericho, "A scanning force microscope with a fiber-optic-interferometer displacement

For example, as long ago as 1988 an AFM using a fiber-optic interferometer as the cantilever displacement sensor and a Fabry-Pérot cavity several microns in size produced low thermal drift (~5 pm/sec) and reduced susceptibility to laser frequency variation.[359] By 2005, Hoogenboom et al.[360] reported a Fabry-Pérot interferometer for detecting the deflection of micrometer-sized cantilevers that provided a noise floor of 1 fm/√Hz at 1 MHz. Notes Hoogenboom:[361] "There is a general tendency to further miniaturize cantilevers for atomic force microscopy and cantilever sensing applications, thus reducing the effect of thermal noise on the measurement. Using a Fabry-Pérot interferometer, sub-picometer oscillations of small cantilevers can be detected in vacuum. The interferometer can easily be aligned using a three-axis piezo-electric motor, and is particularly suited for atomic force microscopy."

2.3.1.3.4 Fizeau and Gires-Tournois Interferometers

A modified version of the Fabry-Pérot interferometer is the Fizeau interferometer (Figure 2-33), where the second mirror is totally reflective, and slightly tilted. The reflected light is used (e.g. with an angled beam splitter) e.g. for characterizing optical components. The Fizeau interferometer is similar to a Fabry-Pérot interferometer in that they both consist of two reflecting surfaces. But in a Fizeau interferometer the two surfaces are usually much less than totally reflecting (typically 4% to 30%) so that secondary reflections don't contribute greatly to the fringe contrast. An angled beam splitter captures the reference and measurement beams. Fizeau interferometers are commonly used for measuring the shape of an optical surface – e.g., where a fabricated lens or mirror is compared to a reference piece with the same shape. The reference piece is often realized by a diffractive optical element, as this can be manufactured by

---

sensor," Rev. Sci. Instrum. 62(1991):1280-1284. A. Ruf, M. Abraham, M. Lacher, K. Mayr, T. Zetterer, "A Miniaturised Fabry Perot AFM Sensor," 8th International Conference on Solid-State Sensors and Actuators, IMM Institute of Microtechnology GmbH, 25-29 June 1995, Eurosensors IX: Transducers '95, Vol 1, pp. 660-663. L. Howard, J. Stone, J. Fu, "Real-time displacement measurements with a Fabry-Perot cavity and a diode laser," Precis. Eng. 25(October 2001):321-335. Shao-Kang Hung, En-Te Hwu, Mei-Yung Chen, Li-Chen Fu, "Design and Experiment of Range-Extended Fiber Fabry-Perot Interferometer Utilizing the Second Harmonic Displacement Modulation," Proceedings of IEEE/ASME International Conference on Advanced Intelligent Mechatronics (EI), 2005, pp. 88-92. B.W. Hoogenboom, P.L.T.M. Frederix, J.L. Yang, S. Martin, Y. Pellmont, M. Steinacher, S. Zaech, E. Langenbach, H.-J. Heimbeck, A. Engel, H.J. Hug, "A Fabry-Perot interferometer for micrometer-sized cantilevers," Appl. Phys. Lett. 86(2005):074101; http://eprints.ucl.ac.uk/9619/1/9619.pdf.

[358] "ATOMIC FORCE MICROSCOPES – AFM", AttoCube, 2008; http://www.attocube.com/nanoSCOPY/AFM/fundamentals.htm.

[359] D. Rugar, H.J. Mamin, R. Erlandsson, J.E. Stern, B.D. Terris, "Force microscope using a fiberoptic displacement sensor," Rev. Sci. Instrum. 59(1988):2337-2340.

[360] B.W. Hoogenboom, P.L.T.M. Frederix, J.L. Yang, S. Martin, Y. Pellmont, M. Steinacher, S. Zaech, E. Langenbach, H.-J. Heimbeck, A. Engel, H.J. Hug, "A Fabry-Perot interferometer for micrometer-sized cantilevers," Appl. Phys. Lett. 86(2005):074101; http://eprints.ucl.ac.uk/9619/1/9619.pdf.

[361] http://www.london-nano.com/content/contactlcn/lcndirectory/hoogenboombart/.

lithographic methods which inherently warrants high precision. Fizeau interferometers are also used in fiber optic sensors for measuring pressure, temperature, strain, etc.

Figure 2-33. Drawing of a Fizeau interferometer[362]

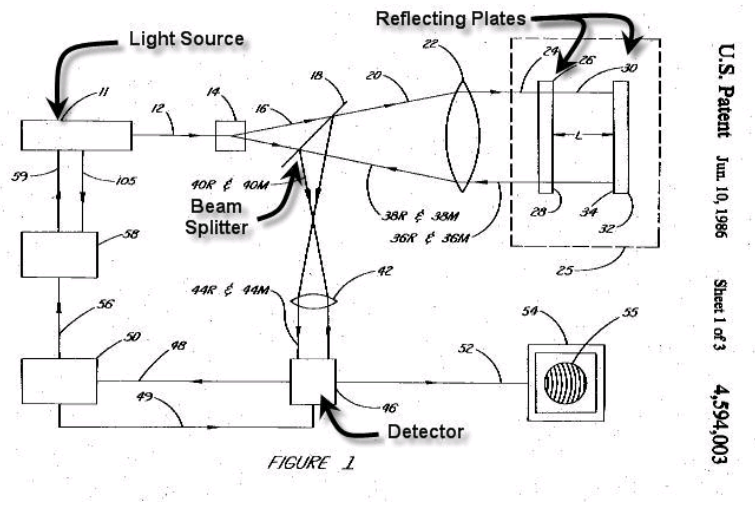

Another special kind of Fabry-Pérot interferometer, used for dispersion compensation, is the Gires-Tournois interferometer. A Gires−Tournois interferometer is an optical standing-wave resonator designed for generating chromatic dispersion.

2.3.1.3.5 Fiber-Based Fabry-Pérot Interferometers

Note that all the interferometer types discussed above can also be implemented with optical fibers. Instead of beam splitters, one then uses fiber couplers. A potential difficulty is that the polarization state of light may change during propagation in the fiber. This often requires one to include a fiber polarization controller (which may occasionally have to be readjusted) or to use polarization-maintaining fibers. Also note that temperature changes in the fibers can affect the optical phase shifts.[363] Some interferometers called "common-path interferometers" use a common beam path but different polarizations for the two beams. This has the advantage that fluctuations of the geometric path length do not affect the interferometer output, whereas the interferometer can be a sensitive detector for birefringence.

As described by Oh[364] in connection with FP fiber-based sensors, the Fabry-Pérot interferometer consists of two parallel reflectors separated by a fixed distance. A monochromatic optical wave

---

[362] http://en.wikipedia.org/wiki/File:Fizeau_Picture.JPG.

[363] Encyclopedia of Laser Physics and Technology; http://www.rp-photonics.com/interferometers.html.

[364] Ki Dong Oh, "Chapter 2 – Extrinsic Fabry-Perot Interferometer Measuring Magnetic Field," in Optical Fiber Fabry-Perot Interferometer based Sensor Instrumentation System for Low Magnetic Field

incident upon an etalon at an arbitrary angle to the normal of the mirror (semi-transparent reflector) will experience multiple reflections within the mirrors. The intensity distribution of the reflected and refracted interfering beams using an etalon generates a set of fringes for each case. The distance of interfering peak or bottom of the fringe is dependent on the spacing between the etalon mirrors and the inverse wavelength of the light. Hence, the basic function of the F-P interferometer is to transform wavelength into an displacement. The main advantages of F-P interferometers based on optical fiber over the other sensor configurations such as Michelson, Mach-Zehnder, and Sagnac interferometers are lightness and compactness, high reliability, low cost, and ease in fabrication. Hence optical fiber based Fabry-Pérot (FP) sensors have been used for measuring temperature, strain, vibration, acoustic waves, and magnetic fields. The measurement of voltage and pressure were done by using an etalon based FP configuration. Beside this classic etalon based configuration, there are several ways to fabricate the Fabry-Pérot cavity such as using Bragg gratings in or on the fiber, other inline fiber configurations to enhance environmental durability,[365] and air-glass interfaces at the fiber ends as the reflectors. When an etalon sensor is fabricated in a continuous length of fiber using a pair of semireflective splices, the optical wave resides inside the fiber so that the sensing mechanism is **intrinsic**. The FP sensors based on air-glass reflectors are referred to as **extrinsic** F-P interferometers (EFPI) (Figure 2-34). The **extrinsic** Fabry-Pérot interferometer does not have the polarization rotation problem which is inherent in **intrinsic** FP interferometers since the light leaves the air-glass interface and is reflected back through the air gap between the reflectors.

Figure 2-34. Typical EFPI sensor structure.[366]

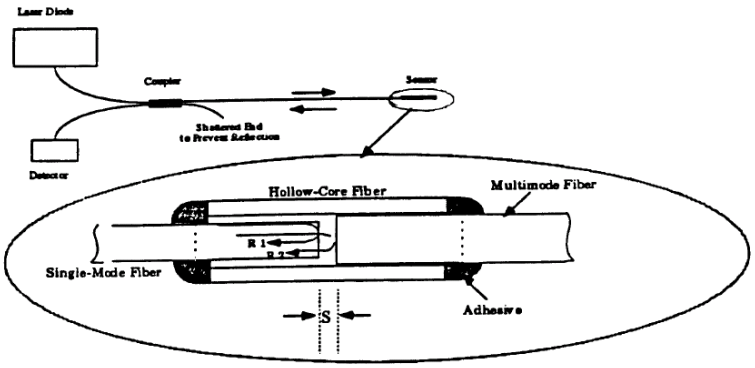

Measurement, PhD dissertation, Dept. of Electrical and Computer Engineering, Virginia Polytechnic Institute, 18 December 1997; http://scholar.lib.vt.edu/theses/available/etd-11198-54532/unrestricted/ch2.pdf.

[365] T. Wei, Y. Han, H.L. Tsai, H. Xiao, "Miniaturized fiber inline Fabry-Perot interferometer fabricated with a femtosecond laser," Opt Lett. 33(15 March 2008):536-538.

[366] Ki Dong Oh, "Chapter 2 – Extrinsic Fabry-Perot Interferometer Measuring Magnetic Field," in Optical Fiber Fabry-Perot Interferometer based Sensor Instrumentation System for Low Magnetic Field Measurement, PhD dissertation, Dept. of Electrical and Computer Engineering, Virginia Polytechnic Institute, 18 December 1997; http://scholar.lib.vt.edu/theses/available/etd-11198-54532/unrestricted/ch2.pdf

A typical EFPI sensor configuration is shown in Figure 2-34. The light from a laser source propagates along an input/output single mode fiber to the Fabry-Pérot cavity that is formed by the input/output and the target fibers. A fraction of this incident light, approximately 4 %, is reflected at the output endface of the input/output fiber back into the fiber. The light transmitted out of the input/output fiber projects onto the fiber endface of the target fiber. The reflected light from the target fiber is partially recoupled into the input/output fiber. The interference between the two reflections produces interfering fringes as the air gap distance is changed.

Yu[367] observes that most fiber-based FP interferometers (FFPI) exploit a low-finesse FP cavity to simplify the sensor fabrication and to take advantage of the two-beam interference approximation in the sensor demodulation.[368] An FP interferometer, rigorously speaking, is a multibeam interference device. But because a low-finesse FFPI consists of two interfaces with a reflectivity less than 4%, its higher order interferences in the cavity are weak and often negligible, and therefore it can be approximately treated as a two-beam interference device. In some applications, medium,[369] high finesse,[370] or even asymmetric[371] FP interferometers have also been used to achieve higher sensitivity, increase the signal amplitude, reduce the source power requirement, and sometimes avoid other unwanted interferences.

2.3.1.3.6 Pound-Drever-Hall Technique

The Pound-Drever-Hall (PDH) technique[372] is an application of frequency modulation spectroscopy to detect the resonances of an optical cavity by demodulating the beam reflected from the cavity. The PDH technique is often part of a control system which regulates the frequency of a laser to match the resonance condition of a cavity. Named after R.V. Pound, Ronald Drever, and John L. Hall, the technique was described in 1983 by Drever, Hall and others

---

[367] Bing Yu, Anbo Wang, Gary Pickrell, "Analysis of Fiber Fabry-Perot Interferometric Sensors Using Low-Coherence Light Sources," J. Lightwave Technology 24(April 2006):1758-1767.

[368] P.C. Beard, T.N. Mills, "Extrinsic optical-fiber ultrasound sensor using a thin polymer film as a low-finesse Fabry-Perot interferometer," Appl. Opt. 35(February 1996):663-675. J.L. Santos, D.A. Jackson, "Optical fiber sensing with a low-finesse Fabry-Perot cavity," Appl. Opt. 31(1992):7361-7366.

[369] M.N. Inci, S.R. Kidd, J.S. Barton, J.D.C. Jones, "Fabrication of single-mode fiber optic Fabry-Perot interferometers using fusion spliced titanium dioxide optical coatings," Meas. Sci. Technol. 3(July 1992):678-684. B. Yu, D.W. Kim, J. Deng, H. Xiao, A. Wang, "Fiber Fabry-Perot sensors for partial discharge detection in power transformers," Appl. Optics 42(June 2003):3241-3250.

[370] C.E. Lee, W.N. Gibler, R.A. Atkins, H.F. Taylor, "In-line fiber Fabry-Perot interferometer with high-reflectivity internal mirrors," J. Lightwave Technology 10(October 1992):1376-1379.

[371] M.A. Chan, S.D. Collins, R.L. Smith, "A micromachined pressure sensor with fiber-optic interferometric readout," Sens. Actuators A, Phys. 43(May 1994):196-201.

[372] "Pound-Drever-Hall technique," http://en.wikipedia.org/wiki/Pound-Drever-Hall_technique.

working at the University of Glasgow and the U.S. National Bureau of Standards,[373] and had similarities to an older frequency-modulation technique used for microwave cavities.[374] In recent years the Pound-Drever-Hall technique has become a mainstay of modern laser frequency stabilization and is the basis of many of types of precision laser stabilization. Prominently, the field of interferometric gravitational wave detection depends critically on enhanced sensitivity afforded by optical cavities.[375]

Figure 2-35. Schematic of Pound-Drever-Hall (PDH) setup.[376]

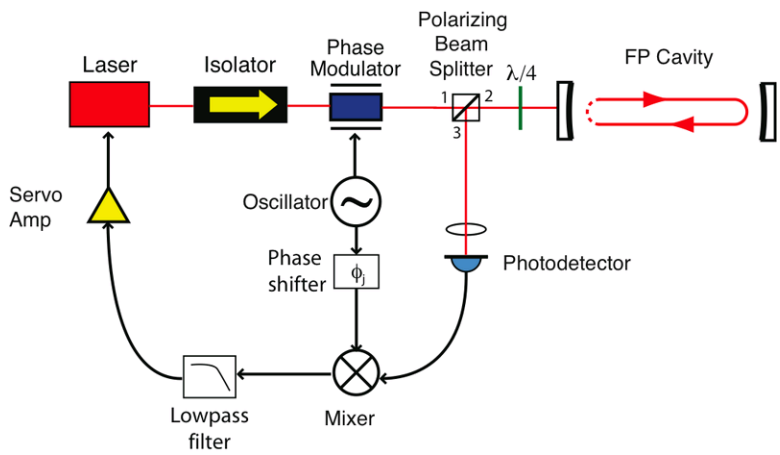

PDH addresses the problem that all lasers demonstrate some kind of frequency wander. This is an artifact of temperature variations which change laser cavity lengths, laser driver current and voltage fluctuations, atomic transition widths, and many other factors. PDH locking offers one possible solution to this problem by actively tuning the laser to match the resonance condition of a stable reference cavity. As shown in Figure 2-35, phase modulated light consisting of a carrier frequency and two side bands – well outside the FWHM (full-width half-maximum) of the cavity – is directed onto a two mirror cavity. Light reflected off the cavity is measured using a high speed photodetector, the reflected signal consisting of the two unaltered side bands along with a

---

[373] R.W.P. Drever, J.L. Hall, F.V. Kowalski, J. Hough, G.M. Ford, A.J. Munley, H. Ward, "Laser Phase and Frequency Stabilization Using an Optical Resonator," Appl. Phys. B 31(June 1983):97-105.

[374] Eric D. Black, "An introduction to Pound-Drever-Hall laser frequency stabilization," Am. J. Phys. 69(January 2001):79-87; http://elmer.tapir.caltech.edu/ph237/week13/BlackAJP01.pdf.

[375] Alex Abramovici, William E. Althouse, Ronald W.P. Drever, Yekta Gürsel, Seiji Kawamura, Frederick J. Raab, David Shoemaker, Lisa Sievers, Robert E. Spero, Kip S. Thorne, Rochus E. Vogt, Rainer Weiss, Stanley E. Whitcomb, Michael E. Zucker, "LIGO: The Laser Interferometer Gravitational-Wave Observatory," Science 256(17 April 1992):325-333; http://www.sciencemag.org/cgi/reprint/256/5055/325.pdf.

[376] "Pound-Drever-Hall technique," http://en.wikipedia.org/wiki/Pound-Drever-Hall_technique.

phase shifted carrier component. This light is then measured using a photodetector and is mixed down with a phase-shifted local oscillator, then low-pass filtered. The resulting electronic readout signal gives a measure of how far the laser carrier is off resonance with the cavity, allowing a control system to apply corrective adjustments.

2.3.1.4 Sagnac Interferometry

The Sagnac effect (also called Sagnac interference), named after French physicist Georges Sagnac, is a phenomenon encountered in interferometry that is elicited by rotation.[377] The Sagnac effect manifests itself in a setup called ring interferometry or a Sagnac interferometer (Figure 2-36). A beam of light is split and the two beams are made to follow a trajectory in opposite directions. To act as a ring the trajectory must enclose an area. On return to the point of entry, the light is allowed to exit the apparatus in such a way that an interference pattern is obtained. The position of the interference fringes changes as a function of, and is dependent upon, the angular velocity of the setup.

Figure 2-36. Schematic representation of a Sagnac interferometer.[378]

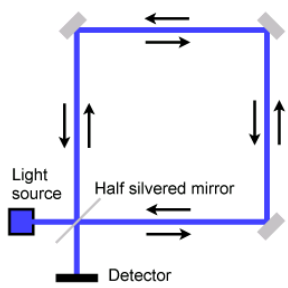

2.3.1.5 Heterodyne Interferometry

Heterodyne interferometers (Section 2.3.1.5) and homodyne interferometers (Section 2.3.1.6) are the two main families of optical interferometer.

Interferometric methods based on heterodyne techniques are of ancient vintage in AFM.[379] In heterodyne detection, one modulates, usually by a frequency shift, one of two beams prior to detection. A special case of heterodyne detection is optical heterodyne detection, which detects

---

[377] "Sagnac Effect," Wikipedia, Spetember 2009; http://en.wikipedia.org/wiki/Sagnac_effect.

[378] "Sagnac Effect," Wikipedia, Spetember 2009; http://en.wikipedia.org/wiki/Sagnac_effect.

[379] Y. Martin, C.C. Williams, H.K. Wickramasinghe, "Atomic force microscope-force mapping and profiling on a sub 100-A scale," J. Appl. Phys. 61(1987):4723-4729.

the interference at the beat frequency. A signal of interest at some frequency is non-linearly mixed with a reference "local oscillator" that is set at a close-by frequency. The desired outcome is the "difference frequency" or beat frequency, which carries the information (amplitude, phase, and frequency modulation) of the original higher frequency signal, but is oscillating at a lower more easily processed carrier frequency. The AC signal now oscillates between the minimum and maximum levels every cycle of the beat frequency. Since the modulation is known, the relative phase of the measured beat frequency can be measured very precisely even if the intensity levels of the beams are (slowly) drifting. This phase is identical in value to the phase one measures in the homodyne case. There are additional benefits of optical heterodyne detection, such as an improved signal to noise ratio when one of the beams is weak.

In a typical heterodyne metrology system, a laser output is split into measurement and local arms, and one arm is frequency shifted with respect to the other. The measurement beam is mixed at the detector with a frequency-shifted local oscillator beam to produce a beat frequency whose phase is readily measured. The inner core of the measurement beam is returned by the target retroreflector, while the outer annulus is returned by the reference mirror. The returned beams mix with the local oscillator beam at the target and reference detectors. The phase difference between the beat frequencies obtained from the two detectors is sensitive to the displacement between the reference and the target, while any other optical path fluctuations within the metrology system are eliminated.

According to Peggs and Yacoot:[380] A heterodyne interferometer uses two polarized beams having slightly different frequencies. This is usually achieved using either a Zeeman-stabilized laser, or a single-frequency laser with an acousto-optic modulator. A polarizing beam-splitter is used to separate the two beams: one beam becomes the reference beam and the other is used as the measurement beam. The two beams traverse their respective paths, are recombined in the beam-splitter, and then pass through a polarizer set at 45° to the polarization axes of the two beams. As the measurement arm of the interferometer changes its length at acoustic frequencies, there will be Doppler shifting of the optical frequency of the beam in the measurement arm. This results in a change in the difference in frequency between the two beams that have passed through the interferometer. This difference is then compared with the frequency difference between the two beams prior to them entering the beam-splitter to yield a phase difference corresponding to the distance moved by the measurement arm of the interferometer. Ideally, this variation in phase with respect to the change in path length in the measurement arm should be a perfectly linear effect; however, there are many factors which introduce nonlinearities. The many sources of nonlinearity in heterodyne interferometers have been listed by Rosenbluth and Bobroff[381] and were further discussed and extended by Bobroff.[382] These sources included misalignment of laser

---

[380] G.N. Peggs, A. Yacoot, "A review of recent work in sub-nanometre displacement measurement using optical and X-ray interferometry," Philos Transact A Math Phys Eng Sci. 360(15 May 2002):953-968; http://journals.royalsociety.org/content/nj5d8xydfdy8b85d/fulltext.pdf.

[381] A.E. Rosenbluth, N. Bobroff, "Optical sources of non-linearity in heterodyne interferometers," Precis. Engng. 12(1990):7-11.

[382] N. Bobroff, "Recent advances in displacement measuring interferometry," Meas. Sci. Technol. 4(1993):907-926.

polarization axes with respect to the beam-splitter, ellipticity of the light from the laser source, differential transmission between the two arms of the interferometer, rotation of the plane of polarization by the retro-reflectors, leakage of light with the unwanted polarization through the beam-splitter, and lack of geometrical perfection of the wave plates used. After extensive analysis, Rosenbluth and Bobroff[383] concluded that frequency mixing was not important unless it was asymmetric between the two arms of the interferometer. The sources of nonlinearity in a heterodyne interferometer give rise to two periodic errors: a first-order phase harmonic having a period of one cycle per fringe and a second-order harmonic with a period of two cycles per fringe. Such sources of uncertainty can, if uncorrected, give rise to errors of several nanometers in the accuracy with which measurements can be made.

Xie and Wu[384] developed a theoretical matrix-based analysis of the unwanted elliptical polarization output of a Zeeman-stabilized laser where they concluded that it was due mainly to anisotropy in the laser cavity. Their measurements, using several lasers, showed that the orthogonality errors between the two polarization states were between 4° and 7°, which would give rise to errors in length measurement of 3.5 nm and 6 nm. They extended their work[385] to include the interferometer itself and explained how it would be possible to compensate for non-orthogonality and elliptical polarization in a heterodyne interferometer by using a Babinet-Soleil compensator in front of the beam-splitter.

At about the same time, Hou and Wilkening[386] presented an analysis of the effects of mixing due to non-orthogonality of polarization directions and elliptic incident radiation. They detected, and compensated for, phase errors by using a "double-phase-measurement" technique in which the output of the optical interferometer is measured as two output signals with a 90° phase shift between them – variations of the phase difference between these two signals being a measure of the nonlinearity. This work was continued by Hou and Zhao[387] who measured drift in the nonlinearity and compensated for it by using the "double-phase-measurement" technique. The correction of such drift is important in interferometer systems having low thermal drift.

De Freitas and Player[388] published a detailed vector model, produced using Jones matrices, of the errors in a heterodyne interferometer. They showed, in contrast to Rosenbluth and Bobroff[389],

---

[383] A.E. Rosenbluth, N. Bobroff, "Optical sources of non-linearity in heterodyne interferometers," Precis. Engng. 12(1990):7-11.

[384] Y. Xie, Y. Wu, "Elliptical polarization and nonorthogonality of stabilized Zeeman laser output," Appl. Opt. 28(1989):2043-2046.

[385] Y. Xie, Y. Wu, "Zeeman laser interferometer errors for high precision measurements," Appl. Opt. 31(1992):881-884.

[386] W. Hou, G. Wilkening, "Investigation and compensation of the nonlinearity of heterodyne interferometers," Prec. Eng. 14(1992):91-98.

[387] W. Hou, X. Zhao, "Drift of nonlinearity in the heterodyne interferometer," Precis. Engng. 16(1994):25-35.

[388] J.M. De Freitas, M.A. Player, "Importance of rotational beam alignment in the generation of second harmonic errors in laser heterodyne interferometry," Meas. Sci. Technol. 4(1993):1173-1176. J.M. De

that rotational beam alignment was important and that misalignment of orthogonal input states was responsible for the second harmonic periodical error observed by Sutton.[390] De Freitas[391] widened the scope of his previous models to consider the effects of birefringence and dichroism on an "ideal" heterodyne interferometer free of other sources of nonlinearity. He favored the matrix-based vector models over the simpler approach developed by Wu and Su[392] to produce a plane-wave scalar model for nonlinearity in both homodyne and heterodyne interferometers. The matrix methods are more rigorous since the depolarization, birefringence, dichroism and other similar phenomena can be described in terms of the electric field vector. Nevertheless, both the scalar and vector methods can be used to provide realistic estimations of the errors in heterodyne interferometers.

Stone and Howard[393] devised an ingenious method of measuring the periodic errors by rotating the cube corner in one path of the optical interferometer through a measured angle to introduce a predicted nonlinearity and comparing it with the measured value. The interferometer under examination was a commercial design in which the cube corner could be coupled directly to the beam-splitter. Although the authors of the paper were encouraged to note that the periodic error measured on the interferometer under test was of the order of ±300 pm, they pointed out that other interferometers could exhibit errors as large as ±15 nm. Discrepancies of such a size emphasize the importance of evaluating the performance of the individual interferometers used for very demanding applications. The method described by Stone and Howard does, however, suffer from the disadvantage that it requires the measurement of an angle from an external reference and is therefore not suited to being used to optimize a system in situ.

Badami and Patterson[394] adopted a completely different approach for the evaluation of an interferometer system by observing the frequency output of the interferometer. The retroreflector in the reference arm of their interferometer was driven at a constant speed of a few millimeters per second, which produced a frequency separation between the desired signal and the harmonics

---

Freitas, M.A. Player, "Polarization effects in heterodyne interferometry," J. Mod. Opt. 42(1995):1875-1899.

[389] A.E. Rosenbluth, N. Bobroff, "Optical sources of non-linearity in heterodyne interferometers," Precis. Engng. 12(1990):7-11.

[390] C.M. Sutton, "Non-linearity in length measurement using heterodyne laser Michelson interferometry," J. Phys. E 20(1987):1290-1292.

[391] J.M. De Freitas, "Analysis of laser source birefringence and dichroism on nonlinearity in heterodyne interferometry," Meas. Sci. Technol. 8(1997):1356-1359.

[392] C.-M. Wu, C.-S. Su, "Nonlinearity in measurements of length by optical interferometry," Meas. Sci. Technol. 7(1996):62-68.

[393] J.A. Stone, L.P. Howard, "A simple technique for observing periodic nonlinearities in Michelson interferometers," Precis. Engng. 22(1998):220-232.

[394] V.G. Badami, S.R. Patterson, "A frequency domain method for the measurement of nonlinerarity in heterodyne interferometry," Precis. Engng. 24(2000):41-49.

associated with the system's nonlinearity. By careful alignment they were able to reduce the second-order harmonic to ~2 nm and the first-order harmonic to 0.5 nm. The advantage of their method lies in the fact that no phase measuring electronics are required, thereby facilitating a direct measurement of interferometer errors. The uncertainties associated with the electronic systems that they used for the frequency analysis gave rise to errors very much smaller than the signals being measured. However, this approach to measuring nonlinearity is only suited to systems that can be driven at a sufficiently high speed to generate a phase shift between the desired signal and those due to nonlinearity.

As noted by Wu,[395] the periodic nonlinearity, ranging from tens of nanometers to a few nanometers in heterodyne interferometry limits its usage in high accuracy measurements.[396] This result from frequency mixing and polarization mixing is caused by the ellipticity and nonorthogonality of the laser beams, the imperfection of the beam splitters, the nonperfect alignment between laser beam axes and splitter axes, and the ghost reflections from the interfaces used between the different components.[397] While great efforts have been made to reduce these kind of errors,[398] only the heterodyne interferometers with two spatially separated polarization beams can provide periodic nonlinearity as low as a few tens of picometers in real time.[399]

2.3.1.6 Homodyne Interferometry

Interferometric methods based on homodyne techniques also date back to the earliest experiments in AFM.[400] In homodyne optical interferometry, the reference radiation (i.e., the local oscillator)

---

[395] C.M. Wu, "A generalized, periodic nonlinearity-reduced interferometer for straightness measurements," Rev Sci Instrum. 79(June 2008):065101.

[396] C.M. Wu, J. Lawall, R.D. Deslattes, "Heterodyne interferometer with subatomic periodic nonlinearity," Appl. Opt. 38(1999):4089-4094.

[397] C.M. Wu, "Periodic nonlinearity resulting from ghost reflections in heterodyne interferometry," Opt. Commun. 215(2003):17-23. C.M. Wu, S.T. Lin, J. Fu, "Heterodyne interferometer with two spatial-separated polarization beams for nanometrology," Opt. Quantum Electron. 34(2002):1267-1276. C.M. Wu, J. Lawall, R.D. Deslattes, "Heterodyne interferometer with subatomic periodic nonlinearity," Appl. Opt. 38(1999):4089-4094. R.C. Quenelle, "Nonlinearity in interferometric measurements," Hewlett-Packard J. 34(1983):10.

[398] W. Hou, G. Wilkening, "Investigation and compensation of the nonlinearity of heterodyne interferometers," Prec. Eng. 14(1992):91-98. C.M. Sutton, "Non-linearity in length measurement using heterodyne laser Michelson interferometry," J. Phys. E 20(1987):1290-1292. R.C. Quenelle, "Nonlinearity in interferometric measurements," Hewlett-Packard J. 34(1983):10. Y. Gursel, "Laser metrology gauges for OSI," Proc. SPIE 1947(1993):188-197.

[399] C.M. Wu, "Periodic nonlinearity resulting from ghost reflections in heterodyne interferometry," Opt. Commun. 215(2003):17-23. C.M. Wu, S.T. Lin, J. Fu, "Heterodyne interferometer with two spatial-separated polarization beams for nanometrology," Opt. Quantum Electron. 34(2002):1267-1276.

[400] G.M. McClelland, R. Erlandsson, S. Chiang, "Atomic force microscopy: General principles and a new implementation," Vol. 6, in: D.O. Thompson, D.E. Chimenti, eds., Review of Progress in Quantitative

is derived from the same source as the signal before the modulating process. That is, the interference occurs between two beams at the same wavelength (or carrier frequency). The phase difference between the two beams results in a change in the intensity of the light on the detector. Measuring the resulting intensity of the light after the mixing of these two light beams is known as homodyne detection. For example, in a laser scattering measurement, the laser beam is split into two parts. One is the local oscillator and the other is sent to the system to be probed. The scattered light is then mixed with the local oscillator on the detector. This arrangement has the advantage of being insensitive to fluctuations in the frequency of the laser. Usually the scattered beam will be weak, in which case the (nearly) steady component of the detector output is a good measure of the instantaneous local oscillator intensity and therefore can be used to compensate for any fluctuations in the intensity of the laser.

According to Peggs and Yacoot:[401] In contrast to the heterodyne interferometer, the homodyne interferometer uses a single-frequency polarized beam. In a typical homodyne interferometer, the measurement arm contains a $\lambda/4$ plate, which results in the measurement and reference beams having a phase separation of 90°. After traversing their respective paths, the two beams recombine in the beam-splitter. This combined beam is then divided in two using a 45° polarizing beam-splitter. The two signals have a phase difference of 90° and provide sufficient information to measure both a displacement and its direction.

In common with the heterodyne interferometer, the homodyne interferometer also suffers from nonlinearity, giving rise to periodic first- and second-order harmonic errors. If the signals were perfect sine and cosine signals and of equal amplitude, it would be possible to plot the sine and cosine signals against each other and obtain a circle, with its center at coordinates (0, 0). The angle of the radius vector with respect to the abscissa would be equal to the phase difference of the interfering beams, thereby giving a measurement of the displacement in the measurement arm. In reality the resultant plot tends to an ellipse rather than a circle (for reasons discussed below). Heydemann[402] and Birch[403] showed how, if the equation of the ellipse were known, the differences between the ellipse and the "theoretical" circle could be calculated and expressed in terms of offsets and phase errors in the interferometer signals. The ellipse could then be fitted to a circle to correct for the nonlinearity present and enable sub-nanometer optical fringe division to be realized.

Non-Destructive Evaluation, Plenum, New York, 1987, p. 307. R. Erlandsson, G.M. McClelland, C.M. Mate, S. Chiang, "Atomic force microscopy using optical interferometry," J. Vac. Sci. Technol. 6(1988):266-270.

[401] G.N. Peggs, A. Yacoot, "A review of recent work in sub-nanometre displacement measurement using optical and X-ray interferometry," Philos Transact A Math Phys Eng Sci. 360(15 May 2002):953-968; http://journals.royalsociety.org/content/nj5d8xydfdy8b85d/fulltext.pdf.

[402] Peter L.M. Heydemann, "Determination and correction of quadrature fringe measurement errors in interferometers," Appl. Opt. 20(1981):3382-3384.

[403] K.P. Birch, "Optical fringe subdivision with nanometric accuracy," Precis. Engng. 12(1990):195-198.

Augustyn and Davis[404] produced a detailed theoretical analysis of the periodic errors associated with homodyne interferometers. They note that the main sources of uncertainty can be attributed to polarization mixing caused by imperfections in the polarizing beam-splitters. In more sophisticated homodyne interferometers the beam containing the signals from both the reference and measurement arms is divided into two components. Each of the two beams passes through a polarizing beam-splitter and the four beams produced have phase differences of 0°, 90°, 180° and 270° with respect to each other. Augustyn and Davis concluded that the accuracies of the 0° and 90° position measurements were not affected by polarization mixing and that phase angle error in the other beams (180° and 270°) was likely to be smaller than that observed in heterodyne interferometers.[405]

Greco et al.[406] described a design of homodyne polarization interferometer in which the laser power instability was corrected. They also considered the merits of looking at all four signals rather than just the 0° and 90° signals. They concluded that when four signals were analysed it was possible to compensate more effectively for laser power instabilities and uncorrelated noise in the system. If, however, the interferometer noise error were to approach the shot noise level, i.e., quantum noise, the four-signal approach would offer no advantages over the two-signal approach.

Wu et al.[407] pointed out (as had Birch[408] earlier) that as well as polarization mixing, other "set factors" such as unequal gain of the detectors, imbalance of the two beams, and lack of quadrature between the two signals can contribute to errors in the interferometer measurements. They analysed these errors and used an ellipse-fitting routine (in a manner similar to that described by Birch) to correct their signal. Verification of their model was performed using a homodyne interferometer whose stability was shown to be 270 pm.

Petru and Cip[409] used Jones matrices to model the behavior of a homodyne interferometer. They tested the linearity of their interferometer system by using a Soleil-Babinet optical compensator

---

[404] W. Augustyn, P. Davis, "An analysis of polarization mixing in distance measuring interferometers," J. Vac. Sci. Technol. B 8(1990):2032-2036.

[405] N. Bobroff, "Residual errors in laser interferometry from air turbulence and nonlinearity," Appl. Opt. 26(1987):2676-2682.

[406] V. Greco, C. Lemmi, S. Ledesma, G. Molesini, F. Quercioli, "Multiphase homodyne interferometry: analysis of some error sources," Appl. Opt. 34(1995):2207-2213. V. Greco, S. Ledesma, G. Molesini, F. Quercioli, "Accurate polarization interferometer," Rev. Scient. Instrum. 66(1995):3729-3734.

[407] C. Wu, C. Su, G. Peng, "Correction of nonlinearity in one-frequency optical interferometry," Meas. Sci. Technol. 7(1996):520-524.

[408] Franco Chiaravalloti, Leo Gross, Karl-Heinz Rieder, Sladjana M. Stojkovic, André Gourdon, Christian Joachim, Francesca Moresco, "A rack-and-pinion device at the molecular scale," Nature Materials 6(2007):30-33; http://www.nature.com/nmat/journal/v6/n1/abs/nmat1802.html.

[409] F. Petru, O. Cip, "Problems regarding linearity of data of a laser interferometer with a single-frequency laser," Precis. Engng. 23(1999):39-50. O. Cip, F. Petru, "A scale-linearization method for precise laser interferometry," Meas. Sci. Technol. 11(2000):133-141.

in the input beam to generate a known phase shift between the two polarizations in the interferometer. Their system had a linearity of ±500 pm. Eom et al.[410] also used the well-known ellipse-fitting routines to correct for nonlinearity, and their system achieved subnanometric linearity over a measuring range of 100 mm using commercially available interface cards to collect the signals and dynamically compensate for the nonlinearity.

Both homodyne and heterodyne frequencies are mainly employed for measuring a displacement. The homodyne interferometer offers the same laser light frequency for both the reference and the measurement arms, and is a dc-type instrument, therefore containing a substantial amount of noise from the low frequency band. In contrast, the heterodyne interferometer employs a different frequency for each arm. This is an ac-type instrument having the advantages of being noise immune and having longrange measurement ability. Therefore, the heterodyne interferometer is the best candidate for displacement measurements with accuracy at the nanometer level.[411]

2.3.1.7 Factors Affecting Optical Interferometry Accuracy

Besides the issues addressed in the two preceding Sections, there are also several other factors that affect the accuracy of optical interferometry. Our discussion is again drawn from Peggs and Yacoot.[412]

(A) **Environment**. The uncertainties due to the characteristics of the ambient air and hence refractive index are the largest contributors to the overall uncertainty budget for an optical interferometer working in the ambient air. One must not only correct for changes in absolute values of temperature, atmospheric pressure and impurities such as hydrocarbons present in an industrial environment, but also try to minimize local variations (turbulence) which can dramatically change the refractive index of the air through which the laser beam propagates.[413] The conventional way of minimizing these effects is to make the measurement and the reference paths as geometrically similar as possible, with the minimum dead path in the measurement arm. Shielding the air path completely and thereby minimizing the influence of turbulence can make

---

[410] T. Eom, J. Kim, K. Jeong, "The dynamic compensation of nonlinearity in a homodyne laser interferometer," Meas. Sci. Technol. 12(2001):1734-1738.

[411] C.M. Wu, "A generalized, periodic nonlinearity-reduced interferometer for straightness measurements," Rev Sci Instrum. 79(June 2008):065101.

[412] G.N. Peggs, A. Yacoot, "A review of recent work in sub-nanometre displacement measurement using optical and X-ray interferometry," Philos Transact A Math Phys Eng Sci. 360(15 May 2002):953-968; http://journals.royalsociety.org/content/nj5d8xydfdy8b85d/fulltext.pdf.

[413] N. Bobroff, "Residual errors in laser interferometry from air turbulence and nonlinearity," Appl. Opt. 26(1987):2676-2682.

an additional reduction.[414] The effects of the variations in the refractive index of the ambient air over that part of the laser paths that is not compensated is normally accounted for by applying a modified version of Edlen's equations.[415]

In most cases, in order to minimize the influences of the ambient air, ultra-high-accuracy measurements are conducted in a vacuum system; but for some applications the use of helium, whose refractive index has a low sensitivity to changes in temperature, as the medium through which the laser beam propagates, has been successful in reducing uncertainties.[416] Operation in UHV minimizes all of these uncertainties. SPM instruments in highly controlled environments that are secluded from external perturbations (e.g., temperature, acoustic, liquid) by multiple layers of isolation and by operating at low temperature and ultrahigh vacuum can passively achieve extreme stability, e.g., drift rates of ~1 pm/min.[417]

(B) **Alignment of Interferometer Optics**. Many practical interferometer configurations make extensive use of plane mirrors for the targets in measuring systems. The attraction is that multiple pass optics can be used to enhance the resolution to some extent and the plane mirrors can be used as surfaces along which straightness measurements can be made. However, it is not widely realized that both the alignment between the laser interferometer and the direction of motion, and the alignment between the laser interferometer coordinate system and that of the plane mirror target are critical misalignments giving rise to a cosine error.[418]

(C) **Diffraction Effects**. The finite diameter of the laser beams (~0.5 mm) propagating through the interferometer gives rise to uncertainties at the one part in 10^9. This is as a result of Fresnel diffraction causing a bending of nominally plane wavefronts. Mana[419] and Bergamin et al.[420] have built upon existing theoretical treatments, performed measurements using a

---

[414] Andrew Yacoot, Michael J Downs, "The use of x-ray interferometry to investigate the linearity of the NPL Differential Plane Mirror Optical Interferometer," Meas. Sci. Technol. 11(2000):1126-1130.

[415] Andrew Yacoot, Michael J Downs, "The use of x-ray interferometry to investigate the linearity of the NPL Differential Plane Mirror Optical Interferometer," Meas. Sci. Technol. 11(2000):1126-1130. K.P. Birch, M.J. Downs, "Correction to the updated Edlen equation for the refractive index of air," Metrologia 31(1994):315-316. G. Bonsch, E. Potulski, "Measurement of the refractive index of air and comparison with the modified Edlen equations," Metrologia 35(1998):133-139.

[416] J.B. Bryan, "Design and construction of an ultraprecision 84 inch diamond turning machine," Prec. Eng., 1(1979):13-17.

[417] B.C. Stipe, M.A. Rezaei, W. Ho, "Single-molecule vibrational spectroscopy and microscopy," Science 280(1998):1732-1735.

[418] N. Bobroff, "Critical alignments in plane mirror interferometry," Precis. Engng. 15(1993):33-38.

[419] G. Mana, "Diffraction effects in optical interferometers illuminated by laser sources," Metrologia 26(1989):87-93.

[420] A. Bergamin, G. Cavagnero, G. Mana, "Quantized positioning of X-ray interferometers," Rev. Scient. Instrum. 68(1997):17-22. A. Bergamin, G. Cavagnero, G. Mana, "Observation of Fresnel diffraction in a two-beam laser interferometer," Phys. Rev. A 49(1994):2167-2173. A. Bergamin, G. Cavagnero, L.

combination of X-ray and optical interferometry, and provided details of how to compensate for diffraction effects.

(D) **Photon Bounce**. Fujimoto et al.[421] considered the effects of light bounce, i.e., parasitic low reflectivity reflections, in a polarizing interferometer. Such reflections can shift the position of fringe maxima. These authors showed that in the worst case (for their configuration) the effect of the phenomenon was 0.040 ppm.

(E) **Quantum Effects**. The factors described so far that contribute to nonlinearity can be explained using classical physics. The ultimate limits of optical interferometry are governed by quantum physics. The two sources of quantum mechanical noise are photon-counting error (also known as shot noise) and radiation pressure. Only photon counting error is significant and it manifests itself as noise in the detector and variations in the laser power amplitude. The effects of the quantum noise have been studied by Meers and Strain[422] and Stevenson et al.[423] Interferometers are now being designed where the quantum noise limit is being approached. Lawall and Kessler[424] showed (Section 4.6.3.1) that if the classical detector noise (for a typical commercial detector) was combined with the quantum laser amplitude noise (shot noise) the quadrature sum of the components was 0.57 pm.

2.3.2 Combination Optical Source/Detector

Several other optical methods have been tried, such as positioning a laser diode close to the cantilever wherein the sensor acts as a combined light source and light detector. Perhaps the best-known example is Laser Feedback Interferometry (LFI), which features a simple, single-axis optical arrangement that requires minimal optical components while providing high sensitivity at low light levels. Because the frequency selectivity of the laser, LFI is far less sensitive to incoherently reflected light than are other forms of interferometry that require all the scattered light to be collected by a photodetector.

Despite an increased understanding of the behavior of lasers in the presence of optical feedback, there have been only a few uses of LFI concentrated mostly in applications to atomic force and

---

Cordiali, G. Mana, "A Fourier optics model of two-beam scanning laser interferometers," Eur. Phys. J. D 5(1999):433-440.

[421] H. Fujimoto, G. Mana, K. Nakayama, "Light bounces in two-beam scanning laser interferometers," Jpn. J. Appl. Phys. 39(2000):2870-2875.

[422] B.J. Meers, K.A. Strain, "Modulation, signal and quantum noise in optical interferometers," Phys. Rev. A 44(1991):4693-4703.

[423] A.J. Stevenson, M.B. Gray, H.A. Bachor, D.E. McCelland, "Quantum-noise-limited interferometric phase measurements," Appl. Opt. 32(1993):3481-3493.

[424] John Lawall, Ernest Kessler, "Michelson interferometer with 10 pm accuracy," Rev. Scient. Instrum. 71(2000):2669-2676. http://link.aip.org/link/?RSINAK/71/2669/1.

optical microscopy.[425] In one early example from 1988 for AFMs, Sarid et al.[426] described "a compact scanning-force microscope in which the element that senses the amplitude of vibration of a tip interacting with force gradients is the cavity of a single-mode laser diode and its integrally built photodiode."

In 1999 Ovryn and Andrews[427] used light fed back into a laser cavity for interferometric position sensing, and reported: "The operating characteristics of a novel phase-shifting interferometer are presented. Interference arises by reflecting the light from a sample back into the cavity of a cw He-Ne laser. Changes in phase and fringe visibility are calculated from an overdetermined set of phase-shifted intensity measurements with the phase shifts being introduced with an electro-optic modulator. The interferometer is sensitive enough to measure displacements below 1 Hz with a rms error of approximately 1 nm **[1000 pm]** from a sample that reflects only 3% of the 28 mW that is incident on its surface. The interferometer is applied to the determination of cantilever bending of a piezoelectric bimorph." These authors modeled the effect of coherent feedback in the He-Ne gas laser cavity as a three-mirror Fabry-Pérot etalon, which is their method for reflecting the light incident on the object back into the laser cavity.

2.3.3 Non-Optical Capacitive Sensors

Capacitive sensing is a technology for detecting proximity, position, etc., based on capacitive coupling effects.[428] Capacitive sensors are noncontact devices capable of high-resolution measurement of the position and/or change of position of any conductive target. The sub-nanometer resolution of high-performance capacitive sensors makes them indispensible in today's nanotechnology world.

---

[425] D. Sarid, D. Iams, V. Weissenberger, L.S. Bell, "Compact scanning-force microscope using laser diode," Opt. Lett. 13(1988):1057-1059. D. Sarid, V. Weissenberger, D. A. Iams, and J. T. Ingle, "Theory of the laser diode interaction in scanning force microscopy," IEEE J. Quantum Electron. 25(1989):1968-1972. D. Sarid, D. A. Iams, J. T. Ingle, V. Weissenberger, "Performance of a scanning force microscope using a laser diode," J. Vac. Sci. Technol. A 8(1990):378-383. A. Bearden, M.P. O'Neill, L.C. Osborne, T.L. Wong, "Imaging and vibrational analysis with laser-feedback interferometry," Opt. Lett. 18(1993):238-240. R. Juskaitis, T. Wilson, N.P. Rea, "Compact confocal interference microscopy," Opt. Commun. 109(1994):167-177. B. Ovryn, J.H. Andrews, "Phase-shifted laser feedback interferometry," Opt. Lett. 23(1998):1078-1080. Ben Ovryn, James H. Andrews, "Measurement of changes in optical path length and reflectivity with phase-shifting laser feedback interferometry," Applied Optics 38(1 April 1999):1959-1967; http://asb.aecom.yu.edu/pdf/ovryn/ovryn_andrews.pdf.

[426] D. Sarid, D. Iams, V. Weissenberger, L.S. Bell, "Compact scanning-force microscope using laser diode," Opt. Lett. 13(1988):1057-1059.

[427] Ben Ovryn, James H. Andrews, "Measurement of changes in optical path length and reflectivity with phase-shifting laser feedback interferometry," Applied Optics 38(1 April 1999):1959-1967; http://asb.aecom.yu.edu/pdf/ovryn/ovryn_andrews.pdf.

[428] X. Zhao, G. Wilkening, H. Marth, K. Horn, "High-accuracy capacitance sensors for positioning of piezoelectric displacement actuator," Proc. Actuator 94(1994):193.

Capacitive sensors use the electrical property of "capacitance" to make measurements. Capacitance is a property that exists between any two conductive surfaces within some reasonable proximity. Changes in the distance between the surfaces changes the capacitance. It is this change of capacitance that capacitive sensors use to indicate changes in position of a target. High-performance displacement sensors use small sensing surfaces and as result are positioned close to the targets (0.25 mm - 2 mm).[429]

Capacitive sensors for use in precision displacement measurement and metrology applications use complex electronic designs to execute complex mathematical algorithms. Unlike inexpensive sensors, these high-performance sensors have outputs which are very linear, stable with temperature, and able to resolve incredibly small changes in capacitance resulting in high resolution measurements of less than one nanometer. Compared to other noncontact sensing technologies such as optical, laser, eddy-current, and inductive, high-performance capacitive sensors have some distinct advantages, including (1) higher resolutions, including subnanometer resolutions; (2) insensitivity to material changes, as capacitive sensors respond equally to all conductors; and (3) less expensive and much smaller than laser interferometers. However, capacitive sensors are not good choice in dirty or wet environment (where eddy-current sensors are ideal), or when a large gap between sensor and target is required (where optical and laser are better).[430]

Capacitance based detectors are widely employed in AFM applications[431] and commercially-available capacitance-based sensors can provide on the order of 100 pm positioning accuracy though these figures can be misleading when considering their possible use in a molecular workstation. For example, one of the best capacitive sensors available anywhere in the world in 2009 is the Physik Instrumente P-363 PicoCube™ XY(Z) Piezo Scanner,[432] which is described as "an ultra-high-performance closed-loop piezo scanning system designed for AFM, SPM and nanomanipulation applications. It combines an ultra-low inertia, high-speed XY/XYZ piezo scanner with non-contact, direct-measuring, parallel-metrology capacitive feedback capable of 50 picometers resolution 5 µm x 5 µm x 5 µm travel range." Unfortunately, these systems generally suffer from rather severe hysteresis effects and can only hold deviation from a repeat trajectory to under a few nanometers of stable accuracy, despite their much better nominal resolution for

---

[429] "Capacitive Sensor Operation and Optimization (How Capacitive Sensors Work and How to Use Them Effectively)," Lion Precision, Capacitive Sensor TechNote LT03-0020, 2009; http://www.lionprecision.com/tech-library/technotes/tech-pdfs/cap-0020-cap-theory.pdf.

[430] "Capacitive Sensor Operation and Optimization (How Capacitive Sensors Work and How to Use Them Effectively)," Lion Precision, Capacitive Sensor TechNote LT03-0020, 2009; http://www.lionprecision.com/tech-library/technotes/tech-pdfs/cap-0020-cap-theory.pdf.

[431] Th. Göddenhenrich, H. Lemke, U. Hartmann, C. Heiden, "Force microscope with capacitive displacement detection," J. Vac. Sci. Technol. 8(1990):383-387. J. Brugger, R.A. Buser, N.F. Rooij, "Micromachined atomic force microprobe with integrated capacitive read-out," J. Micromech. Microeng. 2(1992):218.

[432] "P-363 PicoCube™ XY(Z) Piezo Scanner," 13 July 2009, Physik Instrumente; http://www.physikinstrumente.com/en/products/prdetail.php?sortnr=201650.

single measurements – e.g., the P-363 PicoCube can provide "nanometer accuracy in 1 millisecond with 30-picometer resolution".[433]

2.3.4 Non-Optical Piezo Sensors

The ability of piezoelectric crystals and ceramics to serve as sensors as well as actuators has already been mentioned in Section 2.2.1. For example, piezoresistance is the changing electrical resistance of a material due to applied mechanical stress. The piezoresistive effect differs from the piezoelectric effect in that the piezoresistive effect only causes a change in resistance; it does not produce an electric potential.

Note that some piezo-based displacement detection methods such as piezoresistive sensors[434] and piezoelectric quartz tuning forks (i.e., qPlus sensors; Section 2.1.6) have the advantage of self-sensing (Section 3.2.2.3) – that is, the use of an optical return signal is unnecessary and operation in ultrahigh vacuum and low temperatures is easily implemented.[435]

2.4 Tip-Based Nanofabrication (TBN)

In late 2006, DARPA sponsored at least one preliminary workshop[436] on the subject of Tip-Based Nanofabrication, as reported in the CV of one participant of that workshop (J.J. De Yoreo, Deputy Director, Laboratory Science and Technology Office, Lawrence Livermore Lab). De Yoreo's CV does not indicate that he ever received any DARPA funding for TBN, outside of the workshop itself.

In 2007, DARPA issued a Broad Agency Announcement (BAA) soliciting proposals on Tip-Based Nanofabrication to make nanowires, nanotubes, or quantum dots using functionalized scanning probe tips.[437] In 2008, DARPA funded 8 independent efforts under this program, apparently with a total budget of several tens of millions of dollars, overseen by program manager Dr. Thomas Kenny. The 8 TBN "performers" are the following:

---

[433] "P-363 PicoCube™ XY(Z) Piezo Scanner," 13 July 2009, Physik Instrumente; http://www.physikinstrumente.com/en/products/prdetail.php?sortnr=201650.

[434] M. Tortonese, R.C. Barrett, C. Quate, "Atomic resolution with an atomic force microscope using piezoresistive detection," Appl. Phys. Lett. 62(1993):834-836.

[435] Franz J. Giessibl, "Atomic resolution on Si(111)-(7x7) by noncontact atomic force microscopy with a force sensor based on a quartz tuning fork," Appl. Phys. Lett. 76(13 March 2000):1470; http://dns.ntu-ccms.ntu.edu.tw/references/APPL_PHYS_LETT-76-1470-2000.pdf.

[436] J.J. De Yoreo, "Tip-Based NanoFabrication for Defense Applications," DARPA Workshop, San Francisco, CA, 16-17 November 2006.

[437] T. Kenny, "Tip-Based Nanofabrication (TBN)," Defense Advanced Research Projects Agency (DARPA)/Microsystems Technology Office (MTO), Broad Agency Announcement BAA 07-59, July 2007; http://www.fbo.gov/spg/ODA/DARPA/CMO/BAA07-59/listing.html.

CMU http://www.darpa.mil/mto/programs/tbn/pdf/CMU_TBN.pdf
Cornell http://www.darpa.mil/mto/programs/tbn/pdf/Cornell_TBN.pdf
CWRU http://www.darpa.mil/mto/programs/tbn/pdf/CWRU_TBN.pdf
LBL http://www.darpa.mil/mto/programs/tbn/pdf/LBL_TBN.pdf
NWU http://www.darpa.mil/mto/programs/tbn/pdf/Northwestern_TBN.pdf
UCB http://www.darpa.mil/mto/programs/tbn/pdf/UCB_TBN.pdf
UIUC http://www.darpa.mil/mto/programs/tbn/pdf/UIUC_TBN.pdf
Zyvex http://www.darpa.mil/mto/programs/tbn/pdf/Zyvex_TBN.pdf

Of these, only the Zyvex effort claims atomic precision in any physical dimension, and the other 7 efforts use DNA, peptides, or related "soft" materials that are inapplicable to DMS. An April 2008 webpage at NIST[438] provides a few more details about Rick Silver and NIST's involvement in the Zyvex project:

"The Atom-based Dimensional Metrology Project Awarded Large DARPA Contract
MELs atom-based dimensional metrology project was awarded a five-year, three-phase Defense Advanced Research Projects Agency (**DARPA**) contract to conduct collaborative research in atomically precise positioning, patterning and metrology. NIST is a leading collaborator in the Zyvex-led Atomically Precise Manufacturing (APM) program, one of the **Tip Based Nanofabrication** Programs funded by **DARPA**. NIST will work with Zyvex, The University of Illinois, The University of Texas at Dallas (UTD), and others on Scanning Tunneling Microscopy (STM) tip development and characterization. This will include characterization of tip structures via Field ion microscopy (FIM), Field Emission Microscopy (FEM), x-section scanning electron microscopy (SEM) and Transmission electron microscopy (TEM) techniques as well as characterizing the STM tips operational characteristics on atomic lattices. The atom-based dimensional project has published a number of results in this area over the years and was solicited to participate in the **DARPA** program. MEL will also participate in MicroElectroMechanical systems (MEMS) scanning element design for large arrays of actuated tips as well as help characterize a the 3D Passivation process to be developed at UTD. NIST will help test passivated 3D nanostructures and develop techniques for atomic scale substrate preparation and measurements, processes critical to the success of nanomanufacturing applications. The long term goal of this program is to develop economically viable manufacturing solutions at the nanometer scale that involve atomically precise patterning. Contact: Rick Silver, 301-975-5609."

A European-centered group called EUSPEN **(**European Society for Precision Engineering and Nanotechnology**)**[439] "is a community of leading industrialists and researchers working in the field of precision, micro and nano engineering with representation across 32 countries worldwide." It's focus is on "nano-precision manufacturing, design and build of ultra-precision machine systems, and characterization using metrology systems, instruments and techniques."

---

[438] http://www.mel.nist.gov/wnew/hilights/2008/hlapril08.htm.
[439] http://www.euspen.com/.

A larger international "tip-based nanofabrication" research community is also beginning to coalesce, staging their first international workshop in October 2008 in Taiwan.[440] According to the Conference website:

"Nanofabrication is critical to the realization of the potential benefits of nanotechnology to our society. One enabling technology in nanofabrication is Tip-Based Nanofabrication (TBN), which is through the use of functionalized micro-cantilevers with nanoscale tips. These cantilevered nanotips, basically evolved from scanning probe microscopy (SPM), are able to manipulate environments at nanoscale on the substrates in generating different nanoscale patterns and structures. Many TBN techniques have been developed with different degrees of similarity and success. As a result, the purpose of this first international workshop on TBN is to provide a technical forum for the researchers to discuss the scope and similarity of the TBN technology, to present the state-of-the-art research finding, to foster research collaboration, and to elaborate the needs and challenges facing the TBN community. In addition to the conference proceedings, papers presented in this workshop will be selected and published a special issue in *Journal of Nanoscience & Nanotechnology (JNN)*.[441] The discussion and conclusion of this workshop will also be summarized and disseminated to the TBN community by the workshop organizers. This workshop is sponsored by National Taiwan University of Science and Technology."

A 2008 review of the TBN field by Tseng et al.[442] notes that:

"In TBN, a functionalized cantilevered-tip is the common basic apparatus for performing the tasks of nanofabrication. The nanofabrication applications of three major techniques under the TBN family: atomic force microscopy (AFM), dip-pen nanolithography (DPN), and scanning near-field optical microscopy (SNOM), are studied with the focus on their manipulability over the size, orientation, and position of the nanostructures fabricated. The nanostructures made by these techniques are selectively presented in order to illustrate the versatility and advancement of these tip-based techniques. The information reviewed and illustrated is extrapolated to form the basis for the assessment of the needs and challenges facing the TBN community in the future. A preliminary roadmap over the next seven years is then developed. The prospective approaches and focusing areas for future research and development are also discussed."

The almost exclusive focus of the TBN community at large appears still to be on tip-based methods of fabrication, not on atomic precision *per se*, hence atomically imprecise products are fair game for (and are most commonly sought by) the TBN community.

---

[440] http://www.ntust.edu.tw/tbn2008/.
[441] http://www.aspbs.com/jnn/.

[442] Ampere A. Tseng, Shyankay Jou, Andrea Notargiacomo, T.P. Chen, "Recent Developments in Tip-Based Nanofabrication and Its Roadmap," Journal of Nanoscience and Nanotechnology 8(May 2008):2167-2186.

3. Background on Atomic Force Microscope Systems

AFMs are primarily instruments designed to measure surface topography with a very high spatial resolution. Accordingly, classical AFMs were designed to scan the surfaces of flat / 2D (2.5D) samples. In keeping with the general tendency of combining form/profile measuring instruments with size measuring instruments, recently developed AFM systems are equipped with position measuring sensors for all axes and have been turned into (small) coordinate measuring machines (CMMs) obtaining 3D information from the samples.[443]

In this section the main components and design principles of an AFM system are given followed by an overview of positioning and detection systems after which the imaging and surface sensing process is discussed. The latter is defined by the probe and its interaction with the surface. The probe and the sample have to be understood as a unit – they cannot be treated separately. This aspect may be highlighted as the decisive difference compared to macroscopic coordinate measuring machines: the interaction between probe and sample and the influence of control parameters and environmental conditions of this interaction affect the final result (in relative terms) much more strongly than in the macroscopic world – i.e. the whole system including sample has to be investigated.[444]

The following discussion (in Chapter 3) borrows liberally from the excellent 2006 review of scanning force microscopy for dimensional metrology by Danzebrink et al.[445]

3.1 General Structure and Function of AFMs

The main components of an AFM (Figure 3-1) are:

(1) Probe: a fine tip for the investigation of the sample properties;

(2) Feedback Sensor: detects small changes of the tip or cantilever position (i.e., proportional to the tip-sample interaction);

(3) Z Scanner: keeps the probe under constant conditions (usually at a constant value of the interaction used for control) while scanning the sample surface;

(4) XY Scanner: displaces the probe (scanning probe mode) or alternatively the sample (scanning sample mode) in equidistant steps or continuously at a constant speed;

(5) XY Coarse Positioning: positions and aligns the sample to bring the region of interest on the sample into the reach of the XY scanner; and

(6) Z Coarse Approach: decrease the distance between sample and probe to a value that

---

[443] H.-U. Danzebrink, L. Koenders, G. Wilkening, A. Yacoot, H. Kunzmann, "Advances in Scanning Force Microscopy for Dimensional Metrology," CIRP Annals - Manufacturing Technology 55(2006):841-878..

[444] H.-U. Danzebrink, L. Koenders, G. Wilkening, A. Yacoot, H. Kunzmann, "Advances in Scanning Force Microscopy for Dimensional Metrology," CIRP Annals - Manufacturing Technology 55(2006):841-878..

[445] H.-U. Danzebrink, L. Koenders, G. Wilkening, A. Yacoot, H. Kunzmann, "Advances in Scanning Force Microscopy for Dimensional Metrology," CIRP Annals - Manufacturing Technology 55(2006):841-878..

allows the Z actuator to bring probe and sample sufficiently close so that they interact.

In order to allow positioning in a larger volume, the positioning unit often consists of a dual-stage arrangement with coarse and fine stages. The probing system also consists of different actuating components to move the probe. When the AFM is operated in a dynamic mode (Section 2.1.5) an additional actuator is needed to oscillate the probe at a frequency close to its resonance frequency. In designing an AFM one has the choice of either scanning the sample or the measuring probe. In the case of large objects the sensor head is often moved to the interesting position by (slower) large motion stages, and the actual scan to collect data is then performed by the scanning mechanics integrated in the sensor head.[446]

Figure 3-1. Schematic description of the components of an AFM.[447]

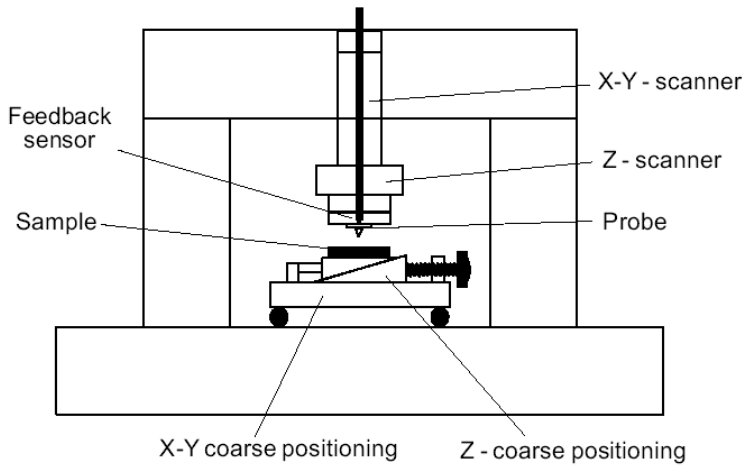

3.1.1 Design Principles

AFMs show lateral and vertical resolutions that are of the order of atomic distances and the sensor structures in the AFM head are extremely delicate. Therefore, AFMs are generally much more sensitive to ambient influences than most other measurement instruments operated over larger measurement ranges. Consequently, both the design of AFMs and the location of their set-up require careful consideration. Temperature changes, turbulence, vibrations, acoustic noise and electronic noise can influence the system significantly and thus lead to drift and noise in the measurement signal.

---

[446] Veeco Instruments, U.S.A., www.veeco.com. PSIA Corp., Sungnam, Korea, www.psiainc.com. Surface Imaging Systems (S.I.S.) GmbH, Herzogenrath, Germany, www.sis-gmbh.com.

[447] H.-U. Danzebrink, L. Koenders, G. Wilkening, A. Yacoot, H. Kunzmann, "Advances in Scanning Force Microscopy for Dimensional Metrology," CIRP Annals - Manufacturing Technology 55(2006):841-878.

3.1.1.1 General Requirements

To ensure that an AFM design is successful, some general and metrologically specific requirements have to be fulfilled during the design process. Among the general characteristics is a stiff linkage between the sample and the sensor head in order to minimise low frequency resonances. The latter limits the bandwidth of the feedback loop that controls the probe-sample distance and determines the maximum scanning speed.[448] Also, the construction and the choice of materials should be such that thermal drift is minimized. Furthermore, the susceptibility of the system to acoustic and electronic noise and contamination as well as temperature variations should be as small as possible. For a metrological AFM the reproducibility of measurements has the highest importance.

Therefore, for AFMs used for dimensional metrology special attention has to be paid to the following topics:

(1) long-term stability of the whole instrument;
(2) small positioning errors of the probe with respect to the sample;
(3) stability of the probe as "detector";
(4) well-known probe-sample interactions;
(5) correct measurement data collection and treatment; and
(6) the possibility to achieve traceability.

3.1.1.2 Thermal Drift

The thermal drift behavior of an AFM can be analysed by the use of the "measurement loop" concept: the shortest possible and metrologically relevant link between tip and sample. The loop is virtually divided into horizontal and vertical sections, each with homogenous thermal behavior (i.e., made from the same material). Figure 3-2A shows the division in vertical (V_n) and horizontal (H_n) directions of the AFM as shown in Figure 3-1. Consider the vertical loop: length changes (caused by temperature changes) of each of these sections are counted positive in the "up going" (left) branch and negative in the "down going" (right) branch. If the same material was used for all sections, the sum of all changes would be zero. However, as this is not possible, the principle idea is to compensate for the thermal behavior of sections in the loop so that a zero effect results, i.e., the gap between tip and sample remains constant. Further details of the effect of thermal drift are given in Section 4.7.2.

---

[448] J.E. Griffith, D.A. Grigg, "Dimensional metrology with scanning probe microscopes," J. Appl. Phys. 74(1993):R83-R109.

Figure 3-2. A. <u>(left)</u> The "measurement loop" of the AFM as shown in Figure 3-1 is the shortest possible and metrologically relevant link between tip and sample. H_i and V_i denote horizontal and vertical sections with homogenous thermal behavior. The sum of length changes has to be kept zero. The sign of length changes are counted clockwise: for the vertical loop, positive in the "up going" branch, and negative in the "down going". B. <u>(right)</u> Comparator' or 'Abbe' error caused by angular deviations during probe scanning.

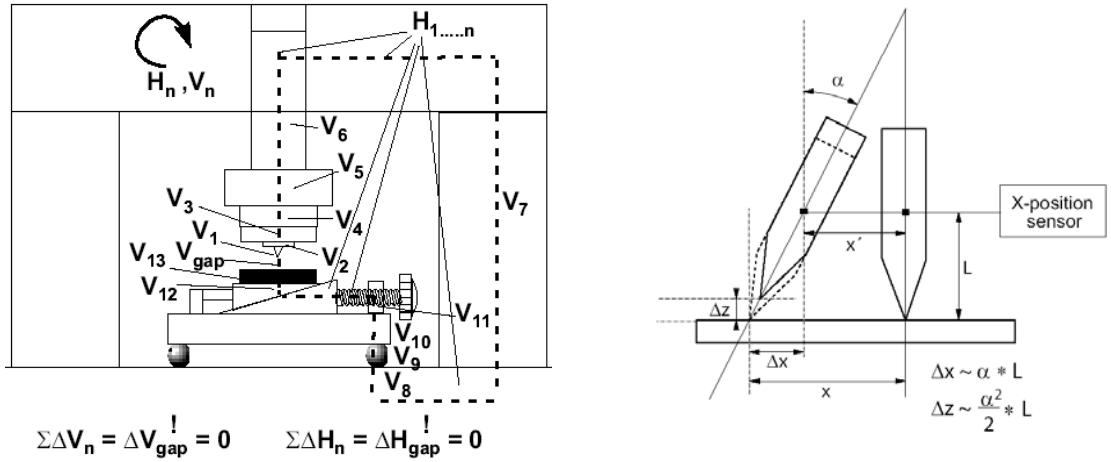

While thermal drifts may be minimized by adhering to this measurement loop principle, the best possible construction of an AFM usually demands some compromises that are not necessarily the best solutions with respect to the desired reduction of thermal drifts. Therefore, AFM users cannot count on optimal thermal behavior of commercial instruments.

3.1.1.3 Positioning Errors

The AFM can be regarded to a certain extent as a small coordinate measuring machine (CMM) in which the probe is moved relative to the object in all three directions. Therefore the movement has 21 degrees of freedom including 3 positioning errors, 6 straightness errors, 9 rotational errors, and 3 squareness errors. In principle, they can be determined and accounted for. Naturally, instruments used for quantitative measurements should have deviations as small as possible. In most cases, the calibration of an AFM is restricted to the three positioning errors and three squareness errors. However, there is a very important measurement error, which is caused by rotational deviations: the "comparator" or "Abbe" error. It appears in cases where, during movement, the position of the tip is not measured at the interaction point, and where tip and/or sample experience changing rotational errors (e.g., tilting). One possible situation is shown in Figure 3-2B, where the position is monitored at a certain distance from the tip ("Abbe offset"), and the angular orientation of the tip is changing during scanning. AFMs with tube scanners suffer badly from this error. In fact, the Abbe error in most instruments is by far the largest contribution to the error budget.

3.1.2 Metrological Instruments

As a consequence of the points discussed in the previous section, a metrological AFM should be designed in a way, such that:

(1) the measurement loop is as small as possible;
(2) the materials in the measurement loop are matched to get a zero thermal effect;
(3) the position of the tip is measured as close as possible to the interaction point (i.e., the "Abbe offset" is close to zero); and
(4) the rotational errors of movement are as small as possible.

There are different approaches to achieving these goals and there is an increasing number of AFMs on the market that offer reasonable solutions. In general, the efforts of commercial providers address the stability (repeatability) issue and they equip their instruments with position monitors for X, Y and Z.[449] If an instrument is stable enough it can be calibrated by artifacts and with care it is possible to reduce significantly the effect of these error sources. Great care is taken in the design of SFMs used by national metrology institutes since these instruments must be able to calibrate artifacts with the smallest achievable uncertainty. These instruments use laser interferometry for displacement measurements and advanced displacement mechanics to minimise "mechanical errors".[450] The basic idea is to measure the relative displacement of tip and sample in all three axes by laser interferometers whose measurement arms are adjusted in a way that they intersect at the interaction point. This well established principle has been investigated and realized in large-scale measurement and manufacturing instruments.[451] Figure 3-3 shows the principle arrangement of a metrology AFM. Here, the sample is scanned in X and Y and moved in Z. The position of the tip is held constant ("Zero detector"). The sample is placed inside a cube mirror corner and the three beams intersect virtually at the interaction point. The laser beams are orthogonal to each other and adjusted parallel to the axes of movement.

A further improvement, which benefits the long-term stability, is to keep the measurement loop small by applying a differential laser interferometer configuration and to attach the reference mirrors of the interferometers to the tip holder. The remaining measurement loop is shown in Figure 3-4. For a complete compensation, one needs to know the resulting thermal expansion coefficient of the mechanical link, and the refractive index of air. Also, as the reflection points on the mirrors are "wandering" during scanning and z-movement, the deviations from flatness of the mirrors have to be known.

---

[449] Veeco Instruments, U.S.A., www.veeco.com. PSIA Corp., Sungnam, Korea, www.psiainc.com. Surface Imaging Systems (S.I.S.) GmbH, Herzogenrath, Germany, www.sis-gmbh.com. Asylum Research, 6310 Hollister Ave, Santa Barbara, CA 93117, USA, http://www.asylumresearch.com.

[450] e.g. 6-axes, long-travel piezo nanopositioning/ scanning stage (P-587) from Physik Instrumente (PI) GmbH, Karlsruhe/Palmbach, Germany, www.pi.ws.

[451] J.B. Bryan, "The Abbe Principle revisited: An updated interpretation," Prec. Eng. 1(1979):129-132. J.B. Bryan, "Design and construction of an ultraprecision 84 inch diamond turning machine," Prec. Eng., 1(1979):13-17.

Figure 3-3. Elimination of the "Abbe error" by adjusting the beams of three laser interferometers in a way that they virtually intersect at the interaction point. The beams are reflected from the three orthogonal planes of a (hollow) mirror cube. (A) principle; (B) realization in the Nano Measuring and Positioning Machine.[452]

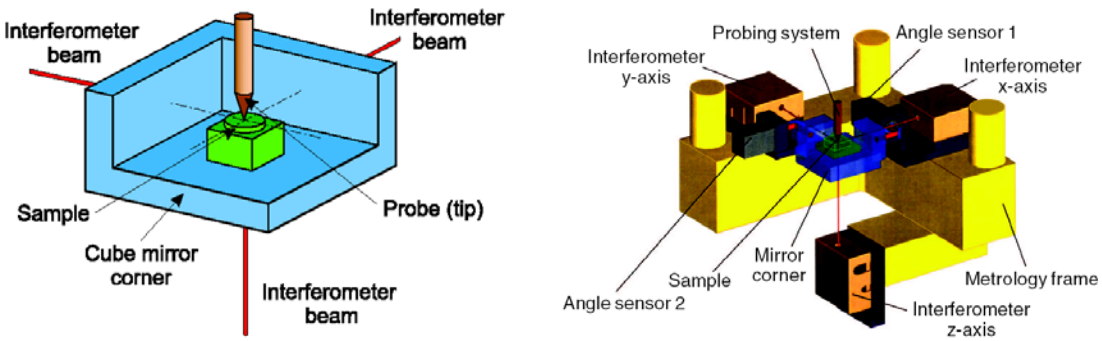

(A) **(B)**

Figure 3-4. (A) Keeping the measurement loop small: Principle arrangement of laser interferometers in X (or Y) and Z directions. The resulting measurement loops are also shown (c.f., Figure 3-2A). (B) Realization of such an arrangement in a metrology AFM.[453]

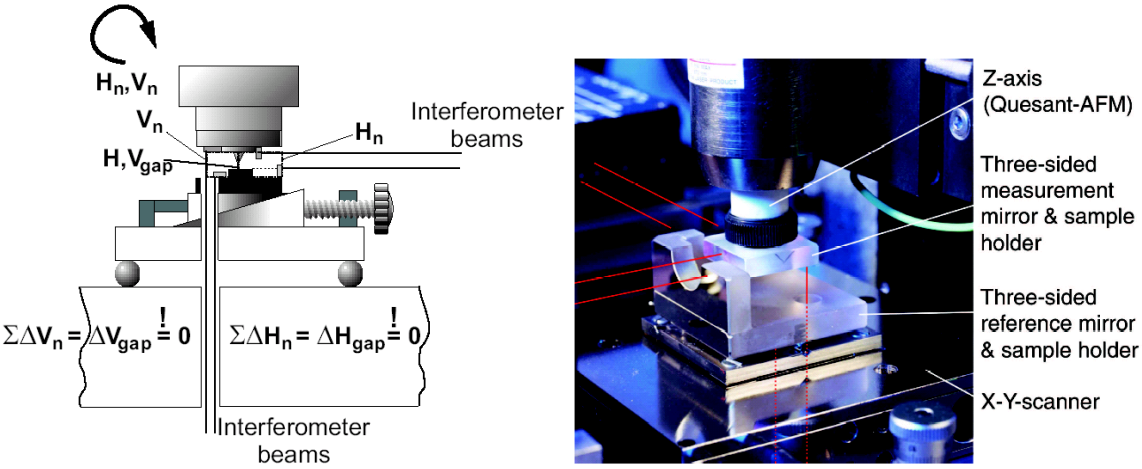

(A) **(B)**

---

[452] G. Jäger, E. Manske, T. Hausotte, H.-J. Büchner, R. Grünwald, W. Schott, "Nanometrology - nanomeasuring machines," Proc. Annual Meeting of ASPE, Crystal City, Virginia, USA, 2001, pp. 23-27. SIOS Meßtechnik GmbH, Ilmenau, Germany, www.sios.de.

[453] J. Haycocks, K. Jackson, "Traceable calibration of transfer standards for scanning probe microscopy," Prec. Eng. 29(2005):168-175.

Several National Metrology Institutes have developed metrologically sound designs with small measurement loops according to the principles outlined in Section 3.1.1.1.[454] Figure 3-4 shows a principle sketch of an AFM of the scanning sample type where laser differential interferometers are used to minimize the measurement loop. Such AFMs fulfill at least the first two necessary prerequisites for quantitative measurements as listed in Section 3.1.1.1. Provided that the other four requirements are also fulfilled, error budgets can be formed and uncertainty figures can be stated.

Uncertainty statements for metrology SFMs are listed in Table 3-1. Some of these claims have been verified by international key comparisons and they have been entered into the "CMC" list which is a collection of reviewed uncertainty statements.[455] We'll discuss these and related systems in greater detail in Section 4.6.

---

[454] J. Haycocks, K. Jackson, "Traceable calibration of transfer standards for scanning probe microscopy," Prec. Eng. 29(2005):168-175. S. Gonda, T. Doi, T. Kurosawa, Y. Tanimura, N. Hisata, T. Yamagishi, H. Fujimoto, H. Yukawa, "Real-time, interferometrically measuring atomic force microscope for direct calibration of standards," Rev. Sci. Instr. 70(1999):3362-3368. Ichiko Misumi, Satoshi Gonda, Qiangxian Huang, Taeho Keem, Tomizo Kurosawa, Akihiro Fujii, Nahoko Hisata, Takeshi Yamagishi, Hirohisa Fujimoto, Ken Enjoji, Sunao Aya, Hiroaki Sumitani, "Sub-hundred nanometre pitch measurements using an AFM with differential laser interferometers for designing usable lateral scales," Meas. Sci. Technol., 16(2005):2080-2090. G.B. Picotto, M. Pisani, "A sample scanning system with nanometric accuracy for quantitative SPM measurements," Ultramicroscopy, 86(2001):247-254. J. Kim, J.W. Kim, B.C. Park, T.B. Eom, C. Kang, "Pitch measurement of one-dimensional gratings using a metrological atomic force microscope," Proc. of the 4th Euspen conference, Glasgow, Scotland, May 31th-June 2nd, 2004, pp. 248-249. R. Dixson, R. Köning, J. Fu, T. Vorburger, B. Renegar, "Accurate dimensional metrology with atomic force microscopy," Proc. SPIE 3998(2000):362-368. M. Bienias, S. Gao, K. Hasche, R. Seemann, K. Thiele, "A metrological scanning force microscope used for coating thickness and other topographical measurements," J. Appl. Phys. A 66(1998):837-842.

[455] Key Comparison Data Base, BIPM, France, http://kcdb.bipm.org.

Table 3-1 Uncertainties (at 95% confidence level) stated by National Metrology Institutes for their metrological SPMs (from Danzebrink)[456]

National Metrology Institute	Instrument			Uncertainties			Remarks
	Meas. range X x Y x Z (μm)	**Scan-ning Type**	**Traceability**	**2(3) D lateral distance L (nm)**	**Mean pitch p of periodic structures (nm)**	**Step height h (nm)**	
AIST/NMIJ, Japan[457]	17.5 x 17.5 x 2.5	sample X/Y/Z	Homodyne laser interferometers in 3 axes		$(0.32^2 + (2 \times 10^{-5} \times p)^2)^{1/2}$ p in nm*	$(0.35^2 + (8.0 \times 10^{-4} \times h)^2)^{1/2}$ h in nm	Purpose-built
AIST/NMIJ, Japan[458]	100 x 100 x 12	sample X/Y/Z	Homodyne laser interferometers in 3 axes		$(0.16^2 + (9.9 \times 10^{-6} \times p)^2)^{1/2}$ p in nm	$(0.31^2 + (2.6 \times 10^{-5} \times h)^2)^{1/2}$ h in nm	Purpose-built
CMS/ITRI, Taiwan	100 x 100 x 10	sample X/Y/Z	Homodyne laser interferometers in 3 axes		0.5 nm		Purpose-built with commercial head
DFM, Denmark	70 x 70 x 6	tip X/Y/Z	Grating and step height certified by Metas and PTB	0.0015 x L L in nm	$(0.36^2 + (1.6 \times 10^{-3} \times p)^2)^{1/2}$ p in nm*	$(0.26^2 + (1.6 \times 10^{-6} \times h)^2)^{1/2}$ h in nm	Most BMCs will be accredited by DANAK soon
IMGC, Italy[459]	30 x 30 x 18	sample X/Y	Capacitive transducers calibrated by	$(3^2 + 1 \times 10^{-3} \times L)^{1/2}$ L in nm	$(2^2 + (1 \times 10^{-3} \times p)^2)^{1/2}$ p in nm*	$(2^2 + (1 \times 10^{-3} \times h)^2)^{1/2}$ h in nm	Home-built

[456] H.-U. Danzebrink, L. Koenders, G. Wilkening, A. Yacoot, H. Kunzmann, "Advances in Scanning Force Microscopy for Dimensional Metrology," CIRP Annals - Manufacturing Technology 55(2006):841-878.

[457] S. Gonda, T. Doi, T. Kurosawa, Y. Tanimura, N. Hisata, T. Yamagishi, H. Fujimoto, H. Yukawa, "Real-time, interferometrically measuring atomic force microscope for direct calibration of standards," Rev. Sci. Instr. 70(1999):3362-3368. S. Gonda, T. Doi, T. Kurosawa, Y. Tanimura, N. Hisata, T. Yamagishi, H. Fujimoto, H. Yukawa, "Accurate topographic images using a measuring atomic force microscope," Applied Surface Science, 144(April 1999):505-509. I. Misumi, S. Gonda, T. Kurosawa, K. Takamasu, "Uncertainty in pitch measurements of onedimensional grating standards using a nanometrological atomic force microscope," Meas. Sci. Technol. 14(7 March 2003):463-471. I. Misumi, S. Gonda, T. Kurosawa, Y. Tanimura, N. Ochiai, J. Kitta, F. Kubota, M. Yamada, Y. Fujiwara, Y. Nakayama, K. Takamasu, "Submicrometre-pitch intercomparison between optical diffraction, scanning electron microscope and atomic force microscope," Meas. Sci. Technol. 14(6 October 2003):2065-2074; http://www.nano.pe.u-tokyo.ac.jp/pdffiles/mst3_12_004.pdf. I. Misumi, S. Gonda, T. Kurosawa, Y. Azuma, T. Fujimoto, I. Kojima, T. Sakurai, T. Ohmi, K. Takamasu, "Reliability of parameters of associated base straight line in step height samples: Uncertainty evaluation in step height measurements using nanometrological AFM," Prec. Eng. 30(2006):13-22. http://www.nmij.jp/dms-std/Paper/2005/Paper 4.pdf.

[458] I. Misumi, S. Gonda, T. Kurosawa, K. Takamasu, "Uncertainty in pitch measurements of onedimensional grating standards using a nanometrological atomic force microscope," Meas. Sci. Technol. 14(7 March 2003):463-471.

[459] G.B. Picotto, M. Pisani, "A sample scanning system with nanometric accuracy for quantitative SPM measurements," Ultramicroscopy, 86(2001):247-254.

			laser interferometers				
KRISS, Korea[460]	100 x 100 x 12	sample X/Y	Heterodyne laser interferometer in X/Y; calibrated capacitive transducer in Z	$(4.3^2 + (2.8 \times 10^{-4} \times L)^2)^{1/2}$ L in nm	$(0.22^2 + (2.8 \times 10^{-4} \times p)^2)^{1/2}$ p in nm	$(0.19^2 + (7.8 \times 10^{-4} \times h)^2)^{1/2}$ h in nm	Modified commercial instrument
LNE, France	300,000 x 300,000 x 50	sample X/Y	Calibrated capacitive transducers for Z axis, interferometers and 2D optical encoders for X and Y axis				Home-built, not yet evaluated as the X-Y stage is not fully characterized
METAS, Switzerland[461]	tip: 70 x 70 5 sample: 380	tip: X/Y/Z sample: X	Homodyne laser interferometer	$(1^2 + (5 \times 10^{-5} \times L)^2)^{1/2}$ L in nm	$5 \times 10^{-5} \times p$ p in nm*	$(1^2 + (5 \times 10^{-3} \times h)^2)^{1/2}$ h in nm*	Commercial metrology AFM head and linear long range stage
MIKES, Finland	100 x 100 x 16	sample X/Y/Z	Position sensors calibrated by interferometry and 1D grids (calibrated by laser diffractometer)	$(3^2 + (1 \times 10^{-3} \times L)^2)^{1/2}$ L in nm		$(0.5^2 + (2 \times 10^{-4} \times h)^2)^{1/2}$ h in nm	Commercial SFM: preliminary characterization going on
NIM, China	70 x 15 x 8	sample X/Y/Z	Homodyne laser interferometers in 3 axes	$(2^2 + (1 \times 10^{-4} \times L)^2)^{1/2}$ L in nm	$(0.5^2 + (1 \times 10^{-4} \times p)^2)^{1/2}$ p in nm	$(1^2 + (1 \times 10^{-4} \times h)^2)^{1/2}$ h in nm	Modified commercial instrument
NIST, USA[462]	50 x 50 x 5	sample X/Y/Z	Heterodyne laser interferometer in X/Y; calibrated capacitive transducer in Z		$(3^2 + (2 \times 10^{-3} \times p)^2)^{1/2}$ p in nm*	$(0.1^2 + (1 \times 10^{-3} \times h)^2)^{1/2}$ h in nm	Commercial SFM head
NMI-VSL, Netherlands[463]	100 x 100 x 20	sample X/Y/Z	Heterodyne laser interferometers	Work in progress;	To be estimated	To be estimated	Home built metrology frame

[460] J. Kim, J.W. Kim, B.C. Park, T.B. Eom, C. Kang, "Pitch measurement of one-dimensional gratings using a metrological atomic force microscope," Proc. of the 4th Euspen conference, Glasgow, Scotland, May 31th-June 2nd, 2004, pp. 248-249.

[461] F. Meli, R. Thalmann, "Long range AFM profiler used for accurate pitch measurements," Meas. Sci. Technol., 9(1998):1087-1092. F. Meli, et al., "Z-calibration of a metrology AFM scanner using an interferometer and a tilting device with linear stage," Proc. of the Third Seminar on Quantitative Microscopy, Lyngby, Denmark, PTB-F-34, 1998, pp. 61-67. F. Meli, "International comparison in the field of nanometrology: Pitch of 1D gratings," Nano4, Proc. of 2nd Int. EUSPEN Conference, Italy, Vol. 1, 2001, pp. 358-361. F. Meli, "Lateral and vertical diameter measurements on polymer particles with a metrology AFM," in: G. Wilkening, L. Koenders, eds., Nanoscale Calibration Standards and Methods, Wiley-VCH, Weinheim, Germany, 2005, pp. 361-374.

[462] R. Dixson, R. Köning, J. Fu, T. Vorburger, B. Renegar, "Accurate dimensional metrology with atomic force microscopy," Proc. SPIE 3998(2000):362-368.

			in 3 axes	goal is 1 nm in 3D			using commercial scanning stage and SPM head
NPL, UK[464]	100 x 100 x 5	sample X/Y	Homodyne laser interferometers in 3 axes		$(0.2^2 + (2 \times 10^{-4} \times p)^2)^{1/2}$ p in nm	$(0.4^2 + (6 \times 10^{-3} \times h)^2)^{1/2}$ h in nm	Modified commercial instrument
PTB, Germany[465]	75 x 15 x 15	sample X/Y/Z	Homodyne laser interferometers in 3 axes			$(1^2 + (5 \times 10^{-4} \times h)^2)^{1/2}$ h in nm*	Modified commercial instrument
PTB, Germany[466]	25,000 x 25,000 x 5,000	sample X/Y/Z	Homodyne laser interferometers in 3 axes		$(0.002^2 + (3 \times 10^{-5} \times p)^2)^{1/2}$ p in nm**	$(0.6^2 + (7.5 \times 10^{-5} \times h)^2)^{1/2}$ h in nm	Combined SFM + piezo stage + nano positioning machine
* Entry in the CMC (Calibration and Measurement Capabilities of the NMIs), a database published by the BIPM.[467] ** Due to the long measurement range, the uncertainty of the mean pitch value is extremely small.							

3.1.3 Commercial Instruments

According to their structure, AFMs can be divided into scanning probe, scanning sample, separated XY and Z scanning motion and combined tip and sample scanning systems. Scanning sample systems are widely used in commercial SPMs because they are simpler than other systems. However, these systems have limitations on sample size and sample mass. Compared with the conventional three-axis tube scanner-based structure, scan-systems with separated XY and Z scanner (e.g., flexure XY scanner and tube Z scanner) not only increase scanning speed by a factor of ten, but also show very small non-linearity errors. The combined tip and sample scanning systems provide not only more flexibility, but also larger scan ranges both in the horizontal and in the vertical dimension.

The linearity of scanners is improved by software or by external sensors. Inexpensive open-loop systems with software corrections may depart from true linear behavior by as much as 10%, and closed-loop systems equipped with capacitive sensors, strain gauge sensors, or optical scan-

---

[463] K. Dirscherl, K.R. "Traceable probing with an AFM," in: G. Wilkening, L. Koenders, eds., Nanoscale Calibration Standards and Methods, Wiley-VCH, Weinheim, Germany, 2005, pp. 95-108.

[464] J. Haycocks, K. Jackson, "Traceable calibration of transfer standards for scanning probe microscopy," Prec. Eng. 29(2005):168-175.

[465] L. Koenders, R. Bergmans, J. Garnaes, J. Haycocks, N. Korol, T. Kurosawa, F. Meli, B.C. Park, G.S. Peng, G.B. Picot, E. Prieto, S. Gao, B. Smereczynska, T. Vorburger, G. Wilkening, "WGDM-7: Preliminary comparison on nanometrology according to the rules of CCL key comparisons. Nano 2 Step height standards," Metrologia Technical Report, 40(2003):04001.

[466] L. Koenders, P. Klapetek, F. Meli, G.B. Picotto, "Comparison on step height measurements in the nano and micrometre range by Scanning Force Microscopes," Metrologia Technical Report 43(2006):04001.

[467] Key Comparison Data Base, BIPM, France, http://kcdb.bipm.org

correction systems can reduce the total non-linearity of the system to less than 1%. Lateral scan ranges of commercial AFMs are mostly from 0.5 µm to about 100 µm, and vertical scan ranges are of the order of 10 µm. Most AFM systems offer different scanners for different scan ranges in order to keep the range/resolution ratio constant. The data acquisition software collects images with sizes up to 4096 × 4096 pixels, and image processing software enables quantitative statistical analysis. Also, calibration often is supported by appropriate routines. According to the area of application, AFM systems can be divided into those that are predominantly used in research laboratories and those that are used in industry (close to production). Industrial AFMs are an essential inspection tool in the semiconductor industry for the measurement of surface roughness, trench width, depth, side wall slope, line width, etc. Industrial AFMs often feature advanced automatic operation. For instance, some systems can automatically find optimal feedback parameters and scanning speeds for a given sample size and surface. Also, they often have extended positioning ranges. Systems are equipped with XY stages of 200 mm × 200 mm up to 1100 mm × 1300 mm for measurements on wafers or flat panel displays].[468]

The trend of commercial manufacturers in designing commercial AFMs is to work towards attaining higher accuracy, higher measurement speed and to meet special demands of customers. Besides developing AFM itself, some manufacturers integrate AFM with other instruments, such as conventional optical microscopy, scanning near-field optical microscopy (SNOM) or scanning electrom microscopy (SEM), or Raman microscopes.

3.2 Scanning Systems

In order to determine the dimensions of a nano structure, a three dimensional measurement has to be carried out, i.e., measurand (sample) and sensor have to be positioned with respect to each other in three dimensions and in such a way that all necessary information can be collected. In practice, the 3D positioning is often split into a movement of the measurand and of the detection system, with the positioning in the z-direction accomplished by the detection system – either intrinsically, or together with the z-axis of the instrument.

Positioning comprises two aspects:[469] movement or "displacement" to a position, requiring a positioning system (Section 3.2.1), and subsequent measurement of the proper position reached, requiring a detection system (Section 3.2.2). More specifically, to make a high-accuracy picopositioner system, we need an apparatus capable of performing a precise positioning displacement (Section 3.2.1) and a second apparatus for measuring the displacement to very high precision (Section 3.2.2).

---

[468] Veeco Instruments, U.S.A., www.veeco.com. PSIA Corp., Sungnam, Korea, www.psiainc.com.

[469] G. Wilkening, Positionierungen in der Nanotechnologie, VDI-Bericht 1530 Sensoren und Meßsysteme, VDI Verlag Düsseldorf, 2000.

3.2.1 Positioning Systems

Traditionally, SPMs have a coarse static positioning range with no (or only moderately accurate) position measurement, and often a quite restricted scanning range. Positioning apparatuses can be divided roughly into two categories:

(1) Positioning apparatus with sub-nanometer resolution and restricted positioning range of a few 100 µm at most.
(2) Positioning apparatus with a large positioning range and resolution in the micrometer range.

The first category is dominated by the flexure hinge principle, while the second comprises sliding or rolling guides.

In order to achieve the desired resolution and positioning range it might be necessary to combine both principles, for example, a flexure hinge stage on a plane table with air bearings. A solution which in principle covers both – that is, high resolution *and* large range – is the so-called nano positioning machine.[470] Of course, large positioning ranges require large mechanical structures and hence such apparatuses have low resonance frequencies. Table 3-2 lists the possible scanning systems used in AFMs, together with their properties.

Except for some of the monolithic scanning stages made from metal or silicon, the scanning stages listed in Table 3-2 all show distinct deviations from perfect rectangular and straight motion. The approaches that do not use piezo ceramics as guiding element material normally show very good repeatability; hence their behavior is predictable and can be calibrated. However, except for the micro-mechanical scanner which has to be looked at as a special case, all state-of-the-art AFMs use piezo ceramics as actuator material, and hence suffer from its pronounced non-ideal properties.

Table 3-2. Positioning apparatuses with flexure hinges, with at least 2D displacements (from Danzebrink)[471]

Guiding Element		Actuation	Positioning Resolution (pm)	Displacement Range up to (µm x µm)	Realizations and Remarks
Principle	**Material**				
Monolithic	Piezo ceramic	active guiding element (piezo)	< 100	100 x 100	Tube scanner; characteristic for conventional SPMs[472] and "credit card"-AFM[473]

[470] G. Jäger, E. Manske, T. Hausotte, H.-J. Büchner, R. Grünwald, W. Schott, "Nanometrology - nanomeasuring machines," Proc. Annual Meeting of ASPE, Crystal City, Virginia, USA, 2001, pp. 23-27. SIOS Meßtechnik GmbH, Ilmenau, Germany, www.sios.de.

[471] H.-U. Danzebrink, L. Koenders, G. Wilkening, A. Yacoot, H. Kunzmann, "Advances in Scanning Force Microscopy for Dimensional Metrology," CIRP Annals - Manufacturing Technology 55(2006):841-878.

Monolithic	Al, steel, Invar, Si	extension actuator (generally piezo)	100	100 x 100	Scanning stages for SPMs, micro-lithography, nano- and micro-manufacturing, measuring instruments in general[474]
Micro-mechanical – monolithic	Si	electrostatic	< 100	10 x 10	Micro-mechanical scanner for micro-SPMs and micro-optical applications[475]
Composite	Piezo ceramic	active piezo-bimorph, parallel spring guiding	< 100	30 x 30	Bimorph scanner for SPMs[476]
Composite	Piezo ceramic	active guiding element (piezo)	< 100	10 x 10	Tripod scanner: characteristic for early STMs and SPMs for surface research[477]
Composite	Spring steel	extension of bending actuators (generally piezo)	100	≥ 100 x 100	Scanning tables with larger displacement-to-outer-dimension ratio; multi-dimensional displacements; displacements in combination with rotations;[478] used in a number of up-to-date SPMs

---

[472] G. Binnig, D.P.E. Smith, "Single-tube three-dimensional scanner for scanning tunneling microscopy," Rev. Sci. Instr. 57(1986):1688-1689. J.E. Griffith, G.L. Miller, C.A. Green, D.A. Grigg, P.E. Russell, "A scanning tunneling microscope with a capacitance-based position monitor," J. Vac. Sci. Technol. B 8(1990):2012-2027.

[473] A. Bergander, W. Driesen, T. Varidel, J.-M. Breguet, "Monolithic piezoelectric actuators for miniature robotic systems," 9th Intl. Conf. on New Actuators (Actuator 2004), pp. 114-117.

[474] R. Glöß, P. Pertsch, "Systeme der Nanopositionierung," Feinwerk & Messtechnik, 107(1999):64-68. E. Furokawa, M. Mizuno, D. Doi, "Development of a flexure-hinged translation mechanism driven by two piezoelectric stacks," JSME Int. Journ. C 38(1995):743-748. Nano Positioning Product Overview; Queensgate Ltd., Bracknell, UK; www.queensgate.com. Nanopositioning 1998; Physik Instrumente (PI) GmbH, Karlsruhe/Palmbach, Germany, www.pi.ws. S. Gonda, T. Kurosawa, Y. Tanimura, "Mechanical performance of a symmetrical, monolithic three-dimensional fine-motion stage for nanometrology," Meas. Sci. Technol. 10(1999):986-993.

[475] F. Ayela, J. Chaussy, T. Fournier, E. Menegaz, "A micromachined actuator for nanopositioning in two dimensions," Sens. and Act., 76(1999):459-462. J.A. Heimberg, T. Zijlstra, E.W.J.M. Van der Drift, D.G. Van Loon, E. DeKuyper, H.J. Hug, J.W.M. Trenken, "New scanning probes for nanotribology," Proc. 2nd Seminar Quantitative Microscopy, PTB-Bericht-F-30, 1997, pp. 25-31.

[476] P. Muralt, D.W. Pohl, W. Denk, "Wide-range, low-operating-voltage, bimorph STM: Application as potentiometer," IBM J. Res. Develop. 30(1986):443-450. X. Zhao, "Scanning probe microscope with high resolution capacitive transducers," PTB-Bericht-F-32, Braunschweig. Wirtschaftsverlag. NW, Verl. für Neue Wiss., Bremerhaven, 1998.

[477] G. Binnig, H. Rohrer, "Scanning tunneling microscopy," Helv. Phys. Acta, 55(1982):726-735; G. Binnig, C.F. Quate, Ch. Gerber, "Atomic force microscope," Phys. Rev. Lett. 56(1986):930-933.

[478] Nano Positioning Product Overview; Queensgate Ltd., Bracknell, UK; www.queensgate.com. Nanopositioning 1998; Physik Instrumente (PI) GmbH, Karlsruhe/Palmbach, Germany, www.pi.ws. K. Lieberman, N. Ben-Ami, A. Lewis, "A fully integrated near-field optical, far-field optical and normal-force scanned probe microscope," Rev. Sci. Instr. 67(1996):3567- 3572.

Note that there appear to be acceptable positioning technologies (primarily piezo-based) that can actively position AFM tips to an accuracy of better than 100 pm over ranges of 10-100 microns, as will be required for our molecular workstation.

3.2.2 Detection Systems

The second part of positioning is the measurement of the position. This is accomplished with suitable transducers, such as inductive, capacitive, or optical sensors. As with the positioning apparatus, the applicable sensors depend on the positioning range. Some methods are principally suited only for ranges of a few 100 µm, whereas others cover the range of up to 100 mm and more. Sometimes, and especially in low-resolution AFMs, movement and position measurement are merged. However, the use of the control voltage of a piezo as a position indicator is afflicted with pronounced non-ideal properties (see below).

3.2.2.1 Survey of Detection Systems

Table 3-3 lists methods that may be used for position measurements, as compiled by Danzebrink et al.[479] in 2005-2006. Interferometers are the first choice when traceability is needed. In commercial SPMs, capacitive, strain gauge and simple intensity-optical transducers are most often used. All other sensors mentioned need calibration, which in most cases has to be accomplished in situ, as the actual mounting conditions influence their properties. That having been said, care must be taken when using optical interferometry to remove the sources of error associated with them.

In AFM the imaging contrast is evaluated from force interactions between probe and sample. These forces result in a displacement or a change of the dynamic behavior of the probe. The "geometrical response" can be measured with sub-nanometre resolution. In the ideal realization, forces would be detected at the place of the tip/sample interaction. In reality, the motion of the tip is mostly measured by monitoring the movement of the cantilever arm, which carries the tip.

In the first AFM, the deflection of the cantilever was measured with an STM[480] – the backside of the cantilever was metalized, and a tunneling tip was brought close to it to measure the deflection.[481]

---

[479] H.-U. Danzebrink, L. Koenders, G. Wilkening, A. Yacoot, H. Kunzmann, "Advances in Scanning Force Microscopy for Dimensional Metrology," CIRP Annals - Manufacturing Technology 55(2006):841-878.

[480] G. Binnig, D.P.E. Smith, "Single-tube three-dimensional scanner for scanning tunneling microscopy," Rev. Sci. Instr. 57(1986):1688-1689.

[481] G. Binnig, C.F. Quate, Ch. Gerber, "Atomic Force Microscopy," Phys. Rev. Lett. 56(3 March 1986):930-933.

Table 3-3. Position measurement methods with reproducible resolution of <50 nm (from Danzebrink)[482]

Principle		Possible number of axes	Reso-lution	Rel. meas. range	Measure-ment range	Remarks
Capacitive		multi	100 pm	2 x 10^{-5}	≤ 300 µm	arrangements with 2 "active" capacitor plates show better resolution than those with one plate "earthed"[483]
						segmented plate structures in the XY plane[484]
Inductive		one	several 1000 pm	10^{-4}	some 100 µm	"LVDT" ; integrated or modular arrangement with free suspended magnetic core
Intensity-optical		multi	several 1000 pm	10^{-4}	some 100 µm	light intensity varying with displacement[485]
Incre-mental-optical	linear	one	1000 pm	10^{-8}	≤ 100 mm	Phase grating on Zerodur with interferential reading head[486]
	2D	two	10,000 pm	10^{-7}	≤ 100 mm x 100 mm	Phase grating on glass with interferential reading head[487]
		two	100 pm	10^{-4}	1 µm x 1 µm	crystalline lattice (e.g., HOPG) with STM- or AFM-based reading head[488]

---

[482] H.-U. Danzebrink, L. Koenders, G. Wilkening, A. Yacoot, H. Kunzmann, "Advances in Scanning Force Microscopy for Dimensional Metrology," CIRP Annals - Manufacturing Technology 55(2006):841-878.

[483] Nano Positioning Product Overview; Queensgate Ltd., Bracknell, UK; www.queensgate.com. Nanopositioning 1998; Physik Instrumente (PI) GmbH, Karlsruhe/Palmbach, Germany, www.pi.ws. X. Zhao, "Scanning probe microscope with high resolution capacitive transducers," PTB-Bericht-F-32, Braunschweig. Wirtschaftsverlag. NW, Verl. für Neue Wiss., Bremerhaven, 1998.

[484] P.W. Kolb, R.S. Decca, H.D. Drews, "Capacitive sensor for micropositioning in two dimensions," Rev. Sci. Instr. 69(1998):310-312. K.R. Koops, R. Banning, P.M.L.O. Scholte, W. Chr. Heerens, J.M.T.A. Adriaens, W.L. de Koning, "Sub-Angstrom resolution position feedback and control in Scanning Probe Microscops," Proc. 2nd Seminar Quantitative Microscopy, PTB-Bericht-F-30, 1997, pp. 32-39.

[485] DI "new" Metrology head, and older Park head with optical sensor for z-axis, both cited in: H.-U. Danzebrink, L. Koenders, G. Wilkening, A. Yacoot, H. Kunzmann, "Advances in Scanning Force Microscopy for Dimensional Metrology," CIRP Annals - Manufacturing Technology 55(2006):841-878.

[486] e.g., Dr. Johannes Heidenhain GmbH, Traunreut, Germany, http://www.heidenhain.de; Heidenhain (company), http://www.heidenhain.com/.

[487] e.g., Dr. Johannes Heidenhain GmbH, Traunreut, Germany, http://www.heidenhain.de; Heidenhain (company), http://www.heidenhain.com/.

[488] H. Kawakatsu, T. Higuchi, "A dual tunneling unit scanning tunneling microscope," J. Vac. Sci. Technol. 8(January 1990):319-323. M. Aketagawa, K. Takada, N. Takeshina, K. Yamada, J.-D. Lee, "Long atomic imaging over a 5-µm-long region using an ultralow thermally drifted dual-tunneling-unit scanning tunneling microscope in a thermostabilized cell," Rev. Sci. Instr. 70(1999):133-136. M. Aketagawa, K. Takada, P. Rerkkumsup, Y. Togawa, H. Honda, "Real-time atomic encoder using scanning tunnelling microscope and regular crystalline surface," Meas. Sci. Technol. 17(2006):513-518.

Strain gauge		multi	1000 pm	10^{-5}	some 100 μm	strain gauge attached to flexures of guiding apparatus
Multi-beam inter-ferometer		one	100 pm 10 pm *	10^{-7}	< 1 mm	Fabry-Pérot Interferometer; demands highest guiding quality; operational modes: quasi-continuous and discrete (λ/2 steps)
Two-beam-inter-fero-meter	Triple reflector	one	1000 pm	10^{-9} **	some m	Homodyne and heterodyne interferometers; moderate guiding quality needed[489]
	Plane mirror	multi	300 pm	10^{-9} **	≤ 1 m	good guiding and mirror quality necessary[490]
	Fiber	multi	300 pm	10^{-6}	< 500 μm	fiber arrangement with integrated splitter and fiber exit plane as reference mirror[491]
X-ray interfer-ometer		one	< 100 pm	10^{-5}	< 10 μm	Extreme guiding quality necessary; generally, monolithic flexure hinge arrangement from Si;[492] in combination with optical interferometer measurement ranges of up to mm[493]
* Highest resolution in the discrete mode ** In vacuum, and with lasers stabilized on absorption lines						

Subsequent designs used optical (e.g., beam-bounce, interferometer) methods[494] for measuring the cantilever deflection. The deflection of silicon cantilevers is most commonly measured by optical detection through an interferometer or by bouncing a light beam of the cantilever and measuring its deflection (optical beam-deflection[495] or "beam bounce method"). In this case a light beam is reflected from the back side of the cantilever towards a 4-segment photodetector, allowing both, bending and twisting deflections of the cantilever to be detected.[496]

---

[489] Linear interferometers and plane mirror interferometers are available from a number of suppliers.

[490] Linear interferometers and plane mirror interferometers are available from a number of suppliers.

[491] D. Rugar, H.J. Mamin, R. Erlandsson, J.E. Stern, B.D. Terris, "Force microscope using a fiberoptic displacement sensor," Rev. Sci. Instrum. 59(1988):2337-2340. Surface Imaging Systems (S.I.S.) GmbH, Herzogenrath, Germany, www.sis-gmbh.com.

[492] G. Basile, P. Becker, A. Bergamin, G. Cavagnero, A. Franks, K. Jackson, U. Kuetgens, G. Mana, E.W. Palmer, M. Stedman, J. Stümpel, A. Yacoot, G. Zosi, "COXI – A Combined Optical and Xray Interferometer for high precision dimensional metrology," Proc. Roy. Soc. Lond. A 456(2000):701-729.

[493] P. Becker, J. Stümpel, "X-ray optics in metrological application," Metrologia 27(1990):127-132.

[494] L. Howald, Rasterkraftmikroskopie an Silizium und Ionenkristallen im Ultrahochvakuum, Ph.D. thesis, Universitat Basel, Switzerland, 1994.

[495] G. Meyer, N.M. Amer, "Simultaneous measurement of lateral and normal forces with an optical-beam-deflection atomic force microscope," Appl. Phys. Lett. 53(1988):1045-1047. S. Alexander, L. Hellemans, O. Marti, J. Schneir, V. Elings, P.K. Hansma, M. Longmire, J. Gurley, "An atomic-resolution atomic-force microscope implemented using an optical lever," J. Appl. Phys. 65(1989):164-167.

[496] D. Sarid, Scanning Force Microscopy, 2nd Ed., Oxford University Press, New York, 1994.

Interferometric methods are based on homodyne[497] or heterodyne[498] techniques. There are also a number of solutions that use a fibre-optic interferometer,[499] where the cleaved end of a single-mode optical fibre and the cantilever act as a Fabry-Pérot interferometer. For this arrangement, noise figures of a few 10^{-4} Å/Hz$^{1/2}$ have been reported. The latter is also used in commercial AFMs.[500] Other methods using a laser diode placed close to the cantilever, such as a combined light source and light detector[501] or capacitance based detectors[502] and other non-optical methods (i.e., Section 2.3.3, Section 2.3.4) have been applied.

Other work began using electrical methods (piezoresistive, piezoelectric)[503] for measuring the cantilever deflection. The deflection of piezoresistive cantilevers is usually measured by making them part of a Wheatstone bridge.[504] Like piezoresistive sensors, quartz tuning forks (i.e., qPlus sensors) have the advantage of self-sensing – in these cases, the use of optics is not necessary and operation in ultrahigh vacuum and low temperatures is easily implemented.[505]

---

[497] G.M. McClelland, R. Erlandsson, S. Chiang, "Atomic force microscopy: General principles and a new implementation," Vol. 6, in: D.O. Thompson, D.E. Chimenti, eds., Review of Progress in Quantitative Non-Destructive Evaluation, Plenum, New York, 1987, p. 307. R. Erlandsson, G.M. McClelland, C.M. Mate, S. Chiang, "Atomic force microscopy using optical interferometry," J. Vac. Sci. Technol. 6(1988):266-270.

[498] Y. Martin, C.C. Williams, H.K. Wickramasinghe, "Atomic force microscope-force mapping and profiling on a sub 100-A scale," J. Appl. Phys. 61(1987):4723-4729.

[499] D. Rugar, H.J. Mamin, R. Erlandsson, J.E. Stern, B.D. Terris, "Force microscope using a fiberoptic displacement sensor," Rev. Sci. Instrum. 59(1988):2337-2340. P.J. Mulhern, T. Hubbert, C.S. Arnold, B.L. Blackford, M.H. Jericho, "A scanning force microscope with a fiber-optic-interferometer displacement sensor," Rev. Sci. Instrum. 62(1991):1280-1284.

[500] Surface Imaging Systems (S.I.S.) GmbH, Herzogenrath, Germany, www.sis-gmbh.com.

[501] D. Sarid, D. Iams, V. Weissenberger, L.S. Bell, "Compact scanning-force microscope using laser diode," Opt. Lett. 13(1988):1057-1059.

[502] Th. Göddenhenrich, H. Lemke, U. Hartmann, C. Heiden, "Force microscope with capacitive displacement detection," J. Vac. Sci. Technol. 8(1990):383-387. J. Brugger, R.A. Buser, N.F. Rooij, "Micromachined atomic force microprobe with integrated capacitive read-out," J. Micromech. Microeng. 2(1992):218.

[503] M. Tortonese, R.C. Barrett, C. Quate, "Atomic resolution with an atomic force microscope using piezoresistive detection," Appl. Phys. Lett. 62(1993):834-836.

[504] M. Tortonese, R.C. Barrett, C. Quate, "Atomic resolution with an atomic force microscope using piezoresistive detection," Appl. Phys. Lett. 62(1993):834-836.

[505] Franz J. Giessibl, "Atomic resolution on Si(111)-(7x7) by noncontact atomic force microscopy with a force sensor based on a quartz tuning fork," Appl. Phys. Lett. 76(13 March 2000):1470; http://dns.ntu-ccms.ntu.edu.tw/references/APPL_PHYS_LETT-76-1470-2000.pdf.

Table 3-3 suggests that there are only two measurement technologies that can definitively measure displacements to a precision under 100 pm as we require, over 10-100 micron ranges, though both are listed as only being "one-axis" systems. Those two technologies are:

(1) X-ray interferometry is capable of <100 pm precision over 10 micron ranges; extreme guiding quality is necessary, and generally uses monolithic flexure hinge arrangement from Si].[506] Combined optical and X-ray interometry (COXI) can attain measurement ranges of up to mm.[507]

(2) Multi-beam interferometry, in particular Fabry-Pérot interferometry, is capable of 10 pm precision in vacuum over 1 mm ranges. This also demands the highest guiding quality, and has two operational modes: quasi-continuous and discrete (λ/2-steps).

One commentator[508] briefly summarizes the pro's and con's in comparing these two approaches as follows:

X-ray Interferometry

Pro: Large displacements; "simple" set-up (CW laser)
Con: Limited resolution; cyclic errors

Fabry-Pérot Cavity

Pro: Ultra-high resolution; no cyclic errors
Con: Limited displacements; sensitive to air pressure (not relevant when using vacuum systems)

Three other detection systems that are listed in Table 3-3 are known to be capable of a measurement precision of 100-300 pm. This is close, within a factor of 2-10X of the 20-50 pm resolution needed for a reliable molecular workstation system, hence it is possible that these technologies might be sufficiently improveable to enable them to reach the required technical goals for a molecular workstation. The three systems include:

(1) Capacitive sensing can already be used with multiple axes and can achieve a resolution of 100 pm over ranges up to 300 microns.

(2) Incremental optical detection with two axes can reach a resolution of 100 pm over a 1 micron range, using a crystalline lattice with an STM or AFM reading head.

(3) Two-beam interferometry with multiple axes can achieve a resolution of 300 pm over a 1 meter range using the plane mirror approach (good guiding and mirror quality are necessary)

---

[506] P. Becker, J. Stümpel, "X-ray optics in metrological application," Metrologia 27(1990):127-132.

[507] G. Basile, P. Becker, A. Bergamin, G. Cavagnero, A. Franks, K. Jackson, U. Kuetgens, G. Mana, E.W. Palmer, M. Stedman, J. Stümpel, A. Yacoot, G. Zosi, "COXI – A Combined Optical and Xray Interferometer for high precision dimensional metrology," Proc. Roy. Soc. Lond. A 456(2000):701-729.

[508] P. Becker, J. Stümpel, "X-ray optics in metrological application," Metrologia 27(1990):127-132.

or over a 500 micron range using the fiber approach (fiber arrangement includes an integrated splitter and fiber exit plane as the reference mirror).

3.2.2.2 Optical Detection Systems

Beam deflection and optical interferometry have relative advantages and disadvantages. It is important to realise that while both methods are equally sensitive,[509] beam deflection and optical interferometry measure different quantities. Optical interferometry measures only the vertical motion of the cantilever. If an appropriate design is used, this measurement can be restricted to only the vertical motion of the tip and not that of the whole detection system. On the other hand, beam deflection measures the bending of the cantilever in the longitudinal axis along with the twisting of the cantilever around the longitudinal axis so one can obtain a measure of the cantilever motion in two axes. However, unless special care is taken with the design of the system, the beam deflection system will also be sensitive to the vertical motion of the whole detection system and this will lead to a small but significant error in vertical measurements. Furthermore, careful alignment of the quadrant photodiode with respect to the motion of the deflected beam is necessary to avoid cross-talk between the two axes.[510] With both methods it is important to ensure that the size of the light spot illuminating the cantilever is smaller than the width of the cantilever. Otherwise, stray light will impinge on the sample and can lead to unwanted reflections and interference resulting in erroneous signals.

The general advantages of optical detection methods are their high sensitivity and fast response. Drawbacks related to the use of light include the previously mentioned parasitic interference, influences due to the variable quality of the reflective side of the cantilever (e.g., roughness, waviness, local reflectivity), and the need for precise beam alignment. For some applications, these drawbacks can make it desirable to investigate other methods such as self-sensing cantilevers (Section 3.2.2.3) and even self-actuated cantilevers (Section 3.2.2.4).

3.2.2.3 Self-Sensing SPM Probes

Instead of detecting the movement and position of the tip by optical methods it is possible to monolithically integrate the bending detection system and even the actuation into the sensor probe itself. Although there are some commercially available probes with integrated functions,[511] more work is needed in this area to push the general acceptance and a broader application for this type of probes.

---

[509] C.A.J. Putman, B. de Grooth, N.F. van Hulst, J. Grave, “A detailed analysis of the optical beam deflection technique for use in atomic force microscopy,” J. Appl. Phys. 72(1992):6-12.

[510] S. Fujisawa, H. Ogiso, “Compensation of cross talk in the optical lever deflection method used in atomic force microscopy,” Rev. Sci. Instrum. 74(2003):5115-5117.

[511] Such probes are available from a number of companies, e.g., “DMASP - Micro-Actuated Silicon Probes” by Veeco Instruments, piezoresistive cantilevers by Seiko Instruments Inc., and Nascatec GmbH.

The so-called "self-sensing" AFM probes directly convert their bending into a measurable electrical signal. The detection principle may be based on integrated capacitive[512] or piezoresistive[513] sensor elements or a piezoelectric signal[514] proportional to the bending of the cantilever or sensor arm. The mechanics of self-sensing probing heads could be made very compact[515] since there is no need for additional alignment of light beams as in the case of beam deflection or interferometry. This improves the user-friendliness of the system and alignment must not be repeated whenever the probe has to be changed, or when mechanical drift had caused a shift between beam and probe. The latter is especially important for operation in vacuum or low temperature conditions. Also, it is assured that the motion of the cantilever alone is detected and not that of the whole detection system. These compact heads can be used for demanding measurements such as roughness of sidewalls and can be easily combined with other instruments.

The piezoresistive detection scheme (based on a strain gauge principle) has been implemented for displacement or strain measurements in a number of other sensor applications (e.g., sensors for pressure, acceleration, temperature) and its restrictions are well-known: electronic noise (Johnson and 1/f-Hooge), temperature sensitivity, and heat dissipation.[516] (Self-sensing microcantilevers use piezoresistive displacement transduction,[517] replacing the usual

---

[512] Th. Göddenhenrich, H. Lemke, U. Hartmann, C. Heiden, "Force microscope with capacitive displacement detection," J. Vac. Sci. Technol. 8(1990):383-387. J. Brugger, R.A. Buser, N.F. Rooij, "Micromachined atomic force microprobe with integrated capacitive read-out," J. Micromech. Microeng. 2(1992):218.

[513] M. Tortonese, H. Yamada, R.C. Barrett, C.F. Quate, "Atomic force microscopy using a piezoresistive cantilever," Proceedings of Transducers '91, IEEE 91, CH2817-5, 1991, p. 448. R. Linnemann, T. Gotszalk, L. Hadjiiski, I.W. Rangelow, "Characterisation of a cantilever with an integrated deflection sensor," Thin Solid Films 264(1995):159-164. R. Jumpertz, J. Schelten, O. Ohlsson, F. Saurenbach, "Bridge configuration of piezoresistive devices for scanning force microscopes," Sensors and Actuators A 70(1998):88-91.

[514] J. Tansock, C.C. Williams, "Force measurement with a piezoelectric cantilever in a scanning force microscope," Ultramicroscopy 42(1992):1464-1469. T.C. Itoh, T. Suga, "Development of a force sensor for atomic force microscopy using piezoelectric thin films," Nanotechnology 4(1993):218-224. R.G. Beck, M.A. Eriksson, M.A. Topinka, R.M. Westervelt, K.D. Maranowski, A.C. Gossard, "GaAs/AlGaAs self-sensing cantilevers for low temperature scanning probe microscopy," Appl. Phys. Lett. 73(1998):1149-1151.

[515] C. Dal Savio, S. Dejima, H.-U. Danzebrink, T. Gotszalk, "3D metrology with a compact scanning probe microscope based on self-sensing cantilever probes," Meas. Sci. Technol. 18(2006):S328-S333.

[516] M. Tortonese, R.C. Barrett, C. Quate, "Atomic resolution with an atomic force microscope using piezoresistive detection," Appl. Phys. Lett. 62(1993):834-836.

[517] M. Tortonese, R.C. Barrett, C. Quate, "Atomic resolution with an atomic force microscope using piezoresistive detection," Appl. Phys. Lett. 62(1993):834-836.

semiconducting piezoresistive layer with a thin metal film.[518]) All in all, theoretical investigations[519] show that the sensitivity of the piezoresistive detection systems is one order of magnitude poorer (typically 10^{-3} Å/Hz$^{1/2}$) in comparison to that of optical systems (typically 10^{-4} Å/Hz$^{1/2}$). On the other hand, piezoelectric sensors are based on thin films of material with much higher piezoelectric constants than quartz. The advantage of such piezoelectric sensors versus piezoresistive sensors is that the latter dissipate energy in the mW range, whereas there is negligible energy dissipation in piezoelectric sensors.[520] This reduces drift effects and may make piezoelectrics especially useful for dimensional measurements. Regardless of possible advantageous properties as a sensor, piezoelectric films are most commonly used for the actuation of probes.

3.2.2.4 Self-Actuated SPM Probes

Not only deflection-sensing elements can be integrated in the cantilever, but also configurations comprising actuators for resonance excitation and for the Z-direction feedback. A number of systems use the piezoelectric actuator for Z-direction feedback and either the same piezoelectric element[521] or an additional piezoresistive configuration[522] for sensing. Fully integrated cantilevers comprising actuators for Z-direction feedback motion, dynamic mode excitation, and

---

[518] Mo Li, H.X. Tang, M.L. Roukes, "Ultra-sensitive NEMS-based cantilevers for sensing, scanned probe and very high-frequency applications," Nature Nanotechnology 2(2007):114-120; http://nano.caltech.edu/publications/papers/NatNanotech2007-Li.pdf.

[519] E. Meyer, "Atomic force microscopy," Prog. Surf. Sci. 41(1992):3-49.

[520] Franz J. Giessibl, "Advances in atomic force microscopy," Rev. Mod. Phys. 75(2003):949-983.

[521] T.C. Itoh, C. Lee, T. Suga, "Deflection detection and feedback actuation using a self-excited piezoelectric $Pb(Zr,Ti)O_3$ microcantilever for dynamic scanning force microscopy," Appl. Phys. Lett. 69(1996):2036-2038. S. Watanabe, T. Fujii, "Micro-fabricated piezoelectric cantilever for atomic force microscopy," Rev. Sci. Instrum. 67(1996):3898-3903.

[522] S.C. Minne, Ph. Flueckiger, H.T. Soh, C.F. Quate, "Atomic force microscope lithography using amorphous silicon as a resist and advances in parallel operation," J. Vac. Sci. Technol. B 13(1995):1380-1385. S.C. Minne, G. Yaralioglu, S.R. Manalis, J.D. Adams, J. Zesch, A. Atalar, C.F. Quate, "Automated parallel high-speed atomic force microscopy," Appl. Phys. Lett. 72(1998):2340-2342.

detection of beam bending are based on piezoelectric elements[523] and a combination of thermal bimorphs (actuators) and MOS piezoelectric stress sensors.[524]

Another important class of self-sensing/self-actuated AFM probes are based on quartz crystals. Quartz tuning forks (aka. "qPlus sensors"), as one example, have been used as force sensors in several applications.[525] In operation, this quartz is excited to swing in response to an electric AC voltage with the proper frequency applied – just like the tuning fork in a quartz clock. The measurement of the distance between probe and surface and thus imaging the surface is performed by recording the current flowing through the quartz. This current is proportional to the lever arm vibration amplitude and is sensitive to changes in the damping when the distance between tip and surface varies. Quartz tuning forks have many attractive properties – among which the greatest benefits are their high frequency stability and their high Q factor.[526] Tuning forks are available in a wide range of sizes, and a wide selection of tips can be mounted on one of the two prongs. However, the mass of the tip and the interaction with the sample breaks the symmetry of the tuning fork geometry. This problem can be avoided by fixing one of the two beams to a high-mass substrate with a low-loss material, thus turning the fork into a cantilever geometry.[527] A combination of a V-shaped cantilever glued between both prongs of a tuning fork has been realized as well.[528] As another possibility to overcome the imbalance due to the extra mass of the tip, a micro-machined quartz fork with a monolithically integrated tip has been

---

[523] T.C. Itoh, C. Lee, T. Suga, "Deflection detection and feedback actuation using a self-excited piezoelectric $Pb(Zr,Ti)O_3$ microcantilever for dynamic scanning force microscopy," Appl. Phys. Lett. 69(1996):2036-2038. S.C. Minne, S.R. Manalis, C.F. Quate, "Parallel atomic force microscopy using cantilevers with integrated piezoresistive sensors and integrated piezoelectric actuators," Appl. Phys. Lett. 67(1995):3918-3920. C. Lee, T. Itoh, T. Suga, "Self-excited piezoelectric PZT microcantilevers for dynamic SFM with inherent sensing and actuating capabilities," Sensors and Actuators A 72(1999):179-188.

[524] T. Akiyama, U. Staufer, N.F. de Rooij, D. Lange, C. Hagleitner, O. Brand, H. Baltes, A. Tonin, H.R. Hidber, "Integrated atomic force microscopy array probe with metal-oxide-semiconductor field effect transistor stress sensor, thermal bimorph actuator, and on-chip complementary metal-oxidesemiconductor electronics," J. Vac. Sci. Technol. B 18(2000):2669-2675.

[525] P. Güthner, U.C. Fischer, K. Dransfeld, "Scanning near field accoustic microscopy," Appl. Phys. B: Laser Opt. 48(1989):89-92. K. Bartzke, T. Antrack, K.-H. Schmidt, E. Dammann, C. Schatterny, "The needle-sensor, microchemical detector for atomic force microscopy," Intl. J. Optoelectron. 8(1993):669-676. G. Goch, R. Volk, "Contactless surface measurement with a new acoustic sensor," Annals of CIRP 43(1994):487-490.

[526] Franz J. Giessibl, "Advances in atomic force microscopy," Rev. Mod. Phys. 75(2003):949-983.

[527] Franz J. Giessibl, "Advances in atomic force microscopy," Rev. Mod. Phys. 75(2003):949-983.

[528] T. Akiyama, U. Staufer, N.F. de Rooij, P. Frederix, A. Engel, "Symmetrically arranged quartz tuning fork with soft cantilever for intermittent contact mode atomic force microscopy," Rev. Sci. Instrum. 74(2003):112-117.

proposed.[529] An oscillating probe shank measuring 7 µm in diameter and several mm in length has been fixed to a tuning fork to allow mapping of high-aspect ratio features on a sample.[530]

Not only tuning forks but also quartz discs (aka. quartz-crystal resonators or QCRs) with resonance frequencies in the range of MHz were equipped with sharp tips and used as AFM probes.[531] One possible way to reduce the high stiffness that most of the quartz sensor geometries/solutions have in common is to fabricate AFM probes based on thin quartz cantilevers.[532]

3.2.2.5 Multiple SPM Probes and Probe Arrays

Reduction of measurement time is a prerequisite for the further integration of SFMs into industrial production lines. One possibility for increasing scan speed is to use a whole array of sensors so that different points on the sample can be probed in parallel. A requirement for such multiple cantilever systems is individual self-sensing and self-actuated cantilever probes. Not only the acquisition rate but also the scanning range is increased due to the extended positions of the probes.

One of the first SFM multi-cantilever arrangements consisted of 5 self-sensing piezoresistive cantilevers without individual Z-actuation.[533] In a next step the same group published two independently distance controlled cantilevers equipped with integrated piezoelectric Z-actuators.[534] A row of 50 cantilevers with 200 µm pitch allowed a scan speed equivalent to 4 mm/sec for a single cantilever. However, only 4 cantilevers out of the 50 were actively feedback controlled by the computer at that time.[535] In further developments the control electronics were

---

[529] H. Hida, M. Shikida, K. Fukuzawa, A. Ono, K. Sato, K. Asaumi, Y. Iriye, D. Cheng, K. Sato, "Proposal of new type of micro-machined quartz tuning fork AFM probe," Proc. of 18th IEEE Intl. Conference on Micro Electro Mechanical Systems, Piscataway, NJ, USA, 2005. pp. 323-326.

[530] M.B. Bauza, R.J. Hocken, S.T. Smith, S.C. Woody, "Development of a virtual probe tip with an application to high aspect ratio microscale features," Rev. Sci. Instrum. 76(2005):095112.

[531] Y. Seo, J.H. Park, J.B. Moon, W. Jhe, "Fast-scanning shear-force microscopy using a highfrequency dithering probe," Appl. Phys. Lett. 77(2000):4274-4276.

[532] T. Ono, Y.C. Lin, M. Esashi, "Scanning probe microscopy with quartz crystal cantilever," Appl. Phys. Lett. 87(2005):074102.

[533] S.C. Minne, Ph. Flueckiger, H.T. Soh, C.F. Quate, "Atomic force microscope lithography using amorphous silicon as a resist and advances in parallel operation," J. Vac. Sci. Technol. B 13(1995):1380-1385.

[534] S.C. Minne, S.R. Manalis, C.F. Quate, "Parallel atomic force microscopy using cantilevers with integrated piezoresistive sensors and integrated piezoelectric actuators," Appl. Phys. Lett. 67(1995):3918-3920.

[535] S.C. Minne, G. Yaralioglu, S.R. Manalis, J.D. Adams, J. Zesch, A. Atalar, C.F. Quate, "Automated parallel high-speed atomic force microscopy," Appl. Phys. Lett. 72(1998):2340-2342.

fabricated as an on-chip circuitry in CMOS technology together with a piezoresistive/ thermal bimorph cantilever array,[536] but still in the latter system only 4 cantilevers out of 10 are actively controlled. Obviously, considerably more effort is required to develop on-chip control circuitry for the control electronics for a larger number of cantilevers.

A well known example of a 2-dimensional array is the "Millipede" developed for data storage applications at IBM Research (Rüschlikon, Switzerland).[537] However, Millipede's 1024 (32 x 32) silicon cantilevers (most recently: 64 x 64) are not actively distance controlled. The distance between cantilever and surface is determined by measuring the heat flow through the cantilever (read process), while the writing process is performed by heating of the tip and locally deforming the surface. Active probe arrays of 10,000 independently-actuated microscope tips have been developed by Mirkin's group at Northwestern University for dip-pen nanolithography[538] using DNA-based "ink". Almost any desired 2D shape can be drawn using 10 tips in concert. Another microcantilever array manufactured by Protiveris Corp. has millions of interdigitated cantilevers on a single chip.[539]

Besides data storage, multiple levers can serve simply as a reservoir for remote SFM applications[540] or in the case of different properties it could be used for testing of material properties; equipped with functionalized tips other properties may be tested, too.[541]

---

[536] T. Volden, CMOS-Integrated cantilevers for biosensing and probe microscopy, Ph.D. thesis, Diss. ETH No. 15984, 2005; cited in: H.-U. Danzebrink, L. Koenders, G. Wilkening, A. Yacoot, H. Kunzmann, "Advances in Scanning Force Microscopy for Dimensional Metrology," CIRP Annals - Manufacturing Technology 55(2006):841-878.

[537] M.I. Lutwyche, M. Despont, U. Drechsler, U. Dürig, W. Häberle, H. Rothuizen, R. Stutz, R. Widmer, G.K. Binnig, P. Vettiger, "Highly parallel data storage system based on scanning probe arrays," Appl. Phys. Lett. 77(2000):3299-3301.

[538] 435. D. Bullen, S. Chung, X. Wang, et al., "Development of parallel dip pen nanolithography probe arrays for high throughput nanolithography," Symposium LL: Rapid Prototyping Technologies, Materials Research Society Fall Meeting; 2-6 Dec 2002; Boston, MA. Proc. MRS, Vol. 758, 2002; http://mass.micro.uiuc.edu/publications/papers/84.pdf.

[539] Protiveris Corp.. "Microcantilever arrays," 2003; http://www.protiveris.com/cantilever_tech/microcantileverarrays.html.

[540] Phoenix Mars Lander, 2007; http://phoenix.lpl.arizona.edu/technology/meca.php.

[541] T. Volden, CMOS-Integrated cantilevers for biosensing and probe microscopy, Ph.D. thesis, Diss. ETH No. 15984, 2005; cited in: H.-U. Danzebrink, L. Koenders, G. Wilkening, A. Yacoot, H. Kunzmann, "Advances in Scanning Force Microscopy for Dimensional Metrology," CIRP Annals - Manufacturing Technology 55(2006):841-878. H.P. Lang, R. Berger, C. Andreoli, J. Brugger, M. Despont, P. Vettiger, Ch. Gerber, J.K. Gimzewski, J.P. Ramseyer, E. Meyer, H.-J. Güntherodt, "Sequential position readout from arrays of micromechanical cantilever sensors," Appl. Phys. Lett. 72(1998):383-385.

3.3 Cantilevers and Tips

In contrast to STM probes that simply consist of a sharpened metallic wire, AFM probes are more complex and a large variety of different geometries and materials exist. The most commonly used AFM probes are still cantilever probes having a sharp protruding tip.

3.3.1 Cantilever Beams

Historically the first cantilevers were fabricated manually from thin metal foils[542] or small bent metal wires.[543] The corresponding tips were created by gluing diamond fragments to the foil cantilevers or electrochemically etching the wires to a sharp point. The first mass-produced cantilevers were built from silicon nitride (Si_3N_4) or silicon dioxide (SiO_2)[544] and monocrystalline silicon.[545] Since then the basic fabrication steps for standard cantilevers have not changed. Due to the fact that the processing methods have been developed from semiconductor technology, cantilevers together with integrated tips are now consistently produced in large numbers and thus at reasonable prices.[546] Apart from the materials mentioned before, cantilevers made from tungsten, nickel and other materials are also in use for special applications.[547]

---

[542] G. Binnig, H. Rohrer, "Scanning tunneling microscopy," Helv. Phys. Acta, 55(1982):726-735; G. Binnig, C.F. Quate, Ch. Gerber, "Atomic force microscope," Phys. Rev. Lett. 56(1986):930-933.

[543] G.M. McClelland, R. Erlandsson, S. Chiang, "Atomic force microscopy: General principles and a new implementation," Vol. 6, in: D.O. Thompson, D.E. Chimenti, eds., Review of Progress in Quantitative Non-Destructive Evaluation, Plenum, New York, 1987, p. 307.

[544] T.R. Albrecht, S. Akamine, T.E. Carver, C.F. Quate, "Microfabrication of cantilever styli for the atomic force microscope," J. Vac. Sci. Technol. A 8(1990):3386-3396. S. Akamine, R.C. Barrett, C.F. Quate, "Improved atomic force microscope images using microcantilevers with sharp tips," Appl. Phys. Lett. 57(1990):316-318.

[545] O. Wolter, Th. Bayer, J. Greschner, "Micromachined silicon sensors for scanning force microscopy," J. Vac. Sci. Technol. B 9(1991):1353-1357.

[546] Veeco Instruments, U.S.A., www.veeco.com. NanoWorld AG, Neuchatel, Switzerland, www.nanoworld.com. NT-MDT Co., Zelenograd, Moscow, Russia, www.ntmdt.ru.

[547] D. Sarid, "Tapping-mode scanning force microscopy: Metallic tips and samples," Computational Materials Science 5(1996):291-297. W. Kulisch, A. Malave, W. Scholz, C. Mihalcea, E. Oesterschulze, G. Lippold, "Fabrication of integrated diamond cantilevers with tips for SPM applications," Diamond and Related Materials 6(1997):906-911. T. Fujii, Y. Miyahara, H. Bleuler, H. Yamada, A. Tonoli, S. Watanabe, S. Carabelli, "Lead zirconate titanate cantilever for noncontact atomic force microscopy," Applied Surface Science 140(1999):428-431. J.L. Hazel, V.V. Tsukruk, "Spring constants of composite ceramic/gold cantilevers for scanning probe microscopy," Thin Solid Films 339(1999):249-257. A.H. Sorensen, U. Hvid, M.W. Mortensen, K.A. Morch, "Preparation of platinum iridium scanning probe microscopy tips," Rev. Sci. Instrum. 70(1999):3059-3067. T. Hantschel, S. Slesazeck, P. Niedermann, P. Eyben, W. Vandervorst, "Integrating diamond pyramids into metal cantilevers and using them as electrical AFM probes," Microelectronic Engineering 57-58(2001):749-754.

In general, cantilevers used in AFM should meet the following criteria:[548]

(1) low normal spring constant (low longitudinal stiffness);
(2) high resonance frequency;
(3) high quality factor of the cantilever (*Q* value);
(4) high lateral spring constant (high transversal stiffness);
(5) short cantilever length;
(6) prepared for deflection sensing (smooth, reflective back side or self-sensing elements); and
(7) small electrical resistance to make sure that no electric charging of the tip occurs.

Some of these criteria are contradictory and the absolute values have to be matched with the measurement applications (e.g., when materials of different hardness are to be investigated). But in general, probes are available and fabricated with a variety of parameters.

The requirement to perform a non-destructive measurement of the surface defines the stiffness and detection sensitivity needed. The inter-atomic force constants of the tip and sample define the limits to prevent a plastic deformation of both. For solid materials the force constants k are on the order of 10 N/m[549] (in biological samples, they can be as small as 0.1 N/m). Thus typical values for k in the static mode are 0.01 - 5 N/m.[550] As a result, a deflection detection sensitivity of 100 pm would allow detecting forces in the range of 100 pN for a 1 N/m cantilever. For dynamic AFM modes, force constants of hundreds of N/m are usually chosen to reduce noise and increase stability.[551] In these cases much higher force detection sensitivity is needed.

The mechanical resonance frequency of the cantilever, as another parameter, should have values significantly larger than 10 kHz.[552] Otherwise, a slow dynamic performance of the cantilevers may limit the scanning rate of the whole AFM system. Especially for dimensional metrology, fast imaging rates are needed to reduce measurement times and the influence of thermal drift. The combined requirement of a high resonance frequency and a low stiffness is generally achieved by reducing the size and therefore the mass of the cantilevers.[553] Conventional scanning

---

[548] T.R. Albrecht, S. Akamine, T.E. Carver, C.F. Quate, "Microfabrication of cantilever styli for the atomic force microscope," J. Vac. Sci. Technol. A 8(1990):3386-3396.

[549] D. Rugar, P. Hansma, "Atomic force microscopy," Phys. Today, 43(October 1990):23-30.

[550] Franz J. Giessibl, "Advances in atomic force microscopy," Rev. Mod. Phys. 75(2003):949-983.

[551] Franz J. Giessibl, "Advances in atomic force microscopy," Rev. Mod. Phys. 75(2003):949-983.

[552] T.R. Albrecht, S. Akamine, T.E. Carver, C.F. Quate, "Microfabrication of cantilever styli for the atomic force microscope," J. Vac. Sci. Technol. A 8(1990):3386-3396.

[553] V. Thien Binh, N. Garcia, A.L. Lavanuyk, "A mechanical nanosensor in the gigahertz range: where mechanics meets electronics," Surf. Sci. Lett. 301(10 January 1994):L224-L228. H. Kawakatsu, S. Kawai, D. Saya, M. Nagashio, D. Kobayashi, H. Toshiyoshi, H. Fujita, "Towards atomic force microscopy up to 100 MHz," Rev. Sci. Instrum. 73(2002):2317-2320.

rate is not as important in DMS systems, which will largely use dead-reckoning pick-and-place operations in place of swath-scanning.

A high quality factor is especially important for dynamic AFM modes. On the one hand, a high *Q* increases sensitivity, while on the other hand high *Q* reduces the measurement bandwidth of the system at least when amplitude modulation (AM) techniques are implemented.[554] Thus frequency modulation (FM) methods are most commonly preferred for high-*Q* AFM probes.[555]

3.3.2 Cantilever Characterization

Cantilever beams are characterized by their dimensions and by other constants such as mass, resonance frequency, and spring constant. In dimensional metrology, the knowledge of the tip shape in conjunction with the applied force is mandatory. In addition, for the investigation of soft samples (e.g., in the field of life sciences) it is important to evaluate the true forces applied. These constants are mainly determined from geometrical and material properties but the achieved accuracies are very limited.

Many papers have been published on methods to determine the spring constant k_z of AFM cantilevers. There are three categories of methods used for this determination:

(1) dimensional parameters,
(2) static experiments, and
(3) dynamic experiments.

A theoretical comparison of dimensional aspects of these methods has been performed by Clifford et al.[556] After reviewing analytical equations in several papers and comparing the results with finite element analysis (FEA) calculations, they found that the equations of Neumeister and Ducker[557] showed the best agreement.

Hoffmann et al.[558] presented an experimental solution by calibrating the stiffness of AFM cantilevers using a microforce calibration setup based on a high precision 1D stage and a

---

[554] T.R. Albrecht, P. Grütter, D. Horne, D. Rugar, "Frequency modulation detection using high-q cantilevers for enhanced force microscope sensitivity," J. Appl. Phys., 69(1991):668-673.

[555] F.J. Giessibl, S. Hembacher, M. Herz, C. Schiller, J. Mannhart, "Stability considerations and implementation of cantilevers allowing dynamic force with optimal resolution: the qPlus sensors," Nanotechnology 15(2004):79-86.

[556] C.A. Clifford, M.P. Seah, "Cantilever spring constants via dimensional methods for nanomechanical analysis," Nanotechnology 16(2005):1666-1680.

[557] J.M. Neumeister, W.A. Ducker, "Lateral, normal, and longitudinal spring constants of atomic force microscopy cantilevers," Rev. Sci. Instrum. 65(1994):2527-2531.

[558] W. Hoffmann, S. Loheide, T. Kleine-Besten, U. Brand, A. Schlachetzki, "Method of characterising micro mechanical beams and its calibration for the application in micro force measurement systems," Proc. MicroTec, 2000, pp. 819-823.

compensation balance with 100 nN resolution. Doering et al.[559] improved this calibration setup using a higher-resolving compensation balance leading to 1 nN force resolution. Behrens et al.[560] described the design, fabrication and test of cantilever-type sensors for active microforce calibration. The cantilever comprises a probing tip at its free end where a force can be applied which is measured using a piezoresistive strain gauge at the cantilever suspension. Cumpson et al.[561] have developed a compact and easy-to-use reference artifact for the calibration of contact cantilevers by bulk micromachining of silicon, which they call a microfabricated array of reference springs (C-MARS). The C-MARS device spans the range of spring constants from 25 N/m down to 0.03 N/m, allowing almost any contact-mode AFM cantilever to be calibrated easily and rapidly. Gibson et al.[562] compared three different methods for the calibration of the spring constant of two different types of silicon beam-shaped AFM cantilevers to determine each method's accuracy, ease of use, and potential destructiveness. Dai et al.[563] described the high-precision probing-force calibration of a stylus probe using a calibrated silicon beam microforce transfer standard. These reference artifacts[564] are commercially available with stiffness values from 5 N/m up to 1000 N/m. A review of traceable calibration for indentation and AFM is given by Pratt et al.[565]

3.3.3 Tip Shape

The most critical element in a scanning AFM is the tip that senses the sample surface (Figure 3-5). For highest resolution, the very end of this tip should ideally end in one atom interacting

---

[559] L. Doering, U. Brand, E. Peiner, I. Behrens, "Calibration of micro force setting standards using a new nano force calibration device," Proc. of Micro System Technologies MST, 2003, pp. 492-494.

[560] I. Behrens, L. Doering, E. Peiner, "Piezoresistive cantilever as portable micro force calibration standard," J. Micromech. Microeng. 13(2003):171-177.

[561] P.J. Cumpson, C.A. Clifford, J. Hedley, "Quantitative analytical atomic force microscopy: a cantilever reference device for easy and accurate AFM spring-constant calibration," Meas. Sci. Technol. 15(2004):1337-1346.

[562] C.T. Gibson, D.A. Smith, C.J. Roberts, "Calibration of silicon atomic force microscope cantilevers," Nanotechnology 16(2005):234-238.

[563] G. Dai, U. Brand, L. Doering, H.-U. Danzebrink, "Probing force calibration of stylus instruments using force calibration standards," 2006, to be published; cited in: H.-U. Danzebrink, L. Koenders, G. Wilkening, A. Yacoot, H. Kunzmann, "Advances in Scanning Force Microscopy for Dimensional Metrology," CIRP Annals - Manufacturing Technology 55(2006):841-878.

[564] J. Frühauf, H. Trumpold, "Silicon standards for assessment and calibration of stylus probes," Annals of the CIRP 51(2002):475-478.

[565] J.R. Pratt, J.A. Kramar, D.B. Newell, D.T. Smith, "Review of SI traceable force metrology for instrumented indentation and atomic force microscopy," Meas. Sci. Technol. 16(2005):2129-2137.

strongly with the atoms of the sample via short-range repulsive forces.[566] Since long-range forces are present as well, the tip geometry near to the peak of the tip influences the force measurement.

Figure 3-5. (A) Typical cantilever with sharp silicon tip (PTB); (B) ion beam sharpened silicon tip with carbon nanotube (NPL).[567]

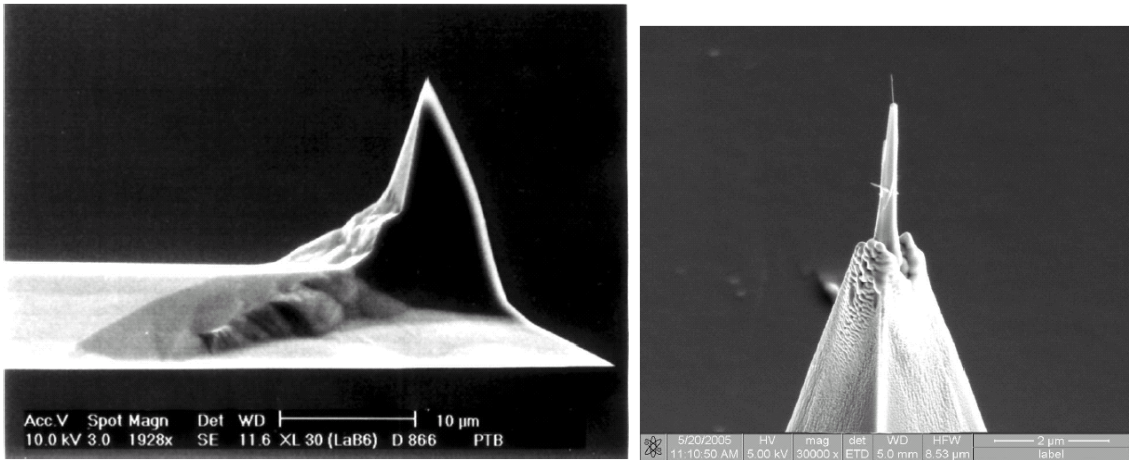

(A) **(B)**

The overall tip shape is determined by the fabrication method; i.e., for Si_3N_4-tips, symmetrical pyramids; for Si-tips, irregular polyhedrals. As a result, Si tips are usually sharper than Si_3N_4 tips because they are directly formed by anisotropic etch steps rather than using an etch pit as a mold for deposited materials. Furthermore, the original tip geometry can be tailored to the intended use within wide ranges. Instruments for high resolution generally require tips with very small radii of curvature and very sharp apex angles. In some cases the tip shape can be improved by sharpening the tips via oxidation processes. Another controllable method is to modify the tips by ablation/deposition using focused ion beams (FIB)[568] or e-beams.[569] FIB-modified tips are commercially available having half-cone angles of < 3 degrees over lengths of several microns, yielding aspect ratios of approximately 10:1. One step even further towards the ultimate imaging

---

[566] Franz J. Giessibl, "Advances in atomic force microscopy," Rev. Mod. Phys. 75(2003):949-983.

[567] H.-U. Danzebrink, L. Koenders, G. Wilkening, A. Yacoot, H. Kunzmann, "Advances in Scanning Force Microscopy for Dimensional Metrology," CIRP Annals - Manufacturing Technology 55(2006):841-878.

[568] Veeco Instruments, U.S.A., www.veeco.com. NanoWorld AG, Neuchatel, Switzerland, www.nanoworld.com.

[569] Commercial supplier of EBD tips: NanoTools www.nano-tools.com, NT-MDT www.ntmdt.ru. D.J. Keller, C. Chih-Chung, "Imaging steep, high structures by scanning force microscopy with electron beam deposited tips," Surf. Sci. 268(1992):333-339.

resolution are AFM probes with a carbon nanotube (CNT) at their tip.[570] Single-walled nanotubes (SWNTs) can have diameters as small as 0.7 nm and lengths of several microns, thus reaching the highest aspect ratio possible (Figure 3-5B). The nanotubes themselves are ideal in terms of a reproducible shape because their atomic structure is defined by a self-assembly process. The biggest problem is how to attach or grow a CNT at a specifically desired position, and having a fixed direction and length, on the end of a cantilever probe. Different techniques have been proposed[571] and only "hand-made" tips are available at the moment. It is also possible that the PALE process currently being pursued by Zyvex could produce atomically precise tips, albeit in silicon or germanium rather than diamond (see further discussion in Section 4.2.4).

It has been shown[572] that SWNT probes can achieve a lateral resolution as small as 2 nm. For measurements on rough surfaces, tips made of multi-walled nanotubes (MWNTs) must show no detectable degradation in lateral resolution even after more than 15 hours of continuous scanning on a Si_3N_4 surface. This has been confirmed by Larsen[573] who found that CNTs have at least 20 times the lifetime of etched silicon probes. This long life, plus the lack of debris at the tip and the ability to probe deep holes and valleys, make CNT tips ideal for surface metrology.

For critical dimension (CD) metrology where the measurement of sidewalls is necessary, special probes with horizontally protruding structures or flared ends have been developed and tested.[574] The so-called "3-point" tips implemented by Nyyssonen et al.[575] had diameters of approximately 200 nm and were used for measurements inside 300-nm-wide trenches. Another solution is a kind of a boot-shaped tip ("CD tip") whose front part is basically a post with a small thin disk on

---

[570] H.J. Dai, J.H. Hafner, A.G. Rinzler, D.T. Colbert, R.E. Smalley, "Nanotubes as nanoprobes in scanning probe microscopy," Nature 384(1996):147-150.

[571] J.H. Hafner, C.L. Cheung, T.H. Oosterkamp, C.M. Lieber, "High-yield assembly of individual single-walled carbon nanotube tips for scanning probe microscopies," J. Phys. Chem. B 105(2001):743-746. T. Ono, H. Miyashita, M. Esashi, "Electric-field-enhanced growth of carbon nanotubes for scanning probe microscopy," Nanotechnology 13(2002):62-64. S. Tseng, C. Tsai, C. Lee, C. Tsai, S. Chen, C. Liang, G. Hsieh, W. Lin, "Fabrication of individual aligned carbon nanotube for scanning probe microscope," Journal of Physics: Conference Series 10(2005):186-189. C.V. Nguyen, Q. Ye, M. Meyyappan, "Carbon nanotube tips for scanning probe microscopy: fabrication and high aspect ratio nanometrology," Meas. Sci. Technol. 16(2005):2138-2146.

[572] C.V. Nguyen, K.J. Chao, R.M.D. Stevens, L. Delzeit, A. Cassell, J. Han, M. Meyyappan, "Carbon nanotube tip probes: stability and lateral resolution in scanning probe microscopy and application to surface science in semiconductors," Nanotechnology 12(2001):363-367.

[573] T. Larsen, K. Moloni, F. Flack, M.A. Eriksson, M.G. Lagally, C.T. Black, "Comparison of wear characterisitics of etched-silicon and carbon nanotube atomic force microscopy probes," Appl. Phys. Lett. 50(2002):1996-1998.

[574] D. Nyyssonen, L. Landstein, E. Coombs, "Two-dimensional atomic force microprobe trench metrology system," J. Vac. Sci. Technol. B 9(1991):3612-3616. Y. Martin, H.K. Wickramasinghe, "Toward accurate metrology with scanning force microscopes," J. Vac. Sci. Technol. B 13(1995):995-2335.

[575] D. Nyyssonen, L. Landstein, E. Coombs, "Two-dimensional atomic force microprobe trench metrology system," J. Vac. Sci. Technol. B 9(1991):3612-3616.

top.[576] By 2006 there were many different tips commercially available with disk diameters down to 60 nm and post lengths of a few 100 nm.[577] Special tip wear-resistant coatings have been developed and tested for this type of probe.[578]

For applications where a high resistance to tip wear is necessary, diamond coated tips[579] and also single crystal diamond tips[580] are commercially available (Section 4.2.1, Table 4-1). Both types may be used in nanoindentation measurements as well. Specially functionalized tips have been developed to achieve more than geometrical information from the sample. For instance, metallization as well as special hydrophobic coatings[581] or other additional preparation steps provide access to different kinds of interactions. Here one has to distinguish between those probes and methods where the specific interaction introduces forces, and those methods where the force sensing principle is used to keep the tip within a close distance to the surface. One prominent example for the latter is a probe for scanning near-field optical microscopy (SNOM/NSOM).[582]

As described above there is a large variety of different cantilever/tips available for many applications. For dimensional measurements the most important properties are stability of tip shape and high aspect ratio. However, traditionally AFMs are "profilometer-type" instruments which means that surfaces are measured from one side only, hence a controlled rotation of the tip is a challenge and only realistic for self-sensing systems. Very specialized probes and control methods are needed for 3D measurements of objects.

For applications requiring such 3D measurements of objects, the AFM tip or the sample is moved in X and Y directions while the sample's topography is detected along the Z-axis. These measurements produce a set of raster points in the XY plane with assigned Z heights which are usually taken and used for data processing or "3D" representations. However, the 3D images obtained in such a way are not really equal to the true 3D surface of the sample due to three limitations:

---

[576] Y. Martin, H.K. Wickramasinghe, "Methods of imaging sidewalls by atomic force microscopy," Appl. Phys. Lett. 64(1994):2498-2500. Team Nanotec GmbH, Villingen-Schwenningen, Germany, www.team-nanotec.de

[577] Team Nanotec GmbH, Villingen-Schwenningen, Germany, www.team-nanotec.de

[578] H. Liu, D. Klonowski, D. Kneeburg, G. Dahlen, M. Osborn, T. Bao, "Advanced atomic force microscopy probes: Wear resistant designs," J. Vac. Sci. Technol. B 23(2005):3090-3093.

[579] NanoWorld AG, Neuchatel, Switzerland, www.nanoworld.com, NT-MDT Co., Zelenograd, Moscow, Russia, www.ntmdt.ru.

[580] Micro Star Technologies, Huntsville, U.S.A., www.microstartech.com.

[581] Veeco Instruments, U.S.A., www.veeco.com.

[582] U.C. Fischer, "Scanning near field optical microscopy," in: R. Wiesendanger, ed., Scanning Probe Microscopy: Analytical Methods, Springer-Verlag, Berlin, 1998.

(1) the acquired SFM image is typically a combination of both the original surface topology and the used-tip shape, known as the "tip dilation";

(2) there are "dead regions" where the tip never reaches the actual surface, for instance at vertical flanks or even undercut regions of the sample; and

(3) only few data points are obtained over the vertical regions of the structures because the raster points are distributed with nearly equal-distance in the XY plane.

True 3D AFM scanning is demanded increasingly, e.g., in the metrology and processing of photomasks where the parameters such as bottom/middle/top critical dimensions (CD), wall angle, depth, linewidth variability, and edge location need to be determined very accurately. Several techniques have been proposed and developed in the last 20 years in order to get the true 3D surface of the samples, directly addressing the three limitations described above. Apart from the offline methods that are applied to deal with the "tip dilation" aspect, two different kinds of methods can be generally adopted to reduce the "dead region" of AFM measurements.

The first method is to tilt the tip with respect to the sample (tilting of sample is also possible but is usually more difficult). However, this method has the handicap that only one sidewall of the structure can be measured. To avoid this problem, Mancevski et al.[583] have proposed a set-up comprising two tilted AFM probes as a caliper.

The second method is to employ a special kind of tip which usually comprises horizontally-protruding structures at its tip region. Martin et al.[584] discuss the detection method for these types of probes. The idea is to measure the surface slope in a dynamic mode by vibrating the probe not only in Z (vertical) but also in X (horizontal) directions. This technique has been successfully transferred into a commercially available CD-AFM for photomask metrology.[585] A disadvantage of the boot-shaped tip is its relatively large tip radius in the horizontal direction which limits its lateral resolution, e.g., for line-edge roughness measurements.[586] Recently Dai et al.[587] developed a novel type of AFM probe allowing one to image vertical sidewalls with high lateral resolution (Figure 3-6). In their configuration, a horizontal AFM cantilever is micro-assembled with a vertical AFM cantilever having a sharp AFM tip at its end. Depending on the angle between the two cantilevers, even undercut features and 3D microstructures (e.g., micro-gears) can be

---

[583] V. Mancevski, P.F. McClurem, "Development of a dual-probe Caliper™ CD-AFM for near modelindependent nanometrology," Proc. SPIE 4689(2003):83.

[584] Y. Martin, H.K. Wickramasinghe, "Methods of imaging sidewalls by atomic force microscopy," Appl. Phys. Lett. 64(1994):2498-2500.

[585] G. Dahlen, M. Osborn, N. Okulan, W. Foremann, A. Chand, J. Foucher, "Tip characterization and surface reconstruction of complex structures with critical dimension atomic force microscopy," J. Vac. Sci. Technol. B 23(2005):2297-2303.

[586] N. Orji, T.V. Vorburger, J. Fu, R.G. Dixson, et al., "Line edge roughness metrology using atomic force microscopes," Meas. Sci. Technol. 16(2005):2147-2154.

[587] G. Dai, H. Wolff, F. Pohlenz, H.U. Danzebrink, G. Wilkening, "Novel atomic force probe for sidewall scanning of nano and micro structures," Appl. Phys. Lett. 88(2006):171908.

measured. Methods[588] have been discussed to increase the number of measurement points at the sidewall regions of structures. Using this technique, the tip can be scanned and servo-controlled with respect to the sample in two dimensions, e.g., along the X and Z directions. As a result, the raster points in the XY plane are no longer distributed with equal distances.

Figure 3-6. "Assembled cantilever probe" (ACP) applied for measurements of micro-gears. Tip "t_a" measures the sidewall of the gear tooth, while tip "t_b" is applied for measuring the upper surface of the gear.[589]

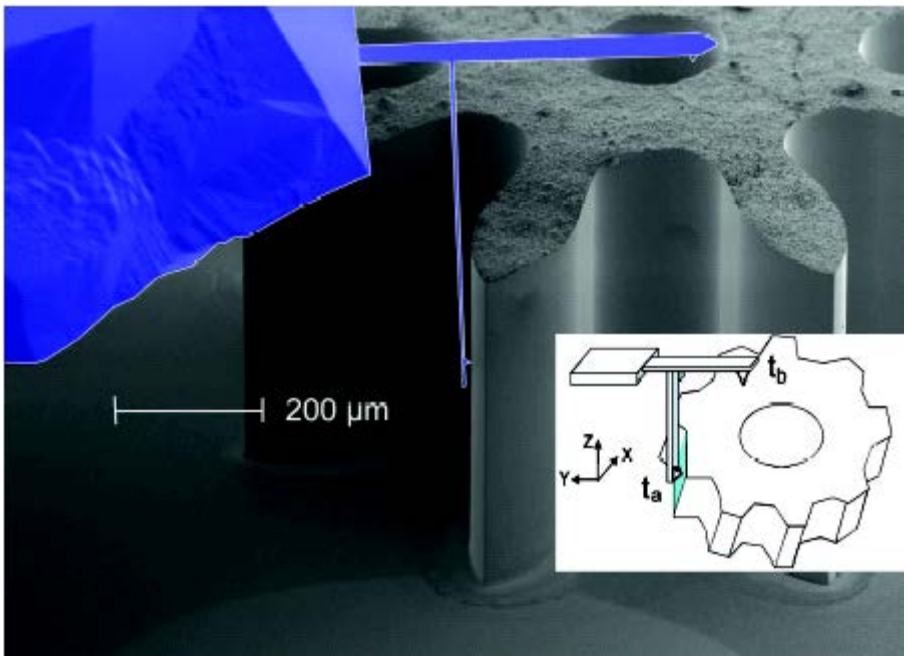

Although the studies in the field of scanning probe microscopy are booming, feasible and practically applicable techniques for true 3D AFM scanning are still rather limited; the development of new probes and methods for 3D nanometrology remains a critical issue.

---

[588] D. Nyyssonen, L. Landstein, E. Coombs, "Two-dimensional atomic force microprobe trench metrology system," J. Vac. Sci. Technol. B 9(1991):3612-3616. Y. Martin, H.K. Wickramasinghe, "Methods of imaging sidewalls by atomic force microscopy," Appl. Phys. Lett. 64(1994):2498-2500.

[589] G. Dai, H. Wolff, F. Pohlenz, H.U. Danzebrink, G. Wilkening, "Novel atomic force probe for sidewall scanning of nano and micro structures," Appl. Phys. Lett. 88(2006):171908.

3.3.4 Tip Characterizers

The uncertainties for step height and pitch measurements are now in the sub-nanometer range.[590] In both cases the measurements are independent of the tip shape as long as the structure is not too small and the tip is stable. On the other hand, for measurements of shape, width (CD) or roughness the tip directly influences the measured profiles. To evaluate the true shape, width, or surface profile it is mandatory to know the tip shape, or better, the effective tip shape. For atomic force microscopy the fine tip is crucial to the spatial resolution of structures on the sample, but it must be accepted that this tip is naturally not infinitely fine, i.e., no delta function. Thus the geometry and the physical characteristics of the probe together with the interaction between probe and sample are of substantial importance for dimensional measurements. Special artifacts known as tip characterizers have been developed for the in-line measurement of tip shape (Figure 3-7). The idea is based on a reconstruction of the tip shape from measuring data obtained when scanning the tip across the characterizer. Various mathematical techniques have been developed over the years to evaluate the tip shape from images.

There are two types of evaluation methods depending upon whether the characterizer shape is known or not. If the characterizer's shape is known, then its influence can be accounted for and hence the shape of the tip can be derived. Mathematical solutions based on a process analogous to de-convolution had been derived in the form of differential equations[591] or Legendre Transformation,[592] but later on a more convenient method was developed. The method known as "envelope-method" or "morphological method" was described independently by a number of different authors in varying mathematical forms.[593] The measurement of a sample by a tip formally corresponds to a morphological operation and can be described as dilation. Consequently, after performing erosion, the reconstructed surface is obtained, which is identical to the imaged surface in an ideal case. Wang et al.[594] used the neural network technique to quantify the sample assuming that tip properties are known. The disadvantage of this method is

---

[590] J.M. Neumeister, W.A. Ducker, "Lateral, normal, and longitudinal spring constants of atomic force microscopy cantilevers," Rev. Sci. Instrum. 65(1994):2527-2531.

[591] G. Reiss, F. Schneider, J. Vancea, H. Hoffmann, "Scanning tunneling microscopy on rough surfaces: Deconvolution of constant current images," Appl. Phys. Lett. 57(1990):867-869.

[592] D. Keller, "Reconstruction of STM and AFM images distorted by finite-size tips," Surf. Sci. 253(1991):353-364.

[593] J.S. Villarubia, "Tip characterization for dimensional metrology," in: B. Bushan, H. Fuchs, S. Hosaka, eds., Applied Scanning Probe Methods I, Springer Verlag, 2004, pp. 47-168. S. Dongmo, M. Troyon, P. Vautrot, E. Delain, N. Bonnet, "Blind reconstruction methods of scanning tunneling and atomic force microscopy images," J. Vac. Sci. Technol. B 14(1996):1552-1556. P.M. Williams, K.M. Shakesheff, M.C. Davies, D.E. Jackson, C.J. Roberts, S.J.B. Tendler, "Blind reconstruction of scanning probe image data," J. Vac. Sci. Technol. B 14(1996):1557-1562. J.S. Villarubia, "Algorithms for scanned probe microscope image simulation, surface reconstruction, and tip estimation," J. Res. Natl. Inst. Stand. Technol. 102(1997):425-454.

[594] W.L. Wang, D.J. Whitehouse, "Application of neural networks to the reconstruction of scanning probe microscope images distorted by finite-size tips," Nanotechnology 6(1997):45-51.

that the calibration standards must be used relatively often for precise measurements – a rather time-consuming process.

Several types of tip characterizers have been developed, most[595] with geometrically well-defined shapes.[596] The so-called Si nanoedge is well-known.[597] This specimen consists of a row of sharp knife-edges with nominal tip radii of 5 nm. Due to its 2D character it is likely to be more stable than spike arrays. However, like other 2D characterizers it can only be used to evaluate the probe in one direction. Martin and Wikramasinghe estimated that the artifact allows CD-measurements to an accuracy of approximately 3 nm.[598] Huebner et al.[599] also developed several kinds of silicon standards for tip characterization with certified structures. Common features of this sample are fine-linewidth structures with sharp edges. The linewidth as determined directly by optical means has an uncertainty of 10 nm, which significantly limits the uncertainty of the reconstruction of the tip shape from the profiles.

NIST has developed a novel tip characterization sample referred to as "single-crystal critical dimension reference material". Due to its crystalline nature, it was possible to use the silicon lattice constant as the source of width information when measured with TEM. With this sample, a tip width determination with an uncertainty of less than 1 nm has been reported.[600] Nanoparticles such as nano-colloids or gold nano-spheres[601] have also proven helpful for studying the tip at its very end, with tip radius uncertainties in the low-nanometer range. The dimensions

---

[595] NanoWorld AG, Neuchatel, Switzerland, www.nanoworld.com. NT-MDT Co., Zelenograd, Moscow, Russia, www.ntmdt.ru.

[596] J.S. Villarubia, "Tip characterization for dimensional metrology," in: B. Bushan, H. Fuchs, S. Hosaka, eds., Applied Scanning Probe Methods I, Springer Verlag, 2004, pp. 47-168.

[597] Y. Martin, H.K. Wickramasinghe, "Toward accurate metrology with scanning force microscopes," J. Vac. Sci. Technol. B 13(1995):995-2335.

[598] Y. Martin, H.K. Wickramasinghe, "Toward accurate metrology with scanning force microscopes," J. Vac. Sci. Technol. B 13(1995):995-2335.

[599] U. Huebner, W. Morgenroth, H.G. Meyer, T. Sulzbach, B. Brendel, W. Mirandé, "Downwards to metrology in nanoscale: determination of the AFM tip-shape with wellknown sharp-edged calibration structures," Appl. Phys. A 76(2003):913-917. U. Hübner, W. Morgenroth, R. Boucher, H.G. Meyer, T. Sulzbach, B. Brendel, W. Mirandé, E. Buhr, G. Ehret, T. Fries, G. Kunath-Fandrei, R. Hild, "Prototypes of new nanoscale CD-standards for high resolution optical microscopy and AFM," Proc. of 5th EUSPEN Int. Conference, F. Chevrier (ed.), 1(2005):185-188.

[600] R. Dixson, J. Fu, N. Orji, W. Guthrie, R. Allen, M. Cresswell, "CD-AFM Reference metrology at NIST and SEMATECH," Proc. SPIE 5752(2005):324.

[601] J. Vesenka, S. Manne, R. Giberson, T. Marsh, E. Henderson, "Colloidal gold particles as an incompressible atomic force microscope imaging standard for assessing the compressibility of biomolecules," Biophys. J. 65(1993):992-997. S. Czerkas, T. Dziomba, H. Bosse, "Comparison of different methods of SFM tip shape determination for various characterisation structures and types of tip," in: G. Wilkening, L. Koenders, eds., Nanoscale Calibration Standards and Methods, Wiley-VCH, Weinheim, Germany, 2005, pp. 311-320.

of such tiny particles can (1) be controlled during the fabrication process, (2) are given by nature (e.g., natural self-organization, uniform crystallites), or (3) can be determined by a method different from AFM, e.g. straylight.

Figure 3-7. Reconstruction of tip geometry and its uncertainty by bringing the unknown tip into contact with a specially-shaped tip characterizer artifact already present on the test surface.[602]

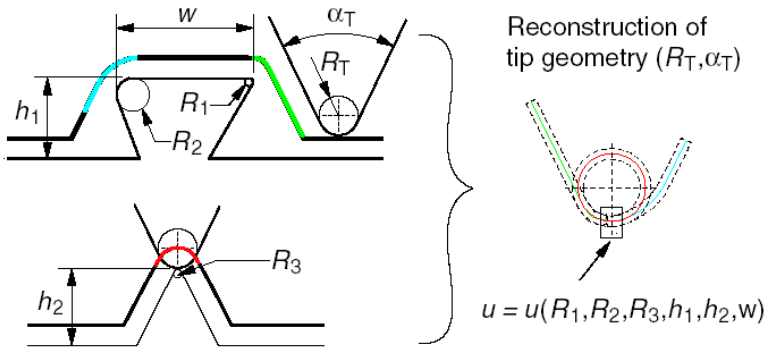

The second method – required when the characterizer geometry is not independently known – can be used to estimate upper limits to the tip dimensions. This method, in which the sample produces an image of the tip, is a special case of the more general blind reconstruction independently developed by Villarubia,[603] Dongmo et al.[604] and Williams,[605] as reviewed elsewhere.[606] In this method, one estimates the geometry of the tip using the data measured during the scanning of a sample. The approach is based on the assumption that the image of the shape of the tip is always a component of the topological maps of a sample that can be generated by means of dilation. An iterative algorithm is thus able to permit an estimation of the maximum dilation of the tip, providing a first, qualitative estimation of the geometric properties of the tip apex – including symmetry, opening angle, flank profile, and tip radius R. It relies upon

---

[602] H.-U. Danzebrink, L. Koenders, G. Wilkening, A. Yacoot, H. Kunzmann, "Advances in Scanning Force Microscopy for Dimensional Metrology," CIRP Annals - Manufacturing Technology 55(2006):841-878.

[603] J.S. Villarubia, "Tip characterization for dimensional metrology," in: B. Bushan, H. Fuchs, S. Hosaka, eds., Applied Scanning Probe Methods I, Springer Verlag, 2004, pp. 47-168.

[604] S. Dongmo, M. Troyon, P. Vautrot, E. Delain, N. Bonnet, "Blind reconstruction methods of scanning tunneling and atomic force microscopy images," J. Vac. Sci. Technol. B 14(1996):1552-1556.

[605] P.M. Williams, K.M. Shakesheff, M.C. Davies, D.E. Jackson, C.J. Roberts, S.J.B. Tendler, "Blind reconstruction of scanning probe image data," J. Vac. Sci. Technol. B 14(1996):1557-1562.

[606] J.S. Villarubia, "Algorithms for scanned probe microscope image simulation, surface reconstruction, and tip estimation," J. Res. Natl. Inst. Stand. Technol. 102(1997):425-454.

characterizers having one or more sharp features that image all or part of the tip. The simplest forms of such characterizers are spikes[607] or edges[608] but other suitably sharp objects are also used to deliberately produce an image of the tip. For probes with complicated tip shapes, Dahlen et al.[609] recently presented the reconstruction of complex tips for the case of the so-called re-entrant AFM, i.e., an SFM with feedback control active not only in Z, but equally also in X and Y[610] – a system designed to probe sharp edges also by lateral approaches with active feedback loop. A 2004 review summarizes all aspects of the use of characterizers in dimensional metrology.[611]

All methods mentioned above suffer from the fact that they provide only outer limits of the tip shape, and do not discriminate effects due to the interaction between tip and sample. Any changes in the tip characterizer's structure during the measurement are allocated to the effective tip shape.[612] Measuring the tip by SEM or TEM can reveal the geometrical form of a non-interacting tip, which can be changed significantly by interaction forces during test scans. [613] But such off-line measurements are rather time consuming and require additional handling of the tip with the risk of subsequent damage or contamination (e.g., carbon deposition from an e-beam).

---

[607] L. Montelius, J.O. Tegenfeldt, P. van Heerens, "Direct observation of the atomic force microscopy tip using inverse atomic force microscopy imaging," J. Vac. Sci. Technol. B 12(1994):2222-2226. A.L. Bogdanov, D. Erts, B. Nilsson, H. Olin, "Fabrication of arrays of nanometer size test structures for scanning probe microscope tips characterization," J. Vac. Sci. Technol. B 12(1994):3681-3684.

[608] H.K. Wickramasinghe, Y. Martin, "Toward accurate metrology with scanning force microscopes," J. Vac. Sci. Technol. B 3(1995):2335-2339.

[609] G. Dahlen, M. Osborn, N. Okulan, W. Foremann, A. Chand, J. Foucher, "Tip characterization and surface reconstruction of complex structures with critical dimension atomic force microscopy," J. Vac. Sci. Technol. B 23(2005):2297-2303. K. Miller, A. Chand, G. Dahlen, B. Todd, "Tip characterization for CD-AFM: getting to 2 nm, 3 sigma," Metrology, Inspection, and Process for Microlithography XVI, D.J.C. Herr, ed., Proc. SPIE 4689(2002):863-868.

[610] Y. Martin, H.K. Wickramasinghe, "Methods of imaging sidewalls by atomic force microscopy," Appl. Phys. Lett. 64(1994):2498-2500.

[611] J.S. Villarubia, "Tip characterization for dimensional metrology," in: B. Bushan, H. Fuchs, S. Hosaka, eds., Applied Scanning Probe Methods I, Springer Verlag, 2004, pp. 47-168.

[612] F. Meli, "Lateral and vertical diameter measurements on polymer particles with a metrology AFM," in: G. Wilkening, L. Koenders, eds., Nanoscale Calibration Standards and Methods, Wiley-VCH, Weinheim, Germany, 2005, pp. 361-374. S. Czerkas, T. Dziomba, H. Bosse, "Comparison of different methods of SFM tip shape determination for various characterisation structures and types of tip," in: G. Wilkening, L. Koenders, eds., Nanoscale Calibration Standards and Methods, Wiley-VCH, Weinheim, Germany, 2005, pp. 311-320. T. Machleidt, R. Kästerner, K. Franke, "Reconstruction and geometric assessment of AFM tips," in: G. Wilkening, L. Koenders, eds., Nanoscale calibration standards and methods, Wiley-VCH, Weinheim, Germany, 2005, pp. 297-310.

[613] D. Taatjes, A. Quinn, M. Lewis, E. Bovill, "Quality assessment of atomic force microscopy probes by scanning electron microscopy: Correlation of tip structure with rendered Images," Micros. Res. and Tech. 44(1999):312-326.

Also, both SEM and TEM are limited to producing only 2D images and the electron scattering efficiency at the boundaries is low.[614]

Using SEM imaging and the well-approved "three-sample method", Meli[615] has shown the difference between "static" and "effective" tip shape. Czerkas et al.[616] used gold spheres as reference objects to demonstrate this difference. Both experiments show that the static geometry of the tip is only one part of the components of tip related effects that need to be taken into account for a precise description of a measurement. A non-negligible effect may be caused by the interaction forces that can either temporarily or permanently modify the tip shape by elastic or plastic deformation. (Using a theoretical approach based on molecular dynamics (MD) based calculations, Abraham et al.[617] investigated the relaxation of Si(001)-2x1 and graphite[618] surfaces in the presence of a silicon tip, and Landman et al.[619] applied MD to investigate the interaction between a nonreconstructed Si(111) surface and a silicon tip and between a gold tip and a nickel surface and vice versa. These studies show[620] that for forces on the order of ~1 nN the AFM image reflects the surface topography, but tip-induced atomic relaxations lead to a reduction of the image corrugation, whereas much larger forces on the order of ~10 nN can lead to a physical rearrangement of the tip or of substrate atoms, e.g., the creation of interstitials in silicon occurs.)

Additionally, strong adhesion may cause tip wear, and capillary forces due to water films may strongly influence ambient measurements. As a consequence, tip radii (i.e., the shape of the very tip end) may be defined to about a few nanometers, but traditionally the complete shape (tip end plus flanks) cannot be defined better than to about 5 nm resolution.

---

[614] C.G. Frase, W. Häßler-Grohne, E. Buhr, K. Hahm, H. Bosse, "Analysis and comparison of CD-SEM edge oparators: A contribution to feature width metrology," in: G. Wilkening, L. Koenders, eds., Nanoscale calibration standards and methods, Wiley-VCH, Weinheim, Germany, 2005, pp. 385-403.

[615] F. Meli, R. Thalmann, "Long range AFM profiler used for accurate pitch measurements," Meas. Sci. Technol., 9(1998):1087-1092. F. Meli, "Application of a metrology AFM profiler for various dimensional measurands," JMO, Fine mechanics and optics, Czech Republic, ISSN 0447-6441, Vol. 47/6-7(2002):180-189.

[616] S. Czerkas, T. Dziomba, H. Bosse, "Comparison of different methods of SFM tip shape determination for various characterisation structures and types of tip," in: G. Wilkening, L. Koenders, eds., Nanoscale Calibration Standards and Methods, Wiley-VCH, Weinheim, Germany, 2005, pp. 311-320.

[617] F.F. Abraham, I.P. Batra, S. Ciraci, "Effect of tip profile on atomic-force microscope images: A model study," Phys. Rev. Lett. 60(1988):1314-1317.

[618] Farid F. Abraham, Inder P. Batra, "Theoretical interpretation of atomic-force-microscope images of graphite," Surf. Sci. 209(2 February 1989):L125-L132.

[619] U. Landman, W.D. Luedtke, M.W. Ribarsky, "Structural and dynamical consequences of interactions in interfacial systems," J. Vac. Sci. Technol. A 7(1989):2829-2839.

[620] E. Meyer, R.M. Overney, K. Dransfeld, T. Gyalog, "Normal forces at atomic scale in nanoscience friction and rheology on the nanometer scale," World Scientific, Singapore, 1998; cited in: H.-U. Danzebrink, L. Koenders, G. Wilkening, A. Yacoot, H. Kunzmann, "Advances in Scanning Force Microscopy for Dimensional Metrology," CIRP Annals - Manufacturing Technology 55(2006):841-878.

3.3.5 Tip Registration

In his 2008 EPSRC Fellowship proposal,[621] P. Moriarty describes experiments to test the concept of "deterministic epitaxy" wherein each atom is placed in position via a deterministic computer-controlled trajectory, using an automated atom-by-atom assembly via scanning probe technology. One major practical challenge is the relocation of a single atomic site on a sample which may be several millimetres square in area – e.g., after abstracting an H atom from a passivated surface, we must revisit this same atomic lattice site after moving the tip a significant distance or, in some cases, exchanging samples or tips. This requires a viable methodology for relocating atomic sites on a macroscopic sample. Moriarty's proposed approach is to use local scanning probe oxidation, under ambient (or high relative humidity) conditions, of hydrogen-passivated diamond samples to form arrays of oriented micron-scale features resembling tiny arrowheads. These can act as "registration marks" to guide the tip to a micron scale region at the center of the sample surface, allowing that region to be used as a workspace for a lengthy sequence of site specific mechanosynthetic reactions at or near the same atomic site.

Local oxidation of hydrogen-passivated Si(111) surfaces using scanning probes has been shown experimentally[622] and the same technique can be applied, with very little modification, to H:C(100) surfaces[623] to form nanoscale and microscale oxide regions. The Nottingham group has previously developed registration mark protocols and successfully located the same molecular scale regions following removal and subsequent replacement of the sample in an STM.[624] Figure 3-8A shows an image of etched registration marks formed via e-beam lithography on an Si(100) surface. Combining e-beam lithography patterning with the requirement for atomically clean surfaces, although possible,[625] is immensely time-consuming and difficult, hence local scanning probe oxidation is used to form the features. Until very recently this technique would have been too slow to generate a sufficiently large array of registration marks, but the video-rate AFM system recently developed by Infinitesima (and available in the Nottingham Nanoscience Centre) enables rapid nanolithographic patterning of hydrogen-passivated silicon and diamond over distances of 100s of microns.[626]

---

[621] Philip Moriarty, "Digital Matter?: Towards Mechanised Mechanosynthesis," EPSRC Fellowship Proposal, March 2008, 9 pp.

[622] Christopher P. Martin, Matthew O. Blunt, Emmanuelle Pauliac-Vaujour, Andrew Stannard, Philip Moriarty, Ioan Vancea, Uwe Thiele, "Controlling Pattern Formation in Nanoparticle Assemblies via Directed Solvent Dewetting," Phys. Rev. Lett. 99(14 September 2007):116103.

[623] T. Kondo, M. Yanagisawa, et al., "Nanolithographic modification of diamond," Diam. Rel. Mat. 11(2002):1788-1796.

[624] A.W. Dunn, B.N. Cotier, A. Nogaret, P. Moriaty, P.H. Beton, "Molecular scale alignment strategies: An investigation of Ag adsorption on patterned fullerene layers," Appl. Phys. Lett. 71(1997):2937-2939.

[625] A.W. Dunn, B.N. Cotier, A. Nogaret, P. Moriaty, P.H. Beton, "Molecular scale alignment strategies: An investigation of Ag adsorption on patterned fullerene layers," Appl. Phys. Lett. 71(1997):2937-2939.

[626] A.D.L. Humphris, M.J. Miles, J.K. Hobbs, "A mechanical microscope – high-speed atomic force microscopy," Appl. Phys. Lett. 86(2005):034106.

Accurate registration of AFM tip location requires that the entire system must be properly positionally calibrated. Since the AFM is an instrument with 3D capabilities it is desirable to have standards at one's disposal that allow the whole measurement volume to be calibrated in one operation. Attempts were made to use etch pits in a silicon (111) plane (wafer). These negative pyramids, produced by anisotropic etching, show well-known flank angles and could, e.g., be used to calibrate the Z-axis[627] and to determine the rectangularity of the Z-axis to the XY scanning plane.[628] This method is based on the assumption that the side areas of the pyramids are perfect lattice planes, but investigations revealed local deviations due to inhomogeneities in the etching process[629] so the practical application might be very limited for 3D studies of the scanner behavior.

Figure 3-8. (A) Registration marks formed by e-beam lithography on a Si(100) surface.[630] (B) Example for a 3D standard: SEM image of a pyramidal structure with landmarks, up to 10-μm tall.[631]

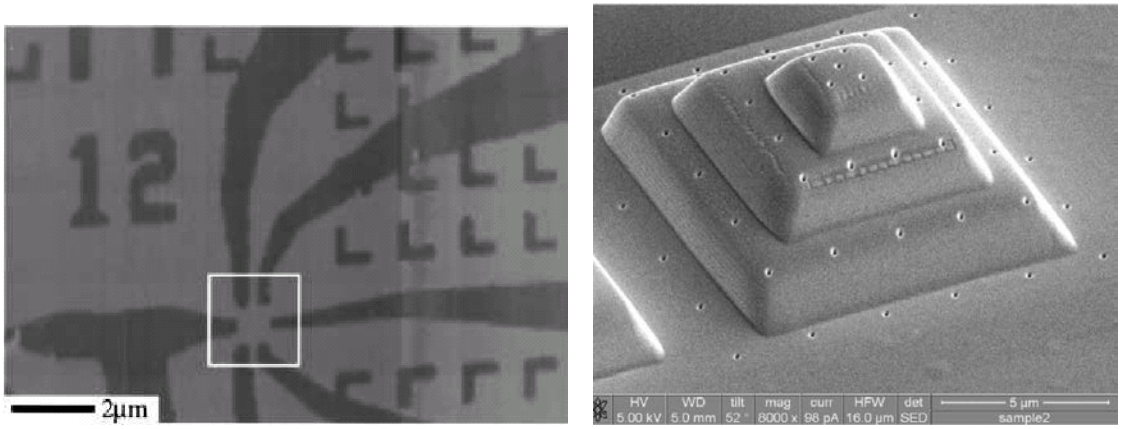

(A) **(B)**

---

[627] NT-MDT Co., Zelenograd, Moscow, Russia, www.ntmdt.ru.

[628] J. Garneas, A. Kühle, L. Nielsen, F. Borsetto, "True three-dimensional calibration of closed loop scanning probe microscopes," in: G. Wilkening, L. Koenders, eds., Nanoscale calibration standards and methods, Wiley-VCH, Weinheim, Germany, 2005, pp. 193-204.

[629] X. Min, T. Dziomba, L. Koenders, to be published; cited in: H.-U. Danzebrink, L. Koenders, G. Wilkening, A. Yacoot, H. Kunzmann, "Advances in Scanning Force Microscopy for Dimensional Metrology," CIRP Annals - Manufacturing Technology 55(2006):841-878.

[630] A.W. Dunn, B.N. Cotier, A. Nogaret, P. Moriaty, P.H. Beton, "Molecular scale alignment strategies: An investigation of Ag adsorption on patterned fullerene layers," Appl. Phys. Lett. 71(1997):2937-2939.

[631] M. Ritter, M. Hemmleb, O. Sinram, J. Albertz, H. Hohenberg, "A versatile 3D calibration object for various micro-range measurement methods," Proceedings ISPRS 2004, Istanbul, Turkey.

Positional 3D calibrations may be better achieved using novel micrometer-sized 3D calibration structures (Figure 3-8B) as proposed and recently realised as prototypes by Ritter et al.[632] These objects have features that act as reference markers or "nanomarks" that could serve as distinguishable reference points for the calibration not only of SPMs, but also of various other 3D micro-range measurements methods such as SEM (especially SEM stereogrammetry) and optical methods such as confocal laser-scanning microscopy (CLSM). They consist of a pyramid of up to 10 µm height with several terraces having reference points on each terrace which serve as nanomarks. The 3D calibration object was fabricated using gas-assisted focused ion beam (FIB) metal deposition. The spatial data of the non-symmetrically distributed markers were obtained by high-precision AFM and serve as reference points for the calibration of the user's instrument. For AFM this standard can be used to calibrate the lateral as well as the vertical scale of the scanner at once; in addition, it allows one to determine rectangularity errors of the XY plane and of the Z-axis to the XY plane, which is a practical advantage of such standards compared to the established types of SPM standards. The accuracy depends critically on the shape and quality of the steps and markers as well as on the calibration by AFM.

The landmark-based concept of these standards requires all measured coordinates of the nanomarkers to be compared with their respective reference values as stated, e.g., in the calibration certificate delivered with the standard.[633] Such a comparison of the coordinates of a whole set of nanomarkers requires automated data processing that matches the measured coordinates with the reference data by calculating at least the translator vector in all three directions, three angles of rotation and three scaling factors (nine degrees of freedom). Depending on the number of points and stability of this matching fit, this method also allows one to determine coupling factors between the axes together with higher degrees of freedom, e.g., parameters that quantify the distortion of the AFM scanning system. For DMS work requiring high positional precision registration, landmarks with detectable fixed features at the nanometer or sub-nanometer scale should be used in place of traditional micron-scale standards. (See also the additional comments in Section 4.4.)

3.4 Combination AFM Displacement Systems

The combination of various displacement systems with measuring instruments brings many advantages. For instance, to build a metrological AFM, the AFM is usually combined with a high-precision translation stage to alleviate the problems of non-linearity associated with the piezo elements of the AFM. Nevertheless, these translation stages have limitations, either with precision or scanning (and hence measurement) range.

---

[632] M. Ritter, M. Hemmleb, O. Sinram, J. Albertz, H. Hohenberg, "A versatile 3D calibration object for various micro-range measurement methods," Proceedings ISPRS 2004, Istanbul, Turkey.

[633] Martin Ritter, Thorsten Dziomba, Axel Kranzmann, Ludger Koenders, "A landmark-based 3D calibration strategy for SPM," Meas. Sci. Technol. 18(2007):404-414.

For sub-nanometer or sub-Angstrom resolution the AFM can be combined with an X-ray interferometer (Section 3.4.1). AFMs attached to coordinate measuring machines have also been set up for applications where large 3D specimens must be investigated at certain locations in more detail (Section 3.4.2). If a larger measuring range is required, or if there is a need to measure small areas at selective regions within a large sample area, the AFM can be combined with a large-range positioning stage, creating a Large-Range AFM (Section 3.4.3). This normally is an XY table equipped with suitable position measurement sensors. Instruments of this kind are commercially available and are used especially in the semiconductor and flat panel industries, though in most cases the positioning accuracy is limited to a few microns.

3.4.1 AFM and X-ray Interferometry

Although traceability of an AFM in all three axes can be achieved using optical interferometry to measure displacements, the non-linearity in optical interferometers will ultimately provide a limit to their measurement capability. To overcome this problem, the AFM has been combined with an X-ray interferometer.[634]

X-ray interferometry is a technique originally developed by Bonse and Hart.[635] Its potential for metrology was demonstrated by Hart[636] (who measured distances up to 0.1 micron with ±2 pm precision) and has subsequently been exploited by several national metrology institutes.[637] When combined with an AFM, the X-ray interferometer can be regarded as a linear high-resolution translation stage that makes displacements in discrete steps of 192 pm – a displacement corresponding to the lattice spacing of the (220) planes in silicon that is directly traceable to the meter.[638] A further development of this work was to combine an AFM with the Combined Optical and X-ray Interferometer (COXI) facility, jointly developed by NPL, PTB and IMGC.[639] (See Section 4.6.2.1 for an extensive description of this system.) COXI was originally developed as a facility for calibrating displacement transducers. The instrument can be thought of as a Vernier-type device where the coarse scale is an optical interferometer for measuring long-range displacements up to 1 mm in steps of optical fringes of 158 nm. The X-ray interferometer is used to interpolate optical fringes in 192 pm steps with a working range of up to 10 µm. Thus displacements of an AFM tip within the 1 mm range could be measured in steps as a combination

---

[634] Andrew Yacoot, Ulrich Kuetgens, Ludger Koenders, Thomas Weimann, "A combined STM and x-ray interferometer," Meas. Sci. Technol. 12(2001):1660-1665.

[635] U. Bonse, M. Hart, "An x-ray interferometer," Appl. Phys. Lett. 6(1965):155-156. U. Bonse, M. Hart, "Principles and design of Laue case X-ray interferometers," Z. Phys. 88(1965):154-164.

[636] M. Hart, "An Ångstrom ruler," Br. J. Appl. Phys. 1(1968):1405-1408.

[637] A. Yacoot, "Metrological applications of X-ray interferometry," in G. Wilkening, L. Koenders, eds., Nanoscale calibration standards and methods, Wiley-VCH, Weinheim, Germany, 2005, pp. 38-44.

[638] P.J. Mohr, B.P. Taylor, "CODATA recommended values for the fundamental physical constants," Rev. Mod. Phys. 72(2000):351-435.

[639] P. Becker, J. Stümpel, "X-ray optics in metrological application," Metrologia 27(1990):127-132.

of integer numbers of X-ray and optical fringes. Danzebrink[640] opines that "the combination of such techniques is complicated and probably remains within the remit of national metrology institutes," but the unrivalled resolution and accuracy of the X-ray interferometer makes it a valuable tool in the quest for AFM measurements with lower uncertainty and a leading contender in the design of the first molecular manufacturing workstation.

3.4.2 AFM and CMM

An AFM has been mounted on a coordinate measuring machine (CMM) to extend its working range, thereby achieving free positioning of the AFM in the space covered by the CMM.[641] This integrated system can be used for surface mapping.[642] The CMM is used to reposition the AFM probe in between measurements that are stitched together thereby over a continuous region much larger than the range normally scanned by the AFM. Correct stitching independently from the positioning errors of the CMM is obtained though optimization of the cross-correlation between two adjacent overlapping surface areas. In one study in 2004, an uncertainty of 0.8% was achieved for the case of surface mapping across an area 1.2 mm wide by combining of 49 single AFM images as shown in Figure 3-9.[643]

---

[640] H.-U. Danzebrink, L. Koenders, G. Wilkening, A. Yacoot, H. Kunzmann, "Advances in Scanning Force Microscopy for Dimensional Metrology," CIRP Annals - Manufacturing Technology 55(2006):841-878.

[641] N. Kofod, "Validation and industrial application of AFM," Ph. D Thesis, Department of Manufacturing Engineering and Management, Technical University of Denmark and Danish Fundamental Metrology, 2002. L. De Chiffre, H.N. Hansen, N. Kofod, "Surface topography characterization using an atomic force microscope mounted on a coordinate measuring machine," Annals of CIRP 48(1999):463-466.

[642] H.N. Hansen, P. Bariani, L. De Chiffre, "Modelling and measurement uncertainty estimation for integrated AFM-CMM Instrument," Annals of the CIRP 55(2005). L. De Chiffre, F. Marinello, P. Bariani, H.N. Hansen, "Surface mapping with an AFM-CMM, Integrated system and stitching software," Proceedings of 4th EUSPEN International Conference, 2004, pp. 326-327. J.C. Wyant, J. Schmit, "Large field of view, high spatial resolution, Surface Measurements," International Journal of Machine Tools & Manufacture 38(1998):691-698. K. Yanagi, M. Hasegawa, S. Hara, "A computational method for stitching a series of 3D surface topography data measured by microscope-type surface profiling instruments," Proc. of 3rd EUSPEN Int. Conference, 2(2002):653-656. S.H. Huerth, H.D. Hallen, "Quantitative method of image analysis when drift is present in a scanning probe microscope," J. Vac. Sci. Technol. 21(2003):714-718. P. Bariani, "Dimensional metrology for microtechnology", Ph.D. Thesis, Department of Manufacturing Engineering and Management, Technical University of Denmark, 2004.

[643] P. Bariani, "Dimensional metrology for microtechnology", Ph.D. Thesis, Department of Manufacturing Engineering and Management, Technical University of Denmark, 2004.

Figure 3-9. 3D plot of an AFM image (1.2 mm x 1.2 mm in size) composed of 49 single scans stitched together.[644]

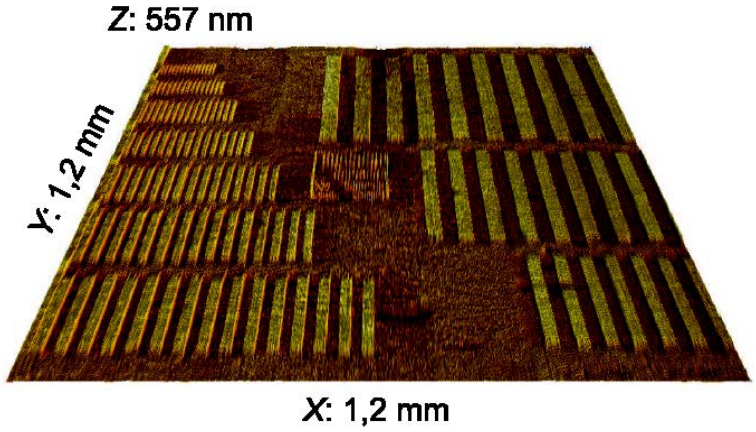

3.4.3 Large-Range AFMs

The term "Large-Range AFMs" should be understood as referring to instruments that allow AFM imaging over the whole range of several millimeters – in contrast to ordinary combinations of AFM head plus coarse positioning stage. The first prominent example of an APM-based metrology instrument that is designed to achieve sub-nanometer resolution over a macroscopic area of 50 mm x 50 mm is called the Molecular Measuring Machine or M^3.[645] (See Section 4.6.1.1 for an extensive description of this system.) The goal of M^3 is to achieve 1 nm combined uncertainty for point-to-point measurements within the full working area.

Another system (long-range scanning system or LORS; Section 4.6.1.3) is a magnetically suspended six degree-of-freedom precision motion control stage with a travel range of 25 mm x 25 mm x 0.1 mm.[646]

At PTB a large-range SPM (LR-SPM; see Section 4.6.1.2) has been developed with a measurement volume of 25 mm × 25 mm × 5 mm.[647] To obtain the large range scanning

---

[644] P. Bariani, "Dimensional metrology for microtechnology", Ph.D. Thesis, Department of Manufacturing Engineering and Management, Technical University of Denmark, 2004.

[645] E.C. Teague, "The National Institute of Standards and Technology molecular measuring machine project:. metrology and precision engineering design," J. Vac. Sci. Technol. B 7(1989):1898-1902. John A. Kramar, "Nanometre resolution metrology with the Molecular Measuring Machine," Meas. Sci. Technol., 16(2005):2121-2128.

[646] M. Holmes, R. Hocken, D. Trumper, "The long-range scanning stage: a novel platform for scanned-probe microscopy," Precis. Eng. 24(July 2000):191-209.

capability, the sample is moved in this case by a combined motion system which consists of a fast Z-piezo positioning stage (Z-PPS) and a ball-bearing positioning stage.[648] All six degrees of freedom of the motion stage are measured directly by interferometers (with a resolution of 80 pm) and angle sensors (with a resolution < 0.01 arc-seconds). During the measurement process the AFM probe tip (so also the measurement point) is always located at the intersection point of the three interferometer beams, which reduces the Abbe errors to a minimum.

3.5 Noise, Environmental Isolation, and Measurement Uncertainty

In order to make high accuracy traceable measurements not only a well designed and characterized instrument is required, but also the instrument must be operated in a suitable environment that has minimum influence on the measurement.

Intrinsic electronic noise is the main source of measurement noise. Its level can be amplified by electronic interference with external sources. The dynamic behavior of an AFM also depends strongly on its excitation by ambient vibrations – both acoustic and mechanical. Mechanical vibrations from the floor must be damped by means of passive or active tables. A damping table and AFM form a complicated coupled mechanical system[649] and it is advisable to follow the manufacturers' suggestions when setting up such a system. Acoustic noise raises the measurement noise level and specific narrow-band acoustic excitation may influence measurements dramatically. Sufficient temperature stability is also a prerequisite for high quality dimensional measurements.

There is no general rule for the required level of stability, since different AFM designs show different susceptibility and particular measurement tasks demand different degrees of stability. In practice, a suitable enclosure is indispensable for high quality measurements and can go a long way towards eliminating the effects of many external disturbances. Enclosures should be designed in such a way that they damp acoustic and electronic interference as well as temperature fluctuations. For highest effectiveness, enclosures should cover the complete set-up, including the AFM and the anti-vibration table or platform.

An acoustic chamber comprising an aluminum box with bituminous coating and cellular foam plastic insulation, as used with the modified SIS Nanostation nc-AFM[650] in the PTB cleanroom

---

[647] G. Dai, F. Pohlenz, H.-U. Danzebrink, M. Xu, K. Hasche, G. Wilkening, "Metrological large range scanning probe microscope," Rev. Sci. Instrum. 75(2004):962-969; http://www.physikinstrumente.com/en/news/pdf/large range scanning probe microscope.pdf.

[648] G. Jäger, E. Manske, T. Hausotte, H.-J. Büchner, R. Grünwald, W. Schott, "Nanometrology - nanomeasuring machines," Proc. Annual Meeting of ASPE, Crystal City, Virginia, USA, 2001, pp. 23-27.

[649] J.C. Wyant, J. Schmit, "Large field of view, high spatial resolution, Surface Measurements," International Journal of Machine Tools & Manufacture 38(1998):691-698.

[650] Surface Imaging Systems (S.I.S.) GmbH, Herzogenrath, Germany, www.sis-gmbh.com.

center,[651] reduces the integrated noise to one third. A massive sample holder helps to reduce noise further. The drawback of such an acoustic chamber is that it might also act as a thermal insulator, thereby preventing any heat generated inside the chamber from escaping. The heat sources and the time constants of the temperature change need to be determined so that appropriate countermeasures can be taken. (At minimum, these time constant should be taken into account when defining operation guidelines, e.g., to determine the idle time needed after opening/closing the chamber to reach temperature equilibrium.)

Such temperature dependence can be avoided or at least minimized in the course of construction of an AFM system by taking great care in designing the measuring loop – so that the probe's position relative to the sample does not change with temperature at all or at least not in all three directions. This is usually achieved by selecting materials with a low thermal expansion coefficient and by designing the measurement loop to be as small as possible.

The uncertainty for AFM in dimensional measurements must be calculated following the rules of the Guide to the Expression of Uncertainty in Measurement (GUM).[652] The properties of the instrument and the experimental set-up must be taken into account as well as the properties of the standard and of the sample. Except for a few instruments equipped with laser interferometers the axes have to be calibrated using certified standards. For these instruments the uncertainty components should be divided into components associated with the calibration of the instrument (i.e., uncertainty of calibrated standards used, non-linearity of the instrument, angular motion of translation stages (scanner and/or Z-axis) and Abbe offset), the measurement sample (i.e., alignment, noise and drift, cross-talk between XY and Z-axis, remaining non-linearity of the scanner, tip wear/shape, repeatability), and the evaluation (i.e., roughness and homogeneity of standard and sample, temperature of the standard, evaluation method).

In most practical cases, the dynamic effects contribute significantly to the overall measurement uncertainty. The scanning speed can affect the cross talk between axes and many scanning systems can be described quite well by a set of both scan-rate and scan-range dependent correction factors.[653] It is generally mandatory to check the dynamic behavior of the scan system carefully during – or better, before – the instrument is calibrated. If the dynamic behavior appears too unsystematic to allow determination of a set of speed-related correction factors, then these dynamic influences must be accounted for in the overall uncertainty budget.

---

[651] T. Dziomba, L. Koenders, G. Wilkening, M. Flemming, A. Duparré, "Development of a calibration guideline for scanning probe microscopes," Technisches Messen. 72(2005):295-307.

[652] ISO/BIPM Guide to the Expression of Uncertainty in Measurements (GUM), Corrected and reprinted, 1995, BSI, London; Geneva, ISO.

[653] T. Dziomba, L. Koenders, H.-U. Danzebrink, G. Wilkening, "Lateral & vertical calibration of SPM and their measurement uncertainty," in: M. Dietzsch, ed., Proceed. of the XIth Intl. Colloq. on Surfaces, Chemnitz, Shaker Verlag, Aachen, Germany, 2004, pp. 117-128.

More information about uncertainty budget calculations is available for height,[654] for pitch (horizontal feature spacing),[655] or for combined height/pitch measurements.[656] Marinello et al.[657] have summarized the many sources of distortions that occur in AFM scanning systems (Table 3-4). The numerous positioning errors are surveyed and systematized in the ISO GUM[658] standards (see above).

---

[654] F. Meli, R. Thalmann, "Long range AFM profiler used for accurate pitch measurements," Meas. Sci. Technol., 9(1998):1087-1092. L. Koenders, R. Bergmans, J. Garnaes, J. Haycocks, N. Korol, T. Kurosawa, F. Meli, B.C. Park, G.S. Peng, G.B. Picotto, E. Prieto, S. Gao, B. Smereczynska, T. Vorburger, G. Wilkening, "WGDM-7: Preliminary comparison on nanometrology according to the rules of CCL key comparisons. Nano 2 Step height standards," Metrologia Technical Report, 40(2004):04001. H. Edwards, J. Joergensen, J. Dagata, Y. Strausser, J. Schneir, "Influence of data analysis and other factors on the short-term stability of vertical scanning probe microscope calibration measurements," J. Vac. Sci. Technol. B 16(1998):633-644.

[655] I. Misumi, S. Gonda, T. Kurosawa, Y. Tanimura, N. Ochiai, J. Kitta, F. Kubota, M. Yamada, Y. Fujiwara, Y. Nakayama, K. Takamasu, "Submicrometre-pitch intercomparison between optical diffraction, scanning electron microscope and atomic force microscope," Meas. Sci. Technol. 14(6 October 2003):2065-2074; http://www.nano.pe.u-tokyo.ac.jp/pdffiles/mst3_12_004.pdf. I. Misumi, S. Gonda, T. Kurosawa, K. Takamasu, "Uncertainty in pitch measurements of onedimensional grating standards using a nanometrological atomic force microscope," Meas. Sci. Technol. 14(7 March 2003):463-471. F. Meli, "International comparison in the field of nanometrology: Pitch of 1D gratings," Nano4, Proc. of 2nd Int. EUSPEN Conference, Italy, Vol. 1, 2001, pp. 358-361. T. Dziomba, W. Häßler-Grohne, H. Bosse, H.-U. Danzebrink, G. Wilkening, "Influence of nanostandard properties on calibration procedures of SPMs," Proc. 4th Int. EUSPEN Conference, 2(2003):491-494. J. Joergensen, J. Jensen, J. Garnaes, "Lateral metrology using scanning probe microscopes, 2D pitch standards & image processing," Appl. Phys. A 66(1998):847-852.

[656] N. Kofod, "Validation and industrial application of AFM," Ph. D Thesis, Department of Manufacturing Engineering and Management, Technical University of Denmark and Danish Fundamental Metrology, 2002. T. Dziomba, L. Koenders, H.-U. Danzebrink, G. Wilkening, "Lateral & vertical calibration of SPM and their measurement uncertainty," in: M. Dietzsch, ed., Proceed. of the XIth Intl. Colloq. on Surfaces, Chemnitz, Shaker Verlag, Aachen, Germany, 2004, pp. 117-128. R. Dixson, A. Guerry, M. Bennett, T. Vorburger, M. Postek, in Metrology Inspection, and Process, Control for Microlithography XVI, Danile J.C. Herr, ed., Proc. SPIE 4689(2002):313-335.

[657] F. Marinello, P. Bariani, S. Carmignato, E. Savio, "Geometrical modelling of scanning probe microscopes and characterization of errors," Meas. Sci. Technol. 20(2009):084013.

[658] ISO/BIPM Guide to the Expression of Uncertainty in Measurements (GUM), Corrected and reprinted, 1995, BSI, London; Geneva, ISO.

Table 3-4. Main AFM distortions. The third column indicates (proportionally to the number of arrows) if a compensation or an improvement is possible through instrument calibration or post-processing operations.[659]

Source	Distortion	Systematicity
Scanning system	Positioning (21 errors)	↑↑↑
	Scaling	↑↑↑
	Nonlinearity	↑↑
	Resolution	↑
	Drift	↑↑
	Hysteresis	↑
	Creep	–
	Aging	–
	Sampling synchronization	↑
Probing system	Mode switching	–
	Cantilever dynamics	↑
	Convolution	↑↑
	Tip wear	↑
	Unsampled parts	–
	Cantilever reflectivity	–
	Surface or probe deformations	–
Environment	Noise	↑
	Vibrations	–
	Temperature	–
	Humidity	–
	Contaminations	↑
Data processing	Filtering	↑
	Levelling	↑↑↑

[659] F. Marinello, P. Bariani, S. Carmignato, E. Savio, "Geometrical modelling of scanning probe microscopes and characterization of errors," Meas. Sci. Technol. 20(2009):084013.

4. Key Enabling Technologies for the Molecular Workstation

The completion of the Minimal Toolset paper[660] provides a first cut at the required operations that a DMS molecular manufacturing system must perform. Further analysis of alternative tooltips and strategems to be employed in the bootstrap development sequence leading to a full diamondoid manufacturing system will result in an elucidation of the system specifications for the first molecular workstation. These specifications will define the number of tooltips and surfaces needed, the number of DOFs needed for each tooltip and for the workpiece surface, the ranges of motion and forces required to perform the specified diamondoid mechanosynthesis (DMS) operations, the precision of motion for each DOF of each tooltip or surface, and so forth. With these specifications in hand, we can then proceed to a comprehensive molecular workstation design effort.

However, even without these detailed specifications that will soon be in our possession, enough is already known today about the required capabilities of the molecular workstation to allow identification of the nine key enabling technologies that will be involved in a comprehensive workstation design effort. These key enabling technologies are:

(1) workspace surfaces (Section 4.1),
(2) atomically sharp tooltips (Section 4.2),
(3) tooltip handles, tool chucks, and toolrack (Section 4.3),
(4) tooltip positional registration (Section 4.4),
(5) SPM positioning systems (Section 4.5),
(6) metrological SPM systems (Section 4.6),
(7) environmental isolation (Section 4.7),
(8) ancillary facilities (Section 4.8), and
(9) control software (Section 4.9).

During the design process, we will select the most suitable of the available technical options for each required capability, and these choices must then be integrated into our workstation system design so that all required performance specifications are satisfied. It is expected that some number of design iterations may be needed to arrive at a workable system with acceptable tradeoffs among the numerous design and performance constraints.

4.1 Workspace Surfaces

To perform reliable DMS operations within the interior working environment of the molecular workstation, aka. the "workspace", we will require atomically flat surfaces (Section 4.1.1), feedstock presentation surfaces (Section 4.1.2), disposal surfaces (Section 4.1.3), DMS fabrication (Section 4.1.4),and release (Section 4.1.5) surfaces, a nanopart gripper tool capable of

---

[660] Robert A. Freitas Jr., Ralph C. Merkle, "A Minimal Toolset for Positional Diamond Mechanosynthesis," J. Comput. Theor. Nanosci. 5(May 2008):760-861; http://www.molecularassembler.com/Papers/MinToolset.pdf.

detaching finished parts from the build surface (Section 4.1.6), and the ability to rapidly scan all those surfaces (Section 4.1.7).

4.1.1 Atomically Flat Surfaces

Performing DMS will require starting with well-behaved atomically flat surfaces upon which workpieces can be reliably fabricated, feedstock molecules can be precisely positioned, and waste molecules can be disposed of one by one in specific locations. Hence one key technology for the molecular workstation is the ability to create or procure atomically flat surfaces.

A flat depassivated diamond surface[661] may be required to serve as a hydrogen dump[662] (transient H atom source and sink), and a flat depassivated germanium surface[663] may be required for positionally precise methane, acetylene or digermane presentation. Both diamond[664] and germanium[665] "flat" surfaces can be produced using currently available bulk chemical vapor deposition (CVD) techniques.

In the case of diamond, as early as 1995 Kühnle and Weis[666] had shown that atomically flat diamond surfaces with no damage layer below, having residual roughness of ~2 Å RMS independent of crystal orientation, could be produced by mechanochemical superpolishing of diamond substrates using $NaNO_3$ or KNO_3 as oxidizing agents (for use in diamond electronics which needs atomically flat and damage-free diamond substrates for the growth of doped and undoped homoepitaxial layers of high crystalline quality). By 1998 Hayashi et al.[667] had obtained an atomically flat C(100) diamond surface via hydrogen-plasma treatment, with AFM revealing the resulting diamond surface to consist of successive terraces with atomic steps running parallel to the C(110) direction. By 1999, the same group was able to grow homoepitaxial C(100) diamond films with atomically flat surface with mean roughness of 0.4 Å over areas as large as

---

[661] A.V. Hamza, G.D. Kubiak, R.H. Stulen, "The role of hydrogen on the diamond C(111)-(2 x 1) reconstruction," Surface Sci. 206(1988):L833-L844.

[662] Robert A. Freitas Jr., Ralph C. Merkle, "A Minimal Toolset for Positional Diamond Mechanosynthesis," J. Comput. Theor. Nanosci. 5(May 2008):760-861; http://www.molecularassembler.com/Papers/MinToolset.pdf.

[663] V.I. Davydov, Germanium, Gordon and Breach, New York, 1966.

[664] Jes Asmussin, D.K. Reinhard, eds., Diamond Films Handbook, Marcel Dekker, New York, 2002.

[665] K.-S. Huang, T.-S. Ku, D.-S. Lin, "Growth process of Ge on Si(100)-(2x1) in atomic-layer epitaxy from Ge_2H_6," Phys. Rev. B56(1997):4878; http://www.cc.nctu.edu.tw/~dslin/Gesi100.pdf

[666] J. Kühnle, O. Weis, "Mechanochemical superpolishing of diamond using $NaNO_3$ or KNO_3 as oxidizing agents," Surface Science 340(10 October 1995):16-22.

[667] Kazushi Hayashi, Sadanori Yamanaka, Hideyuki Watanabe, Takashi Sekiguchi, Hideyo Okushi, Koji Kajimura, "Atomic force microscopy study of atomically flat (001) diamond surfaces treated with hydrogen plasma," Applied Surface Science 125(2 January 1998):120-124.

4x4 mm^2 (the whole region of the substrate), using the microwave plasma chemical vapor deposition method at a low CH_4 concentration of 0.025% in a CH_4 and H_2 mixed gas system.[668] Tokuda et al.[669] also achieved homoepitaxial growth of diamond C(111) films by microwave plasma-enhanced chemical vapor deposition, in which lateral film growth forms atomically flat surfaces that include atomically flat terraces over several hundred nanometer widths with single-bilayer steps of C(111) diamond. The same group has fabricated a nanometer scale height standard by using an atomically controlled diamond surface consisting of an equilateral triangular island with 2.06-Å bi-atomic layer steps of (111) diamond on an atomically flat surface.[670]

As for germanium, atomically smooth Ge(111) samples with ~0.15 Å surface undulations have been used in STM work since the late 1980s.[671] Gregory et al.[672] has used repetitive Ar^+ ion bombardment for ~1 hr followed by ~20 min resistive heating (annealing) of a germanium crystal under ultrahigh vacuum conditions to produce large, atomically flat (1x1) regions on a Ge(111) crystal face. More recently, Qin et al.[673] prepared an atomically smooth Ge(100) surface on a large scale by deposition of submonolayer Ge on a Ge(100) surface at 300 °C, which repairs the missing dimer defects produced during enhanced energy ion bombardment and annealing of the substrate. Tsui et al.[674] cleaned a semi-insulating Ge(100) sample using the standard RCA method, then degassed it at 600 °C under UHV conditions. A growth-anneal cycle was then employed to prepare a Ge(100) buffer layer of 380 Å thick, preceding the growth of a ternary CoMn-doped Ge combinatorial film wherein during each cycle, a thin Ge layer (typically 30-100 Å) was deposited at 250 °C and then annealed at 600 °C. The resulting surface was atomically smooth across the entire substrate with (2x1) surface reconstructions, as determined by real-time

---

[668] H. Watanabe, D. Takeuchi, S. Yamanaka, H. Okushi, K. Kajimura, T. Sekiguchi, "Homoepitaxial diamond film with an atomically flat surface over a large area," Diamond and Related Materials 8(July 1999):1272-1276.

[669] Norio Tokuda, Hitoshi Umezawa, Sung-Gi Ri, Masahiko Ogura, Kikuo Yamabe, Hideyo Okushi, Satoshi Yamasaki, "Atomically flat diamond (111) surface formation by homoepitaxial lateral growth," Diamond and Related Materials 17(July-October 2008):1051-1054.

[670] Norio Tokuda, Hitoshi Umezawa, Hiromitsu Kato, Masahiko Ogura, Satoshi Gonda, Kikuo Yamabe, Hideyo Okushi, Satoshi Yamasaki, "Nanometer Scale Height Standard Using Atomically Controlled Diamond Surface," Appl. Phys. Express 2(2009):055001.

[671] R.S. Becker, J.A. Golovchenko, B.S. Swartzentruber, "Atomic-scale surface modifications using a tunneling microscope," Nature 325(1987):419-421.

[672] B.W. Gregory, S. Thomas, S.M. Stephens, R.A. Dluhy, L.A. Bottomley, "Preparation of atomically smooth germanium substrates for infrared spectroscopic and scanning probe microscopic characterization of organic monolayers," Langmuir 13(1997):6146-6150; http://www.chem.uga.edu/dluhy/pdf%20files/ge_atm_ir.pdf

[673] Zhihui Qin, Dongxia Shi, Wei Ji, Shijin Pan, Hong-Jun Gao, "Processing of an atomically smooth Ge(001) surface on a large scale," Nanotechnology 17(14 May 2006):2396-2398.

[674] F. Tsui, B.A. Collins, L. He, A. Mellnik, Y. Zhong, S. Vogt, Y.S. Chu, "Combinatorial synthesis and characterization of a ternary epitaxial film of Co and Mn doped Ge(001)," Applied Surface Science 254(2007):709-713.

scanning reflection high-energy electron diffraction (RHEED) measurements. Wistey et al.[675] achieved low-temperature (350-420 °C) growth of atomically smooth Ge films (2-4 Å roughness) directly on Si(100) via gas-source molecular beam epitaxy.

Of course, our standards for "flatness" are extraordinarily high. Achieving true atomic flatness over large areas of diamond and germanium is still fairly challenging and the practical difficulties should not be underestimated. For instance, as part of Philip Moriarty's 5-year $3M experimental program (2008-2013) to conduct the first diamond mechanosynthesis experiments[676] following the DMS proposals of Freitas and Merkle,[677] a key additional collaboration was established with Chris Pakes at La Trobe University, Victoria, Australia to provide atomically flat passivated diamond surfaces within the context of an Australian Research Council-funded project,[678] since La Trobe had built up considerable expertise on hydrogen-passivated diamond surfaces prepared using microwave plasmas. However, in 2009 Moriarty privately reported that the initial samples of diamond C(100) surface provided by Pakes were not sufficiently atomically flat for DMS work and that Pakes was attempting to improve the process further.

Atomically flat surfaces have also been produced using many other materials. For example, in 1995 Yoshimoto et al.[679] prepared atomically ultrasmooth sapphire (0001) surfaces (crystalline α-Al_2O_3) by annealing in air at temperatures between 1000-1400 °C. These surfaces have atomic steps ~2 Å in height and typically show atomically flat terraces measuring 50-100 nm in width, as determined quantitatively by atomic force microscopy and ion scattering spectroscopy and confirmed via theory using molecular dynamics simulations. The terrace width and atomic step height of the ultrasmooth surfaces were controlled on an atomic scale by changing the annealing conditions and the crystallographic surface of substrates, and the obtained ultrasmooth surface was stable in air. Relatively large plates of this flat-sapphire material have been prepared for macroscale biological tests of various kinds.[680] Kuroda et al.[681] have fabricated an atomically flat

---

[675] M.A. Wistey, Y.-Y. Fang, J. Tolle, A.V.G. Chizmeshya, J. Kouvetakis, "Chemical routes to Ge/Si(100) structures for low temperature Si-based semiconductor applications," Appl. Phys. Lett. 90(19 February 2007):082108.

[676] "Nanofactory Collaboration Colleague Awarded $3M to Conduct First Diamond Mechanosynthesis Experiments," press release, Nanofactory Collaboration, 11 August 2008; http://www.molecularassembler.com/Nanofactory/Media/PressReleaseAug08.htm.

[677] Robert A. Freitas Jr., Ralph C. Merkle, "A Minimal Toolset for Positional Diamond Mechanosynthesis," J. Comput. Theor. Nanosci. 5(May 2008):760-861; http://www.molecularassembler.com/Papers/MinToolset.pdf.

[678] Philip Moriarty, "Digital Matter?: Towards Mechanised Mechanosynthesis," EPSRC Fellowship Proposal, March 2008, 9 pp.

[679] M. Yoshimoto, T. Maeda, T. Ohnishi, H. Koinuma, O. Ishiyama, M. Shinohara, M. Kubo, R. Miura, A. Miyamoto, "Atomic-scale formation of ultrasmooth surfaces on sapphire substrates for high-quality thin-film fabrication," Appl. Phys. Lett. 67(30 October 1995):2615-2617.

[680] K. Yoshida, M. Yoshimoto, K. Sasaki, T. Ohnishi, T. Ushiki, J. Hitomi, S. Yamamoto, M. Sigeno, "Fabrication of a New Substrate for Atomic Force Microscopic Observation of DNA Molecules from an Ultrasmooth Sapphire Plate," Biophys. J. 74(April 1998):1654-1657.

silicon surface with straight atomic steps and a very uniform terrace width of 140-150 nm over the entire surface of a large 200-mm-diameter silicon wafer. Jia et al.[682] have grown atomically flat lead (Pb) metal ultrathin films on Si(111) semiconductor substrates, as Pb atoms are known to terminate Si(111) surface dangling bonds and to reduce the surface energy significantly;[683] Wang et al.[684] have also fabricated Pb nanowires having atomically smooth surfaces. Hegner et al.[685] have produced atomically flat (~2 Å) gold films with ultralarge atomically flat areas (2.25 μm^2; also, 25 μm^2 areas at ~3 Å) using a method called "template-stripped gold" in which the epitaxial growth of gold on mica is followed by thermal deposition of gold onto freshly cleaved mica sheets, then gluing to a piece of Si wafer, then chemically or consecutively mechanically stripping the mica down to a fresh gold surface. Numerous other atomically flat surfaces – e.g., of platinum,[686] silver,[687] silicon carbide (SiC),[688] graphite,[689] Te,[690] GaAs (110),[691] TiO_2,[692]

---

[681] R. Kuroda, T. Suwa, A. Teramoto, R. Hasebe, S. Sugawa, T. Ohmi, "Atomically Flat Silicon Surface and Silicon/Insulator Interface Formation Technologies for (100) Surface Orientation Large-Diameter Wafers Introducing High Performance and Low-Noise Metal–Insulator–Silicon FETs," IEEE Transactions on Electron Devices 56(February 2009):291-298.

[682] Jin-Feng Jia, Shao-Chun Li, Yan-Feng Zhang, Qi-Kun Xue, "Quantum Size Effects Induced Novel Properties in Two-Dimensional Electronic Systems: Pb Thin Films on Si(111)," J. Phys. Soc. Jpn. 76(2007):082001.

[683] Ing-Shouh Hwang, Tien-Chih Chang, Tien T. Tsong, "Growth Mechanism and Morphology of Ge on Si(111) Surfaces," Paper A9.4, Session A9: Poster Session, Strained Epitaxial Films, 3 December 1997, MRS Symposium A: Evolution of Surface Morphology and Thin-Film Microstructure, 1-4 December 1997; http://www.mrs.org/s_mrs/doc.asp?CID=14865&DID=86243.

[684] L.L. Wang, X.C. Ma, P. Jiang, Y.S. Fu, S.H. Ji, J.F. Jia, Q.K. Xue, "Uniform Pb nanowires of magic thickness on Si(111) controlled by elastic interaction and quantum size effects," Phys. Rev. B 74(2006):073404.

[685] Martin Hegner, Peter Wagner, Giorgio Semenza, "Ultralarge atomically flat template-stripped Au surfaces for scanning probe microscopy," Surface Science 291(1 July 1993):39-46.

[686] M.L. Hildner, T.J. Minvielle, R.J. Wilson, "Epitaxial growth of ultrathin Pt films on basal-plane sapphire: the emergence of a continuous atomically flat film," Surface Science 396(20 January 1998):16-23.

[687] Arthur R. Smith, Kuo-Jen Chao, Qian Niu, Chih-Kang Shih, "Formation of Atomically Flat Silver Films on GaAs with a 'Silver Mean' Quasi Periodicity," Science 273(12 July 1996):226-228.

[688] V. Ramachandran, M.F. Brady, A.R. Smith, R.M. Feenstra, D.W. Greve, "Preparation of atomically flat surfaces on silicon carbide using hydrogen etching," Journal of Electronic Materials 27(April 1998):308-312; http://www.cmu.edu/physics/stm/publ/5/sic1.pdf.

[689] Paolo Lacovig, Monica Pozzo, Dario Alfe, Paolo Vilmercati, Alessandro Baraldi, Silvano Lizzit, "Growth of Dome-Shaped Carbon Nanoislands on Ir(111): The Intermediate between Carbidic Clusters and Quasi-Free-Standing Graphene," Phys. Rev. Lett. 103(16 October 2009):166101. Johann Coraux, Alpha T. N'Diaye, Martin Engler, Carsten Busse, Dirk Wall, Niemma Buckanie, Frank-J Meyer zu Heringdorf, Raoul van Gastel, Bene Poelsema, Thomas Michely, "Growth of graphene on Ir(111)," New J. Phys. 11(4

$SrTiO_3$,[693] $LiNbO_3$ and $LiTaO_3$ substrates,[694] and step-free surface regions on metal W(110), Ru(0001), Cu(100), and Fe(100) single crystals[695] – have also been prepared.

Another well-known technology for producing atomically flat surfaces is atomic layer epitaxy (ALE) (Section 4.2.3) and the associated technique of patterned ALE (PALE) (Section 4.2.4), in which self-limiting monolayers can be deposited to create atomically flat surfaces that are one atomic layer thick, using various metals and semiconductor materials such as Si, Ge, SiO_2, and the like. ALE and PALE are described at length in the sections cited above, so those discussions will not be repeated here.

4.1.2 Feedstock Presentation Surface

Performing DMS will require using atomically flat surfaces (Section 4.1.1) to hold feedstock molecules in fixed position at a temperature that permits little or no surface migration, enabling the toll manipulation system to acquire feedstock molecules at need via blind pick-and-place operations. This implies a need for feedstock molecules to bond to such a **presentation surface** tightly enough not to migrate or boil off, but loosely enough so that a DMS tool can bond more tightly to them, and thus remove them reliably from the presentation surface. The original

---

February 2009):023006. "Fabricating Large-Area Sheets of Single-Layer Graphene by CVD," NASA's Jet Propulsion Laboratory, 1 August 2008; http://www.techbriefs.com/component/content/article/2992.

[690] Jie-Ren Ku, Ruxandra Vidu, Pieter Stroeve, "Mechanism of Film Growth of Tellurium by Electrochemical Deposition in the Presence and Absence of Cadmium Ions," J. Phys. Chem. B 109(2005):21779-21787.

[691] Ji-Won Oh, Masahiro Yoshita, Hidefumi Akiyama, Loren N. Pfeiffer, Ken W. West, "Step-edge kinetics driving the formation of atomically flat (110) GaAs surfaces," Appl. Phys. Lett. 82(17 March 2003):1709-1711; http://aki.issp.u-tokyo.ac.jp/oh/pdf/APL01709.pdf

[692] R. Nakamura, N. Ohashi, A. Imanishi, T. Osawa, Y. Matsumoto, H. Koinuma, Y. Nakato, "Crystal-face dependences of surface band edges and hole reactivity, revealed by preparation of essentially atomically smooth and stable (110) and (100) n-TiO(2) (rutile) surfaces," J. Phys. Chem. B 109(10 February 2005):1648-1651.

[693] Jaewan Chang, Yoon-Seok Park, Sang-Koog Kim, "Atomically flat single-terminated $SrTiO_3$ (111) surface," Appl. Phys. Lett. 92(18 April 2008):152910.

[694] G.H. Lee, "Realization of ultrasmooth surface with atomic scale step structure on $LiNbO_3$ and $LiTaO_3$ substrates," Optics Express 10(1 July 2002):556-560; http://www.opticsinfobase.org/DirectPDFAccess/AE7A1D3B-BDB9-137E-CFDDB1D7919B4843_69328.pdf?da=1&id=69328&seq=0.

[695] F. El Gabaly, N.C. Bartelt, A.K. Schmid, "Preparing arrays of large atomically flat regions on single crystal substrates," J. Phys.: Condens. Matter 21(2009):314019.

proposal[696] was to use a flat depassivated germanium surface decorated with methyl groups (CH_3), acetylene (C_2H_2) or bare carbon dimers (C_2) as the feedstock carbon source, or with digermane (Ge_2H_6) groups as the feedstock germanium source, or with passivating H atoms as the feedstock hydrogen source.

If it proves possible to employ atomically sharp metal tips (Section 4.2.2), the range of required tooltip motions (along with the number of tips and DOFs) may be greatly reduced. However, metal-C and metal-Ge bonds are apparently somewhat weaker than Ge-C and Ge-Ge bonds, hence we will require a feedstock presentation surface other than Ge that binds more weakly to the C- and Ge-based feedstock molecules. One possibility under investigation is the use of a lead (Pb) surface to which the C- and Ge-based feedstock molecules could be bonded. Atomically flat lead surfaces are experimentally accessible (Section 4.1.1). It is true that the surface diffusion of Ge atoms is greater on Pb surface than on Si surfaces,[697] or most likely than on Ge surfaces; on the other hand, Ge atom surface migration on Si(100) is negligible below ~475 K,[698] so at LN2 temperatures or below, the diffusion of Ge on Pb surfaces could be extremely low. Atomically flat transition metal surfaces are another possibility for presentation surfaces, but positional stability (surface migration) remains a possible problem.

Any presentation surface must satisfy at least two important constraints.

First, it must satisfy the feedstock release criterion: $F_{FT} > (F_{FS} + \Delta F)$, where F_{FT} = the threshold scission force for the feedstock-to-tooltip bond, F_{FS} = the threshold scission force for the feedstock-to-surface bond, and ΔF = the minimum force differential required to ensure the minimum acceptable threshold energy differential for a given operating temperature (e.g., ΔF = 0.64 nN to ensure a +0.40 eV energy differential at 300 K, or ΔF = 0.32 nN to ensure a +0.20 eV energy differential at 77 K).[699] This ensures that the feedstock molecule can be reliably removed from the presentation surface using the intended tooltip.

Second, a carbon feedstock presentation surface must also satisfy the carbide exclusion criterion. In convention chemical vapor deposition (CVD) diamond growth processes, in order to form adherent diamond films it is a customary requirement that the substrate material should be

---

[696] Robert A. Freitas Jr., Ralph C. Merkle, "A Minimal Toolset for Positional Diamond Mechanosynthesis," J. Comput. Theor. Nanosci. 5(May 2008):760-861; http://www.molecularassembler.com/Papers/MinToolset.pdf.

[697] Ing-Shouh Hwang, Tien-Chih Chang, Tien T. Tsong, "Growth Mechanism and Morphology of Ge on Si(111) Surfaces," Paper A9.4, Session A9: Poster Session, Strained Epitaxial Films, 3 December 1997, MRS Symposium A: Evolution of Surface Morphology and Thin-Film Microstructure, 1-4 December 1997; http://www.mrs.org/s_mrs/doc.asp?CID=14865&DID=86243

[698] Y.-W. Mo, R. Kariotis, B.S. Swartzentruber, M.B. Webb, M.G. Lagally, "Scanning tunneling microscopy study of diffusion, growth, and coarsening of Si on Si(001)," J. Vac. Sci. Technol. A 8(January 1990):201-206. See also: Y.-W. Mo, M.B. Webb, M.G. Lagally (unpublished, cited in Mo et al., 1990).

[699] Robert A. Freitas Jr., Ralph C. Merkle, "A Minimal Toolset for Positional Diamond Mechanosynthesis," J. Comput. Theor. Nanosci. 5(May 2008):760-861; http://www.molecularassembler.com/Papers/MinToolset.pdf.

capable of forming a carbide layer to a certain extent, since diamond CVD on nondiamond substrates usually involves the formation of a thin carbide interfacial layer upon which the diamond then grows. The carbide layer is viewed as a "glue" which promotes diamond growth and aids its adhesion by (partial) relief of interfacial stresses caused by lattice mismatch and substrate contraction.[700] However, the ideal presentation surface for carbon feedstock molecules is a substrate that resists or prohibits carbide formation. The absence of carbide on the presentation surface (a) discourages downgrowth of C-based feedstock molecule into the substrate, (b) helps maintain the isolation of the feedstock molecule prior to acquisition by the tooltip, and (c) facilitates feedstock molecule separation from the presentation surface. On the basis of carbide exclusion, potential presentation surface materials including metals, alloys and pure elements can be subdivided into three broad classes,[701] in descending order of preference:

(1) *Carbide Exclusion*. Most preferred are metals such as Cu, Sn, Pb, Ag and Au, as well as non-metals such as Ge and sapphire/alumina (Al_2O_3), that have little or no solubility or reaction with C. These materials do not form a carbide layer, so during CVD any diamond layer that might try to form will not adhere well to the surface (which is known as a way to make free-standing diamond films, as the films will often readily delaminate after deposition). These are probably the best materials for a presentation surface upon which to preposition C-based feedstock molecules.

(2) *Carbon Solvation*. Possibly acceptable at low temperature are metals such as Pt, Pd, Rh, Ni, Ti and Fe, which exhibit substantial mutual solubility or reaction with C (all industrially important ferrous materials such as iron and stainless steel cannot be diamond coated using simple CVD methods).[702] During CVD, a substrate composed of these metals acts as a carbon sink whereupon deposited carbon dissolves into the surface, forming a solid solution. This dissolution transports large quantities of C into the bulk, rather than remaining at the surface where it can promote diamond nucleation.[703] Often diamond growth on the surface only begins after the substrate is completely saturated with carbon, with carbide finally appearing on the surface; clearly it is not acceptable if the feedstock molecule dissolves into the presentation surface.

(3) *Carbide Formation*. Metals such as Ti, Zr, Hf, V, Nb, Ta, Cr, Mo, W, Co, Ni, Fe, Y, Al, and certain other rare-earth metals can form carbide during CVD. In some metals, such as Ti, the interfacial carbide layer continues growing during diamond deposition and can become

---

[700] Paul W. May, "Diamond thin films: a 21st-century material," Phil. Trans. R. Soc. Lond. A 358(2000):473-495; http://www.chm.bris.ac.uk/pt/diamond/pdf/rscreview.pdf.

[701] Paul W. May, "Diamond thin films: a 21st-century material," Phil. Trans. R. Soc. Lond. A 358(2000):473-495; http://www.chm.bris.ac.uk/pt/diamond/pdf/rscreview.pdf. B. Lux, R. Haubner, "Nucleation and growth of low-pressure diamond," in: R.E. Clausing, L.L. Horton, J.C. Angus, P. Koidl, eds., Diamond and Diamond-like Films and Coatings, Plenum Press, New York, 1991, pp. 579-609.

[702] Paul W. May, "Diamond thin films: a 21st-century material," Phil. Trans. R. Soc. Lond. A 358(2000):473-495; http://www.chm.bris.ac.uk/pt/diamond/pdf/rscreview.pdf.

[703] Paul W. May, "Diamond thin films: a 21st-century material," Phil. Trans. R. Soc. Lond. A 358(2000):473-495; http://www.chm.bris.ac.uk/pt/diamond/pdf/rscreview.pdf.

hundreds of microns thick. Non-metals such as B and Si, and Si-containing compounds such as SiO_2, quartz and Si_3N_4, also form carbide layers, and substrates composed of carbides themselves, such as SiC, WC and TiC, are particularly amenable to diamond deposition.[704] Surface nucleation rates (cm^{-2} hr^{-1}) on stable carbide-forming substrates (Si, Mo, W) are 10-100 times higher than on carbide-resistant substrates,[705] and surface nucleation density (cm^{-2}) on Mo is about 10 times higher than on other carbide-forming substrates (Si, Ni, Ti, Al) under similar deposition conditions.[706] It remains to be investigated whether carbide formation in these materials will continue to occur at the low temperatures believed neceessary for reliable DMS operations.

The solubility of Ge-based feedstock molecules into the chosen presentation surface material must also be investigated, and a similar acceptance criterion applied.

4.1.3 Disposal Surface

Atomically flat **disposal surfaces** will securely bond waste molecules (or spent disposable tooltips like CCH groups, in the case of metal tips), ensuring that these items cannot migrate in a positionally uncontrolled manner and poison DMS feedstock molecules or active tooltips located elsewhere in the system. The original proposal[707] was to use a flat depassivated diamond surface such as C(110) or C(100) as hydrogenophilic surfaces where excess H atoms left over from DMS reactions could be dumped.

A disposal surface should satisfy the waste molecule release criterion: $F_{MS} > (F_{MT} + \Delta F)$, where F_{MS} = the threshold scission force for the molecule-to-surface bond, F_{MT} = the threshold scission force for the molecule-to-tooltip bond, and ΔF is defined as before (Section 4.1.2).

For disposal surfaces, carbide exclusion (and Ge exclusion, etc.) materials should again be preferred because we desire that waste atoms should remain where they are placed on the disposal surface, and neither migrate across nor dissolve into that surface.

---

[704] Paul W. May, "Diamond thin films: a 21st-century material," Phil. Trans. R. Soc. Lond. A 358(2000):473-495; http://www.chm.bris.ac.uk/pt/diamond/pdf/rscreview.pdf.

[705] B.V. Spitzyn, L.L. Bouilov, B.V. Derjaguin, "Vapor Growth of Diamond on Diamond and Other Surfaces," J. Crystal Growth 52(1981):219-226.

[706] J.W. Kim, Y.J. Baik, K.Y. Eun, in: Y. Tzeng, M. Yoshikawa, M. Murakawa, A. Feldman, eds., Applications of Diamond Films and Related Materials, Elsevier Sci. Publ., New York 1991, p. 399.

[707] Robert A. Freitas Jr., Ralph C. Merkle, "A Minimal Toolset for Positional Diamond Mechanosynthesis," J. Comput. Theor. Nanosci. 5(May 2008):760-861; http://www.molecularassembler.com/Papers/MinToolset.pdf.

4.1.4 DMS Fabrication Surface

The objective of the molecular workstation is to build diamondoid nanoscale objects, aka. "nanoparts", on a fabrication surface using some combination of positionally controlled DMS tooltips and reaction sequences. To accomplish this, the existing DMS toolset must be able to deposit the first carbon-containing moiety (e.g., a CH_3 group) onto an atomically flat fabrication surface, and this initial moiety must not detach as the tooltip is subsequently withdrawn. This first step creates an initial "seed" structure on the surface upon which the rest of the growing nanopart can be built. This relationship between tooltips, the fabrication surface and the nanopart must persist throughout all subsequent reaction sequences that are employed to build the nanopart. In other words, the fabrication surface must continuously satisfy the nanopart fabrication criterion: $F_{NS} > (F_{NT} + \Delta F)$, where F_{NS} = the threshold scission force for the nanopart-to-surface bond, F_{NT} = the threshold scission force for the nanopart-to-tooltip bond, and ΔF is defined as before (Section 4.1.2).

Note that the end of a self-assembled metal tip (e.g., a pyramidal Ir tip with the apical atom and some number of apical crystal planes removed), an ALE- or PALE-fabricated tip which is terminated with a flat plane rather than a point, or even the end of an atomically imprecise asperity tip (if it can be adequately characterized) could in principle serve as a fabrication surface. In this case, the fabricated product object might itself be an atomically sharp tip, a tooltip-mounted gripper mechanism, or some similar structure or simple device. Another (albeit less desirable) alternative would be a diamond shard cleaved so as to expose any desired plane at the tip, giving a flat surface to build upon. Flawless CVD-grown diamonds from companies such as Apollo or Gemesis could be used for the cleaving operation, or perhaps the end of a tip could be ion-milled or etched to be atomically flat, normal to the shard tip.

For large, flat fabricated nanoparts having extensive areas in bonding contact with the fabrication surface, a mismatch in the crystal lattice constant[708] between the nanopart contact wall and the fabrication surface may greatly reduce the bonding opportunities between nanopart and substrate, although it is also true that an extensive interfacial misfit would also facilitate nanopart detachment (Section 4.1.5) from the fabrication surface. For nanoparts having only a few contact points with the fabrication surface and where the nanopart is mostly positioned up and away from the fabrication surface, lattice mismatch should pose no serious problems.

4.1.5 Release Surface

After the nanopart has been molecularly manufactured on a fabrication surface (Section 4.1.4) using a molecular workstation, there are two possibilities.

---

[708] Hiromu Shiomi, Naoji Fujimori, "Method for producing single crystal diamond film," U.S. Patent 5,387,310, 7 February 1995. Wei Zhu, Peichun Yang, Jeffrey T. Glass, "Method of fabricating oriented diamond films on nondiamond substrates and related structures," U.S. Patent 5,449,531, 12 September 1995.

The first possibility is that the workstation can only build nanoparts that must remain permanently affixed to surfaces. This approach would still allow the workstation to fabricate many useful products, but its versatility would be sharply limited and so a second-generation workstation would have to be designed and built that was able to make detachable nanoparts – which is the ultimate objective of this phase of nanofactory development.

The second possibility is that the workstation can build nanoparts that can be detached from the fabrication surface, allowing the nanopart to be carried off and elsewhere incorporated into nanomachines. This detachment process must be purely mechanical and not chemical (e.g., acid etching, sacrificial layers, etc.) in nature, in order to preserve positional control of the finished nanopart at all times. To achieve mechanical detachment, we require a release surface and a nanopart gripper tool (Section 4.1.6) that satisfy the nanopart release criterion: $F_{NG} > (F_{NS} + \Delta F)$, where F_{NG} = the threshold scission force for the nanopart-to-gripper bond, F_{NS} = the threshold scission force for the nanopart-to-surface bond, and ΔF is defined as before (Section 4.1.2). This is the desired capability of the molecular workstation.

A releasable fabrication surface is a surface upon which diamondoid nanostructures may be positionally fabricated and then mechanically removed without destroying either the release surface or the fabricated nanostructure. Original concepts for releasable fabrication surfaces included:

(1) Build structures on a hydrogenated C(111) surface which is punctuated by an occasional Ge-substituted bridgehead atom, making an array of well-separated "weakly sticky points" from which parts may be readily separated. A rigid structure under construction will need at least two such attachment points to prevent the nanopart-in-progress from spinning, and a third attachment point will prevent rocking and maintain good positional control during the performance of positionally controlled DMS reaction sequences. Van der Waals forces between nanopart and passivated fabrication surface can be reduced by elevating the Ge radical sites to the apexes of low pyramidal piers having the same surface number density.

(2) Use shaped H-terminated diamond "pits" or "cups" to hold single-adamantane molecules or related molecular precursors via predominantly van der Waals forces, upon which larger nanostructures are then constructed, then pulled out of the cup. A single Ge substituent atom in the base of the cup may provide a weak covalent anchor point for the growing structure. In a more sophisticated system, the cup may be in two halves that are pressed together to apply mechanical restraint to the precursor molecule, and the halves may be pre-shaped to provide large barriers to rotation of the trapped molecule (especially if the molecule has significant geometric asymmetries and/or the experiments are conducted at reduced temperatures). The halves can also be used to detach the finished nanostructure from the surface.

(3) Build nanopart structures directly onto the chemically active apexes of multiple repositionable radical-tipped jigs or auxiliary manipulators that will hold the growing nanopart. Once the nanopart is finished and fixture detachment is required, the jigs or manipulators can be pulled off of the finished part one by one in the right sequence and at the right angles, and the revealed radical sites on the nanopart passivated as soon as they appear. The key advance here would be to demonstrate that we could start with a simple non-cage diamondoid seed structure – e.g., a methyl group on the end of a GM tool – and build up a whole cage structure just from that, effectively eliminating the need for a formal fabrication release surface.

The design, modeling, simulation, fabrication and physical testing of workpiece release surfaces and the nanoparts to be built upon those surfaces should address the following key technical issues:

(A) Need to design nanoparts to allow easy gripping and manipulation.

(B) Need efficient parts presentation schemes.

(C) Need to devise complete DMS fabrication sequences to build nanoparts and/or their intermediate structures on piers or detachable surfaces, and then pick them up.

(D) Need to verify that nanoparts may be held sufficiently rigidly on the release surface during DMS fabrication steps (e.g., to within the required 0.2-0.5 Å positional accuracy limits),[709] while allowing convenient and nondestructive removal of the nanopart from the surface once fabrication is complete.

(E) Investigate the possibility of controlled or reversible parts adhesivity during positionally controlled assembly.

(F) Investigate possible schemes for nanopart palletization (transport jigs of standardized shape and size to permit standardized handling, but that can easily release the affixed nanopart).

Our subsequent thinking is that even when building a nanopart on a diamond surface, if the three bonded attachment points are well enough separated and if we can tilt either the nanopart or the gripper-nanopart pullaway vector, then each of the three bonds can be individually targeted and sequentially pulled apart, one by one. In this case, the many bonds throughout the interior of the nanopart and the many bonds between gripper and nanopart would be collectively far stronger than any single C-C bond between nanopart and surface, which bond would undergo scission. Repeating this procedure on the other 2 bonds then frees the nanopart. In such a scenario, no special release surface is required because the C-C bonds between nanopart and fabrication surface are sufficiently widely separated to allow independent targeting for scission. Alternatively, if it is possible to establish the initial seed moiety and then to build the rest of the nanopart on an atomically flat metal fabrication surface, the still weaker bonds that metals provide could make the nanopart detachment process even easier.

Thermal release has also been proposed but is undesirable because of the serious risk of positionally uncontrolled movements or structural reconfigurations. This proposal derives from the usual requirement during CVD growth of diamond films that the substrate material should have a thermal expansion coefficient comparable with that of diamond, since at the high growth temperatures currently used, a substrate will tend to expand, and thus the diamond coating will be grown upon and bonded directly to an expanded substrate. Upon cooling, the substrate will contract back to its room temperature size, whereas the diamond coating, with its very small expansion coefficient, will be relatively unaffected by the temperature change, causing the

---

[709] Robert A. Freitas Jr., Ralph C. Merkle, "A Minimal Toolset for Positional Diamond Mechanosynthesis," J. Comput. Theor. Nanosci. 5(May 2008):760-861; http://www.molecularassembler.com/Papers/MinToolset.pdf.

diamond film to experience significant compressive stresses from the shrinking substrate, leading to bowing of the sample, and/or cracking, flaking or even delamination of the entire film.[710] To help detach nanoparts, a nondiamond fabrication surface upon which diamond nanoparts were constructed and in bonded contact over a large interfacial contact area could incorporate the maximum possible thermal expansion mismatch between the substrate and the diamond, producing the largest possible thermal stresses upon cooling that could facilitate nanopart separation from the nondiamond fabrication surface. However, this approach would positionally uncontrolled radical sites that could lead to unplanned nanopart surface reconstructions, hence this method should not be employed in the workstation design. We should however remain alert to the possible impact of lattice mismatches between nanoparts and fabrication surfaces.

4.1.6 Nanopart Gripper Tool

We need a nanopart gripper tool that can apply sufficient force in the correct directions to detach a finished nanopart from a fabrication surface, after which the gripper tool must bind the nanopart strongly enough from at least three points of attachment to ensure that nanopart position and orientation can be continuously controlled during transport of the nanopart. Gripping mechanisms can be either passive, using only bonding patterns, or active, using an actuated mechanism of some kind.

Among passive mechanisms, one interesting possibility would be to use an isolated self-assembled metal tip to directly grip a nanopart and perform the detachment operation. However, metal-carbon bonds are generally weaker than C-C or Ge-C bonds, so the nanopart release criterion is unlikely to be satisfied unless at least three covalent bonding points are employed to ensure adequate positional control, but it is unclear how to fabricate a three-point metal tooltip. The GeRad tool or a discharged DCB6Ge (DimerP) tool could be used as bonding grippers but appear to have an insufficient number of attachment points. Also, a gripper that employs covalent bonding points will inevitably require dehydrogenation of the three attachment points on the nanopart (risking unwanted possible surface rearrangements) prior to gripper bonding to the nanopart, and will also require rehydrogenation of the three attachment points following nanopart transport, after the gripper has been detached from the nanopart.

A related possibility would be to fabricate all nanoparts so that each one possesses a complementary pyramidal hole large enough to allow a pyramidal metal tip to grip the part by docking into the hole, thus providing a positionally controllable 3-D gripping force solely via van der Waals forces rather than by covalent bonding. This would eliminate the risk of surface rearrangements and also the need for hydrogen abstraction/donation operations on a nanopart every time the nanopart is transported.

Among active mechanisms for tooltip gripper, we could design and develop an actuated atomically precise end-effector directly onto the apex of a bulk-manufactured scanning probe tip, with the gripper able to be actuated into closed (gripping) or open (nongripping) states. The gripping state must be mechanically strong enough: (1) to hold an atomically precise nanopart

---

[710] Paul W. May, "Diamond thin films: a 21st-century material," Phil. Trans. R. Soc. Lond. A 358(2000):473-495; http://www.chm.bris.ac.uk/pt/diamond/pdf/rscreview.pdf.

without slip during DMS operations or (2) to remove a nanopart from the release surface. Micromechanical grippers with multiple independently-actuated fingers have already been experimentally demonstrated with positional control of a few nanometers at each fingertip.[711]

One conceptual design for a reversible gripper device might employ a T-shaped member that slides along a race on the bottom leg of a second larger L-shaped member, with a two-position latch corresponding to gripped and ungripped states. The design would include a mechanical barrier preventing movement away from either state, once occupied, with said barrier surmountable by laterally pushing the traveling member to the left (from the right side) to open the gripper, or to the right (from the left side) to close the gripper. The mechanical sliding force to overcome the barrier could be supplied either (1) by using the manipulator to which the gripper is attached to press against a nubbin or protrusion in the workspace environment (e.g., near or attached to the toolrack), or (2) by using a second manipulator to press against the first at the appropriate location and direction to trigger a change of mechanical state in the gripper. Gripping of an object would be mediated entirely by van der Waals forces, but the gripper surface contours could be design to maximally positionally constrain the gripped nanopart by incorporating cavities and protrusions that are shape-complementary to the nanopart intended to be gripped.

The design, modeling, simulation, fabrication and physical testing of gripper mechanisms (and the nanoparts which they will be capable of gripping) will address several key technical issues. Theoretical analyses of nanopart gripper design should include:

(A) Positionally controlled grippers must be designed that can grab and then manipulate finished nanoparts, whether to transport them elsewhere or to further manipulate them in a series of assembly steps, such as a parts insertion operation (a peg pushed into a complementary hole) or other similar assembly operation, in which small parts are mechanically combined to make larger compound nanoparts which include van der Waals bonding.

(B) The grippers should also be able to firmly and reliably grip toolheads (Section 4.3.2) and jigs (Section 4.3.3), and to retrieve them from, or replace them into, the toolrack (Section 4.3.4). Handled tools intended to be used for the purpose of constructing compound nanomachines from their component parts might be significantly different in design from handled tools intended to be used for mechanosynthesis. For example, mechanosynthetic tooltips will usually have almost exclusively covalent-bond-forming reactivity, whereas tooltips intended to be used for assembly work may employ primarily van der Waals or other weak bonding systems for parts gripping, though weak covalent bonding (e.g., dative bonds, Sn-C bonds, etc.) might also be used.

(C) The actuated gripper mechanism needs methods for attachment to the picopositioning system (e.g., via a bulk-made scanning probe tip) while provably retaining rigidity and an ability to actuate the gripper.

---

[711] Sandeep Krishnan, Laxman Saggere, "A multi-fingered micromechanism for coordinated micro/nano manipulation," J. Micromech. Microeng. 17(March 2007):576-585, http://www.iop.org/EJ/abstract/0960-1317/17/3/021. See also: "Micromanipulator makes its debut", 21 February 2007, http://nanotechweb.org/articles/news/6/2/19/1.

Experimental work to demonstrate a working nanopart gripper should include:

(D) Development of SPM technology to enable nanopart assembly work.

(E) Need a reversible nanopart gripper as an end-effector on an SPM tip. The gripper should be capable of remote and/or conditional actuation. The gripper should be able to grab a nanopart and hold it with at least 3-point contact so that the nanopart is translationally and rotationally fully constrained while it is being gripped.

(F) SPM systems to be used for assembly work may require less positional placement precision but an ability to apply greater forces, and in more complex directions (e.g., twisting motions that apply circular or helical torques, threading/insertion motions. etc.). Making an atomically precise product out of nanometer-scale nanoparts does not necessarily require atomic precision in nanopart positioning, but rather only enough positional precision to distinguish the desired assembly structure from adjacent pathological assembly structures.

(G) Ideally need an actuation methodology that could be controlled in parallel and is potentially scalable.

(H) Need a specific experimental demonstration in which the gripper mechanism is fabricated onto (or otherwise mated with) a bulk scanning probe tip, and then the tip is actuated so as to grab a nanopart off of a release surface and then setting it down in a different place on the surface.

4.1.7 Rapid Surface Scanning

One final criterion for using presentation, fabrication, and disposal surfaces is the ability to at least initially scan each surface and map it to atomic precision using SPM, so that the precise location of all features and contents of the surfaces are known, thus enabling the SPM to return later (blindly) to the same spot and pick up or drop off the appropriate molecule. Typical scan speeds for such surfaces to the required resolution should be on the order of ~100 sec/μm^2 as previously discussed in Section 1.5. Ideally, this scanning can be performed using the same tips as are used in the DMS reactions (e.g., atomically sharp metal tips); if not, then a separate scanning tip or scanning tool must be provided for this purpose.

4.2 Atomically Sharp Tooltips

To perform atomically precise DMS operations, we need tooltips that are as sharp as possible, in order to reduce the positional and orientational uncertainty of the reactive sites at the tip as these tips are brought together, recharged, or applied to a workpiece. The sharpest possible tip terminates in a single atom. A related but less well-defined requirement is that the tips must have the highest possible aspect ratio to maximize steric accessability of tips to other tips and to workpieces; however, an excessively high aspect ratio can produce larger-amplitude mechanical vibrations at the apex of a very long lever arm, reducing positional certainty at the tip and thus decreasing reaction reliability. Longer lever arms also mechanically resonate at lower frequencies that could be relevant on the timescale of DMS operations – e.g., ~10 MHz for a 2-micron long, 20-nm-wide, diamond rod. Aspect ratio is an important secondary consideration

that demands further detailed analysis, but such analysis is beyond the scope of the preliminary technology assessment presented here.

It should be noted that fully atomically precise tooltips are not strictly required to undertake the initial workstation development effort. All that is needed is sufficient atomic sharpness and a good aspect ratio. However, high-aspect atomically-sharp tooltips that are also atomically precise should be manufacturable by the initial molecular workstation, and one important product of this system will be the fabrication of better tooltips that could be employed in later generations of the workstation design in order to improve precision, speed, and reliability of the system. In other words: we don't need fully atomically precise tips to bootstrap the first instantiation of the workstation, but once we have the first operational workstation, we'll be able to use it to build fully atomically precise tips that are also high-aspect and atomically-sharp.

Aspect ratio is sometimes alternatively described[712] in terms of the "flank angle" of a tip, as indicated by α in the drawing below (Figure 4-1).

Figure 4-1. Definition of "flank angle" aspect ratio.[713]

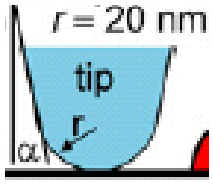

Following a general survey of currently available ultra-sharp SPM tips (Section 4.2.1) we describe four possible methods for obtaining atomically sharp tips that could be used for DMS in the molecular workstation, including single-atom metallic SPM tips (Section 4.2.2), ALE-coated single-atom SPM tips (Section 4.2.3), atomically-precise single-atom tooltips from PALE (Section 4.2.4), graphene dome tips on iridium surface (Section 4.2.5), and atomically-imprecise tooltips (Section 4.2.6).

---

[712] P. Colombi, I. Alessandri, P. Bergese, S. Federici, L.E. Depero, "Self-assembled polystyrene nanospheres for the evaluation of atomic force microscopy tip curvature radius," Meas. Sci. Technol. 20(2009):084015.

[713] P. Colombi, I. Alessandri, P. Bergese, S. Federici, L.E. Depero, "Self-assembled polystyrene nanospheres for the evaluation of atomic force microscopy tip curvature radius," Meas. Sci. Technol. 20(2009):084015.

4.2.1 Survey of Ultrasharp SPM Tips

Ultrasharp, and preferably atomically precise, scanning probe tips are needed to reliably perform positionally controlled mechanosynthetic reactions. Atomically-precise diamondoid pyramidal tooltip geometries (e.g., Figure 1-5, Section 1.2; Figure 4-25, Section 4.5.3) – that may require atomically precise molecular manufacturing to fabricate – will allow the close tooltip proximation required for DMS, but current scanning probe tips with a sub-nanometer radius of curvature should allow 2-tip operations in free space and may allow multi-tip operations near surfaces. A 2008 survey (Table 4-1) of available ultra-sharp tips – generally defined as having a radius of curvature of 10-20 nm (~50-100 carbon atoms) or less – revealed that sub-nanometer tips are already available in many materials, including diamond and CNTs, and that three-atom and one-atom tungsten tips[714] have been fabricated (though tungsten has a tendency to oxidize).

Another important consideration is that these early tips (the ultra-sharps) must also have an adequate aspect ratio – that is, they need to be sufficiently long and pointed. A good range of "high aspect ratio" tips are commercially available, with some providing ratios as high as 20:1 (especially the nanotube-based tips). For example, Ahner et al.[715] used ultra-sharp tungsten tips[716] to place four independent probes on the facet faces of selected single Ge nanodots, and on various assemblies of dots, with a positional accuracy of better than 5 nm. Olbrich et al.[717] have fabricated high aspect ratio (7:1) diamond tips using focused ion beam methods, although the tip radius is rather large (~30 nm) and milling of the tip left a 10-20 nm thick nonconducting amorphous carbon layer that had to be etched away by pure HNO_3 to expose the diamond surface. As tips get very long and narrow, the amplitude of their lateral vibrations increases, injecting more uncertainty into the apex position; as tips get shorter, their aspect ratio declines which increases the risk of handle collision during close proximation. The optimum technical tradeoff must be determined in order to select the best tips for the workstation development efforts.

---

[714] Moh'd Rezeq, Jason Pitters, Robert Wolkow, "Tungsten nanotip fabrication by spatially controlled field-assisted reaction with nitrogen," J. Chem. Phys. 124(28 May 2006):204716, http://www.aip.org/png/2006/264.htm (image), http://www.phys.ualberta.ca/~wolkow (movie).

[715] Joachim Ahner, Olivier Guise, Hubertus Marbach, Jeremy Levy, Jr. Yates, "The Nanoworkbench: Electron transport on Ge/Silicon Surfaces. First Results," [N14.005] Session N14 - Microscopic Techniques. ORAL session, Wednesday morning, March 05, Room 8C, Austin Convention Center, APS Meeting March 2003, http://flux.aps.org/meetings/YR03/MAR03/baps/abs/S4940.html.

[716] Olivier L. Guise, Joachim W. Ahner, Moon-Chul Jung, Peter C. Goughnour, John T. Yates Jr., "Reproducible Electrochemical Etching of Tungsten Probe Tips," Nano Letters 2(2002):191-193; http://pubs.acs.org/cgi-bin/abstract.cgi/nalefd/2002/2/i03/abs/nl010094q.html.

[717] A. Olbrich, B. Ebersberger, C. Boit, Ph. Niedermann, W. Hänni, J. Vancea, H. Hoffmann, "High aspect ratio all diamond tips formed by focused ion beam for conducting atomic force microscopy," J. Vac. Sci. Tech. B 17(July 1999):1570-1574; http://link.aip.org/link/?JVTBD9/17/1570/1.

Table 4-1. Experimentally Attainable or Commercially Available Ultra-Sharp Probe Tips for Scanning Probe Microscopy			
Probe Tip Manufacturer or Experimentalist Group	**Probe Tip Product**	**Probe Tip Radius**	**Image of Tip**
Silicon			
Tao et al.[718]	experimental tip	< 20 nm	
Park Systems[719]	HART0-#-05	10 nm	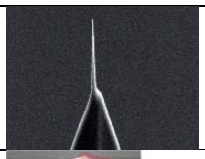
Nanochip[720]	data storage cantilever tips	10 nm	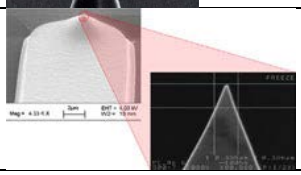
Park et al.[721]	experimental tip	< 10 nm	

[718] Y. Tao, R. J. Fasching, F. B. Prinz, "Ultra-sharp High-aspect-ratio Probe Array for SECM and AFM Analysis," 2003, http://www-rpl.stanford.edu/goto-publication/138; Ye Tao, Rainer J. Fasching, Fritz B. Prinz, "Ultrasharp high-aspect-ratio probe array for SECM and AFM Analysis," Proceedings of SPIE, Vol. 5389, Smart Structures and Materials 2004: Smart Electronics, MEMS, BioMEMS, and Nanotechnology, Vijay K. Varadan, ed., July 2004, pp. 431-442.

[719] Park Systems (http://www.parkafm.com/) SPM Tool Box; HART0-#-05, http://www.psiastore.com/product.sc?categoryId=11&productId=98

[720] Kevin Bullis, "Higher-Capacity Memory: A new type of memory could soon be available to device makers," Technology Review, 12 February 2008; http://www.technologyreview.com/Nanotech/20192/. See also Nanochip website: http://www.nanochipinc.com/.

[721] Jaehong Park, Kidong Park, Byoungdoo Choi, Kyo-In Koo, Seung-Joon Paik, Sangjun Park, Jongpal Kim, Dong-Il Dan Cho, "A novel fabrication process for ultra-sharp, high-aspect ratio nano tips using (111) single crystalline silicon," 12th International Conference on Transducers, Solid-State Sensors, Actuators and Microsystems, 2003, Vol. 2, 8-12 June 2003, pp. 1144-1145.

Nanosensors[722]	Pointprobe® Silicon-SPM-Sensors	< 10 nm	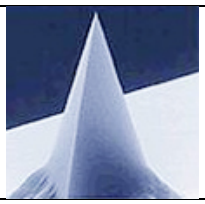
Innovative Solutions[723]	ISB-BudgetSensors	< 10 nm	
NanoWorld®[724]	AR5-NCHR Cantilevers	< 10 nm	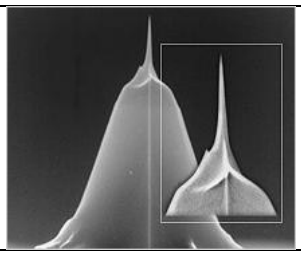
ASM[725]	various tips	< 10 nm	
Applied NanoStructures[726]	HART0-1	< 10 nm	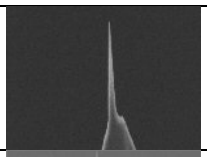
Veeco[727]	Super Cone Probes	< 10 nm	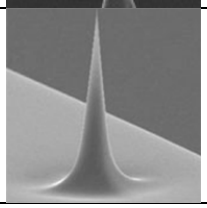

---

[722] Nanosensors™ Probes, Pointprobe® Silicon-SPM-Sensors http://www.nano-tools.com/php/cantilever.php?g_id=2&t_id=18.

[723] Innovative Solutions Bulgaria (ISB-BudgetSensors) Sofia, Bulgaria.

[724] NanoWorld® POINTPROBE® sensors, https://ssl.jpk.com/cantilevers/images/ar5.jpg; Type AR5-NCHR Cantilevers, https://ssl.jpk.com/cantilevers/csc_article_details.php?nPos=0&saArticle[ID]=29&VID=NyVAykQ2RMEgcnrx.

[725] Advanced Surface Microscopy, Inc. (ASM) Indianapolis, IN.

[726] Applied NanoStructures, high aspect ratio probe tips, HART0-1; http://www.2spi.com/catalog/spec_prep/high-aspect-ratio-AFM-probe-tips.shtml.

[727] IBMSC – Super Cone Probes https://www.veecoprobes.com/probe_detail.asp?ClassID=28.

Park Systems[728]	FORTA-10	5-6 nm	
Park Systems[729]	SICONA-10	5-6 nm	
Park Systems[730]	ACLA-10	5-6 nm	
MikroMasch[731]	GP AFM probe STING probe (DP14)	5-10 nm	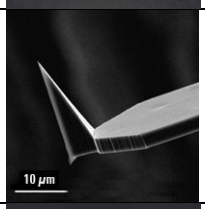
Park Systems[732]	ACTA-10	5-6 nm	
Park Systems[733]	NCHR (610-#051)	2-5 nm	

[728] Park Systems (http://www.parkafm.com/) SPM Tool Box; FORTA-10, http://www.psiastore.com/product.sc?categoryId=7&productId=95.

[729] Park Systems (http://www.parkafm.com/) SPM Tool Box; SICONA-10, http://www.psiastore.com/product.sc?categoryId=6&productId=94.

[730] Park Systems (http://www.parkafm.com/) SPM Tool Box; ACLA-10, http://www.psiastore.com/product.sc?categoryId=4&productId=92.

[731] MikroMasch http://www.spmtips.com/, GP AFM probe http://www.spmtips.com/products/cantilevers/datasheets/gp, DP14/GP series http://www.spmtips.com/dp140/gp.

[732] Park Systems (http://www.parkafm.com/) SPM Tool Box; ACTA-10, http://www.psiastore.com/product.sc?categoryId=4&productId=93.

[733] Park Systems (http://www.parkafm.com/) SPM Tool Box; NCHR (610-#051), http://www.psiastore.com/product.sc?categoryId=4&productId=102.

Veeco[734]	TESP-SS - ESP Series Probes - Super Sharp Tip	2-5 nm	
NanoScience Instruments[735]	ACL-SS Super Sharp Dynamic Mode AFM Probes	2-3 nm	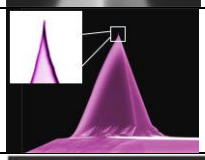
Nanosensors[736]	SuperSharpSilicon™	< 2 nm	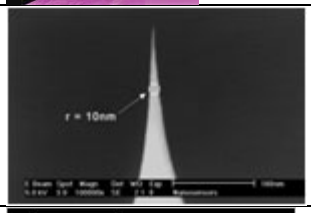
NanoWorld®[737]	SSS-NCH Cantilevers	< 2 nm	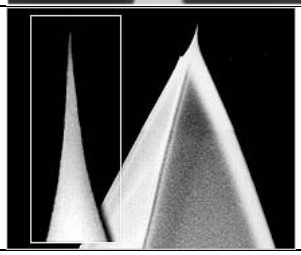
Marcus et al.[738]	experimental tip	~1 nm	
Ding et al.[739]	field emission tip	~0.75 nm	

---

[734] TESP-SS - ESP Series Probes - Super Sharp Tip; https://www.veecoprobes.com/probe_detail.asp?ClassID=111.

[735] NanoScience Instruments, "ACL-SS Super Sharp Dynamic Mode AFM Probes" AC / tapping mode - 225 micron Long cantilever - Super Sharp tip; http://store.nanoscience.com/store/pc/viewCategories.asp?idCategory=83.

[736] Nanosensors http://www.nanosensors.com/ ; http://www.nanosensors.com/products_overview.html SuperSharpSilicon™ http://www.nanosensors.com/products_overview.html#SSS (Image) Writeup on SSS is at: http://www.nanosensors.com/SuperSharpSilicon.pdf.

[737] NanoWorld®, Tip shape: Super Sharp, https://ssl.jpk.com/cantilevers/images/sss.jpg Type SSS-NCH Cantilevers https://ssl.jpk.com/cantilevers/csc_article_details.php?nPos=0&saArticle[ID]=45&VID=NyVAykQ2RMEgcnrx.

[738] R.B. Marcus, T.S. Ravi, T. Gmitter, K. Chin, D. Liu, W.J. Orvis, D.R. Ciarlo, C.E. Hunt, J. Trujillo, "Formation Of Silicon Tips with < 1 nm Radius," Appl. Phys. Lett. 56(15 January 1990):236-238; http://www.ece.ucdavis.edu/HuntGroup/Publications/APL_Marcus_AtomSharp.pdf. See also: Yongxia Zhang, Yanwei Zhang, T.S. Sriram, R.B. Marcus, "Formation of single tips of oxidation-sharpened Si," Appl. Phys. Lett. 69(30 December 1996):4260.

Tungsten			
Fujita et al.[740]	experimental tip	5 nm	
Guise et al.[741]	electrochemical etch	5 nm	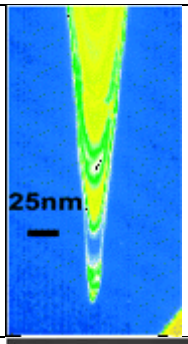
Lucier[742]	three-atom apex W(111) tip	< 0.6 nm	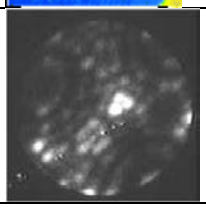
Chen,[743] Binh[744]	single-atom "Teton tip"	~0.3 nm (single-atom tip)	

---

[739] Ding Meng, Sha Guobin, A.I. Akinwande, "Silicon field emission arrays with atomically sharp tips: turn-on voltage and the effect of tip radius distribution," IEEE Transactions on Electron Devices 49(December 2002):2333-2342.

[740] Jun-ichi Fujita, Yuta Ikeda, Satoshi Okada, Kodai Higashi, Shotaro Nakazawa, Masahiko Ishida, Shinji Matsui, "In-situ Visualization of Local Field Enhancement in an Ultra Sharp Tungsten Emitter under a Low Voltage Scanning Transmission Electron Microscope," Japanese Journal of Applied Physics 46(2007):L498-L501; http://jjap.ipap.jp/link?JJAP/46/L498/.

[741] Olivier L. Guise, Joachim W. Ahner, Moon-Chul Jung, Peter C. Goughnour, John T. Yates Jr., "Reproducible Electrochemical Etching of Tungsten Probe Tips," Nano Letters 2(2002):191-193; http://pubs.acs.org/cgi-bin/abstract.cgi/nalefd/2002/2/i03/abs/nl010094q.html.

[742] Anne-Sophie Lucier, "Preparation and Characterization of Tungsten Tips Suitable for Molecular Electronics Studies," M.S. Thesis, Center for the Physics of Materials, Department of Physics, McGill University, Montreal, Quebec, Canada, February 2004; http://www.physics.mcgill.ca/~peter/theses/lucier.pdf. See also: Anne-Sophie Lucier, Henrik Mortensen, Yan Sun, and Peter Grütter, "Determination of the atomic structure of scanning probe microscopy tungsten tips by field ion microscopy," Phys. Rev. B 72, 235420 (2005).

[743] C.J. Chen, Introduction to Scanning Tunneling Microscopy, Oxford University Press, 1993.

[744] V.T. Binh, "In Situ Fabrication and Regeneration of Microtips for Scanning Tunnelling Microscopy," J. Microsc. 152(November 1988):355-361.

Rezeq et al.[745]	single-atom tip (FIM image)	~0.3 nm (inside centermost ring)	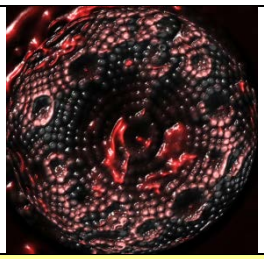
Diamond/DLC			
Wang et al.[746]	solid diamond	< 50 nm	
Nanosensors[747]	diamond-coated silicon	10 nm	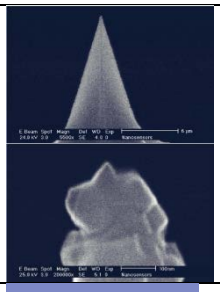
Nanotools[748]	T-EAR M* 8-40 (high dense carbon over silicon nitride)	~10 nm	
Nanotools[749]	Universal Type U3 (high dense carbon over silicon nitride)	~10 nm	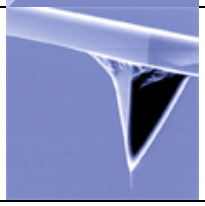

[745] Moh'd Rezeq, Jason Pitters, Robert Wolkow, "Tungsten nanotip fabrication by spatially controlled field-assisted reaction with nitrogen," J. Chem. Phys. 124(28 May 2006):204716, http://www.aip.org/png/2006/264.htm (image), http://www.phys.ualberta.ca/~wolkow (movie).

[746] Zongli Wang, Changzhi Gu, Junjie Li, Zheng Cui, "A novel method for making high aspect ratio solid diamond tips," Microelectronic Engineering 78-79(March 2005):353-358.

[747] Nanosensors: Diamond Coated Silicon-SPM-Sensors Pointprobe®; http://www.nanosensors.com/Diamond.pdf.

[748] Nanotools Scanning Probes, "Supersharp Probes," http://www.nano-tools.com/.

[749] Nanotools Scanning Probes, "Supersharp Probes," http://www.nano-tools.com/.

Advanced Diamond Technologies, Inc.[750]	NaDiaProbe™ (ultrananocrystalline (~5 nm) diamond)	7-12 nm	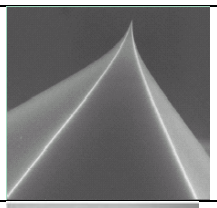
Mesa & Magonov[751]	solid diamond experimental tips	5 nm	
Nanotools[752]	Supersharp (high dense carbon over silicon nitride)	2-3 nm	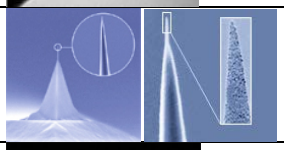
Veeco[753]	Diamond-Like Carbon Spike Probe	1 nm *(asperity)* 5 nm *(tip)*	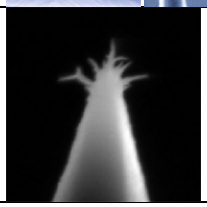
NT-MDT[754]	Super sharp Diamond-Like Carbon (DLC) tips	≤ 1 nm	
Carbon Nanotube Tips			
Dai et al.[755]	MWCNT	5-20 nm	

[750] Advanced Diamond Technologies, Inc., "NaDiaProbe™ – Monolithic Diamond AFM Probes," accessed March 2008; http://www.thindiamond.com/downloads/NaDiaProbe.pdf.

[751] Bernard Mesa, Sergei Magonov, "Novel diamond/sapphire probes for scanning probe microscopy applications," Journal of Physics: Conference Series 61(2007):770-774; http://www.microstartech.com/index/mesa-magonov.pdf.

[752] Nanotools Scanning Probes, "Supersharp Probes," http://www.nano-tools.com/.

[753] "Diamond-Like Carbon Spike Probes," https://www.veecoprobes.com/probe_detail.asp?ClassID=12.

[754] NT-MDT (Molecular Devices and Tools for Nanotechnology, Moscow, Russia, http://www.ntmdt.com), "Super sharp Diamond_Like Carbon (DLC) tips," from their "SPM Probe and Accessories" catalog, 2008; http://www.ntmdt.com/download/accessories_catalog.pdf.

NanoScience Instruments[756]	Carbon Nanotube AFM Tips	5-15 nm	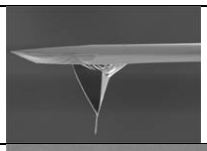
Xidex[757]	MWCNT	~10 nm	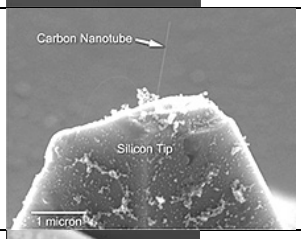
Cheung et al.[758]	MWCNT	3-8 nm	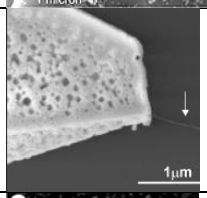
Zhang et al.[759]	tubular graphite cones	2-10 nm	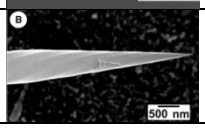
Lieber et al.[760]	MWCNT	3-5 nm	

---

[755] Hongjie Dai, Jason H. Hafner, Andrew G. Rinzler, Daniel T. Colbert, Richard E. Smalley, "Nanotubes as Nanoprobes in Scanning Probe Microscopy," Nature 384(1996):147-151; http://web.archive.org/web/20020609154706/http://cnst.rice.edu/TIPS_rev.htm.

[756] NanoScience Instruments, "Carbon Nanotube AFM Tips," CNTek™ AFM Probes; http://www.nanoscience.com/products/carbon_nanotube_probes.html.

[757] "AMRC Research Leads to Promising Nanotechnology Application for Chip Industry," (23 February, 2005), Advanced Materials Research Center, SEMATECH; http://www.amrctx.org/news/20050223.htm.

[758] Chin Li Cheung, Jason H. Hafner, Charles M. Lieber, "Carbon nanotube atomic force microscopy tips: Direct growth by chemical vapor deposition and application to high-resolution imaging," Proc. Natl. Acad. Sci. USA 97(11 April 2000):3809-3813; http://www.pubmedcentral.nih.gov/articlerender.fcgi?artid=18098.

[759] Guangyu Zhang, Xin Jiang, Enge Wang, "Tubular Graphite Cones," Science 300(18 April 2003):472-474; http://www.scienceonline.org/cgi/content/full/300/5618/472.

[760] Charles M. Lieber, Adam T. Woolley, Jong-in Hahm, David Housman, "Direct haplotyping using carbon nanotube probes," United States Patent 20020146714, 10/10/2002, http://freepatentsonline.com/20020146714.html; see also (WO/2002/022889) Direct Haplotyping Using Carbon Nanotube Probes, http://www.wipo.int/pctdb/en/wo.jsp?IA=US2001042138&DISPLAY=DESC.

Martinez et al.[761]	MWCNT sharpened to SWCNT radius	~0.9 nm	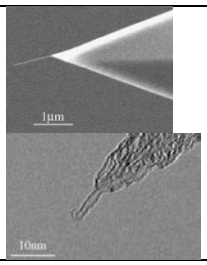
Nguyen et al.[762]	SWCNT	0.7 nm	
Hafner et al.[763]	SWCNT	0.5-1.4 nm	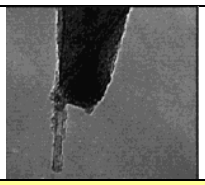
Other			
Zhu et al.[764]	Fe_2O_3 nanoflakes	12-22 nm	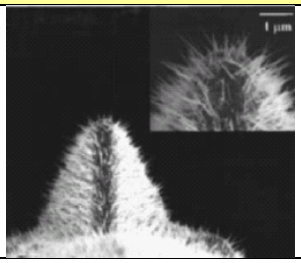
Lee et al.[765]	ZnO piezo tip	< 15 nm	

[761] J. Martinez, T.D. Yuzvinsky, A.M. Fennimore, A. Zettl, R. Garcia, C. Bustamante, "Length control and sharpening of atomic force microscope carbon nanotube tips assisted by an electron beam," Nanotechnology 16(2005):2493-2496; http://socrates.berkeley.edu/~tyuz/pub/nanotechnology16.pdf.

[762] Cattien V. Nguyen, Kuo-Jen Chao, Ramsey M.D. Stevens, Lance Delzeit, Alan Cassell, Jie Han, M. Meyyappan, "Carbon nanotube tip probes: stability and lateral resolution in scanning probe microscopy and application to surface science in semiconductors," Nanotechnology 12(September 2001):363-367; http://www.iop.org/EJ/abstract/0957-4484/12/3/326/.

[763] J.H. Hafner, C.L. Cheung, T.H. Oosterkamp, C.M. Lieber, "High-Yield Assembly of Individual Single-Walled Carbon Nanotube Tips for Scanning Probe Microscopies," J. Phys. Chem. B. 105(2001):743-746; http://cmliris.harvard.edu/publications/2000s/2001/jPCB105_743.pdf.

[764] Y.W. Zhu, T.Yu, C.H. Sow, Y.J. Liu, A.T.S. Wee, X.J. Xu, C.T. Lim, J.T.L. Thong, "Efficient field emission from -Fe_2O_3 nanoflakes on an atomic force microscope tip,"Appl. Phys. Lett. 87(2005):023103; http://www.ntu.edu.sg/home/yuting/papers/APL_Fe2O3%20on%20AFM%20tip.pdf.

[765] S.H. Lee, S.S. Lee, J.-J. Choi, J.U. Jeon, K. Ro, "Fabrication of a ZnO piezoelectric micro cantilever with a high-aspect-ratio nano tip," Microsystem Technologies 11(June 2005):416-423.

Asylum Research[766]	aluminum tip	< 15 nm	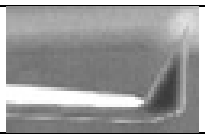
Libioulle et al.[767]	platinum tip	~5 nm	
Ermanoski et al.[768]	faceted clean iridium	~0.3 nm (single-atom tip; schematic at lower right)	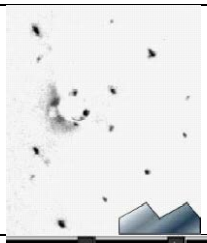
Fu et al.,[769] Madey et al.,[770] Kuo et al.,[771] Itagaki et al.[772]	Pd-coated tungsten	~0.3 nm (single-atom tip)	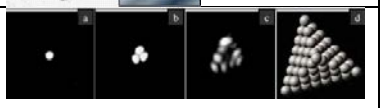

4.2.2 Plan A: Single-Atom Metallic SPM Tips

Atomically sharp and stable tips are of great importance in scanning probe microscopy. Many ways to produce sharp tips of various materials for SPM have been developed, including electrolytic (electrochemical) polishing/etching, chemical polishing/etching, ion milling, cathode sputtering, whisker growth, electron-beam deposition, flame polishing, mechanical sharpening,

---

[766] Asylum Research, AC160BN, High Aspect Ratio, AC Mode; http://www.asylumresearch.com/Products/Levers/AC160BN.shtml.

[767] L. Libioulle, Y. Houbion, J.-M. Gilles, "Very sharp platinum tips for scanning tunneling microscopy," Rev. Sci. Instrum. 66(January 1995):97.

[768] Ivan Ermanoski, Kalman Pelhos, Wenhua Chen, Jamie S. Quinton, Theodore E. Madey, "Oxygen-induced nano-faceting of Ir(210)," Surf. Sci. 549(10 January 2004):1-23.

[769] T.-Y. Fu, L.C. Cheng, C.H. Nien, T.T. Tsong, "Method of creating a Pd-covered single-atom sharp W pyramidal tip: Mechanism and energetics of its formation," Phys. Rev. B 64(15 September 2001):113401; http://www.phys.sinica.edu.tw/~nano/publication/223.pdf.

[770] Theodore E. Madey, Kalman Pelhos, Qifei Wu, Robin Barnes, Ivan Ermanoski, Wenhua Chen, Jacek J. Kolodziej, John E. Rowe, "Nanoscale surface chemistry," Proc. Nat. Acad. Sci. USA 99(2002):6503-6508; http://www.physics.rutgers.edu/~wchen/Madey_page/Full_Publications/PDF/madey_PNAS_2002.pdf.

[771] H.S. Kuo, I.S. Hwang, T.-Y. Fu, J.Y. Wu, C.C. Chang, T.T. Tsong, "Preparation and characterization of single-atom tips," Nano Lett. 4(December 2004):2379-2382; http://aao.sinica.edu.tw/download/publication_e/Year2005/math04.pdf.

[772] T. Itagaki, E. Rokuta, H.-S. Kuo, K. Nomura, T. Ishikawa, B.-L. Cho, I.-S. Hwang, T.T. Tsong, C. Oshima, "Stabilities in field electron emissions from noble-metal covered W nano-tips: apex structure dependence," Surface and Interface Analysis 39(2006):299-303.

cutting, machining, fragmenting, and so on.[773] As previously noted, the sharpest possible tip terminates in a single atom. Leaving aside the question of aspect ratio, the survey presented in Section 4.2.1 reveals that a number of single-atom SPM tips have been fabricated and widely used by experimentalists for decades, since the first (tungsten) single-atom tip was made in 1986.[774] Most currently-known single-atom tips are metal-based, ranging from pure metals to more complex metal-containing structures such as Pt/Ir-$H_3PW_{12}O_{40}$.[775] Examples from Table 4-1 include:

(1) **Iridium:** 1-atom tip, clean-faceted.[776] Oxygen chemisorbs dissociatively on Ir(210) at room temperature, forming pyramid-shaped facets with (311) and (110) orientations on the oxygen-covered Ir(210) surface when annealed to $T \geq 600$ K. The surface remains faceted for substrate temperatures $T < 850$ K; for $T > 850$ K, the substrate structure reverts to the oxygen-covered (210) planar state and does so reversibly, provided that oxygen is not lost due to desorption or via chemical reactions upon which the planar (210) structure remains. A clean oxygen-free faceted surface can be prepared through the use of low temperature surface cleaning methods: using CO oxidation, or reaction of H_2 to form H_2O, oxygen can be removed from the surface while preserving ("freezing") the clean faceted structure, which remains stable for $T < 600$ K.[777] DFT simulations of Ir facet stability have been reported.[778]

(2) **Tungsten:** 1-atom tip; FIM image[779] and "Teton tip".[780] This technique for fabricating nanotips is based on spatially controlling the reaction of nitrogen gas with the surface atoms of a tungsten tip in a field ion microscope (FIM); confining this field-assisted etching

---

[773] Allan J. Melmed, "Art and Science and other Aspects of Making Sharp Tips," J. Vac. Sci. Technol. B 9(March/April 1991):601-608.

[774] H.W. Fink, "Mono-atomic tips for scanning tunneling microscopy," IBM J. Res. Develop. 30(1986):460-465. H.W. Fink, "Point Source for Ions and Electrons," Physica Scripta 38(1988):260-263.

[775] In K. Song, John R. Kitchin, Mark A. Barteau, "$H_3PW_{12}O_{40}$-functionalized tip for scanning tunneling microscopy," PNAS 99(30 April 2002):6471-6475; http://www.pnas.org/content/99/suppl.2/6471.full.

[776] Ivan Ermanoski, Kalman Pelhos, Wenhua Chen, Jamie S. Quinton, Theodore E. Madey, "Oxygen-induced nano-faceting of Ir(210)," Surf. Sci. 549(10 January 2004):1-23.

[777] Ivan Ermanoski, Kalman Pelhos, Wenhua Chen, Jamie S. Quinton, Theodore E. Madey, "Oxygen-induced nano-faceting of Ir(210)," Surf. Sci. 549(10 January 2004):1-23.

[778] P. Kaghazchi, T. Jacob, I. Ermanoski, W. Chen, T.E. Madey, "First-principles studies on oxygen-induced faceting of Ir(210)," ACS Nano. 2(June 2008):1280-1288.

[779] Moh'd Rezeq, Jason Pitters, Robert Wolkow, "Tungsten nanotip fabrication by spatially controlled field-assisted reaction with nitrogen," J. Chem. Phys. 124(28 May 2006):204716, http://www.aip.org/png/2006/264.htm (image), http://www.phys.ualberta.ca/~wolkow (movie).

[780] C.J. Chen, Introduction to Scanning Tunneling Microscopy, Oxford University Press, 1993. V.T. Binh, "In Situ Fabrication and Regeneration of Microtips for Scanning Tunnelling Microscopy," J. Microsc. 152(November 1988):355-361.

reaction to the shank enables the production of single-atom tips.[781] A 3-atom tungsten W(111) tip has also been reported.[782]

(3) **Palladium-coated tungsten**: 1-atom tip.[783] Single-atom sharp pyramidal W tips, wrapped in a Pd overlayer, having atom-perfect wedges can be routinely and repeatedly created using a surface-science technique and are thermally stable up to 1000 K because of the exceptionally large surface-energy anisotropy of the Pd covered W(111) surface; the W tip is covered with only one physical monolayer of Pd.[784] The trap barrier for the top Pd atom on Pd trimer is much greater than 2.8 eV.[785] The deep trap is due to the formation of an exceptionally stable four-atom Pd cluster at the pyramid tip driven by the large surface-energy anisotropy of the Pd-covered W surfaces.[786]

---

[781] Moh'd Rezeq, Jason Pitters, Robert Wolkow, "Tungsten nanotip fabrication by spatially controlled field-assisted reaction with nitrogen," J. Chem. Phys. 124(28 May 2006):204716, http://www.aip.org/png/2006/264.htm (image), http://www.phys.ualberta.ca/~wolkow (movie).

[782] Anne-Sophie Lucier, "Preparation and Characterization of Tungsten Tips Suitable for Molecular Electronics Studies," M.S. Thesis, Center for the Physics of Materials, Department of Physics, McGill University, Montreal, Quebec, Canada, February 2004; http://www.physics.mcgill.ca/~peter/theses/lucier.pdf. See also: Anne-Sophie Lucier, Henrik Mortensen, Yan Sun, and Peter Grütter, "Determination of the atomic structure of scanning probe microscopy tungsten tips by field ion microscopy," Phys. Rev. B 72, 235420 (2005).

[783] T.-Y. Fu, L.C. Cheng, C.H. Nien, T.T. Tsong, "Method of creating a Pd-covered single-atom sharp W pyramidal tip: Mechanism and energetics of its formation," Phys. Rev. B 64(15 September 2001):113401; http://www.phys.sinica.edu.tw/~nano/publication/223.pdf. Theodore E. Madey, Kalman Pelhos, Qifei Wu, Robin Barnes, Ivan Ermanoski, Wenhua Chen, Jacek J. Kolodziej, John E. Rowe, "Nanoscale surface chemistry," Proc. Nat. Acad. Sci. USA 99(2002):6503-6508; http://www.physics.rutgers.edu/~wchen/Madey_page/Full_Publications/PDF/madey_PNAS_2002.pdf. H.S. Kuo, I.S. Hwang, T.-Y. Fu, J.Y. Wu, C.C. Chang, T.T. Tsong, "Preparation and characterization of single-atom tips," Nano Lett. 4(December 2004):2379-2382; http://aao.sinica.edu.tw/download/publication_e/Year2005/math04.pdf. T. Itagaki, E. Rokuta, H.-S. Kuo, K. Nomura, T. Ishikawa, B.-L. Cho, I.-S. Hwang, T.T. Tsong, C. Oshima, "Stabilities in field electron emissions from noble-metal covered W nano-tips: apex structure dependence," Surface and Interface Analysis 39(2006):299-303.

[784] T.-Y. Fu, L.C. Cheng, C.H. Nien, T.T. Tsong, "Method of creating a Pd-covered single-atom sharp W pyramidal tip: Mechanism and energetics of its formation," Phys. Rev. B 64(15 September 2001):113401; http://www.phys.sinica.edu.tw/~nano/publication/223.pdf.

[785] Roland Stumpf, Matthias Scheffler, "Theory of self-diffusion at and growth of Al(111)," Phys. Rev. Lett. 72(1994):254-257. Erratum: Phys. Rev. Lett. 73(1994):508.

[786] T.-Y. Fu, L.C. Cheng, C.H. Nien, T.T. Tsong, "Method of creating a Pd-covered single-atom sharp W pyramidal tip: Mechanism and energetics of its formation," Phys. Rev. B 64(15 September 2001):113401; http://www.phys.sinica.edu.tw/~nano/publication/223.pdf.

(4) **Silicon:** field emission tip, 3-4 atoms at tip.[787] The tip radius has a log-normal distribution with a peak at 0.75 nm, an expected value of 1.8 nm, and a shape parameter of 0.74 nm, which was achieved by isotropic etching of silicon and low-temperature oxidation sharpening.[788]

4.2.2.1 Fabrication and Availability

As noted by Kuo et al.,[789] single-atom tips (SATs) used in SPM can achieve good spatial resolution and allow manipulation of single atoms, but such tips have proven very difficult to prepare. Traditional methods[790] for preparing single-atom tips required special equipment and tedious procedures in ultra-high vacuum (UHV), and the tips could not be produced reliably. Even if a single-atom tip was obtained, the tip usually did not last long because its structure was not thermodynamically or chemically stable. It has long been known that ultrathin **Pd, Pt, Au, Ir, or Rh** films grown on a W(111) surface could form three-sided pyramids with (211) facets upon annealing in UHV.[791] (The bcc W(111) and Mo(111) surfaces are morphologically unstable when covered by monolayer films of certain metals (including Rh, Pd, Ir, Pt, Au), and they

---

[787] Ding Meng, Sha Guobin, A.I. Akinwande, "Silicon field emission arrays with atomically sharp tips: turn-on voltage and the effect of tip radius distribution," IEEE Transactions on Electron Devices 49(December 2002):2333-2342.

[788] Ding Meng, Sha Guobin, A.I. Akinwande, "Silicon field emission arrays with atomically sharp tips: turn-on voltage and the effect of tip radius distribution," IEEE Transactions on Electron Devices 49(December 2002):2333-2342.

[789] H.S. Kuo, I.S. Hwang, T.-Y. Fu, J.Y. Wu, C.C. Chang, T.T. Tsong, "Preparation and characterization of single-atom tips," Nano Lett. 4(December 2004):2379-2382; http://aao.sinica.edu.tw/download/publication_e/Year2005/math04.pdf.

[790] H.W. Fink, "Mono-atomic tips for scanning tunneling microscopy," IBM J. Res. Develop. 30(1986):460-465. H.W. Fink, "Point Source for Ions and Electrons," Physica Scripta 38(1988):260-263. Vu Thien Binh, S.T. Purcell, N. Garcia, J. Doglioni, "Field-emission electron spectroscopy of single-atom tips," Phys. Rev. Lett. 69(1992):2527-2530. V.T. Binh, N. Garcia, "On the electron and metallic ion emission from nanotips fabricated by field-surface-melting technique – experiments on W and Au tips," Ultramicroscopy 42-44(1992):80-90. K. Nagaoka, H. Fujii, K. Matsuda, M. Komaki, Y. Murata, C. Oshima, T. Sakurai, "Field emission spectroscopy from field-enhanced diffusion-growth nano-tips," Appl. Surf. Sci. 182(5 October 2001):12-19.

[791] K.J. Song, R.A. Demmin, C. Dong, E. Garfunkel, T.E. Madey, "Faceting Induced by an Ultrathin Film: Pt on W(111)," Surf. Sci. Lett. 227(1990):L79. K.J. Song, C.Z. Dong, T.E. Madey, "Faceting of tungsten(111) Induced by Ultrathin Palladium Films," Langmuir 7(December 1991):3019-3026; http://pubs.acs.org/doi/abs/10.1021/la00060a019. T.E. Madey, J. Guan, C.H. Nien, C.Z. Dong, H.S. Tao, R.A. Campbell, "Faceting Induced by Ultrathin Metal Films on W(111) and Mo(111): Structure, Reactivity, and Electronic Properties," Surf. Rev. Lett. 3(1996):1315-1328. T.E. Madey, C.H. Nien, K. Pelhos, J.J. Kolodziej, I.M. Abdelrehim, H.S. Tao, "Faceting induced by ultrathin metal films: structure, electronic properties and reactivity," Surface Science 438(1999):191-206; http://www.isr.umd.edu/gwrubloff/teaching/enma490fall03/resources/current/_final_report/120203_Anne/ref_11.pdf.

become "nanotextured" upon annealing at T > 700 K: the surface becomes covered by nanoscale three-sided pyramids with mainly (211) facets.[792] All the elements that are observed to induce faceting have Pauling electronegativities >2.0.)

In 2001, Fu and Tsong[793] demonstrated that Pd-covered W(111) single-atom tips could be created by the same faceting process – i.e., by by evaporating a Pd monolayer on a tungsten tip and then annealing the tip in ultra-high vacuum (UHV). The major advantage of this method is that the faceting is a thermodynamic process, so that when the tip is destroyed it could be regenerated through simple annealing. Most importantly, the stacking of the single-atom tip remains the same after each regeneration, ensuring a long operating lifetime. This success also implies that other noble metals (such as Pt, Ir, Rh, and Au) grown on W(111) tips may also form single-atom tips through a similar procedure.

However, two requirements in this preparation procedure made its application less convenient. First, prior to the noble metal deposition a clean W surface had to be prepared in UHV, which requires applying a very high electric field or a very high temperature to remove surface impurity atoms. Second, an evaporator has to be installed inside the UHV chamber to evaporate a noble metal film onto the clean W tip, and most laboratory setups don't have room for an evaporator.

In 2004, Kuo et al.[794] demonstrated a new, simple, and easily reproducible method of preparing single-atom tips in which both the preparation of a clean W tip surface and the deposition of a noble metal film are carried out in an electrochemical cell. This tip can be stored in ambient conditions for a long time. After the tip is transferred into a vacuum chamber and following a gentle annealing, a single-atom tip with the atomic structure identical to the one prepared by vacuum evaporation can be obtained (Figure 4-2).

---

[792] T.E. Madey, C.H. Nien, K. Pelhos, J.J. Kolodziej, I.M. Abdelrehim, H.S. Tao, "Faceting induced by ultrathin metal films: structure, electronic properties and reactivity," Surface Science 438(1999):191-206; http://www.isr.umd.edu/gwrubloff/teaching/enma490fall03/resources/current/_final_report/120203_Anne/ref_11.pdf.

[793] T.-Y. Fu, L.C. Cheng, C.H. Nien, T.T. Tsong, "Method of creating a Pd-covered single-atom sharp W pyramidal tip: Mechanism and energetics of its formation," Phys. Rev. B 64(15 September 2001):113401; http://www.phys.sinica.edu.tw/~nano/publication/223.pdf.

[794] H.S. Kuo, I.S. Hwang, T.-Y. Fu, J.Y. Wu, C.C. Chang, T.T. Tsong, "Preparation and characterization of single-atom tips," Nano Lett. 4(December 2004):2379-2382; http://aao.sinica.edu.tw/download/publication_e/Year2005/math04.pdf. Hong-Shi Kuo, Ing-Shouh Hwang, Tsu-Yi Fu, Yu-Chun Lin, Che-Cheng Chang, Tien T. Tsong, "Noble Metal/W(111) Single-Atom Tips and Their Field Electron and Ion Emission Characteristics," Japanese Journal of Applied Physics 45(2006):8972-8983; http://www.phys.sinica.edu.tw/~nano/publication/Ing-Shouh%20HWANG/Noble%20MetalW(111)%20Single-Atom%20Tips%20and%20Their%20Field%20Electron.pdf.

Figure 4-2. <u>Left:</u> Procedure for preparation of single-atom tips: <u>(a)</u> A single crystal W(111) tip is prepared through electrochemical etching; <u>(b)</u> the tip is covered with nail polish except for the tip apex; <u>(c)</u> the native oxide at the tip apex is reduced through cathodic cleaning in an electrochemical cell; <u>(d)</u> a noble metal film is electroplated on the tip; <u>(e)</u> the nail polish is removed though cleaning in acetone; <u>(f)</u> after being transferred into vacuum, the tip is annealed and the plated noble metal atoms diffuse to other parts of the tip; <u>(g)</u> when the tip is covered by only one physical layer of a noble metal, a pyramidal single-atom tip builds up spontaneously.[795] <u>Right:</u> Optical micrograph of a W(111) tip after it is covered with a nail polish (scale bar: 0.1 mm).[796]

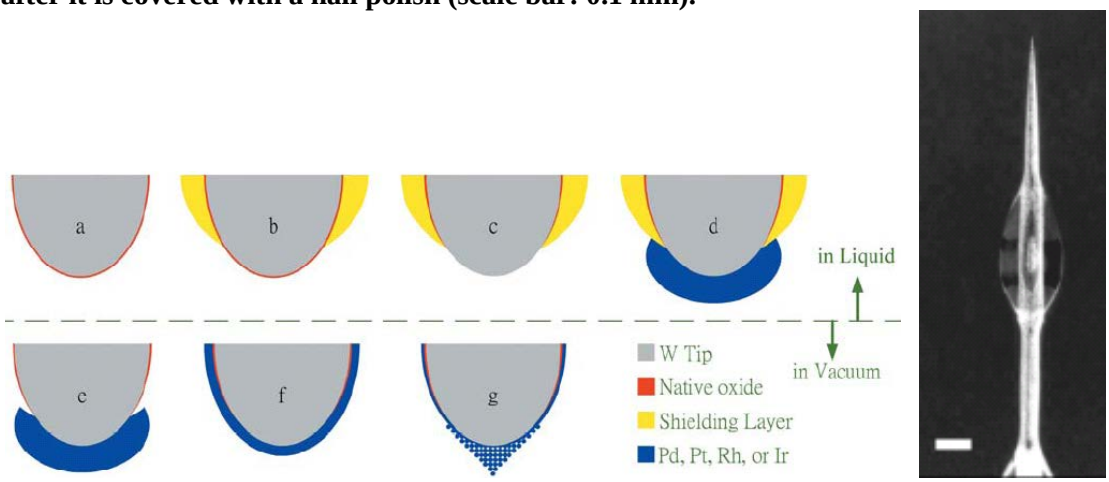

Kuo et al.[797] detail their process as follows:

"The procedure for preparing SATs using our new method can be divided into two parts: the liquid and vacuum processes."

---

[795] H.S. Kuo, I.S. Hwang, T.-Y. Fu, J.Y. Wu, C.C. Chang, T.T. Tsong, "Preparation and characterization of single-atom tips," Nano Lett. 4(December 2004):2379-2382; http://aao.sinica.edu.tw/download/publication_e/Year2005/math04.pdf.

[796] Hong-Shi Kuo, Ing-Shouh Hwang, Tsu-Yi Fu, Yu-Chun Lin, Che-Cheng Chang, Tien T. Tsong, "Preparation of Single-Atom Tips and Their Field Emission Behaviors," e-J. Surf. Sci. Nanotech. 4(2006):233-238; http://www.phys.sinica.edu.tw/~nano/publication/Ing-Shouh%20HWANG/Preparation%20of%20Single-Atom%20Tips%20and%20Their%20Field%20Emission%20Behaviors.pdf.

[797] Hong-Shi Kuo, Ing-Shouh Hwang, Tsu-Yi Fu, Yu-Chun Lin, Che-Cheng Chang, Tien T. Tsong, "Noble Metal/W(111) Single-Atom Tips and Their Field Electron and Ion Emission Characteristics," Japanese Journal of Applied Physics 45(2006):8972-8983; http://www.phys.sinica.edu.tw/~nano/publication/Ing-Shouh%20HWANG/Noble%20MetalW(111)%20Single-Atom%20Tips%20and%20Their%20Field%20Electron.pdf.

"In the liquid process, a (111) orientated single crystal W wire of 0.13 mm diameter (purity 99.999%, FEI Co.) is electrochemically polished to a needle shape in KOH solution with an AC voltage. The tip is inspected using either an optical microscope or an electron microscope to ensure sharpness. The apex of the needle is approximately hemispherical with an average radius of curvature of 50 nm. After polishing, the tip surface is covered with a thin native oxide layer, which has to be removed before the plating of a noble metal film. To decrease the total amount of the material to be deposited (plating metal), we use nail polish to shield the tip from the electrolyte except for the apex part. The shielded tip is immersed into 0.1M HCl (15 mL) and held at -0.6V (SCE) to reduce the surface oxide for about 3 min. Subsequently, a small amount of the plating electrolyte (15 mL) is introduced into the electrochemical cell under the same cathodic polarization conditions. Faradic current is in situ monitored during the electrochemical process, and the deposition time is controlled to within 10^{-15} s. At t ~ 195 s, the tip is removed from the plating bath, and the current drops to zero, indicating the end of the electrochemical reaction."

"Before transferring the electroplated tip into our laboratory-built UHV FIM/FEM chamber, we use acetone to remove the nail polish covering on the tip. The chamber has a base pressure of about 1 x 10^{-10} torr. Only heat treatments are used for degassing the tip as well as for faceting. The temperature of the tip is measured with an optical pyrometer. After a proper heat treatment (~1000 K), a He-Ne gas mixture with a pressure of 2 x 10^{-5} torr is utilized as an image gas for FIM observations. By FIM, we can examine the atomic structure of the tip surface. Typically, a positive high voltage is applied to the tip and carefully and slowly increased for observing atomic images as well as for field evaporating surface atoms."

"After degassing a Pd-plated tip in UHV at 700 K for 5 min, we obtain an FIM image of the tip. Since the tip apex is covered with a Pd multilayer, a longer period of annealing than that for the vacuum evaporation of Pd is required for extra Pd atoms to diffuse to the tip shank. After annealing at 1000 K for 20 min, an ordered atomic structure starts to appear. If the tip is annealed for additional 5 min, a perfect bcc atomic structure centered around (111) can be clearly identified, suggesting that a Pd pseudomorphic overlayer is formed on the W(111) tip surface. The tip is further annealed to 1000 K for 5 min, and the image of a single-atom tip is observed. This topmost atom can be field-ionized and field-evaporated by further increasing the positive voltage of the tip, known as field evaporation. Once the top-layer atom is removed, the atomic structure of the second atomic layer is revealed. With field evaporation, the atomic structure of the tip can be examined layer by layer."

Kuo et al used a field ion microscope (FIM) to study the atomic stacking of single-atom tips. Figure 4-3 shows FIM images of Pd-covered W(111) single-atom tips. Only one atom is seen on the topmost layer (Figure 4-3a). The second atomic layer was studied by applying a stronger electric field to remove the topmost atom (field evaporation), causing the second layer consisting of three atoms to be exposed (Figure 4-3b). With another field evaporation, the third layer consisting of 10 atoms was observed (Figure 4-3c). Figure 4-3d and Figure 4-3e show the next two layers, and a hard sphere model for this pyramidal tip is drawn in Figure 4-3f. After several field evaporations the tip apex was destroyed, but a single-atom tip with the same stacking could be regenerated simply by annealing to 1000 K, as shown in Figure 4-3(g-i). Kuo's experiments indicated that this process could be repeated tens of times.

Figure 4-3. (a)-(e) FIM images showing the structure of a Pd-covered W(111) single-atom tip: (a) the top layer; (b) the second layer; (c) the third layer; (d) the fourth layer; and in (e) the pyramidal structure is destroyed; (f) a 3-D hard-sphere model of the pyramidal nanotip; (g)-(i) FIM images showing the structure of a regenerated Pd-covered W(111) single-atom tip: (g) the top layer; (h) the second layer; (i) the third layer.[798]

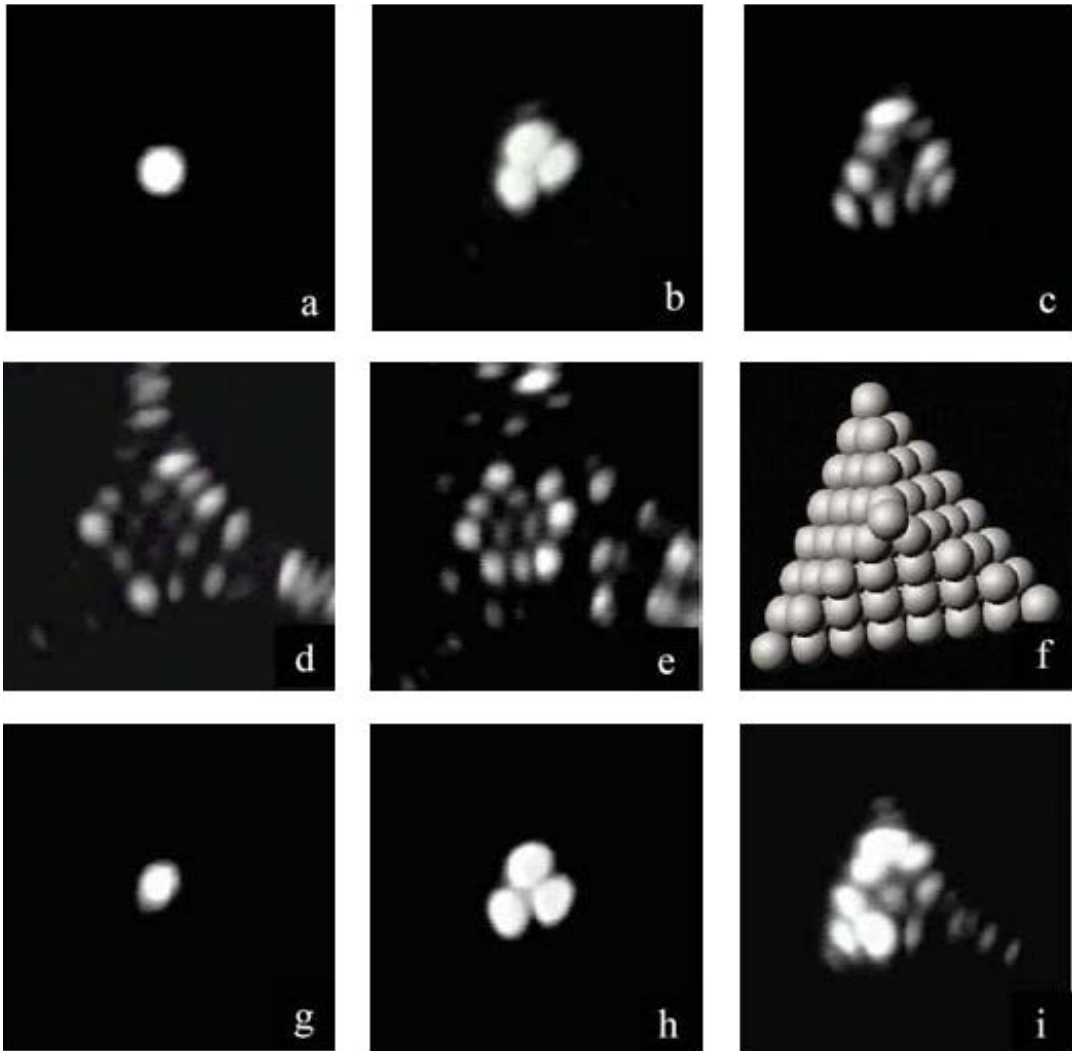

Figure 4-4 shows FIM images of Pt-covered W(111) and Rh-covered W(111) single-atom tips prepared by a similar procedure. The atomic structures are very similar to that of the Pd-covered W(111) single-atom tip, and they all are regenerable. These results further indicate that Kuo's electroplating approach can be applied to other faceting systems to produce single-atom tips.

---

[798] H.S. Kuo, I.S. Hwang, T.-Y. Fu, J.Y. Wu, C.C. Chang, T.T. Tsong, "Preparation and characterization of single-atom tips," Nano Lett. 4(December 2004):2379-2382; http://aao.sinica.edu.tw/download/publication_e/Year2005/math04.pdf.

Figure 4-4. (a)-(c) FIM images showing the structure of a Pt-covered W(111) single-atom tip: (a) the top layer; (b) the second layer; (c) the third layer; and (d)-(f) FIM images showing the structure of a Rh-covered W(111) single-atom tip: (d) the top layer; (e) the second layer; (f) the third layer.[799]

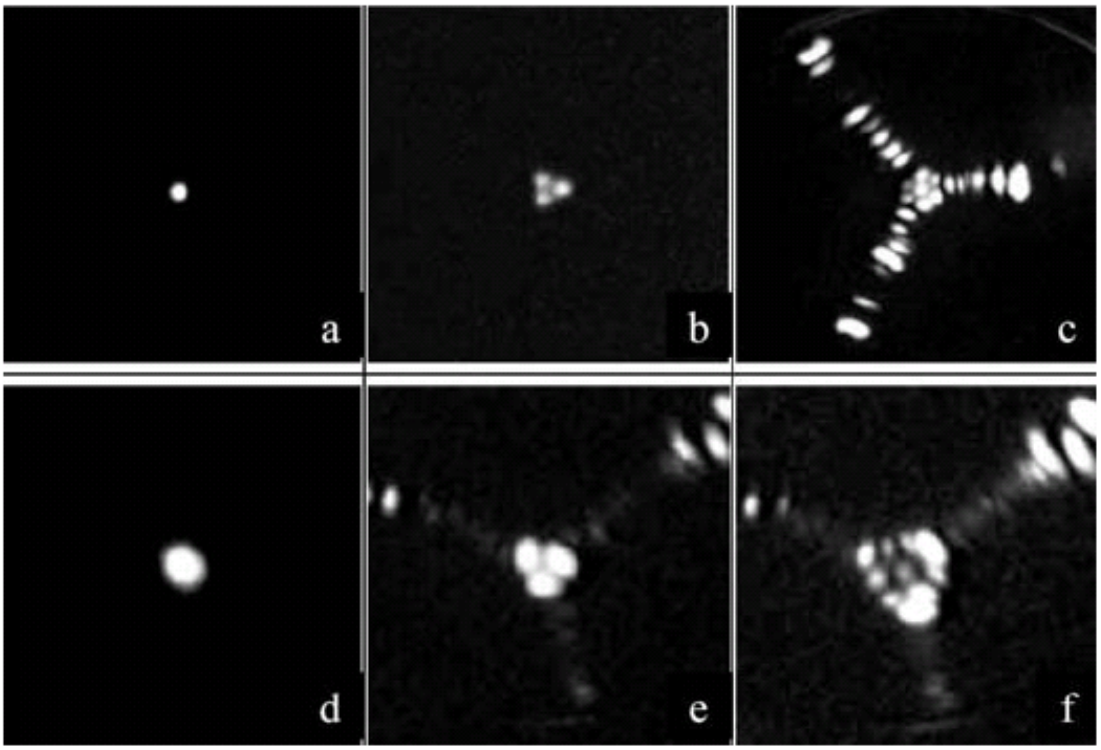

According to Kuo et al.,[800] for a Pt-plated W(111) tip, a SAT can also be obtained simply by annealing at 1100 K in vacuum. The atomic stacking of the Pt/W(111) tip is the same as that of the Pd/W(111) tip, and both SATs can be regenerated. For Pd- and Pt-covered SATs, this is a major stacking sequence with 1, 3, and 10 atoms from the top to the deeper layer. However, there is a second stacking sequence with 1, 6, and 15 atoms. This sequence is seldom observed (<10%) for Pd/W(111) and Pt/W(111) SATs, but it is more often observed for Rh/W(111) and Ir/W(111) SATs. An example is shown in Figure 4-5. After annealing, a Rh electroplated tip at 1100 K for 30 min, we obtain a Rh-covered SAT with a stacking sequence of 1, 3, and 10 atoms, as shown in

---

[799] H.S. Kuo, I.S. Hwang, T.-Y. Fu, J.Y. Wu, C.C. Chang, T.T. Tsong, "Preparation and characterization of single-atom tips," Nano Lett. 4(December 2004):2379-2382; http://aao.sinica.edu.tw/download/publication_e/Year2005/math04.pdf.

[800] Hong-Shi Kuo, Ing-Shouh Hwang, Tsu-Yi Fu, Yu-Chun Lin, Che-Cheng Chang, Tien T. Tsong, "Noble Metal/W(111) Single-Atom Tips and Their Field Electron and Ion Emission Characteristics," Japanese Journal of Applied Physics 45(2006):8972-8983; http://www.phys.sinica.edu.tw/~nano/publication/Ing-Shouh%20HWANG/Noble%20MetalW(111)%20Single-Atom%20Tips%20and%20Their%20Field%20Electron.pdf.

Figure 4-5(a-c). After the field evaporations, the tip is annealed at 1100 K again to recover the single-atom sharpness. The barriers blocking transition between the two stacking sequences are higher than most energies commonly encountered in DMS, e.g., ~3 eV for pyramidal Rh-coated W tips and ~2.7 eV for pyramidal Ir-coated W tips (Figure 4-6A).[801]

Figure 4-5. FIM images showing two types of Rh-covered W(111) single-atom tip: (a) The first layer consists of one atom. (b) The second layer consists of 3 atoms. (c) The third layer consists of 10 atoms. (d) Top view model of tip with 1-3-10 stacking sequence. (e) The first layer consists of 1 atom. (f) The second layer consists of 6 atoms. (g) The third layer consists of 15 atoms; (h) Top view model of tip with 1-6-15 stacking sequence.[802]

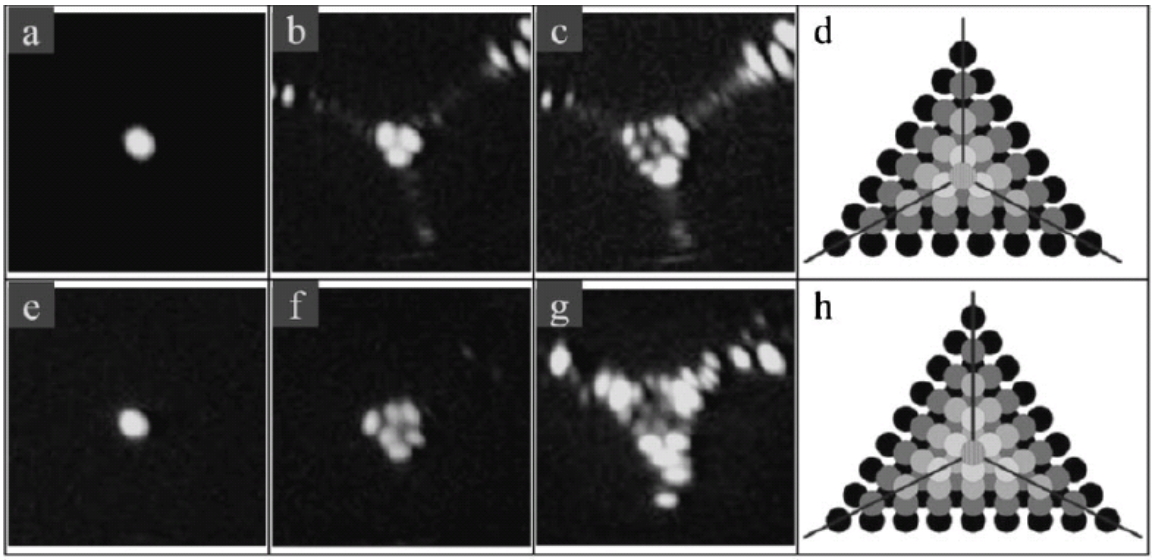

[801] Tsu-Yi Fu, Yu-Chun Lin, Hong-Shi Kuo, Ing-Shouh Hwang, Tien T. Tsong, "Study of two types of Ir or Rh covered single atom pyramidal W tips," Surface Science 601(2007):3992-3995; http://www.phys.sinica.edu.tw/~nano/eng/publication/Fu-2007.pdf.

[802] Hong-Shi Kuo, Ing-Shouh Hwang, Tsu-Yi Fu, Yu-Chun Lin, Che-Cheng Chang, Tien T. Tsong, "Noble Metal/W(111) Single-Atom Tips and Their Field Electron and Ion Emission Characteristics," Japanese Journal of Applied Physics 45(2006):8972-8983; http://www.phys.sinica.edu.tw/~nano/publication/Ing-Shouh%20HWANG/Noble%20MetalW(111)%20Single-Atom%20Tips%20and%20Their%20Field%20Electron.pdf.

Figure 4-6A. Potential energy diagram showing calculated activation barriers for different structures of Rh-covered (left) and Ir-covered (right) single-atom W pyramidal tips.[803]

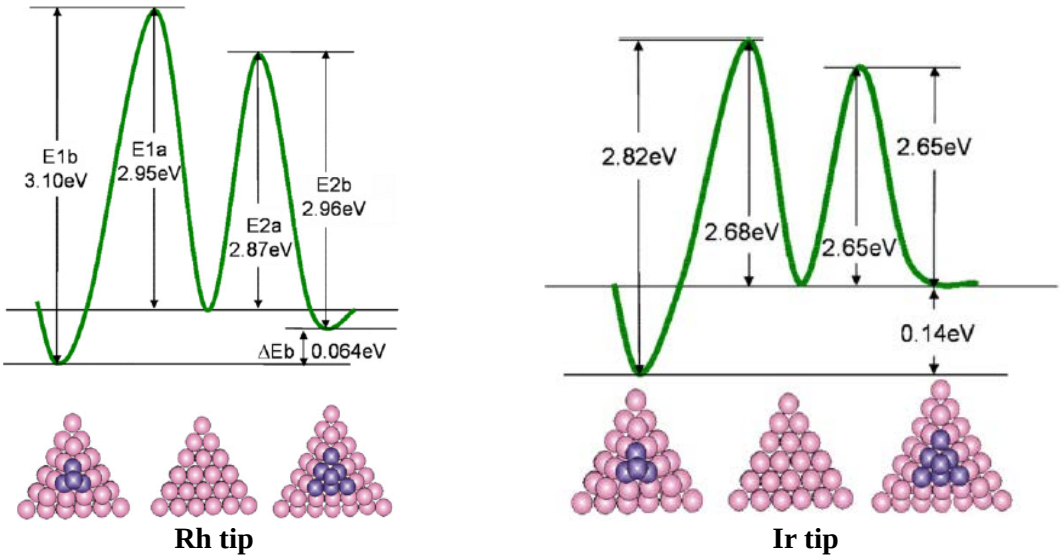

Figure 4-6B. Schematic view of nano-pyramids terminated with a single atom of Pd, Pt, Au and Rh grown on the W<111> tip. The {211} facet face covers the pyramid. The angle between the <111> tip orientation and the direction normal to {210} face is 19.5◦ and the angle between the tip orientation and the directions normal to the rid lines is 10◦. The shape of pyramids is not so sharp in comparison with that of the remolding single-atom tip, of which the pyramids are surrounded by {110} facet faces.[804]

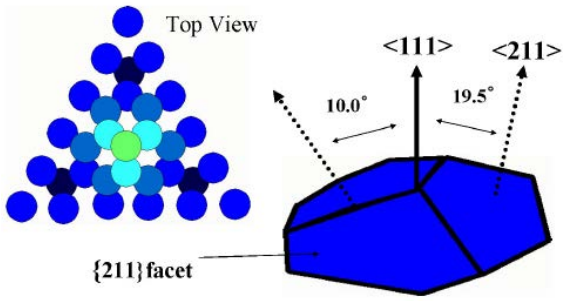

---

[803] Tsu-Yi Fu, Yu-Chun Lin, Hong-Shi Kuo, Ing-Shouh Hwang, Tien T. Tsong, "Study of two types of Ir or Rh covered single atom pyramidal W tips," Surface Science 601(2007):3992-3995; http://www.phys.sinica.edu.tw/~nano/eng/publication/Fu-2007.pdf.

[804] Chuhei Oshima, Eiji Rokuta, Takahiro Itagaki, Tsuyosi Ishikawa, Bokurai Cho, Hong-Shi Kuo, Ing-Shouh Hwang, Tien T. Tsong, "Demountable Single-Atom Electron Source," e-J. Surf. Sci. Nanotech. 3(9 December 2005):412-416; http://www.phys.sinica.edu.tw/~nano/publication/Ing-Shouh%20HWANG/Demountable%20Single-Atom%20Electron%20Source.pdf.

One limitation on these tips is that their aspect ratio is not uniform – the metal pyramids are very sharp, but these lie atop tip termini that have much large radii of curvature (Figure 4-6B).[805] Thus it would be ideal if all two-tip reactions and high-angle approaches to the workpiece could be eliminated from our DMS reaction sequence schedule to avoid steric congestion at the worksite.

In summary, the collaboration of Kuo et al.[806] (with participants at Academia Sinica, National Tsing Hua University, and National Taiwan Normal University, all in Taiwan) has developed a new, simple, and easily reproducible method of preparing single-atom tips. By electroplating a thin noble metal film onto a single-crystal W (111) tip, a single-atom tip can be obtained after a simple annealing in vacuum, that can be used as single-atom field emitters.[807] These noble metal-plated W(111) tips can survive in ambient conditions for months before transfer into a vacuum system, are both thermally and chemically stable, can be regenerated when accidentally damaged, and maintain a small extension angle and the same atomic stacking each time they are regenerated. By 2006-8,[808] the group had succeeded in preparing Pd/W(111), Pt/W(111), Rh/W(111), Au/W(111), and Ir/W(111) single-atom tips, and they believed that their method

---

[805] Chuhei Oshima, Eiji Rokuta, Takahiro Itagaki, Tsuyosi Ishikawa, Bokurai Cho, Hong-Shi Kuo, Ing-Shouh Hwang, Tien T. Tsong, "Demountable Single-Atom Electron Source," e-J. Surf. Sci. Nanotech. 3(9 December 2005):412-416; http://www.phys.sinica.edu.tw/~nano/publication/Ing-Shouh%20HWANG/Demountable%20Single-Atom%20Electron%20Source.pdf.

[806] H.S. Kuo, I.S. Hwang, T.-Y. Fu, J.Y. Wu, C.C. Chang, T.T. Tsong, "Preparation and characterization of single-atom tips," Nano Lett. 4(December 2004):2379-2382; http://aao.sinica.edu.tw/download/publication_e/Year2005/math04.pdf.

[807] T. Itagaki, E. Rokuta, H.-S. Kuo, K. Nomura, T. Ishikawa, B.-L. Cho, I.-S. Hwang, T.T. Tsong, C. Oshima, "Stabilities in field electron emissions from noble-metal covered W nano-tips: apex structure dependence," Surface and Interface Analysis 39(2006):299-303. E. Rokuta, T. Itagaki, D. Miura, T. Moriyama, T. Ishikawa, B.-L. Cho, T.Y. Fu, T.T. Tsong, C. Oshima, "Atomic-scale field emitter with self-repairable function and thermodynamically stable structure: FEM study on Pd-covered nanopyramids on W<1 1 1> tips," Applied Surface Science 251(15 September 2005:205-209. E. Rokuta, H.-S. Kuo, T. Itagaki, K. Nomura, T. Ishikawa, B.-L. Cho, I.-S. Hwang, T.T. Tsong, C. Oshima, "Field emission spectra of single-atom tips with thermodynamically stable structures," Surface Science 602(2008):2508-2512; http://www.phys.sinica.edu.tw/~nano/publication/Rokuta-SS-2008.pdf.

[808] Hong-Shi Kuo, Ing-Shouh Hwang, Tsu-Yi Fu, Yu-Chun Lin, Che-Cheng Chang, Tien T. Tsong, "Noble Metal/W(111) Single-Atom Tips and Their Field Electron and Ion Emission Characteristics," Japanese Journal of Applied Physics 45(2006):8972-8983; http://www.phys.sinica.edu.tw/~nano/publication/Ing-Shouh%20HWANG/Noble%20MetalW(111)%20Single-Atom%20Tips%20and%20Their%20Field%20Electron.pdf. Tsu-Yi Fu, Yu-Chun Lin, Hong-Shi Kuo, Ing-Shouh Hwang, Tien T. Tsong, "Study of two types of Ir or Rh covered single atom pyramidal W tips," Surface Science 601(2007):3992-3995; http://www.phys.sinica.edu.tw/~nano/eng/publication/Fu-2007.pdf. Yu-Wen Liao, L.H. Chen, K.C. Kao, C.-H. Nien, Minn-Tsong Lin, Ker-Jar Song, "Faceting and defaceting phase transitions of Pd/W(111)," Phys. Rev. B 75(2007):125428; http://web.phys.ntu.edu.tw/nanomagnetism/eng/pdf/060-PRB75-125428-2007.pdf. Hong-Shi Kuo, Ing-Shouh Hwang, Tsu-Yi Fu, Yu-Chun Lin, Che-Cheng Chang, Tien T. Tsong, "Preparation of Single-Atom Tips and Their Field Emission Behaviors," e-J. Surf. Sci. Nanotech. 4(2006):233-238; http://www.phys.sinica.edu.tw/~nano/publication/Ing-Shouh%20HWANG/Preparation%20of%20Single-Atom%20Tips%20and%20Their%20Field%20Emission%20Behaviors.pdf.

could also be used for the preparation of noble-metal/Mo(111) pyramidal tips, as one physical monolayer of a noble metal also induces a similar faceting transition on a Mo(111) substrate.[809]

Another method for making atomically sharp tips was demonstrated in 2009 by Gross et al.,[810] who prepared metal tips to which a single CO molecule was bonded and then employed to produce images of a surface-bound pentacene molecule with atomic resolution. In this work, tip fabrication began with a cut 50-μm-thick PtIr wire whose apex was coated with copper by means of controlled indentations into a Cu substrate, producing an atomically imprecise Cu coating at the tip apex. An atomically sharp silver or gold tip was then obtained by accreting Ag or Au atoms, one by one, to the tip. To pick up a Au or Ag atom,[811] the tip was first positioned above a single Au or Ag adatom from a population of such atoms previously sputtered onto a NaCl(2 ML)/Cu(111) surface. Then, starting from a typical set point of I = 2 pA, V = 200 mV, the tip was approached to the adatom by about 4 Å, and the event of picking up the atom was observed as a sudden jump in the tunneling current. Multiple numbers of Au or Ag adatoms were picked up deliberately with the tip by repeating this process a number of times until a stable and atomically sharp metallic tip was obtained (Figure 4-7). Such tips can be characterized by imaging single Au or Ag adatoms as circular protrusions that exhibit a comparably small frequency shift of about $\Delta f = (2\pm1)$ Hz at a tunneling set point of I = 2 pA, V = 200 mV above NaCl(2 ML)/Cu(111).

It is unknown whether the Ag or Au metal atoms self-assemble to form a neat pyramidal geometry at the tip, but apparently these tips can be fabricated on an ad hoc basis with at least one prominent atomically sharp protrusion. Imaging scans using the plain metal tips produces images with very poor resolution, but the subsequent pickup of a CO molecule by the atomically sharp metal tip permits good-quality atomic resolution images to be obtained. The ability of these metal-CO structures to survive use as scanning tips for significant periods of time suggests that the stability of Ag or Au tips might also be sufficient for DMS, and perhaps the characteristics of these tips can be improved by high-temperature annealing. Further investigation of these possibilities appears warranted.

A few other groups are also doing work with single-atom tips,[812] including the Atom-Based Standards and Fabrication project at NIST.[813]

---

[809] K.J. Song, J.C. Lin, M.Y. Lai, Y.L. Wang, "Faceting Phase Transitions of. Mo(111) Induced by Pd, Au, and Oxygen Overlayers," Surf. Sci. 327(1995):17-32.

[810] Leo Gross, Fabian Mohn, Nikolaj Moll, Peter Liljeroth, Gerhard Meyer, "The Chemical Structure of a Molecule Resolved by Atomic Force Microscopy," Science 325(28 August 2009):1110-1114; http://www.sciencemag.org/cgi/content/full/325/5944/1110.

[811] Jascha Repp, Gerhard Meyer, Fredrik E. Olsson, Mats Persson, "Controlling the Charge State of Individual Gold Adatoms," Science 305(23 July 2004):493-495.

[812] Moh'd Rezeq, Christian Joachim, N. Chandrasekhar, "Nanotip apex modification with atomic precision and single atom tips restoration," Microelectronic Engineering 86(April-June 2009):996-998. Shin Fujita, Hiroshi Shimoyama, "Thermal-field treatment for creating single-crystal tungsten tips with ultimate sharpness," J. Vac. Sci. Technol. B 26(March 2008):738-744. T.Y. Fu, W.J. Weng, T.T. Tsong, "Dynamic study of W atoms and clusters on W(111) surfaces," Applied Surface Science 254(30 September 2008):7831-7834.

Figure 4-7. Idealized structure of an atomically sharp gold tip (top left), and the same Au tip after pickup of a CO molecule to obtain atomically precise imaging (top right). AFM (qPlus, 20 pm amplitude) images of a pentacene molecule (a chain of 5 benzene rings) using a plain Ag tip (bottom left) and a metal tip with CO attached (bottom right) are also shown.[814]

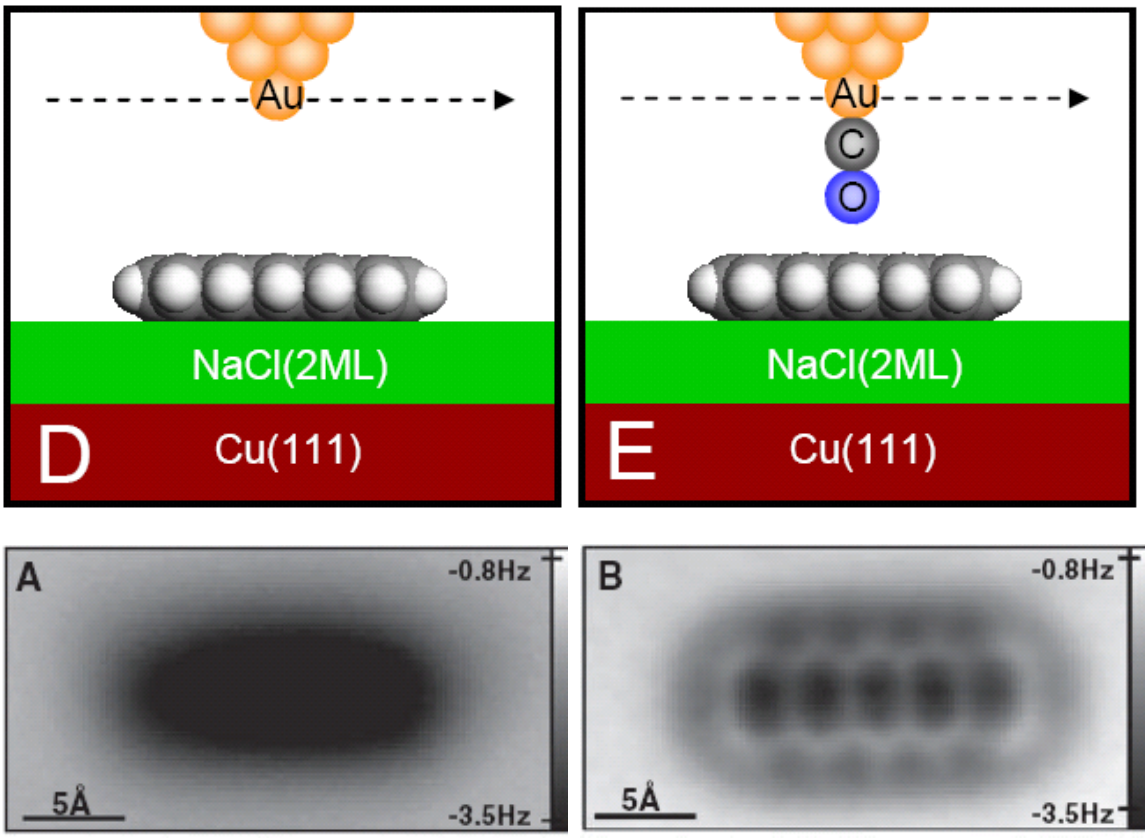

4.2.2.2 DMS Reaction Energetics Using Metal Tips

One key threshold issue requiring investigation is whether metal single-atom tips can reliably perform DMS operations analogous to those described by Freitas and Merkle in the minimal

---

[813] "Atom-Based Standards and Fabrication," Manufacturing Engineering Laboratory, NIST, 28 May 2009; http://www.nist.gov/mel/ped/nm/absf.cfm.

[814] Leo Gross, Fabian Mohn, Nikolaj Moll, Peter Liljeroth, Gerhard Meyer, "The Chemical Structure of a Molecule Resolved by Atomic Force Microscopy," Science 325(28 August 2009):1110-1114; http://www.sciencemag.org/cgi/content/full/325/5944/1110.

toolset paper using diamondoid tips.[815] A definitive answer will require a high-quality analysis of numerous reaction sequences involving the proposed metal tips, coupled with experimental data. Since such detailed analysis is likely to be time-consuming and computationally expensive, we can perform an initial screening of candidate metal tip atoms to determine the priority order of investigation of specific elements as potential tip atoms.

To this end, we performed a brief series of simple DFT calculations using the LANL2DZ basis set, with $H_2Mx\bullet$ and $H_3Mz\bullet$ radical clusters representing a single-atom tip model using either metal element Mx (= $_{45}$Rh, $_{47}$Ag, $_{73}$Ta, $_{75}$Re, $_{77}$Ir, $_{79}$Au) having an odd number of electrons or metal element Mz (= $_{42}$Mo, $_{44}$Ru, $_{46}$Pd, $_{74}$W, $_{76}$Os, $_{78}$Pt) having an even number of electrons,[816] covering all 5th row and 6th row transition metals.

For each single-atom metal tip, we investigated three basic mechanosynthetic operations:

(1) Is the abstraction of a $CH_2\bullet$ group from a Ge, Sn, or Pb presentation surface exoergic as desired, using the isobutane models $(GeH_3)_3Ge\text{-}CH_2\bullet$, $(SnH_3)_3Sn\text{-}CH_2\bullet$, and $(PbH_3)_3Pb\text{-}CH_2\bullet$ to represent a $CH_2\bullet$ group bonded to a germanium, tin, or lead presentation surface?

(2) Can a methylene-loaded metal tip, modeled simply as $H_2Mx\text{-}CH_2\bullet$ or $H_3Mz\text{-}CH_2\bullet$, reliably transfer the $CH_2\bullet$ group onto an adamantane bridgehead radical site, converting a $C_{10}H_{15}\bullet$ cage into a methylated $C_{10}H_{15}\text{-}CH_2\bullet$ structure? (We also calculate the dissociation energy of the $CH_2\bullet$ group from the metal tip in each case – the energy is positive in all cases.)

(3) Can a hydrogen-loaded metal tip, modeled simply as $H_2Mx\text{-}H$ or $H_3Mz\text{-}H$, reliably donate the H group onto an adamantane bridgehead radical site, converting a $C_{10}H_{15}\bullet$ workpiece into a fully passivated $C_{10}H_{16}$ cage?

The results of our DFT simulations for 12 transition metal elements are given in Table 4-2 below. Our two leading candidates are **Ru** and **Ir** (Figure 4-8), the only two elements in the table with numbers that "work". Of these two, the Ru tip must be regarded as the leading contender. Ru is the most "energetically balanced", with its exoergicity for $CH_2\bullet$ abstraction from a Pb surface (-0.63 eV) almost equal to its exoergicity for $CH_2\bullet$ donation to a diamondoid radical site (-0.86 eV). The only problem with Ru is that the fabrication of single-atom pyramidal Ru tips has not yet been reported in the literature. However, such fabrication seems likely to be possible because:

---

[815] Robert A. Freitas Jr., Ralph C. Merkle, "A Minimal Toolset for Positional Diamond Mechanosynthesis," J. Comput. Theor. Nanosci. 5(May 2008):760-861; http://www.molecularassembler.com/Papers/MinToolset.pdf.

[816] Several larger multi-metal-atom test tip structures failed to converge and thus could not be used for this initial screening. Even these modest-sized 3-4 atom tips would not fully converge in all cases. Several elements (Pt, Pd, W, Ag) energetically prefer to form H_2 out of two of the H atoms that are proxying metal atoms deeper into the tip structure, a physically unrealistic result. Some elements (Au, Ag) prefer to allow one of the H atoms to migrate to the $CH_2\bullet$ radical site to make a passivated CH_3, also not a physically realistic configuration.

Table 4-2. Energetics of Basic Diamondoid Mechanosynthesis Operations using Single-Atom Metal Tips (blue = exoergic, red = endoergic)

Single-Atom Tip Element	**Atomic No.**	----- *Abstract* -----				----- *Donate* -----		
		CH_2• from Ge (eV)	**CH_2• from Sn (eV)**	**CH_2• from Pb (eV)**	**CH_2• Dissoc. Energy (eV)**	**CH_2• onto Adam• (eV)**	**H onto Adam• (eV)**	**H Dissoc. Energy (eV)**
W	74	-2.84	-3.20	-3.67	+6.15	+2.18	-1.12	+3.05
Re	75	-2.54	-2.90	-3.37	+5.85	+1.88	-1.02	+3.15
Ta	73	-2.07	-2.43	-2.90	+5.38	+1.41	-1.33	+2.85
Mo	42	-1.90	-2.26	-2.73	+5.21	+1.24	-1.78	+2.40
Os	76	-0.83	-1.19	-1.66	+4.13	+0.17	-1.22	+2.96
Ir	77	-0.40	-0.76	-1.23	+3.70	-0.27	-1.00	+3.18
Ru	44	+0.20	-0.16	-0.63	+3.11	-0.86	-1.83	+2.35
Rh	45	+1.04	+0.68	+0.21	+2.27	-1.70	-1.42	+2.76
Pt	78	+1.29	+0.93	+0.46	+2.01	-1.95	-1.80	+2.37
Au	79	+2.02	+1.66	+1.19	+1.28	-2.68	-5.25*	-0.71*
Pd	46	+2.27	+1.91	+1.44	+1.03	-2.94	-1.82	+2.36
Ag	47	+2.63	+2.27	+1.80	+0.67	-3.29	-2.76	+1.42

* suspect data – no zero-point correction, and only unconverged AuH_3 structure was available

Figure 4-8. (A) LANL-minimized Ir tip carrying CH_2• payload (model as H_2IrCH_2); (B) Ru tip carrying CH_2• payload (model as H_3RuCH_2); C = black, H = white, Ir/Ru = purple.

(A) (B)

(a) $_{44}$Ru, like $_{77}$Ir, has a high Pauling electronegativity of 2.2 (see Table 4-3);

(b) pyramidal tips have been reported for $_{44}$Ru's two neighboring 5th-row elements $_{45}$Rh and $_{46}$Pd that also have a Pauling electronegativity of 2.2; and

(c) faceting of Ru monolayers on W(111) surfaces upon high-temperature annealing has been observed experimentally,[817] although there can be some alloy formation due to tungsten atom migration. From the paper:[818] "W atoms that diffuse into the Ru overlayer upon deposition at 300 K encounter a barrier as more Ru is deposited. As the Ru coverage increases above 1 ML, the intermixing [alloying] signal is attenuated, indicating that W atoms do not diffuse further into the overlayer during deposition at 300 K. When annealing to low temperatures, an intermixing peak is observed and is associated with an intermixed, reconstructed, planar W(111) surface. However, this Ir/W feature disappears when the sample is annealed to temperatures that induce faceting [~750 K], but higher temperatures that induce both faceting and planar surfaces to coexist cause the Ir/W intermixing peak to reappear." This suggests that it should be possible to create non-alloyed pure Ru facets on W(111) tips by annealing to the intermediate ~750 K temperature.

Table 4-3. Pattern of Workable Energies as a Function of Position in the Periodic Table (green = experimental single-atom tip reported available for this element)

5th-Row ELEMENT:	Nb	Mo	Tc	Ru	Rh	Pd	Ag
atomic number	*41*	*42*	*43*	*44*	*45*	*46*	*47*
Pauling electronegativity	*1.6*	*1.8*	*1.9*	*2.2*	*2.2*	*2.2*	*1.9*
CH_2● abstraction from Pb	n/a	-2.73	n/a	-0.63	+0.21	+1.44	+1.80
CH_2● donation to AdamRad	n/a	+1.24	n/a	-0.86	-1.70	-2.94	-3.29
6th-Row ELEMENT:	Ta	W	Re	Os	Ir	Pt	Au
atomic number	*73*	*74*	*75*	*76*	*77*	*78*	*79*
Pauling electronegativity	*1.5*	*1.7*	*1.9*	*2.2*	*2.2*	*2.2*	*2.4*
CH_2● abstraction from Pb	-2.90	-3.67	-3.37	-1.66	-1.23	+0.46	+1.19
CH_2● donation to AdamRad	+1.41	+2.18	+1.88	+0.17	-0.27	-1.95	-2.68

[817] M.J. Gladys, G. Jackson, J.E. Rowe, T.E. Madey, "High resolution photoemission study of growth, alloying, and intermixing of ultrathin ruthenium films on W(111) and W(211)," Surface Science 544(2003):193-208; http://www.physics.rutgers.edu/~madey/Publications/Full_Publications/PDF//madey_SS_2003_G.pdf.

[818] M.J. Gladys, G. Jackson, J.E. Rowe, T.E. Madey, "High resolution photoemission study of growth, alloying, and intermixing of ultrathin ruthenium films on W(111) and W(211)," Surface Science 544(2003):193-208; http://www.physics.rutgers.edu/~madey/Publications/Full_Publications/PDF//madey_SS_2003_G.pdf.

The Ir tip also works but is less energetically balanced: it has superior CH_2● abstraction energetics (i.e., -0.40 eV even from a Ge presentation surface) but its CH_2● donation energy is only marginal at -0.27 eV, thus the tip may donate reliably at 80 K but not at 300 K.

Two other candidate elements (**Os** and **Rh**) are close to being energetically workable – their apparently unworkable numbers may lie within the margin of error for computations using the LANL basis set, so these candidates should also be investigated further. If the LANL error is as large as 0.86 eV in the appropriate direction, it is also remotely possible that a **Pt** tip might be workable. The other seven elements appear fairly solidly unworkable due to their evident thermodynamic inability to either abstract or donate a CH_2● group from the appropriate surface.

The pattern of workable energies as a function of position in the Periodic Table is suggested by the progression shown in Table 4-3. A workable tooltip requires both abstraction *and* donation to be exoergic (negative energy). Elements that have already been fabricated into single-atom tips are indicated in green.

Regarding larger cluster models for tips, a brief literature search revealed that DFT simulations are commonly undertaken on free "tetra-iridium" (Ir_4) clusters where the four Ir atoms are arranged in a tetrahedron, giving an Ir-Ir bondlength of about 2.5 Å in the simulations.[819] The literature also describes simulations of supported Rh_6 clusters[820] and an "almost regular" octahedron of 6 Ru atoms;[821] M_{10} models for the metals Ru, Os, Rh, Ir, Pd, Pt, Cu, Ag, and Au;[822] M_{13} models, with "hexagonal Pt-group metal surfaces (Pt, Ir, Pd, Rh, and Ru)... modeled chiefly as 13-atom metal clusters";[823] Rh_{13}, Rh_{19}, and Rh_{43} clusters;[824] and so forth.

---

[819] Anna Maria Ferrari, Konstantin M. Neyman, Markus Mayer, Markus Staufer, Bruce C. Gates, Notker Rösch, "Faujasite-Supported Ir_4 Clusters: A Density Functional Model Study of Metal−Zeolite Interactions," J. Phys. Chem. B 103(1999):5311-5319. Galina P. Petrova, Georgi N. Vayssilova, Notker Rösch, "Density functional modeling of reverse hydrogen spillover on zeolite-supported tetrairidium clusters," Chem. Phys. Lett. 444(27 August 2007):215-219.

[820] Galina P. Petrova, Georgi N. Vayssilova, Notker Rösch, "Density functional modeling of reverse hydrogen spillover on zeolite-supported tetrairidium clusters," Chem. Phys. Lett. 444(27 August 2007):215-219.

[821] Gerald B. Ansell, M.E. Leonowicz, Michelle A. Modrick, "The crystal structure of $Ru_6Cu_2C(CO)_{16}(MeCN)_2$," Acta Crystallographica Section A: Foundations of Crystallography 14(1981):C-150; http://journals.iucr.org/a/issues/1981/a1/00/a43044/a43044.pdf.

[822] C.-T. Au, C.-F. Ng, M.-S. Liao, "Methane dissociation and syngas formation on Ru, Os, Rh, Ir, Pd, Pt, Cu, Ag, and Au : A theoretical study," J. Catalysis 185(1999):12-22.

[823] Marc T. M. Koper, Rutger A. van Santen, Sally A. Wasileski, Michael J. Weaver, "Field-dependent chemisorption of carbon monoxide and nitric oxide on platinum-group (111) surfaces: Quantum chemical calculations compared with infrared spectroscopy at electrochemical and vacuum-based interfaces," J. Chem. Phys. 113(8 September 2000):4392-4407.

[824] Zhi-Qiang Li, Yuichi Hashi, Jing-Zhi Yui, K Ohno, Y Kawazoe, "Electronic and magnetic properties of embedded Rh clusters in Ni matrix," J. Phys.: Condens. Matter 7(11 September 1995):7367-7372.

Based on these clues, we constructed a tetrahedral Ir_4 cluster in which every Ir atom has 3 bonds to neighboring Ir atoms (Figure 4-9), a similar tetrahedron for Rh_4, and an octahedral Ru_6 cluster in which every Ru atom has 4 bonds to nearest-neighbor Ru atoms (Figure 4-10). The tetrahedral structure for Ir_4, along with its -H and -CH_2● variants, were successfully optimized in DFT using the LANL basis set, yielding the results shown in Table 4-4 below. (Rh_4 and Ru_6 also successfully optimized, but the Rh_4-H, Rh_4-CH_2●, Ru_6-H and Ru_6-CH_2● structures all failed to converge even using "Loose" criteria.)

Figure 4-9. (A) LANL minimized tetrahedron iridium cluster model of empty Ir tip (modeled as Ir_4, filename = Ir4tetraSP.hin); (B) LANL minimized tetrahedron iridium cluster tip carrying H atom payload (modeled as Ir_4H, filename = Ir4tetraHSP.hin); (C) LANL almost-minimized tetrahedron iridium cluster tip carrying CH_2● payload (modeled as Ir_4CH_2, filename = Ir4tetraCH2SP.hin); C = black, H = white, Ir = purple.

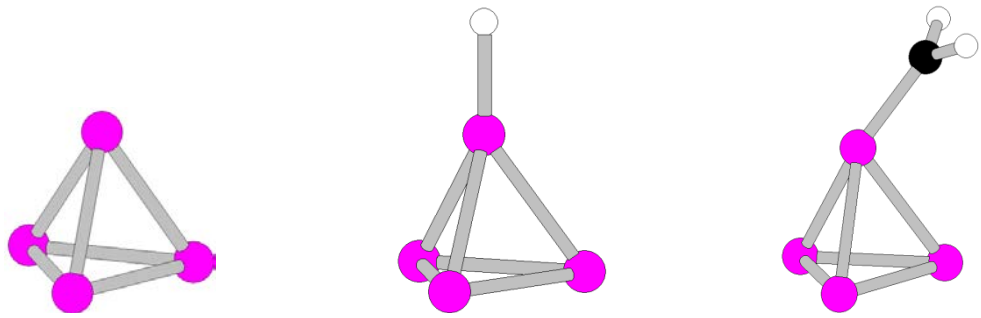

(A) (B) (C)

Figure 4-10. (A) LANL minimized octahedron ruthenium cluster model of empty Ru tip (modeled as Ru_6, filename = Ru6SP.hin); (B) MM+ minimized octahedron ruthenium cluster tip carrying H atom payload (modeled as Ru_6H, filename = Ru6H.hin); (C) MM+ minimized octahedron ruthenium cluster tip carrying CH_2● payload (modeled as Ru_6CH_2, filename = Ru6CH2.hin); C = black, H = white, Ru = purple.

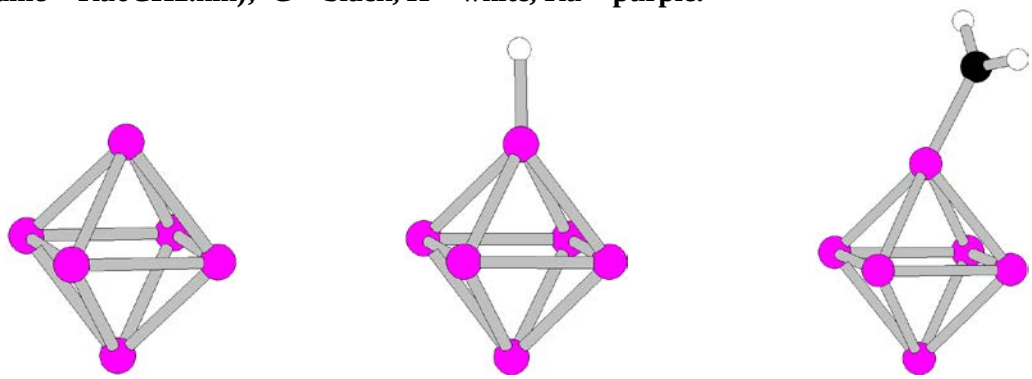

(A) (B) (C)

As a result, only the Ir tip cluster model produced usable results. Comparing these results to the data from Table 4-2 in Table 4-4, we find that the CH_2● transfer energetics has improved slightly for the larger Ir tip, as Ir_4 is now predicted to donate CH_2● to AdamRad almost up to 300 K (this

requires a -0.40 eV threshold). The larger message here is that the two sets of data are generally in good agreement, indicating that the smaller tip models used in Table 4-2 may be adequate for a first-cut analysis.

Table 4-4. Energetics of basic diamondoid mechanosynthesis operations using larger single-atom metal tips (blue = exoergic, red = endoergic)

Single-Atom Tip	Atomic No.	----- *Abstract* -----				----- *Donate* -----		
		CH_2• from Ge (eV)	CH_2• from Sn (eV)	CH_2• from Pb (eV)	CH_2• Dissoc. Energy (eV)	CH_2• onto Adam• (eV)	H onto Adam• (eV)	H Dissoc. Energy (eV)
H_2Ir tip	77	-0.40	-0.76	-1.23	+3.70	-0.27	-1.00	+3.18
Ir_4 tip	77	-0.28	-0.64	-1.11	+3.59	-0.38	-1.68	+2.49

Thus it appears possible that noble metal tips can be used to perform at least some of the critical DMS reactions for the initial bootstrap effort that the first molecular workstation will represent. Later on, we can use the workstation to fabricate atomically precise and atomically sharp diamondoid tips.

4.2.2.3 Bond Strength and Scission Forces with Metal Tips

While it is good news that at least two single-atom metal tips evidently produce good energetics for DMS reactions, we know that even apparently energetically unworkable DMS tips can still reliably perform their desired function if appropriate bond scission forces are available.[825] Thus the next question regarding plausibility is whether these metal tips can provide bond scission forces that lie usefully intermediate between the moiety/presentation-surface bond scission force and the moiety/workpiece bond scission force. If such intermediate bond scission forces are available, then the single atom metal tip may be able to perform its desired function even if the reaction energetics appear modestly unfavorable.

If the proposal is to use single-atom metal tips in the first-generation molecular workstation, then the key threshold issue is whether the bond strengths and scission forces of metal tips comprising, e.g., Ir-Ir or Pt-Pt metallic bonds, compare favorably to similar measures for C-C bonds, and whether metal-C, metal-Ge and metal-H bonds might provide the same range of workability as do C-C, C-Ge and C-H bonds.

---

[825] Jingping Peng, Robert A. Freitas Jr., Ralph C. Merkle, James R. Von Ehr, John N. Randall, George D. Skidmore, "Theoretical Analysis of Diamond Mechanosynthesis. Part III. Positional C_2 Deposition on Diamond C(110) Surface using Si/Ge/Sn-based Dimer Placement Tools," J. Comput. Theor. Nanosci. 3(February 2006):28-41; http://www.MolecularAssembler.com/Papers/JCTNPengFeb06.pdf.

For covalent bonds under large tensile load a useful simple empirical relation for potential energy V as a function of internuclear distance r, based on standard experimental values for bond energy D_e (= potential well depth = bond dissociation energy + zero point vibrational energy), bond length r_0, and bond stretching stiffness k_s, is the Morse function,[826] or $V_{Morse} = D_e \{ (1 – \exp[-\beta(r - r_0)])^2 - 1\}$ where $\beta = (k_s / 2D_e)^{1/2}$, hence the exertable tensile force $F(r) = -(\partial/\partial r) V_{Morse} = 2\beta D_e \{\exp[-2\beta(r - r_0)] - \exp[-\beta(r - r_0)]\}$ which reaches a maximum (F_{max}) at the Morse function inflection point $r_i = r_0 + ((\ln 2) / \beta)$, that is, at $F_{max} = F(r_i)$.

According to the CRC Handbook,[827] the gas phase bond energy (diatomic gas phase) is 460 kJ/mole for C-Ge, 607 kJ/mole for C-C, 598 kJ/mole for Pt-C and 632 kJ/mole for Ir-C. No data was readily available at WebElements for Ir-Ir or Pt-Pt. For the **C-C bond**, D_e = 3.47 eV,[828] r_0 = 1.523 Å,[829] k_s = 440 N/m,[830] giving F_{max} = **5.53 nN**. For the **C-Ge bond**, D_e = 2.44 eV,[831] r_0 = 1.950 Å,[832] k_s = 270 N/m,[833] giving F_{max} = **3.63 nN**. By comparison, for the **Ir-C bond**, assuming D_e = 3.6 eV, r_0 = 2.0 Å, and k_s = 440 N/m (assumed same as C-C) would give F_{max} = **5.7 nN**; for the **Pt-C bond**, assuming D_e = 3.4 eV, r_0 = 2.0 Å, and k_s = 440 N/m (assumed same as C-C) would give F_{max} = **5.5 nN**. However, this estimate for the Ir-C bond differs substantially from a more detailed DFT trajectory calculation for this bond that suggests an Ir-C scission force of only 2.94 nN, indicating the necessity of a more detailed analysis of the parameters used in the above equations. One preliminary result appears to be that the Ir-C bond is relatively weak, so

---

[826] Philip M. Morse, "Diatomic molecules according to the wave mechanics. II. Vibrational levels," Phys. Rev. 34(1 July 1929):57-64; http://prola.aps.org/abstract/PR/v34/i1/p57_1.

[827] J.A. Kerr, in: D.R. Lide, ed., CRC Handbook of Chemistry and Physics 1999-2000: A Ready-Reference Book of Chemical and Physical Data, 81st edition, CRC Handbook of Chemistry and Physics, CRC Press, Boca Raton, Florida, USA, 2000.

[828] Donald F. McMillen, David M. Golden, "Hydrocarbon bond dissociation energies," Annu. Rev. Phys. Chem. 33(1982):493-532.

[829] HyperCube, Inc., HyperChem Computational Chemistry, Publication HC70-00-04-00, January 2002; MM2 (1991) parameter set (/runfiles/mmpstr.txt and /runfiles/mmpben.txt) contributed by Norman Allinger.

[830] HyperCube, Inc., HyperChem Computational Chemistry, Publication HC70-00-04-00, January 2002; MM2 (1991) parameter set (/runfiles/mmpstr.txt and /runfiles/mmpben.txt) contributed by Norman Allinger.

[831] M. Lesbre, P. Mazerolles, J. Stage, The Organic Compounds of Germanium, John Wiley & Sons, New York, 1971.

[832] HyperCube, Inc., HyperChem Computational Chemistry, Publication HC70-00-04-00, January 2002; MM2 (1991) parameter set (/runfiles/mmpstr.txt and /runfiles/mmpben.txt) contributed by Norman Allinger.

[833] HyperCube, Inc., HyperChem Computational Chemistry, Publication HC70-00-04-00, January 2002; MM2 (1991) parameter set (/runfiles/mmpstr.txt and /runfiles/mmpben.txt) contributed by Norman Allinger.

the Ir tip should easily donate C- and Ge-based moieties to diamondoid structures, but a weaker-bonding presentation surface (e.g., perhaps Pb or an appropriate transition metal) might be needed to allow a bare Ir tip to pick up the feedstock molecule in the first place.

Although we haven't performed a comprehensive literature search, mechanical bond scission forces between transition metals and C/Ge atoms appear not to have been widely investigated. Lacking good literature on the subject, a preliminary computational survey seems prudent. Some experimental data does exist for metal-metal bond scission energies. For example, Figure 4-11 shows cohesive energy (the energy required to extract one atom out of the bulk lattice) for various transition metals compared to bulk carbon and germanium – four of the five leading candidates from Table 4-2 have atom extraction energies intermediate between C and Ge.

Figure 4-11. Experimentally measured cohesive energies of transition metals.[834] Tabular data for metals was read off the graph; tabular data for C, Si, and Ge.[835]

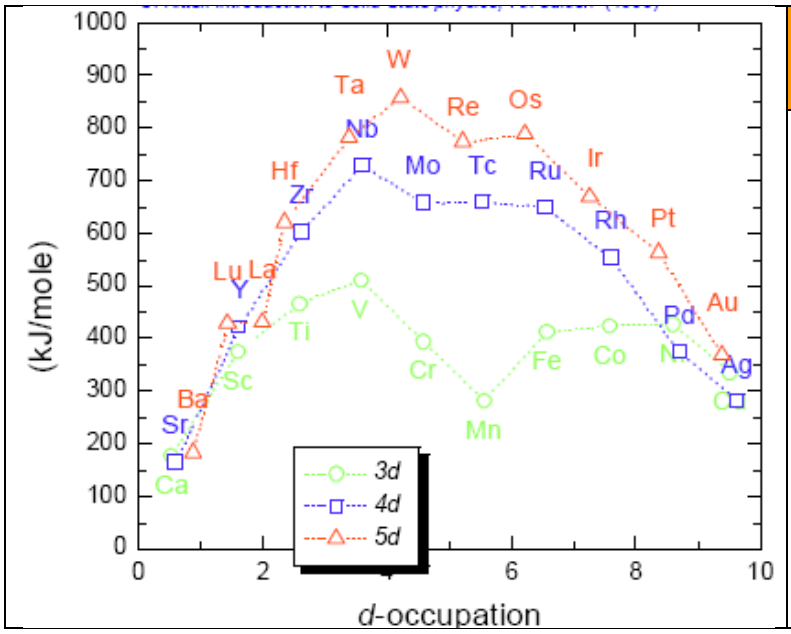

Metal or Atom	Cohesive Energy		
	kJ/ mole	*zJ/ atom*	*eV/ atom*
W	850	1410	8.80
Os	790	1310	8.18
Ta	785	1300	8.11
Re	775	1290	8.05
C	710	1180	7.37
Ir	675	1120	6.99
Mo	660	1100	6.87
Ru	650	1080	6.74
Pt	565	940	5.87
Rh	550	910	5.68
Si	447	742	4.63
Ge	372	617	3.85
Pd	370	615	3.84
Au	365	605	3.78
Ag	280	465	2.90

---

[834] C. Kittel, Introduction to Solid State Physics, 7th Edition, 1996. Cited in: Hans L. Skriver, "Computational Materials Physics," slide presentation, Center for Atomic-Scale Materials Physics CAMP-DTU Lyngby, 2003; http://www.imprs-am.mpg.de/summerschool2003/skriver.pdf.

[835] Philip Peter Rushton, "Cohesive Energies. Table 3.3: Cohesive energies (in eV/atom) calculated using the LDA, PW91 and HCTH," Towards a Non-Local Density Functional Description of Exchange and Correlation, University of Durham, U.K., PhD Thesis, November 2002; http://cmt.dur.ac.uk/sjc/thesis_ppr/node50.html.

However, in molecular mechanics the bond scission force is related to bond energy via the bond stretching stiffness parameter k_s for each type of bond, and that parameter is currently unknown for the bonds of interest. To estimate the bond scission force for M-C, M-Ge, and M-M transition metal bonds, we would need to perform a series of relatively simple DMS trajectory calculations for each bond type. In each trajectory calculation, two bonded structures would first be optimized using LANL for metal atoms and 6-31G(d) or better for the nonmetal atoms C, Ge, and H. The equilibrium M-C, M-Ge, or M-M bondlength is recorded as r_0 and the equilibrium energy is recorded as E_0. The two structures are then incrementally pulled apart along mutually co-axial but opposite paths until the bond of interest breaks, where bond breakage is defined as occurring at the Morse function inflection point r_i, and the energy recorded at the inflection point is E_i. The bond scission force is then estimated as $F_{scission} \approx (E_i - E_0) / (r_i - r_0)$.

The first structure for each trajectory run might be either: (1) a tetrahedral M_4 cluster (Figure 4-9A) where M = Mx (= $_{45}$Rh, $_{47}$Ag, $_{73}$Ta, $_{75}$Re, $_{77}$Ir, $_{79}$Au), or (2) an octahedral M_6 cluster (Figure 4-10A) where M = Mz (= $_{42}$Mo, $_{44}$Ru, $_{46}$Pd, $_{74}$W, $_{76}$Os, $_{78}$Pt). The second structure for each trajectory run could be either: (1) a single-cage Adam tooltip molecule (-$C_{10}H_{15}$) with a bridgehead C atom bonded to one M atom (testing the M-C bond), (2) a single-cage GeRad tooltip molecule (-GeC_9H_{15}) with the bridgehead Ge atom bonded to one M atom (testing the M-Ge bond), or (3) a metal cluster (M_4 or M_6) identical to the first structure with a bond between one M atom from each structure (testing the homotypic M-M bond). Since there are 12 possible first structures and 3 possible second structures, this suggests 36 separate trajectory calculations as illustrated in Figure 4-12. Each of these calculations consists of an initial structure optimization followed by a series of pull-apart structure optimizations that runs until the bond of interest breaks. For comparison we must also do 3 additional "benchmark" sets – an Adam-Adam, Adam-GeRad, and GeRad-GeRad pull-apart series to estimate the C-C, C-Ge, and Ge-Ge scission forces that has previously been calculated by other means – and 4 additional "presentation" sets using SnRad and PbRad to estimate the Sn-Ge, Pb-Ge, C-Sn, and C-Pb bond scission forces. Thus there are a total of 43 unique trajectory calculation sets to be run, allowing the compilation of a table showing 43 separate bond scission force estimates.

Note that in Figure 4-8A, Figure 4-9C and Figure 4-10C, the geometry-optimized CH_2● moiety appears to be significantly tilted relative to a co-axial line passing through the metal cluster. If this bent geometry persists with the adamantane cage (or the second metal cluster) after the initial geometry optimization, then the two structures might have to be moved into a co-axial configuration prior to the pull-apart sequence if scission forces become focused on a single shoulder bond during the scission event and rip apart either the metal cluster or the adamantane cage. A coaxial configuration could be calculated by specifying a C_3 symmetry condition during the energy minimization. (In the ideal case, distributing scission forces evenly across all three shoulder atoms would avoid the breaking of any bonds other than the bond of interest.) In the case of a bent configuration in an unconstrained optimized geometry, the energy of the straightened coaxial configuration should be recorded as $E_{coaxial}$ so that the impact of the bending energy ($E_{coaxial} - E_0$) on the total scission energy ($E_x - E_0$) can be assessed.

Figure 4-12. Generic structures for bond scission testing: (A) $Mx_3Mx\text{-}CC_9H_{15}$ (6 variants), (B) $Mx_3Mx\text{-}GeC_9H_{15}$ (6 variants), (C) $Mx_3Mx\text{-}MxMx_3$ (6 variants), (D) $Mz_5Mz\text{-}CC_9H_{15}$ (6 variants), (E) $Mz_5Mz\text{-}GeC_9H_{15}$ (6 variants), (F) $Mz_5Mz\text{-}MzMz_5$ (6 variants), and (G) $H_{15}C_9C\text{-}CC_9H_{15}$ (1 variant), (H) $H_{15}C_9Ge\text{-}GeC_9H_{15}$ (1 variant), and (I) $H_{15}C_9C\text{-}GeC_9H_{15}$, (C, Sn, Pb for contact atom on left group with Ge on right group; Sn, Pb for contact atom on right group with C on left group; 5 variants). C = black, Ge = yellow, H = white, Ru = purple.

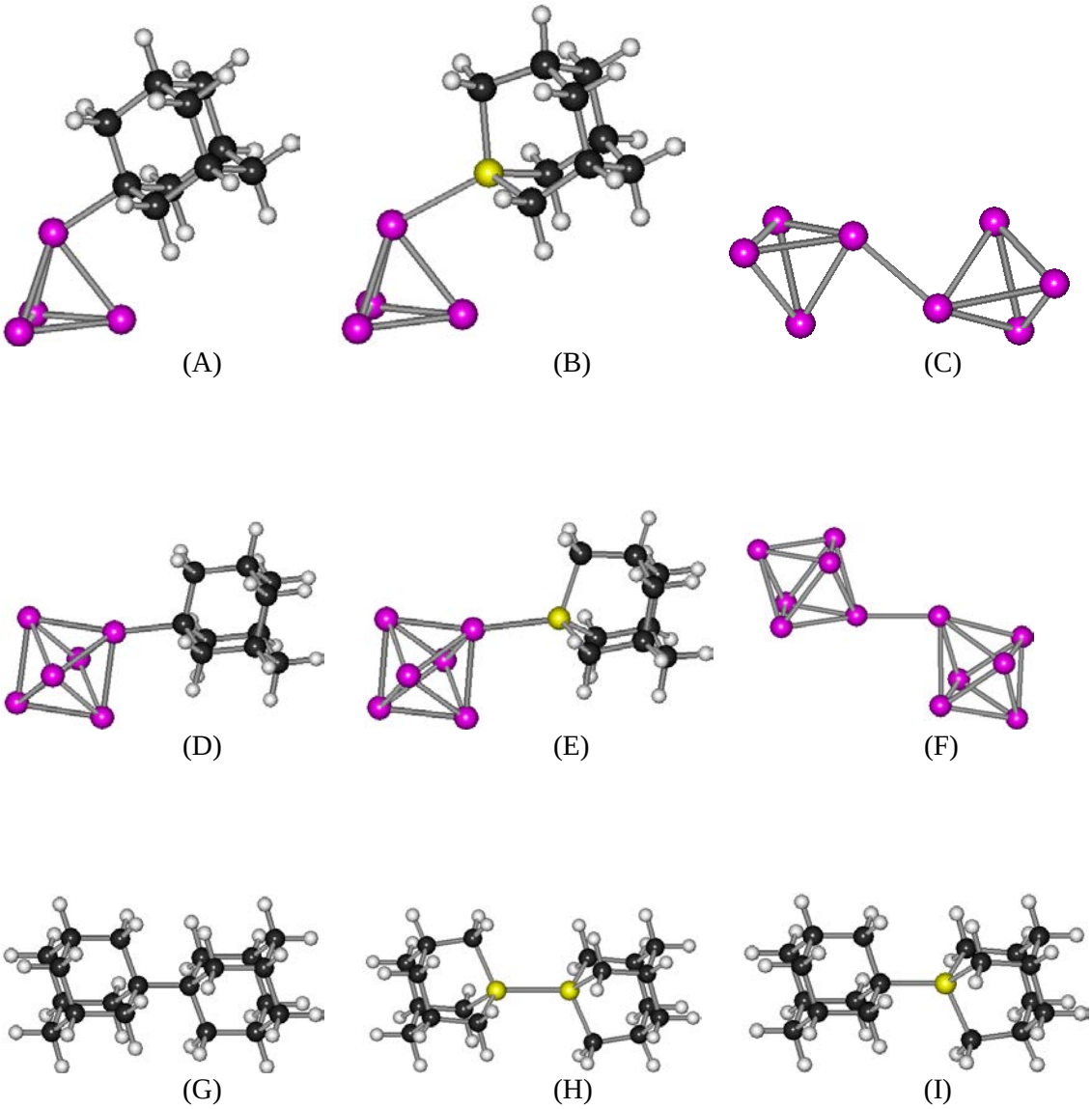

A related question is whether these tips possess enough mechanical strength to maintain their own physical integrity and structural stability during the mechanical DMS operations they would be asked to perform. A literature search needs to be done on this. For instance, observations of Ir atoms adsorbed on Ir(100) shows that islands of Ir of more than 6-7 atoms are stable.[836] One early computational study[837] that simulated SPM tips using molecular dynamics found that "many metallic single-atomic tips are unstable during the scan at a tip load well below typical experimental values," but at least one DFT study has reported the apparent stability of Ir facets.[838] Careful simulations will be needed for all tip configurations that we plan to use in the molecular workstation.

4.2.2.4 Other Aspects of Using Single-Atom Metal Tips

Besides atomic sharpness, noble-metal single-atom tips have two other benefits from the standpoint of molecular workstation design if an electrically conductive presentation surface is employed: (1) conductive metal tips can in principle be used for STM scanning to achieve very precise positional registration so that we're not completely reliant on our metrology system which will be in its earliest incarnation and thus imperfect in its operation (i.e., a belt-and-suspenders approach seems prudent, whenever possible); and (2) the STM scanning capability afforded by metal tips might also be used to map in detail the distribution of feedstock molecules and other features of presentation surfaces at the beginning of the DMS process.

4.2.3 Plan B: ALE-Coated Single-Atom SPM Tips

As an alternative to single-atom metal tips that are often prepared by applying a metal thin film over a tungsten tip (Section 4.2.2.1), the tips described in Section 4.2.2 could possibly be coated instead with a single monolayer of silicon atoms, yielding (in principle) a single Si atom, or perhaps just a few Si atoms, at the tip (Figure 4-13). These would hopefully be better in quality than the silicon field emission tips[839] previously mentioned in Section 4.2.1 and Table 4-1, and would provide more reliable tips that the current practice among experimentalists of banging single-atom Ir-W tips into silicon surface until one Si atom at random comes to reside on the tip, among the jumble of other Si atoms collecting there, thus providing single-atom resolution with a silicon tip (Section 2.1.3.4). Silicon tip chemistry for DMS is the basis of our original bootstrap

---

[836] P.R. Schwoebel, Peter J. Feibelman, "Extraction of Ir – Ir adatom interaction strengths on Ir(100) from field ion microscopy of iridium cluster structures," Surface Science 216(1 June 1989):263-269.

[837] Sun M. Paik, Sihong Kim, Ivan K. Schuller, "Method of determining tip structure in atomic force microscopy," Phys. Rev. B 44(1991):3272-3276.

[838] P. Kaghazchi, T. Jacob, I. Ermanoski, W. Chen, T.E. Madey, "First-principles studies on oxygen-induced faceting of Ir(210)," ACS Nano. 2(June 2008):1280-1288.

[839] Ding Meng, Sha Guobin, A.I. Akinwande, "Silicon field emission arrays with atomically sharp tips: turn-on voltage and the effect of tip radius distribution," IEEE Transactions on Electron Devices 49(December 2002):2333-2342.

proposal, hence single-atom Si tips should work as or more reliably than single-atom metal tips, all else equal.

Figure 4-13. Illustration of tip building sequence using ALE to deposit silicon (red atoms) on a tungsten tip (blue atoms) using hydrogen (white atoms) as the passivating agent.

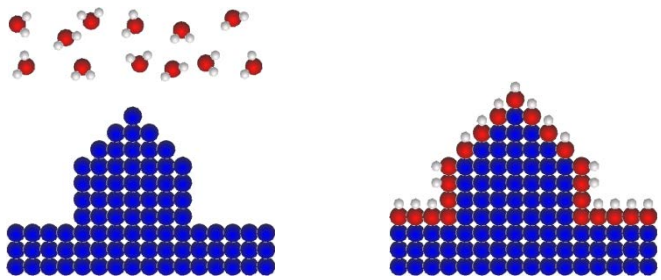

As noted by Randall,[840] Atomic Layer Epitaxy (ALE) of Si is an experimentally-demonstrated cyclic Chemical Vapor Deposition (CVD) process that deposits a monolayer (or a well defined fraction of a monolayer) per ALE cycle. The deposition self-limits due to the Si atoms that bind epitaxially to the surface, carrying with them an atom or molecule that "protects" the newly deposited surface from further deposition. In another part of the ALE cycle, the protecting or passivating species are globally removed from the surface, effectively deprotecting the surface and allowing a subsequent monolayer of atoms to be deposited in the next ALE cycle. In several cases, notably using disilane Si_2H_6 as a precursor gas, the passivating species is H. A patterned Si ALE process (Section 4.2.4) then is accomplished by replacing the global removal of H with a patterned removal of H. ALE cycles then will only deposit Si in the areas that have been deprotected via atomically precise H depassivation lithography, providing atomic resolution in all three dimensions.

One ALE technique involves using two different passivating species where one may be selectively removed without disturbing the other. For instance, both Cl and H will successfully passivate Si (100) surfaces. H will desorb from the Si surface at lower temperatures than Cl. By using the patterned Cl layer to first passivate a Si surface, ALE may be used to grow Si in that patterned area. If the ALE process is one that uses hydrogen as the passivating chemistry, then the ALE process may be continued without additional patterning by using temperature as the depassivating process for the H passivated Si. Because the Cl will remain in place, then the ALE process will only grow Si in the area that was originally patterned in the Cl passivation layer. The process may be continued for as many deposition cycles as desired for that pattern.

Numerous ALE processes have been developed for Si and Ge with a wide variety of precursors (e.g., SiH_4, Si_2H_4, $SiCl_2H_2$, GeH_4, Ge_2H_6, $GeH_2(CH_3)_2$, $GeCl_4$). Further investigation is

---

[840] John Randall, "Atomically Precise Manufacturing Processes," Paper 01, Part 3, Proceedings of the Roadmap Working Group, Foresight/Battelle Nanotechnology Roadmap, 2007.

required to determine if silicon ALE is available (or can be developed) for reliably depositing Si monolayer onto single-atom tip metal surfaces such as Ir, Pt, or W.

4.2.4 Plan C: Atomically-Precise Single-Atom Tooltips from PALE

Patterned Atomic Layer Epitaxy, or PALE, might be used to produce almost atomically-precise atomically-sharp tooltips to greatly improve the efficiency of the initial bootstrapping process for DMS – after which DMS could be used to fabricate fully atomically-precise atomically-sharp nanoscale tooltips for later generations of the molecular workstation. At least one company (Zyvex) has received a patent on the process and was actively pursuing experimental development work using grants from private and government sources totalling ~$25M as of 2009.

Patterned atomic layer epitaxy (PALE) is a positionally-controlled variant of atomic layer deposition (ALD) or atomic layer epitaxy (ALE). ALE is a cyclic Chemical Vapor Deposition (CVD) type process that deposits a monolayer (or a well defined fraction of a monolayer) per ALE cycle (Section 4.2.3). Note that ALE is often considered to be a special case of ALD: the focus of ALE is depositing epitaxial layers, meaning perfect crystal structure, whereas ALD seeks to deposit one layer at a time with the focus on film uniformity, not single crystal structure.

Notes Aaltonen:[841] "ALD is a gas phase thin film deposition method which can be regarded as a special modification of the more widely used chemical vapor deposition (CVD) technique. In ALD, the precursors are led into the reaction chamber in alternate pulses while in CVD, the precursors are led into the reaction chamber simultaneously. The alternate precursor pulses in ALD are separated by inert gas purging (in flow type reactors) or by evacuation of the reactor (in high-vacuum type reactors). The precursors react with the surface groups on the substrate, or chemisorb on the substrate surface. In properly chosen process conditions, the surface reactions are self-limiting, which leads to highly controlled film growth. If the surface reactions become saturated, a constant film growth rate is obtained over the whole substrate surface, and films with excellent conformality and good large-area uniformity are obtained. The set of successive pulses of two or more precursors, separated by purge periods, is called an ALD cycle. The film growth rate is usually measured as the film thickness obtained during one ALD cycle. The film thickness can be easily and accurately controlled by the number of the applied growth cycles."

Atomic layer epitaxy technologies for Si on Si substrate,[842] insulating SiO_2 on Si substrate,[843] P/B doping on SiGe,[844] Si on Ge,[845] and semiconductor on silver substrate[846] are well known, but the

---

[841] Titta Aaltonen, "Atomic Layer Deposition of Noble Metal Thin Films", Academic Dissertation, Helsinki 2005; http://www.cambridgenanotech.com/theses/Atomic%20Layer%20Deposition%20of%20Noble%20Metal%20Thin%20Films.pdf.

[842] Titta Aaltonen, "Atomic Layer Deposition of Noble Metal Thin Films", Academic Dissertation, Helsinki 2005; http://www.cambridgenanotech.com/theses/Atomic%20Layer%20Deposition%20of%20Noble%20Metal%20Thin%20Films.pdf.

ALD of metals on Si and SiO_2 substrates has traditionally been quite challenging. Even so, by 2005 a large number of metallic elements (Al, Co, Cu, Fe, Ir, Mo, Ni, Pd, Pt, Rh, Ru, Ta, Ti, W) had been deposited either by using a thermally activated process or with additional activation.[847]

PALE, which has been proposed by researchers at Zyvex,[848] is an extension of ALD or ALE in which scanning probe technology is employed for positional control to selectively deprotect specific atomic sites on a surface (Figure 4-14), after which atomic layer epitaxy is used to add a single atomic layer of a second material from the vapor phase at the positionally selected depassivated sites in a CVD-type reaction with an ambient gas (Figure 4-15). Repeating this process can allow atomically precise three-dimensional structures to be built up one atomic layer at a time. For example, Lyding's group at the Beckman Institute has successfully grown silicon nanostructures by selectively depassivating a hydrogen-terminated silicon surface at atomically precise locations using Feedback Controlled Lithography,[849] then depositing silicon onto the sites

---

[843] Ofer Sneh, Steven M. George, "Thermal Stability of Hydroxyl Groups on a Well-Defined Silica Surface," J. Phys. Chem. 99(1995):4639-4647; http://pubs.acs.org/cgi-bin/abstract.cgi/jpchax/1995/99/i13/f-pdf/f_j100013a039.pdf?sessid=6006l3. S. Morishita, Y. Uchida, M. Matsumura, "Atomic-Layer Chemical-Vapor-Deposition of SiO_2 by Cyclic Exposures of $CH_3OSi(NCO)_3$ and H_2O_2," Jpn. J. Appl. Phys. 34(1995):5738-5742; http://jjap.ipap.jp/link?JJAP/34/5738. O. Sneh, M.L. Wisem A.W. Ott, L.A. Okada, S.M. George, "Atomic layer growth of SiO_2 on Si(100) using $SiCl_4$ and H_2O in a binary reaction sequence," Surf. Sci. 334(1995):135-152. J.W. Klaus, A.W. Ott, J.M. Johnson, S.M. George, "Atomic layer controlled growth of SiO_2 films using binary reaction sequence chemistry," Appl. Phys. Lett. 70(3 March 1997):1092; http://link.aip.org/link/?APPLAB/70/1092/1. Kei-ichi Yamaguchi, Shigeru Imai, Naoto Ishitobi, Masashi Takemoto, Hidejiro Miki, Masakiyo Matsumura, "Atomic-layer chemical-vapor-deposition of silicon dioxide films with an extremely low hydrogen content," Applied Surface Science 130-132(June 1998):202-207. Eva Aro, Suvi Haukka, Marko Tuominen, "Atomic-Layer-Chemical-Vapor-Deposition of Films That Contain Silicon Dioxide," European Patent EP1248865, Filing Date 12/04/2000; www.freepatentsonline.com/EP1248865.html.

[844] B. Tillack, "Atomic layer doping of SiGe," Proceedings of the Twelfth European Conference on Chemical Vapour Deposition, 1999, Journal de Physique IV: Proceedings 1(1999):295-305.

[845] Keiji Ikeda, Satoshi Sugahara, Yasutaka Uchida, Tomonori Nagai, Masakiyo Matsumura, "Formation of an atomically abrupt Si/Ge hetero-interface," Japanese Journal of Applied Physics 37(1998):1311-1315.

[846] M. Luisa Foresti, Francesca Forni, Massimo Innocenti, Francesca Loglio, Giovanni Pezzatini, "Deposition and characterization of ultrathin layers of compound semiconductors on Ag(111)," Abstr. Papers, Am. Chem. Soc. (2001), 221st COLL-345.

[847] Antti Niskanen, Radical Enhanced Atomic Layer Deposition of Metals and Oxides, Academic Dissertation, Helsinki, 2006; https://oa.doria.fi/dspace/bitstream/10024/2729/1/radicale.pdf. See also: A. Niskanen, T. Hatanpää, K. Arstila, M. Leskelä, M. Ritala, "Radical Enhanced Atomic Layer Deposition of Metallic Silver Films," submitted to Mater. Chem. 2006.

[848] J.N. Randall et al, "Patterned atomic layer epitaxy," United States Patent 20050223968, 13 October 2005. See also: Mikko Ritala, Markku Leskelä, "Atomic layer epitaxy – a valuable tool for nanotechnology?" Nanotechnology 10(March 1999):19-24.

[849] M.C. Hersam, G.C. Abeln, J.W. Lyding, "An approach for efficiently locating and electrically contacting nanostructures fabricated via UHV-STM lithography on Si(100)," Microelectronic Engineering 47(June 1999):235-237. See also: Mark C. Hersam, Nathan P. Guisinger, and Joseph W. Lyding, "Silicon-

from the gas phase, demonstrating that atomically precise deprotection is possible with an STM tip that is not itself atomically precise.

This process has been developed by Lyding's group at the Beckman Institute. Silicon nanostructures[850] and copper phthalocyanine (Cu(Pc)) and norbornadiene[851] were successfully grown by selectively depassivating a hydrogen-terminated silicon surface at atomically precise locations using Feedback Controlled Lithography, then depositing the atoms or molecules by adsorption onto the sites from the gas phase. The work by Lyding and Hersam[852] demonstrates that atomic precision deprotection is possible with an STM tip that is not atomically precise, but is simply capable of atomic resolution imaging. However, reliable manufacturing will require a reproducible tooltip.

Figure 4-14. Site specific hydrogen desorption. (a) The feedback {z} and tunneling current {I} signals are monitored as a function of time while patterning at 3V, 2 nA; hydrogen atom desorption is clearly observed as a ~1.5 Å step in z and occurs in ~0.005 sec.[853] (c) 3 x 3 array of individual dangling bonds nanopatterned with feedback controlled lithography on Si(100)-2x1:H in ultra-high vacuum.[854]

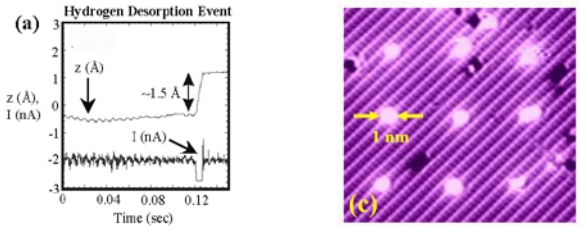

Based Molecular Nanotechnology," Seventh Foresight Conference on Molecular Nanotechnology, 15-17 Oct. 1999, Santa Clara, CA. http://www.foresight.org/conferences/mnt7/Papers/Hersam/index.html.

[850] Joseph Lyding, "Silicon-Based (Carbon) Nanotechnology," seminar presented at the University of Sheffield, 27 January 2004. http://www.shef.ac.uk/sheffield/jsp/polopoly.jsp?a=15946.

[851] Hersam, Mark C.; Guisinger, Nathan P.; and Lyding, Joseph W. 1999a. "Silicon-Based Molecular Nanotechnology," Seventh Foresight Conference on Molecular Nanotechnology, 15-17 Oct. 1999, Santa Clara, CA. http://www.foresight.org/conferences/mnt7/Papers/Hersam/index.html.

[852] M.C. Hersam, G.C. Abeln, J.W. Lyding, "An approach for efficiently locating and electrically contacting nanostructures fabricated via UHV-STM lithography on Si(100)," Microelectronic Engineering 47(June 1999):235-237.

[853] M.C. Hersam, G.C. Abeln, J.W. Lyding, "An approach for efficiently locating and electrically contacting nanostructures fabricated via UHV-STM lithography on Si(100)," Microelectronic Engineering 47(June 1999):235-237. See also: Mark C. Hersam, Nathan P. Guisinger, and Joseph W. Lyding, "Silicon-Based Molecular Nanotechnology," Seventh Foresight Conference on Molecular Nanotechnology, 15-17 Oct. 1999, Santa Clara, CA. http://www.foresight.org/conferences/mnt7/Papers/Hersam/index.html.

[854] Mark Hersam, "Conductive Scanning Probe Microscopy Nanopatterning," The Hersam Research Group: Single Molecule Sensing, Characterization, and Actuation, 2007; http://www.hersam-group.northwestern.edu/nanopatterning.html.

Figure 4-15. Silicon patterned ALE at Zyvex: (A) STM tip removes H atoms from the Si surface; (B) a precursor gas is used to dose the surface, whereupon protected Si atoms are deposited only where H has been removed; (C) Completed deposition is verified, then the deprotection and patterning is repeated. Below: Experimental demonstration of PALE by Joe Lyding – room temperature, 10^{-8} torr disilane, 10 minutes/row, 5V-1nA / 7V-1nA / 6V-1nA, 6 nm high features.

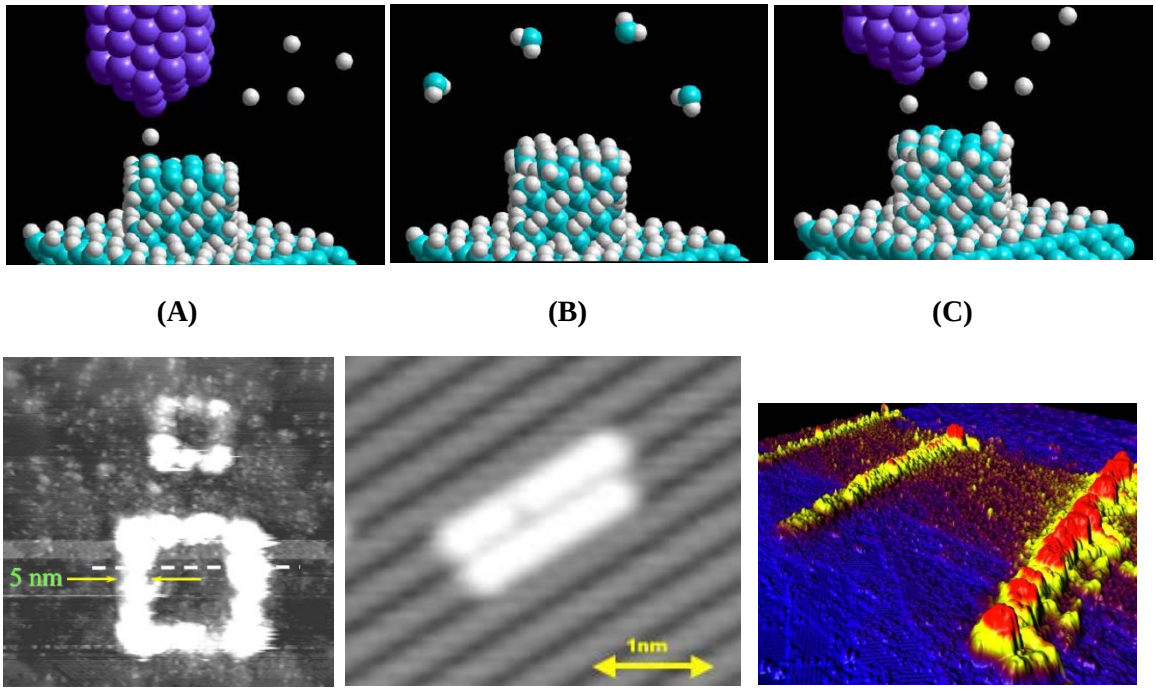

In March 2008, Zyvex announced that it had assembled $15 million in funding for its Atomically Precise Manufacturing Consortium. The project includes a mixture of funding from the Defense Advanced Research Projects Agency, the Texas Emerging Technology Fund and cost sharing from the team members. "Increasing the precision of manufacturing has driven both technology and science for the past couple of centuries and what we are doing is just an extension of that drive," said John Randall, vice president of Zyvex Labs, the prime contractor for the research project. "What is revolutionary is having digital control over where we add atoms to a robust solid material." In addition to UT Dallas and Zyvex, the research team includes the University of Illinois at Urbana-Champaign, the University of North Texas, the University of Central Florida, the University of Texas at Austin, the National Institute of Standards and Technology, General Dynamics, Molecular Imprints Inc. and Integrated Circuit Scanning Probe Instruments.

The Atomically Precise Manufacturing Project currently consists of three coordinated efforts: MicroAutomation, Molecularly Precise Tools, and Patterned Atomic Layer Epitaxy. The latter initiative is perhaps the most important to Nanofactory Corporation's diamondoid nanofactory program. Notes Randall: "Atomic layer deposition builds amorphous materials; atomic layer epitaxy (ALE) builds crystalline materials. Start with a protected (passivated) surface: every available bond has a hydrogen atom. If you deprotect the surface, removing the hydrogen, then you can deposit a layer of atoms. If you choose the right precursor gas, you add only one monolayer which is protected as it's added. Then you can deprotect and add exactly one more

layer of atoms. There are a number of precursor gases available. There are literally hundreds of systems to grow things with atomic precision in one dimension. Now, if you combine this with the ability to deprotect the surface in selected locations....With a scanning tunneling microscope, you can remove single hydrogen atoms with atomic precision. If you do this layer by layer, you can build 3D structures. Professor Joe Lyding at University of Illinois has done repeated desorption/deposition."

According to a Zyvex website:[855] "The Patterned Atomic Layer Epitaxy Project will combine two known experimental techniques to produce atomically precise nanostructures. In our view, this is the best approach to a molecular assembler that can make reasonable progress before molecularly precise tools are available. We have identified a target process and material system that will be capable of producing complex, atomically precise (in all three dimensions) nanostructures in a robust material. The prototype reactors will not be massively parallel and will be capable of only limited output. We have identified several approaches to massive parallelism that will be evaluated as we develop the prototype tools. The prototype system, even with its limited capabilities, will be able to produce valuable products that require only very small atomically precise structures. When the APM Project produces a superior tip for patterning, this will greatly improve patterned atomic layer epitaxy and enable its scale-up to large parallelism. However, such tools will also enable significant progress in molecular pick and place technology. Zyvex will constantly be evaluating the best path to a massively parallel molecular assembler."

Notes Randall:[856] For a Si process two different passivation layers would be required, one (passivation A) that is a robust mask that can be patterned with Atomic Precision and would be stable while an ALE process that used a different passivation chemistry (passivation B) was used to deposit Si in that patterned area. Part of that requirement would be for passivation B to be cleanly removed from the Si surface repeatably (every ALE cycle) with some global depassivation process while not removing passivation A. One technique involves using two different passivating species, where one may be selectively removed without disturbing the other, as already described in Section 4.2.3). The process may be continued for as many deposition cycles as desired for that pattern. Control of the growth on the sidewalls of the ALE grown structure may be an issue.

A Dual Material ALE process could also have a reduced patterning requirement as well as a number of other advantages. Consider an atomically flat section of Ge (100) that was passivated with some species that can be patterned. An ALE process is used to deposit a monolayer of Si in the patterned layer. (Note that heteroepitaxy of Si on Ge and Ge on Si has been established with ALE processes.) At this point a dual material ALE process could be used to selectively deposit Si on Si and Ge on Ge where the cyclic process would alternatively deposit a monolayer of Si and a monolayer of Ge. In this way the growth surface would stay atomically flat and there would be no sidewalls to contend with. After a designed number of deposited monolayers, the pattern could be changed and complex 3D heterostructures could be created. Since there are very selective etches to remove Ge, the Ge material could be used as a sacrificial layer, allowing for releasable 3D

---

[855] Zyvex research activities, accessed March 2008; http://www.zyvex.com/Research/activities.html.

[856] John Randall, "Atomically Precise Manufacturing Processes," Paper 01, Part 3, Proceedings of the Roadmap Working Group, Foresight/Battelle Nanotechnology Roadmap, 2007.

structures. Thus a dual material ALE process such as Si/Ge would be able to create releasable complex 3D structures. Simple atomically precise Si artifacts such as a wall of silicon a known number of atoms wide and tall would be an excellent CD standard for SEMs or AFMs. Several other atomically precise standards could be produced. The cost of producing a single metrology standard even with a single STM tip doing the patterning could be easily under $1000.

According to an online article[857] by Tihamer Toth-Fejel on 6 October 2009, giving an update on the Zyvex TPN effort: "The Zyvex-led Atomically Precise Manufacturing Consortium has recently met their DARPA-funded Tip-Based Nanofabrication project's Phase I metrics by writing 100 dangling bond wires, half of them 36.6 nm x 3.5 nm and half 24.5 nm x 3.5 nm in 5.66 minutes. [These "wires" are just lines of depassivation positionally etched on hydrogenated silicon surface, each line ~10 atoms wide.] That is 1.5 million atoms per hour, but the error rate was ±6.4%, which is unacceptable for [molecular manufacturing] (unless they implement error correction, which for Patterned Atomic Layer Epitaxy may or may not be easy because the high mobility of hydrogen at the operating temperature of the process)."

According to further comments by Tihamer Toth-Fejel on 20 October 2009 at the Lifeboat Foundation blog, in response to an assertion that "Zyvex is working on atomically perfect quantum dots (with size control ot 0.2 nanometers)": "It's not just the precise size, but also the shape. Second, there is the precise placement and orientation of those QDs....Zyvex was thinking about building quantum dots at the beginning of the project, but we are no longer concentrating on them (unless someone here can think of a killer application that only requires a few thousand perfect quantum dots, at $1 each)....The big problem with using our method–Patterned Atomic Layer Epitaxy–to make quantum dots is that all the applications for QDs (e.g. solar cells, biological labeling, etc.) are analogous to putting pebbles in concrete. With the possible exception of quantum dot cellular automata, there is no reason that quantum dots need to be atomically precise. In other words, it's not economically worthwhile to use Patterned ALE for QDs; not even close. As I stated at the Unither Nanomedicine Conference (assuming we succeed in phase III), the estimated costs for building bulk amounts of anything using Patterned ALE are astronomical – a one-person dose of Freitas respirocytes would optimistically cost $360 quadrillion. That's the bad news. But nanoimprint might lower that cost by about one magnitude. A primitive bootstrap, in which the STM array would be used to build another array with smaller, and more numerous probe tips, would require about 16 weeks of build time, plus an indeterminate amount of research time, possibly reducing the cost of one dose of respirocytes by two magnitudes. Only 15 generations to go!... I'm just making assumptions and cranking numbers here. We still need to achieve atomic precision at a rate of 10 million atoms/hour for $300 by 2012, and there are some serious technical barriers that must be overcome. Plus there is the additional problem that Patterned ALE can't do error correction after the ALE step (though it can do it during/after the patterning step)."

"Once PALE is a proven technology, perhaps by 2012 (according to Zyvex estimates as of 2009, and comments by Toth-Fejel), our Plan C is to build a PALE tip from scratch on an atomically flat silicon SPM tip using the Zyvex process, once they can do it. We assume that we can build

---

[857] Tihamer Toth-Fejel, "Productive Nanosystems and the 2009 Financial Meltdown," Nanotechnology-Now, 6 October 2009; http://www.nanotech-now.com/columns/?article=357.

or obtain, say, a rectangular silicon rod of dimensions 1 μm x 1 μm x 1 mm long, where the tip end of the rod tapers down to a 10 nm x 10 nm square surface that is atomically flat. Very crudely, an isoceles triangle (in cross-section) with a $\theta = 60^o$ apex tip angle has a height H equal to halfwidth W/2 divided by the tangent of the half-angle θ/2, therefore the PALE tip height is $H = (W/2) / \tan(\theta/2) = (10\text{ nm} / 2) / \tan(60^o / 2) = 8.66$ nm for a tip with a flat 10 nm x 10 nm flat end on which the tip is built up layer by layer using PALE (Figure 4-16). If the silicon layers are Si(110) crystal planes and are, say, 1.92 Å apart, then to build up a 8.66 nm stack made of these layers will require 8.66 nm / (0.192 nm/layer) ≈ 45 layers to be laid down by PALE. At ~1 hour/layer, this does not seem excessive."

Figure 4-16. Illustration of atomically-sharp silicon tip-building sequence using PALE to deposit silicon on silicon (red atoms) using hydrogen (white atoms) as the passivating agent. The dehydrogenated sections in every other frame is created via positionally-controlled SPM tip-based electrical desorption.

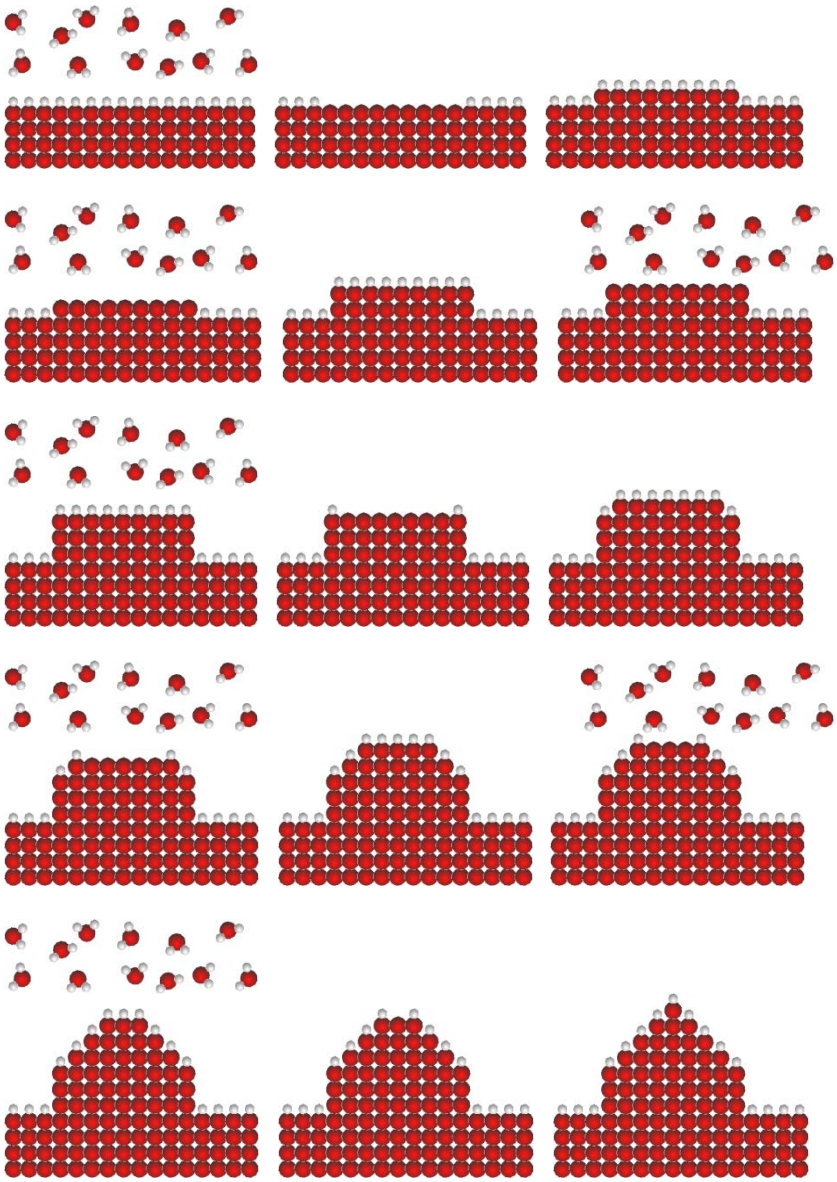

4.2.5 Plan D: Graphene Dome Tips on Ir(111) Surface

Another alternative is to make use of the semi-deterministic growth of graphene domes on Ir(111) surface recently reported by Lacovig et al.[858] A combination of high-resolution photoelectron spectroscopy and ab initio calculations showed that carbon nanoislands formed during the growth of a long-range ordered graphene layer on Ir(111) assume a peculiar domelike shape (Figure 4-17). The researchers studied, both experimentally and via confirmatory DFT-based computational simulations using VASP, the aggregation of carbon atoms into graphene clusters (1) upon annealing to different temperatures an Ir(111) surface saturated with C_2H_4 at 300 K and (2) during C_2H_4 exposure at 820 K, 970 K, and 1270 K. These two procedures resulted in different morphologies of the C clusters as seen with STM:[859] In the second (high-temperature) case the clusters grow exclusively at step edges because of rapid C diffusion and occupation of preferred configurations, but in the first (low temperature) case flat C island formation takes place also on the terraces and an overall coverage of 0.29 ML is obtained. The transition from carbidic C to a low interacting graphene layer proceeds via formation of dome-shaped C nanoislands whose interaction with the Ir substrate takes place only at the cluster edge.

The geometry of a single (n = 1) honeycomb ring (Figure 4-17A) is quite simple: The C atoms, placed in bridge sites, sit in a planar configuration with a C-Ir distance of 1.62 Å and the symmetry axes oriented along the (101) direction. However, an increase in n has drastic effects on cluster morphology. The cluster with n = 3 abandons the flat configuration and bends upwards assuming a domelike shape: the central C atom is now at a distance of 2.53 Å from the Ir surface, and only the C atoms at the periphery remain close to the Ir substrate. This process is paralleled by a rotation of the symmetry axes by 11°. For still larger cluster sizes the unsticking process goes on further: the top C atoms for n = 7 and n = 19 move apart by 2.63 Å and 3.13 Å, respectively, while the cluster undergoes further rotation, not too far from the value of 30° of a graphene layer with a C-C distance of 1.42 Å. Even for a very small C island, the interaction of Ir atoms placed just below the center of the dome is very small (Figure 4-17B). Only the Ir atoms directly bonded with the C atoms at the cluster edge strongly.[860]

---

[858] Paolo Lacovig, Monica Pozzo, Dario Alfe, Paolo Vilmercati, Alessandro Baraldi, Silvano Lizzit, "Growth of Dome-Shaped Carbon Nanoislands on Ir(111): The Intermediate between Carbidic Clusters and Quasi-Free-Standing Graphene," Phys. Rev. Lett. 103(16 October 2009):166101.

[859] Johann Coraux, Alpha T. N'Diaye, Martin Engler, Carsten Busse, Dirk Wall, Niemma Buckanie, Frank-J Meyer zu Heringdorf, Raoul van Gastel, Bene Poelsema, Thomas Michely, "Growth of graphene on Ir(111)," New J. Phys. 11(4 February 2009):023006.

[860] Paolo Lacovig, Monica Pozzo, Dario Alfe, Paolo Vilmercati, Alessandro Baraldi, Silvano Lizzit, "Growth of Dome-Shaped Carbon Nanoislands on Ir(111): The Intermediate between Carbidic Clusters and Quasi-Free-Standing Graphene," Phys. Rev. Lett. 103(16 October 2009):166101.

Figure 4-17. (A) Left: Calculated structural models of the C clusters formed by n honeycomb rings with (a) n = 1, (b) n = 3, (c) n = 7, and (d) n = 19; Ir_i (i = 1; . . . ; 6) and C_j (j = 1; . . . ; 4) represent different Ir and C local configurations, respectively; the distance of the central C atoms from the Ir substrate as well as the orientation of the cluster with respect to the (101) direction of Ir(111) are also shown. (B) Right: Evolution of the binding energy/atom as a function of the ratio of C atoms at the periphery N_P and the total number N_T in each C cluster.[861]

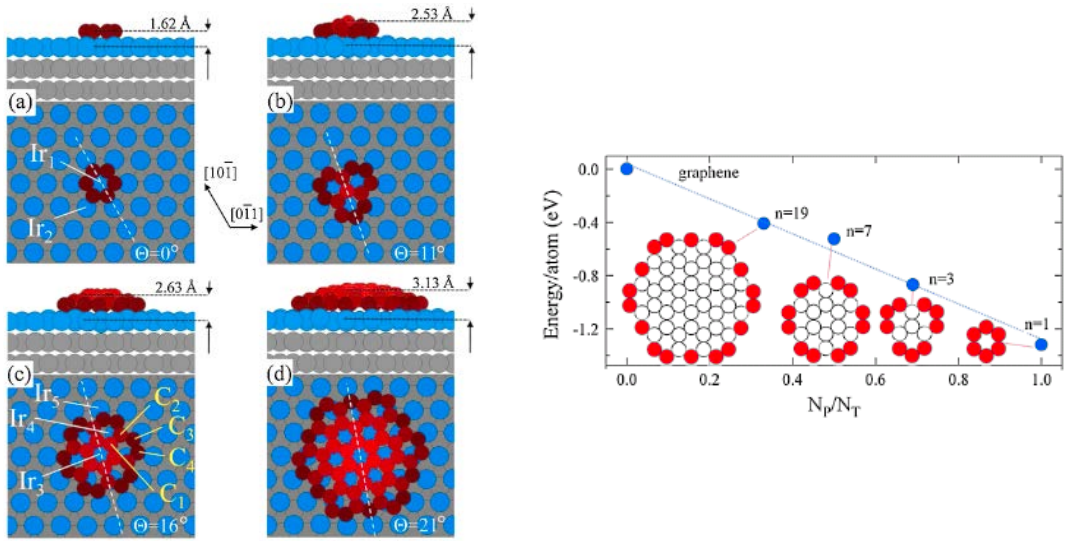

If this process can be closely controlled, a graphene dome of specific n might be self-assembled on a flat Ir surface (e.g., at the apex of a truncated conical probe), with the intent to use the most apical C atom at the center of the dome structure as the DMS bonding atom of a low-aspect-ratio but atomically deterministic DMS tip.

4.2.6 Plan E: Atomically-Imprecise Tooltips

As our least favored but probably still-viable alternative, Plan E is to employ the sub-nanometer asperity (Figure 4-18) (and related) tips shown in Table 4-1. These won't be as reliable and are not atomically precise, but they should work well enough to get the job done if enough trials are attempted. In this case, the obvious strategy using these tips would be to build atomically precise replacement tips as quickly as possible.

---

[861] Paolo Lacovig, Monica Pozzo, Dario Alfe, Paolo Vilmercati, Alessandro Baraldi, Silvano Lizzit, "Growth of Dome-Shaped Carbon Nanoislands on Ir(111): The Intermediate between Carbidic Clusters and Quasi-Free-Standing Graphene," Phys. Rev. Lett. 103(16 October 2009):166101.

Figure 4-18. Probe sharpness determines resolution. DNA strand diameter (~2 nm) can be resolved[862] using a ~1 nm DLC spike-probe tip.[863] Small unwound single-strand DNA fragments can be seen (bold arrow on scan) and even the helical pitch of the DNA molecule can be resolved (thin arrows).

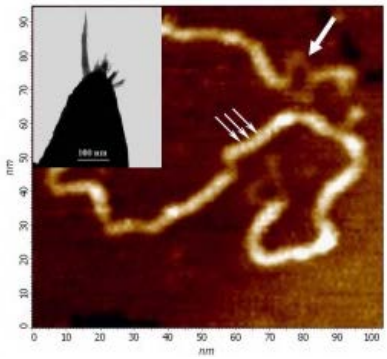

This approach restricts us to diamond, DLC, carbon nanotube, or silicon tips that are already commercially available "off the shelf". Especially noteworthy is the NT-MDT[864] diamond-like carbon (DLC) spike-probe tip with an asperity that is only a few carbon atoms wide at the tip. This tip has been used by Klinov et al.[865] to scan short poly(dG)-poly(dC) DNA fragments deposited on modified HOPG (highly oriented pyrolytic graphite), enabling them to detect single-stranded regions in double-stranded poly(dG)-poly(dC) and double-stranded and single-stranded regions in poly(dG)-poly(dG)-poly(dC) triplexes, as well as to resolve the helical pitch of the triplex molecules (Figure 4-18).

It may also be possible similarly to grow metallic asperity-like tips that might be suitable for DMS. For example, in 2009 Sun et al.[866] synthesized ultrathin single crystal platinum nanowires

---

[862] Dmitry Klinov, Benjamin Dwir, Eli Kapon, Natalia Borovok, Tatiana Molotsky, Alexander Kotlyar, "High-resolution atomic force microscopy of duplex and triplex DNA molecules," Nanotechnology 18(6 June 2007):225102. "DNA in nanotechnology," 2007; http://www.nanovip.com/node/4971.

[863] NT-MDT (Molecular Devices and Tools for Nanotechnology, Moscow, Russia, http://www.ntmdt.com), "Super sharp Diamond_Like Carbon (DLC) tips," from their "SPM Probe and Accessories" catalog, 2008; http://www.ntmdt.com/download/accessories_catalog.pdf.

[864] NT-MDT (Molecular Devices and Tools for Nanotechnology, Moscow, Russia, http://www.ntmdt.com), "Super sharp Diamond_Like Carbon (DLC) tips," from their "SPM Probe and Accessories" catalog, 2008; http://www.ntmdt.com/download/accessories_catalog.pdf.

[865] Dmitry Klinov, Benjamin Dwir, Eli Kapon, Natalia Borovok, Tatiana Molotsky, Alexander Kotlyar, "High-resolution atomic force microscopy of duplex and triplex DNA molecules," Nanotechnology 18(6 June 2007):225102.

[866] Shuhui Sun, Gaixia Zhang, Yu Zhong, Hao Liu, Ruying Li, Xiaorong Zhou, Xueliang Sun, "Ultrathin single crystal Pt nanowires grown on N-doped carbon nanotubes," Chem. Commun. (2009):7048-7050.

(Figure 4-18A) with diameters of 2.5 nm and lengths up to 100 nm on nitrogen-doped CNTs (N-CNTs) using a straightforward wet-chemical method in environmentally friendly water solution at room temperature, without using any stabilizing agent.

Figure 4-18A. Single-crystal platinum asperities grown on CNT.[867]

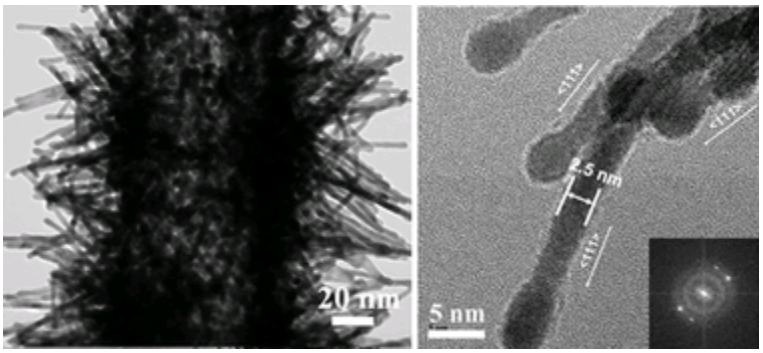

Ge nanocrystals grown on Si(100)-(2x1) surfaces by molecular beam epitaxy (MBE) also are observed to form a relatively high density of Ge islands with small "pyramids," "domes," and "facetted domes" of various sizes co-existing in the film.[868] Scanning tunneling microscopy (STM) and high resolution cross-sectional transmission electron microscopy (XTEM) studies[869] reveal that a large fraction of these islands, especially the dome-shaped Ge islands, have an aspect ratio of ~1(diameter):1 (height), but this is likely too blunt to be useful for DMS bootstrapping tips. These are somewhat similar to the Ge "hut" structures described in Section 4.4 and shown in Figure 4-20, below.

---

[867] Shuhui Sun, Gaixia Zhang, Yu Zhong, Hao Liu, Ruying Li, Xiaorong Zhou, Xueliang Sun, "Ultrathin single crystal Pt nanowires grown on N-doped carbon nanotubes," Chem. Commun. (2009):7048-7050.

[868] Bhattacharjeea, Anupam Roya, Jay Ghataka, P.V. Satyama, B.N. Deva, "Ultrasmall Ge islands with low diameter-to-height aspect ratio on Si(100)-(2x1) surfaces," Applied Surface Science 256(30 October 2009):356-360; http://www.sciencedirect.com/science?_ob=ArticleURL&_udi=B6THY-4W7YXMH-F&_user=10&_rdoc=1&_fmt=&_orig=search&_sort=d&_docanchor=&view=c&_searchStrId=1102988067&_rerunOrigin=scholar.google&_acct=C000050221&_version=1&_urlVersion=0&_userid=10&md5=93d7077e3462b4f62a914d920d9fc656.

[869] Bhattacharjeea, Anupam Roya, Jay Ghataka, P.V. Satyama, B.N. Deva, "Ultrasmall Ge islands with low diameter-to-height aspect ratio on Si(100)-(2x1) surfaces," Applied Surface Science 256(30 October 2009):356-360; http://www.sciencedirect.com/science?_ob=ArticleURL&_udi=B6THY-4W7YXMH-F&_user=10&_rdoc=1&_fmt=&_orig=search&_sort=d&_docanchor=&view=c&_searchStrId=1102988067&_rerunOrigin=scholar.google&_acct=C000050221&_version=1&_urlVersion=0&_userid=10&md5=93d7077e3462b4f62a914d920d9fc656.

4.3 Tooltip Handles, Tool Chucks, and Toolrack

4.3.1 Tooltip Handles and MEMS-Based qPlus Toolheads

The tooltip handle is a structure that permits atomically precise positional control and manipulation of an atomically sharp tooltip. In an advanced DMS system, a tooltip handle might be very simple, perhaps consisting of an extended block of diamondoid that is covalently attached to a high-aspect atomically-precise diamondoid tooltip, yielding a complete tool suitable for DMS. One such possible tool, as illustrated in Figure 1-5, might measure 2.7 nm x 2.8 nm x 5.2 nm, would be atomically precise, and could be self-registering (Section 4.4) when retrieved from a toolrack.

In the initial molecular workstation, the tool handle will be significantly larger, likely macroscale, to facilitate easy handling, attachment, and electrical connection. The current method of choice for SPM is the qPlus sensor pioneered by Giessibl[870] (Section 2.1.6). In this system, the tip is glued onto the free tine of a quartz tuning fork using silver solder that can only tolerate being heated to about 150 °C. This precludes the option of baking out the entire system at a higher temperature to facilitate establishment of good vacuum (Section 4.7.1). This is, therefore, our least desirable option: using an existing Omicron (or related) commercial qPlus sensor to which a tip is glued. Such tools are not only atomically imprecise but are physically messy, variable in size, and contain low-melting-point glue preventing high-temperature bakeout. (Note that Andreas Heinrich at IBM Almaden, in partnership with Giessibl, used a qPlus AFM system with a single-atom Ir tip that achieved a 20 pm resonator amplitude,[871] which Heinrich says[872] they obtained by cutting the conventional free tuning fork tine in half, apparently yielding a record-high tip stiffness on the order of 20,000 N/m. Apparently there is no ongoing effort at IBM Almaden to move into 3D with SPMs, nor is there any SPM-based metrology work. They are doing all metal-on-metal (tip/workpiece) work, due to their primary interest in memory circuits and Giant MagnetoResistive (GMR) racetrack structures.)

Ideally, we would like to fabricate a monolithic qPlus sensor to which the tooltip is integrally bonded, with the entire tooltip + handle unit being fabricated by conventional lithography as a monolithic unit, possibly combined with some modest post-processing steps. In this case, the tip, the tuning fork, the handle base, and all the electrical connections would be manufactured integrally to the monolithic sensor using conventional lithographic processes. The tuning fork

---

[870] F.J. Giessibl, "Atomic Resolution of the Silicon (111)-(7x7) Surface by Atomic Force Microscopy," Science 267(1995):68-71. F.J. Giessibl, "High-Speed Force Sensor for Force Microscopy and Profilometry Utilizing a Quartz Tuning Fork", Applied Physics Letters 73(1998):3956-3958. Franz J. Giessibl, "Advances in atomic force microscopy," Rev. Mod. Phys. 75(2003):949-983.

[871] Markus Ternes, Christopher P. Lutz, Cyrus F. Hirjibehedin, Franz J. Giessibl, Andreas J. Heinrich, "The Force Needed to Move an Atom on a Surface," Science 319(22 February 2008):1066-1069.

[872] Andreas J. Heinrich, IBM Almaden; personal communication with Robert A. Freitas Jr. and Ralph C. Merkle, 15 July 2009.

would be made of lithographically depositable pure silicon but would have to be precisely oriented crystallographically.

Photolithographic etching of miniature quartz tuning fork resonators is well-established[873] and thin-film piezo-based tuning fork resonators have been fabricated using depositional lithography.[874] Integration of such forks with other components of the qPlus sensor has apparently not yet been accomplished. However, a lithographically mass-produced quartz tuning fork wafer using polymer tips to make tuning fork sensors has been demonstrated for scanning force microscope imaging in the dynamic mode.[875]) Also, Epson Toyocom (Kanagawa, Japan) announced in late 2008[876] that they had perfected a semiconductor-like photolithography process called Quartz MEMS (QMEMS) using quartz wafers in a semiconductor-like fab, employing a process involving photolithography, etching, metallization and sacrificial-layer removal – the same steps that are involved with silicon MEMS chips, but using the quartz material. This process has been used to make QMEMS tuning-fork resonators below 2 mm, the point at which traditional cutting and beveling no longer works.

The most difficult challenge would seem to be lithographically fabricating a relatively long metal tip as an integral component of a silicon-based structure. Hasegawa et al.[877] have developed a precise atomic force microscope (AFM) lithography to attach an FIB-milled (focused ion beam) glass-coated tungsten tip to a quartz tuning fork controlled by noncontact AFM. There are other references in the literature dating as far back as the 1980s[878] describing the deposition of metallic

---

[873] J.H. Staudte, "Subminiature quartz tuning fork resonator," Proc. 27th Annual Freq.Contr. Symp., 1973, pp. 50-54. See also: "Microresonator packaging and tuning," U.S. Patent No. 3,766,616, 23 October 1973. Sungkyu Lee, "Photolithography and Selective Etching of an Array of Quartz Tuning Fork Resonators with Improved Impact Resistance Characteristics," Jpn. J. Appl. Phys. 40(2001):5164-5167. Jun Xu, Bo You, Xin Li, Jing Ma, "A high sensitivity quartz tuning fork temperature sensor," NEMS2009, 4th IEEE International Conference on Nano/Micro Engineered and Molecular Systems, 2009, pp. 616-619.

[874] Atsushi Isobe, Nobuhiko Shibagaki, Kengo Asai, Hisanori Matsumoto, "Thin film tuning-fork type inflection resonator and electric signal processing element," USPTO Application # 20070182291, 9 August 2007; http://www.freshpatents.com/Thin-film-tuning-fork-type-inflection-resonator-and-electric-signal-processing-element-dt20070809ptan20070182291.php.

[875] T. Akiyama, U. Staufer, N.F. de Rooij, L. Howald, L. Scandella, "Lithographically defined polymer tips for quartz tuning fork based scanning force microscopes," Microelectronic Engineering 57-58(September 2001):769-773.

[876] R. Colin Johnson, "QMEMS process said to shrink quartz crystals," EETimes, 21 November 2008; http://www.eetimes.com/news/latest/showArticle.jhtml?articleID=212101405 and http://www.planetanalog.com/news/showArticle.jhtml?articleID=212101478.

[877] Yukio Hasegawa, Kotone Akiyama, Masayuki Hamada, Toyoaki Eguchi, Toshu An, Yasunori Fujikawa, Toshio Sakurai, "Functional probes for scanning probe microscopy," paper Q36.00004 (12 March 2008), Session Q36: Focus Session: Advances in Scanned Probe Microscopy III: Force Methods, 2008 APS March Meeting, 10-14 March 2008, New Orleans, Louisiana, http://meetings.aps.org/Meeting/MAR08/Event/79069.

[878] Edward M. King, Kurt E. Gsteiger, Joseph S. Raby, "Method for selective deposition of tungsten on silicon," U.S. Patent No. 4,595,608, 17 June 1986; http://www.freepatentsonline.com/4595608.html.

tungsten directly onto silicon surface, confirming this method may be viable for adding a tungsten starter tip to a lithographically-fabricated MEMS-based qPlus sensor assembly. With a monolithic qPlus sensor in hand, the tungsten tip could then be coated and annealed with self-pyramidalizing iridium tips as described in Section 4.2.2.1 – assuming that atomically sharp Ir tips, or similar, prove feasible for DMS in the molecular workstation.

An almost equally attractive approach would be to fabricate the atomically sharp metal tooltip and the MEMS-based qPlus-sensor-handle separately, but designed so that the tooltip could be easily inserted and permanently fastened to the qPlus-sensor-handle using a strong mechanical interlock. This approach would allow tooltip and handle to be fabricated using two different (possibly incompatible) manufacturing processes, then manually joined later using a single assembly step (i.e., inserting tooltip into handle) that is irreversible and provides an extremely rigid connection between tooltip and handle. Again, the tip locking mechanism, the tuning fork, the base and all electrical connections could be manufactured integrally to the monolithic sensor using conventional lithographic processes and probably fabricated to at least micron-scale tolerances, providing a tool of fairly uniform size, geometry, stiffness and frequency response from one tip to another.

Tyrrell et al.[879] have also affixed a diamond probe to a qPlus sensor.

4.3.2 Tool Chucks

The tool chuck is an end-effector, possibly MEMS-based, that is affixed to and directly (mechanically) manipulated by the AFM positioning system. The chuck has two states – closed (grasping a tool handle) and open (not grasping a tool handle) – and is capable of picking up DMS tools from a toolrack; holding the tool firmly during subsequent transport, registration, and tool use; then returning the tool to the toolrack for storage, for later use. The tool chuck may be electrically or mechanically actuated, and it may be permanently affixed to an AFM tip or its may be separable from the tip in the manner of a jig (Section 4.3.3). The tool chuck is conceptually (and possibly physically) similar to the nanopart gripper tool described earlier (Section 4.1.6) – the gripper tool grabs nanoparts from the fabrication surface, whereas the tool chuck grabs DMS tools from the toolrack (Section 4.3.4). Gripping tools is slightly different from gripping nanoparts, though it is also true that all nanotools (nanoscale tools) are by definition also nanoparts, since the workstation should be able to make them. Depending on the exact system design, these two devices may be very similar or even identical in configuration; if certain configurations of metal tips can be used, the need for a tool chuck may be minimized.

Ideally, the tool chuck will enable automated tool exchange within the workstation volume without breaking vacuum. Leang and Taylor[880] have designed and fabricated a multifunctional

---

[879] James W.G. Tyrrell, Dmitri V. Sokolov, Hans-Ulrich Danzebrink, "Development of a scanning probe microscope compact sensor head featuring a diamond probe mounted on a quartz tuning fork," Meas. Sci. Technol. 14(2003):2139-2143.

[880] Curtis R. Taylor, Kam K. Leang, "Design and Fabrication of a Multifunctional Scanning Probe with Integrated Tip Changer for Fully Automated Nanofabrication," Paper 2617, 2008 ASPE Annual Meeting;

scanning probe with an integrated tip changer for fully automated nanofabrication. Though not directly applicable to our molecular workstation, their paper[881] illustrates the design, optimization, and fabrication of an active cantilever probe with an automated ability to interchange probe tips (tools) – for example, from chemically functionalized tips for biological printing/characterization to nanowire tips for high resolution metrology to dynamic tips that can be used for nanomachining, manipulation, or material modification (Figure 4-19A). By simply switching tips, the probe can be used for nano deposition, patterning, machining, and metrology in a single platform without the need for an operator to physically remove/replace the cantilever as in traditional scanning probe microscopy (SPM).

The design models macroscale computer numerical control (CNC) manufacturing in which CNC machines are fully automated allowing for rapid tool changes without operator interruption. Located at the distal end of an SPM cantilever is an electrically activated microgripper (thermal actuator) (Figure 4-19B), which is designed to automatically load/unload tips from an array of available tools. A thermal-proximity sensing scheme is proposed to determine the relative location between the microgripper and tool tip to enable automated loading/unloading of tool tips. After using finite element analysis to optimize the cantilever dynamic response, gripper actuation, and overall probe dimensions, the cantilever was fabricated using a MEMS-based silicon micromachining process. The ability to provide fully automated on-demand probe tip changes will improve the overall efficiency of probe-based nanofabrication, allow for multifunctional probe capabilities, and improve process reliability and quality by enabling the ability to replenish/replace worn or chemically fouled tips in an efficient manner. In particular, the proposed design (1) enhances throughput by reducing the time it takes to replace/replenish a tool tip after extensive use (from ~ 5 minutes by manual changing to less than ~ 1 minute or less by automation), for example replacing a worn or chemically-fouled tip – the design virtually eliminates the need for a human operator to change/replace the SPM probe; (2) expands the functionality of probe-based fabrication via interchangeable tools for multi-functional fabrication, for example, an array of tool tips for nanoindentation, dip-pen nanolithography, in-situ high resolution metrology, material deposition, etc.; (3) enables fully automated and programmable changing of tool tips, as well as fully automated nanofabrication, in particular, for applications that involve more than one type of fabrication technique; (4) provides a method for scalability – an array of such cantilevers can be automated for large-scale parallel operation; and (5) provides robust (repeatable and controlled) fabrication procedures because contaminated, chemically fouled, and/or damaged tips can quickly be changed.

Figure 4-19C shows the layout of the envisioned workspace as well as the thermal-proximity concept. In particular, the heated gripper will be positioned over the calibration zone and slowly lowered until there is a noticeable change in thermal response due to conduction of thermal

---

http://www.leang.com/academics/pubs/LeangKK_2008_ASPE.pdf. Kam K. Leang, Curtis R. Taylor, "A novel multifunctional SPM probe with modular quick-change tips for fully automated probe-based nanofabrication," Proceedings of 2009 NSF Engineering Research and Innovation Conference, Honolulu, Hawaii, 22-25 June 2009.

[881] Curtis R. Taylor, Kam K. Leang, "Design and Fabrication of a Multifunctional Scanning Probe with Integrated Tip Changer for Fully Automated Nanofabrication," Paper 2617, 2008 ASPE Annual Meeting; http://www.leang.com/academics/pubs/LeangKK_2008_ASPE.pdf.

energy between the calibration feature and integrated sensor. By using the heated gripper as a thermal-proximity sensor, it can be rastered at constant height above the tool-tip array (X and Y) to determine the approximate location of the tool tips relative to the jaws of the gripper. This information will be used to automatically position the AFM active cantilever at the correct (XYZ) location to enable loading/unloading of tips (Figure 4-19D).

Figure 4-19. (A) Top Left: Concept drawing showing active cantilever probe and modular tool tips. (B) Top Right: Prototype design of cantilever probe with integrated thermally actuated gripper (electrodes and chip base not shown). (C) Bottom Left: Envisioned fabrication workspace, which consists of a platform containing sample and modular tool tips with a calibration zone (home position). The gripper is actuated by the AFM piezoactuator for scanning. (D) Bottom Right: Front and top view of thermal gripper hovering over tool tips. The relative location between gripper and tool tip is determined using thermal proximity sensing: monitoring the thermal behavior of the gripper as it moves over the calibration zone and tool tips.[882]

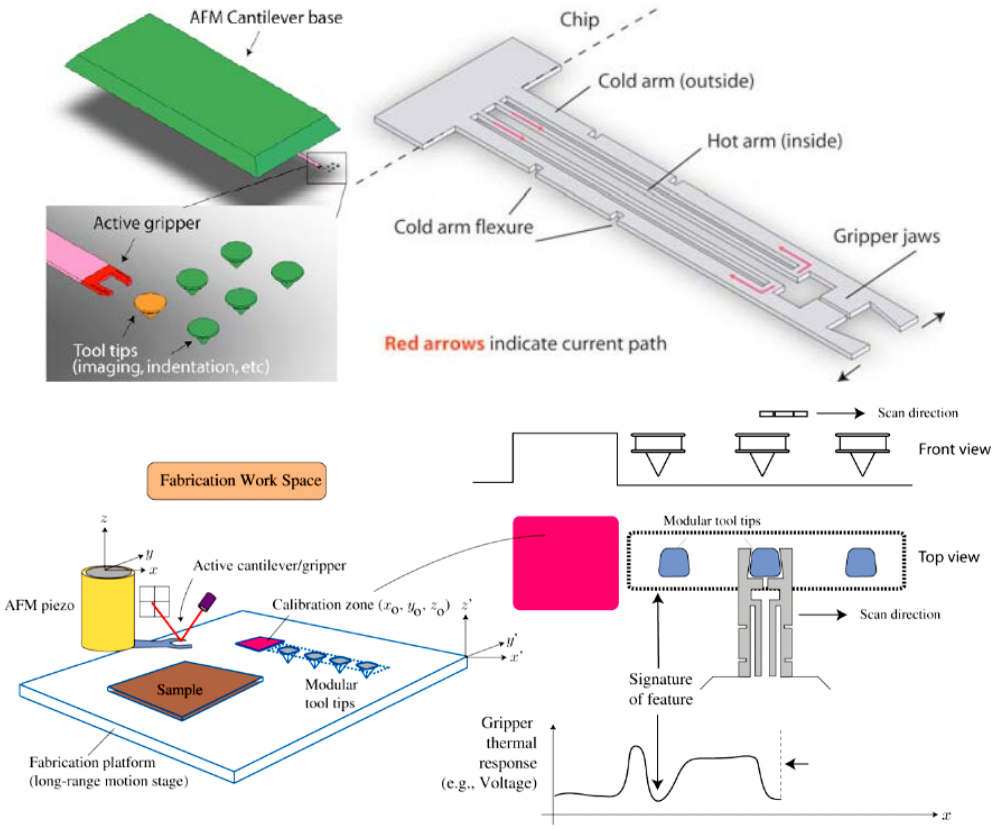

[882] Curtis R. Taylor, Kam K. Leang, "Design and Fabrication of a Multifunctional Scanning Probe with Integrated Tip Changer for Fully Automated Nanofabrication," Paper 2617, 2008 ASPE Annual Meeting; http://www.leang.com/academics/pubs/LeangKK_2008_ASPE.pdf.

Perhaps somewhat more relevant to our workstation design effort, Tyrrell et al.[883] have developed a compact scanning probe microscope sensor head using a mechanical design that allows positioning of the probe relative to the microscope objective and the swift exchange of quartz tuning fork sensors. Additionally, the design permits rotation of the sensor so that its orientation with respect to the sample may be changed.

4.3.3 Tool Jigs

A jig is a fixture, present in the workspace, that can be manipulated by a tool to perform some useful function. Typically a jig will be used to hold a nanopart-in-progress at some desired angle or position.

It may be possible to eliminate one or more tips or DOFs by substituting a jig whose function can substitute for the function of the missing tip or DOF. For example, if one tip is needed to hold a portion of a structure fixed in space while another tip moves around it doing some other task, a jig could be made to perform the same task. The one tip would first put the jig in place, then perform the other task, then remove the jig, so that only one tip was needed instead of two, thus greatly simplifying the workstation manipulator system at the cost of added operational complexity and the need to build and maintain jigs inside the workspace.

It is also possible that a feature could be added to the fabrication surface (Section 4.1.4) or to other surfaces present inside the workspace volume that could serve as a mechanosynthetic jig. For example, a bulk-buildable Ge notch or ledge feature present on a Ge presentation surface could provide a one-step H abstraction tool recharge jig. The spent HAbstH tool would be brought up to the ledge in a particular orientation, placed into contact with the structure such that the distal C on the tool became bonded to a ledge Ge atom while an off-ledge Ge came into abstraction range of the waste hydrogen atom, and then pulled away from the ledge making a recharged HAbst and leaving the waste H bonded to the jig structure – thus avoiding the need for two GeRad tips to participate in this reaction sequence (RS5).[884] Such a jig might allow us to reduce the minimum DMS tip count by one tip, and it might also let us eliminate two of the four presentation surfaces: the H dump could be eliminated and the Ge surface having the ledge jigs could also be littered with GeH_3 and CH_3 groups, thus these two feedstock molecules would need only one presentation surface, not two.

---

[883] James W.G. Tyrrell, Dmitri V. Sokolov, Hans-Ulrich Danzebrink, "Development of a scanning probe microscope compact sensor head featuring a diamond probe mounted on a quartz tuning fork," Meas. Sci. Technol. 14(2003):2139-2143.

[884] Robert A. Freitas Jr., Ralph C. Merkle, "A Minimal Toolset for Positional Diamond Mechanosynthesis," J. Comput. Theor. Nanosci. 5(May 2008):760-861; http://www.molecularassembler.com/Papers/MinToolset.pdf.

4.3.4 Toolrack

The toolrack is rack inside the vacuum workspace where all tools are stored when not in use. The toolrack allows the tools to be stored such that they are not directly exposed to vacuum while they are stored – once plugged into its slot, the handle makes a good seal with the frame of the rack, and the tip of the tool where an exposed radical may reside lies in a fully enclosed volume where it will be maximally protected from stray contaminant molecules. The floor of each slot in the rack can contain getters, if this is deemed useful. The toolrack should space the tools far enough apart that the tool chuck has sufficient clearance to be able to remove or replace tools when neighboring tool slots on either side of the desired tool are occupied by seated tools.

4.4 Tooltip Positional Registration

One major practical challenge of DMS is the relocation of a single atomic site on a sample which may be several mm^2 in area – e.g., after abstracting an H atom from a passivated surface, we must revisit this same atomic lattice site to add, say, a methyl group, after moving the tip a significant distance or in some cases exchanging tips. This requires a viable methodology for relocating atomic sites on a macroscopic sample. Some existing techniques for tip registration, usually involving identification of surface landmarks, have already been described at length in Section 3.3.5 so we will not repeat that discussion here. Assuming we use a qPlus sensor of some kind in the workstation design, the vibratory-sensing qPlus feature will be actively employed only during a tip registration operation (i.e., looking for a known surface feature). For the rest of the time, the qPlus resonator will be turned off and the sensor will be used only as a rigid tip that is moved around the workspace using dead reckoning provided by the high-precision metrology system (Section 4.6).

Printing landmarks on or near the fabrication surface appears to be the leading strategy. On germanium presentation surfaces, such landmarks might include self-assembled metastable Ge hut clusters (Figure 4-20)[885] (after they have been scanned and mapped; Section 4.1.7) – whose formation and growth, and the distribution of strain around their base, are fascinating problems, as is their peculiar propensity to form (501)-facets as their sides,[886] e.g., when Ge atoms are added to Si(100) surface in 4-6 monolayer thickness.[887] Ge hut clusters could also be employed as single-motion H abstraction tool recharge sites. Potential landmarking structures on metal presentation surfaces might include self-assembled metal pyramids that are observed for Ir, Pd, and some other metals (Section 4.2.2.1).

---

[885] Y.-W. Mo, D.E. Savage, B.S. Swartzentruber, M.G. Lagally, "Kinetic Pathway in Stranski-Krastanov Growth of Ge on Si(001)," Phys. Rev. Lett. 65(20 August 1990):1020-1023.

[886] http://www.cmmp.ucl.ac.uk/~drb/Thesis/Masterch8.html.

[887] Y.-W. Mo, D.E. Savage, B.S. Swartzentruber, M.G. Lagally, "Kinetic Pathway in Stranski-Krastanov Growth of Ge on Si(001)," Phys. Rev. Lett. 65(20 August 1990):1020-1023.

Figure 4-20. <u>Left:</u> An STM image of "hut" clusters formed (number density typically ~7 x $10^{10}/cm^2$)[888] when 4-6 layers of germanium are grown on silicon, with the hut sides running along (100)-like directions (which are elastically soft) and the faces all (501)-like; image courtesy of Ilan Goldfarb.[889] <u>Right:</u> STM images of a single Ge "hut" cluster – (a) perspective image with a scan area of 40 nm x 40 nm, showing a hut height of 2.8 nm; (b) curvature-mode grey-scale image, showing the crystal structure on all four facets as well as the dimer rows in the 2D Ge layer around the cluster; the 2D layer dimer rows are 45° to the axis of the cluster.[890]

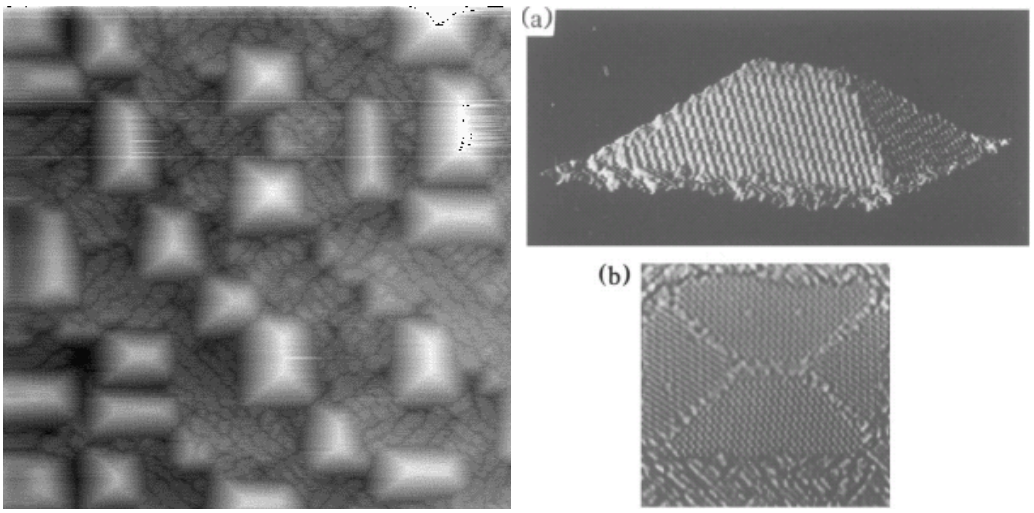

If metal tips can be used in the molecular workstation, this may greatly reduce or even eliminate the need to change tooltips, possibly also greatly reducing the required freqency of tooltip positional re-registration.

It should also be noted that the use of nanoscale tools (e.g., Figure 1-4) which are stored in slot holes of a specific size and orientation in a toolrack (Section 4.3.4) can allow automatic self-registration every time a tool is picked up or returned to the toolrack. For example, if a tool: (1) is designed with a pyramidal tip geometry, (2) has a pyramidal base that is ~2 nm wide, (3) has only a ~0.5 nm wide region near the apex of the pyramid that is chemically active (e.g., exposed radical sites are present), and (4) has gotten less than 1.5 nm out of lateral alignment, then upon inserting a tool into the rack the pyramidal faces on the tip will guide the tool correctly into its hole, automatically recentering the tool to the proper XY position relative to the toolrack. (A

---

[888] Y.-W. Mo, D.E. Savage, B.S. Swartzentruber, M.G. Lagally, "Kinetic Pathway in Stranski-Krastanov Growth of Ge on Si(001)," Phys. Rev. Lett. 65(20 August 1990):1020-1023.

[889] http://www.cmmp.ucl.ac.uk/~drb/Thesis/Masterch8.html.

[890] Y.-W. Mo, D.E. Savage, B.S. Swartzentruber, M.G. Lagally, "Kinetic Pathway in Stranski-Krastanov Growth of Ge on Si(001)," Phys. Rev. Lett. 65(20 August 1990):1020-1023.

simple stop-ledge at the bottom of the hole allows self-registration in the Z-direction as well.) Of course, a misalignment that large would never be allowed to accumulate because it would render all DMS tooltip operations pathological. But more typical nonpathological cumulative positioning errors on the order of 20-50 pm could be periodically auto-corrected in this manner. One would not even have to pickup or release a tool – simply inserting a compliantly gripped tool into the rack, adjusting tool position to restore a zero compliance force, re-setting the XYZ positioning counters, then withdrawing the gripped tool would suffice to quickly re-register the tool position without the need to make any complex SPM-based measurements or calculations.

4.5 SPM Positioning Systems

4.5.1 Actuator Systems

SPM actuators such as piezos and the like will allow us to position a tooltip, tool, or tool chuck to 20-50 pm accuracy over 10-100 micron or larger excursions. A 2004 survey of commercially available systems appears in Table 2-3 in Section 2.2.5. These positioning systems – reviewed at length in Section 2.2 – can operate independently of our ability to actually measure the exact displacement that they produce. Thus the positioning system can be relatively sloppy and hysteretic as long as the metrology system (Section 4.6) is precise enough for reliable dead-reckoning. The same considerations also apply to workpiece and presentation surface positioners.

Piezoelectric actuators, used in AFM, are made of polycrystalline materials and possess a number of imperfections (hysteresis, non-linearity, etc.) that limit the accuracy of their translation.[891] One of the possible solutions for the calibration of AFM scanners and TEM microscopes is the use of linear hysteresis-free piezoelectric actuators based on single crystals.[892] The control of the motion of such actuators can be performed using the dynamic phase microscopy (DPM) method described by Tichinsky et al.[893] Dynamic phase microscopy has been applied to measurements of nanometer-scale and subnanometer-scale displacements of a piezoelectric scanner. This scanner, which was designed for calibration purposes for scanning probe microscopy and TEM, exhibited a linear and hysteresis-free translation in the **50-2000 pm** range.

Tichinsky's "Nanotester" cell (Figure 4-21A) is designed to generate vertical or horizontal displacements in the 0-20 nm and 0-60 nm ranges, respectively. These are the motions of a surface of a central block carrying a piezoelectric single crystal in the horizontal and vertical cells. An electronic block (not shown) supplied voltage (±1 kV) to the cells to cause the crystal

---

[891] V. Giurgiutiu, R. Pomirleanu, C.A. Rogers, "Energy-based comparison of solid-state actuators," University of South California, Report #USCOME-LAMSS-2000-12, 2000.

[892] Boston Piezo-Optics, Inc., Bellingham, MA; http://www.bostonpiezooptics.com.

[893] V.P. Tichinsky, A.V. Kretushev, P.N. Luskinovich, "Dynamic phase microscopy: measurements of translational displacements at sub-nanometer scale," Optical Society of America, 2006; http://arxiv.org/ftp/physics/papers/0608/0608093.pdf.

motion. These cells are calibrated with a coherent phase microscope called "Airyscan"[894] with a He-Ne laser ($\lambda = 632.8$ nm) as the source in a setup described in Figure 4-21B. An optical-path difference was measured using the modulation method with a position-sensitive photodetector-dissector image tube. In static images, the microscope provided a sensitivity of ~500 pm and a spatial resolution up to 100 nm, with a sampling rate limited to modulation frequency 1 kHz (or 1 ms/pixel). This instrument was used for dynamic phase measurements in which the 3D surface pattern was represented by a function h(X,Y,t), where h = optical path difference measured by the interferometer and X,Y = surface coordinates. Most of the calibration operations for displacements in the nanometer range require low electric and vibration noise environment and high temperature stability eliminating thermal drift.

Figure 4-21. (A) Left: Design and photo of dynamic "Nanotester" standard. (B) Right: Setup of Coherent Phase Microscope "Airyscan"; measurements of an optical-path difference are carried out by compensational method in each point consistently scanning images; optical-path difference values normalized on the wavelength are collected in computer memory.[895]

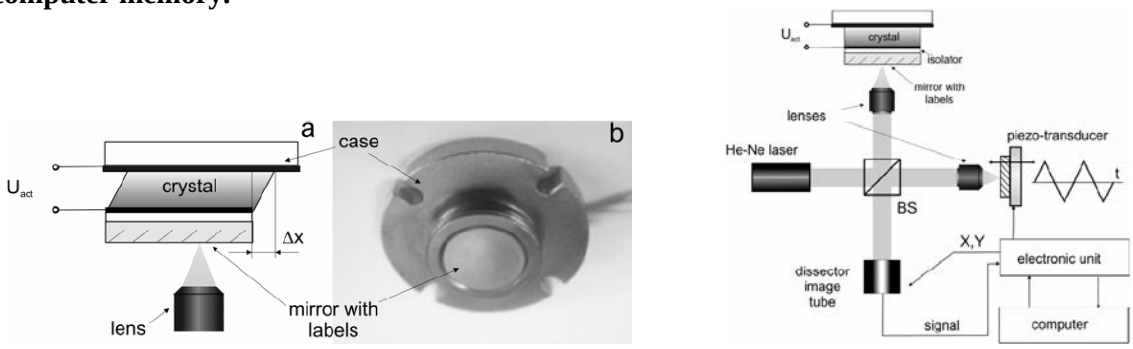

Reducing the hysteresis loop typical for piezoceramics (Figure 4-22a) requires a low noise level, high accuracy, and stability of the instruments. Using an ordinary piezoceramic transducer, the measurement of axial movements as height alterations with fixation of zero values (Figure 4-22b) indicates that the hysteresis (the difference of zero values) amounts to 20 nm, whereas similar measurements using DPM on the "Nanotester" (Figure 4-22c) indicate the practical absence of hysteresis ($\delta X <$ **200 pm**).[896]

---

[894] V.P. Tychinsky, G.E. Kufal, T.V. Vyshenskaja, E.V. Perevedentseva, S.L. Nikandrov, "Measurement of submicron 'Airyscan' laser phase microscope," Quantum Electronics 27(1997):735-739. V.P. Tychinsky, "Coherent phase microscopy of intracellular processes," Physics-Uspekhi 44(2001):617-629.

[895] V.P. Tichinsky, A.V. Kretushev, P.N. Luskinovich, "Dynamic phase microscopy: measurements of translational displacements at sub-nanometer scale," Optical Society of America, 2006; http://arxiv.org/ftp/physics/papers/0608/0608093.pdf.

[896] V.P. Tichinsky, A.V. Kretushev, P.N. Luskinovich, "Dynamic phase microscopy: measurements of translational displacements at sub-nanometer scale," Optical Society of America, 2006; http://arxiv.org/ftp/physics/papers/0608/0608093.pdf.

As noted by Hu et al.,[897] the characteristics of piezoelectric translators (PZTs) that make them appropriate actuators for precision positioning applications include fast frequency response, high stiffness, high resolution, smooth motion, and miniature size. Since the maximum expansion of a conventional PZT is only about 0.1% of its length, a displacement amplifier is usually integrated with an actuator in compact micropositioning devices to achieve motion ranges up to hundreds of microns with several nanometers resolution (equivalent to ~1 micron motion range at ~10 pm of resolution). A variety of displacement amplifiers for PZTs have been proposed in the research community.[898]

Figure 4-22. Measurements of hysteresis: (a) Typical hysteresis loop for piezoceramics is cause of positioning ambiguity. (b) Measurements of hysteresis of an ordinary piezoceramic transducer verified adequateness of the method. (c) Measurements show hysteresis-free translations using "Nanotester" standard.[899]

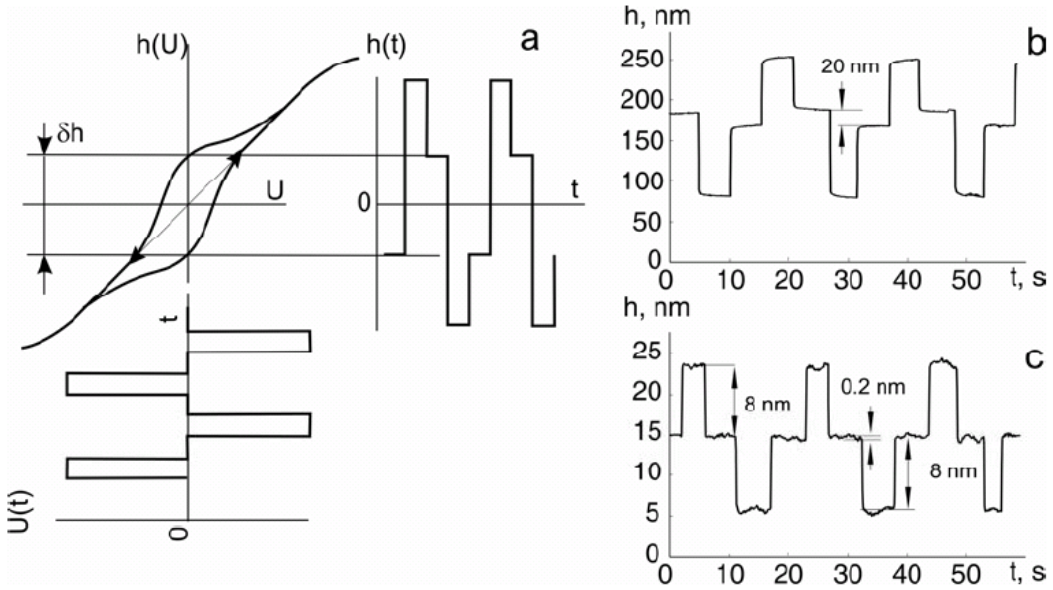

[897] Kaixuan Hu, Jung H Kim, James Schmiedeler, Chia-Hsiang Menq, "Design, implementation, and control of a six-axis compliant stage," Rev Sci Instrum. 79(February 2008):025105.

[898] T. King, M. Pozzi, A. Manara, "Piezoactuators for 'real world' applications. Can they deliver sufficient displacement?" Power Eng. J. 14(June 2000):105-110.

[899] V.P. Tichinsky, A.V. Kretushev, P.N. Luskinovich, "Dynamic phase microscopy: measurements of translational displacements at sub-nanometer scale," Optical Society of America, 2006; http://arxiv.org/ftp/physics/papers/0608/0608093.pdf.

A number of micropositioning stages with nanometer resolution have been developed using piezoactuated compliant mechanisms.[900] Single-axis examples include Scire and Teague's stage that achieved a 50 μm range,[901] Yang et al.'s device in which a novel lever design orthogonally transferred actuator motion to yield a 200 μm range,[902] Choi et al.'s stage featuring an amplifier with multiple flexure hinges,[903] and Chang et al.'s micropositioner using multiple Scott-Russell linkages.[904] Gao et al.[905] developed a two-axis stage utilizing two-grade amplifiers to achieve about 40 μm of displacement in two orthogonal directions. Most three-degree-of-freedom (DOF) stages developed to date have been for in-plane motion. Examples include Lu et al.'s fully parallel mechanism,[906] and Ryu et al.'s stage featuring optimized double compound mechanical lever amplifiers.[907] In contrast, Kim et al.[908] developed a 3-DOF atomic force microscope scanner that provided for three orthogonal translations. Liu et al.[909] constructed a 6-DOF micromanipulator based on a Gough-Stewart platform, the forward kinematics of which were too complex to solve in real time. Gao and Swei[910] resolved the forward kinematics issue with a different 6-DOF manipulator design, but its range of motion was small because no displacement

---

[900] Kaixuan Hu, Jung H Kim, James Schmiedeler, Chia-Hsiang Menq, "Design, implementation, and control of a six-axis compliant stage," Rev Sci Instrum. 79(February 2008):025105.

[901] F.E. Scire, E.C. Teague, "Piezodriven 50-μm Range Stage with Subnanometer Resolution," Rev. Sci. Instrum. 49(December 1978):1735-1740.

[902] R. Yang, M. Jouaneh, R. Schweizer, "Design and characterization of a low-profile micropositioning stage," Precis. Eng. 18(1996):20-29.

[903] S.B. Choi, S.S. Han, Y.S. Lee, "Fine motion control of a moving stage using a piezoactuator associated with a displacement amplifier," Smart Mater. Struct. 14(February 2005):222-230.

[904] S.H. Chang, B.C. Du, "A precision piezodriven micropositioner mechanism with large travel range," Rev. Sci. Instrum. 69(1998):1785-1791.

[905] P. Gao, S.-M. Swei, Z. Yuan, "A new piezodriven precision micro-positioning stage utilizing flexure hinges," Nanotechnology 10(1999):394-398.

[906] T.-F. Lu, D.C. Handley, Y.K. Yong, C. Eales, "A three-DOF compliant micromotion stage with flexure hinges," Ind. Robot 31(2004):355-361.

[907] J.W. Ryu, D.-G. Gweon, K.S. Moon, "Optimal design of a flexure hinge based XYθ wafer stage," Precis. Eng. 21(1997):18-28.

[908] D. Kim, D. Kang, J. Shim, I. Song, D. Gweon, "Optimal design of a flexure hinge-based XYZ atomic force microscopy scanner for minimizing Abbe errors," Rev. Sci. Instrum. 76(2005):073706.

[909] Xin-Jun Liu, Jinsong Wang, Feng Gao, Li-Ping Wang, "On the design of 6-DOF parallel micro-motion manipulators," Proceedings of the 2001 IEEE/RSJ International Conference on Intelligent Robots and Systems, Maui, Hawaii, USA, 29 Oct. - 3 Nov. 2001, pp. 343-348.

[910] P. Gao, S.-M. Swei, "A six-degree-of-freedom micro-manipulator based on piezoelectric translators," Nanotechnology 10(1 December 1999):447-452.

amplifiers were used with the piezoelectric actuators. Seugling et al.[911] also developed a 6-DOF stage with a relatively small workspace. Chao et al.[912] achieved a large motion range with a series-parallel architecture at the expense of resolution reduction to 50 nm for the X and Y translations and significant machine thickness in the vertical direction. Hu et al.[913] (Section 4.6.1.9) developed a compact, piezoactuated 6-axis compliant stage with a large motion range, nanometer resolution, and an integrated real-time visual feedback measurement system.

4.5.2 Commercial Positioning Systems

Thayer[914] has provided a good summary of the commercial vendors of AFM systems, current as of August 2009, but few if of these systems are readily adaptable for any kind of DMS work under low-temperature UHV conditions. Some representative picoscale-resolution positioning systems (and their best available positional resolution) that were commercially available in 2009 include:

(1) **Physik Instrumente (PI)**.[915] P-363 PicoCube™ XY(Z) Piezo Scanner, 5 x 5 x 5 µm Travel Range, 50 Picometer Resolution, Vacuum-Compatible Versions available. (Another statement on the site claims a bit better performance, "Nanometer Accuracy in 1 Millisecond with 30-Picometer Resolution PicoCube™ systems provide resolution of **30 pm** and below".[916]

(2) **Mad City Labs**: Their commercial off-the-shelf Nano-Mini positioning stage[917] provides **20 pm** resolution over a 10 micron range of motion. Product Description: The Nano-Mini is one of the smallest flexure guided nanopositioning stages available. Designed for optimum performance on a small footprint, this stage uses an innovative mini-cross section multilayer piezo ceramic which allows for a stiff stage to translate 10 microns with picometer precision. This unique design makes it ideal for applications in precision metrology and microscopy. Internal position sensors utilizing proprietary PicoQ™ technology provide absolute, repeatable position measurement with picometer accuracy under closed loop control. Available in

---

[911] Richard M. Seugling, Thomas LeBrun, Stuart T. Smith, Lowell P. Howard, "A six-degree-of-freedom precision motion stage," Rev. Sci. Instrum. 73(2002):2462-2468.

[912] D. Chao, G. Zong, R. Liu, "Design of a 6-DOF Compliant Manipulator Based on Serial-Parallel Architecture," Proceedings of the 2005 IEEE/ASME International Conference on Advanced Intelligent Mechatronics (AIM 2005), Monterey, California, USA, Vol. 1, July 2005, pp. 765-770.

[913] Kaixuan Hu, Jung H Kim, James Schmiedeler, Chia-Hsiang Menq, "Design, implementation, and control of a six-axis compliant stage," Rev Sci Instrum. 79(February 2008):025105.

[914] Ann M. Thayer, "Nanotech Toolkit," Chemical and Engineering News 87(10 August 2009):12-17; http://pubs.acs.org/cen/coverstory/87/8732cover.html.

[915] http://www.physikinstrumente.com/en/.

[916] http://www.physikinstrumente.com/en/products/prdetail.php?sortnr=201650.

[917] http://www.madcitylabs.com/nanomini.html.

titanium or invar. "Stackable for XY motion" means this is a 1D positioner only. Their Nano-P15[918] has **30 pm** resolution over a 15 micron range of motion, and their Nano-OP30[919] has **60 pm** resolution over a 30 micron range of motion.

(3) **NanoWave Inc.**[920] "MIT startup NanoWave Inc. announced today[921] that their groundbreaking position measurement technology has reached the highest level of measurement precision ever achieved with any technology on the market today. Furthermore, these measurements were taken outside of a cleanroom environment and without environmental controls, highlighting the robustness of the system. The latest test model of the NanoWave Scanning Probe Position Encoder (NW SPPE) demonstrated approximately **13 pm** resolution (standard deviation at 300 Hz bandwidth within 1 sec. frame) using a 1.6 μm pitch grating. The SPPE can be adapted to cover a wide range of precision needs ranging from 5 nanometers to less than 10 picometer resolution. Dr. Tetsuo Ohara co-founded NanoWave in 1995 with business partner, Renee Buck, for the sole purpose developing a practical and commercially viable position measurement systems capable of subnanometer to picometer precision. NanoWave Inc. has been awarded three phases of NSF SBIR (Small Business Innovation Research) grants." At the company website, last updated in 2007: "SPPE-1000 (**7.6 pm** resolution incremental linear encoder)":[922] Atomic scale (7.6 pm), ultra-precision position encoder based on NanoWave's patents and FPGA engine, with white paper,[923] technical blog,[924] and product manual[925] (last updated October 2008); however, repeatability is only listed as "<10 nm".

(4) **Renishaw**.[926] The company sells Laser (interferometer) encoders[927] and an XY Plane Mirror system,[928] which offer "ppb frequency stability and ultra low cyclic error, allowing output resolutions to **38.6 pm**."

---

[918] http://www.madcitylabs.com/nanopseries.html.

[919] http://www.madcitylabs.com/nanoopseries.html.

[920] http://www.nanowave.com.

[921] NanoWave Inc. "NanoWave Inc. Breakthrough – Attains Picometer-Resolution Position Measurement System for True...," Thursday, 12 June 2003, Business Wire; press release at http://www.allbusiness.com/electronics/computer-equipment-computer-scanners/5797393-1.html.

[922] http://www.nanowave.com/Overview.htm.

[923] http://nanowave.com/files/SPPE_1000_wp.pdf.

[924] http://nanowave.com/blog/category/productinformation/sppe-1000/.

[925] http://www.nanowave.com/pdf/SPPE.pdf.

[926] http://www.renishaw.com/.

[927] http://www.renishaw.com/en/6404.aspx.

[928] http://www.renishaw.com/en/6483.aspx.

(5) **Asylum Research**.[929] The company sells its CypherAFM system which it proclaims is "The World's Highest Resolution AFM" (images, below):[930]

The CypherAFM provides closed loop atomic resolution using sensors in all three axes and is said to achieve positioning accuracies better than **60 pm** in X, Y and Z, presumably using very accuracy capacitive sensors. This produces images such as the one below, an image of graphite atoms using a closed loop STM over a 6 nm scan. The system provides closed loop imaging from tens of microns down to atomic scales, with <20 pm deflection noise (all noise measurements are quoted as average deviation (A_{dev}) in a 0.1 Hz to 1 KHz bandwidth). Scan Range: XY range is 30/40 µm (closed/open loop). Z range is 5/7 µm (closed/open loop). NPS™ Sensor Noise: Digital LVDT sensors. XY noise is <60 pm, Z noise is <50 pm. Vibration Immunity: <10 pm coupling into deflection for 1 mm/s^2 floor acceleration. XY Sample Drift: <20/150 nm/$^\circ$ C (with/without temperature control module). Out-of-Plane Motion: Tilt is <10 nm per micron of travel. Bow is <10 nm over full scan range.

Instrument isolation includes the following: Vibration: Included passive vibration isolation with f_o = 7 Hz, Q~1. The Cypher AFM exhibits exceptional vibration immunity for high resolution work in labs with floor accelerations > 1mm/s^2. Additional isolation may be needed for unusually noisy environments. Acoustic: Included acoustic enclosure provides 20dB of isolation. Temperature: Included enclosure allows for 0.1° C temperature stabilization with optional temperature control module. However, they provide no information on hysteresis or on scan resolution over large transit ranges; this is likely where the system becomes noncompetitive.

Some additional information on Asylum Research and the Cypher AFM product line:[931]

"In 1999, work on single-molecule force measurements was taking off, and a team of scientists founded Santa Barbara, Calif.-based Asylum Research. They came from Digital Instruments after it was acquired by Veeco, which then bought Thermo's and IBM's AFM

---

[929] http://www.asylumresearch.co.uk.

[930] "Introducing the Cypher™ AFM," http://www.asylumresearch.co.uk/Products/Cypher/Cypher.shtml. See also: "Pushing the envelope in atomic force microscopy," NanoWerk, 12 November 2009; http://www.nanowerk.com/spotlight/spotid=13498.php.

[931] Ann M. Thayer, "Nanotech Toolkit," Chemical and Engineering News 87(10 August 2009):12-17; http://pubs.acs.org/cen/coverstory/87/8732cover.html.

businesses and remains a major provider of metrology and process equipment to the electronics industry."

"Asylum wanted to maintain a spirit of innovation and invention, founder and Chief Executive Officer Jason Cleveland says. Six months after its formation, the firm debuted its first molecular force probe for biophysics research and has since added other SPM products. "We focus exclusively on AFMs for the high-end R&D market," Cleveland says, emphasizing technology development and product support by Ph.D.-level staff."

"In late 2008, Asylum launched the Cypher AFM. While other providers were tweaking older systems or focusing on AFMs that could handle large samples, such as semiconductor wafers, Asylum designed Cypher from the ground up for faster scanning, more accurate positional control, and the highest resolution possible on small samples, says Monteith G. Heaton, Asylum's executive vice president for marketing and business development."

"Speed is a limiting factor for AFMs. To scan faster, Cypher's probe-holding cantilevers, at less than 10 μm, are an order of magnitude shorter than typical ones. Response to Cypher has been "phenomenal," Heaton says, but the privately owned company doesn't give sales figures. With operations around the world, Asylum employs about 60 people."

(6) **Queensgate Instruments**.[932] The NPS-XYZ-100A/15A option incorporates an integrated Z axis stage to provide a solid XYZ arrangement. This arrangement offers over 120 microns of closed loop travel in X and Y with over 16 microns of closed loop travel in the z axis. Sub-nm accuracy is **~100 pm**. The linearity and hysteresis errors are typically 0.01%, which means that to have a 20 pm error on a given round trip path, that path cannot exceed 20 pm / 0.0001 = 200 nm in length; that is, it cannot be more than 100 nm out, followed by 100 nm back to the starting point. That's not much travel distance at our requisite accuracy. We're obviously going to need a metrology system. The position noise is 250 pm in XY, 100 pm in Z; that's not very good – the PI system is probably better.

4.5.3 SPM-Based Multi-Tip and Multi-DOF Systems

A minimum of three independent high-precision SPM-based picopositioners are needed to perform many of the diamondoid mechanosynthesis (DMS) reaction sequences that have been identified[933] for building diamond nanostructures. Manipulators having multiple degrees of freedom (DOF), including tip translation in all three Cartesian dimensions and at least one – and often two – rotational dimensions, also (very conservatively) appear to be required to consummate all foundational DMS reactions[934] (Table 4-5) and likely most nanopart assembly

---

[932] http://www.nanopositioning.com/.

[933] Robert A. Freitas Jr., Ralph C. Merkle, "A Minimal Toolset for Positional Diamond Mechanosynthesis," J. Comput. Theor. Nanosci. 5(May 2008):760-861; http://www.molecularassembler.com/Papers/MinToolset.pdf.

[934] Robert A. Freitas Jr., Ralph C. Merkle, "A Minimal Toolset for Positional Diamond Mechanosynthesis," J. Comput. Theor. Nanosci. 5(May 2008):760-861; http://www.molecularassembler.com/Papers/MinToolset.pdf.

operations as well. Hence a multi-tip 4-5 DOF SPM-based manipulator system[935] may be required to build a sufficiently functional workstation system. Our plan is to start with a 1-tip 3-DOF system and then upgrade to systems with more tips and perhaps more DOFs, possibly culminating with a 3-4 tip 3-5 DOF-per-tip system.

Table 4-5. Number of Freitas-Merkle[936] Reaction Sequences* Nominally Executable Using a Given Multiplicity of Independent Positionally-Controlled Tooltips with a Given Number of Degrees of Freedom (DOF)

Degrees of Freedom per Tooltip	Number of Available Tooltips				Totals for All Tooltips
	1 tooltip	2 tooltips	3 tooltips	4 tooltips	
1 DOF	RS59 (2)				1 (2)
2 DOF					0 (0)
3 DOF	RS1,RS2,RS46 (47)	RS47,RS48 (5)			5 (53)
4 DOF	RS12,RS13,RS14, RS20b,RS24,RS25, RS26,RS27,RS37, RS40,RS49,RS50, RS51 (34)	RS3,RS4,RS9, RS10b,RS11b,RS15, RS20a,RS21,RS22, RS23,RS28b,RS38, RS39,RS42,RS52 (113)	RS16b (1)		29 (152)
5 DOF		RS7,RS19,RS29, RS30,RS31,RS32, RS45,RS63 (33)	RS5,RS6,RS8, RS10a,RS11a,RS17, RS28a,RS33,RS34, RS35,RS41,RS44, RS53,RS54,RS55, RS58,RS61,RS62, RS64,RS65 (71)	RS16a,RS18,RS36, RS43,RS56,RS57, RS60 (9)	35 (113)
6 DOF					0 (0)
Totals for All DOFs	17 (83)	25 (151)	21 (77)	7 (9)	70 (320)

* Reaction Sequences are designated as: a = workpiece on tooltip/manipulator, b = workpiece on fabrication surface. (The number of individual reactions that can be executed with a given tip/DOF capability are given in parens.)

Building a multi-tip system (Figure 4-23) is more challenging than a single-tip system in terms of system geometry and stability. Experimentally, the first opposable STM tip pair was fabricated by MacDonald's group in 1991 using the Cornell Nanofabrication Facility,[937] and two-handed

---

[935] Shuji Hasegawa, "Chapter 12. Multiprobe SPM," in: Seizo Morita, ed., Roadmap of Scanning Probe Microscopy, Springer Berlin Heidelberg, 2007, pp. 95-100.

[936] Robert A. Freitas Jr., Ralph C. Merkle, "A Minimal Toolset for Positional Diamond Mechanosynthesis," J. Comput. Theor. Nanosci. 5(May 2008):760-861; http://www.molecularassembler.com/Papers/MinToolset.pdf.

[937] J. Jason Yao, Susanne C. Arney, Noel C. MacDonald, "Fabrication of high frequency two-dimensional nanoactuators for scanned probe devices," J. Microelectromech. Syst. 1(March 1992):14-22.

coordinated micromanipulation under the view of an SEM was reported in 1993.[938] In 2005, Xidex reported opposable AFM dual-tip calipers for metrology, with each cantilever probe tiltable in up to three rotational degrees of freedom allowing tips to touch each other's apices and to access vertical and re-entrant feature sidewalls, using tips with 10 nm radius of curvature and a 10° cone angle but without closed-loop control.[939] In 2005 a dual probe system available from Nanonics allowed two tips to approach within 10 nm of each other,[940] and other dual-tip SPM systems have been described in the experimental literature.[941] In 1998, Zyvex demonstrated the first simultaneous coordinated operation of three independently controlled AFM tips within the same workspace at different orientations;[942] a successor 4-tip system was designed as early as 1999 and finally offered as a commercial product starting in 2003. A three-probe AFM was employed experimentally in 2001 by Watanabe et al.[943] A 4-tip STM was used for condutivity measurements in 2005.[944]

---

[938] Hiroshi Morishita, Yotaro Hatamura, "Development of ultra micro manipulator system under stereo SEM observation," Proc. 1993 IEEE/RSJ Intl. Conf. on Intelligent Robots and Systems, 26-30 July 1993, Yokohama, Japan, Volume 3, pp. 1717-1721.

[939] V. Mancevski, P.F. McClure, "Development of a dual-probe Caliper™ CD-AFM for near model-independent nanometrology," Proc. of the SPIE. Metrology, Inspection and Process Control for Microlithography XVI, 4-7 March 2003 Vol. 4689, pp. 83-91; http://www.xidex.com/Xidex%20Caliper%20CD%20AFM%20SPIE%202002.pdf. P.F. McClure, V. Mancevski, "Calibration of a dual-probe NanoCaliper™ AFM for CD metrology," SPIE Microlithography 2005 Conference, San Jose California, February 27-March 4, 2005; http://www.xidex.com/Xidex%20SPIE%205752-100.pdf.

[940] "The MultiView 3000," Nanonics Imaging Ltd., 2005; http://www.nanonics.co.il/main/prod_item.php?ln=en&item_id=146&cat=5&sub_cat=22.

[941] H. Grube, B.C. Harrison, J.F. Jia, J.J. Boland, "Stability, resolution, and tip imaging by a dual-probe scanning tunneling microscope," Rev. Sci. Instr. 72(December 2001):4388-4392. H. Okamoto, D.M. Chen, "An ultrahigh vacuum dual-tip scanning tunneling microscope operating at 4.2 K," Rev. Sci. Instr. 72(December 2001):4398-4403. K. Takami, J. Mizuno, M. Akai-kasaya, A. Saito, M. Aono, Y. Kuwahara, "Conductivity measurement of polydiacetylene thin films by double-tip scanning tunneling microscopy," J. Phys. Chem. B 108(2004):16353-16356.

[942] MinFeng Yu, Mark J. Dyer, George D. Skidmore, Henry W. Rohrs, Xue Kun Lu, Kevin D. Ausman, James Von Ehr, Rodney S. Ruoff, "3 dimensional manipulation of carbon nanotubes under a scanning electron microscope," 6th Foresight Nanotechnology Conference, November 1998; http://www.foresight.org/Conferences/MNT6/Papers/Yu/index.html. Robert F. Service, "AFMs wield parts for nanoconstruction," Science 282(27 November 1998):1620-1621.

[943] H. Watanabe, C. Manabe, T. Shigematsu, K. Shimotani, M. Shimizu, "Single molecule DNA device measured with triple-probe atomic force microscope," Appl. Phys. Lett. 79(2001):2462.

[944] Olivier Guise, Hubertus Marbach, John T. Yates, Jr., Moon-Chul Jung, Jeremy Levy, Joachim Ahner, "Development and performance of the nanoworkbench: A four tip STM for conductivity measurements down to submicrometer scales," Rev. Sci. Instrum. 76(2005):045107, http://www.nanotechnik.com/fileadmin/public/publications/ahner_rsi2005.pdf.

Figure 4-23. Multiprobe SPM-based systems commerically available from Nanonics, Zyvex, Omicron, and RHK Technology.

Nanonics[945] MV4000 Multi-Probe SPM

Zyvex[946] S100 Nanomanipulator

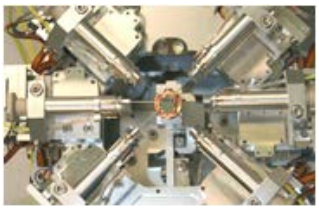

Zyvex dProber™

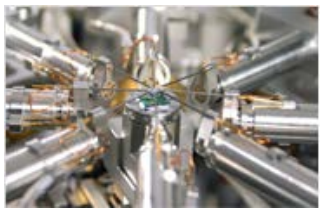

Zyvex nProber™

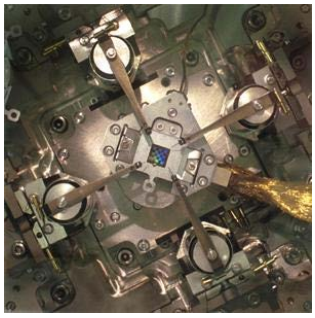

Omicron[947] UHV Nanoprobe

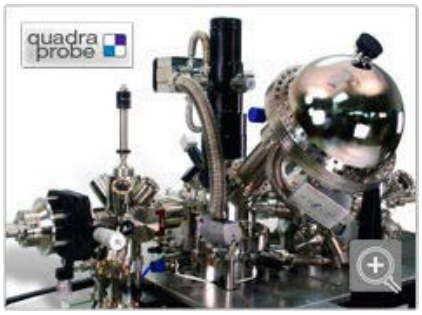

RHK Technology[948] QuadraProbe

---

[945] "Nanonics' MultiView 4000 Multi-Probe Scanned Probe Microscopy (SPM) Systems," Nanonics Imaging Ltd., 3 September 2008, http://www.nanonics.co.il/new-product-announcement-the-multiview-4000-multiprobe-.html; Alexander Kirkwood, "Nanonics Imaging Ltd - MV4000 multiprobe SPM," Microscopy and Analysis, 1 September 2006; http://www.microscopy-analysis.com/cgi-bin/item.cgi?id=356; see image at http://www.photonics.com/images/spectra/newprods/2006/October/Nanonics_FourTowers2.jpg.

[946] "S100", http://www.zyvex.com/Products/S100_Features.html; "sProber™", http://www.zyvex.com/Products/sProber_Features.html; "dProber™", http://www.zyvex.com/Products/dProber_Features.html; "nProber™", http://www.zyvex.com/Products/nProber_Features.html.

In 2006, Nanonics introduced the MV4000 Multiprobe SPM to allow four SPM tips to be brought to within 10 nm of each other throughout a volume of 160 microns x 160 microns in XY and 130 microns in Z,[949] and four-tip SPM systems are now being reported in the experimental literature[950] and by other manufacturers such as Omicron[951] and RHK Technology[952] (Figure 4-23). By 2008, Zyvex had expanded their 3-DOF nanomanipulator line[953] to 4-probe (S100 and sProber™), 6-probe (dProber™) and 8-probe (nProber™) systems, and MultiProbe's AFP II Nanoprober system[954] allows up to six MP II probe heads to be placed with 100 nm of each other in a sample area of dimension ~10 cm. In 2008, Gorman et al.[955] described a design for a 4-tip microscale assembly system, to be fabricated on a single chip, that includes four MEMS-based nanomanipulators (each composed of an XYZ nanopositioning mechanism with an attached nanoprobe) positioned around a centrally located port for introducing nanostructure samples (Figure 4-24). The prototype manipulator demonstrated sequences of 50 nm steps with ±7 nm resolution; open-loop nanopositioning control can presently achieve this precision only for ±1 micron tip excursions, but a closed-loop controller is being developed that should significantly improve repeatability.[956]

---

[947] "UHV Nanoprobe," Omicron Vacuumphysik GmbH, Taunusstein, Germany; http://www.omicron.de/products/spm/multi_technique_spms/uhv_nanoprobe/index.html.

[948] "QuadraProbe 4 Probe System," RHK Technology, 2008; http://www.rhk-tech.com/4probe.php.

[949] "Nanonics' MultiView 4000 Multi-Probe Scanned Probe Microscopy (SPM) Systems," Nanonics Imaging Ltd., 3 September 2008, http://www.nanonics.co.il/new-product-announcement-the-multiview-4000-multiprobe-.html; Alexander Kirkwood, "Nanonics Imaging Ltd - MV4000 multiprobe SPM," Microscopy and Analysis, 1 September 2006; http://www.microscopy-analysis.com/cgi-bin/item.cgi?id=356; see image at http://www.photonics.com/images/spectra/newprods/2006/October/Nanonics_FourTowers2.jpg.

[950] Shinya Yoshimoto, Yuya Murata, Keisuke Kubo, Kazuhiro Tomita, Kenji Motoyoshi, Takehiko Kimura, Hiroyuki Okino, Rei Hobara, Iwao Matsuda, Shin-ichi Honda, Mitsuhiro Katayama, Shuji Hasegawa, "Four-Point Probe Resistance Measurements Using PtIr-Coated Carbon Nanotube Tips," Nano Lett. 7(2007):956-959; http://www-surface.phys.s.u-tokyo.ac.jp/papers/2007/Yoshimoto07-NanoLetters.pdf.

[951] "UHV Nanoprobe," Omicron Vacuumphysik GmbH, Taunusstein, Germany; http://www.omicron.de/products/spm/multi_technique_spms/uhv_nanoprobe/index.html.

[952] "QuadraProbe 4 Probe System," RHK Technology, 2008; http://www.rhk-tech.com/4probe.php.

[953] "S100", http://www.zyvex.com/Products/S100_Features.html; "sProber™", http://www.zyvex.com/Products/sProber_Features.html; "dProber™", http://www.zyvex.com/Products/dProber_Features.html; "nProber™", http://www.zyvex.com/Products/nProber_Features.html.

[954] MultiProbe, Inc., "AFP II Core System," accessed January 2008, http://www.multiprobe.com/products/.

[955] Jason J. Gorman, Yong-Sik Kim, András E. Vladár, Nicholas G. Dagalakis, "Design of an on-chip microscale nanoassembly system," Int. J. Nanomanufacturing 1(2007):710-721.

[956] Jason J. Gorman, Yong-Sik Kim, András E. Vladár, Nicholas G. Dagalakis, "Design of an on-chip microscale nanoassembly system," Int. J. Nanomanufacturing 1(2007):710-721.

Figure 4-24. Schematic representations of: (A) Top Left: microscale nanoassembly cell with 2 × 2 array of XYZ nanomanipulators; (B) Top Right: multiple nanoprobes working in a shared workspace; and (C) Bottom: an actual fabricated microscale XYZ nanomanipulator prototype. Images from Gorman et al.[957]

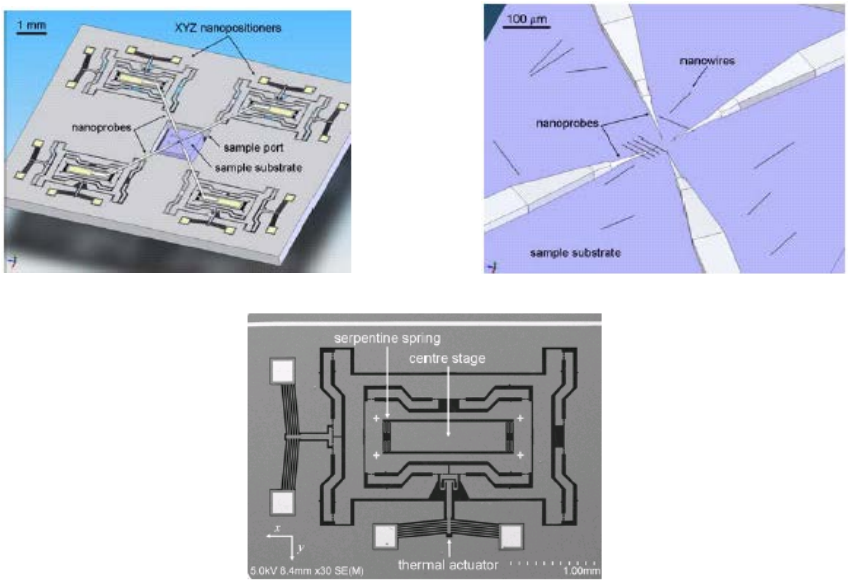

Building a 4-DOF or a 5-DOF system will also be more challenging than building a 3-DOF system. The smallest 6-DOF SPM-based nanopositioner system may be the 6-axis Piezo Nanopositioning P-587 (Figure 4-25A) manufactured by Physik Instrumente.[958] The P-587 has an 800 x 800 x 200 micron linear range with a resolution of ~10^{-5} x travel range (e.g., 80 Å or 8000 pm over 800 microns of linear travel) – with XY linearity of 0.004% (0.4 Å or 40 pm over 1 micron of linear travel) and Z linearity of 0.01% (1 Å or 100 pm over 1 micron of linear travel) – and rotation ranges of 3 mrad, 3 mrad, and 10 mrad (~0.6 deg) with a typical closed-loop linearity in rotation of 0.2% (~2 µrad). Rotation stages with 5 µrad (0.0003 deg) rotational increments with 240 µrad (0.014 deg) of backlash are commercially available.[959] A few microscale 6-axis

---

[957] Jason J. Gorman, Yong-Sik Kim, András E. Vladár, Nicholas G. Dagalakis, "Design of an on-chip microscale nanoassembly system," Int. J. Nanomanufacturing 1(2007):710-721.

[958] Physik Instrumente, "P-587 6-Axis, Long-Travel Piezo Nanopositioning / Scanning Stage with Parallel Metrology," accessed January 2008, http://www.physikinstrumente.com/en/products/prdetail.php?sortnr=201600 and datasheet at http://www.physikinstrumente.com/en/pdf/P587_Datasheet.pdf.

[959] Physik Instrumente, "M-060 · M-061 · M-062, Series Rotation Stages with Worm Gear Drive," accessed January 2008, http://www.physikinstrumente.com/en/products/prdetail.php?sortnr=703100; see also http://www.physikinstrumente.com/en/pdf/M060_Datasheet.pdf.

mechanisms comprised of rigid links and sliding bearings have been built,[960] but while these devices may achieve work volumes comparable to their size, bearing friction and bearing/joint gaps limit the achievable positional resolution to several microns.

Figure 4-25. (A) Left: Image of Physik Instrumente's P-587 piezo-driven nanopositioning/scanning stage with 6-axis digital controller, which is perhaps the smallest known 6-DOF SPM-based nanopositioner system.[961] (B) Middle: Image of Physik Instrumente's vacuum-compatible M-824 compact 6-Axis Parallel Kinematics hexapod nanoposiitoner.[962] (C) Right: Image of Physik Instrumente's M-840 HexaLight™ 6-axis micropositioning system.[963]

(A) (B) (C)

Hexapod or Stewart-platform type nanomanipulators are generally rare in commercial systems, probably due to limited demand, but there appear to be no fundamental technical barriers to substantial improvements in resolution and repeatability in such systems. Physik Instrumente's

---

[960] B. Jokiel, G.L. Benavides, L.F. Bieg, J.J. Allen, "Planar and spatial three degree-of-freedom micro-stages in silicon MEMS," in: Proceedings of the 2001 Annual Meeting of the American Society for Precision Engineering, 2001, pp. 32-35. H. Bamberger, M. Shoham, "A new configuration of a six degree-of-freedom parallel robot for MEMS fabrication," in: Proceedings of the 2004 IEEE International Conference on Robotics and Automation, 2004, pp. 4545-4550.

[961] Physik Instrumente, "P-587 6-Axis, Long-Travel Piezo Nanopositioning / Scanning Stage with Parallel Metrology," accessed January 2008, http://www.physikinstrumente.com/en/products/prdetail.php?sortnr=201600 and datasheet at http://www.physikinstrumente.com/en/pdf/P587_Datasheet.pdf.

[962] Physik Instrumente, "M-824 Compact 6-Axis Parallel Kinematics Microrobot," accessed January 2008, http://www.physikinstrumente.com/en/products/prdetail.php?sortnr=700815 and datasheet at http://www.physikinstrumente.com/en/pdf/M824_Datasheet.pdf.

[963] Physik Instrumente, "M-840 HexaLight™ 6-Axis-Parallel Kinematics Microrobot," accessed January 2008, http://www.physikinstrumente.com/en/products/prdetail.php?sortnr=700810 and datasheet at http://www.physikinstrumente.com/en/pdf/M840_Datasheet.pdf.

vacuum-compatible M-824 six-axis parallel-kinematics hexapod[964] is a coarser 6-DOF manipulator (Figure 4-25B) with a travel range of 45 mm and 25° of rotation, and with 7 nm resolution but a minimum incremental motion of 300 nm and a repeatability of only ±500 nm, the related 6-DOF M-840 six-axis hexapod (Figure 4-25C) has an actuator resolution of 16 nm but a repeatability of only ±2000 nm.[965] 6-DOF micromanipulators have been described in the literature,[966] including one medical micromanipulator with a 20 micron movement range and a 20 nm resolution,[967] Stewart platform micromanipulators,[968] and a 6-DOF dual micromanipulator system.[969] Another related system is the 6-axis μHexFlex microscale nanopositioner demonstrated by Chen and Culpepper.[970] Their 3-mm prototype (Figure 4-26) proved capable of 8.4 micron x 12.8 micron x 8.8 micron translational displacements (with a ~20-30 nm noise level) and 19.2 mrad x 17.5 mrad x 33.2 mrad (1.1° x 1.0° x 1.9°) angular displacements. Although its angular range is quite limited, the modular design might readily lend itself for use in close-packed 4-tip systems. A 5-DOF three-nanomanipulator system is probably also within the state of the art but may require considerably greater development effort than a 3-DOF system.

---

[964] Physik Instrumente, "M-824 Compact 6-Axis Parallel Kinematics Microrobot," accessed January 2008, http://www.physikinstrumente.com/en/products/prdetail.php?sortnr=700815 and datasheet at http://www.physikinstrumente.com/en/pdf/M824_Datasheet.pdf.

[965] Physik Instrumente, "M-840 HexaLight™ 6-Axis-Parallel Kinematics Microrobot," accessed January 2008, http://www.physikinstrumente.com/en/products/prdetail.php?sortnr=700810 and datasheet at http://www.physikinstrumente.com/en/pdf/M840_Datasheet.pdf.

[966] Eric Pernette, Simon Henein, Ivo Magnani, Reymond Clavel, "Design of parallel robots in microrobotics," Robotica 15(1997):417-420; Quan Zhou, Petteri Korhonen, Jukka Laitinen, Sami Sjövall, "Automatic dextrous microhandling based on a 6-DOF microgripper," Journal of Micromechatronics 3(September 2006):359-387.

[967] S. Guo, J. Wang, "A New Human-Scale Tele-Operating System For Biomedical Applications," International Journal of Robotics and Automation 22(2007):#206-1008.

[968] Feng Gao, Zhang Jianjun, Chen Yulong, Jin Zhenlin, "Development of a new type of 6-DOF parallel micro-manipulator and its control system," Robotics, Intelligent Systems and Signal Processing 2(8-13 October 2003):715-720; http://ieeexplore.ieee.org/xpls/abs_all.jsp?tp=&arnumber=1285672&isnumber=28679.

[969] Gilgueng Hwang, Peter Tamas Szemes, Noriaki Ando, Hideki Hashimoto, "A Realization of Autonomous Rectilinear Movement on 6 D.O.F Parallel Micromanipulator," Nippon Kikai Gakkai Robotikusu, Mekatoronikusu Koenkai Koen Ronbunshu 2004: 1A1-H-44; Gilgueng Hwang, Peter Tamas Szemes, Noriaki Ando, Hideki Hashimoto, "Development of a single-master multi-slave tele-micromanipulation system," Advanced Robotics 21(March 2007):329-349.

[970] S.-C. Chen, M.L. Culpepper, "Design of a six-axis micro-scale nanopositioner – μHexFlex," Precision Engineering 30(2006):314-324; http://pcsl.mit.edu/2_72/documents/microHexFlex.pdf.

Figure 4-26. (A) Closeup of 6-axis μHexFlex microscale nanopositioner and (B) the 6-DOF nanopositioner shown with its electrical connections. Alternative conceptual schemes for this general manipulator motif include: (C) parallel flexures, (D) series flexures, and (E) amplifying bow flexures. Images from Chen and Culpepper.[971]

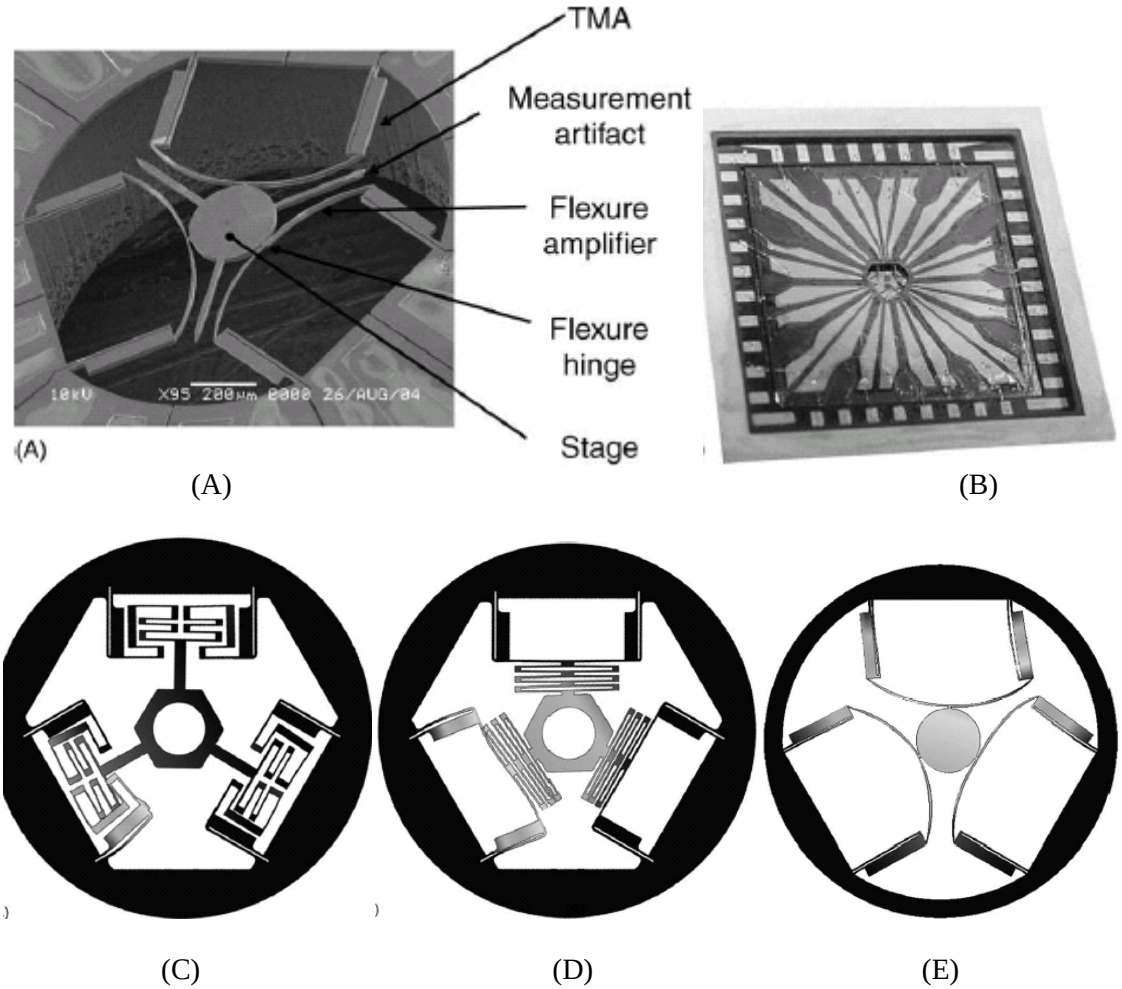

Any multitool SPM system must provide adequate clearance when juxtaposed near a workpiece. With two exceptions, all primary and auxiliary tools in the minimal DMS toolset[972] are mounted on simple pyramidal diamond handles consisting of stacked planes of adamantane cages. The simplest 1, 2, 3,... adamantane stack (Figure 4-27A) has an aspect angle of ~60°, which may be considered typical for most tooltypes in our toolset. The two exceptions are the DimerP tool,

---

[971] S.-C. Chen, M.L. Culpepper, "Design of a six-axis micro-scale nanopositioner – μHexFlex," Precision Engineering 30(2006):314-324; http://pcsl.mit.edu/2_72/documents/microHexFlex.pdf.

[972] Robert A. Freitas Jr., Ralph C. Merkle, "A Minimal Toolset for Positional Diamond Mechanosynthesis," J. Comput. Theor. Nanosci. 5(May 2008):760-861; http://www.molecularassembler.com/Papers/MinToolset.pdf.

essentially a fused double GeRad tool, which requires a handle with a ~60° aspect angle in the common dimension and ~140° in the transverse dimension, and the two-handled HTrans tool, similarly at ~60-90° x ~140-160°, adjustable by manipulating the component HAbst and GeRad handles independently.

For tool operations in free space, the 360° of available planar angle can conservatively accommodate at most four proximated tools (4 x 60° = 240°), again occupying only 2/3 of available planar angle. However, tools arranged tetrahedrally rather than coplanarly use only half of the effectively available 120° tetrahedral angle between each pair, leaving extra room for positional and rotational adjustments during mechanosynthetic operations. A tetrahedral arrangement of 4 tooltips on a single workpiece may be regarded as 3 coplanar tools at 120° separation with any single tool positioned above the plane, with that single tool having much of an entire hemisphere of free space in which to maneuver. Purely for illustrative purposes, the most severe geometry (Figure 4-27B) occurs when four proximated DimerP tools whose C_2 dimer payloads are shown bonded in an energetically unstable cubane configuration (while the addition of the fourth DimerP tool is exoergic by -1.03 eV, subsequent retraction of this tool retrieves the donated C_2 dimer because such retrieval is strongly exoergic compared to C_2 deposition).

Figure 4-27. (A) Adam tooltip mounted on pyramidal handle, (B) four DimerP tooltips forced into unstable cubane geometry in free space, and two handled DimerP tools in close (C) and more distant (D) apposition on a workpiece surface.

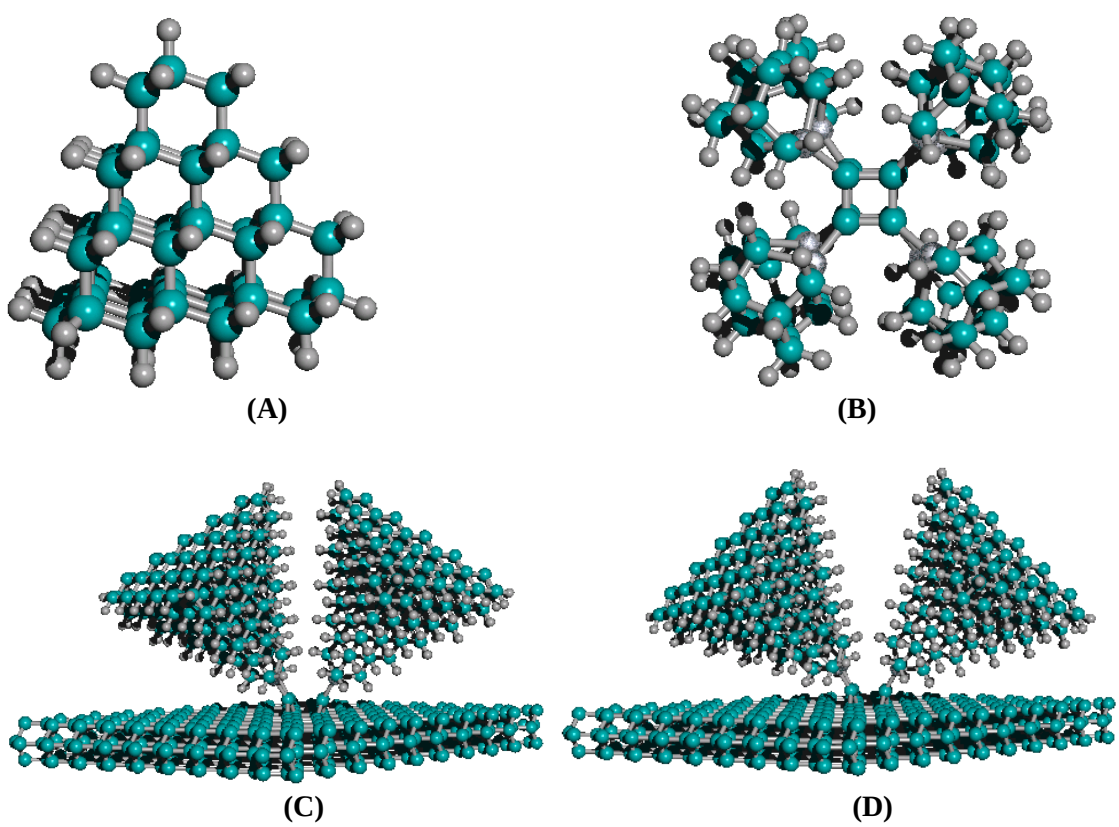

For tool operations in the proximity of a flat surface, the 180° of available planar angle can conservatively accommodate at most two proximated tools (60° + 60° = 120°), occupying only 2/3 of available planar angle, since three proximated tools would occupy the entire 180° planar angle, leaving no room for positional or rotational adjustments during mechanosynthetic operations. The most severe instance is again illustrated by two proximated DimerP tools on a flat C(110) surface. In Figure 4-27C, the two tools are very close (~5° relative angle), yielding an estimated van der Waals intertool attraction of ~1.3 nN which is reduced to ~0.4 nN when the tools are tipped to a ~30° relative angle as in Figure 4-27D. (Adhesive force is crudely estimated by integrating the Israelachvili relation[973] for opposed planar surfaces across the entire tool height for the two nearest tipped central planes taken as the width of 3 adamantane cages on each tool, and taking the Hamaker constant as ~3.4 x 10^{-19} J for diamond surface.)

4.6 Metrological SPM Systems

The molecular workstation will be a modified version of a scanning probe-based metrology system. Section 4.6.1 surveys high-precision large-range SPM-based whole metrology systems of the general type that would be necessary to implement the molecular workstation – though none that have been built to date could implement all the objectives of our workstation. Subsequent sections review the many different metrology system approaches that could be employed in a molecular workstation, including combined optical and X-ray interferometry (COXI) systems (Section 4.6.2), Michelson interferometry systems (Section 4.6.3), Fabry-Pérot interferometry systems (Section 4.6.4), digitally enhanced heterodyne interferometry (Section 4.6.5), various astronomy-oriented metrological interferometer systems (Section 4.6.6), multimode waveguide interferometry systems (Section 4.6.7), electron interferometry (Section 4.6.8), non-interferometric backscatter detection (Section 4.6.9), and other metrological approaches (Section 4.6.10), as summarized in Section 4.6.11.

4.6.1 High-Precision Large-Range SPM-Based Systems

The scanning probe microscopy-based workstation system described in Section 1.5 has not yet been experimentally demonstrated but is believed to lie within the existing or developable state-of-the-art. Given the recognized importance of developing a high-precision measurement infrastructure for nanotechnology, many national metrology institutes worldwide have already initiated ongoing efforts in the development of high-quality SPM-based metrology instruments.[974]

---

[973] Jacob N. Israelachvili, Intermolecular and Surface Forces, Second Edition, Academic Press, NY, 1992.

[974] J. Schneir, T.H. McWaid, J. Alexander, B.P. Wilfley, "Design of an atomic force microscope with interferometric position control," J. Vac. Sci. Technol. B 12(1994):3561-3566; F. Meli, R. Thalmann, "Long-range AFM profiler used for accurate pitch measurements," Meas. Sci. Technol. 9(1998):1087-1092; M. Bienias, S. Gao, K. Hasche, R. Seemann, K. Thiele, "A metrological scanning force microscope used for coating thickness and other topographical measurements," Appl. Phys. A 66(1998):S837-S842; S. Gonda, T. Doi, T. Kurosawa, Y. Tanimura, N. Hisata, T. Yamagishi, H. Fujimoto, H. Yukawa, "Real-time, interferometrically measuring atomic force microscope for direct calibration of standards," Rev. Sci. Instrum. 70(1999):3362-3368; R.K. Leach, J. Haycocks, K. Jackson, A. Lewis, S. Oldfield, A. Yacoot,

The metrological performance of many of these SPM systems was first compared by Breil et al.[975] in a study that included both standard and special metrological SPMs and clearly showed the need for active metrology sensors to achieve the necessary measurement accuracy. Most of the instruments surveyed operate over sub-millimeter ranges, but there are a few large-range (≥25 mm) interferometer-based SPM metrology instruments and stages that have also been developed.[976] Many of these have already been summarized in Table 3-1.

A successful molecular workstation needs two primary metrological technologies:

(1) Large-Range Picopositioning Devices. We need actuators that can move the AFM cantilever, toolhead, tool chuck, or end effector through the precise movements needed to perform DMS operations. These movements will include coarse movements over the micron-to-millimeter length scale, and fine movements over the picometer-to-nanometer length scale. Movements may include linear displacements and possible rotational displacements of DMS tool or tool handles. Various actuator technologies have already been reviewed in Section 4.5 and Section 2.2.

(2) Large-Range Picometrology Devices. We need a large-scale position detection system capable of measuring repeated 0.1-10 mm excursions between feedstock, registration, and workpiece sites, providing 20-50 pm placement accuracy over many cycles, ideally with the fewest possible number of periodic recalibrations during a sequential run of DMS tool handling operations. Typically this is called "displacement metrology" (the science of accurately

---

"Advances in traceable nanometrology at the National Physical Laboratory," Nanotechnology 12(2001):R1-R6; G.B. Picotto, M. Pisani, "A sample scanning system with nanometric accuracy for quantitative SPM measurements," Ultramicroscopy 86(2001):247-254; I. Misumi, S. Gonda, T. Kurosawa, K. Takamasu, "Uncertainty in pitch measurements of one-dimensional grating standards using a nanometrological atomic force microscope," Meas. Sci. Technol. 14(2003):463-471; Andrew Yacoot, Ludger Koenders, "From nanometre to millimetre: a feasibility study of the combination of scanning probe microscopy and combined optical and x-ray interferometry," Meas. Sci. Technol. 14(2003):N59-N63; M. Bisi, E. Massa, A. Pasquini, G. B. Picotto, M. Pisani, "Nanometrology at the IMGC", in: Günter Wilkening, Ludger Koenders, eds., Nanoscale Calibration Standards and Methods, Wiley-VCH Verlag GmbH & Co. KGaA, 2005; H.-U. Danzebrink, L. Koenders, G. Wilkening, A. Yacoot, H. Kunzmann, "Advances in Scanning Force Microscopy for Dimensional Metrology," CIRP Annals - Manufacturing Technology 55(2006):841-878; K.R. Koops, M.G.A. van Veghel, G.J.W.L. Kotte, M.C. Moolmanration, "Strategies for scanning probe metrology," Meas. Sci. Technol. 18(January 2007):390-394; M. Ritter, T. Dziomba, A. Kranzmann, L. Koenders, "A landmark based 3D calibration strategy for SPM," in: Measurement Science and Technology, IOP, Bristol, 2007, pp. S404-S414.

[975] R. Breil, T. Fries, J. Garnaes, J. Haycocks, D. Huser, J. Joergensen, W. Kautek, L. Koenders, N. Kofod, K.R. Koops, R. Korntner, B. Lindner, W. Mirande, A. Neubauer, J. Peltonen, G.B. Picotto, M. Pisani, H. Rothe, M. Sahre, M. Stedman, G. Wilkening, "Intercomparison of scanning probe microscopes," Precis. Eng. 26(July 2002):296-305.

[976] M. Holmes, R. Hocken, D. Trumper, "The long-range scanning stage: a novel platform for scanned-probe microscopy," Precis. Eng. 24(2000):191-209; "Nano Positioning and Nano Measuring Machine," SIOS Messtechnik, GmbH, http://www.sios.de; G. Dai, L. Jung, F. Pohlenz, H.-U. Danzerbrink, R. Krueger-Sehm, K. Hasche, G. Wilkening, "Measurement of micro-roughness using a metrological large range scanning force microscope," Meas. Sci. Technol. 15(2004):2039-2046.

measuring how far apart two physical objects are) by metrologists to distinguish it from other closely related techniques such as length metrology (lengths of objects) or surface profilometry (measuring surface textures). Large-range displacement devices are the primary topic of this Section.

Here we briefly review a dozen or so complete large-range SPM-based metrology systems that have been designed, constructed and operated by the national metrology laboratories around the world (and a few others). None of these complete systems provides the positional precision needed for the molecular workstation – the best of which achieve only ~1000 pm repeatable accuracy over long travels, which is 20-fold to 50-fold poorer than the 20-50 pm we require – but they are nonetheless good examples of what a complete system might look like. It seems likely that our molecular workstation will have many elements in common with these setups, at least at the systems level of organization.

4.6.1.1 Molecular Measuring Machine (M^3) at NIST (U.S.)

One good example of a high-performance metrology instrument is the Molecular Measuring Machine (M^3) project[977] at the National Institute of Standards and Technology (NIST), the details of which are both illuminating and representative of such systems and thus will be presented here at length. M^3 is a 1-tip 3-DOF (degrees of freedom) SPM- and Michelson interferometer-based metrology instrument designed to achieve 1 nanometer measurement uncertainty for point-to-point measurements over a 50 mm x 50 mm working area, and thus "to achieve sub-nanometer-scale metrology over centimeter-scale areas...[and] to be able to repeatably locate any specific atom within the 50 mm by 50 mm measurement area, and measure the distance between it and any other atom." According to a description[978] of M^3 published in 2005 by John Kramar, leader of the NIST Nanoscale Metrology Group:

"Key design requirements that must be accentuated because of the large range-over-resolution goal are vibration isolation, machine stiffness and low noise in the control electronics, which together are needed to minimize the positional noise. For measurement accuracy, care must also be taken to design for motion accuracy and repeatability, and high-stability temperature control to minimize measurement uncertainty due to thermal expansion effects. In addition, we have chosen to operate in a vacuum environment, both to reduce sample contamination and adsorbed overlayers, and to remove measurement errors in the interferometers due to changes in the refractive index of the ambient air."

---

[977] E. Clayton Teague, "The National Institute of Standards and Technology Molecular Measuring Machine Project: Metrology and precision engineering design," J. Vac. Sci. & Technol. A 8(September 1990):3876-3877; J. Kramar, J. Jun, W. Penzes, F. Scire, C. Teague, J. Villarrubia, E. Amatucci, D. Gilsinn, "The Molecular Measuring Machine," Proceedings of the 1998 International Conference on Mechatronic Technology, 30 November – 2 December 1998, Hsinchu, Taiwan (ICMT'98), pp. 477-487, http://www.isd.mel.nist.gov/documents/amatucci/ICMTreal.pdf; John A. Kramar, "Nanometre resolution metrology with the Molecular Measuring Machine," Meas. Sci. Technol. 16(2005):2121-2128.

[978] John A. Kramar, "Nanometre resolution metrology with the Molecular Measuring Machine," Meas. Sci. Technol. 16(2005):2121-2128.

"For the basic machine core structure, a spherical geometry was chosen to maximize stiffness and symmetry, which also gives improved thermal uniformity and stability. The core is 350 mm in diameter, made out of pure copper, again for thermal uniformity and for long-term creep stability. The planar motion is generated separately as one-dimensional (1D) motions of the sample relative to the core (X-axis carriage), and orthogonally, of the probe relative to the core (Y-axis carriage) (Figure 4-28). Avoiding stacked stages avoids position-dependent cross-talk between the axes, simplifying the error mapping of the planar motion into two 1D maps. To achieve the desired range over resolution, each axis of motion is a combination of a coarse motion and fine motion stage. Here stacked stages are used, but the small range of the fine motion stage, and the resulting limited mass shift, is small enough that the effect on the attitude of the coarse motion stage should be negligible. For repeatability, the coarse motion stages are guided by slideways. The motion is generated by linear piezoceramic stepper motors, from which sub-micrometer position control is readily achieved over the 50 mm linear range. The piezoceramic motors also have a decided advantage over electromagnetic stepper motors in terms of minimal heat generation. The fine motion stages are guided by parallel flexure elements and have a range of about 10 microns. They are driven directly by piezoceramics, with any parasitic lateral drive motion somewhat decoupled by means of a flexible coupling element. The fine stage resolution is limited only by the noise on the control electronics and high voltage amplifiers, and for highest resolution work, the noise can be scaled down by scaling down the motion range." Note that the M^3 system has a far greater range of motion (50 mm range) that is strictly required for the molecular workstation proposed here (1-100 micron range).

Figure 4-28. Illustration of the Molecular Measuring Machine (M^3) project: Cut-away view of the Molecular Measuring Machine. Courtesy of John Kramar.

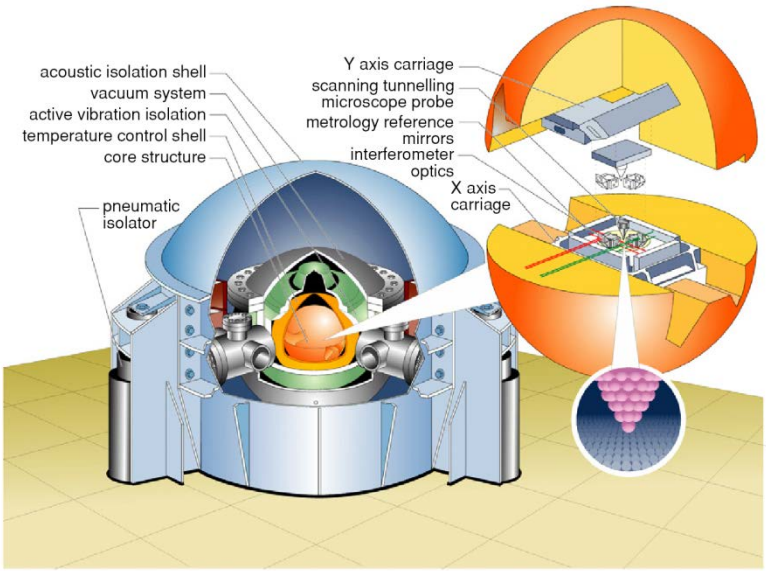

"The relative motion of the upper and lower fine motion stages, carrying the probe and sample respectively, is measured using a 2D displacement measuring interferometer system (Figure 4-29). The interferometers measure differentially the combined motion of the coarse and fine stages, giving a continuous metric independent of what portion of the total motion was generated by the fine or coarse stages. (For error mapping, the position of each fine motion stage is also

measured relative to its coarse motion stage, using a capacitance gauge.) The reference mirrors for the interferometer are the inside surfaces of a highly accurate, low-expansion-coefficient metrology box, inside of which lies the sample. The interferometer beam-splitter optic assemblies are carried by the upper carriage on the same mounting plate that carries the probe system, suspended inside the metrology box."

Figure 4-29. Illustration of the Molecular Measuring Machine (M^3) project: Differential interferometer beam path view – the position of the central assembly is measured with respect to the metrology box, with the input and output beams directed along the motion axis of the central assembly. Courtesy of John Kramar.

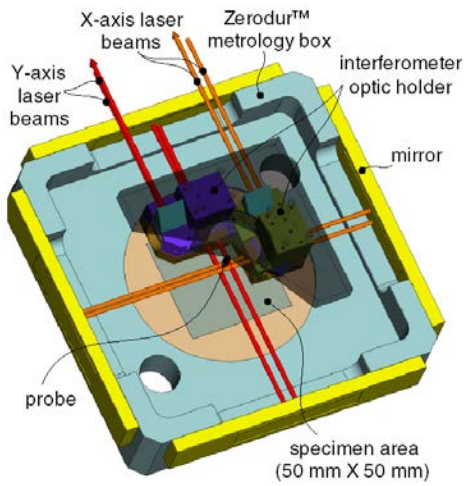

"A scanning probe microscope is used as the sample imaging probe system for M^3. The probe system is comprised of coarse and fine motion stages, a capacitance gauge position sensor, and the probe itself (Figure 4-30). It was in-house designed to meet the various constraints, notable among them the very limited available space. The coarse motion stage is a cylindrical piezoceramic linear stepper motor that operates in the vertical axis with a 3 mm range. The grounded or open circuit clamping force is sufficient to keep the motor slug from sliding down when the power is removed. Built into this motor slug is the vertical, 5 micron range fine motion stage, having flexure-guided motion, and driven by a piezoceramic through a decoupling mechanism of a ball between two flats. The elements of the fine motion stage had to be folded back through the coarse motion stage to accommodate the space constraints. There is no horizontal (scan) motion built into the probe system, because any such motion would not be measured by the interferometer system; all horizontal scanning either drives the metrology box containing the sample or drives the entire upper assembly that includes the probe system along with the interferometer optics, as already described. The vertical fine motion is measured relative to the vertical coarse motion stage using a capacitance gauge that is calibrated *ex situ* against an interferometer. For a given measurement, the vertical range is limited to that provided by the guided fine motion stage. The vertical coarse motion is only crudely guided by the cylindrical housing in which the motor slug runs, and is not considered to be sufficiently characterized or repeatable to use during measurements, since it is within the metrology loop."

Figure 4-30. Illustration of the Molecular Measuring Machine (M^3) project: Probe actuator assembly exploded views, showing separately the detail of the coarse and fine motion mechanisms: The coarse motion is a linear piezo stepping motor; the fine motion is a folded, piezo-driven, flexure-guided system, with a capacitance gauge sensor. Courtesy of John Kramar.

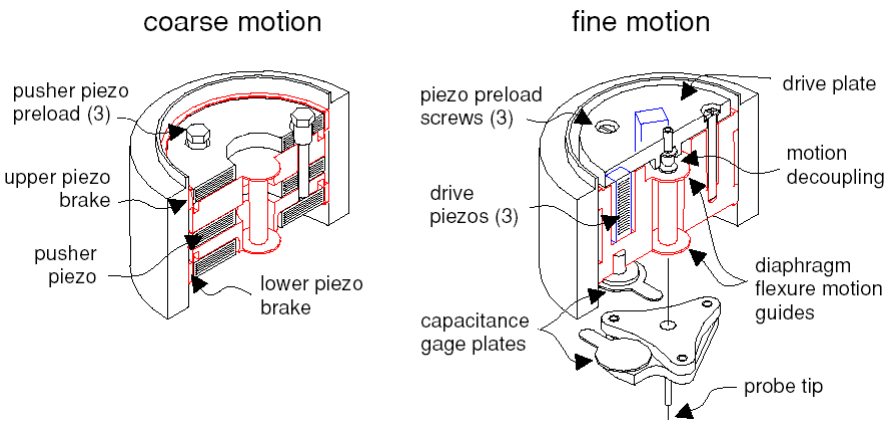

"The machine core assembly is enclosed in layers of environmental isolation and control, as illustrated in (Figure 4-28). The first layer is a temperature control shell. This is a gold-coated copper sphere about 50 mm larger in diameter than the machine core, spiral-wrapped with polyimide-insulated copper wire at a 6 mm spacing. The shell has three doors on rails to allow the removal and replacement of the coarse motion carriages. To maintain a stable temperature at 20 °C, the room is kept at 17 °C ± 0.01 °C, and the current through the heater shell wire is controlled. There are several thermocouples distributed about the temperature control shell and the machine core to monitor the temperature, as well as platinum resistance thermometers on the probe mounting plate and near the sample. The control scheme is to maintain stability through thermal inertia and by keeping a constant heat load. Between the large thermal mass of the copper core and the weak coupling between it and the temperature control shell, the temperature rise time for the system is on the order of one day. Temperature stability of ±0.001 °C has been demonstrated."

"The next layer of environmental control is an active vibration isolation system. For this, the payload is suspended inside an outer shell, kinematically constrained by means of six actuator rods in the Mallock[979] suspension configuration, each actuator having an accompanying accelerometer mounted as nearly as possible coaxially, on the suspended inner mass. Different vibration compensation control algorithms have been implemented using a digital signal processor (DSP),[980] which have good effect when the vibration environment is noisy, for example

---

[979] R.S. Whipple, "The design and construction of scientific instruments," Trans. Opt. Soc. Lond. 22(1921):35-52.

[980] K.-J. Lan, J.-Y. Yen, J.A. Kramar, "Active vibration isolation for a long range scanning tunneling microscope," Asian J. Control 6(2004):179-186; K.-J. Lan, J.-Y. Yen, J.A. Kramar, "Sliding mode control

when the turbomolecular pump is operating. In the quieter environment in which we more typically operate, the performance of the active system is limited by the sensor noise, and is less useful. The entire instrument described to this point is contained in a vacuum system equipped with a turbo pump for roughing and eight symmetrically placed ion pumps for quiet operation. Several of the machine components will not withstand the bake out temperatures needed to achieve ultra-high vacuum levels; a typical base pressure reached is 10^{-5} Pa (~10^{-7} torr). The vacuum system is contained in an environmental control chamber that can be hermetically sealed to provide further acoustic isolation. This chamber is supported by pneumatic isolators having level control and a damped natural resonance of about 1 Hz."

"We have recently moved this instrument to our new Advanced Metrology Laboratory.[981] The new laboratory space is in a building that is completely underground. The laboratory is a class 100 clean room with ±0.01 °C temperature control, and yet is acoustically quiet. The instrument rests on a pneumatically supported concrete slab that is in a pit under the walk-on floor. Most of the electronics and power supplies that drive the instrument are located in an adjacent control room. The control system for M^3 runs on multiple DSPs on a VME (Versa Module Europa) backplane. The VME processor cards each have mezzanine input/output boards for reading from and controlling the instrument. The overall system control is done from a desktop computer that communicates with the VME through a bus adaptor. Code for the DSPs is developed on the desktop computer. User interface and top level control is done in the Matlab programming environment on the desktop computer. Our closed-loop positioning control has some noise at the few tenths of nanometers [~300 pm] level and at relatively low bandwidth due in part to what we believe to be a second-order effect caused by laser pointing instability due to turbulence. In order to decrease this source of noise in the interferometer measurements, we are currently developing a system for delivering the laser beams to the in-vacuum interferometer using fibre optics."

The Advanced Metrology Laboratory (Figure 4-31) was completed in 2003 and is a suite of 5 large buildings, including two that are 40 feet underground. From the AML brochure:[982] "27 specialized AML laboratories offer the ultimate in vibration isolation. These modules are located about 12 meters (40 feet) below ground level in structurally isolated building wings, a first line of defense against vibration. Instruments sit atop specially designed, heavy mass isolation slabs supported on pneumatic "air springs." An isolated, raised floor system spans over the pit containing each isolation slab so that researchers can run their experiments without affecting the isolation systems."

---

for active vibration isolation of a long range scanning tunneling microscope," Rev. Sci. Instrum. 75(2004):4367-4373.

[981] Advanced Measurement Laboratory 2004; http://www.nist.gov/public affairs/amlbrochure.htm; The National Institute of Standards and Technology Advanced Measurement Laboratory, Gaithersburg, MD; http://www.nanobuildings.com/projects/nist/.

[982] Advanced Measurement Laboratory 2004; http://www.nist.gov/public affairs/amlbrochure.htm; The National Institute of Standards and Technology Advanced Measurement Laboratory, Gaithersburg, MD; http://www.nanobuildings.com/projects/nist/.

According to NANObuildings.com, the AML cost $235M and had 536,500 SF of floor space, implying a rough cost per square foot of $438/SF. By this measure (which naively assumes a constant cost per SF as a function of size), a future proprietary 5000 SF West Coast facility (e.g., in the San Francisco Bay Area foothills) might cost about $2.2M plus land cost (probably another $800K), or a ~$3M total, to build.

Further detailed analysis of the molecular workstation system will be needed to determine the degree of vibration isolation required for the workstation to perform according to specifications.

Figure 4-31. Advanced Metrology Laboratory (AML) at NIST

Two other instruments are being used for traceable AFM measurements at NIST: a custom in-house metrology AFM called the calibrated AFM (C-AFM), and a second instrument called the commercial critical dimension AFM (CD-AFM).[983] The C-AFM has displacement metrology for all three axes traceable to the 633 nm wavelength of the iodine-stabilized He-Ne laser. In the current generation of this system (as of 2006), the relative standard uncertainty of pitch and step height measurements was approximately 1.0×10^{-3} for pitches at the micron scale and step heights at the 100 nm scale. The CD-AFM has the capability of measuring vertical sidewalls and thus complements the C-AFM. Although it does not have intrinsic traceability, the CD-AFM can be calibrated using standards measured on other instruments (such as the C-AFM) and the CD-AFM is used primarily for linewidth measurements of near-vertical structures – as of 2006, with relative standard uncertainties of ~0.2% for pitch measurements and ~0.4% for step height measurements. It is possible to calibrate the CD-AFM tip width with a 1 nm standard uncertainty with the assistance of the NIST single crystal critical dimension reference material (SCCDRM) project.

---

[983] Ronald Dixson, Ndubuisi G. Orji, Joseph Fu, Michael Cresswell, Rich Allen, Will Guthrie, "Traceable atomic force microscope dimensional metrology at NIST," Proc. SPIE 6152(2006):61520P.

4.6.1.2 Large-Range Scanning Probe Microscope (LR-SPM) (Germany)

During 2000-9 the German national metrology institute, Physikalisch-Technische Bundesanstalt (PTB) (current group leader Hans-Ulrich Danzebrink), with the Technische Universitaet Ilmenau (Germany) developed a metrological large-range scanning probe microscope (M-LRSPM) (aka. metrological large-range scanning force microscope or Met-LRSFM) having a resolution of less than **100 pm** over the entire positioning and measurement range of having a measurement volume of **25 mm x 25 mm x 5 mm**.[984] To obtain the large range scanning capability, the sample is moved in this case by a combined motion system which consists of a fast Z-piezo positioning stage (Z-PPS)[985] and a ball-bearing positioning stage[986] – creating a dual-stage positioning system

---

[984] G. Jäger, E. Manske, T. Hausotte, H.-J. Büchner, R. Grünwald, W. Schott, "Nanometrology - nanomeasuring machines," Proc. Annual Meeting of ASPE, Crystal City, Virginia, USA, 2001, pp. 23-27. G. Dai, F. Pohlenz, H.-U. Danzebrink, M. Xu, K. Hasche, G. Wilkening, "Metrological large range scanning probe microscope," Rev. Sci. Instrum. 75(2004):962-969; http://www.physikinstrumente.com/en/news/pdf/large range scanning probe microscope.pdf. G. Dai, L. Jung, F. Pohlenz, H.-U. Danzebrink, R. Krueger-Sehm, K. Hasche, G. Wilkening, "Measurement of micro-roughness using a metrological large range scanning force microscope," Meas. Sci. Technol. 15(2004):2039-2046. G. Dai, F. Pohlenz, H.-U. Danzebrink, M. Xu, K. Hasche, "A novel metrological scanning probe microscope with a measurement range up to $(25\ \mathrm{mm})^2$," PTB-Bericht F-48(2003):175-182. G. Dai, F. Pohlenz, H.-U. Danzebrink, M. Xu, K. Hasche, G. Wilkening, "Metrological large range scanning probe microscope applicable for traceable calibration of surface textures," in: G. Wilkening, L. Koenders, eds., Nanoscale Calibration Standards and Methods, 2005, pp. 73-92. H.-U. Danzebrink, G. Dai, F. Pohlenz, G. Wilkening, "Overview of the Metrological Scanning Probe Microscopes at PTB," Microscopy and Microanalysis 11(2005):S2-S5. Gaoliang Dai, Frank Pohlenz, Min Xu, Ludger Koenders, Hans-Ulrich Danzebrink, Günter Wilkening, "Accurate and traceable measurement of nano- and microstructures," Measurement Science and Technology 17(2006):545-552. Gaoliang Dai, Frank Pohlenz, Thorsten Dziomba, Min Xu, Alexander Diener, Ludger Koenders, Hans-Ulrich Danzebrink, "Accurate and traceable calibration of two-dimensional gratings," Measurement Science and Technology 18(2007):415-421. G. Dai, F. Pohlenz, H.-U. Danzebrink, K. Hasche, G. Wilkening, "Improving the performance of interferometers in metrological scanning probe microscopes," Meas. Sci. Technol. 15(2004):S444-S450. See also: A. Sikora, D.V. Sokolov, H.-U. Danzebrink, "Scanning probe microscope set-up with interferometric drift compensation," in: G. Wilkening, L. Koenders, eds., Nanoscale Calibration Standards and Methods, 2005, pp. 109-118; G. Dai, F. Pohlenz, H.-U. Danzebrink, M. Xu, K. Hasche, G. Wilkening, "DSP-based metrological scanning probe microscope with direct interferometric position measurement and improved measurement speed," in: G. Wilkening, L. Koenders, eds., Nanoscale Calibration Standards and Methods, 2005, pp. 119-130. T. Hausotte, G. Jager, E. Manske, N. Hofmann, N. Dorozhovets, "Application of a positioning and measuring machine for metrological long-range scanning force microscopy," Proc. SPIE 5878(2005):587802. Gaoliang Dai, Sebastian Butefisch, Frank Pohlenz, Hans-Ulrich Danzebrink, "A high precision micro/nano CMM using piezoresistive tactile probes," Meas. Sci. Technol. 20(2009):084001. T. Hausotte, B. Percle, G. Jager, "Advanced three-dimensional scan methods in the nanopositioning and nanomeasuring machine," Meas. Sci. Technol. 20(2009):084004.

[985] G. Dai, F. Pohlenz, H.-U. Danzebrink, M. Xu, K. Hasche, G. Wilkening, "Metrological large range scanning probe microscope," Rev. Sci. Instrum. 75(2004):962-969; http://www.physikinstrumente.com/en/news/pdf/large range scanning probe microscope.pdf.

[986] G. Jäger, E. Manske, T. Hausotte, H.-J. Büchner, R. Grünwald, W. Schott, "Nanometrology - nanomeasuring machines," Proc. Annual Meeting of ASPE, Crystal City, Virginia, USA, 2001, pp. 23-27.

designed to achieve both a large measurement range and a high measurement speed. The M-LRSPM senses the surface using a stationary fixed atomic force microscope (AFM) head working in contact mode. During operation, lateral scanning of the sample is performed solely by the "nano measuring machine" (NMM)[987] while the Z-motion, controlled by the AFM signal, is carried out by a combination of the NMM and the compact Z-stage. The compact Z-stage, with its high mechanical resonance frequency (greater than 20 kHz), is responsible for the rapid motion while the NMM simultaneously makes slower movements over a larger motion range.

All six degrees of freedom of the motion stage are measured directly by interferometers (with a resolution of 80 pm) and angle sensors (with a resolution < 0.01 arc-seconds). The AFM probe tip (so also the measurement point) is always located at the intersection point of three interferometer measurement beams oriented in X, Y and Z directions, which reduces the Abbe errors to a minimum during the measurement process. To improve real time performance two high-end digital signal processing (DSP) systems are used for NMM positioning and AFM servo control. This system looks to be roughly similar to M^3 (Section 4.6.1.1), except that PTB's original M-LRSPM did not include a vibration-controlled and temperature-controlled environement, and it was not designed for UHV operation.

According to the primary document,[988] Figure 4-32 shows a schematic diagram of the M-LRSPM, consisting of six main blocks:

Block I is a commercially available positioning system with a motion range of 25 mm x 25 mm x 5 mm in X, Y and Z directions, called a nano measuring machine (NMM).

Block II (the circular platform atop the NMM) is a fast Z-axis piezoelectric positioning stage with an extension range of 2 μm. This compact Z-stage is fixed mechanically to the NMM, forming a dual-stage positioning system. The sample to be measured is placed on the moving part of the compact Z-stage. The "dual-stage aspect" of this design is important since high

---

[987] R. Petersen, H. Rothe, D. Hueser, "Large area AFM-scans with the nanometer coordinate measuring machine," Proceedings of the 5th seminar on quantitative microscopy and 1st seminar on nanoscale calibration standards and methods, PTB Bericht PTB-F-44, Braunschweig, Germany, November 2001. G. Jäger, E. Manske, T. Hausotte, et al. "Nanometrology-Nanomeasuring Machines," ASPE Annual Meeting, 10-15 November 2001, Crystal City, Virginia. SIOS Meßtechnik GmbH, Am Vogelherd 46, D-98693 Ilmenau, Germany. Web site: www.sios.de . See also: http://www.sios.de/ENGLISCH/UEBERENG.HTM, http://www.sios.de/ENGLISCH/PRODUKTE/NMM_E.HTM and http://www.sios.de/ENGLISCH/PRODUKTE/NMMBM_E.HTM. G. Jaeger, R. Gruenwald, E. Manske, T. Hausotte, R. Fuessl, "A nanopositioning and nanomeasuring machine: operation – measured results," Nanotechnol. Precis. Eng. 2(2004):81-84. A. Weckenmann, J. Hoffmann, A. Schuler, "Development of a tunnelling current sensor for a long-range nano-positioning device," Meas. Sci. Technol. 19(2008):064002. Gerd Jäger, Eberhard Manske, Tino Hausotte, H.-J. Büchner, "The Metrological Basis and Operation of Nanopositioning and Nanomeasuring Machine NMM-1," tm - Technisches Messen 76(May 2009):227-234.

[988] G. Dai, F. Pohlenz, H.-U. Danzebrink, M. Xu, K. Hasche, G. Wilkening, "Metrological large range scanning probe microscope," Rev. Sci. Instrum. 75(2004):962-969; http://www.physikinstrumente.com/en/news/pdf/large range scanning probe microscope.pdf.

scanning speeds would not be possible if the NMM were operated alone, due to its low resonance frequency.

Figure 4-32. Schematic diagram of M-LRSPM.[989] OD: optical detector for measuring the bending of the cantilever. Pre-Amp: preamplifier for amplifying the electronic signal from the OD. ADC: analog to digital converter. DAC: digital to analog converter. HV-Amp: High voltage amplifier. CSSP: Capacitive sensor signal processing unit. S_0: the setpoint value of the cantilever bending. S_1: the target home position of the PPS. S_2: emergency signal to stop the NMM motion. S_3: the motion target of the NMM in Z-axis. S_4: Commands, data and configurations.

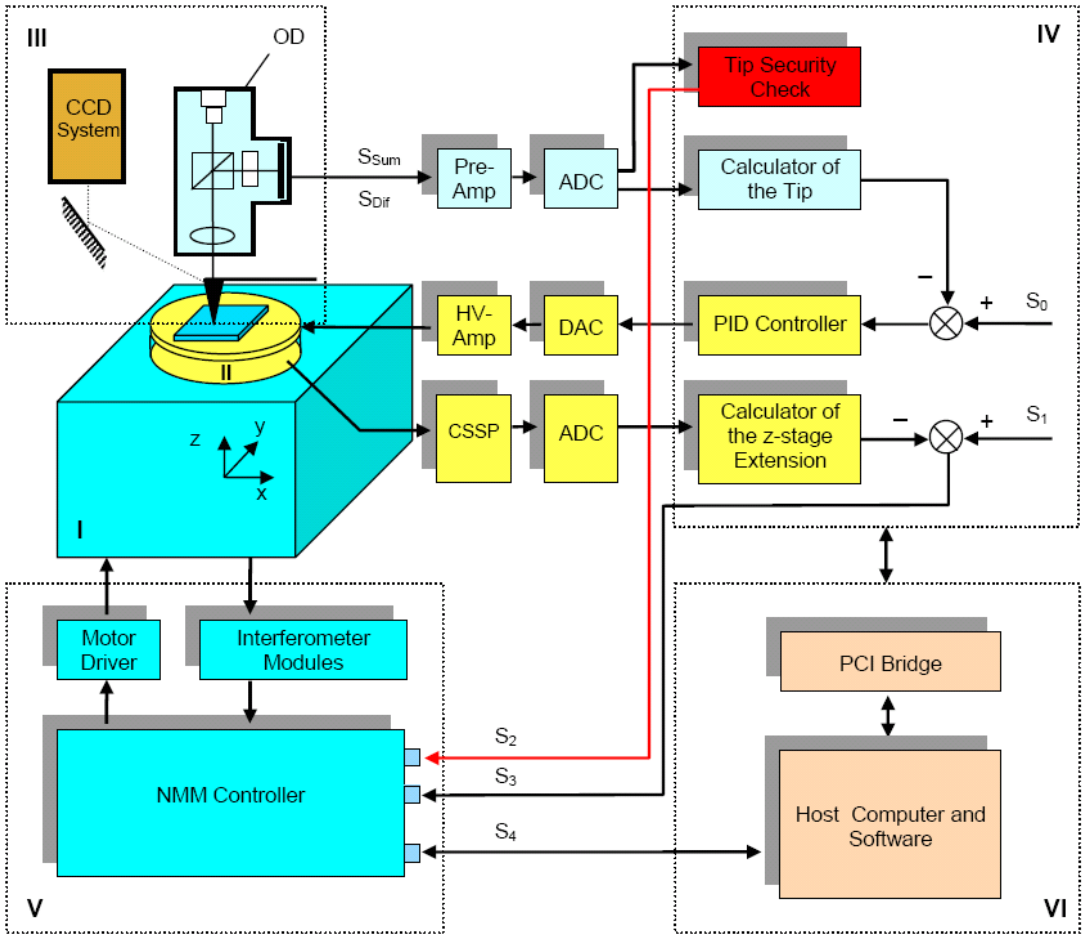

[989] G. Dai, F. Pohlenz, H.-U. Danzebrink, M. Xu, K. Hasche, G. Wilkening, "Metrological large range scanning probe microscope," Rev. Sci. Instrum. 75(2004):962-969; http://www.physikinstrumente.com/en/news/pdf/large range scanning probe microscope.pdf.

Block III is an AFM detection system which consists of an AFM cantilever and holder, an optical detector for measuring the bending of the cantilever and an optical microscope with CCD camera for monitoring tip and sample. The tip of the AFM cantilever is positioned at the intersection of the three interferometer measurement beams of the positioning stage oriented in X, Y and Z directions, therefore reducing the Abbe error to a minimum. The AFM head is fixed to the metrological frame of the NMM by stiff springs in order to reduce vibrations.

Block IV is a high-end DSP system. It acts as a fast real-time controller of the SPM co-ordinating the movement of both the NMM and the compact Z-stage and communicating with Blocks V and VI.

Block V servo-controls the motion of the NMM and includes interferometer modules, another DSP system and motor drivers.

Block VI is the host computer. It communicates with Block IV via a PCI bus and Block V via an USB line. As a host, Block VI collects operational instructions and displays the measurement results.

The measurement setup (Figure 4-33) is enclosed within an acoustic isolating box and placed on a vibration isolation table to attenuate vibrations from the ground and acoustic noise generated by external sources, e.g., the air conditioning systems of neighbouring instruments. Since the complete instrument is located in a segment of the PTB's clean-room center, fans forming part of the air-flow system also act as noise sources. Where possible, heat sources of the instrument are placed outside of the acoustic isolating box to reduce the temperature increase inside the box because a good acoustic isolating box also means a lack of heat dissipation. The instrument's location inside the clean-room center provides excellent temperature stability (better than ± 0.1 K) and cleanliness which avoids dust particle contamination of the working environment.

The principle layout of the NMM is shown schematically in Figure 4-34. It consists of a metrological base (Zerodur frame), a mirror corner and measurement systems that include three interferometers and two angle sensors. To simplify the presentation, the mechanical guiding system and motors are not shown in the figure. The NMM was designed at the Technical University of Ilmenau and produced by SIOS Messtechnik GmbH.[990] The mirror corner, which comprises three high precision planar mirrors attached orthogonally one to each other, moves together with the sample. It is fixed on a stage with motion range of 25 mm x 25 mm x 5 mm in X, Y and Z directions, respectively. This stage consists of three ball bearing guidances driven by electrodynamic motors. The compact Z-stage and the sample are placed on the upper part of the Z-mirror. Because the position of the mirror corner is measured directly by the three interferometers, the location of the sample relative to the metrological base can be measured with high resolution (80 pm) and with traceability to the meter definition. Additionally, the yaw, pitch and roll angles of the sample movement are simultaneously measured by angle sensors. A DSP servo control system based on the measured position and angle is provided to move the sample to

---

[990] SIOS Meßtechnik GmbH, Am Vogelherd 46, D-98693 Ilmenau, Germany. Web site: www.sios.de . See also: http://www.sios.de/ENGLISCH/UEBERENG.HTM, http://www.sios.de/ENGLISCH/PRODUKTE/NMM_E.HTM and http://www.sios.de/ENGLISCH/PRODUKTE/NMMBM_E.HTM.

its target position by driving the kinematic system using the electrodynamic motors. The NMM can position the sample with nanometer accuracy at any point within the measurement range.

Figure 4-33. Photo of the M-LRSPM setup.[991] The system is installed in the clean-room center with the monitors for control and visualization and the M-LRSPM is in the opened acoustic hood – the insert shows the AFM detection system with the optical microscope, the compact Z-stage and the sample table of the NMM.

[991] G. Dai, F. Pohlenz, H.-U. Danzebrink, M. Xu, K. Hasche, G. Wilkening, "Metrological large range scanning probe microscope," Rev. Sci. Instrum. 75(2004):962-969; http://www.physikinstrumente.com/en/news/pdf/large range scanning probe microscope.pdf.

Figure 4-34. Schematic principle of the nano measuring machine (NMM).[992] The detection point coincides with the intersection of three interferometer measurement beams oriented in X, Y and Z directions, an arrangement that reduces Abbe-error to a minimum.

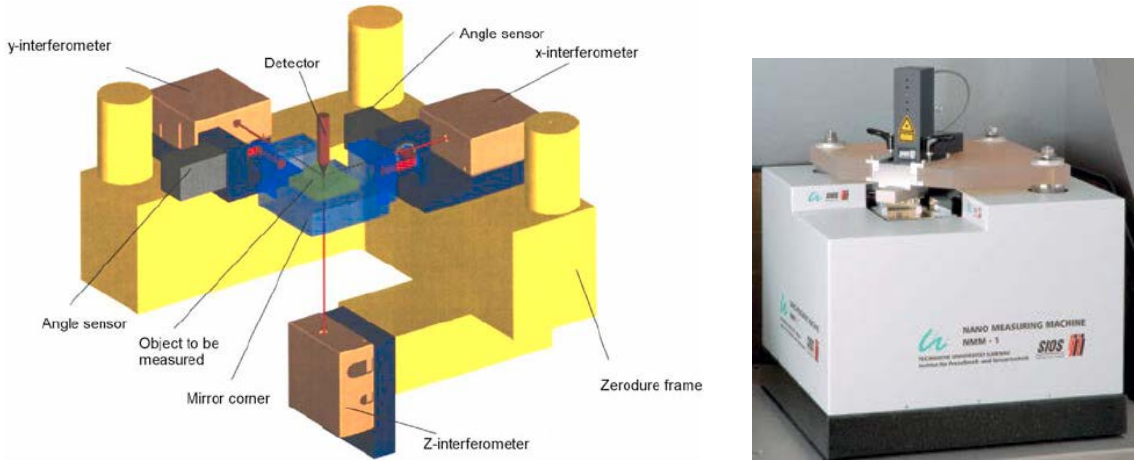

The compact Z-stage is a custom specified product designed and manufactured by Physik Instrumente GmbH.[993] The principle layout of this compact Z-stage is shown in Figure 4-35. It consists mainly of three identical piezoelectric transducers (PZTs) and a capacitive sensor. All mechanical parts are made from Invar to enhance the thermal stability of the instrument. The three parallel PZTs are located symmetrically around the center of the stage, pushing or pulling the moving part with respect to the fixed part over a motion range of about 2 μm. The gap between the moving and the fixed part is measured by the capacitive sensor which is located in the center. The sensor and piezos allow Z-position control with subnanometer resolution. In the device described here only one voltage value is applied to the three parallel PZTs. This can cause unwanted jaw, pitch and roll angle errors due to small physical differences between the three PZTs, but these tilting angles were expected to be less than 0.2" which would produce an unobservable measurement error – if required, an unwanted angle tilt could be compensated by applying different voltages to each PZT. The important advantages of the stage are its compact size, the small mass and the good dynamic performance. Since it has a size of only 30 mm in diameter and 8 mm in thickness its mass is minimized to about 40 g. When combined with the NMM the additional mass is small and the original dynamic performance of the NMM is maintained. Furthermore, because of the high stiffness of the PZTs, the small mass of the moving

---

[992] G. Dai, F. Pohlenz, H.-U. Danzebrink, M. Xu, K. Hasche, G. Wilkening, "Metrological large range scanning probe microscope," Rev. Sci. Instrum. 75(2004):962-969; http://www.physikinstrumente.com/en/news/pdf/large range scanning probe microscope.pdf.

[993] SIOS Meßtechnik GmbH, Am Vogelherd 46, D-98693 Ilmenau, Germany. Web site: www.sios.de . See also: http://www.sios.de/ENGLISCH/UEBERENG.HTM, http://www.sios.de/ENGLISCH/PRODUKTE/NMM_E.HTM and http://www.sios.de/ENGLISCH/PRODUKTE/NMMBM_E.HTM.

part, and the carefully designed preload structure, the stage has a mechanical resonance frequency above 20 kHz. The compact Z-stage performs a fast servo loop along the Z-axis during the scanning procedure so its high control frequency can significantly enhance the scanning speed of the whole positioning system.

Figure 4-35. The compact 2 µm Z-axis piezoelectric positioning stage, consisting of three parallel PZTs located symmetrically around a central capacitive sensor.[994]

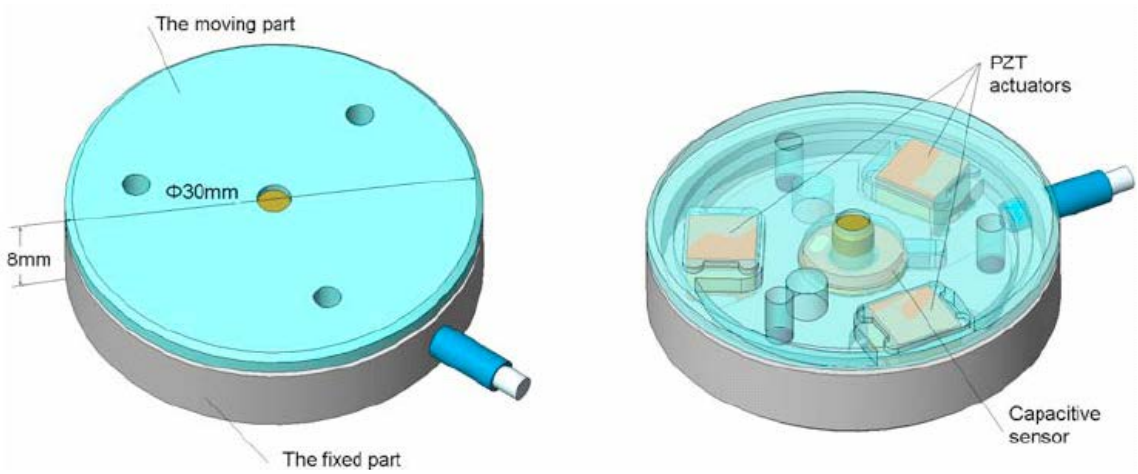

During measurement, the sample surface is detected using an AFM tip in contact mode by monitoring the bending of the cantilever with an optical detector. After preamplification the optical detector signals S_{sum} and S_{diff} are sent to the DSP system, and the results are then fed into the digital PID controller. This control loop maintains the bending of the cantilever at a constant value, defined by the setpoint, by moving the sample rapidly in Z-direction using the compact Z-stage. Simultaneously, the DSP can monitor the extension of the compact Z-stage by sampling the voltage output of the capacitance sensor. To overcome the limitation of measurement range in Z-direction to the extension range of the compact Z-stage (2 µm), the calculated Z-stage position is further compared with the chosen home position of the system to yield a NMM motion target signal (S_3 in Figure 4-32). The S_3 signal indicates how far the NMM should move the sample along the Z-axis relative to its current position. This signal is sent to the NMM controller and the controller responds by commanding the NMM to move along its Z axis. The total motion of the sample is the sum of the motion from both the NMM and the compact Z-stage. As the extension of the compact Z-stage is now controlled relative to its home position and thus comprises the displacement of the NMM, the measurement range along the Z-axis is no longer

---

[994] G. Dai, F. Pohlenz, H.-U. Danzebrink, M. Xu, K. Hasche, G. Wilkening, "Metrological large range scanning probe microscope," Rev. Sci. Instrum. 75(2004):962-969; http://www.physikinstrumente.com/en/news/pdf/large range scanning probe microscope.pdf.

limited by the motion range of the compact Z-stage. The AFM is scanned at a speed of up to 25 μm/sec.

The system has an error of about 2 nm due to nonlinearity of the interferometers, which was asserted to be reducible to <300 pm in future work.[995] The SPM has a p-v noise level of about 3 nm, principally due to vibrational noise originating from the building and other sources of acoustic noise, with further noise reduction asserted to be achievable by using an improved acoustic isolation housing. Thus a single-measurement accuracy around 5 nm can be obtained using this system (potentially reducible to ~1 nm), with multiple averaged measurements of a step-height standard reducing the final measurement uncertainty to 900 pm using the original system,[996] which by 2007 had been reduced to 15 pm for multiple measurements on a 2D grating with a 1 μm pitch.[997]

The latest version of the NMM from SIOS, called the Nano Positioning and Nano Measuring Machine,[998] is claimed to be able to make three-dimensional coordinate measurement in a range of **25 mm x 25 mm x 5 mm** with a resolution of **100 pm**[999] or even **80 pm**[1000] by using three

---

[995] G. Dai, F. Pohlenz, H.-U. Danzebrink, K. Hasche, G. Wilkening, "Improving the performance of interferometers in metrological scanning probe microscopes," Meas. Sci. Technol. 15(2004):S444-S450. See also: A. Sikora, D.V. Sokolov, H.-U. Danzebrink, "Scanning probe microscope set-up with interferometric drift compensation," in: G. Wilkening, L. Koenders, eds., Nanoscale Calibration Standards and Methods, 2005, pp. 109-118; G. Dai, F. Pohlenz, H.-U. Danzebrink, M. Xu, K. Hasche, G. Wilkening, "DSP-based metrological scanning probe microscope with direct interferometric position measurement and improved measurement speed," in: G. Wilkening, L. Koenders, eds., Nanoscale Calibration Standards and Methods, 2005, pp. 119-130.

[996] G. Dai, F. Pohlenz, H.-U. Danzebrink, K. Hasche, G. Wilkening, "Improving the performance of interferometers in metrological scanning probe microscopes," Meas. Sci. Technol. 15(2004):S444-S450. See also: A. Sikora, D.V. Sokolov, H.-U. Danzebrink, "Scanning probe microscope set-up with interferometric drift compensation," in: G. Wilkening, L. Koenders, eds., Nanoscale Calibration Standards and Methods, 2005, pp. 109-118; G. Dai, F. Pohlenz, H.-U. Danzebrink, M. Xu, K. Hasche, G. Wilkening, "DSP-based metrological scanning probe microscope with direct interferometric position measurement and improved measurement speed," in: G. Wilkening, L. Koenders, eds., Nanoscale Calibration Standards and Methods, 2005, pp. 119-130.

[997] Gaoliang Dai, Frank Pohlenz, Thorsten Dziomba, Min Xu, Alexander Diener, Ludger Koenders, Hans-Ulrich Danzebrink, "Accurate and traceable calibration of two-dimensional gratings," Measurement Science and Technology 18(2007):415-421.

[998] SIOS Meßtechnik GmbH, Am Vogelherd 46, D-98693 Ilmenau, Germany. Web site: www.sios.de . See also: http://www.sios.de/ENGLISCH/UEBERENG.HTM, http://www.sios.de/ENGLISCH/PRODUKTE/NMM_E.HTM and http://www.sios.de/ENGLISCH/PRODUKTE/NMMBM_E.HTM.

[999] SIOS Meßtechnik GmbH, Am Vogelherd 46, D-98693 Ilmenau, Germany. Web site: www.sios.de . See also: http://www.sios.de/ENGLISCH/UEBERENG.HTM, http://www.sios.de/ENGLISCH/PRODUKTE/NMM_E.HTM and http://www.sios.de/ENGLISCH/PRODUKTE/NMMBM_E.HTM. C. Recknagel, H. Rothe, "A concept for automated nanoscale atomic force microscope (AFM) measurements using a priori knowledge," Meas. Sci. Technol. 20(2009):084026.

embedded homodyne interferometers – miniaturized laser interferometers as fiber-coupled length measurement devices that work very stably and precisely by using a frequency-stabilized He-Ne laser as the light source combined with compensation for air pressure and temperature variations that can affect the precision of laser wavelength. However, Hausotte et al.[1001] says that while the interferometric length measuring and drive systems of the MMM allow moving the stage with a resolution of less than 100 pm, the positioning uncertainty is only about <10 nm in all three axes. The nanometer coordinate measuring machine (NCMM) developed at the Helmut Schmidt University (HSU)[1002] also uses the NMM from SIOS and has a claimed positioning repeatability of <300 pm.

As with M^3 (Section 4.6.1.1), this is another example where the motions of imperfect actuators are tracked by a very accurate interferometer setup, thus yielding a net high-accuracy positioning system – rather than attempting to design a high-accuracy actuator system directly.

4.6.1.3 LORS and SAMM (Univ. N. Carolina, MIT)

Built during 1995-2001, the original Long-Range Scanning System (LORS)[1003] had a measurement range of 25 mm x 25 mm x 0.1 mm. The key paper by Holmes (Center for Precision Metrology, University of North Carolina, Charlotte, NC, USA), Hocken (also then at

---

[1000] Gaoliang Dai, Sebastian Butefisch, Frank Pohlenz, Hans-Ulrich Danzebrink, "A high precision micro/nano CMM using piezoresistive tactile probes," Meas. Sci. Technol. 20(2009):084001.

[1001] T. Hausotte, B. Percle, G. Jager, "Advanced three-dimensional scan methods in the nanopositioning and nanomeasuring machine," Meas. Sci. Technol. 20(2009):084004.

[1002] C. Recknagel, H. Rothe, "A concept for automated nanoscale atomic force microscope (AFM) measurements using a priori knowledge," Meas. Sci. Technol. 20(2009):084026. Martin Gruhlke, Hendrik Rothe, "Combining nanometrology and coordinate measurement for large-range nanoscale metrology," Proc. SPIE 6648(2007):66480I. M. Gruhlke, C. Recknagel, H. Rothe, "Development features in large-range nanoscale coordinate metrology," Opt. Micro- Nanometrology Microsyst. Technol. II, Proc. SPIE 6995(2008):69950B.

[1003] M. Holmes, R. Hocken, D. Trumper, "The long-range scanning stage: a novel platform for scanned-probe microscopy," Precis. Eng. 24(July 2000):191-209. M. Holmes, D. Trumper, R. Hocken, "Atomic-Scale Precision Motion Control Stage (The Angstrom Stage)," CIRP Annals 44(January 1995); M.L. Holmes, R.J. Hocken, D.L. Trumper, "A Long-Range Scanning Stage (The LORS Project)," Proceedings of 1996 ASPE Annual Meeting, November 1996; M. Holmes, R. Hocken, D. Trumper, "A Long-range Scanning Stage Design," Proc. of ASPE 14(1996); D. Trumper, R. Hocken, M. Holmes, "Analysis and Design of a Long-range Scanning Stage," Proc. of the 1998 NSF Manufacturing Grantees Conference, Monterey, Mexico, January 1998, p. 363; M. Holmes, D. Trumper, R. Hocken, "Magnetically-suspended Stage for Accurate Positioning of Large Samples in Scanned Probe Microscopy," Proceedings of the MAG '98 Industrial Conference and Exhibition on Magnetic Bearings, 5-7 August 1998, pp. 123-132; M.L. Holmes, R.J. Hocken, D.L. Trumper, "The long-range scanning stage: a novel platform for scanned probe microscopy," Precision Eng. 24(2000):191-209; R.J. Hocken, D.L. Trumper, C. Wang, "Dynamics and control of the UNCC/MIT sub-atomic measuring machine," CIRP Ann. 50(2001):373-376.

CPM; formerly of NIST) and Trumper (then at MIT; also involved with the NIST ADM project in 2000) describes a magnetically suspended six degree-of-freedom precision motion control stage with a horizontal positioning noise of less than 600 pm at three sigma and a vertical positioning noise of less than 2200 pm at three sigma. The stage utilizes four levitation linear motors to suspend and servo the moving element (platen) throughout its 25 mm x 25 mm x 0.1 mm range of travel. Position feedback is provided by three plane mirror interferometers and three capacitance probes. The suspended platen (12 kg mass) is floated in oil to enhance the stage's disturbance rejection and to reduce power dissipation in the actuators. The stage has been designed to achieve a positioning accuracy of 10 nm and is used to position samples beneath a scanned probe microscope. The ultimate purpose of this measuring machine is to provide a means of measuring submicron-scale features with nanometer-scale accuracy. The technology can be scaled to larger travels, with accuracy limited primarily by the wavelength instability of the He-Ne light source.

Together with UNC Charlotte, during 2002-2005 Andrew Stein at the MIT Precision Motion Control Laboratory[1004] built a magnetically-suspended stage designed to achieve 100 pm resolution and 1-nm repeatability, but with only 10-nm accuracy over a macroscopic range of 25 mm in X and Y, and 100 microns in Z. To complete this project, called the Sub-Atomic Measuring Machine (SAMM), Stein tried to develop an atomic force microscope head to allow accurate characterization of the performance of the LORS stage. This probe would sense tip-sample separation using a miniature piezoelectric quartz tuning fork. When driven with an AC voltage at its resonant frequency and with a sharp tip mounted to one end, this sensor would resolve topographic features on the atomic scale. Development of integrated metrology with the inherent accuracy of the system was a key design challenge, since scanned probe microscopy typically relies on open-loop control of PZT actuators which may introduce errors due to hysteresis. The RMS noise reported in the early work for the vertical measurement was only ~5 nm.[1005]

Robert Hocken has received the following grants to support this work:

$ 25 K	3/1/97 - 2/28/98	IUCRC Planning-Precision Metrology NSF
$ 380 K	7/1/98-9/30/2003	Precision Metrology – I/UCRC NSF
$ 469 K	5/1/99-4/30/2002	Sub-Atomic Measuring Machine NSF
$ 200 K	7/1/03-9/30/2008	Precision Metrology – I/UCRC NSF
$ 400 K	10/1/03-9/30/08	NSEC:Center for Scalable and Integrated Nano Manufacturing NSF
$ 1500 K	07/01/05-06/30/09	NIRT: Nanometrology for Nanoscale Science and Engineering NSF

[1004] Andrew Stein, "Atomic Force Microscope Probe with Metrology, for Subatomic Measuring Machine (SAMM)," MIT, Precision Motion Control Laboratory, sponsored by National Science Foundation Grant Number DMI-9821003, 2005; http://web.mit.edu/pmc/www/projects.htm. Andrew J. Stein, David L. Trumper, Robert J. Hocken, "A Metrological Atomic Force Microscope," http://www.aspe.net/publications/Annual_2002/PDF/PAPERS/5optmet/959.PDF.

[1005] Andrew J. Stein, David L. Trumper, Robert J. Hocken, "A Metrological Atomic Force Microscope," http://www.aspe.net/publications/Annual_2002/PDF/PAPERS/5optmet/959.PDF.

According to notes for a September 2007 lecture,[1006] Hocken was still working on "the Sub-Atomic Measuring Machine that is being upgraded to picometer precision." As recently as 2008, the SAMM project was still active, as revealed by the following progress report delivered by Hocken and Trumper describing their upgraded system at a 2008 metrology conference:

High Accuracy Atomic Force Microscope for Dimensional Metrology

"The focus of this paper is the design and manufacture of an atomic force microscope capable of nanometer accuracy over 20 micrometers of range. The microscope is designed to interface with an instrument called the Sub-Atomic Measuring Machine (SAMM) developed by Holmes, Hocken, and Trumper. The SAMM uses laser interferometry to measure and control the X-Y position and yaw of a stage which is neutrally buoyant in fluorosilicone oil. The Z position, roll, and pitch of the stage are measured with capacitance sensors. Both sets of direct metrology instruments are capable of sub-nanometer resolution to guide the stage in closed loop positioning control in all six degrees of freedom. The SAMM stage has demonstrated sub-nanometer resolution, 1 nm repeatability, and on the order of 30 nm accuracy over 25mm x 25mm x 100µm travel. We have developed an AFM head with compatible specifications to measure the surface height of a sample while the SAMM raster scans it over its complete range of movement.
The newly developed high accuracy AFM head uses a monolithic flexure to guide an AFM probe tip in one degree of freedom (z axis) while three capacitance sensors measure its displacement. A piezoelectric actuator pushes on the guide flexure through a decoupling flexure. The relative stiffnesses between the guide and decoupling flexures allow us to inhibit secondary rotation and translation error motions of the piezoelectric actuator from propagating into the measurement. Though FEA and experimental results, we have demonstrated that the guide flexure is 18 times more compliant than the decoupling flexure in the intended z direction of motion and over 1500 times mores stiff than the decoupling flexure against unwanted perturbations in the other degrees of freedom. The monolithic construction of both flexures mitigates alignment, mircoslip, and frictional problems commonly found in flexural systems."

"Other sources of error such as the intersection of force and metrology loops as well as thermal stability are examined in detail. Both transient forces derived from changes in momentum as well as repeatable forces derived from the displacement of the flexures are routed in a loop that does not inject deflections into the metrology path. Furthermore, every component in the metrology loop is composed of low expansion Invar or Zerodur. The error brought about by thermal expansion of both steel guide and decoupling flexures is designed to be measured by the capacitance sensors. We expect that the summation of mechanical, thermal, and electrical errors and noise will enable one nanometer positional accuracy. The AFM system is currently being assembled. We expect to report on experimental results in the extended abstract and at the conference presentation."

However, the LORS and SAMM systems don't appear adaptible to our needs because they use a floating oil suspension for the stage that is inconsistent with UHV operating conditions; also, the designed repeatable accuracy is only 10 nm, whereas we need better than 100 pm.

[1006] Robert J. Hocken, Technology Lecture: Nano Scale Dimensional Metrology and Application, Singapore Institute of Manufacturing Technology (SIMTech), 19 September 2007.

4.6.1.4 NMi Nanopositioner (Netherlands)

Within the Dutch standards laboratory (NMi Van Swinden Laboratorium) a traceable atomic force microscope (AFM) is currently being developed that aims for a measurement uncertainty of 1 nm[1007] (Figure 4-36). According to the most recent (2007) paper, the SPM has been constructed using a commercial AFM head that has been embedded in a metrology frame using an accurate 3D translation stage. The position of the AFM probe relative to the sample is determined along three orthogonal measurement axes by three individual laser interferometers. Due to the properties of the 3D translation stage the Abbe offset between the probe position and the measurement axes should remain below 0.1 mm in order to realize an overall measurement uncertainty of 1 nm. The laser interferometers use a four-pass optical configuration so the measurement axis is defined by the virtual center of the four positions of the laserspots onto the plane retro mirror. In order to accurately determine this virtual center and therefore the position of the measurement axis a device has been designed to measure the four laserspot positions of each axis within the SPM. Since the AFM probe position is determined in 3D, accurate calibration of the angles between the measurement axes is important if the measurement error is to be minimized to 1 nm.

A commercial piezo table with three independent translation axes is used. The table has a displacement volume XYZ of 100 microns x 100 microns x 20 microns. A square aperture of 66 x 66 mm^2 in the center of the table provides space for interferometric positioning measurement along the z axis. The pitch, roll, and yaw during translation along the axes are less than 2 arcsec peak-to-peak for the whole range of motion. A commercial interferometric system is used to sample the 3D position of the scan table. The interferometers allow a resolution of approximately 0.16 nm (160 pm), but the optical components of the interferometer introduce a nonlinearity error of 1.4 nm peak-to-peak (calculated) to the measured position. To reduce environmental measurement errors caused by a long dead path, the interferometers are placed 1 mm from the mirrors; the resulting achieveable measurement uncertainty per axis is estimated to be better than 2 nm.[1008]

[1007] K.R. Koops, M.G.A. van Veghel, G.J.W.L. Kotte, M.C. Moolman, "Strategies for scanning probe metrology," Meas. Sci. Technol. 18(January 2007):390-394 http://www.iop.org/EJ/abstract/0957-0233/18/2/S10/. K. Dirscherl, K.R. Koops, "Chapter 7. Traceable Probing with an AFM," in: G. Wilkening, L. Koenders, eds., Nanoscale Calibration Standards and Methods: Dimensional and Related Measurements in the Micro- and Nanometer Range, Wiley-VCH Verlag GmbH & Co., Weinheim, 2005, pp. 95-108; http://books.google.com/books?id=0pSO2IT6YqQC&pg=PA95&lpg=PA95&dq=KR+Koops+Netherlands&source=web&ots=sGX9vZYLtb&sig=GqgnfAOaaaeUq8QmmbbWv6YjXxo&hl=en&sa=X&oi=book_result&resnum=1&ct=result..

[1008] K. Dirscherl, K.R. Koops, "Chapter 7. Traceable Probing with an AFM," in: G. Wilkening, L. Koenders, eds., Nanoscale Calibration Standards and Methods: Dimensional and Related Measurements in the Micro- and Nanometer Range, Wiley-VCH Verlag GmbH & Co., Weinheim, 2005, pp. 95-108; http://books.google.com/books?id=0pSO2IT6YqQC&pg=PA95&lpg=PA95&dq=KR+Koops+Netherlands&source=web&ots=sGX9vZYLtb&sig=GqgnfAOaaaeUq8QmmbbWv6YjXxo&hl=en&sa=X&oi=book_result&resnum=1&ct=result.

Figure 4-36. <u>Left:</u> The low-vibration set-up with the AFM in our new laboratory; a granite pillar is supported by a separate foundation and is isolated from the surrounding floor. <u>Right:</u> The traceable AFM consists of a scanning stage (SS), an invar metrology frame (MF) with a 3D laser interferometer and an AFM head (AH).[1009]

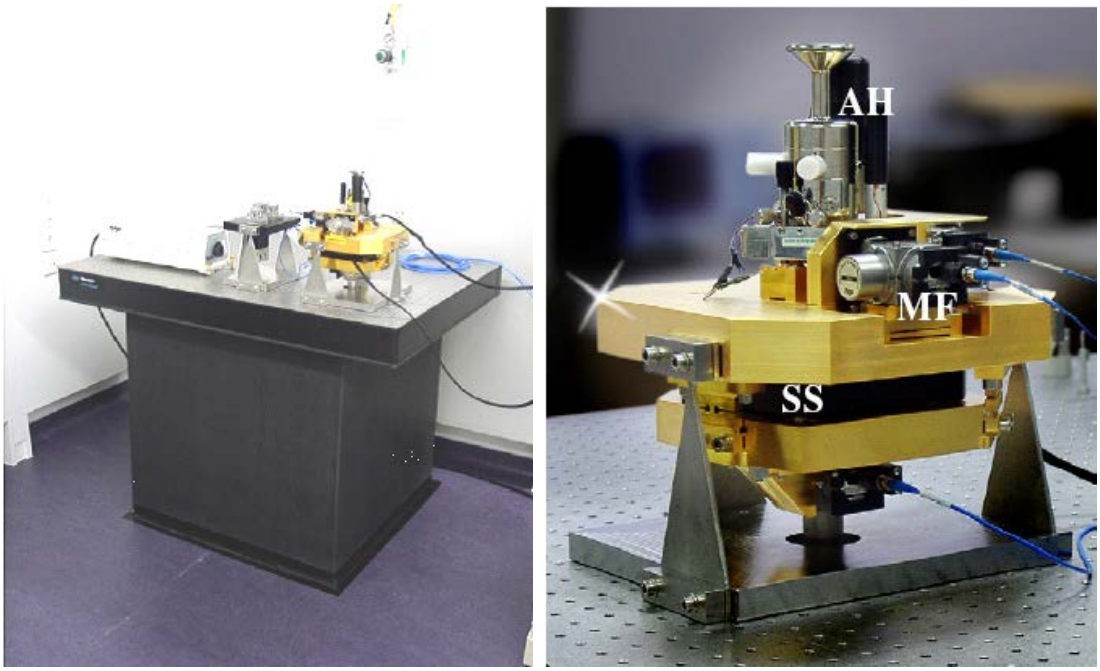

This system provides only 100 microns of travel and targets only 1 nm repeatable positioning accuracy; additionally, in a personal communication[1010] Koops notes that "our system has not been designed for UHV applications."

[1009] K.R. Koops, M.G.A. van Veghel, G.J.W.L. Kotte, M.C. Moolman, "Strategies for scanning probe metrology," Meas. Sci. Technol. 18(January 2007):390-394 http://www.iop.org/EJ/abstract/0957-0233/18/2/S10/.

[1010] K.R. Koops, personal communication to Robert A. Freitas Jr., 23 June 2008.

4.6.1.5 3D Measuring Instrument (BNM-LNE, France)

The BNM-LNE (Bureau National de Metrologie et le Laboratoire National de Métrologie et d'Essais), the national metrology laboratory of France, has a nanometrology program within its Dimensional Metrology division.[1011] A major initiative within this program was a three-dimensional high-accuracy measurement tool (Figure 4-37) intended to serve as a reference metrology instrument traceable to the national standard of length.[1012] The machine was developed as a joint project of the LNE in collaboration with the National Laboratory of Metrology and Testing (ESA) and the Metrology Laboratory and Applied Mathematics (L2MA) ENSAM of Lille.

The instrument's movable mechanical structure offers a displacement capacity through and XYZ range of **300 mm x 300 mm x 50 µm**, with expected measurement uncertainties of **30 nm** for displacements along the X and Y axes and **1 nm** along the Z axis. The object to be measured is moved under an interchangeable sensor. At present LNE can use the instrument with three types of sensor: an atomic force microscope (AFM), an optical microscope, or an optical sensor. However, the machine has been designed to operate with any kind of sensor. The instrument is installed in dedicated premises specifically designed for nanodimensional metrology activities. The system uses piezoelectric actuators, thermal insulation and vibration islation, calibrated capacitive transducers for Z-axis measurement, interferometers and 2D optical encoders for X and Y axis measurements. The system apparently is designed to operate in air, not UHV.

[1011] LNE Dimensional Nanometrology, 2009; http://74.125.19.132/translate_c?hl=en&sl=fr&u=http://www.lne.eu/en/r_and_d/nanometrology/dimensional-nanometrology.asp&prev=/search%3Fq%3DDucourtieux,%2BS.%2BDuhem,%2BF.%2BLarsonnier,%2BJ.%2BSalgado,%2BG.%2BP.%2BVailleau,%2BL.%2BLahousse%26hl%3Den%26sa%3DG&rurl=translate.google.com&usg=ALkJrhjnpETiKYd70y1rCjL78Ru1IjT7jQ.

[1012] S. Ducourtieux, F. Ducourtieux, F. Larsonnier, S. Larsonnier, S. Duhem, L. Duhem, L. Lahousse, J. Lahousse, J. Salgado, J. Salgado, J. David, GP Vailleau, "The research and development in Nanometrology of BNM-LNE," 11th International Congress of Metrology, Toulon, 20-23 October 2003; S. Ducourtieux, S. Duhem, F. Larsonnier, J. Salgado, G. P. Vailleau, L. Lahousse, J. David, "The Nanometrology ESA's research and development program," in Proceedings of the 5th Euspen International Conference, Montpellier, France, Vol. 1, 2005, pp. 131-134; G.P. Vailleau, S. Vailleau, S. Ducourtieux, L. Ducourtieux, L. Lahousse, J. Lahousse, J. David, S. David, S. Leleu, "Implementation of a new architectural design for a machine to measure nanometer resolution," French Metrology 2005-4(2005):35-43; S. Ducourtieux, L. Lahousse, F. Larsonnier, S. Duhem, J. Salgado, J. David, GP. Vailleau, "Program of Research and Development LNE nanometrology: recent results," 12th International Congress of Metrology, Lyon, June 2005; L. Lahousse, "Contribution to the machines to large geometric precision: The concept of information in improving machine performance", Thesis, October 2005; http://74.125.19.132/translate_c?hl=en&sl=fr&u=http://www.lne.eu/compteur/download_these-lahousse.asp&prev=/search%3Fq%3DDucourtieux,%2BS.%2BDuhem,%2BF.%2BLarsonnier,%2BJ.%2BSalgado,%2BG.%2BP.%2BVailleau,%2BL.%2BLahousse%26hl%3Den%26sa%3DG&rurl=translate.google.com&usg=ALkJrhgn9eczLBgK04yPihWJSjE1klU4og.

Figure 4-37. LNE's 3D instrument undergoing preliminary tests[1013]

4.6.1.6 NRC Metrological AFM (Canada)

Brian Eves at the Institute for National Measurement Standards of the Canadian National Research Council (NRC) has designed[1014] a large measurement-volume metrological atomic force microscope (mAFM) and by 2009 the prototype was nearly completed. The design goal for the mAFM is to achieve a measurement volume of **40 mm x 40 mm x 6 mm** with a measurement uncertainty of position of **1 nm** (k = 1). (The stated uncertainty goal does not include the uncertainty contribution of the probe.) The translation of the sample is accomplished with multiple stages which allow for separate coarse and fine motion. Interferometers and

---

[1013] LNE Dimensional Nanometrology, 2009; http://74.125.19.132/translate_c?hl=en&sl=fr&u=http://www.lne.eu/en/r_and_d/nanometrology/dimensional-nanometrology.asp&prev=/search%3Fq%3DDucourtieux,%2BS.%2BDuhem,%2BF.%2BLarsonnier,%2BJ.%2BSalgado,%2BG.%2BP.%2BVailleau,%2BL.%2BLahousse%26hl%3Den%26sa%3DG&rurl=translate.google.com&usg=ALkJrhjnpETiKYd70y1rCjL78Ru1IjT7jQ.

[1014] Brian J. Eves, "Design of a large measurement-volume metrological atomic force microscope (AFM)," Meas. Sci. Technol. 20(2009):084003.

autocollimators are used to measure the position and orientation of the sample. Interestingly, the instrument does not attempt to control position via feedback from the interferometers, thereby allowing use of readily available commercial translation stages and controllers. The mAFM was apparently designed to operate in air, not vacuum.

A diagram of the metrological AFM is shown in Figure 4-38. The mAFM design can be conveniently described in four sections, summarized below: (1) the translation stages, (2) the metrology frame and position sensors, (3) the control system, and (4) the AFM sensor. Most of the following discussion is drawn directly from the paper.[1015]

Figure 4-38. A diagram of the NRC metrological atomic force microscope (mAFM).[1016] For scale, the granite base plate has a diameter of 550 mm.

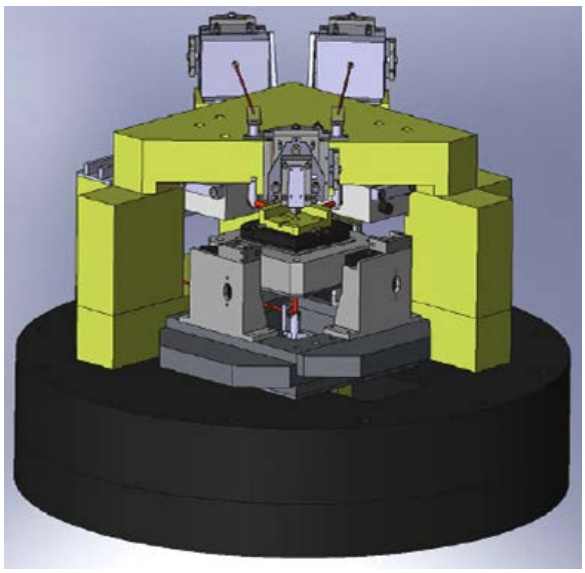

(1) **Translation Stages.** The main design challenge for the mAFM is the large measurement volume, a requirement that adds complexity to the design of the translation stages and increases the magnitude of the uncertainty contribution of the index of refraction of air (absent for *in vacuo* systems), the effects of thermal expansion, and various alignment errors. To minimize this additional complexity, the range over which translation occurs to sub-nanometer accuracy is limited to an area commensurate with a typical AFM scan range. The key is to only *measure* the position with sub-nanometer uncertainty and not to attempt to *control* the position

[1015] Brian J. Eves, "Design of a large measurement-volume metrological atomic force microscope (AFM)," Meas. Sci. Technol. 20(2009):084003.

[1016] Brian J. Eves, "Design of a large measurement-volume metrological atomic force microscope (AFM)," Meas. Sci. Technol. 20(2009):084003.

with low uncertainty. This design approach enables the use of readily available commercial translation stages and changes only the measurement procedure for a specific measurand, when compared to a large scan range system, while not limiting the measurement capabilities of the instrument. The mAFM translation stages move the sample, holding the probe position fixed which enables the relative positions of the interferometers to remain constant with respect to the probe position, thus minimizing the Abbe errors.

A schematic of the translation stages is shown in Figure 4-39. A coarse set of translation stages moves a fine XY translation stage into an approximate position. The coarse XY translation stage is a Steinmeyer KDT180-1 which has a travel range of 100 mm x 100 mm and an encoder resolution of **100 nm**. The coarse Z travel is accomplished with a three-point lift using three Physik Instrumente (PI) M111.1DG stages. They have a travel range of 15 mm, a minimum incremental motion of 50 nm and an encoder resolution of **7 nm**. Constant force springs have been added to reduce the loading due to gravity. A PI P-734 flexure stage is kinematically mounted to the three Z stages and provides 100 µm x 100 µm of travel. Capacitance sensors supply position feedback for the flexure stage with a closed-loop resolution of **300 pm**. The zero of the machine coordinate system is defined by the home position on the KDT180 encoders (X- and Y-axes) and by the average of the encoder readings at the three end limits of the M111.1DG stages (Z-axis). All the translation stages described are predominately made from aluminum in the first prototype. Note that the translation stages described above lack sufficient resolution along the Z-axis to perform AFM measurements. Only coarse translation along the Z-axis is provided in the mAFM, and a separate fine Z-axis stage must be supplied by the AFM head (described later). The separation of the Z-axis motion into two independent translation stages is required to achieve a high positioning bandwidth for AFM operation. The relatively large mass and hence inertia of the sample and sample holder precludes incorporation of the fine Z motion into the translation stage system.

Figure 4-39. Diagram of the translation stages used in the mAFM. The coarse XY stage has a travel range of 100 mm x 100 mm, the coarse Z translators have a travel range of 15 mm and the fine XY stage has a travel range of 100 µm x 100 µm.[1017]

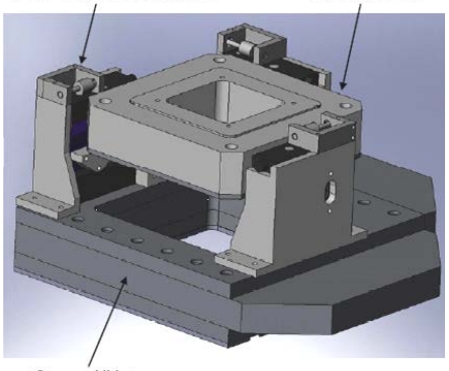

[1017] Brian J. Eves, "Design of a large measurement-volume metrological atomic force microscope (AFM)," Meas. Sci. Technol. 20(2009):084003.

The potential for rotational errors during motion with this translation system is significant. The cause of the errors is the stacking of multiple translation stages upon one another. The three-point lift used for the coarse Z-axis motion is especially problematic as rotations about the X- and Y-axes rely upon the relative consistency of the closed-loop positioning of all three stages. As a means of helping to compensate for the Abbe errors induced by the rotational errors, a set of six piezo actuators are used to generate small rotations about all three axes as shown in Figure 4-40. The rotation stage is mounted on the XY flexure stage and supports the Zerodur sample holder. The top portion of the rotation stage induces rotation about the X- and Y-axes and kinematically supports the sample holder. The bottom half of the stage induces rotations about the Z-axis through three shear piezos and kinematically supports the top half. As well as being used to compensate for the Abbe error, they are also used to help determine the form of the interferometer mirrors. The piezo actuators provide up to 30 μrad of rotation about the X- and Y-axes, and 75 μrad of rotation about the Z-axis.

Figure 4-40. Exploded view of the small angle rotation stage. The three shear piezos induce rotation about the Z-axis, while the other three piezos induce rotations about the X- and Y-axes.[1018]

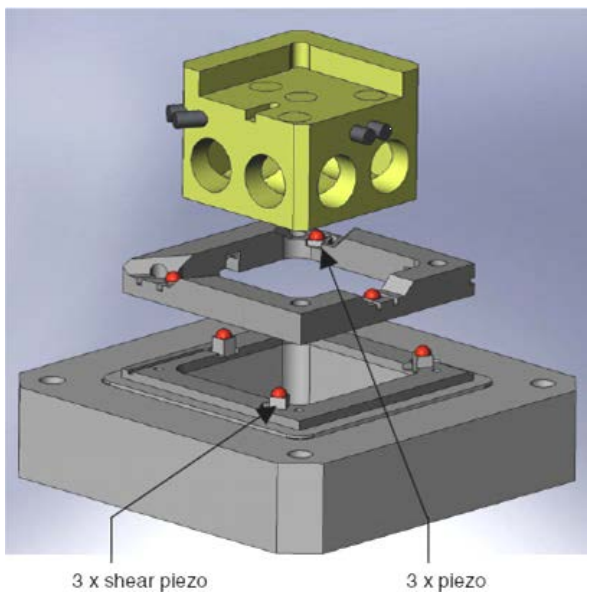

(2) **Metrology Frame and Position Sensors.** Displacement of the sample is measured by three laser interferometers, each of which is a single-pass homodyne interferometer made by SIOS (SP 2000 on custom Invar base) and have an 8-bit interpolation resolution of ~500 pm. Averaging of multiple measurements or the introduction of a 16-bit analog-to-digital converter is

[1018] Brian J. Eves, "Design of a large measurement-volume metrological atomic force microscope (AFM)," Meas. Sci. Technol. 20(2009):084003.

required to achieve the stated uncertainty goal of **1 nm** positioning uncertainty. The lasers are aligned orthogonal to each other and define the three Cartesian axes as shown in Figure 4-41A. The intersection region of the lasers defines the probe position, thus Abbe errors are minimized for probes centered in this region. The interferometers are supported by a relatively large frame which also holds the AFM sensor. The thermal expansion of the frame, which is proportional to the separation distance between the interferometers and the probe, is minimized by using Zerodur as the main construction material. A mirror cube comprises the sample holder and is also made of Zerodur. A pocket machined into the cube defines the sample region. The resonant frequencies of the Zerodur frame determine the level of coupling between external vibrations and the measurement. Note that oscillations of the sample holder due to vibration of the translation stages will not affect the measurement because vibrations of the sample holder will be detected by the interferometers. The main source of noise is expected to be the vertical oscillation of the AFM sensor head and the vertical oscillation of the Z-axis interferometer. Finite element analysis of the frame yields the lowest resonant frequency at approximately 1500 Hz. The vibration-isolation platform upon which the AFM sits has resonant frequencies less than 2 Hz, hence a reduction of vibration by approximately 6 x 10^5 for frequencies between 2-1500 Hz.[1019] A complication to the above simple analysis is the presence of a bending mode of the tabletop at approximately 30 Hz. It is likely that some form of damping, e.g., eddy current damping, will need to be employed to reduce this source of vibration coupling.

Figure 4-41. (A) Left: Metrology frame and arrangement of *XYZ* interferometers for definition of the coordinate system; (B) Right: Design of the autocollimators.[1020]

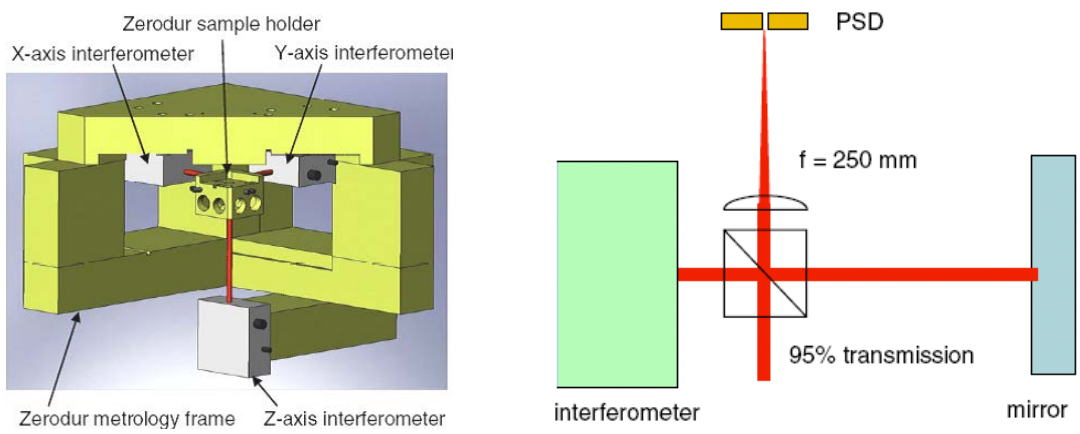

The rotational errors caused by the translation stages are determined by three separate autocollimators which measure the orientation of the mirror cube. A schematic showing the design of the autocollimators is shown in Figure 4-41B. The autocollimators sample a small

---

[1019] C.J. Chen, Introduction to Scanning Tunneling Microscopy, Oxford University Press, New York, 1993, p. 242.

[1020] Brian J. Eves, "Design of a large measurement-volume metrological atomic force microscope (AFM)," Meas. Sci. Technol. 20(2009):084003.

portion of the return interferometer beam intensity and hence measure the orientation of the mirror surface coincident with the position at which the mirror surfaces displacement is measured. Three main measurement capabilities are possible through the use of the autocollimators. The Z-axis autocollimator provides a mechanism for maintaining the orientation of the XY flexure stage as it is traversed up or down the Z-axis. The angle measurements from all three autocollimators orient the sample holder and enable the implementation of an Abbe error correction scheme. Lastly, the autocollimators are used to measure the form error of the mirrors.

(3) **Control System.** The control systems supplied by the manufacturers are used to control the various translation stages described above. We do not attempt to control the position of the sample via the interferometer readings and the sample is free to drift as a function of, for instance, temperature. The synchronization of various translation and measurement subsystems is an important issue and is made more difficult by the use of commercial equipment. It is important that the interferometer measurements, the autocollimator measurements and the AFM position sensor all measure synchronously. A digital signal processor (DSP) is used to coordinate between various sub-systems and also synchronously records the interferometer, autocollimator and AFM head signals with the aide of a 16-channel 16-bit analog-to-digital converter at a maximum rate of 25 kHz. Initial tests on the analog-to-digital converter show that the maximum time delay between any two channels to acquire a sample reading is less than 250 ns, and that the time delay repeatability is less than 10 ns.

(4) **AFM Sensor.** Quartz tuning forks are used as the sensing element for the feedback mechanism of the AFM. Such a system is less complicated to build and incorporate into an AFM sensor when compared to traditional optical force detectors. The use of quartz tuning forks as sensors for force detection in scanning probe microscopy goes back to 1989,[1021] and have been used to achieve atomic resolution images in ultra-high vacuum.[1022] Quartz tuning forks have a number of features which make them attractive for metrology purposes. The sensitivity of the tuning fork resonance frequency to temperature is significantly better than that for silicon cantilevers.[1023] A further benefit is the absence of optical interference effects caused by scattered light off of both the cantilever and surface. Probes attached to the tuning forks will include either etched tungsten tips or micro-fabricated silicon tips.

The AFM sensor comprises a 6-degree-of-freedom stage, a Z-axis flexure stage and a detection system built around a quartz tuning fork. The 6-degree-of-freedom stage is simply for positioning the AFM probe so as to minimize the Abbe offsets and for orienting the Z-axis of the flexure stage approximately to the Z-axis defined by the interferometer. The Z-axis flexure stage (PI P-753.11) has 12 μm of travel with a closed-loop resolution of **50 pm**. As the AFM sensor is part of the metrology loop, both the 6-degree-of-freedom stage and the Z-axis flexure stage are made from Invar. The detection system is a quartz tuning fork coupled to an electronic circuit

---

[1021] P. Güthner, U.C. Fischer, K. Dransfeld, "Scanning near field accoustic microscopy," Appl. Phys. B: Laser Opt. 48(1989):89-92.

[1022] F.J. Giessibl, S. Hembacher, H. Bielefeldt, J. Mannhart, "Subatomic Features on the Silicon(111)-(7x7) Surface Observed by Atomic Force Microscopy," Science 289(2000):422-425.

[1023] Franz J. Giessibl, "Advances in atomic force microscopy," Rev. Mod. Phys. 75(2003):949-983.

that both drives the oscillations of the tuning fork and measures the oscillations via the piezoelectric effect.[1024] A schematic of the sensor head is shown in Figure 4-42. Note that the attachment of the quartz tuning fork to the flexure stage has yet to be finalized and is not accurately portrayed.

Figure 4-42. The diagram of the AFM sensor which comprises a 6-degree-of-freedom translation stage, a Z-axis flexure stage and a quartz tuning fork. Note that the X- and Y-axes are not collinear with the X- and Y-axes of the sample translation stages.[1025]

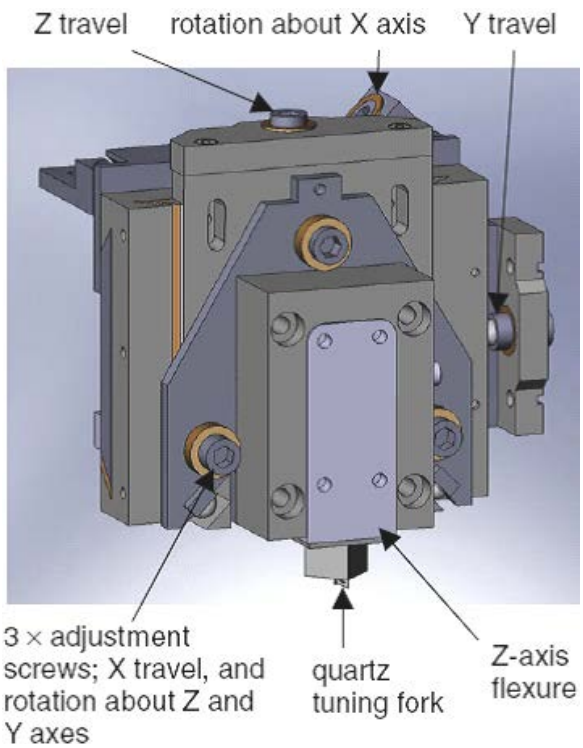

As of September 2008, the stacked translation stages had been assembled and integrated into the custom control software. The components for the autocollimators and the AFM head had been built and were awaiting assembly and a prototype of the metrological frame had been built using aluminum instead of Zerodur. Once the autocollimators, interferometer mounts, translation stages and AFM head have been shown to work, the Zerodur metrology frame will be built based upon the prototype. A significant portion of the software which allows the various control sub-systems to interact had been written and the system was expected to be functioning at a basic

---

[1024] C.L. Jahncke, O. Brandt, K.E. Fellows, H.D. Hallen, "Choosing a preamplifier for tuning fork signal detection in scanning force microscopy," Rev. Sci. Instrum. 75(2004):2759-2761.

[1025] Brian J. Eves, "Design of a large measurement-volume metrological atomic force microscope (AFM)," Meas. Sci. Technol. 20(2009):084003.

level of operation by Fall of 2009. However, it was expected to take until year-end 2011 before the mAFM would be fully characterized and a suitable uncertainty budget developed.

4.6.1.7 Dual-Level Translation Stage (CEA, INM/CNAM, LIRIS, LNIO, France)

The work on picometer-scale displacement control using heterodyne interferometry recently reported (2005-7) by the Chassagne group in France[1026] and described below (Section 4.6.3.10) is part of a larger integrated project in the nanoscience field. The aim of this larger project is to control the displacement of the holding sample of the near field probe microscope over a **1 mm course** and with an **uncertainty of 1 nm**. For this purpose, Chassagne's group plans to use their positioning control method in a dual-level translation stage composed of an air-bearing long-range translation stage with a piezoelectric actuator. The Chassagne group (at LIRIS (University of Versailles) and at INM/CNAM, France) is working in close collaboration with the University of Technology of Troyes (LNIO) and the CEA (LTM).

4.6.1.8 AFM Head for Nano-Measuring Machine (Tsinghua University, China)

From the group's abstract:[1027] "An atomic force microscope (AFM) head designed for nanometrology is accomplished in this study. It is the sensing component of the nano-measuring machine, a nanometrological instrument with a working range of **50 mm x 50 mm x 2 mm**, as well as a part of the metrological system of the instrument. Three reference mirrors are mounted on the head and arranged without Abbe error. Relative displacement of the AFM head and the specimen is measured by interferometers and results are traceable. The optical beam deflection method is used to detect the atomic force. The laser beam is introduced through a single-mode polarization-maintaining optical fiber from an external laser diode. With a compact design, a 100 mm optical lever is realized inside the AFM head that is less than 20 mm in thickness and 200 g in weight. A force-distance curve is obtained using a gauge block in a test. Furthermore, online tests of the measurement of a step scale have been made. According to the calculation and experimental verification, the resolution of our AFM head reaches **50 pm**."

[1026] Luc Chassagne, Suat Topcu, Yasser Alayli, Patrick Juncar, "Highly accurate positioning control method for piezoelectric actuators based on phase-shifting optoelectronics," Meas. Sci. Technol. 16(2005):1771-1777. L. Chassagne, M. Wakim, S. Xu, S. Topcu, P. Ruaux, P. Juncar, Y. Alayli, "A 2D nano-positioning system with sub-nanometric repeatability over the millimetre displacement range," Meas. Sci. Technol. 18(2007):3267-3272. S. Topcu, L. Chassagne, D. Haddad, Y. Alayli, P. Juncar, "Heterodyne interferometric technique for displacement control at the nanometric scale," Rev. Sci. Instrum. 74(2003):4876-4880.

[1027] Mingzhen Lu, Sitian Gao, Qihai Jin, Jianjun Cui, Hua Du, Hongtang Gao, "An atomic force microscope head designed for nanometrology," Meas. Sci. Technol. 18(2007):1735-1739.

4.6.1.9 6-DOF Laser Interferometry (Menq Group, Ohio State Univ.)

The Menq group in the Precision Measurement and Control Laboratory at Ohio State University has constructed a prototype six-axis actuated magnetic levitation stage which has no direct mechanical couplings.[1028] By using both a flat mirror and a retroreflector in each interferometer optical path,[1029] the modified Michelson heterodyne laser interferometer system is capable of simultaneously measuring large transverse motions along and large rotational motions about three orthogonal axes while retaining the inherent precision provided by interferometry. The resolution achieved by the prototype is **1.24 nm** in translation and tens of nanoradians in rotation, over a travel range of **5 mm x 5 mm x 5 mm** in translation and 8° x 8° x 8° in rotation, thus allowing both large rotational and transverse motions while maintaining nanometer resolution.[1030]

In other work by the same group,[1031] a compact six-axis compliant stage employs piezoelectric actuators to achieve six-axis actuation with nanometer resolution (Figure 4-43). Experimental results demonstrate that the six-axis compliant stage has the motion range of 77.42 μm x 67.45 μm x 24.56 μm and 0.93 mrad x 0.95 mrad x 3.10 mrad, with the ability to measure at a resolution of ±5 nm x ±8 nm x ±10 nm and ±10 μrad x ±10 μrad x and ±20 μrad, for X-axis, Y-axis, and Z-axis translation and rotation, respectively.

Figure 4-43. A compact six-axis compliant stage with nanometer resolution.[1032]

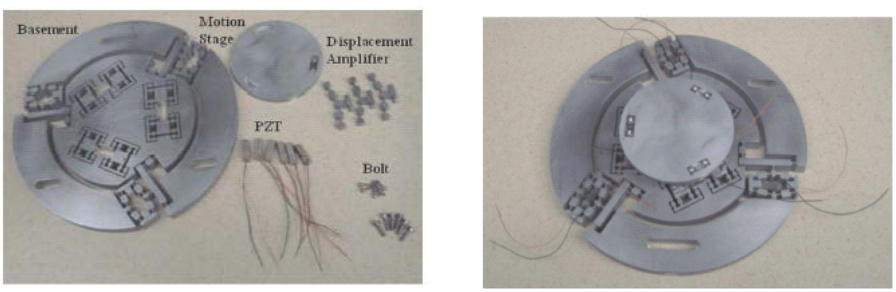

[1028] Zhipeng Zhang, Chia-Hsiang Menq, "Six-Axis Magnetic Levitation and Motion Control," IEEE Trans. Robotics 23(April 2007):196-205.

[1029] J.-H. Zhang, C.-H. Menq, "A linear/angular interferometer capable of measuring large angular motion," Meas. Sci. Technol. 10(December 1999):1247-1253; Chia-Hsiang Menq, Ji-Hua Zhang, Jian Shi, "Design and development of an interferometer with improved angular tolerance and its application to x-y theta measurement," Rev. Sci. Instrum. 71(2000):4633-4638.

[1030] Zhipeng Zhang, Chia-Hsiang Menq, "Laser interferometric system for six-axis motion measurement," Rev. Sci. Instrum. 78(August 2007):083107.

[1031] Kaixuan Hu, Jung H Kim, James Schmiedeler, Chia-Hsiang Menq, "Design, implementation, and control of a six-axis compliant stage," Rev Sci Instrum. 79(February 2008):025105.

[1032] Kaixuan Hu, Jung H Kim, James Schmiedeler, Chia-Hsiang Menq, "Design, implementation, and control of a six-axis compliant stage," Rev Sci Instrum. 79(February 2008):025105.

The group is also investigating: (1) multiaxis atomic force microscopes,[1033] (2) large range linear encoders with 60 pm measurement resolution and measurement accuracy in the nanometer order after calibration (with measurement range is only limited by the size of the reference grating employed),[1034] and (3) experimental demonstration of visually servoed 3-D alignment, in which two microcantilevers are aligned in a 3D workspace with alignment errors below 1 nm (rms) in all axes and with nanostepping of 0.5 nm magnitude along the out-of-plane z-axis also performed between the two microcantilevers.[1035]

4.6.1.10 Parallel-Kinematics Nanopositioner (Univ. of Illinois)

The Ferreira group in the Department of Mechanical Science and Engineering at the University of Illinois at Urbana-Champaign has designed and built a parallel-kinematics XYZ nanopositioning (PKXYZNP) stage for general nanomanipulation and nanomanufacturing applications.[1036] The stage has a low degree-of-freedom monolithic parallel-kinematic mechanism featuring single-axis flexure hinges (Figure 4-44). The stage is driven by piezoelectric actuators and its displacement is detected by capacitance gauges. The control loop is closed at the end effector instead of at each joint, so as to avoid calibration difficulties and to enable high positioning accuracy. Using the capacitive gauges, the stage is capable of about **85 µm of motion** along each axis with a resolution of about **2-4 nm**.[1037]

[1033] G.R. Jayanth, Sissy M. Jhiang, C.H. Menq, "Two-axis probing system for atomic force microscopy," Review of Scientific Instruments 79(2008):023705.

[1034] Y. Huang, C.H. Menq, "Design and Development of a Large Range Linear Encoder with Subnanometer Resolution," Review of Scientific Instruments 77(2006):105104.

[1035] J. Kim, C.H. Menq, "Visually Servoed 3D Alignment of Multiple Objects with Sub-Nanometer Precision," IEEE Transactions on Nanotechnology 7(May 2008):321-330.

[1036] Jingyan Dong, S.M. Salapaka, P.M. Ferreira, "Robust MIMO control of a parallel kinematics nano-positioner for high resolution high bandwidth tracking and repetitive tasks," 46th IEEE Conference on Decision and Control, 12-14 December 2007, pp. 4495-4500. Qing Yao, Jingyan Dong, Placid M. Ferreira, "A novel parallel-kinematics mechanisms for integrated, multi-axis nanopositioning: Part 1. Kinematics and design for fabrication," Precision Engineering 32(January 2008):7-19. Jingyan Dong, Qing Yao, Placid M. Ferreira, "A novel parallel-kinematics mechanism for integrated, multi-axis nanopositioning: Part 2: Dynamics, control and performance analysis," Precision Engineering 32(January 2008):20-33. Jingyan Dong, Srinivasa M. Salapaka, Placid M. Ferreira, "Robust Control of a Parallel- Kinematic Nanopositioner," J. Dyn. Sys. Meas. Control 130(July 2008):041007. Y.H. Jeong, J. Dong, P.M. Ferreira, "Self-calibration of dual-actuated single-axis nanopositioners," Meas. Sci. Technol. 19(2008):045203, doi: 10.1088/0957-0233/19/4/045203.

[1037] Qing Yao, Jingyan Dong, Placid M. Ferreira, "A novel parallel-kinematics mechanisms for integrated, multi-axis nanopositioning: Part 1. Kinematics and design for fabrication," Precision Engineering 32(January 2008):7-19.

Figure 4-44. The PKXYZNP prototype.[1038]

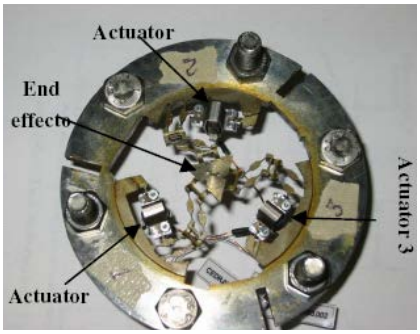

4.6.1.11 LRM-AFM (Singapore)

Within Singapore's National Measurement Laboratory, in 2006 their National Metrology Center (http://www.nmc.a-star.edu.sg/aboutus-programme.htm) announced "...development of nanometrology capabilities in dimensional area....setting up a **large range metrological atomic force microscope** for nanoscale measurement and a micro CMM for 3D measurement of small objects".[1039] According to the press release:

> "SPRING will in mid-2007 start offering nanometrology calibration and measurement services to industry in measurement areas of surface and form – using our **large range metrological atomic force microscope (LRM-AFM)** and micro-CMM facilities. Semiconductor, microelectronics, precision optics and precision engineering industries will be the first to benefit from the new nanometrology infrastructure at SPRING.
>
> As the national metrology authority, SPRING Singapore recognises the critical role that accurate measure.
>
> For a start, $10 million has been set aside to develop the capabilities in dimensional and optical measurements.
>
> From next year, the following new calibration and measurement services will be available to industry:
>
> 6. New nano calibration service for nano linear displacement sensor and nano positioning (piezo-electrical) devices – Linear sensor is used to detect/measure small movement of an object produced by some electrical-mechanical drive mechanism. An **accuracy in the range of sub-nanometre** is required by the most accurate positioning machines used in high-tech industries such as semiconductor, precision engineering, photonics and optics.
>
> 7. New nano calibration service for atomic force microscope (AFM) – AFM is a device that uses a spring-mounted probe to image individual atoms on the surface of a material. With its sub-nanometre resolution, AFM is one of the foremost tools for imaging, measuring and manipulating matter at the nano-scale. In Singapore, there are more than 200 AFMs used in semiconductor, electronics, telecom, biology and other high-tech industries and research institutes."

[1038] Jingyan Dong, S.M. Salapaka, P.M. Ferreira, "Robust MIMO control of a parallel kinematics nano-positioner for high resolution high bandwidth tracking and repetitive tasks," 46th IEEE Conference on Decision and Control, 12-14 December 2007, pp. 4495-4500.

[1039] "S$10 Million Nanometrology Capabilities to support Nanotechnology R&D Sector. Singapore first in ASEAN to develop nanometrology capabilities," Nanometrology Capabilities Media Briefing, 20 October 2006; http://www.spring.gov.sg/Content/PrintPage.aspx?group=nw&id=5a98217c-1771-43c2-aef7-f0fc6abfc189.

Figure 4-45. The Large Range Metrological Atomic Force Microscope.[1040]

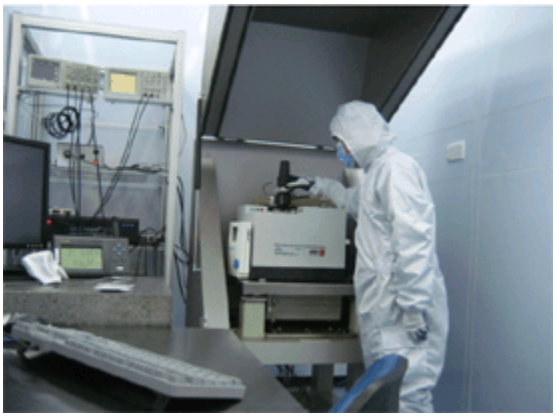

In 2008, NMC was transferred from SPRING Singapore to the Agency for Science, Technology and Research (A*STAR), effective from 1 January 2008.[1041] At the new A*STAR website[1042] we find an image of the LRM-AFM (Figure 4-45) and the following brief description, with no technical references or other details of the device:

"To support the measurement need in the fast moving nanotechnology development, the laboratory has planned its nanoscale capability since 2004. The two recent achievements are the setting up of a **Large Range Metrological Atomic Force Microscope (LRM-AFM)** and a Micro-Coordinate Measuring Machine (Micro-CMM)."

Large Range Metrological Atomic Force Microscope

"AFM is one of the most powerful tools for measurement of surface texture of micro- and nano-structures at sub-nanometre resolution with wide applications in nanotechnology. The LRM-AFM provides direct traceability lacked by commercial AFMs through three laser interferometers installed in its metrological frame. The system is also featured with a very large scanning range and small **uncertainty of better than 10 nm**. An optical probe can replace the AFM head in the system for non-contact measurement."

[1040] A*STAR's website: http://www.nmc.a-star.edu.sg/metrology-LDM-NM.htm.

[1041] "The National Metrology Centre was transferred from SPRING Singapore to the Agency for Science, Technology and Research (A*STAR) on 1 January 2008," http://www.spring.gov.sg/Content/WebPage.aspx?id=29c808ca-454e-42f5-8d77-4993f07a9069.

[1042] A*STAR's website: http://www.nmc.a-star.edu.sg/metrology-LDM-NM.htm.

4.6.1.12 DIU-AFM (Zhang group, Zhejiang University, China)

A dual-imaging-unit atomic force microscope (DIU-AFM) was developed for wide-range length metrology.[1043] In the DIU-AFM, two AFM units were combined, one as a reference unit, and the other a test one. Their probes with Z piezo elements and tips were horizontally set in parallel at the same height to reduce errors due to geometric asymmetry. An XY scanner was attached to an XY block that was able to move in the X direction with a step of about 500 nm. A standard porous alumina film was employed as the reference sample. Both reference sample and test sample were installed at the center of the XY scanner on the same surface and were simultaneously imaged. The two images had the same lateral size, and thus the length of the test sample image could be accurately measured by counting the number of periodic features of the reference one. The XY block together with the XY scanner were next moved in the X direction for about 1.5 micron and a second pair of reference and test images were obtained by activating the scanner. In this way, a series of pairs of images were acquired and could be spliced into two wide-range reference and test images, respectively. Again, the two spliced images were of the same size and the length of test image was measured based on the reference one. Experiments show the ability of the apparatus to make wide-range length metrology measurements based on the hexagonal features of the porous alumina with a periodic length of several tens of nanometers. The DIU-AFM method (having 2 tips present in the workspace) is asserted to be capable of realizing nanometer-order accuracy length metrology when covering a wide range from microns to several hundreds of microns, or even up to millimeter order.

4.6.1.13 Magnetic Levitation Stage (Tsinghua University, China)

A novel magnetic levitation stage that could provide large range motion with nanometer positioning accuracy was proposed in 2004 by another group at Tsinghua University.[1044] The construction, dynamics analysis, measurement system, and control strategy of this stage were presented and discussed in the initial paper. In 2006, further results were reported:[1045] A height measurement and calibration of the stage using a triplex heterodyne interferometer is presented. This measurement system mainly consists of three parts: one 2-frequency He-Ne laser, three heterodyne interferometers, and three phase meters. Each heterodyne interferometer is used to measure the displacement of the magnetic levitation stage in the vertical direction, allowing the nanometer measurement of three degrees of freedom motion for the stage (i.e., translation in the Z-axis and rotations around the X- and Y-axes) using the triplex heterodyne interferometer. Since the three heterodyne interferometers have a common planar reflecting mirror, the

---

[1043] D. Zhang, H. Zhang, X. Lin, "Wide-range length metrology by dual-imaging-unit atomic force microscope based on porous alumina," Microsc. Res. Tech. 64(15 June 2004):223-227.

[1044] Benyong Chen, Junru Wang, Yong Lei, "Progress in large-range and nanoscale micromotion stage," Proc. SPIE 5641(November 2004):348-353.

[1045] Benyong Chen, Guizhen Zhang, Liqiong Zhang, Ting Zhong, "Nanometer measurement of the planar motion of a magnetic levitation stage based on optical heterodyne interferometry," Proc. SPIE 6024(25 January 2006):60241J.

heterodyne interference can ensure good height control for the stage within the entire travel range wherever the stage travels.

4.6.1.14 Nanorobotics Technologies (Univ. Nottingham, UK)

An EPSRC grant for £ 254,379, for a project called "BASIC TECHNOLOGY: Nanorobotics – Technologies for Simultaneous Multidimensional Imaging & Manipulation of Nanoobjects" running from 01 November 2004 to 30 April 2009, was awarded to P.H. Beton and Philip Moriarty at the University of Nottingham, UK. The project partners are listed as the Indian Institute of Science, Nanomagnetics Ltd., National Physical Laboratory (NPL), and QinetiQ (Malvern), who received an additional £ 1,847,850 under related EPSRC Grant GR/S85689/01 and £ 294,805 under related EPSRC Grant GR/S85696/01, for a total expenditure on this project of £ 2,397,034 (about $4M).

The grant description,[1046] which fairly clearly sounds like a positionally controlled SPM system intended to perform nano-assembly operations with multiple DOFs, reads as follows:

> "Novel miniaturised piezo-controlled nanopositioning and nanomanipulation systems, with intelligent mechanical and electronic sensors and control, will be designed and constructed to form a multipurpose NANOLAB to be integrated into the specimen chambers of transmission electron microscopes. Special features of the new nanorobotics technologies will include:
>
> (i) Integration of TEM nanopositioning with in-situ laser interferometry: For sub nm-accuracy measurements of displacements (enabling evaluation of force) with visual observation up to 1 million magnification.
>
> (ii) 5-Degree-of-freedom actuation: Translation in all three cartesian directions xyz will enable a (e.g., tip-shaped) test object to be brought into contact with a (e.g., substrate surface) target object for dynamical mechanical (nanoindentation), chemical and electrical (including STM) testing at the contact point. Additionally rotation in one, possibly two directions, will enable in-situ 3D reconstruction of observed nanostructures by nanotomography. Novel nanotools will be developed for nanoscale manipulation of objects whilst imaging with the TEM.
>
> (iii) Intelligent nanorobot control: High-power vision based computing will allow (near) real-time tracking and automated control of the position and function of the nanorobot arm with respect to a possibly moving target by means of fast image processing algorithms. This feature qualifies our device as a "nanorobot".
>
> We will test our nanorobotics NANOLAB in some of the most promising application areas, including manipulation of fullerenes, magnetic particles, biomaterials/scaffolds, semiconductor and MEMS devices."

In a personal communication in late 2008, Moriarty suggested that his involvement with this project is only peripheral and that he's only loosely involved. Moriarty says that the University of Sheffield is actually the lead organization on this effort and the project had only a short time left to run. Moriarty says that the group has gotten a 4-DOF STM to work, but with an accuracy of only 5-10 nm. In the device, stepper motors rotate an XYZ scanning probe tip which is itself mounted at the center of an annular system that rotates axially inside a TEM tube. This implies

---

[1046] P.H. Beton, Philip Moriarty, "Basic Technology: Nanorobotics - Technologies for Simultaneous Multidimensional Imaging & Manipulation of Nanoobjects," School of Physics & Astronomy, University of Nottingham, EPSRC Reference GR/S85702/01, EPSRC Research Topic Classifications: Control Systems Engineering, Integration and Autonomy, Microsystems, Robotics, Assembly, and Automatic Handling, 01 November 2004 to 30 April 2009, http://gow.epsrc.ac.uk/ViewGrant.aspx?GrantRef=GR/S85702/01. Related grants GR/S85689/01 and GR/S85696/01.

that at least one rotational DOF has been experimentally demonstrated in an SPM positioning system over very large angular displacements, but with only **5-10 nm precision**.

The Univ. of Nottingham website[1047] provides a bit more information, along with an image of the device (Figure 4-46), as follows:

> The STM-TEM and nanoscale electrical testing project is part of the **Nanorobotics - technologies for simultaneous multidimensional imaging and manipulation of nano-objects** research program, a collaboration between the University of Nottingham, the University of Sheffield, and Sheffield Hallam University, funded by the EPSRC. The objective of this program is to combine the previously separate technologies of transmission electron microscopy, nanoindentation, 3D-reconstruction of nano-objects and scanning probe microscopy. At the Nottingham Nanoscience group, we have designed an STM that is compatible with the 2010F JEOL TEM. This STM can fit precisely into the TEM sample holder slot, allowing simultaneous acquisition of both STM and TEM data. This technology offers advantages over normal STM, such as:
>
> * STM can be guided to points of interest via the TEM, particularly useful for manipulation of nano-objects.
> * STM tip shape and structure can be dynamically monitored via TEM during scanning.
> * TEM acquires data regarding the bulk properties of a sample and STM gathers data on the surface structure, simultaneous acquisition of both sets of data provide a more comprehensive examination of a sample.
>
> Throughout instrument's development we have also collaborated with Nanograph Systems,[1048] a spin-off company from the Nottingham Nanoscience group, to produce the software and electronics necessary to perform the experimental techniques required for in-situ STM.

Figure 4-46. The STM-TEM configured for use with the 2010F JEOL TEM.[1049]

A few papers have been published reporting progress on this project.[1050]

[1047] http://www.nottingham.ac.uk/physics/research/nano/content-tech-tem.htm.
[1048] http://www.nanographsystems.co.uk/.
[1049] http://www.nottingham.ac.uk/physics/research/nano/content-tech-tem.htm.

[1050] M.S. Bobji, C.S. Ramanujan, J.B. Pethica, B.J. Inkson, "A miniaturized TEM nanoindenter for studying material deformation in-situ," Meas. Sci. Technol. 17(2006):1324-1329. A.J. Lockwood, J.J. Wang, R. Gay, B.J. Inkson, "Characterising ambient and vacuum performance of a miniaturised TEM nanoindenter for in-situ materials deformation," J. Phys. Conf. Proc. (EMAG2007) 126(2007):012095. X.J. Xu, A. Lockwood, W. Guan, R. Gay, Z. Saghi, J.J. Wang, Y. Peng, B.J. Inkson, G. Möbus, "Full-tilt Electron

4.6.1.15 Directed Reconfigurable Nanomachines (Univ. Nottingham, UK)

An EPSRC grant for £ 219,754, for a project called "Directed Reconfigurable Nanomachines" running from 03 December 2007 to 02 December 2010, was awarded to Philip Moriarty and two other researchers at the University of Nottingham, UK. Other funding included £ 208,318 under related EPSRC Grant EP/F00981X/1 running from 01 April 2008 to 31 March 2011, £ 205,294 under related EPSRC Grant EP/F009410/1 running from 01 November 2007 to 31 October 2010, and £ 80,600 under related EPSRC Grant EP/F010109/1 running from 01 May 2008 to 30 April 2011, for a total expenditure on this project of £ 713,966 (about $1.4M).

The grant description,[1051] which sounds like it is purposed toward a scanning-probe-based positional molecular assembly system, reads as follows:

"We propose a scheme to revolutionise the synthesis of nanodevices, nanomachines, and, ultimately, functional materials via the positional assembly of molecules and nanoscale building blocks. **Computer-directed actuators** will be used to drive (with sub-nanometre to **sub-Angstrom precision**) the elements of a nanosystem along pre-defined and **entirely deterministic trajectories**, thereby achieving structures not accessible by mimicking natural assembly strategies alone. Linkages and bonding between the building blocks will also be initiated, modulated, and -- in some cases -- terminated by direct computer control. Our proposal rests on the parallel development of novel surface-bound, reconfigurable nanoscale building blocks (molecules, functionalised clusters, nanoparticles) and advanced techniques for **automated assembly of matter**. We focus on the generation of two major and immensely challenging functionalities for **positionally-assembled nanomachines**: switchable energy transduction and conformationally-driven motion. Our archetypal system comprises the following units: an energy harvester, a switchable/gateable link, and an optical or mechanical output. By arranging, configuring, and triggering these fundamental units our long-term goal is no less than the fabrication of an autonomous, abiotic nanomachine."

In a personal communication in 2008, Moriarty suggested that his involvement with this project is again only peripheral, that the research does not involve diamond, and that the objects to be manipulated an assembled are mostly large nanoscale entities that are not atomically precise. Also, the techniques of "switchable energy transduction" and "conformationally-driven motion" appear not to include mechanosynthesis, though further details on the intent and progress of this project would be welcome.

Tomography with a Piezo-actuated Rotary Drive," Microscopy Research and Technique 71(September 2008):773-777.

[1051] Philip Moriarty, J.J. Baumberg, Robert G. Jones, "Directed Reconfigurable Nanomachines**,"** School of Physics & Astronomy, University of Nottingham, EPSRC Reference EP/F009852/1, EPSRC Research Topic Classifications: Computational and Theoretical Chemistry, Design and Testing Technology, Theoretical Materials Science, 03 December 2007 to 02 December 2010, http://gow.epsrc.ac.uk/ViewGrant.aspx?GrantRef=EP/F009852/1 . Related grants EP/F00981X/1, EP/F009410/1, and EP/F010109/1.

4.6.1.16 Other Large-Range Systems

(1) In the Rosielle group at Eindhoven University of Technology (TUE) there appear to be three tracks of relevant activity. The first project is a high-precision 3D Coordinate Measuring Machine (CMM).[1052] Although the 50 mm x 50 mm x 4 mm working volume is large, the stated target accuracy for the CMM is only **20-25 nm** which is completely unusable for our purposes.[1053] The second TUE project is NANOMEFOS, which appears to be a technology for measuring the optical surface of a very large telescope mirror to within nanometer accuracy.[1054]

[1052] J.P.M.B. Vermeulen, P.C.J.N. Rosielle, P.H.J. Schellekens, "Innovations in the design and development of ultraprecision Machines," Proc. ASPE (November 1996):631-636. H. Haitjema, P.C.J.N. Rosielle, H. Steijaert, "A Calibration Platform for Generating Parallel Displacements with Nanometre Accuracy," in: H. Kunzmann et al., eds., Progress in Precision Engineering and Nanotechnology, Braunschweig, Germany, 1997, pp. 456-459. M.M.P.A. Vermeulen, "High-Precision 3D Coordinate Measuring Machine," PhD Thesis, Technische Universiteit Eindhoven, 1999 (Advisors: P.H.J. Schellekens, H.F. Van Beek; co-advisor: P.C.J.N. Rosielle). A. Jansen, P.C.J.N. Rosielle, P.H.J. Schellekens, "A fully elastically guided three-dimensional CMM with a measurement volume of 1 cm^3," Monterey, United States, ASPE 1999, pp. 453-456. J.K. van Seggelen, P.C.J.N. Rosielle, P.H.J. Schellekens, "Design of a 3-D CMM with elastically guided z-axis and x,y axis with less than 2 mm ABBE offset," in: Delbressine, Schellekens, Homburg, Haitjema, eds., 3rd International Conference and 4th General Meeting of EUSPEN, Eindhoven, Netherlands, 2002, pp. 29-32. J.K. van Seggelen, P.C.J.N. Rosielle, P.H.J. Schellekens, H.A.M. Spaan, R. Bergmans, "Design of a 3D-Coordinate Measuring Machine for measuring small products in array," in: R.J. Hocken, G.W. Caskey, E.P. Morse, eds., ASPE Summer Topical Meeting on Coordinate Measuring Machines, UNC Charlotte, United States, 2003, pp. 39-42; http://yp.wtb.tue.nl/showabstract.php/3082. J.K. van Seggelen, P.C.J.N. Rosielle, P.H.J. Schellekens, H.A.M. Spaan, R. Bergmans, G. Kotte, "Guides with nanometer repeatability for a 3D CMM," in 4th EUSPEN International Conference and 6th Annual General Meeting, Glasgow, United Kingdom, 2004, pp. 224-225; http://yp.wtb.tue.nl/showabstract.php/4355 J.K. van Seggelen, P.C.J.N. Rosielle, P.H.J. Schellekens, H.A.M. Spaan, R. Bergmans, G. Kotte, "An elastically guided machine axis with nanometer repeatability," Annals of the CIRP 54(2005):487-490. J.K.van Seggelen, "NanoCMM: A 3D Coordinate Measuring Machine with low moving mass for measuring small products in array with nanometer uncertainty," PhD Thesis, TU/e, 2007 (Advisors: M. Steinbuch, P.C.J.N. Rosielle). C. Werner, P.C.J.N. Rosielle, M. Steinbuch, "Design and realization of a long-stroke translation stage for SPM," presentation O2.8, Wednesday, 3 June 2009, 16:10-18:00, Session 2: Ultra Precision Machines & Control, International Conference of the European Society for Precision Engineering and Nanotechnology; http://www.sansebastian2009.euspen.eu/content/News-and-events/euspen-events/San%20Sebastian%202009/San%20Sebastian%20Programme/Session%202_Oral.pdf.

[1053] J.K. van Seggelen, P.C.J.N. Rosielle, P.H.J. Schellekens, H.A.M. Spaan, R. Bergmans, "Design of a 3D-Coordinate Measuring Machine for measuring small products in array," in: R.J. Hocken, G.W. Caskey, E.P. Morse, eds., ASPE Summer Topical Meeting on Coordinate Measuring Machines, UNC Charlotte, United States, 2003, pp. 39-42; http://yp.wtb.tue.nl/showabstract.php/3082.

[1054] R. Henselmans, P.C.J.N. Rosielle, J.P. Kappelhof, "NANOMEFOS (Nanometer Accuracy Non-contact Measurement of Free-form Optical Surfaces)," in: Thomas A. Dow, Kenneth P. Garrard, Alex Sohn, eds., ASPE Winter Topical Meeting on Free-form Optics: Design, Fabrication, Metrology and Assembly, Chapell Hill, North Carolina, United States, 2004, pp. 97-101, http://yp.wtb.tue.nl/showabstract.php/4162. R. Henselmans, P.C.J.N. Rosielle, M. Steinbuch, I.J. Saunders, "Design of a machine for the universal non-contact measurement of large free-form optics with 30 nm uncertainty," in: H. Philip Stahl, ed., Optical Manufacturing and Testing VI, San Diego, United States, 2005, pp. 586919-1-12, http://yp.wtb.tue.nl/showabstract.php/5304. L.A. Cacace, W.D. van Amstel, R. Henselmans, H. de Man,

The third TUE project is an interferometric metrology system for a space satellite called GAIA.[1055] Very impressive picometer-level stability is mentioned (i.e., the position stability requirement of the mirrors is a maximum shift of 1 pm in 6 hours). They are targeting angle-change measurements of ~1 picorad – for a ~1 meter-radius mirror that change would represent ~1 pm of linear motion for that mirror, which is really excellent accuracy.

(2) In the Steinbuch group at Eindhoven University of Technology (TUE), a legged stage has recently been designed but its accuracy is insufficient for our use by at least an order of magnitude. According to the abstract from their 2009 paper:[1056] "Piezoelectric actuators are commonly used for micropositioning systems at **nanometer resolution**. Increasing demands regarding the speed and accuracy are inducing the need for new actuators and new drive principles. A nonresonant piezoelectric actuator is used to drive a stage with 1-DOF through four piezoelectric drive legs. In order to improve the positioning accuracy of the stage, a new drive principle and control strategy for the walking piezomotor are proposed in this paper. The proposed drive principle results in overlapping tip trajectories of the drive legs, resulting in a continuous and smooth drive movement. Gain scheduling feedback in combination with feedforward control further improves the performance of the stage. With the developed drive principle and control strategy, the piezomotor is able to drive the stage at constant velocities between 100 nm/s and 1 μm/s with a tracking error below the encoder resolution of **5 nm**. Constant velocities up to 2 mm/s are performed with tracking errors below 400 nm. Point-to-

---

P.C.J.N. Rosielle, "Development of a new differential confocal optical probe with nanometer accuracy at large acceptance angles for measurement of free-form aspherics," in Proc. of Euspen Annual Meeting, Bremen, Germany, 2007, pp. 168-171. R. Henselmans, L.A. Cacace, P.C.J.N. Rosielle, M. Steinbuch, "Design and realization of a measurement machine for the universal non-contact measurement of large freeform optics with 30 nm uncertainty," in Proc. of Euspen Annual Meeting, Bremen, Germany, 2007, pp. 13-16, http://yp.wtb.tue.nl/showabstract.php/8190. R. Henselmans, L.A. Cacace, P.C.J.N. Rosielle, M. Steinbuch, "Design, realization and testing of the NANOMEFOS non-contact measurement machine for freeform optics," in ASPE Annual Meeting, Portland, Oregon, United States, 2008, http://yp.wtb.tue.nl/showabstract.php/9766.

[1055] A.A. van Veggel, H.J.P. Vink, P.C.J.N. Rosielle, H. Nijmeijer, A.A. Wielders, "Metrology concept design of the GAIA basic angle monitoring system," in: Joseph Antebi, Dietrich Lemke, eds., Astronomical Structures and Mechanisms Technology;, Glasgow, United Kingdom, Proceedings SPIE 5495(2004):11-22, http://yp.wtb.tue.nl/showabstract.php/4861. A.A. van Veggel, A.A. Wielders, H. Brug, van, P.C.J.N. Rosielle, H. Nijmeijer, "Experimental set-up for testing alignments and measurement stability of a metrology system in Silicon Carbide for GAIA," in: Alson E. Hatheway, ed., Optomechanics 2005, San Diego, California, United States, SPIE Proceedings 5877(2005):1-12, http://yp.wtb.tue.nl/showabstract.php/5754. A.A. van Veggel, W.J. Berkhout, M.K. Schalkx, A.A. Wielders, P.C.J.N. Rosielle, H. Nijmeijer, "Experimental evaluation of the stability and mechanical behavior of contacts in Silicon Carbide for the design of the basic angle monitoring system of GAIA," Paper 158, in: Karen Fletcher, ed., European Conference on Spacecraft Structures, Materials and Mechanical Testing, Noordwijk, Netherlands, 2005, http://yp.wtb.tue.nl/showabstract.php/5755. A.A.van Veggel, "The Basic Angle Monitoring system: picometer stability with Silicon Carbide optics," PhD Thesis, TU/e, 2007 (Advisors: H. Nijmeijer, P.C.J.N. Rosielle).

[1056] R.J.E. Merry, N.C.T. de Kleijn, M.J.G. van de Molengraft, M. Steinbuch, "Using a walking piezolegs actuator to drive and control a high precision stage," IEEE/ASME Trans. on Mechatronics 14(2009):21-31, http://yp.wtb.tue.nl/showabstract.php/9634.

point movements between 5 nm and the complete stroke of the stage are performed with a final static error below the encoder resolution."

4.6.2 Combined Optical and X-ray Interferometry (COXI) Systems

The ultimate limits of optical interferometry are governed by quantum physics.[1057] The two sources of quantum mechanical noise are photon-counting error (also known as shot noise) and radiation pressure. Only photon counting error is significant and it manifests itself as noise in the detector and variations in the laser power amplitude. The effects of the quantum noise were studied in the early 1990s,[1058] allowing interferometers to be designed where the quantum noise limit can be approached. Lawell and Kessler[1059] showed that if the classical detector noise (for a typical commercial detector) was combined with the quantum laser amplitude noise (shot noise) the quadrature sum of the components was **0.57 pm** (Section 4.6.3.1). Note that optical laser interferometry has not tended towards using progressively shorter optical wavelengths as a way of improving accuracy as has happened with fabrication techniques in the semiconductor industry. Generally speaking, the costs associated with this approach are far too high and usually other sources of uncertainty are greater.[1060]

In the early 1990s, Basile et al.[1061] and Bergamin et al.[1062] developed an optical interferometer that used phase modulation. In this system, light passed through an electro-optic modulator before entering the optical interferometer. The electro-optic modulator introduced a time modulated phase shift between the two incident polarization states. The output of the interferometer was detected simultaneously with the modulation frequency of the electro-optic modulator. Their system demonstrated a resolution of better than **1 pm** around the zero crossing of the demodulated signal (maxima and minima of the interference pattern) and was limited by

---

[1057] G.N. Peggs, A. Yacoot, "A review of recent work in sub-nanometre displacement measurement using optical and X-ray interferometry," Philos Transact A Math Phys Eng Sci. 360(15 May 2002):953-968; http://journals.royalsociety.org/content/nj5d8xydfdy8b85d/fulltext.pdf.

[1058] B.J. Meers, K.A. Strain, "Modulation, signal and quantum noise in optical interferometers," Phys. Rev. A 44(1991):4693-4703. A.J. Stevenson, M.B. Gray, H.A. Bachor, D.E. McCelland, "Quantum-noise-limited interferometric phase measurements," Appl. Opt. 32(1993):3481-3493.

[1059] John Lawall, Ernest Kessler, "Michelson interferometer with 10 pm accuracy," Rev. Scient. Instrum. 71(2000):2669-2676. http://link.aip.org/link/?RSINAK/71/2669/1.

[1060] G.N. Peggs, A. Yacoot, "A review of recent work in sub-nanometre displacement measurement using optical and X-ray interferometry," Philos Transact A Math Phys Eng Sci. 360(15 May 2002):953-968; http://journals.royalsociety.org/content/nj5d8xydfdy8b85d/fulltext.pdf.

[1061] G. Basile, A. Bergamin, G. Cavagnero, G. Mana, Italian Patent 22558/RCGA, 1989. G. Basile, A. Bergamin, G. Cavagnero, G. Mana, "Phase modulation in high resolution optical interferometry," Metrologia 28(1992):455-461.

[1062] A. Bergamin, G. Cavagnero, G. Mana, "Phase holonomy in optical interferometry," J. Mod. Opt. 39(1992):2053-2074.

shot noise and wavelength stability since at these points high sensitivity and noise rejection are obtained. The driving force for the development of their interferometer was the measurement of the lattice parameter of silicon,[1063] which required that the number of X-ray fringes (192 pm spacing) in an optical fringe be determined.[1064]

Reviewing the field in 2002, Peggs and Yacoot[1065] noted that major strides had been made in the 1990s to improve the fundamental understanding of the sources of uncertainty of optical interferometers, such as the development of matrix and scalar models of the sources of nonlinearity in homodyne and heterodyne systems. They cited several examples where the overall accuracy of the interferometer system approaches the level of tens of picometers, but warned: "Systems operating at the limit of currently achievable accuracy do require a high degree of technical complexity and such interferometers are generally only found in national metrology institutes or research laboratories. Nevertheless, there are commercial systems emerging which have the potential for use in applications that demand nanometric and sub-nanometric accuracy."

In parallel with the developments in optical interferometers, by 2002 X-ray interferometry had emerged as a powerful tool for dimensional metrology at the sub-nanometer level[1066] (e.g., enabling 10-20 pm resolution positional measurements)[1067] and as a reference for verifying the

---

[1063] P. Becker, G. Mana, "The lattice parameter of silicon: a survey," Metrologia 31(1994):203-209. G. Basile, A. Bergamin, G. Cavagnero, G. Mana, "Measurement of the silicon (220) lattice spacing," Phys. Rev. Lett. 72(1994):3133-3136.

[1064] D. Windisch, P. Becker, "Silicon lattice parameters as an absolute scale of length for high precision measurements of fundamental constants," Phys. Status Solidi A 118(1990):379-388. J. Martin, U. Kuetgens, J. Stumpel, P. Becker, "The silicon lattice parameter – an invariant quantity of nature?" Metrologia 35(1998):811-817. Special issue on the 1998 CODATA internationally recommended values, Rev. Mod. Phys. 72(2000).

[1065] G.N. Peggs, A. Yacoot, "A review of recent work in sub-nanometre displacement measurement using optical and X-ray interferometry," Philos Transact A Math Phys Eng Sci. 360(15 May 2002):953-968; http://journals.royalsociety.org/content/nj5d8xydfdy8b85d/fulltext.pdf.

[1066] V.N. Ilyin, N.A. Kobets, S.V. Leshkov, "X-ray interferometers as a means of super-high-precision metrology (review)," J. Appl. Spectroscopy 66(July 1999):481-492, http://www.springerlink.com/content/7h808745265x3021/ . See also: V.N. Ilyin, "Prototype of an x-ray nanodisplacement converter," J. Opt. Technol. 68(April 2001):294-296, http://www.opticsinfobase.org/abstract.cfm?URI=JOT-68-4-294.

[1067] D.G. Chetwynd, D.P. Siddons, D.K. Bowen, "X-ray interferometer calibration of microdisplacement transducers," J. Phys. E: Sci. Instrum. 16(1983):871-874, http://www.iop.org/EJ/abstract/0022-3735/16/9/013; D.K. Bowen, D.G. Chetwynd, D.R. Schwarzenberger, "Sub-nanometre displacements calibration using X-ray interferometry," Meas. Sci. Technol. 1(1990):107-119, http://www.iop.org/EJ/abstract/-search=56807660.11/0957-0233/1/2/002; D.G. Chetwynd, D.R. Schwarzenberger, D.K. Bowen, "Two-dimensional X-ray interferometry," Nanotechnology 1(1990):19-26, http://www.iop.org/EJ/abstract/-search=56807660.10/0957-4484/1/1/004; D.G. Chetwynd, S.C. Cockerton, S.T. Smith, W.W. Fung, "The design and operation of monolithic X-ray interferometers for super-precision metrology," Nanotechnology 2(1991):1-10, http://www.iop.org/EJ/abstract/-search=56807660.9/0957-4484/2/1/001; D.G. Chetwynd, S.M. Harb, N.O. Krylova, S.T. Smith, "The

linearity of conventional high-performance laser interferometers. The main advantage of X-ray interferometers is reduced reliance on the sub-division of optical fringes. Once again, it was noted[1068] that "the technology is sophisticated and therefore is still only accessible to a limited number of highly specialized groups."

Realization of the first x-ray interferometer by Bonse and Hart in 1965[1069] was quickly followed by the explication of a clear path leading to atomic-scale measurement accuracy by Hart in 1968[1070] – his "Angstrom ruler" was an articulated silicon monolith able to scan over an extended, though limited, range (100 nm) and measuring these distances with a precision of ±2 pm. While in principle is is possible to measure displacements up to 1 mm with sub-nanometric accuracy using x-ray interferometry alone, the technological difficulties would be very great. X-ray beam intensities provide such low photon counts that, typically, X-ray displacement measurements are orders of magnitude slower than those made by optical interferometry: the slow scanning speed would make measurement times inconveniently long. Additionally, the longer measurement range would suggest the use of separate crystal X-ray interferometers with all its attendant problems of alignment and sensitivity to perturbations. These problems can be circumvented by limiting the range covered directly by the X-ray interferometer to ~10 microns only, and by measuring the major part of the displacement using optical interferometry.[1071]

The first combined optical and X-ray interferometer (COXI) was realized at the U.S. National Bureau of Standards (NBS) in 1969.[1072] During the early 1990s[1073] and culminating in 2000,[1074]

---

feasibility of extended range monolithic X-ray interferometric calibrators," Nanotechnology 4(1993):183-193, http://www.iop.org/EJ/abstract/-search=56807660.7/0957-4484/4/4/002; D.G. Chetwynd, N.O. Krylova, S.T. Smith, "Metrological x-ray interferometry in the micrometre region," Nanotechnology 7(1996):1-12, http://www.iop.org/EJ/abstract/-search=56807599.5/0957-4484/7/1/001; D.G. Chetwynd, "Nanometrology by x-ray interferometry," Measurements & Control 31(1998):43-47; D.G. Chetwynd, N.O. Krylova, P.J. Bryanston-Cross, Z. Wang, "Applications of x-ray interferometer-generated Moiré patterns," Nanotechnology 9(1998):125-132.

[1068] G.N. Peggs, A. Yacoot, "A review of recent work in sub-nanometre displacement measurement using optical and X-ray interferometry," Philos Transact A Math Phys Eng Sci. 360(15 May 2002):953-968; http://journals.royalsociety.org/content/nj5d8xydfdy8b85d/fulltext.pdf.

[1069] U. Bonse, M. Hart, "An x-ray interferometer," Appl. Phys. Lett. 6(1965):155-156.

[1070] M. Hart, "An Ångstrom ruler," Br. J. Appl. Phys. 1(1968):1405-1408.

[1071] M. Bisi, E. Massa, A. Pasquini, G. B. Picotto, M. Pisani, "Nanometrology at the IMGC", in: Günter Wilkening, Ludger Koenders, eds., Nanoscale Calibration Standards and Methods, Wiley-VCH Verlag GmbH & Co. KGaA, 2005, pp. 22-36.

[1072] Richard D. Deslattes, "Optical and X-Ray Interferometry of a Silicon Lattice Spacing," Appl. Phys. Lett. 15(1969):386-388.

[1073] P. Becker, J. Stümpel, "X-ray optics in metrological application," Metrologia 27(1990):127-132. G. Basile, P. Becker, A. Bergamin, G. Cavagnero, A. Franks, K. Jackson, U. Kuetgens, G. Mana, E.W. Palmer, C.J. Robbie, M. Stedman, J. Stumpel, A. Yacoot, G. Zosi, "COXI - Combined optical and x-ray interferometry for high precision dimensional metrology," Conference Paper, 7th International Precision Engineering Seminar, Kobe, Japan, May 1993, pp. 248-259.

three National Metrological Institutes – the Instituto de Metrologia 'G. Colonnetti' (IMGC) in Italy, the National Physical Laboratory (NPL) in U.K., and the Physikalisch-Technische Bundesanstalt (PTB) in Germany – joined forces to develop an instrument for the measurement of linear displacements with ultra-high accuracy. In their COXI instrument, an X-ray interferometer is coupled with an optical interferometer. The optical interferometer generates a relatively coarse, but very precise scale that can be directly referred to the standard of length, and the X-ray interferometer subdivides each "graduation" of this scale into about 824 precisely equal parts, each of which is equal to the lattice spacing of 192.015497 pm of the (220) planes of an almost perfect silicon lattice. This lattice makes an almost perfect "Angstrom ruler"[1075] over very long ranges because the variation in atomic position in an unstressed crystal is only ±0.000012 pm at 22.5 °C due to residual carbon and oxygen impurities in the silicon. (Atom thermal vibrations within the lattice also occur but at a much higher frequency (e.g., GHz) than the frequency of measurement by the COXI system (e.g., kHz), hence the COXI system reads these atoms as being present at their equilibrium center position.) The COXI instrument allows large displacements to be measured with a rapidity associated with conventional optical interferometry, leaving the relatively slow X-ray interferometer to measure the very small fraction of the required distance by counting the number of X-ray fringes in one optical fringe.

4.6.2.1 The COXI System at NPL/PTB/IMGC (Europe)

Figure 4-47 is a drawing showing the main features of COXI.[1076] The instrument is housed in an underground laboratory, is mounted on a pneumatic anti-vibration table, and is ensconced inside three nested enclosures to provide thermal stability and isolation from radiation and airborne vibrations. The system is operated in air at a pressure of 1 bar and a temperature of 22.5 °C.

[1074] G. Basile, P. Becker, A. Bergamin, G. Cavagnero, A. Franks, K. Jackson, U. Kuetgens, G. Mana, E.W. Palmer, M. Stedman, J. Stümpel, A. Yacoot, G. Zosi, "COXI – A Combined Optical and Xray Interferometer for high precision dimensional metrology," Proc. Roy. Soc. Lond. A 456(2000):701-729.

[1075] M. Hart, "An Ångstrom ruler," Br. J. Appl. Phys. 1(1968):1405-1408.

[1076] G. Basile, P. Becker, A. Bergamin, G. Cavagnero, A. Franks, K. Jackson, U. Kuetgens, G. Mana, E.W. Palmer, M. Stedman, J. Stümpel, A. Yacoot, G. Zosi, "COXI – A Combined Optical and Xray Interferometer for high precision dimensional metrology," Proc. Roy. Soc. Lond. A 456(2000):701-729.

Figure 4-47. The main components of COXI.

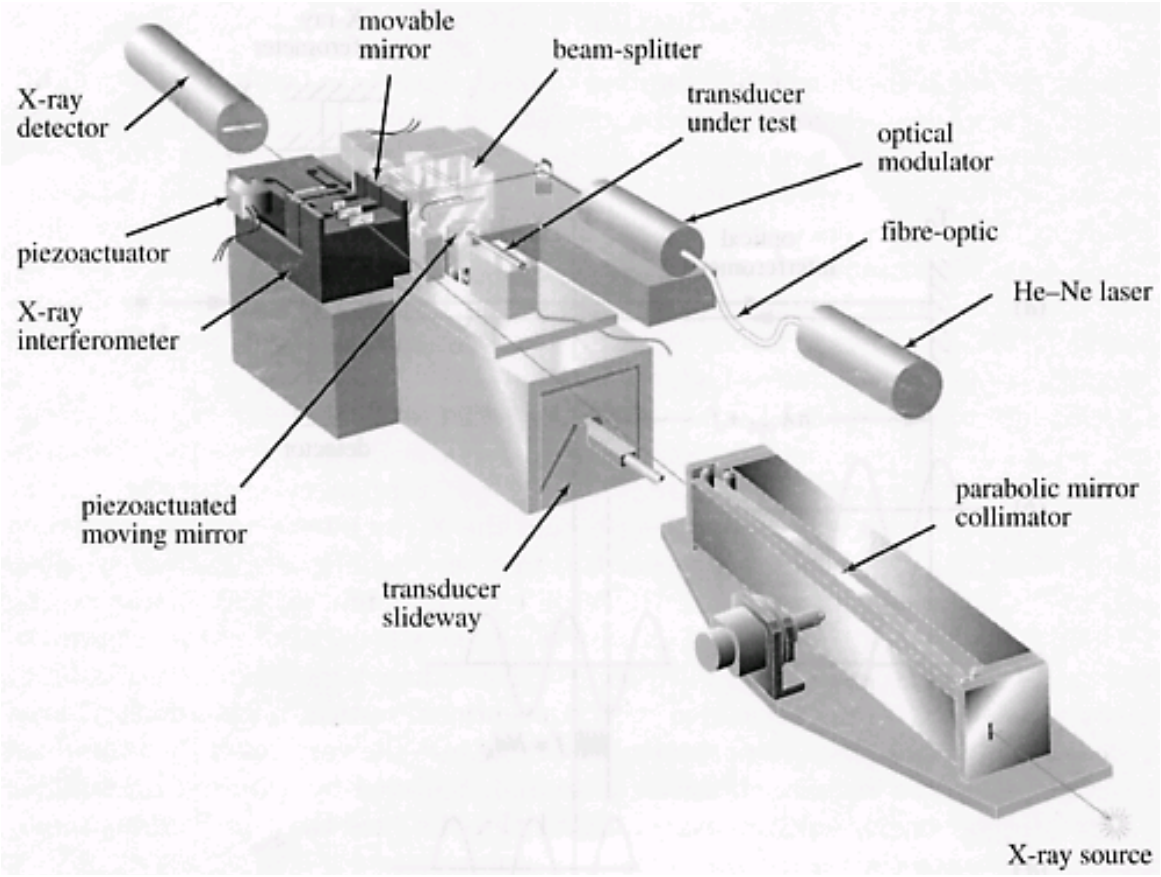

The layout of the X-ray interferometer is shown in Figure 4-48. X-rays generated by the 2 kW X-ray tube are reflected from a cylindrical parabolic mirror collimator, increasing useful beam intensity. The beam then passes through three 1-mm thick lamellae spaced 10-15 mm apart , respectively, that serve as (a) the fixed beam-splitter, (b) the fixed beam combiner, and (c) the moveable fringe analyzer. The lamella are fabricated with their atomic lattice planes normal to the surface. This diffracts X-rays in transmission, generating two coherent beams leaving the exit surface of the beam-splitter at a divergence angle twice the Bragg angle.

Figure 4-48.[1077] **(A) Schematic of Mach-Zehnder X-ray interferometer, with crystal lamella S as the beam-splitter, M acting as two mirrors, and A as the analyzer. (B): Image of the monolithic silicon X-ray interferometer. (C) Schematic diagram, plan view of monolithic X-ray interferometer, with beam-splitter (B), mirror (M) and analyzer (A) lamellae coming out of the plane of the paper towards the reader; X-ray path is dotted line; motion of lamella achieved via piezo-electric transducer (PZT).**

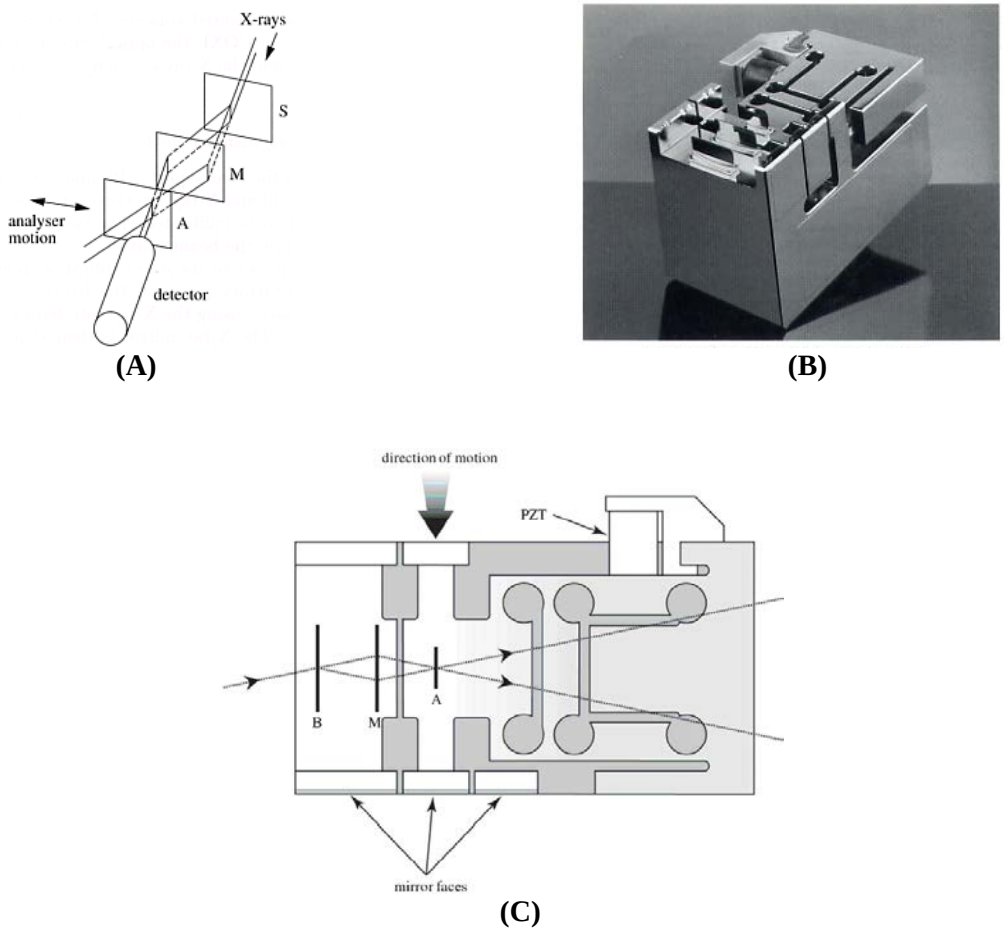

"X-ray interferometers (Figure 4-48) are made from single crystals of silicon. The extremely demanding tolerance with which the components must be aligned has led to most interferometers having a monolithic construction. Silicon is chosen because it is elastic and pure, and defect-free

---

[1077] G. Basile, P. Becker, A. Bergamin, G. Cavagnero, A. Franks, K. Jackson, U. Kuetgens, G. Mana, E.W. Palmer, M. Stedman, J. Stümpel, A. Yacoot, G. Zosi, "COXI – A Combined Optical and Xray Interferometer for high precision dimensional metrology," Proc. Roy. Soc. Lond. A 456(2000):701-729. G.N. Peggs, A. Yacoot, "A review of recent work in sub-nanometre displacement measurement using optical and X-ray interferometry," Philos Transact A Math Phys Eng Sci. 360(15 May 2002):953-968; http://journals.royalsociety.org/content/nj5d8xydfdy8b85d/fulltext.pdf.

crystals in the form of rods in specific crystallographic orientations are readily available. Material is machined away from the top of the original block of silicon to leave three equally spaced thin lamellae, which are usually referred to as the beam-splitter, mirror and analyzer lamella, respectively. Around the third (analyzer) lamella a flexure stage has been machined so that application of a force parallel to the lamellae faces results in displacement of the third lamella. The force is applied using a piezo-electric transducer (PZT) and the complex design of flexure stage ensures that the motion of the analyser lamella is in a straight line parallel to the lamellae faces. The range of the flexure stage is typically a few microns. The orientation of the lamellae is such that crystallographic planes from which X-rays can be diffracted are perpendicular to the faces of the lamellae. In this case the diffraction planes are (220) and the range of the interferometer is 10 microns."[1078]

In use the interferometer is aligned so that X-rays are incident at the Bragg angle and diffracted from the first lamella (i.e., "S" in Figure 4-48A, "B" in Figure 4-48C). Two diffracted beams are produced which are incident on the second lamella (M), from which two more pairs of diffracted beams emerge. The inward pointing beams from each pair recombine at the third lamella (A). The combination of these two beams results in an interference or standing wave pattern whose periodicity is given by the lattice parameter of the planes from which the X-rays have been diffracted. (The period of the fringe pattern is independent of the X-ray wavelength used, unlike the analogous case in visible optics.) Since the lattice parameter of the (220) planes is of the order of 192 pm, the pattern would be very hard to detect. For this reason the third lamella (A) is used to produce a moire fringe pattern between the X-ray beams and the atomic planes in the crystal. Consequently, when the third lamella is displaced through a distance equal to the lattice spacing of the diffracting planes, the intensity of the X-ray beams transmitted through the third lamella cycles through maximum and minimum. By measuring the intensity of the X-ray signal as the third lamella is displaced, one is able to measure the displacement of the flexure stage in terms of the lattice spacing of silicon, which is now regarded as a traceable standard of length.[1079] The X-ray interferometer is physically separated from the translation stage supporting the mirror to which the transducer (whose displacement is to be measured) are coupled. Hence the X-ray interferometer is not subjected to any external forces that could impair its performance.

"At the side of the interferometer, perpendicular to the lamella are three optical mirrors, the center mirror being coupled with the analyser lamella and the other two mirrors being fixed to the main body of the interferometer. These three mirrors are used by the optical interferometer. The X-ray interferometer has a servo system[1080] that allows the flexure stage on the interferometer either to be moved in discrete numbers of X-ray fringes or to be held in a fixed position.

[1078] G.N. Peggs, A. Yacoot, "A review of recent work in sub-nanometre displacement measurement using optical and X-ray interferometry," Philos Transact A Math Phys Eng Sci. 360(15 May 2002):953-968; http://journals.royalsociety.org/content/nj5d8xydfdy8b85d/fulltext.pdf.

[1079] P.J. Mohr, B.P. Taylor, "CODATA recommended values for the fundamental physical constants," Rev. Mod. Phys. 72(2000):351-435.

[1080] A. Bergamin, G. Cavagnero, G. Mana, "Quantized positioning of X-ray interferometers," Rev. Scient. Instrum. 68(1997):17-22.

Additionally, the optical interferometer has a second moving mirror and a servo system that allows the second moving mirror to follow the movement of the X-ray interferometer or move through a set number of optical fringes. Hence it is possible to move the optical interferometer in quantized steps of either optical or X-ray fringes. The transducer under calibration follows the movement of the optical interferometer on COXI. Movements made using COXI can be compared with those measured by the transducer under calibration, and hence errors in the transducer under calibration can be determined."[1081]

The optical layout of COXI is shown in Figure 4-49. The purpose of COXI is to measure the 1-dimensional displacement of the tip of the transducer very accurately. To accomplish this, the light from a frequency-stabilized He-Ne laser is transmitted via a single-mode polarization-preserving fiber to ensure beam quality and pointing stability. This light is fed to an optical beam-splitter that produces two sets of four beams that are incident on and reflected by the X-ray interferometer and the transducer slideway mirrors. There are one moving mirror and two fixed mirrors in both the X-ray and transducer paths of the optical interferometer. One component of the polarized beam impinges twice on the movable mirror of the X-ray interferometer and once on each of the two fixed mirrors of the calibration stage. The other component impinges twice on the movable mirror of the calibration stage and once on each of the two fixed mirrors of the X-ray interferometer. The optical interferometer measures the change in path length resulting from the displacement of the moving mirrors. To ensure maximum mechanical stability of measurement, the fixed mirrors in the transducer branch form part of a monolithic inverted U-shaped member. The movable mirror travels centrally through the arch of the "U". The double-beam system significantly reduces the sensitivity to whole-body translations and rotations of the X-ray interferometer and of the translation stage. It also increases the sensitivity by a factor of two: each optical fringe corresponds to a displacement of $(1/4)\lambda_{opt}$, which is approximately equal to 824 X-ray fringes.

[1081] G.N. Peggs, A. Yacoot, "A review of recent work in sub-nanometre displacement measurement using optical and X-ray interferometry," Philos Transact A Math Phys Eng Sci. 360(15 May 2002):953-968; http://journals.royalsociety.org/content/nj5d8xydfdy8b85d/fulltext.pdf.

Figure 4-49. Schematic of the optical interferometer layout in COXI.[1082] Silicon lamellae are a, b, and c; QWP are quarter wave plates, CC are cube corners, and PSD is a phase-sensitive detector.

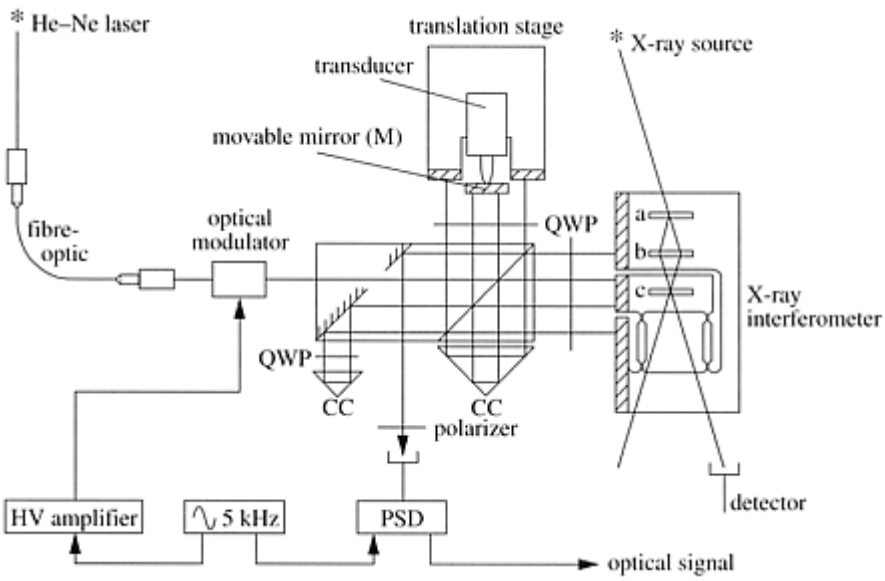

High sensitivity and noise rejection are obtained in the neighborhood of the maxima (brightest) and minima (darkest) of the interference pattern – noise rejection was slightly greater at the minimum, making it the preferred choice. Displacements from consecutive minima can thus be measured with an accuracy limited by the wavelength stability and shot noise.

Figure 4-50 illustrates the operating principle of COXI. Optical interferometry links the measurements made by X-ray interferometry to the standard of length. In optical interferometry the intensity of the fringes is normally closely, but not exactly, sinusoidal. Departures from the perfect sinusoid are a result of imperfect optics, for example as a result of polarization leakage. The spacings of the fringes are nearly equal to the wavelength, or a submultiple of the wavelength of light, depending on the interferometer: a small deviation from the wavelength is due to Fresnel diffraction. Subdivision of the optical fringe spacing by electronic or optical methods may result in a small error due to the departure of the fringe from the sinusoidal form. The measurements of a transducer displacement, consisting of a whole number of optical fringes, can be made with a precision dependent on the accuracy with which a particular feature of the optical fringe can be located. This can be done very precisely at the null point (the point of minimum intensity) of each optical fringe – a count of X-ray fringes in two successive optical fringes showed that the null point of the optical fringe could be located to better than ±0.055 X-ray fringes (±10.6 pm).

[1082] G. Basile, P. Becker, A. Bergamin, G. Cavagnero, A. Franks, K. Jackson, U. Kuetgens, G. Mana, E.W. Palmer, M. Stedman, J. Stümpel, A. Yacoot, G. Zosi, "COXI – A Combined Optical and Xray Interferometer for high precision dimensional metrology," Proc. Roy. Soc. Lond. A 456(2000):701-729.

In optical interferometry the travel distance to be measured generally consists of a whole number of optical fringes and a fraction of an optical fringe. In COXI, the optical interferometer measures the whole number of optical fringes and the X-ray interferometer measures the fractional part of the optical fringe. Polarization encoding makes the interferometer nonlinear between consecutive optical fringe minima. This nonlinearity results from the mixing of the reference and measurement states in the interferometer, but all nonlinearity effects are effectively zero at the optical fringe null points, the setting points used by COXI.

Figure 4-50. COXI operating principle: BS = beam-splitter; T = transducer mirror; X = X-ray interferometer optical mirror.[1083]

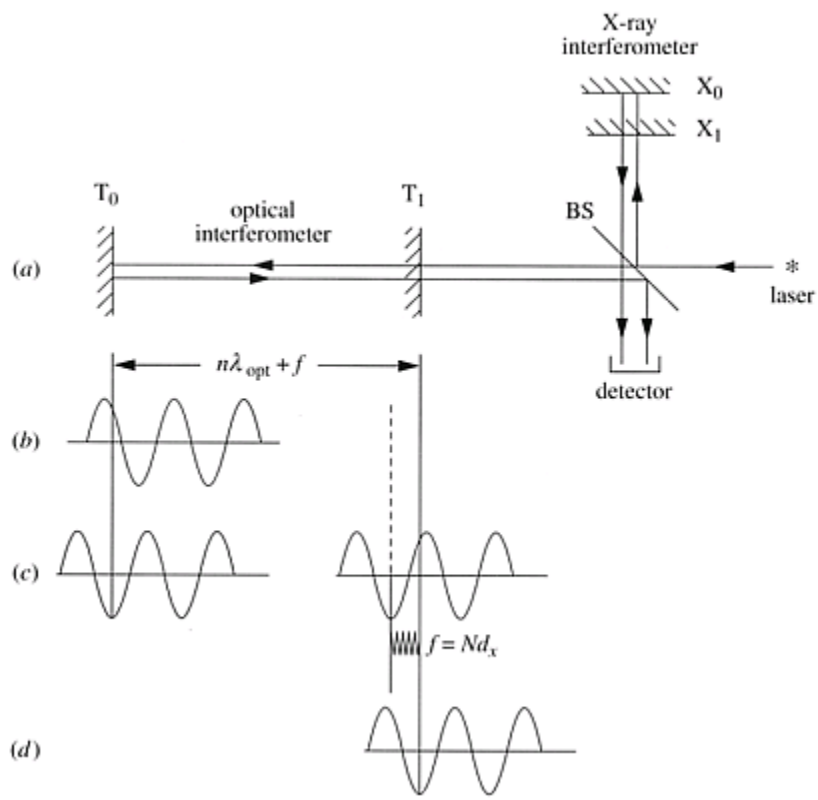

In Figure 4-50a, a laser beam is incident on the beam-splitter BS and is reflected from the moving members T and X of the optical and X-ray interferometers, respectively. T is a mirror attached to the AFM tip whose 1D motions we wish to monitor. The two beams interfere after transmission through and reflection by the beam-splitter. To calibrate the AFM tip position, it is initially set to

---

[1083] G. Basile, P. Becker, A. Bergamin, G. Cavagnero, A. Franks, K. Jackson, U. Kuetgens, G. Mana, E.W. Palmer, M. Stedman, J. Stümpel, A. Yacoot, G. Zosi, "COXI – A Combined Optical and Xray Interferometer for high precision dimensional metrology," Proc. Roy. Soc. Lond. A 456(2000):701-729.

its zero calibration point T_0. In general, this will correspond to some arbitrary point on the fringe, as shown in Figure 4-50b. The fringe pattern is then displaced using the X-ray interferometer mirror to align it with the optical fringe null point (Figure 4-50c). The X-ray mirror is then at position X_0. The AFM tip is then moved to its first translation point T_1. This translation will normally consist of a whole number of optical fringes, $n\lambda_{opt}$, and a fraction, f, of an optical fringe. The number of X-ray fringes, N, in the fractional optical optical fringe is measured by displacing the X-ray mirror to position X_1 to shift the optical fringe to the next null point (Figure 4-50d). The displacement is therefore equal to $n\lambda_{opt} + Nd_X$, where d_X is the silicon lattice spacing. The same procedure is followed as the AFM tip is moved to a succession of translation points, in principle allowing the motion of the AFM tip to be very precisely tracked during nearly continuous motion. X-ray fringe contrast remains good enough for displacements of 7 microns or less, allowing X-ray fringe-counting alone to be used within this range and optical fringe counting to be eliminated, though at multi-micron displacements the total fringe-counting time may be affected. At displacements beyond 7 microns, optical fringe counting must be used in addition to X-ray fringe counting.

<u>To summarize</u>: The COXI system precisely measures the X-axis position of a mirror attached to the end of a 1-DOF linear transducer. After registration of transducer position at some arbitrary origin point within the field of travel of the transducer, COXI measures the displacement from that origin by counting interferometric fringes of two types: optical fringes and X-ray fringes. The stabilized He-Ne optical laser used in COXI has a wavelength of $\lambda \sim 633$ nm and the optical geometry includes four half-paths, hence successive fringes in the optical interferometer component correspond to $\lambda/4 \sim 158$ nm steps, which is the optical step size for COXI. Between each of the adjacent optical fringes (measured from the darkest or null point), the X-ray interferometer produces ~824 successive X-ray fringes corresponding to the silicon lattice spacing of 192 pm, which is the X-ray step size for COXI. Thus the transducer can be coarse-translated over large distances in 158 nm steps using the optical interferometer, then can be fine-translated in 192 pm steps (in the vicinity of any selected optical fringe) using the X-ray interferometer.

More specifically, the reference movable surface (to which the AFM tip is attached) is represented by the back surface of the movable mirror (M) in the calibration arm shown in Figure 4-49. Each translation point will be associated with the number N_0 of the optical order (optical fringes), plus the number n_x of X-ray order (X-ray fringes), plus the fraction f_x of the X-ray fringe, starting from an arbitrary optical order zero:

$$N_0(1) + n_x(1) + f_x(1)\,, \quad N_0(2) + n_x(2) + f_x(2)\,, \quad \ldots \tag{5.1}$$

Hence the measured distance Δl between two successive translation points, the fundamental equation of COXI, corresponds to:

$$\Delta l = \tfrac{1}{4}\,\lambda'(N_0(2) - N_0(1)) + (n_x(2) - n_x(1))d'_{220} + (f_x(2) - f_x(1))d'_{220} \tag{5.2}$$

where λ' and d'_{220} correspond to the laser wavelength (~633 nm) and the silicon lattice spacing (~192 pm) once necessary corrections have been made. The first term in Eqn. 5.2 represents the integer number of optical orders (equal to ¼ λ or ~158 nm), the second term represents the fractional part of the optical order in terms of an integer number of X-ray fringes (at ~192 pm per fringe), and the last term represents the remaining fractional part of the optical order in terms of the fractional part on an X-ray fringe. When operated in the closed-loop mode as in the original

investigation, the last term is treated as zero and the fractional X-ray fringe information is discarded.

For the molecular workstation, we wish to recover the fractional X-ray fringe information to obtain the highest precision possible from the COXI system. This appears to be possible. With mirror collimation of the X-ray source, the X-ray detector receives 60,000 counts/sec at the peak and 20,000 counts/sec at the trough of the approximately sinusoidal measured X-ray intensity (assumed to be photon count) of each X-ray fringe (Figure 4-51). The maximum random variation away from the underlying sinusoidal trend curve appears to be ~5,000 counts/sec or less, which means that successive points on the sine curve that are separated by ~10,000 counts/sec or more have little overlap and thus should be reliably distinguishable from noise. This divides the X-ray sine curve into 8 distinguishable regions. Ignoring possible minor nonlinearities in the X-ray fringes, stepping the COXI system through each of these 8 regions in sequence permits picometric-translation of the transducer through (192 pm / 8 =) 24 pm steps. This is probably the smallest Δf_x that would have practical utility, since such 24 pm steps are of similar magnitude to the 35 pm measurement uncertainty for up to 100 micron displacements at the 95% confidence level that are reported in the COXI paper.[1084] Thus COXI appears to satisfy the basic requirement of 20-50 pm repeatable positioning accuracy for the molecular workstation.

Figure 4-51. X-ray fringes measured by the detector, when intensity is enhanced using the parabolic reflecting mirror (top curve).[1085]

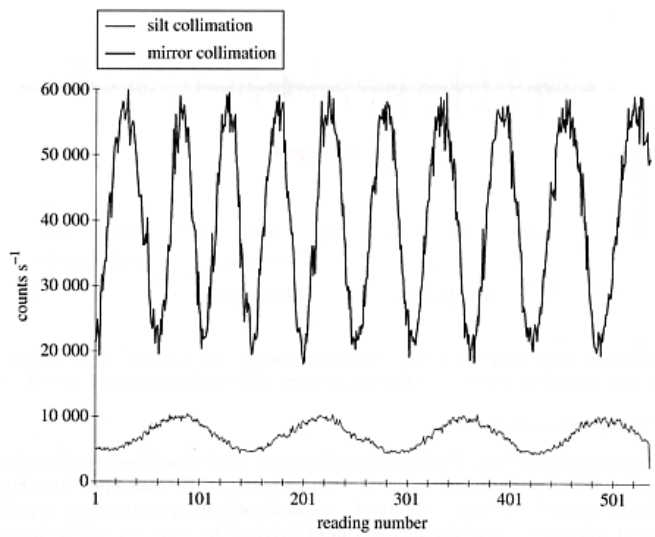

[1084] G. Basile, P. Becker, A. Bergamin, G. Cavagnero, A. Franks, K. Jackson, U. Kuetgens, G. Mana, E.W. Palmer, M. Stedman, J. Stümpel, A. Yacoot, G. Zosi, "COXI – A Combined Optical and Xray Interferometer for high precision dimensional metrology," Proc. Roy. Soc. Lond. A 456(2000):701-729.

[1085] G. Basile, P. Becker, A. Bergamin, G. Cavagnero, A. Franks, K. Jackson, U. Kuetgens, G. Mana, E.W. Palmer, M. Stedman, J. Stümpel, A. Yacoot, G. Zosi, "COXI – A Combined Optical and Xray Interferometer for high precision dimensional metrology," Proc. Roy. Soc. Lond. A 456(2000):701-729.

Note that the X-ray interferometer is not physically connected to the translation stage, which means it can be conveniently located well out of the way of the moving tooltips. The COXI paper[1086] suggests that the optical paths to and from the X-ray interferometer should be as short as possible, in part because these experiments were performed in warm air at 1 atm pressure, not cold vacuum. Operation in UHV (vacuum) should allow this constraint to be considerably relaxed. Nevertheless, each toolholder will still need to have at least one mirror for each DOF it possesses. Each toolholder and its mirrors ideally should be made of one monolithic block of material to eliminate any misalignment effects between these multiple mirrors and the actual tip that is contacting the workpiece surface, but it is also highly likely that 3 DOFs will be required per toolholder and that 3-4 separate toolholders must be present in the workspace, causing the space near the workpiece to get extremely cluttered with mirrors and beams.

Another potential concern is that COXI has a measured drift error of ±13 pm in 400 sec. If this cannot be corrected (e.g., via low temperature operation, *in vacuo*), then in ~1000 sec of operation the system will drift beyond the required minimum positional tolerance of 20-50 pm for DMS work and re-registration of the tip will be required. COXI reports using an X-ray fringe counting rate of 20 fringes/sec.[1087] MHz optical counting rates are commonplace today, so travel time per tip cycle is dominated by the much slower fine- and picometric-translation steps. The average number of fine steps around a known optical fringe is ~824/4 = 206 steps, plus 2 for the picometric steps, giving a typical one-way transit time of (208 steps/transit) / (20 steps/sec) = 10.4 sec/transit, which should allow up to ~100 transits between re-registrations unless the drift problem can be corrected. (Modestly increasing the count rate to 100 fringes/sec would allow ~500 transits between re-registrations.)

It has also been noted[1088] that X-ray interferometers require very delicate adjustment to obtain a high-contrast X-ray interference fringe, and that X-ray interferometers are not commonly used in industry due to the difficulty and high cost of machining pure and precise silicon lamellas and the dangers of working with X-ray radiation.

How fast can we cycle the tooltips to perform DMS operations using a COXI system? According to Basile et al.,[1089] the optical subsystem coarse-drive carriage can be driven at a speed of 1 mm/minute (page 714), presumably while retaining an accurate optical fringe count. This could

---

[1086] G. Basile, P. Becker, A. Bergamin, G. Cavagnero, A. Franks, K. Jackson, U. Kuetgens, G. Mana, E.W. Palmer, M. Stedman, J. Stümpel, A. Yacoot, G. Zosi, "COXI – A Combined Optical and Xray Interferometer for high precision dimensional metrology," Proc. Roy. Soc. Lond. A 456(2000):701-729.

[1087] G. Basile, P. Becker, A. Bergamin, G. Cavagnero, A. Franks, K. Jackson, U. Kuetgens, G. Mana, E.W. Palmer, M. Stedman, J. Stümpel, A. Yacoot, G. Zosi, "COXI – A Combined Optical and Xray Interferometer for high precision dimensional metrology," Proc. Roy. Soc. Lond. A 456(2000):701-729.

[1088] Masato Aketagawa, Yosuke Ikeda, Nuttapong Tanyarat, Masashi Ishige, "Optical encoder calibration using lattice spacing and optical fringe derived from a scanning tunnelling microscope and optical interferometer," Meas. Sci. Technol. 18(February 2007):503-509.

[1089] G. Basile, P. Becker, A. Bergamin, G. Cavagnero, A. Franks, K. Jackson, U. Kuetgens, G. Mana, E.W. Palmer, M. Stedman, J. Stümpel, A. Yacoot, G. Zosi, "COXI – A Combined Optical and Xray Interferometer for high precision dimensional metrology," Proc. Roy. Soc. Lond. A 456(2000):701-729.

presumably be increased by a factor of ~1000 (~1 cm/sec) if we're just going to re-register anyway at the destination and just need sufficient accuracy to find the registration markers. So tool pickup and return to the registration area over a 10 cm round-trip distance should be doable in a round-trip travel time of ~10 sec, plus allowing another 10 sec for tooltip pickup by a (possibly MEMS) locking gripper. Assuming this translates the tip to within 100 microns of the target workspace, we can step at the slower 1 mm/minute for the remaining 100 microns to the registration area, taking another ~6 sec to get there. Once within 1 micron, COXI can do the rest. The X-ray fringes are 192 pm apart and the count rate used in Basile et al. was 20 fringes/sec (page 716), so we're stepping at 3.84 nm/sec with 43 pm accuracy at this point. If we find a registration marker within 38.4 nm, then 10 sec has elapsed; we allow a total of 20 sec to take readings and get the tool positionally re-registered. Add another 20 sec of travel to reach the workpiece and to perform the DMS mechanical reaction, plus another 20 sec to pull away and return to the toolrack and put down the tooltip. The total cycle time is thus about 86 sec per operation – of comparable magnitude to our targeted 100 sec/operation budget (neglecting tooltip recharge time) for our molecular workstation.

Silicon is the material normally used for an x-ray interferometer since it is readily available in a pure and defect free form with a known crystallographic orientation. Another major advantage for metrological applications is that the lattice parameter of silicon has been measured very accurately and is regarded as a traceable standard of length.[1090] Note that substituting large perfect diamond crystals for the large perfect silicon crystals used in the X-ray interferometer would only reduce the X-ray fringe separation from 192 pm to perhaps ~125 pm, which would be a modest but not game-changing improvement.

4.6.2.2 Subsequent COXI Work at NPL (U.K.) and PTB (Germany)

After the culmination of the original international COXI collaboration,[1091] some work was pursued relevant to COXI through 2005-2006 primarily under the direction of Andrew Yacoot at NPL and Ludger Koenders at PTB. Some of this work involved the X-ray interferometric component of the COXI system. For example, in 2000 Yacoot et al.[1092] used the X-ray interferometer from the COXI facility at NPL to investigate the performance of the NPL Jamin Differential Plane Mirror Interferometer. But it was quickly recognized that since the X-ray interferometer is free from the nonlinearities associated with optical interferometry and its

---

[1090] D. Windisch, P. Becker, "Silicon lattice parameters as an absolute scale of length for high precision measurements of fundamental constants," Phys. Status Solidi A 118(1990):379-388. J. Martin, U. Kuetgens, J. Stumpel, P. Becker, "The silicon lattice parameter – an invariant quantity of nature?" Metrologia 35(1998):811-817. Special issue on the 1998 CODATA internationally recommended values, Rev. Mod. Phys. 72(2000).

[1091] G. Basile, P. Becker, A. Bergamin, G. Cavagnero, A. Franks, K. Jackson, U. Kuetgens, G. Mana, E.W. Palmer, M. Stedman, J. Stümpel, A. Yacoot, G. Zosi, "COXI – A Combined Optical and Xray Interferometer for high precision dimensional metrology," Proc. Roy. Soc. Lond. A 456(2000):701-729.

[1092] Andrew Yacoot, Michael J Downs, "The use of x-ray interferometry to investigate the linearity of the NPL Differential Plane Mirror Optical Interferometer," Meas. Sci. Technol. 11(2000):1126-1130.

displacements are traceable to the meter, it is an ideal translation stage for use with scanning probe microscopes.

In one such study during 1999-2000, Koenders and two Chinese collaborators at Tsinghua University[1093] demonstrated the successful operation of a combination of a scanning tunneling microscope (STM) with an X-ray interferometer (XRI), which they called a scanning XRI, to obtain pitch measurements for a structure on a sample using the almost homogeneous silicon lattice spacing ($\Delta d/d<10^{-7}$) as a (secondary) length standard for subnanometer measurements (the so-called "Angstrom ruler").

In another such configuration in 2001, Yacoot, Kuetgens and Koenders[1094] placed a sample on the moving component of the X-ray interferometer used in COXI, after which a scanning tunneling microscope (STM) was placed above the X-ray interferometer as shown in Figure 4-52. This configuration was used to measure the period of a 100 nm grating produced as a standard for SPMs and the period of an 80 nm grating. "The X-ray interferometer is used as a translation stage which moves in discrete steps of 192 pm, the lattice spacing of the silicon (220) planes. Hence, movements are traceable to the definition of the meter and the nonlinearity associated with the optical interferometers used to measure displacement in more conventional metrological scanning probe microscopes (MSPMs) is removed."

[1093] Wang Lin, Ulrich Kuetgens, Peter Becker, Ludger Koenders, Li Dacheng, Cao Mang, "Calibration of standards for precision pitch measurement in the nanometre region by combined scanning tunnelling microscopy and x-ray interferometry," Nanotechnology 10(1999):412-417. W. Lin, L. Dacheng, C. Mang, L. Koenders, U. Kuetgens, P. Becker, "Angstrom Ruler for High-Accuracy Pitch Measurement," Appl. Opt. 39(2000):4535-4539; http://www.opticsinfobase.org/abstract.cfm?URI=ao-39-25-4535.

[1094] Andrew Yacoot, Ulrich Kuetgens, Ludger Koenders, Thomas Weimann, "A combined STM and x-ray interferometer," Meas. Sci. Technol. 12(2001):1660-1665.

Figure 4-52. Schematic diagram of scanning probe microscope combined with an x-ray interferometer:[1095] the STM sits on the three invar rods and is above the X-ray interferometer, with the scanning direction perpendicular to the plane of the paper.

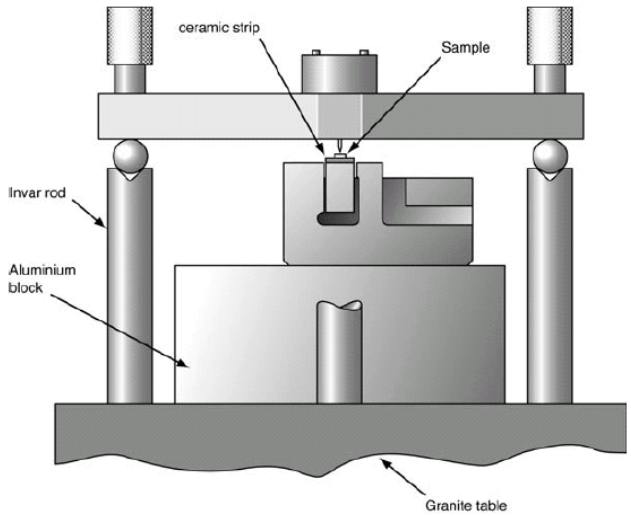

These investigators then employed the entire COXI system to extend the scanning range of an SPM, this time using an atomic force microscope (AFM) instead of an STM. Following a preliminary study[1096] of the use of X-ray interferometry to characterize the non-linearity in an optical encoder displacement measuring system (cyclic errors up to 50 pm were recorded), in 2003 Yacoot and Koenders[1097] published a feasibility study investigating the potential combination of an X-ray interferometer and optical interferometer as a one-dimensional long-range high-resolution scanning stage for an AFM in order to overcome the problems of non-linearity associated with conventional AFMs and interferometers. In this paper, the authors refer to a 3-DOF metrological SPM but concentrate their attention on the feasibility of a 1-DOF metrological SPM. In their experiments they used the previous COXI system already built at NPL as a single-axis translation stage for an AFM; their set-up is a modified version of Figure 4-49, as shown in Figure 4-53 below.

[1095] Andrew Yacoot, Ulrich Kuetgens, Ludger Koenders, Thomas Weimann, "A combined STM and x-ray interferometer," Meas. Sci. Technol. 12(2001):1660-1665.

[1096] Andrew Yacoot, Nigel Cross, "Measurement of picometre non-linearity in an optical grating encoder using x-ray interferometry," Meas. Sci. Technol. 14(2003):148-152.

[1097] Andrew Yacoot, Ludger Koenders, "From nanometre to millimetre: a feasibility study of the combination of scanning probe microscopy and combined optical and x-ray interferometry," Meas. Sci. Technol. 14(2003):N59-N63.

Figure 4-53. Schematic diagram of the Yacoot-Koenders 1-DOF AFM set-up, using COXI; "QWP" = quarter-wave plate.[1098]

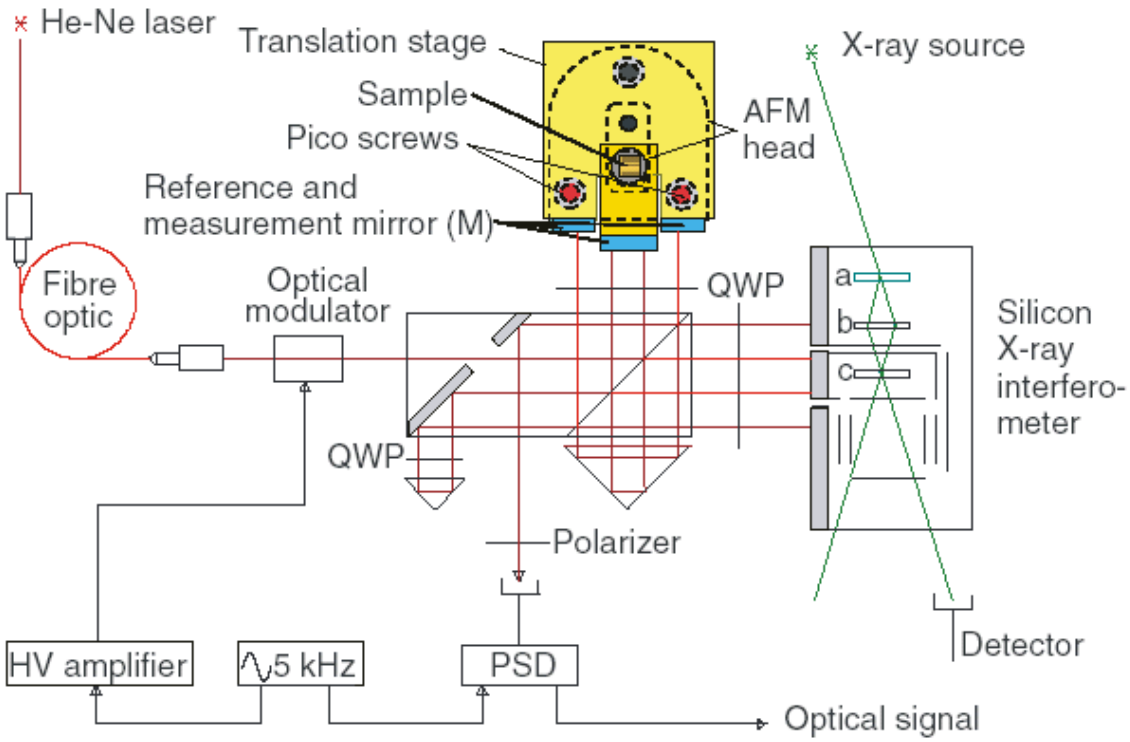

The Yacoot-Koenders experimental set-up[1099] is shown in Figure 4-54 and Figure 4-55 below. The movable mirror (whose position can be accurately tracked by the COXI system) is mounted on a piezo translation stage that can move up to 60 microns; this translation stage is itself mounted on a larger translation stage that can move up to 1 mm. Thus the mirror can be stepped forward or backward along its 1-DOF in optical fringe steps of 158 nm or in x-ray fringe steps of 192 pm. The AFM is then attached to the COXI system to measure the ridge spacing of an optical grating, to test the system. The grating under examination was placed on the optical interferometer translation stage and measurements of the grating period were made over a small range (up to 1 micron) by scanning the x-ray interferometer and simultaneously recording data with the AFM. A displacement was then made using the translation stage for the optical

---

[1098] Andrew Yacoot, Ludger Koenders, "From nanometre to millimetre: a feasibility study of the combination of scanning probe microscopy and combined optical and x-ray interferometry," Meas. Sci. Technol. 14(2003):N59-N63.

[1099] Andrew Yacoot, Ludger Koenders, "From nanometre to millimetre: a feasibility study of the combination of scanning probe microscopy and combined optical and x-ray interferometry," Meas. Sci. Technol. 14(2003):N59-N63.

interferometer over a distance of several hundreds microns followed by more measurements of the grating period using the x-ray interferometer and AFM. The effective resolution with which the grating period could be determined was 500 pm, which is not bad for a first (simple) effort.

Figure 4-54. Holder for sample and small scanning stage for coarse positioning of sample in the Yacoot-Koenders AFM-COXI system.

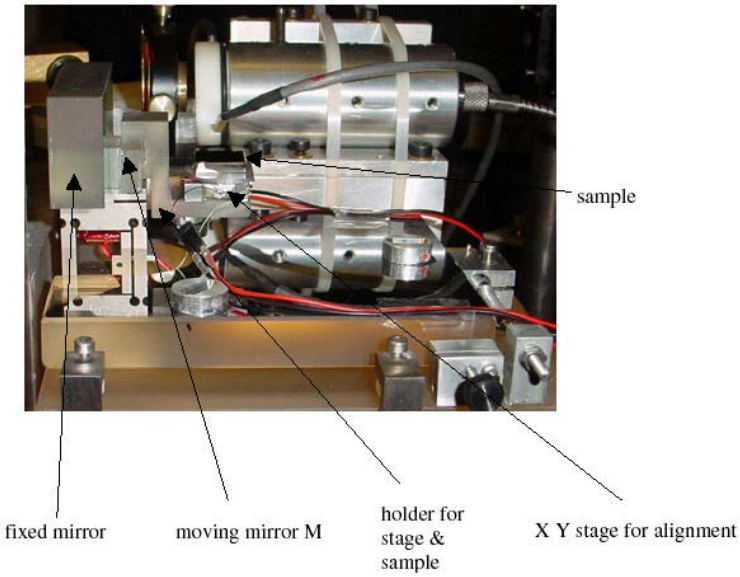

Figure 4-55. AFM mounted above the sample in the Yacoot-Koenders AFM-COXI system.

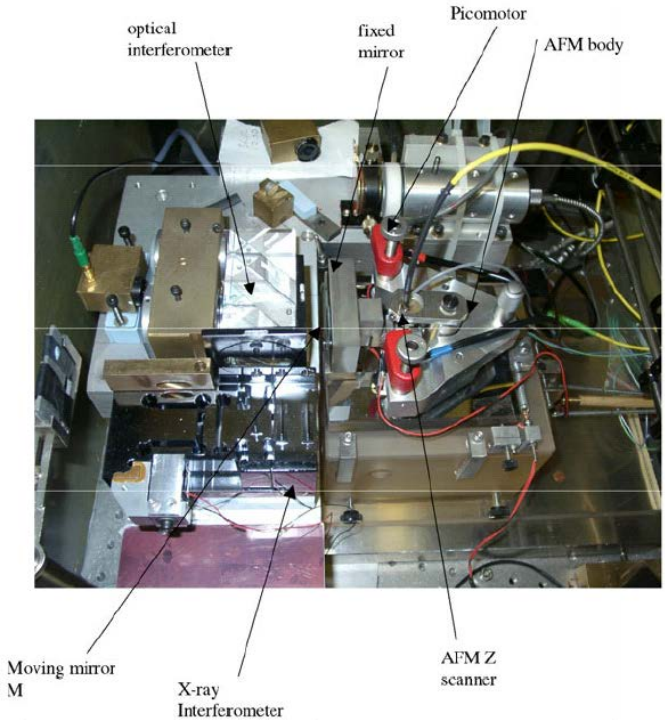

Note the two authors:[1100] "The feasibility study has highlighted the advantages of combining these three instruments as well as the shortcomings of the current configuration of the three instruments. While the measurement of sub-nanometer distances over some hundreds of microns has been successfully demonstrated, the work has also highlighted the extreme sensitivity to temperature drift and the problems associated with sample mounting. Work is currently in progress to improve the temperature control, reduce the AFM's sensitivity to temperature fluctuations, improve the sample mount, make the instrument more user friendly and add traceable metrology to the vertical axis of the AFM [evidently an attempt to add picometer resolution to the vertical movement axis]."

A survey paper explicitly on COXI by Yacoot appeared in 2005,[1101] and during 2004-2007 the NPL/PTB collaborators concentrated on adding "traceable metrology to the vertical axis of the AFM", with the 2007 paper by Yacoot, Koenders and Wolff[1102] concentrating on providing "traceable metrology" for the cantilever tip in the vertical direction, using only (high-resolution homodyne differential) optical interferometry, resulting in the metrological atomic force microscope (MAFM) at NPL. The authors note that this new optical capability for measuring vertical displacements could be mated to the COXI system but had not yet attempted that mating themselves: "The instrument is compatible with an x-ray interferometer, thereby facilitating high resolution one-dimensional scans in the X-direction whose metrology is based on the silicon d220 lattice spacing (192 pm). This paper concentrates on the first stage of the instrument's development and presents some preliminary results validating the instrument's performance and showing its potential." The most recent (2007-2008) papers by Yacoot discuss other issues including the use of artificial neural networks to track positions in an ultrastable optical interferometer[1103] and papers discussing the effects of tip shape[1104] and tip wear[1105] on SPM-based metrology. At a talk in 2006,[1106] Yacoot discussed the "metrological atomic force microscope

---

[1100] Andrew Yacoot, Ludger Koenders, "From nanometre to millimetre: a feasibility study of the combination of scanning probe microscopy and combined optical and x-ray interferometry," Meas. Sci. Technol. 14(2003):N59-N63.

[1101] A. Yacoot, "Metrological applications of X-ray interferometry," in G. Wilkening, L. Koenders, eds., Nanoscale calibration standards and methods, Wiley-VCH, Weinheim, Germany, 2005, pp. 38-44.

[1102] Andrew Yacoot, Ludger Koenders, Helmut Wolff "An atomic force microscope for the study of the effects of tip–sample interactions on dimensional metrology," Meas. Sci. Technol. 18(2007):350-359.

[1103] Richard J. Smith, Chung W. See, Mike G. Somekh, Andrew Yacoot, "Use of artificial neural networks on optical track width measurements," Appl Opt. 46(1 August 2007):4857-4866.

[1104] Andrew Yacoot, Ludger Koenders, "Aspects of scanning force microscope probes and their effects on dimensional measurement," J. Phys. D: Appl. Phys. 41(2008):103001.

[1105] Peter Bakucz, Andrew Yacoot, Thorsten Dziomba, Ludger Koenders, Rolf Krüger-Sehm, "Neural network approximation of tip-abrasion effects in AFM imaging," Meas. Sci. Technol. 19(2008):065101.

[1106] Micro and Nano Technology (MNT) Measurement Club Workshop, Critical Dimension Metrology using SPM, SEM and Related Techniques, Venue: National Physical Laboratory, Hampton Road,

(MAFM) at NPL and the design of the tip-sample interaction AFM (WW-AFM) developed jointly with German national standards laboratory, Physikalisch-Technische Bundesanstalt (PTB). The MAFM is used for traceable calibration of artefacts. The WW-AFM will be used for the examination of tip sample interactions and their effects on dimensional metrology." The joint NPL/PTB work lives on in the European NANOTRACE project described below (Section 4.6.2.4).

To sum up: Yacoot developed COXI along with his German and Italian collaborators by 2000-1. Then he spent from 2002-5 or so working on the 1-DOF COXI/AFM machine with the Germans, whereupon it came to be called the "metrological atomic force microscope" or MAFM. Then he and the Germans spent from 2005-8 adding optical-only interferometric-based metrology ("high-resolution homodyne differential optical interferometry") to the vertical z-axis, thus creating a 2-DOF AFM with COXI-like accuracy (<100 pm?) along the (lateral) x-axis and with optical-interometer-like accuracy (~1-10 nm?) along the (vertical) z-axis. The MAFM site at NPL says: "Atomic force microscopy can be used to calibrate step height standards with nanometre uncertainty and lateral pitch standards with sub nanometre uncertainty."

4.6.2.3 Subsequent COXI Work at IMGC/INRIM (Italy)

Since publication of the landmark COXI paper by Basile et al.[1107] in 2000, the Italian metrology institute IMGC has continued using the entire COXI instrument under the leadership of Dr. Giovanni Mana and Prof. Guido Piragino, but have also apparently not sought to improve it any further. For instance, in 2003 Bergamin et al.[1108] described a design and experimental demonstration of a two-axis tip-tilt platform stacked on a translation stage for COXI. The platform was electronically controlled to compensate for parasitic rotations and straightness errors. "The key characteristic of the platform is the way in which it carries out translations and rotations by sliding. In spite of the potential stop-and-go motion, an x-ray interferometer was successfully operated and guiding errors were kept to within 1 nrad and 1 nm. The platform made it possible to move the x-ray interferometer by up to a couple of millimeters. The combined x-ray and optical interferometer allowed us to investigate the microdynamics of sliding."

By the 2007-2009 funding cycle, IMGC – since renamed the Istituto Nazionale di Ricerca Metrologica or INRIM – had become interested in the precise determination of Avogadro's number, presumably for historical reasons, as part of the International Avogadro Coordination

---

Teddington, Middlesex TW11 0LW, Date: Wednesday 20 September 2006; http://www.npl.co.uk/upload/pdf/programme_PENDNG.pdf.

[1107] G. Basile, P. Becker, A. Bergamin, G. Cavagnero, A. Franks, K. Jackson, U. Kuetgens, G. Mana, E.W. Palmer, M. Stedman, J. Stümpel, A. Yacoot, G. Zosi, "COXI – A Combined Optical and Xray Interferometer for high precision dimensional metrology," Proc. Roy. Soc. Lond. A 456(2000):701-729.

[1108] A. Bergamin, G. Cavagnero, G. Durando, G. Mana, E. Massa, "A two-axis tip-tilt platform for x-ray interferometry," Meas. Sci. Technol. 14(2003):717-723.

(IAC) research project.[1109] According to one grant description,[1110] the existing COXI technology could support "construction of an X-ray interferometer for displacement measurements with picometric resolution: measurement of the a_0 lattice parameter of Si; redetermination of the Avogadro Constant N_A; [and a] proposal for a new kilogram standard." One 2007 paper[1111] from Mana's group reports the further development of the COXI instrumentation: "When external-cavity diode lasers are used in dimensional metrology via optical interferometry, parasitic modes and background radiation deserve careful investigation. This paper gives the relevant measurement equation and explicit formulae for the excess phase of travelling fringes. Particular emphasis is given to potential errors in the measurement of the Si lattice parameter by combined X-ray and optical interferometry." A 2008 paper[1112] from the same group reports that COXI was used to obtain high-quality measurements and provides a detailed discussion of the corrections and uncertainty contributions for the improved COXI system: "A combined X-ray and optical interferometer capable of centimeter displacements has been made to measure the lattice parameter of Si crystals to within a $3x10^{-9}$ (0.003 ppm) relative uncertainty. This paper relates the results of test measurements carried out to assess the capabilities of the apparatus." The most recent 2009 paper[1113] coauthored by the INRIM group and the German PTB group that provided the X-ray interferometer component provides some additional details. The INRIM group developed a guide capable of "interferometer displacements up to 5 cm with guiding errors commensurate with the requirements of atomic-scale positioning and alignment" using the COXI apparatus shown in Figure 4-56.

Notes the 2009 paper:[1114] "With respect to all previous apparatuses, the key development is the extension of the interferometer operation to displacements of 5 cm. This measurement capability is obtained by means of a guide where an L-shaped carriage slides on a quasi-optical rail. An active tripod with three piezoelectric legs rests on the carriage. Each leg expands vertically and shears in the two, X and Y, transverse directions, thus allowing compensation for the sliding errors and electronic positioning of the X-ray interferometer over **six degrees of freedom to atomic-scale accuracy**. Crystal displacement, parasitic rotations and transverse motions are

---

[1109] P. Seyfried, et al., "A determination of the Avogadro constant," Z. Phys. B 87(1992):289-298.

[1110] "Picometria", http://www.centrofermi.it/index.php?pageId=126.

[1111] Gianluca Galzerano, Giovanni Mana, Enrico Massa, "On the effect of broadband emission in external-cavity diode-laser interferometry," Meas. Sci. Technol. 18(2007):1338-1342.

[1112] L. Ferroglio, G. Mana, E. Massa, "Si lattice parameter measurement by centimeter X-ray interferometry," Opt. Express 16(2008):16877-16888; http://www.opticsinfobase.org/abstract.cfm?URI=oe-16-21-16877.

[1113] E. Massa, G. Mana, U. Kuetgens, "Comparison of the INRIM and PTB lattice-spacing standards," Metrologia 46(2009):249-253; http://www.iop.org/EJ/article/0026-1394/46/3/011/met9_3_011.pdf and http://arxiv.org/pdf/0902.0379.

[1114] E. Massa, G. Mana, U. Kuetgens, "Comparison of the INRIM and PTB lattice-spacing standards," Metrologia 46(2009):249-253; http://www.iop.org/EJ/article/0026-1394/46/3/011/met9_3_011.pdf and http://arxiv.org/pdf/0902.0379.

sensed via laser interferometry and by capacitive transducers. Feedback loops provide picometer positioning, nanoradian alignment and interferometer movement with nanometer straightness."

Figure 4-56. Left: Combined X-ray and optical interferometer. Right: Photograph of the WASO 4.2a interferometer (from PTB) – the ruler indicates where the d_{220} measurements were carried out and the remachined area is also visible.[1115]

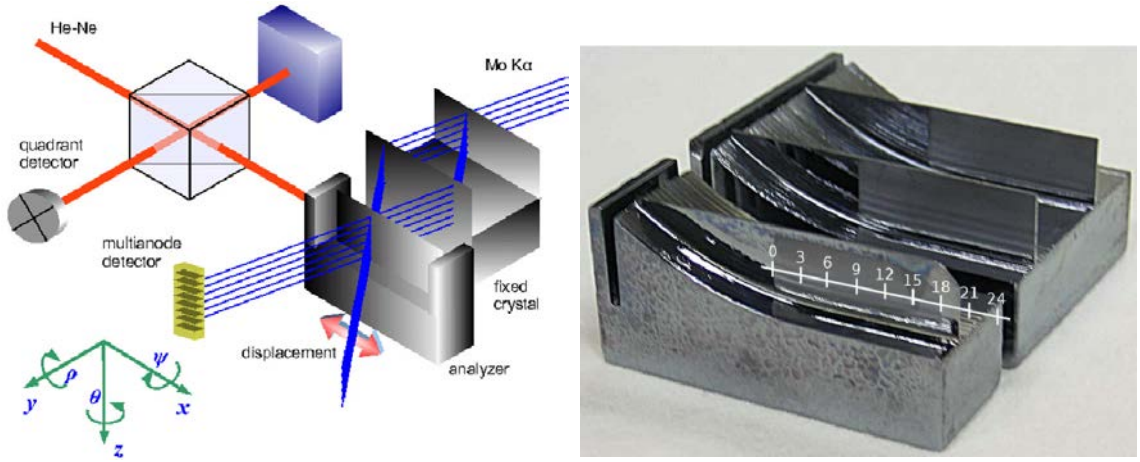

4.6.2.4 EUROMET and the Nanotrace Project (Europe)

The next (expanded) phase of the NPL/PTB collaboration emerged from the following proposal to the European Collaboration in Measurement Standards (EUROMET) program:[1116] "Building on the success of the collaboration between PTB, NPL and IMGC in constructing the combined optical and x-ray interferometer facility (COXI) for calibrating displacement transducers, PTB and NPL are collaborating by combining x-ray interferometry with scanning probe microscopy. This work is proving to be very successful and led to an Institute of Physics Select publication. PTB and NPL have decided to formalize the collaboration and are considering the possibilities for combining optical and x-ray interferometry with scanning probe microscopy. The principal application for the combination of these techniques will be the investigation of long range variations in the periodic structure of artifacts used for the calibration of scanning probe

---

[1115] E. Massa, G. Mana, U. Kuetgens, "Comparison of the INRIM and PTB lattice-spacing standards," Metrologia 46(2009):249-253; http://www.iop.org/EJ/article/0026-1394/46/3/011/met9_3_011.pdf and http://arxiv.org/pdf/0902.0379.

[1116] EUROMET (European Collaboration in Measurement Standards) http://www.euromet.org/cgi-bin/projectsearch.pl?status=specific&SubjectField=LENGTH ; "659. The combination of scanning probe microscopy, optical interferometry and x-ray interferometry," 2008; http://www.euromet.org/cgi-bin/projectfile.pl?prefno=659.

microscopes. Additionally, the collaborators will attempt to seek industrial interest for the development of the combination of these techniques." Yacoot was listed[1117] as the proposer/coordinator for this project (listed as having started in November 2001 and last updated in June 2008).

A U.K government planning document[1118] for the National Measurement System titled "Engineering and Flow Metrology Programme (2008-2011)", dated March 2008, presents a 4-year plan for U.K. metrology programs for which funding was being sought. Two specific projects are of relevance here under Theme 5: Innovative Metrology for Industry.

The first relevant project is titled: "Metrology for atomic force microscopes (AFMs)". According to Section 5.6 of the report (emphasis added):[1119] "The project **provides a metrological infrastructure for Atomic Force Microscopes (AFMs)** enabling reliable traceable measurements to be made using both commercial and metrological AFMs in the UK. This work will build on **world leading capability at NPL for Metrological AFM (MAFM) development** and tip sample interactions. Traceability for AFMs is achieved via NPL's MAFM. **The new NPL designed head for the MAFM will be completed, characterised and commissioned. It will detect cantilever motion extraneous to the servo system providing a more reliable calibration of transfer artefacts overcoming intrinsic problems with the current commercial head.** Software is required for interpolation of data both from periodic and nonperiodic surfaces that cannot be measured optically. To provide better dissemination it is necessary to determine uncertainty sources in commercial AFMs and optimum AFM operating parameters; recently highlighted by ISO TC201 for Scanning Probe Microscopy. This will be done using the existing MAFM, the NPL/PTB developed Tip-Sample Interaction AFM and a number of commercial AFMs. AFM measurements of surface topography need be linked to ISO standards for surface texture measurement. NPL and PTB have already identified several tip sample interaction effects needing quantification and collaborative work will be continued in this area contributing towards the NPL led EURAMET project on the effects of tip sample interactions on dimensional metrology. **The project supports the current paradigm shift in surface metrology towards the examination of structured surfaces that have numerous applications, e.g,,** abrasives, support for tissue, **NEMS devices**."

[1117] EUROMET (European Collaboration in Measurement Standards) http://www.euromet.org/cgi-bin/projectsearch.pl?status=specific&SubjectField=LENGTH ; "659. The combination of scanning probe microscopy, optical interferometry and x-ray interferometry," 2008; http://www.euromet.org/cgi-bin/projectfile.pl?prefno=659.

[1118] "National Measurement System. Engineering and Flow Metrology Programme (2008-2011) for Public Comment, March 2008," NPL 2008-11, http://resource.npl.co.uk/docs/about_npl/nms/engineering_flow.pdf.

[1119] "National Measurement System. Engineering and Flow Metrology Programme (2008-2011) for Public Comment, March 2008," NPL 2008-11, http://resource.npl.co.uk/docs/about_npl/nms/engineering_flow.pdf.

The second project is titled: "X-ray interferometry to support optical metrology". According to Section 5.7 of the report (emphasis added):[1120] "This project provides the necessary co-funding for NPL's participation in **the EMRP project, NANOTRACE**. NPL will be using x-ray interferometry (XRI) to assess the performance and validity of measurement of the next generation of displacement measuring optical interferometers developed by NMIs within Europe. **7 NMIs have joined forces <u>to develop optical interferometers that have a displacement accuracy of 10 pm</u>, representing an uncertainty reduction of one order of magnitude with respect to the present state of the art.** These interferometers are required by NMIs to meet the grand challenges of multidisciplinary metrology: (a) **development and combined application of optical and scanning probe microscopy** for analysis of nano-structured surfaces, nano-particles and photomasks for semiconductor manufacturing (here the contribution is in **developing low uncertainty metrology to be integrated in these systems**); (b)nano-electronics, nano-magnetic and nanoelectro-mechanical systems: **research towards measurement of sub-nm length. The only traceable independent method for verification of performance of these novel optical interferometer designs and the proposed transfer standard is XRI.**

The report[1121] further clarifies NPLs role as follows: "**NPL is leading the NPL-PTB XRI work package**. In previous programmes NPL has measured optical interferometry non-linearity using a combined optical and XRI facility (**COXI**) that was developed jointly with PTB and INRIM. **<u>COXI will be enhanced</u> with more efficient x-ray collimating optics based on polycapillaries and monochromators that will increase useful x-ray signal level, thereby reducing temporal stability requirements**. A digital servo control for the XRI will be developed and software will written for 3 separate data acquisition modes: quantized positioning, continual data collection, and high speed data collection to enable a more rigorous assessment of the performance the interferometers and a transfer standard. Throughout the project close liaison with colleagues from other NMIs will be necessary to ensure that the designs of optical interferometer are compatible with the XRI and that meaningful measurements can be made. **Participation in NANOTRACE places NPL in an ideal position to survey recent advancements in optical interferometry with a view to tackling some of the problems** for practical applications of optical interferometry **such as** alignment, **miniaturisation**, low photon counts and reflections from non-ideal surfaces. **A study will be undertaken with a view to a future project via the rolling formulation process**." Thus the NPL/PTB partnership that is responsible for the "XRI work package" may be developing a high-precision X-ray-interferometry-based AFM positioning system for the Nanotrace project.

In early 2008, the "NanoTrace" project (JRP 1.4) received the requested funding from the European Commission.[1122] A September 2008 presentation at the "NanoScale 2008"

[1120] "National Measurement System. Engineering and Flow Metrology Programme (2008-2011) for Public Comment, March 2008," NPL 2008-11, http://resource.npl.co.uk/docs/about_npl/nms/engineering_flow.pdf.

[1121] "National Measurement System. Engineering and Flow Metrology Programme (2008-2011) for Public Comment, March 2008," NPL 2008-11, http://resource.npl.co.uk/docs/about_npl/nms/engineering_flow.pdf.

[1122] TC-Chair Annual Report 2007/2008 and TC-Length**,** 26 May 2008; Participation in iMERA-Plus, p. 4; http://resource.npl.co.uk/euromet/length/annual_reports/an_rep_2007_2008.pdf.

workshop[1123] titled "Optical interferometry with 10 pm level accuracy – the Project Nanotrace" was co-authored by the following people and institutions: M. Matus and A. Niessner (BEV, Austria); P. Balling, P. Kren, and P. Klapetek (CMI, Czech Republik); A. Lassila (Mikes, Finland); A. Yacoot (NPL, England); G. B. Picotto and M. Pisani (INRIM [formerly IMGC], Italy); J. Flügge and U. Kuetgens (Physikalisch-Technische Bundesanstalt Braunschweig, Germany); and M. Celik and R. Hamid (UME, Turkey). (The presentation was oral; no paper is listed in the special issue of workshop proceedings[1124] due to be published online in June 2009.) Some early results have already been reported by Pisani[1125] (Section 4.6.3.4) and Kren and Balling[1126] (Section 4.6.3.5).

A progress report on Project Nanotrace was published in March 2009 giving results through October 2008.[1127] Nanotrace is a 36-month project that runs from 1 April 2008 through 31 March 2011. The report proclaims that the project "**aims to 10 pm accuracy of displacement metrology** namely by refined optical interferometry. The challenge is an uncertainty reduction of one order of magnitude with respect to the present state of the art....[Given the future metrology requirements for various industries,] interferometer **nonlinearities, noise and stability well below 100 pm** will be necessary. The project will provide a bridge between present state-of-the art of traceable displacement measurements by optical interferometers and future new ways and standards to provide traceability at the atomic scale." It appears that an optical interferometer will be used to achieve project accuracy objectives and that an X-ray interferometer will be used to validate the performance of the optical interferometer. Five "new interferometric techniques" including "combined interferometers" are being pursued independently as possible solutions although it is not explicitly stated that COXI is one of the five; at least one or more approaches involve Fabry-Pérot interferometry (Section 4.6.4).

Three of the five "work packages" are listed as follows:

[1123] "NanoScale 2008" Workshop; Seminar on Quantitative Microscopy and Nanoscale Calibration Standards and Methods, Istituto Nazionale di Ricerca Metrologica (iNRiM), Strada delle Cacce, 91, 10135 Torino, Italy, 22-23 September 2008; http://www.nanoscale.de/docs/nanoscale2008.pdf and http://www.nanoscale.de/docs/NanoScale-2008.pdf.

[1124] http://www.iop.org/EJ/journal/-page=forthart/0957-0233#Special_isNanoScale_.

[1125] Marco Pisani, "A homodyne Michelson interferometer with sub-picometer resolution," Meas. Sci. Technol. 20(2009):084008. See also: M. Pisani, "Interferometer with optical path multiplication for picometer resolution," presentation at NanoScale 2008 conference.

[1126] Petr Kren, Petr Balling, "Common path two-wavelength homodyne counting interferometer development," Meas. Sci. Technol. 20(2009):084009.

[1127] "Publishable JRP Summary for Project T3 J1.4 (NANOTRACE). New Traceability Routes for Nanometrology," EMRP/EURAMET, 6 March 2009, T3.J1.4 JRP NANOTRACE; http://www.euramet.org/fileadmin/docs/EMRP/JRP/JRPnew/T3_J1.4_NANOTRACE__publishable_summary_r2.pdf.

WP2: "**Development of new interferometric techniques"** will be articulated in 5 independent activities each one devoted to the realization and test of new interferometric techniques. Although the goal is the same (to minimize measurement uncertainty at the nanoscale) the techniques to be investigated exploit different technical solutions and/or physical principles. Each one is equally promising and has possible advantages with respect to the others. The pioneering level of the target requires a 360° investigation without an a priori choice of the "best" direction to go.

WP4: "**X-ray interferometer set-up"** is a joint program to implement an existing X-ray interferometer in order to allow its use for the characterization of the interferometers developed in WP2. The X-ray interferometer, based on the silicon crystal atomic lattice, has an intrinsic uncertainty to the picometer level, thus is the ideal instrument to validate new interferometers.

WP5: "Comparison" is to compare each interferometer developed in WP2 directly (for transportable interferometers) or indirectly by means of the transfer standard (for non transportable interferometers) with the X-ray interferometer. The comparison will allow a reliable evaluation of the results. The activity of WP5 will be carried out during the third year.

4.6.2.5 Atomic Displacement Metrology – COXI at NIST (U.S.)

A COXI development effort in the U.S. might have been underway at least as early as 2001, led by John R. Lawall at NIST. According to the NIST website titled "Atomic Displacement Metrology":[1128] "Linear displacement is a primitive component of many fundamental physical and technical measurements, yet its realization with atomic scale refinement and accuracy is difficult. Displacements are related to primary wavelength standards by interferometry, and at the moment, the accuracy of interferometric measurements is at least two orders of magnitude below that of commercially available reference lasers. We are working at improving the understanding and application of interferometry. The one-dimensional displacement of a specially fabricated translation stage will be simultaneously measured by means of heterodyne Michelson interferometry, scanning Fabry-Pérot interferometry, and X-ray interferometry." (NIST apparently has also developed a high-accuracy ion-pumped X-ray interferometer.)

The website continues: "This approach will allow robust control of the systematic errors that currently limit the accuracy of displacement measurements. The translation stage will be controlled in real time by closing a servo loop incorporating multiple Michelson interferometers. We currently are working toward measuring a **displacement of up to 5 centimeters with 50-picometer resolution** in a high-vacuum, vibration-controlled environment. Combining the optical techniques with simultaneous X-ray interferometry will allow us to perform a measurement of the lattice constant of silicon over a longer range than has ever been attempted (COXI). The program will address the metrology requirements of the semiconductor industry in the coming decade and have impacts in science in areas as diverse as gamma-ray spectroscopy and the realization of the kilogram using fundamental constants."

[1128] "Atomic Displacement Metrology," NIST, 2001-2007; http://www.nist.gov/public_affairs/guide/atomic_physics.htm.

However, Lawall's recent success in measuring 25 mm distances to 10 pm accuracy, reported in 2005,[1129] was achieved using Fabry-Pérot techniques (Section 4.6.4.2), not COXI. There appears to be no active COXI development effort currently underway at NIST.

4.6.2.6 2D COXI at KRISS/KAIST (South Korea)

A research group headed by Cheon Il Eom at the Korea Research Institute of Standards and Science (KRISS) in South Korea has been pursuing COXI since at least 1998, and continuing to the present time.[1130] According to early papers:[1131] "In the COXI (Combined Optical and X-ray Interferometer) system, optical and X-ray interferometers are combined to provide a means for the calibration of transducers with the traceability to the standards of length in the sub-nanometer region. The objective of COXI is to provide a means for the calibration of transducers or laser interferometers in the nanometer range in terms of the standards of length. The basic idea of COXI is to combine an X-ray interferometer with an optical interferometer in such a way that one can obtain the Angstrom resolution of the X-ray interferometer over the extended measurement range. The limited measurement range and speed of an X-ray interferometer can be increased in COXI by using the optical interferometer as the main ruler and the X-ray interferometer as a

---

[1129] J.R. Lawall, "Fabry-Perot metrology for displacements up to 50 mm," J. Optical Soc. Amer. A 22(December 2005):2786-2798; http://www.opticsinfobase.org/abstract.cfm?URI=josaa-22-12-2786 . See also: "Physicists measure 'long' distances with picometer accuracy," 2 December 2005; http://www.physorg.com/news8668.html.

[1130] Noh B. Yim, Min Seok Kim, Cheon I. Eom, "Development of a combined optical and x-ray interferometer (COXI) system for nanometrology," Proc. SPIE Vol. 3479, p. 94-101, Laser Interferometry IX: Applications, Ryszard J. Pryputniewicz; Gordon M. Brown; Werner P. Jueptner; Eds., July 1998. Cheon Il Eom, Noh Bin Yim, "Development of a combined optical and X-ray interferometer (COXI)at KRISS," CLEO/Pacific Rim Conference on Lasers and Electro-Optics, 1(1999):62-63. Jinwon Park, Jaegun Jo, Sangho Byun, Jae Wan Kim, Tae Bong Eom and Cheon Il Eom, "Development of a Two-Dimensional Nano-Displacement Measuring System Utilizing a 2D Combined Optical and X-ray Interferometer," Journal of the Korean Physical Society 48(January 2006):28-32. http://length.kriss.re.kr/research/performance.html. Dong-Yeon Lee, Dong-Min Kim, Dae-Gab Gweon, Jinwon Park, "A calibrated atomic force microscope using an orthogonal scanner and a calibrated laser interferometer," Applied Surface Science 253(15 February 2007):3945-3951. D. Kim, D.Y. Lee, D.G. Gweon, "A new nano-accuracy AFM system for minimizing Abbe errors and the evaluation of its measuring uncertainty," Ultramicroscopy 107(Apr-May 2007):322-328. Cheon Il Eom, "Nanometrological Application of X-ray Interferometry," Journal of the Korean Society of Precision Engineering 17(June 2000):40-45. In Korean language. http://length.kriss.re.kr/publication/JKSPE_17_40_2000_iL.pdf. J.W. Park, J.G. Jo, S.H. Byun, J.E. Kim, C.I. Eom, "LVDT calibration using a phase modulation optical interferometer calibrated by an x-ray interferometer [5532-04]," Proc. SPIE 5532(August 2004):28-36. (Interferometry XII: Applications; Wolfgang Osten, Erik Novak, eds.).

[1131] Noh B. Yim, Min Seok Kim, Cheon I. Eom, "Development of a combined optical and x-ray interferometer (COXI) system for nanometrology," Proc. SPIE Vol. 3479, p. 94-101, Laser Interferometry IX: Applications, Ryszard J. Pryputniewicz; Gordon M. Brown; Werner P. Jueptner; Eds., July 1998. Cheon Il Eom, Noh Bin Yim, "Development of a combined optical and X-ray interferometer (COXI)at KRISS," CLEO/Pacific Rim Conference on Lasers and Electro-Optics, 1(1999):62-63.

linear interpolator. This was first suggested and reported by researchers in NPL, PTB, and IMGC. The COXI mainly comprises a laser interferometer, an X-ray interferometer, and a precision translation stage. The laser interferometer used for the COXI instrument was a Michelson type, differential heterodyne interferometer having common optical path. A monolithic x-ray interferometer was made from a silicon single crystal. We have designed a control procedure to operate the COXI instrument for the calibration of nano-transducers and developed a phase demodulator for use with the laser interferometer. The COXI which is under development at the Korea Research Institute of Standards and Science (KRISS) is aimed at a measurement uncertainty of **100 pm over 1 mm range**."

By 2006, Eom's group had demonstrated the first multi-axis COXI system capable of 2-D displacement measurements,[1132] which they call "2D COXI". The system is operated in air and consists of two optical interferometers, an X-ray interferometer, and a flexure stage to control two-dimensional displacements with high accuracy (Figure 4-57). "In principle, an X-ray interferometer in a two-dimensional COXI system should be of a two-dimensional displacement type. However, the manufacturing process of a two-dimensional monolithic X-ray interferometer is complicated and time-consuming. If the problem of complexity in a two- or three-dimensional COXI system is to be overcome, the system must be operated with a one-dimensional X-ray interferometer. To operate a two- or three-dimensional COXI in this manner, two or three optical interferometers are connected to the movable part of the X-ray interferometer. If the 2D COXI is combined with an atomic force microscope (AFM), it has the potential in metrology to measure a two-dimensional line-width or the pitch of a grating specimen."

[1132] Jinwon Park, Jaegun Jo, Sangho Byun, Jae Wan Kim, Tae Bong Eom and Cheon Il Eom, "Development of a Two-Dimensional Nano-Displacement Measuring System Utilizing a 2D Combined Optical and X-ray Interferometer," Journal of the Korean Physical Society 48(January 2006):28-32.

Figure 4-57. Experimental setup of the COXI for the measurement of two-dimensional displacement; X-axis represents horizontal moving and Y -axis vertical moving of XY flexure stage; BS = beam splitter, PBS = polarizing beam splitter, QWP = quarter wave plate, Det = detector.[1133]

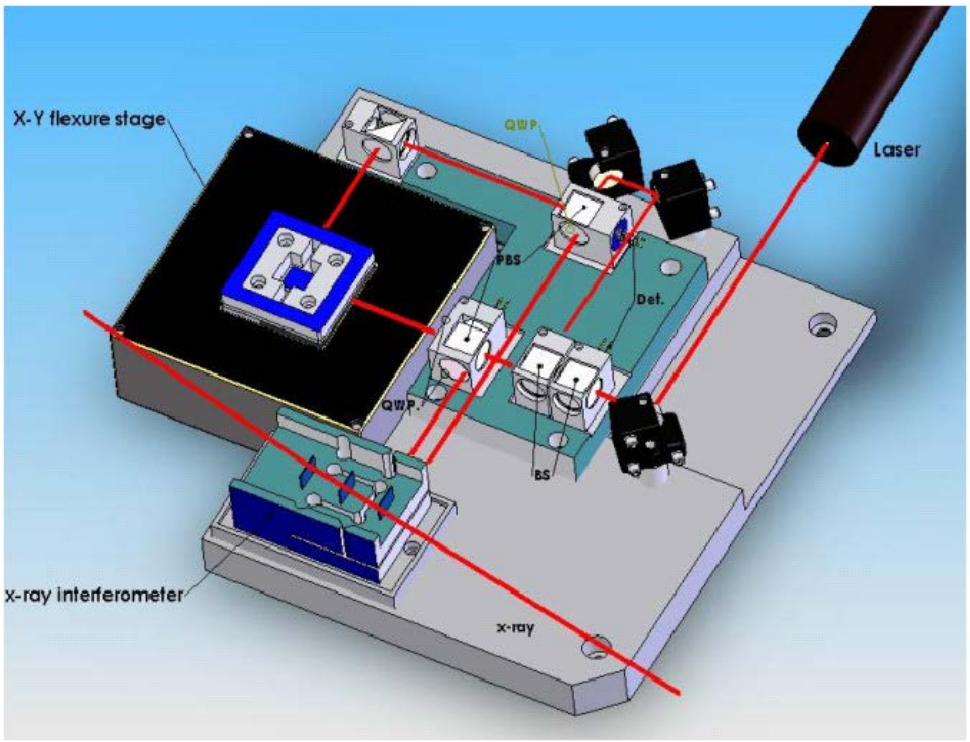

The nano-scale measuring system referred to as the 2D COXI consists of an X-ray and two optical interferometers. The optical interferometers generate signals on a precise scale (316 nm) that are traceable to the length standard, and the signals of the X-ray interferometer can subdivide the signal of the optical interferometer into 1,648 parts (192 pm). The two combined interferometers are able to measure a large displacement with subnanometer accuracy.[1134]

The X-ray interferometer was made from a nearly perfect Si (220) crystal. The X-ray interferometer (Figure 4-58) consists of three thin lamellas: a beam splitter (S), a mirror (M), and an analyzer (A). A monolithic X-ray interferometer with a single parallel spring structure was

---

[1133] Jinwon Park, Jaegun Jo, Sangho Byun, Jae Wan Kim, Tae Bong Eom and Cheon Il Eom, "Development of a Two-Dimensional Nano-Displacement Measuring System Utilizing a 2D Combined Optical and X-ray Interferometer," Journal of the Korean Physical Society 48(January 2006):28-32.

[1134] Jinwon Park, Jaegun Jo, Sangho Byun, Jae Wan Kim, Tae Bong Eom and Cheon Il Eom, "Development of a Two-Dimensional Nano-Displacement Measuring System Utilizing a 2D Combined Optical and X-ray Interferometer," Journal of the Korean Physical Society 48(January 2006):28-32.

designed and manufactured to translate the analyzer lamella. The translation structure was made from a single crystal of silicon to obtain the parallel and rectilinear movements of the analyzer lamella with respect to the other lamellas. The analyzer lamella is moved by a piezoelectric drive, and moves within a range of a few microns. The thickness of the lamellas is 0.6 mm and the dimensions of the X-ray interferometer are 62 mm x 43 mm x 42 mm.[1135] The radiation source for the X-ray interferometer was a water-cooled molybdenum X-ray tube of typical power 1.4 kW. The slit size for the X-ray collimator of the entrance beam setup was 1 mm × 10 mm and the displacement range of the X-ray interferometer was 633 nm. The entire 2D COXI apparatus shown in Figure 4-57 measures approximately 22 cm x 22 cm x 8 cm.

Figure 4-58. Photographs of the X-ray interferometer made at KRISS, at left,[1136] and the lab bench apparatus, at right,[1137] which is operated in air, not in UHV.

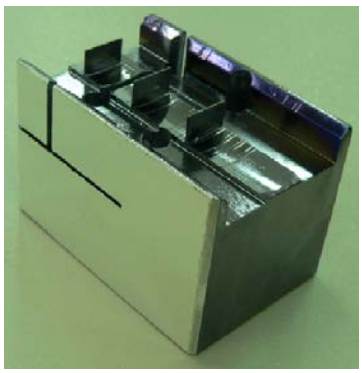

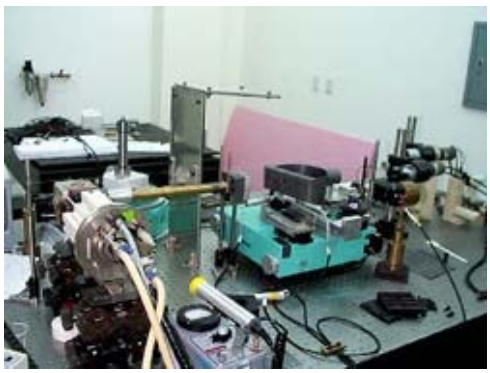

According to the paper,[1138] the X-ray corrected residual displacement errors in X and Y were about ±200 pm over 200 nm travel distances, and about twice that over 633 nm travel distances. However, judging from the uncertainty budget calculated in their Table 1, virtually all of the error comes from just two sources – (1) the refractive index of air, which would be entirely eliminated for operations in UHV when no air is present, and (2) the nonlinearity of the optical system, which could be entirely eliminated if the optical system is employed solely to get close enough to a known atomic-scale fiducial marker to allow precise tip re-registration, after which the X-ray

---

[1135] Jinwon Park, Jaegun Jo, Sangho Byun, Jae Wan Kim, Tae Bong Eom and Cheon Il Eom, "Development of a Two-Dimensional Nano-Displacement Measuring System Utilizing a 2D Combined Optical and X-ray Interferometer," Journal of the Korean Physical Society 48(January 2006):28-32.

[1136] Jinwon Park, Jaegun Jo, Sangho Byun, Jae Wan Kim, Tae Bong Eom and Cheon Il Eom, "Development of a Two-Dimensional Nano-Displacement Measuring System Utilizing a 2D Combined Optical and X-ray Interferometer," Journal of the Korean Physical Society 48(January 2006):28-32.

[1137] http://length.kriss.re.kr/research/performance.html.

[1138] Jinwon Park, Jaegun Jo, Sangho Byun, Jae Wan Kim, Tae Bong Eom and Cheon Il Eom, "Development of a Two-Dimensional Nano-Displacement Measuring System Utilizing a 2D Combined Optical and X-ray Interferometer," Journal of the Korean Physical Society 48(January 2006):28-32.

detection system is used all the rest of the way in to the workpiece. If these two sources of error were entirely eliminated, then the remaining combined standard uncertainty would fall to at most **72 pm**, which would be almost workable for our molecular workstation. This is consistent with the claim in the paper[1139] that "the total uncertainty related to the X-ray interferometer was ±54 pm (k = 2)." One minor problem is that the counting rate of X-ray interference signals in 2D COXI was less than three signals per second due to the restricted bandwidth of the X-ray photon counting chain, at least tenfold slower than the original COXI system[1140] whose X-ray beam intensity was enhanced using a parabolic reflecting mirror (Section 4.6.2.1).

The 2006 paper[1141] concludes: "In the near future, the authors of this study hope to develop a two-dimensional nano-scale pitch or line-width measuring system using the 2D COXI combined with an AFM based on the findings of the present study." By 2007, members of the KRISS group with collaborators at the Korea Advanced Institute of Science and Technology (KAIST) demonstrated[1142] a compact two-dimensional atomic force microscope (AFM) using an orthogonal long-range sample scanner with a 100 μm × 100 μm range,[1143] a calibrated homodyne laser interferometer, and a commercial AFM head developed for use in the nano-metrology field. The conventional homodyne laser interferometer was used to measure the X and Y displacements of the sample, while being compensated via an X-ray interferometer to reduce the nonlinearity of the optical interferometer, yielding an AFM tip uncertainty of ±300 pm.[1144]

[1139] Jinwon Park, Jaegun Jo, Sangho Byun, Jae Wan Kim, Tae Bong Eom and Cheon Il Eom, "Development of a Two-Dimensional Nano-Displacement Measuring System Utilizing a 2D Combined Optical and X-ray Interferometer," Journal of the Korean Physical Society 48(January 2006):28-32.

[1140] G. Basile, P. Becker, A. Bergamin, G. Cavagnero, A. Franks, K. Jackson, U. Kuetgens, G. Mana, E.W. Palmer, M. Stedman, J. Stümpel, A. Yacoot, G. Zosi, "COXI – A Combined Optical and Xray Interferometer for high precision dimensional metrology," Proc. Roy. Soc. Lond. A 456(2000):701-729.

[1141] Jinwon Park, Jaegun Jo, Sangho Byun, Jae Wan Kim, Tae Bong Eom and Cheon Il Eom, "Development of a Two-Dimensional Nano-Displacement Measuring System Utilizing a 2D Combined Optical and X-ray Interferometer," Journal of the Korean Physical Society 48(January 2006):28-32.

[1142] Dong-Yeon Lee, Dong-Min Kim, Dae-Gab Gweon, Jinwon Park, "A calibrated atomic force microscope using an orthogonal scanner and a calibrated laser interferometer," Applied Surface Science 253(15 February 2007):3945-3951.

[1143] D. Kim, D.Y. Lee, D.G. Gweon, "A new nano-accuracy AFM system for minimizing Abbe errors and the evaluation of its measuring uncertainty," Ultramicroscopy 107(Apr-May 2007):322-328.

[1144] Dong-Yeon Lee, Dong-Min Kim, Dae-Gab Gweon, Jinwon Park, "A calibrated atomic force microscope using an orthogonal scanner and a calibrated laser interferometer," Applied Surface Science 253(15 February 2007):3945-3951.

4.6.2.7 XROI at NRLM/NMIJ (Japan)

A research group headed by Hiroyuki Fujimoto and Kan Nakayama at the National Research Laboratory of Metrology (NRLM) in Japan pursued COXI starting in the early 1990s[1145] primarily for the purpose of determining the precise lattice constant of Si, possibly as part of the international effort to determine Avogadro's number. (By 2004, Fujimoto was at the National Metrology Institute of Japan (NMIJ) in AIST, the successor organization to NRLM.)

In 1993, the Japanese group at NRLM constructed a combined X-ray/optical interferometer, called an "XROI", with a new translation stage and a preliminary measurement was made of the (220) lattice spacing of a silicon crystal in air[1146] and in vacuum using upgraded instruments in 1994.[1147] An alternative design of optical interferometer with picometer sensitivity, also for use with an X-ray interferometer and using a Pockels cell for phase modulation, was presented by by the group in 1995.[1148] According to the abstract: "**Picometer interferometry of moving objects is demonstrated experimentally** over the frequency range 0 to 160 Hz. Active feedback is adopted to reduce the lowest frequency noise component due to coupling between geometrical fluctuations of the laser beam incident on the interferometer optics and imperfections in its optical elements. Passive measures to reduce the noise due to thermally induced changes of optical elements both in the geometrical arrangement and in the optical properties are introduced by decreasing the sensitivity to temperature change. With these methods the resultant **noise is reduced to 3 pm**." The group's combined X-ray and optical interferometer measured the lattice spacing d_{220} of a silicon crystal to a relative uncertainty of 0.160 ppm in 1995[1149] and 0.050 ppm

---

[1145] K. Nakayama, H. Fujimoto, M. Tanaka, K. Kuroda, "Silicon lattice measurement with an improved X-ray/optical interferometer," IEEE Trans. Instrum. and Meas. 42(1993):401-404. K. Nakayama, H. Fujimoto, M. Tanaka, G. Misawa, "Silicon lattice measurement with an X-ray/optical interferometer in a vacuum [Avogadro constant determination]," Digest. 1994 Conference on Precision Electromagnetic Measurements, 27 Jun - 1 Jul 1994. pp. 510-511. H. Fujimoto, T. Mitsuru, K. Nakayama, "Noise reduction in an optical interferometer for picometer measurements," IEEE Trans. Instrum. Meas. 44(April 1995):471-474. Hiroyuki Fujimoto, Kan Nakayama, Mitsuru Tanaka, Guento Misawa, "Absolute Measurement of Lattice Spacing d(220) in Floating Zone Silicon Crystal," Jpn. J. Appl. Phys. 34(1995):5065-5069; http://jjap.ipap.jp/link?JJAP/34/5065/. K. Nakayama, H. Fujimoto, "Progress in the measurement of lattice spacing d(220) of silicon," IEEE Transactions on Instrumentation and Measurement 46(April 1997):580-583.

[1146] K. Nakayama, H. Fujimoto, M. Tanaka, K. Kuroda, "Silicon lattice measurement with an improved X-ray/optical interferometer," IEEE Trans. Instrum. and Meas. 42(1993):401-404.

[1147] K. Nakayama, H. Fujimoto, M. Tanaka, G. Misawa, "Silicon lattice measurement with an X-ray/optical interferometer in a vacuum [Avogadro constant determination]," Digest. 1994 Conference on Precision Electromagnetic Measurements, 27 Jun - 1 Jul 1994. pp. 510-511.

[1148] H. Fujimoto, T. Mitsuru, K. Nakayama, "Noise reduction in an optical interferometer for picometer measurements," IEEE Trans. Instrum. Meas. 44(April 1995):471-474.

[1149] Hiroyuki Fujimoto, Kan Nakayama, Mitsuru Tanaka, Guento Misawa, "Absolute Measurement of Lattice Spacing d(220) in Floating Zone Silicon Crystal," Jpn. J. Appl. Phys. 34(1995):5065-5069; http://jjap.ipap.jp/link?JJAP/34/5065/.

in 1997.[1150] As recently as 2007, Fujimoto and Nakayama[1151] were still focused on refining the silicon lattice parameter but it was unclear if they are still actively pursuing XROI system development in 2009.

4.6.2.8 Summary of COXI-Based Systems

COXI has demonstrated 35 pm measurement uncertainty over 100 micron round-trip displacement paths in 1 dimension (1 DOF) at the 95% confidence level with a drift rate of ~2 pm/min (European NPL/PTB/IMGC group, Sections 4.6.2.1-4.6.2.3; European Nanotrace Project, Section 4.6.2.4), and 2-dimensional COXI (2 DOFs) has also been demonstrated experimentally albeit with somewhat poorer precision (the South Korean KRISS/KAIST group, Section 4.6.2.6); Yacoot's group at NPL/PTB, Section 4.6.2.2). COXI-based detection has also been demonstrated on AFM systems (the NPL/PTB group, Section 4.6.2.2).

Thus it appears that COXI could provide positional detection of sufficient precision to enable dead-reckoning pick-and-place DMS operations (without continuous sensory feedback, though likely requiring periodic re-registration), in a molecular workstation to be used for atomically precise DMS-based molecular manufacturing.

4.6.3 Michelson Interferometry Systems

This Section describes methods for measuring displacements using conventional Michelson interferometry that have been proposed or demonstrated that are capable of picometer resolution.

4.6.3.1 Lawall-Kessler Differential Optical Interferometry (NIST, U.S.)

Heterodyne or homodyne interferometers can be directly used to measure nanometer or sub-nanometer displacements, or can be used to calibrate displacement sensors, such as capacitive sensors, inductive sensors, and holographic scales. But while heterodyne or homodyne interferometer systems can guarantee traceability of measurement, it is difficult to achieve sub-nanometer accuracy because of nonlinear errors;[1152] special efforts must be made to remove

---

[1150] K. Nakayama, H. Fujimoto, "Progress in the measurement of lattice spacing d(220) of silicon," IEEE Transactions on Instrumentation and Measurement 46(April 1997):580-583.

[1151] H. Fujimoto, G. Mana, K. Nakayama, "A Possible Solution for the Discrepancy Between the INRIM and NMIJ Values of the Si Lattice-Parameter," IEEE Transactions on Instrumentation and Measurement 56(April 2007):351-355.

[1152] C.-M. Wu, C.-S. Su, "Nonlinearity in measurements of length by optical interferometry," Meas. Sci. Technol. 7(1996):62-68. C.-M. Wu, R.D. Deslattes, "Analytical modeling of the periodic nonlinearity in heterodyne interferometry," Appl. Opt. 37(1998):6696-6700.

periodic nonlinearity.[1153] In 2000 Lawall and Kessler[1154] at the National Institute for Standards and Technology (NIST) demonstrated a new optical heterodyne Michelson differential interferometer design with a resolution (periodic nonlinearities) of **10 pm** whose theoretically achievable accuracy over a **1 mm range** was limited mainly by residual periodic errors and the laser's stability. This paper provides many useful insights and thus we draw from it extensively, below.

Michelson interferometry is the most widely used technique for accurate displacement measurements over length scales of nanometers to meters. The essence of the method is to measure the phase of an optical wave as a target reflector is moved, and to infer the displacement of the reflector in terms of the known wavelength λ of the laser used. Nominally a phase advance of 2π corresponds to a displacement of $\lambda/2$; very high accuracy requires corrections for such factors as the index of refraction of air (except in vacuum) and diffraction. Nevertheless, the characteristic feature of Michelson interferometry for length metrology is to infer a displacement from a phase measurement.[1155]

Each 2π phase change corresponds to an advance from one interference fringe to the next fringe. Optical interferometric techniques for nanometer measurement involve the use of subdivision of interference fringes (within 2π) to achieve high measurement accuracy and resolution.[1156] These subdivisions in various interferometers can be classified into two main types – optical and electronic. Optical subdivision utilizes an appropriate optical configuration design or features of optical elements to achieve fringe subdivision. For example, the optical subdivision factor of 1/4 is obtained in a heterodyne interferometric system by use of a three-longitudinal-mode He-Ne laser.[1157] An optical subdivision factor of 1/8 is obtained by use of a four-path Michelson

---

[1153] S. Gonda, T. Doi, T. Kurosawa, Y. Tanimura, N. Hisata, T. Yamagishi, H. Fujimoto, H. Yukawa, "Real-time, interferometrically measuring atomic force microscope for direct calibration of standards," Rev. Sci. Instr. 70(1999):3362-3368. T. Keem, S. Gonda, I. Misumi, Q. Huang, and T. Kurosawa, "Removing nonlinearity of a homodyne interferometer by adjusting the gains of its quadrature detector systems," Appl. Opt. 43(2004):2443-2448. T. Eom, T. Choi, K. Lee, H. Choi, S. Lee, "A simple method for the compensation of the nonlinearity in the heterodyne interferometer," Meas. Sci. Technol. 13(2002):222-225. M. Sawabe, F. Maeda. Y. Yamaryo, T. Simomura, Y. Saruki, T. Kubo, H. Sakai, S. Aoyagi, "A new vacuum intrerferometric comparator for calibrating the fine linear encoders and scales," Precision Eng. 28(2004):320-328.

[1154] John Lawall, Ernest Kessler, "Michelson interferometer with 10 pm accuracy," Rev. Scient. Instrum. 71(2000):2669-2676. http://link.aip.org/link/?RSINAK/71/2669/1.

[1155] John Lawall, Ernest Kessler, "Michelson interferometer with 10 pm accuracy," Rev. Scient. Instrum. 71(2000):2669-2676. http://link.aip.org/link/?RSINAK/71/2669/1.

[1156] Benyong Chen, Xiaohui Cheng, Dacheng Li, "Dual-wavelength interferometric technique with subnanometric resolution," Appl Opt. 41(1 October 2002):5933-5937.

[1157] T. Yokoyama, T. Araki, S. Yokoyama, N. Suzuki, "A subnanometre heterodyne interferometric system with improved phase sensitivity using a three-longitudinal-mode He–Ne laser," Meas. Sci. Technol. 12(2001):157-162.

interferometer,[1158] and an optical subdivision factor of 1/24 can be achieved with a nonsymmetrical double grating.[1159] Electronic subdivision mainly uses electrical techniques to subdivide the intensities or phases of interference fringes to achieve fringe subdivision. For example, the electronic subdivision factor can reach up to 1/1000 in phase-shifting interferometry[1160] or, by use of a fast analog-to-digital converter[1161] or a calibration technique,[1162] the electronic subdivision factors of from 1/100 to 1/2000 can be obtained with CCDs.[1163] The subdivision factor of 1/2048 can be achieved by a combination of optical and electronic subdivisions.[1164]

With the advent of state-of-the-art digital signal processing (DSP) technology, it has now become possible to make rapid phase measurements with a resolution of 0.01° (one part in 36,000) with readily available commercial equipment. At the wavelength most often used for such displacement measurements, $\lambda = 633$ nm, this corresponds to a resolution of $(\lambda/2)/(36{,}000) \sim 9$ pm. Since conventional commercial interferometers available in the early 2000s fell far short of this resolution, it was natural to ask if it is feasible to adapt this DSP technology to Michelson interferometry and meaningfully interpolate optical fringes by a factor of 36,000. Lawall and Kessler[1165] showed that it is indeed possible to do so – achieving with their design a resolution of less than 10 pm, about two orders of magnitude better than was possible with a commercial interferometer based on a Zeeman-stabilized laser.

[1158] O. Cip, F. Petru, "Compensation method for the scale linearization of the high-precision laser interferometer," in: M. Hrabovsky, A. Strba, W. Urbanczyk, eds., 11th Slovak-Czech-Polish Optical Conference on Wave and Quantum Aspects of Contemporary Optics, Proc. SPIE 3820(1998):144-153.

[1159] H. Lu, J. Cao, S. Su, G. Tang, "Displacement sensor with nonsymmetrical double gratings," in: D. Jiang, A. Wang, eds., International Conference on Sensors and Control Techniques, Proc. SPIE 4077(2000):40-43.

[1160] R. Onodera, Y. Ishi, "Two-wavelength phase-shifting interferometry insensitive to the intensity modulation of dual laser diodes," Appl. Opt. 33(1994):5052-5061.

[1161] J.W. Brault, "New approach to high-precision Fourier transform spectrometer design," Appl. Opt. 35(1996):2891-2896.

[1162] K.P. Birch, "Optical fringe subdivision with nanometric accuracy," Precis. Engng. 12(1990):195-198.

[1163] P. Long, W. Pei, D. Hsu, "Direct subdivision of moire fringe with CCD," in: D. Wang, ed., International Conference on Optoelectronic Science and Engineering '90, Proc. SPIE 1230(1990):165-166. B. Chen, D. Li, R. Zhu, "Algorithm for automatic tracing of interference fringes and its application to nanometer measurement," Opt. Technique 27(2001):223-225, 228.

[1164] O. Cip, F. Petru, "Compensation method for the scale linearization of the high-precision laser interferometer," in: M. Hrabovsky, A. Strba, W. Urbanczyk, eds., 11th Slovak-Czech-Polish Optical Conference on Wave and Quantum Aspects of Contemporary Optics, Proc. SPIE 3820(1998):144-153.

[1165] John Lawall, Ernest Kessler, "Michelson interferometer with 10 pm accuracy," Rev. Scient. Instrum. 71(2000):2669-2676. http://link.aip.org/link/?RSINAK/71/2669/1.

There are two general types of measurement errors in Michelson interferometry that limit the ability to accurately interpolate between fringes – statistical (or random) errors and systematic errors.

The **statistical errors** in fringe interpolation are due to laser amplitude noise and detector noise.[1166] Regarding the laser amplitude noise, heterodyne techniques allow the signal to be placed at a frequency high enough that the laser amplitude noise is entirely due to quantum statistics, i.e., the "shot noise".[1167] The resolution of a Michelson interferometer limited solely by shot noise is given by:[1168]

$$dx_{quantum} = (1/4\pi)\,(2hc\lambda B/\eta P)^{1/2}$$

where $h = 6.63 \times 10^{-34}$ J-sec (Planck constant) and $c = 3 \times 10^{8}$ m/sec (speed of light), B is the measurement bandwidth, η is the detector quantum efficiency, and P is the laser optical power available. Regarding the classical detector noise, the limiting resolution may be shown to be inversely proportional to the signal to noise ratio as follows:

$$dx_{classical} = (\lambda/4\pi)\,(NEP/P)\,B^{1/2}$$

where NEP is the noise equivalent power of the detector; $(NEP)(B^{1/2})$ is the amount of light necessary to produce a dc signal equal to the RMS output noise level.[1169] A typical commercial photodetector (e.g., the ThorLabs PDA 150 detector)[1170] has NEP ~ 7 pW/√Hz and a quantum efficiency of $\eta \sim 0.8$; at a wavelength of $\lambda = 633$ nm the quantum noise dominates the detector noise above a power level of ~62 μW.[1171] Taking for concreteness a laser power of P = 100 μW and a measurement bandwidth of B = 10 KHz,[1172] the uncertainty due to shot noise is

---

[1166] John Lawall, Ernest Kessler, "Michelson interferometer with 10 pm accuracy," Rev. Scient. Instrum. 71(2000):2669-2676. http://link.aip.org/link/?RSINAK/71/2669/1.

[1167] J. Hall, L. Hollberg, T. Baer, H. Robinson, "Optical heterodyne saturation spectroscopy,"Appl. Phys. Lett. 39(1981):680-682. B.J. Meers, K.A. Strain, "Modulation, signal and quantum noise in interferometers," Phys. Rev. A 44(1991):4693-4703.

[1168] L.F. Vitushkin, M.Z. Smirnov, "Combined displacement interferometers," Opt. Spectrosc. 60(1986):379. Andrew J. Stevenson, Malcolm B. Gray, Hans-A. Bachor, David E. McClelland, "Quantum-noise-limited interferometric phase measurements," Appl. Opt. 32(1993):3481-3493.

[1169] John Lawall, Ernest Kessler, "Michelson interferometer with 10 pm accuracy," Rev. Scient. Instrum. 71(2000):2669-2676. http://link.aip.org/link/?RSINAK/71/2669/1.

[1170] John Lawall, Ernest Kessler, "Michelson interferometer with 10 pm accuracy," Rev. Scient. Instrum. 71(2000):2669-2676. http://link.aip.org/link/?RSINAK/71/2669/1.

[1171] John Lawall, Ernest Kessler, "Michelson interferometer with 10 pm accuracy," Rev. Scient. Instrum. 71(2000):2669-2676. http://link.aip.org/link/?RSINAK/71/2669/1.

[1172] John Lawall, Ernest Kessler, "Michelson interferometer with 10 pm accuracy," Rev. Scient. Instrum. 71(2000):2669-2676. http://link.aip.org/link/?RSINAK/71/2669/1.

$dx_{quantum}$ = 0.44 pm and that due to detector noise is $dx_{classical}$ = 0.36 pm. Adding these in quadrature gives a total measurement uncertainty of **0.57 pm**, corresponding to fringe interpolation of one part in 555,000. Thus statistical considerations allow fringe interpolation well beyond a factor of 36,000 even with modest laser powers and bandwidths of tens of KHz.

The **systematic errors** in fringe interpolation limit the resolution of displacement-measuring interferometers to well above the level allowed by statistical considerations. Such systematic errors are well known[1173] and easy to observe by simply performing a linear scan over many fringes – since the error will be the same for every fringe, this error will be periodic with a Fourier spectrum containing the fundamental fringe frequency and harmonics. Thus Fourier analysis of the residuals allows a direct measure of the systematic errors made in fringe interpolation.

One traditional approach to practical Michelson interferometry for displacement measurement is the heterodyne interferometer in which two co-propagating beams of nominally orthogonal polarizations, separated in frequency by ν_0 = 2 MHz, are generated by means of a Zeeman-stabilized helium-neon laser with λ = 633 nm (Figure 4-59).[1174] The beams are separated by a polarizing beamsplitter, and the two beams propagate in separate arms of a conventional Michelson interferometer, one of which incorporates the target reflector. The reflected beams are combined, a beat signal is detected with a frequency of $\nu \sim \nu_0$, and comparison of the phase evolution of this signal with respect to that of the reference signal at ν_0 allows one to infer the displacement.[1175] By working at a heterodyne frequency of ν_0 = 2 MHz, the desired information is placed in a spectral region at which the laser is shot-noise limited. Nevertheless, it is found in practice that it is not useful to interpolate fringes beyond about one part in 300, wherein Fourier spectra of the residuals from a linear scan show systematic errors at the nanometer level. The primary cause of these systematic errors is optical cross-talk between the measurement and reference channels due to imperfect correlation between frequency and polarization ("polarization mixing") in Zeeman-stabilized laser interferometry. While brute-force approaches can ameliorate the situation,[1176] significant improvement requires a different methodology.

[1173] N. Bobroff, "Recent advances in displacement measuring interferometry," Meas. Sci. Technol. 4(1993):907-926.

[1174] J.N. Dukes, G.B. Gordon, "A two-hundred-foot yardstick with graduations every microinch," Hewlett-Packard J. 21(December 1970):2-8. C.M. Wu, J. Lawall, R.D. Deslattes, "Heterodyne interferometer with subatomic periodic nonlinearity," Appl. Opt. 38(1999):4089-4094.

[1175] C.M. Wu, J. Lawall, R.D. Deslattes, "Heterodyne interferometer with subatomic periodic nonlinearity," Appl. Opt. 38(1999):4089-4094.

[1176] E.G. Kessler, "Sub-Nanometer Metrology for X-Ray and Gamma-Ray Wavelength Measurements," in Proceedings: ASPE Spring Topical Meeting on Precision Interferometric Metrology (ASPE, Tucson, 1992), pp. 49-52.

Figure 4-59. Beam configuration for commercial interferometer based on Zeeman-stabilized laser.[1177]

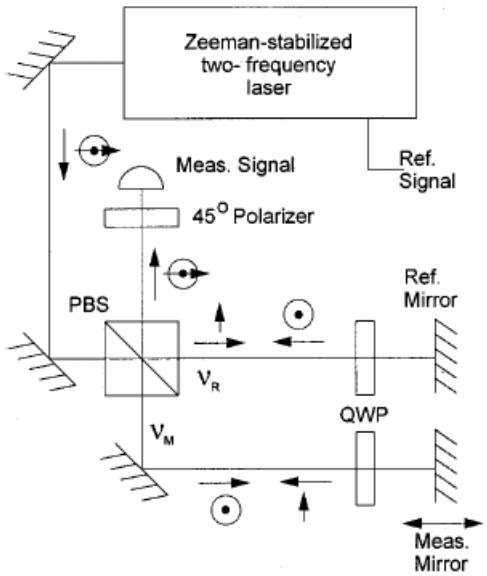

Pioneering work in this area was done by Tanaka,[1178] who proposed generating the frequency difference required for heterodyne interferometry by means of acousto-optic modulators rather than a two-mode Zeeman-stabilized laser; his scheme is in principle completely free of polarization mixing, though later work with this method[1179] claimed a departure from linearity below 100 pm. Other two-frequency laser systems based on acousto-optic frequency shifting[1180] were devised for displacement metrology and at least one[1181] was commercialized. Interferometers based on these laser sources, however, were still susceptible to polarization mixing when the co-propagating modes of different frequencies were separated by a (nonideal) polarizing beam splitter. A more recent interferometer using two acousto-optic modulators for

---

[1177] John Lawall, Ernest Kessler, "Michelson interferometer with 10 pm accuracy," Rev. Scient. Instrum. 71(2000):2669-2676. http://link.aip.org/link/?RSINAK/71/2669/1.

[1178] M. Tanaka, T. Yamagami, K. Nakayama, "Linear interpolation of periodic error in a heterodyne laser interferometer at subnanometer levels," IEEE Trans. Instrum. Meas. 38(1989):552-554.

[1179] K. Nakayama, M. Tanaka, F. Shiota, K. Kuroda, "Precision Physical Measurements and Nanometrology," Metrologia 28(1992):483-502.

[1180] G. Sommargren, "A new laser measurement system for precision metrology," Precis. Eng. 9(1987):179-184. P. Dirksen, J.v.d. Werf, W. Bardoel, "Novel two-frequency laser," Precis. Eng. 17(April 1995):114-116.

[1181] G. Sommargren, "A new laser measurement system for precision metrology," Precis. Eng. 9(1987):179-184.

difference-frequency generation was presented by Wu[1182] (Section 4.6.3.13) and demonstrated by creating a synthetic displacement using a pressure cell; systematic errors at the 20 pm level were found and were attributed largely to parasitic reflections.

In 2000 Lawall and Kessler[1183] demonstrated a new interferometer design for measuring differential displacement (Figure 4-60). Like the configurations of Tanaka and Wu, the design used two acousto-optic modulators for heterodyne frequency generation and was free of polarization mixing. It used a minimal number of optical components in order to reduce the number of parasitic reflections. In addition, it was particularly well adapted to the use of simple mirrors rather than corner cube retroreflectors, which is advantageous in many applications. Finally, like the design of Wu, the beams striking the measurement and reference mirrors are of the same frequency, providing theoretically perfect insensitivity to common-mode displacement. With this interferometer Lawall and Kessler demonstrated a **residual systematic error of ~7.4 pm**, corresponding to a fringe interpolation factor greater than 36,000.

Figure 4-60. Two parallel beams generated by beamsplitter BS pass without Bragg diffraction through the acousto-optic modulators on account of their polarization; upon returning, their polarizations have been flipped by the quarter-wave plate and the beams are diffracted and frequency shifted by ν_M and ν_R; the beams interfere to generate a heterodyne signal at frequency ν_M-ν_R; the homodyne signal allows counting integral numbers of optical fringes at a wider bandwidth than might be allowed with the heterodyne electronics.[1184]

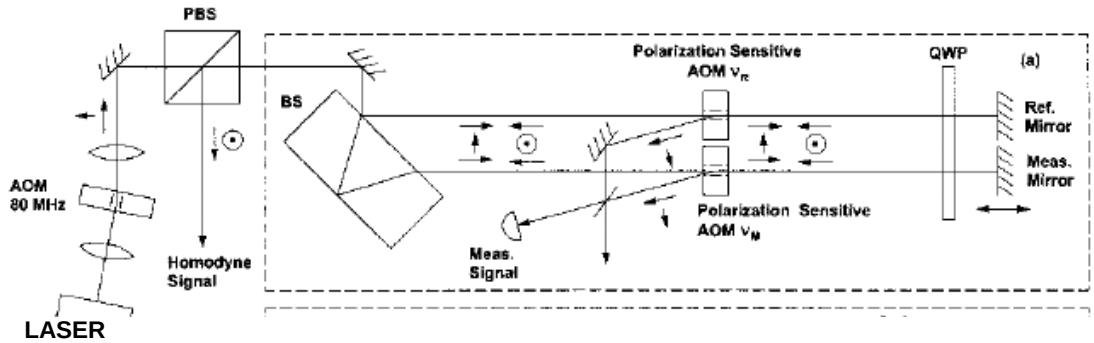

[1182] C.M. Wu, J. Lawall, R.D. Deslattes, "Heterodyne interferometer with subatomic periodic nonlinearity," Appl. Opt. 38(1999):4089-4094.

[1183] John Lawall, Ernest Kessler, "Michelson interferometer with 10 pm accuracy," Rev. Scient. Instrum. 71(2000):2669-2676. http://link.aip.org/link/?RSINAK/71/2669/1.

[1184] John Lawall, Ernest Kessler, "Michelson interferometer with 10 pm accuracy," Rev. Scient. Instrum. 71(2000):2669-2676. http://link.aip.org/link/?RSINAK/71/2669/1.

In the Lawall-Kessler apparatus (Figure 4-60), horizontally polarized light from a single-mode polarization-stabilized laser is collimated after passing through an acousto-optic modulator (AOM) or Faraday isolator in order to minimize optical feedback. After passing through a polarizing beamsplitter (PBS), the light strikes a specially coated beamsplitter (BS) that splits it into two parallel beams of equal intensity and the same polarization. One of these beams is the "measurement" beam and the other one serves as the "reference" beam; each one passes through its own acousto-optic modulator, and the AOMs are driven at rf frequencies ν_M and ν_R, respectively. The AOM-to-mirror distance is ~45 cm. The AOMs have a Bragg angle that is polarization dependent and the angle is set so as to effectively diffract vertical polarization, thus the incident (horizontally polarized) light is transmitted without diffraction. The light passes through a quarter-wave plate (QWP) before striking the separate measurement and reference mirrors (~1.2 cm apart), and on retroreflection through the QWP its polarization is flipped to vertical. The reflected beams are then diffracted by the AOMs and combined on a beamsplitter. The resulting signal has a frequency near the difference of AOM drive frequencies ν_M-ν_R, but in general slightly offset owing to the instantaneous Doppler shift resulting from relative motion between the measurement and reference mirrors. (The AOMs are driven with synthesizers at 39.98 and 40.02 MHz, respectively, giving an optical heterodyne frequency of 40 kHz.) This signal is demodulated with respect to an electronic signal at the exact difference frequency ν_M-ν_R, and the phase evolution of the demodulated signal is directly proportional to the relative displacement.[1185] The zero-order diffraction sent back towards the laser is reflected by the polarizing beam splitter, minimizing optical feedback.

Note that the zero-order retroreflected beams interfere to provide a homodyne signal. This is potentially useful for applications in which the target mirror will be moved at high speed (exceeding the measurement bandwidth of the heterodyne detector) between measurements. By means of a simple level-crossing detector, the integral number of optical fringes can be measured at the homodyne port as the mirror is scanned, while the high-resolution heterodyne output can be read when the target mirror has slowed to the point that the signal falls within its measurement bandwidth. Thus, the homodyne signal provides coarse resolution (an integral number of half wavelengths) while the heterodyne signal interpolates fringes at the beginning and end of the scan.

In a typical linear scan, ~60 fringes were scanned in 1.87 sec for a total displacement of 19 μm. A commercial interferometer gave peak-to-peak residual errors of ~3 nm (Figure 4-61A); the RMS amplitudes of the NIST interferometer are all but invisible when shown alongside those of the commercial interferometer (Figure 4-61B). Figure 4-61C shows them on an expanded scale: four distinct peaks are visible at 32.5, 60, 65, and 89 Hz; only the peaks at 32.5 and 65 Hz represent systematic fringe interpolation errors in the interferometer. The amplitudes of the peaks at 32.5 and 65 Hz are 4.5 pm and 5.8 pm RMS, respectively, resulting in a total error of ~7.4 pm RMS. This is over two orders of magnitude better than the commercial interferometer and corresponds to fringe interpolation by ~42,000.

[1185] C.M. Wu, J. Lawall, R.D. Deslattes, "Heterodyne interferometer with subatomic periodic nonlinearity," Appl. Opt. 38(1999):4089-4094.

Figure 4-61. (A) Left: Residuals of commercial interferometer after suppressing frequencies below 8 Hz. (B) Center: Fourier transform of residuals; the largest peak is at fringe frequency $\nu_{fringe} = 2v/\lambda \sim 32.5$ Hz; residuals from NIST interferometer have been multiplied by 10 in order to make them visible. (C) Right: Fourier transform of pm-level residuals from NIST interferometer on an expanded scale; the largest peak is at 60 Hz.[1186]

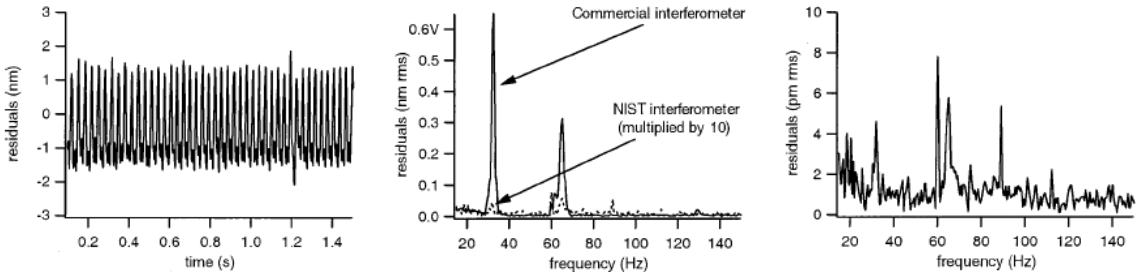

Lawall and Kessler[1187] note that the accuracy of measurements performed using their interferometer is limited by both the residual periodic errors and the accuracy with which the laser wavelength is known; the latter (system accuracy) in turn is a question of the optical frequency and the spatial mode. For concreteness, consider a stabilized laser with a fractional frequency accuracy of 10^{-8}. If collimated to a waist of 0.5 mm, the effective wavelength near the waist will differ from that of an ideal plane wave by ~4 x 10^{-8} on account of diffraction,[1188] and it is probably realistic to account for this and to consider the wavelength to be known at the level of 10^{-8}. Thus measurements over a range of 1 mm would have an accuracy limited at the level of 10 pm by the laser and a similar amount by the interferometer. The accuracy of measurements of displacements much larger than 1 mm would be limited largely by the laser, while measurements of smaller displacements would be primarily limited by the interferometer. In practice, issues such as beam quality, environmental isolation, materials properties, and measurement speed would also be important factors entering into the consideration of maximum achievable accuracy.

[1186] John Lawall, Ernest Kessler, "Michelson interferometer with 10 pm accuracy," Rev. Scient. Instrum. 71(2000):2669-2676. http://link.aip.org/link/?RSINAK/71/2669/1.

[1187] John Lawall, Ernest Kessler, "Michelson interferometer with 10 pm accuracy," Rev. Scient. Instrum. 71(2000):2669-2676. http://link.aip.org/link/?RSINAK/71/2669/1.

[1188] J.-P. Monchalin, M. Kelly, J. Thomas, N. Kurnit, A. Szoke, F. Zernike, P. Lee, A. Javan, "Accurate laser wavelength measurement with a precision two beam scanning Michelson interferometer," Appl. Opt. 20(1981):736-757.

4.6.3.2 Tunable-Laser Michelson Interferometer at NIST (U.S.)

During 2002-4, a group at NIST led by Richard Silver[1189] developed a new implementation of a Michelson interferometer capable of resolution on the order of 20 pm in conjunction with an STM (Figure 4-62). This method uses a tunable diode laser as the light source with the diode laser wavelength continuously tuned to fix the number of fringes in the measured optical path. The diode laser frequency is measured by beating against a reference laser. High speed, accurate frequency measurements of the beat frequency signal enables the diode laser wavelength to be measured with nominally 20 pm resolution. The new interferometer design is lightweight and has been mounted directly on an ultra-high vacuum scanning tunneling microscope capable of atomic resolution. In 2004, Silver's group[1190] reported the simultaneous acquisition of an atomic resolution image while the relative lateral displacement of the STM tip along the sample distance is measured with the new tunable diode laser Michelson interferometer. Atomic resolution on the order of 10 pm can be achieved because of the ability to perform highly accurate frequency measurements over a measurable range of 165 nm in this configuration. With 20 pm steps the maximum scan rate is 20 nm/sec, or ~1 minute per micron of travel assuming a maximum counting rate of about 1KHz; however, in the configuration used here the **20 pm accuracy** can only be maintained over a **range of ~165 nm**. (The researchers believe this limited range could be extended, in principle: "If one allows mode hopping, and keeps track of the number of modes hopped and the change in the optical path difference, significantly larger scanning distances are possible.")

[1189] H. Zhou, B. Damazo, S. Gonda, R.M. Silver, "Developing Atomic-resolution Measurements using a Tunable Diode Laser-based Interferometer," 2003; http://www.aspe.net/publications/Annual_2003/PDF/4INTERF/1333.PDF. R.M. Silver, H. Zhou, S. Gonda, B. Damazo, J. Jun, C. Jensen, L. Howard, "Atomic-resolution measurements with a new tunable diode laser-based interferometer," Opt. Eng. 43(2004):79-86. James D. Gilsinn, Bradley N. Damazo, Richard Silver, Hui Zhou, "A Macro-Micro Motion System for a Scanning Tunneling Microscope," (2002) http://www.mel.nist.gov/publications/get_pdf.cgi?pub_id=821683.

[1190] R.M. Silver, H. Zhou, S. Gonda, B. Damazo, J. Jun, C. Jensen, L. Howard, "Atomic-resolution measurements with a new tunable diode laser-based interferometer," Opt. Eng. 43(2004):79-86.

Figure 4-62. A photograph of the UHV STM with the interferometer mounted on the floating stage, damped; the entire STM and interferometer is mounted on an 8-inch conflat flange for vacuum mounting.[1191]

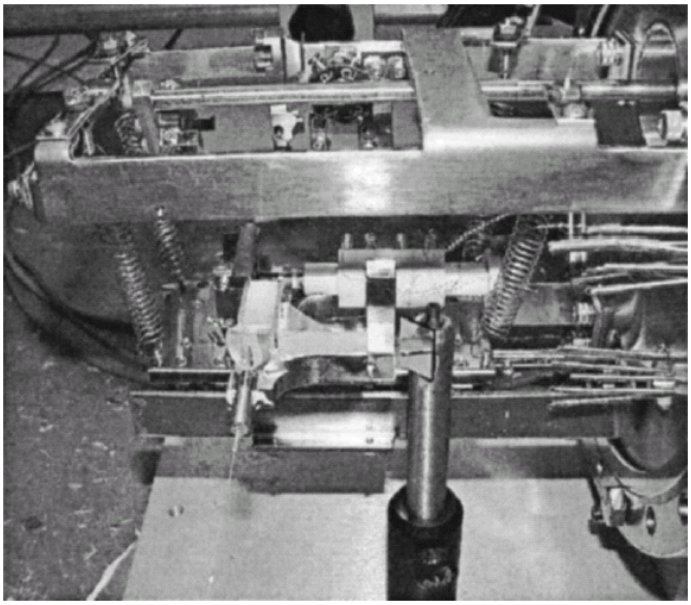

The basic principle of this measurement system is that the output frequency of a tunable diode laser is adjusted so that as the measurement arm of a Michelson interferometer is scanned, there is no movement of the fringe signal.[1192] Figure 4-63 is a schematic of the optical apparatus and measurement and control strategy.

The fringe signal arises in this apparatus from a differential measurement of the reference arm signal against the measurement arm signal. To track the laser diode frequency, a portion of the beam is split off and beat against a reference stabilized He-Ne laser. This allows the diode laser wavelength to have a direct, unbroken traceability path. The beat frequency signal is logged synchronously with the acquisition of the STM images. This is a homodyne interferometer system and only a single frequency is used in the interferometer portion of the system. The heterodyne (two-frequency) portion of the measurement is completely independent of the interferometer and measurement mirrors. This measurement requires no fringe interpolation since it is based on the number of fringes being held constant in the optical path difference between the reference arm and the measurement arm in a "static" sequence.

[1191] R.M. Silver, H. Zhou, S. Gonda, B. Damazo, J. Jun, C. Jensen, L. Howard, "Atomic-resolution measurements with a new tunable diode laser-based interferometer," Opt. Eng. 43(2004):79-86.

[1192] L. Howard, J. Stone, J. Fu, "Real-time displacement measurements with a Fabry-Perot cavity and a diode laser," Precis. Eng. 25(October 2001):321-335.

Figure 4-63. General methodology for tracking the measurement mirror motion and the general hardware functions; the reference measurement process is also shown between the He-Ne and diode laser.[1193]

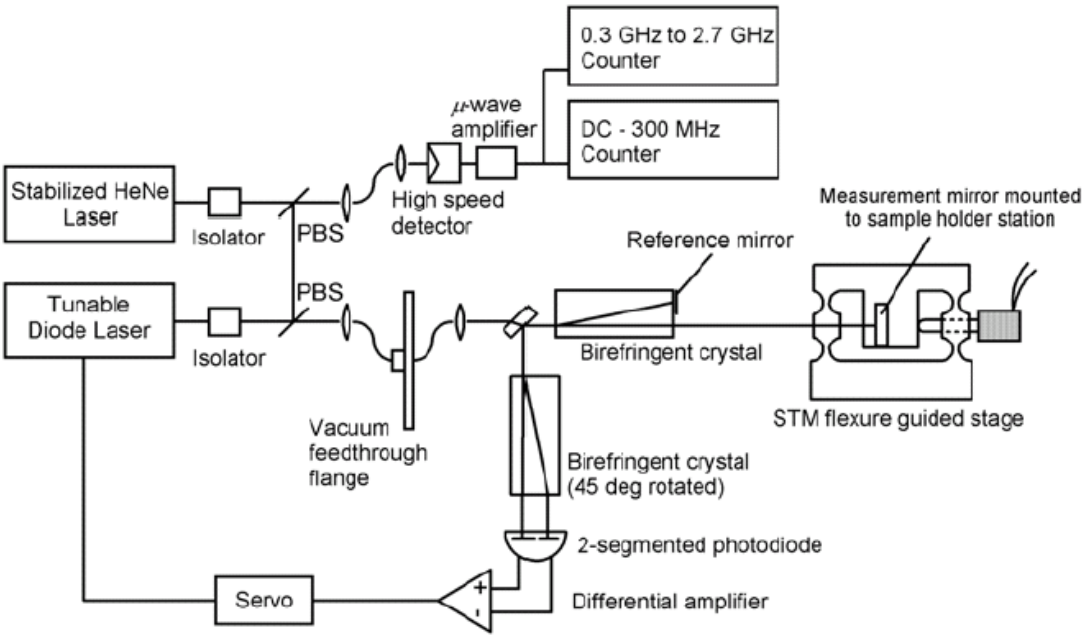

The calibration of the system is obtained by counting the number of fringes in the optical path difference between the reference and measurement arms. The number of fringes is determined by the wavelength of the diode laser and the path difference. This distance determines the scan range for the interferometer, when no mode hopping is allowed, based on the tunable diode laser range.[1194] Although mode hopping can be allowed, it is simplest to explain the principle with a fixed fringe measurement. The optical path difference can be obtained by scanning the diode laser frequency with a stationary measurement stage, and monitoring its wavelength based on the He-Ne reference. This is accomplished by "mapping" a fringe of the differential intensity signal of the interferometer at the bicell detector while scanning the diode laser wavelength. The diode laser frequency is simultaneously beat against the He-Ne laser. The bicell intensity signal of one full or half fringe is then plotted against the beat frequency signal. The map of the diode laser wavelength against the bicell detector intensity pattern results in a unique number of wavelengths making up the optical path difference.

[1193] R.M. Silver, H. Zhou, S. Gonda, B. Damazo, J. Jun, C. Jensen, L. Howard, "Atomic-resolution measurements with a new tunable diode laser-based interferometer," Opt. Eng. 43(2004):79-86.

[1194] Y. Zhu, H. Matsumoto,T. O'ishi, "Arm-length measurement of an interferometer using the optical-frequency-scanning technique," Applied Optics 30(1991):3561-3562. G.P. Barwood, P. Gill, W.R.C. Rowley, "Laser diodes for length determination using swept-frequency interferometry," Meas. Sci. Technol. 4(September 1993):988-994.

As noted by Gilsinn et al.[1195] and Silver et al.,[1196] the goal of using the interferometer system is to make 20 pm resolution measurements of the sample without degrading the atomic resolution imaging performance of the STM. The STM used in this work is a modified commercial instrument which is routinely capable of atomically resolved imaging. The vertical and lateral noise floors are typically 0.1 Å (10 pm) and 0.3 Å (30 pm), respectively. The STM itself is mounted on a floating Invar stage suspended by springs with an eddy current damping mechanism. The STM system resides in an Ultra-High Vacuum (UHV) facility, which typically operates in the 1.33 x 10^{-8} Pa (1 x 10^{-10} torr) range. The detachable sample holder and tip carrier allow sample/tip exchanges quite easily in UHV without breaking vacuum. A 2-micron range of travel piezo device is integrated into the sample stage.

For their first tunable-laser Michelson interferometer, Silver et al.[1197] calculated total measurement uncertainty components as shown in Table 4-6. For a total tip displacement of Δl = 100 nm, the nine error sources total up to: 4.3 pm + 0.02 pm + 1.0 pm + 0.04 pm + 3 pm + 61.0 pm + 87.0 pm + 2 pm + 0.23 pm = 158.59 pm. The largest components of error are the "cosine error" and the "straightness of vertical motion". For Δl = 1 micron, the nine error sources total up to: 4.3 pm + 0.2 pm + 10.0 pm + 0.04 pm + 3 pm + 610.0 pm + 870.0 pm + 2 pm + 2.3 pm = 1501.84 pm. These errors are about an order of magnitude too large to be useful in a successful DMS molecular workstation. Apparently the same NIST group later constructed a second-generation instrument to reduce some of the larger sources of error[1198] (though no publication reporting these results has yet been found): "A second-generation STM interferometer configuration has been assembled, which allows interferometer alignment on the bench. The new flexure-guided motion design eliminates the largest error components in this first set of measurements."

[1195] James D. Gilsinn, Bradley N. Damazo, Richard Silver, Hui Zhou, "A Macro-Micro Motion System for a Scanning Tunneling Microscope," (2002) http://www.mel.nist.gov/publications/get_pdf.cgi?pub_id=821683.

[1196] R.M. Silver, H. Zhou, S. Gonda, B. Damazo, J. Jun, C. Jensen, L. Howard, "Atomic-resolution measurements with a new tunable diode laser-based interferometer," Opt. Eng. 43(2004):79-86.

[1197] R.M. Silver, H. Zhou, S. Gonda, B. Damazo, J. Jun, C. Jensen, L. Howard, "Atomic-resolution measurements with a new tunable diode laser-based interferometer," Opt. Eng. 43(2004):79-86.

[1198] R.M. Silver, H. Zhou, S. Gonda, B. Damazo, J. Jun, C. Jensen, L. Howard, "Atomic-resolution measurements with a new tunable diode laser-based interferometer," Opt. Eng. 43(2004):79-86.

Table 4-6. Examination of the uncertainty components for the tunable-laser Michelson interferometer, for Silver et al.;[1199] values are analyzed in accordance with the distances measured for the atomic measurement example presented.

Influence parameters	Estimated value	Contribution in picometers
Short term fluctuation of the reference laser	140 kHz	4.3
Systematic error of the wavelength of the reference laser	10^{-7}	$2\times10^{-7}\cdot\Delta\ell$
Determination of the optical path difference	10^{-5}	$1\times10^{-5}\cdot\Delta\ell$
Frequency measurements	5×10^{-7}	0.04
Noise of the diode laser	100 kHz	3
Cosine error		$6.1\times10^{-4}\cdot\Delta\ell$
Straightness of vertical motion	$0.05\tan\theta$	$8.7\times10^{-4}\cdot\Delta\ell$
Thermal drift in the mechanical distance between the interferometer and the STM tip	3.6 nm/h	2
Temperature variation of sample	1 K	$2.3\times10^{-6}\cdot\Delta\ell$

4.6.3.3 Calibrated AFM at NIST (U.S.)

Starting in at least 1994, NIST and Park Scientific Instruments undertook a joint effort[1200] to develop an AFM system capable of making accurate dimensional measurements, called the

---

[1199] R.M. Silver, H. Zhou, S. Gonda, B. Damazo, J. Jun, C. Jensen, L. Howard, "Atomic-resolution measurements with a new tunable diode laser-based interferometer," Opt. Eng. 43(2004):79-86.

[1200] J. Schneir, T.H. McWaid, J. Alexander, B.P. Wilfley, "Design of an atomic force microscope with interferometric position control," J. Vac. Sci. Technol. B 12(1994):3561-3566; F. Meli, R. Thalmann, "Long-range AFM profiler used for accurate pitch measurements," Meas. Sci. Technol. 9(1998):1087-1092; M. Bienias, S. Gao, K. Hasche, R. Seemann, K. Thiele, "A metrological scanning force microscope used for coating thickness and other topographical measurements," Appl. Phys. A 66(1998):S837-S842; S. Gonda, T. Doi, T. Kurosawa, Y. Tanimura, N. Hisata, T. Yamagishi, H. Fujimoto, H. Yukawa, "Real-time, interferometrically measuring atomic force microscope for direct calibration of standards," Rev. Sci. Instrum. 70(1999):3362-3368; R.K. Leach, J. Haycocks, K. Jackson, A. Lewis, S. Oldfield, A. Yacoot, "Advances in traceable nanometrology at the National Physical Laboratory," Nanotechnology 12(2001):R1-R6; G.B. Picotto, M. Pisani, "A sample scanning system with nanometric accuracy for quantitative SPM measurements," Ultramicroscopy 86(2001):247-254; I. Misumi, S. Gonda, T. Kurosawa, K. Takamasu, "Uncertainty in pitch measurements of one-dimensional grating standards using a nanometrological atomic force microscope," Meas. Sci. Technol. 14(2003):463-471; Andrew Yacoot, Ludger Koenders, "From nanometre to millimetre: a feasibility study of the combination of scanning probe microscopy and combined optical and x-ray interferometry," Meas. Sci. Technol. 14(2003):N59-N63; M. Bisi, E. Massa, A. Pasquini, G. B. Picotto, M. Pisani, "Nanometrology at the IMGC", in: Günter Wilkening, Ludger Koenders, eds., Nanoscale Calibration Standards and Methods, Wiley-VCH Verlag GmbH & Co. KGaA, 2005; H.-U. Danzebrink, L. Koenders, G. Wilkening, A. Yacoot, H. Kunzmann, "Advances in Scanning Force Microscopy for Dimensional Metrology," CIRP Annals - Manufacturing Technology 55(2006):841-878; K.R. Koops, M.G.A. van Veghel, G.J.W.L. Kotte, M.C. Moolmanration, "Strategies for scanning probe metrology," Meas. Sci. Technol. 18(January 2007):390-394; M. Ritter, T.

"calibrated AFM" or (C-AFM). According to the abstract: "The C-AFM has been constructed as much as possible out of commercially available components. We use a flexure stage driven by piezoelectric transducers for scanning, heterodyne interferometers to measure the X and Y displacements of the sample, a capacitance sensor (calibrated with a third interferometer) to measure the Z displacement of the sample as driven by a piezoelectric actuator, and a commercially available AFM control system. The control system has two feedback loops which read from the X and Y interferometers, respectively, and adjust the piezoelectric voltages to keep the X-Y scan position accurate."

Further development continued from 1999 through at least 2007.[1201] For instance, by 1999 the group achieved 0.2 nm (**200 pm**) expanded uncertainty on a **20 nm step**, and achieved 0.008 nm **(8 pm)** expanded uncertainty in the measurement of the approximately 0.3 nm single atom step on Si.[1202] The C-AFM had metrology traceable to the International System of Units meter for all three axes. However, it appears that after 2001 the research direction shifted from "calibrated AFM" to "critical dimension AFM", with a sharper focus on the semiconductory industry rather than trying to push deeper into picometer territory.[1203]

Dziomba, A. Kranzmann, L. Koenders, "A landmark based 3D calibration strategy for SPM," in: Measurement Science and Technology, IOP, Bristol, 2007, pp. S404-S414.

[1201] R. Dixson, R. Köning, J. Fu, T. Vorburger, B. Renegar, "Accurate dimensional metrology with atomic force microscopy," Proc. SPIE 3998(2000):362-368. Ronald G. Dixson, Rainer G. Koening, Vincent W. Tsai, Joseph Fu, Theodore V. Vorburger, "Dimensional metrology with the NIST calibrated atomic force microscope," Proc. SPIE 3677(1999):20. Ronald G. Dixson, Ndubuisi G. Orji, Joseph Fu, Vincent Tsai, Ellen D. Williams, Raghu Kacker, Theodore V. Vorburger, Hal L. Edwards, Debra Cook, Paul E. West, Ralph Nyffenegger, "Silicon single atom steps as AFM height standards," Proc. SPIE 4344(2001):157. Ronald L. Jones, Tengjiao Hu, Eric K. Lin, Wen-li Wu, Diego M. Casa, N. G. Orji, Theodore V. Vorburger, Patrick J. Bolton, George G. Barclay, "Subnanometer wavelength metrology of lithographically prepraed structures: a comparison of neutron and X-ray scattering," Proc. SPIE 5038(2003):191. Ronald Dixson, Ndubuisi G. Orji, James Potzick, Joseph Fu, Richard A. Allen, Michael Cresswell, Stewart Smith, Anthony J. Walton, Andreas Tsiamis, "Photomask applications of traceable atomic force microscope dimensional metrology at NIST," Proc. SPIE 6730(2007):67303D.

[1202] Ronald G. Dixson, Rainer G. Koening, Vincent W. Tsai, Joseph Fu, Theodore V. Vorburger, "Dimensional metrology with the NIST calibrated atomic force microscope," Proc. SPIE 3677(1999):20. Ronald G. Dixson, Ndubuisi G. Orji, Joseph Fu, Vincent Tsai, Ellen D. Williams, Raghu Kacker, Theodore V. Vorburger, Hal L. Edwards, Debra Cook, Paul E. West, Ralph Nyffenegger, "Silicon single atom steps as AFM height standards," Proc. SPIE 4344(2001):157.

[1203] Ronald L. Jones, Tengjiao Hu, Eric K. Lin, Wen-li Wu, Diego M. Casa, N. G. Orji, Theodore V. Vorburger, Patrick J. Bolton, George G. Barclay, "Subnanometer wavelength metrology of lithographically prepraed structures: a comparison of neutron and X-ray scattering," Proc. SPIE 5038(2003):191. Ronald Dixson, Ndubuisi G. Orji, James Potzick, Joseph Fu, Richard A. Allen, Michael Cresswell, Stewart Smith, Anthony J. Walton, Andreas Tsiamis, "Photomask applications of traceable atomic force microscope dimensional metrology at NIST," Proc. SPIE 6730(2007):67303D.

In 2006, Robert Celotta reported[1204] that NIST possessed the ability to stabilize an STM to 0.002 Å (0.2 pm). Note that this is not repeatable placement precision but rather "stability" in the sense of low-amplitude vibrations around the positional set point.

4.6.3.4 Multiple-Reflection Michelson Interferometer at INRIM (Italy)

Since an optical interferometer fringe is typically hundreds of nanometers long, to perform measurements on the picometer scale means that the optical fringe must be subdivided into tens of thousands of parts. In practice, this process encounters a number of issues which limit the resolution and the accuracy of interferometers at small scales – e.g., quantum noise, electronic noise, and nonlinearity of the optical fringes limit practical measurements resolution to tenths of a nanometer. Different solutions have been investigated and are proposed for future research in order to increase interferometer resolution, mainly based on the refinement of the optical system, the electronics, and the fringe analysis algorithms.[1205] A joint research project financed by the European Community called "Nanotrace" (Section 4.6.2.4) is entirely dedicated to this subject.[1206]

In work reported by Pisani,[1207] a heterodyne Michelson interferometer based on an optical set-up allowing multiple reflection between two plane mirrors performs the multiplication of the optical path by a factor N, proportionally increasing the resolution of the measurement and potentially enabling **direct sub-nanometer resolution**. By late 2008 a multiplication factor of almost two orders of magnitude had already been demonstrated with a simple set-up, using a technique that

---

[1204] Robert Celotta, "Enabling Nanotechnology: An Introduction to NIST's New Center for Nanoscale Science & Technology," presentation at the SME Conference: "The Next Industrial Revolution: Nanotechnology & Manufacturing," Oak Ridge, TN, 24 August 2006; http://www.sme.org/cgi-bin/get-evdoc.pl?&&001640&000007&020104&&SME&.

[1205] W. Hou, G. Wilkening, "Investigation and compensation of the nonlinearity of heterodyne interferometers," Prec. Eng. 14(1992):91-98. Peter L.M. Heydemann, "Determination and correction of quadrature fringe measurement errors in interferometers," Appl. Opt. 20(1981):3382-3384. M. Tanaka, T. Yamagami, K. Nakayama, "Linear interpolation of periodic error in a heterodyne laser interferometer at subnanometer levels," IEEE Trans. Instrum. Meas. 38(1989):552-554.

[1206] EMRP T3.J1.4.NANOTRACE "New traceability routes for nanometrology," http://www.emrponline.eu.

[1207] Marco Pisani, "A homodyne Michelson interferometer with sub-picometer resolution," Meas. Sci. Technol. 20(2009):084008. See also: M. Pisani, "Interferometer with optical path multiplication for picometer resolution," presentation at NanoScale 2008 conference. M. Pisani, M. Astrua, "Angle amplification for nanoradian measurements," Appl Opt. 45(10 March 2006):1725-1729. Marco Pisani, "Multiple reflection Michelson interferometer with picometer resolution," Opt. Express 16(December 2008):21558-21563; http://www.opticsexpress.org/viewmedia.cfm?uri=oe-16-26-21558&seq=0.

can be applied to any interferometric measurement where the classical interferometer limits due to fringe nonlinearities and quantum noise are an issue.[1208]

In one demonstration of this technique,[1209] a simple autocollimating multireflection configuration can provide an amplification factor that can be exploited to measure ultra small angles. (This method to amplify the rotation angle of a mirror, based on multiple reflections between two quasi-parallel mirrors, allows measurement of rotations of fractions of nanoradians.[1210]) If the angle is small but can be held constant, the same configuration can be used to detect very small linear displacements. The apparatus (Figure 4-64) is based on a heterodyne Michelson interferometer fed with two orthogonally polarized, frequency shifted beams (the beam generation is not shown in the picture). A beam splitter (BS) extracts a portion of the beam to generate a reference beat signal on detector D1. The beam is then split by a polarizing beam splitter (PBS). One beam is reflected by a fixed mirror M (the reference arm), while the second beam (the measurement arm) enters the two-mirror arrangement hitting mirror A at an incidence angle α. Here the second beam undergoes a series of reflections between the two mirrors. At each reflection, the incidence angle of the beam is reduced by an amount β, the angle between the two mirrors. If α/β is an integer N, then after N+1 reflections the incidence angle is zero and the beam is reflected back on itself; after another N reflections, it returns back towards the PBS. Here the second beam is finally recombined with the reference beam, thus generating a beat signal on detector D2. The phase difference $\Delta\varphi$ between the two beat signals is the interferometer output, allowing detection of small linear displacements of mirror B.[1211]

[1208] Marco Pisani, "Multiple reflection Michelson interferometer with picometer resolution," Opt. Express 16(December 2008):21558-21563; http://www.opticsexpress.org/viewmedia.cfm?uri=oe-16-26-21558&seq=0.

[1209] Marco Pisani, "Multiple reflection Michelson interferometer with picometer resolution," Opt. Express 16(December 2008):21558-21563; http://www.opticsexpress.org/viewmedia.cfm?uri=oe-16-26-21558&seq=0.

[1210] M. Pisani, M. Astrua, "Angle amplification for nanoradian measurements," Appl Opt. 45(10 March 2006):1725-1729.

[1211] Marco Pisani, "Multiple reflection Michelson interferometer with picometer resolution," Opt. Express 16(December 2008):21558-21563; http://www.opticsexpress.org/viewmedia.cfm?uri=oe-16-26-21558&seq=0.

Figure 4-64. <u>Left</u>: Simplified schematic of the multireflection heterodyne interferometer. <u>Right</u>: Picture of the experimental apparatus. In the larger picture mirror A is visible (mounted on the translation stage on the rotary table), facing mirror B; the λ/4 plate, the lens and the back of the fixed mirror are visible on the right; the beam is coming from the top right corner; in the frame, a detail of the multireflection pattern is seen from the opposite side].[1212] <u>Below:</u> Two other views of the apparatus.[1213]

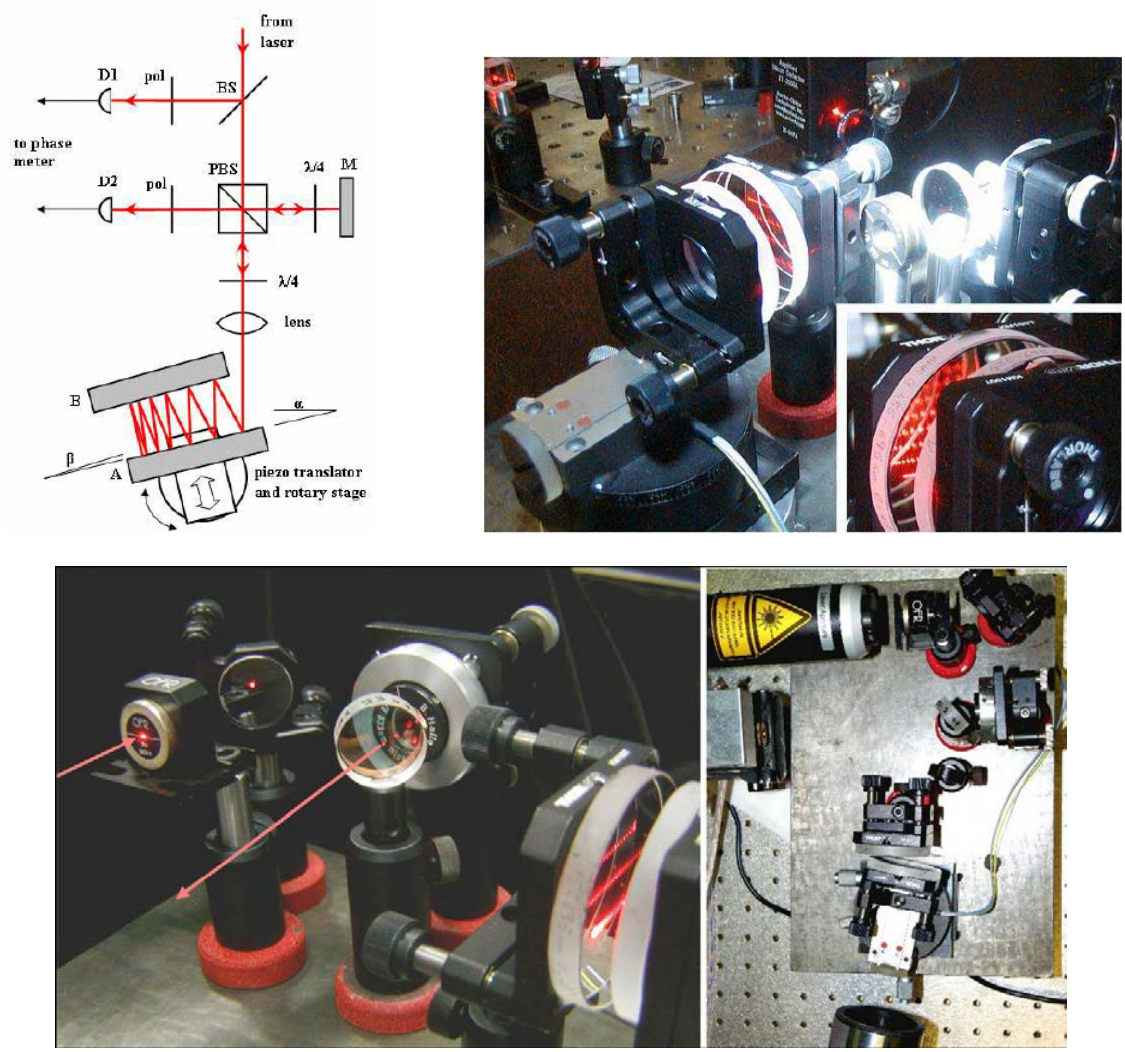

[1212] Marco Pisani, "Multiple reflection Michelson interferometer with picometer resolution," Opt. Express 16(December 2008):21558-21563; http://www.opticsexpress.org/viewmedia.cfm?uri=oe-16-26-21558&seq=0.

[1213] Marco Pisani, "A homodyne Michelson interferometer with sub-picometer resolution," Meas. Sci. Technol. 20(2009):084008. See also: M. Pisani, "Interferometer with optical path multiplication for picometer resolution," presentation at NanoScale 2008 conference.

The heterodyne interferometer is based on a He-Ne frequency stabilized linearly polarized laser source; the high-reflectivity dielectric-coated mirrors are 2 inches in diameter, one of which is translated using a piezo actuator with capacitive feedback (Physik Instrumente P-753). If the waist of the beam coincides with the (N+1)th orthogonal reflection then the entering and the outgoing beams will have the same size, a condition obtained with an achromatic doublet having f = 400 mm using an optical wavelength of 632.8 nm and an incidence angle $\alpha \approx 10°$ in a practical realization that yields N > 60. Based on the multiple reflection between two plane mirrors, the set-up can be implemented on both heterodyne and homodyne interferometers without any substantial changes in the existing fringe counting system (phasemeter). The homodyne interferometer behaves as if the laser had a wavelength N times shorter ($\lambda \approx 10.5$ nm in this work) with the result that non-linearity issues are reduced and resolution is enhanced by the same factor. The gain can be in principle increased to a larger factor, limited only by the dimension and the quality (planarity and reflectivity) of the mirrors.[1214]

The noise limit level for this apparatus is below 20 fm $Hz^{-1/2}$. In one test with N = 100, a modulation with 400 pm peak-to-peak amplitude and 0.5 Hz frequency was applied to one of the two mirrors by means of an open loop piezoelectric actuator. Figure 4-65 shows the interferometer output. The signal is sampled at 1 kHz and observed on a 10 Hz bandwidth. Although the residual mirror vibration effect is clearly visible, the sensitivity of the setup can be appreciated, with an apparent repeatable resolution in the **20-50 pm** range.

Notes Pisani:[1215] "Today commercial interferometers have accuracies that hardly reach the 100 pm level, while an accuracy to the 10 pm level is demanded. The periodic nonlinearity due to the unequal intensity and out-of-quadrature of the sin/cos signals in the homodyne interferometers and to the optical mixing of the two beam frequency components in the two arms of the heterodyne interferometer is the most important error source with measurements in the nanometric range.

[1214] Marco Pisani, "Multiple reflection Michelson interferometer with picometer resolution," Opt. Express 16(December 2008):21558-21563; http://www.opticsexpress.org/viewmedia.cfm?uri=oe-16-26-21558&seq=0.

[1215] Marco Pisani, "A homodyne Michelson interferometer with sub-picometer resolution," Meas. Sci. Technol. 20(2009):084008. See also: M. Pisani, "Interferometer with optical path multiplication for picometer resolution," presentation at NanoScale 2008 conference.

Figure 4.65. Response of the interferometer to a square wave displacement having 0.5 Hz frequency and 400 pm peak-to-peak amplitude, low pass filtered at 10 Hz; the residual ripple is due to mechanical vibration of the mirror assembly.[1216]

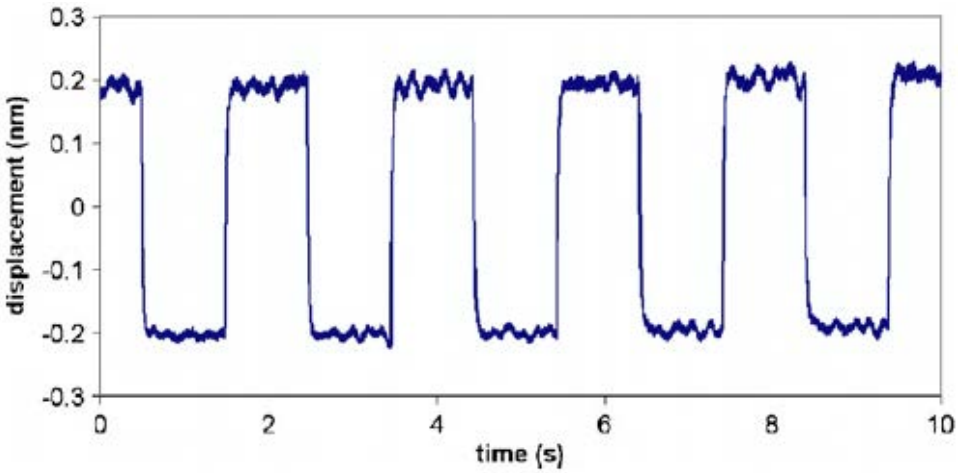

Much work has been done in the last decades to improve interferometer performance by reducing the nonlinearity effects.[1217] Proposed methods are based on refined optical paths which minimize

---

[1216] Marco Pisani, "A homodyne Michelson interferometer with sub-picometer resolution," Meas. Sci. Technol. 20(2009):084008. See also: M. Pisani, "Interferometer with optical path multiplication for picometer resolution," presentation at NanoScale 2008 conference.

[1217] A.E. Rosenbluth, N. Bobroff, "Optical sources of non-linearity in heterodyne interferometers," Precis. Engng. 12(1990):7-11. W. Hou, G. Wilkening, "Investigation and compensation of the nonlinearity of heterodyne interferometers," Prec. Eng. 14(1992):91-98. J.M. De Freitas, "Analysis of laser source birefringence and dichroism on nonlinearity in heterodyne interferometry," Meas. Sci. Technol. 8(1997):1356-1359. V.G. Badami, S.R. Patterson, "A frequency domain method for the measurement of nonlinerarity in heterodyne interferometry," Precis. Engng. 24(2000):41-49. Peter L.M. Heydemann, "Determination and correction of quadrature fringe measurement errors in interferometers," Appl. Opt. 20(1981):3382-3384. M. Tanaka, T. Yamagami, K. Nakayama, "Linear interpolation of periodic error in a heterodyne laser interferometer at subnanometer levels," IEEE Trans. Instrum. Meas. 38(1989):552-554. G. Dai, F. Pohlenz, H.-U. Danzebrink, K. Hasche, G. Wilkening, "Improving the performance of interferometers in metrological scanning probe microscopes," Meas. Sci. Technol. 15(2004):S444-S450. See also: A. Sikora, D.V. Sokolov, H.-U. Danzebrink, "Scanning probe microscope set-up with interferometric drift compensation," in: G. Wilkening, L. Koenders, eds., Nanoscale Calibration Standards and Methods, 2005, pp. 109-118; G. Dai, F. Pohlenz, H.-U. Danzebrink, M. Xu, K. Hasche, G. Wilkening, "DSP-based metrological scanning probe microscope with direct interferometric position measurement and improved measurement speed," in: G. Wilkening, L. Koenders, eds., Nanoscale Calibration Standards and Methods, 2005, pp. 119-130. Han Haitjema, Suzanne J.A.G. Cosijns, N.J.J. Roset, Maarten J. Jansen, "Improving a commercially available heterodyne laser interferometer to sub-nm uncertainty," Proc. SPIE 5190(2003):347-354. C.M. Wu, J. Lawall, R.D. Deslattes, "Heterodyne interferometer with subatomic periodic nonlinearity," Appl. Opt. 38(1999):4089-4094. A. Sacconi, G.B. Picotto, W. Pasin, "The IMGC calibration setup for microdisplacement actuators," IEEE Trans. Instrum. Meas. 48(1999):483-487. S. Cosijns, H. Haitjema, P. Schellekens, "The influence of polarization states on non-linearities in laser interferometry," Proc. 3rd EUSPEN Conf. 2(2002):593-596. Tae Bong Eom et al., "A simple method for

or nullify polarization mixing, on numeric or electronic techniques to compensate for nonlinearities, on integration of a capacitive sensor to interpolate the optical fringes, and on the use of a tunable laser in order to operate at fixed phase. Although excellent results have been obtained, all these interferometers are more complex than the basic Michelson interferometer. Alternative methods based on the use of the atomic lattice constant as a measurement reference are rather complex as well.[1218] The method proposed here, based on a classical Michelson interferometer, consists in multiplying the optical path by means of a folded path, in order to virtually reduce the laser wavelength and consequently reduce the errors associated with the subdivision of the optical fringes."

4.6.3.5 Dual Optical Wavelength Interferometer (Czech Metrology Institute)

As part of the European NanoTrace Project (Section 4.6.2.4), Kren and Balling[1219] at the Czech Metrology Institute report on the development of the common path two-wavelength (633 nm and 532 nm) homodyne counting interferometer, which uses two differential interferometers designed to eliminate optical path drifts and fluctuations. Their short-term instability is projected to be in the order of tens of pm in the single wavelength path difference and below **10 pm** in the difference of these two wavelength path differences, allowing better real-time validation of interferometer fringe interpolation with measurement of displacements up to 100 μm even under ambient air conditions.

The interferometer is suitable for the measurement of a relative displacement of target mirrors. The difference between 633 nm and 532 nm elliptic corrected measurements has a noise floor below 10 pm. The mid-term drift of the interferometer was tested with a single target mirror. Its drift of 20 pm/sec is large (~4 nrad/sec) but smooth enough that its influence on displacement

---

the compensation of the non-linearity in the heterodyne interferometer," Meas. Sci. Technol. 13(2002):222-225. G.B. Picotto, "Interferometric calibration of microdisplacement actuators," Proc. SPIE 5190(2003):355-360. V. Korpelainen, A. Lassila, "Self-calibration of non-linearities of laser interferometer and capacitive sensor combination for an interferometrically traceable AFM device," Proc. EUSPEN (Glasgow, UK, 31 May - 2 June 2004), pp. 256-257. J. Flugge, R. Koning, H. Bosse, "Measurement of high resolution interferential encoders using the PTB nanometer comparator," in: G. Wilkening, L. Koenders, eds., Nanoscale Calibration Standards and Methods: Dimensional and Related Measurements in the Micro- and Nanometer Range, Wiley, New York, 2005, pp. 404-409.

[1218] G. Basile, P. Becker, A. Bergamin, G. Cavagnero, A. Franks, K. Jackson, U. Kuetgens, G. Mana, E.W. Palmer, M. Stedman, J. Stümpel, A. Yacoot, G. Zosi, "COXI – A Combined Optical and Xray Interferometer for high precision dimensional metrology," Proc. Roy. Soc. Lond. A 456(2000):701-729. Masato Aketagawa, Hiroshi Honda, Masashi Ishige, Chaikool Patamaporn, "Two-dimensional encoder with picometre resolution using lattice spacing on regular crystalline surface as standard," Meas. Sci. Technol. 18(February 2007):342-349. Andrew Yacoot, Michael J Downs, "The use of x-ray interferometry to investigate the linearity of the NPL Differential Plane Mirror Optical Interferometer," Meas. Sci. Technol. 11(2000):1126-1130.

[1219] Petr Kren, Petr Balling, "Common path two-wavelength homodyne counting interferometer development," Meas. Sci. Technol. 20(2009):084009.

measurements below 10 pm can be reduced using the authors' drift removal procedure (Figure 4-66). The maximum speed of displacement consistent with high accuracy was also investigated. Up to 50 pm changes in correction estimation were measured for speeds higher than about 100 μm/sec (which would be a >300 Hz fringe counting frequency), so speeds lower than 10 μm/sec (<30 Hz fringe counting frequency) must be used with this method.

Figure 4-66. The mid-term stability of the 633 nm interferometer with a single target mirror common to both interferometric arms without (thin line) and with (bold line) drift removal.[1220]

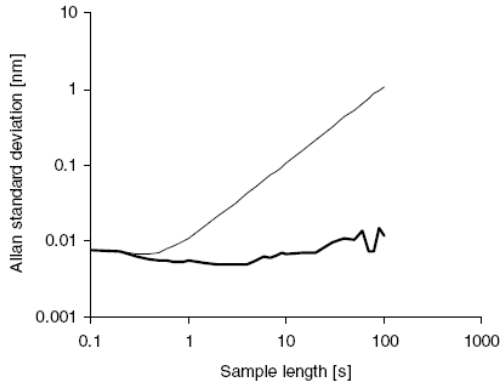

The authors conclude:[1221] "The realized setup has suitable rigidity and stability to be used for a measurement with uncertainties below 30 pm and displacements up to 100 μm. The quality of homodyne signals is also sufficient to provide linearization of fringe interpolation at this level. The time interval of recalculations of elliptic correction parameters in the order of tens of seconds is sufficient to provide a displacement measurement without a significant nonlinearity error. These results imply that the development of the dual optical wavelength interferometer will be successful."

4.6.3.6 AFM with Three-Axis Laser Interferometer (Japan)

The Gonda group[1222] at the National Metrology Institute of Japan has pursued development of a nanometrological AFM using a homodyne laser Michelson-based optical differential

---

[1220] Petr Kren, Petr Balling, "Common path two-wavelength homodyne counting interferometer development," Meas. Sci. Technol. 20(2009):084009.

[1221] Petr Kren, Petr Balling, "Common path two-wavelength homodyne counting interferometer development," Meas. Sci. Technol. 20(2009):084009.

[1222] S. Gonda, T. Doi, T. Kurosawa, Y. Tanimura, N. Hisata, T. Yamagishi, H. Fujimoto, H. Yukawa, "Real-time, interferometrically measuring atomic force microscope for direct calibration of standards," Rev. Sci. Instr. 70(1999):3362-3368. S. Gonda, T. Doi, T. Kurosawa, Y. Tanimura, N. Hisata, T. Yamagishi, H. Fujimoto, H. Yukawa, "Accurate topographic images using a measuring atomic force microscope," Applied Surface Science, 144(April 1999):505-509. I. Misumi, S. Gonda, T. Kurosawa, K.

interferometry measurement system on 3 axes, as reported in the literature during 1999-2006. So far they have fielded three related systems – one with an XYZ measurement range of 17.5 μm x 17.5 μm x 2.5 μm,[1223] a second with an XYZ measurement range of 100 μm x 100 μm x 12 μm,[1224] and a third which is a critical-dimension AFM or CD-AFM system.[1225] This system achieves its high accuracy by employing specialized digital signal processing techniques.

Takamasu, "Uncertainty in pitch measurements of onedimensional grating standards using a nanometrological atomic force microscope," Meas. Sci. Technol. 14(7 March 2003):463-471. I. Misumi, S. Gonda, T. Kurosawa, Y. Tanimura, N. Ochiai, J. Kitta, F. Kubota, M. Yamada, Y. Fujiwara, Y. Nakayama, K. Takamasu, "Submicrometre-pitch intercomparison between optical diffraction, scanning electron microscope and atomic force microscope," Meas. Sci. Technol. 14(6 October 2003):2065-2074; http://www.nano.pe.u-tokyo.ac.jp/pdffiles/mst3_12_004.pdf. I. Misumi, S. Gonda, T. Kurosawa, Y. Azuma, T. Fujimoto, I. Kojima, T. Sakurai, T. Ohmi, K. Takamasu, "Reliability of parameters of associated base straight line in step height samples: Uncertainty evaluation in step height measurements using nanometrological AFM," Prec. Eng. 30(2006):13-22. http://www.nmij.jp/dms-std/Paper/2005/Paper4.pdf. Satoshi Gonda, Kazuto Kinoshita, Hironori Noguchi, Hajime Koyanagi, Tsuneo Terasawa, "Compact high-resolution homodyne interferometer for nanometer-scale multidimensional AFM metrology," in Wolfgang Osten, Erik Novak, eds., Interferometry XII: Applications, Proc. SPIE 5532(2004):229-236. Satoshi Gonda, Kazuto Kinoshita, Hironori Noguchi, Tomizo Kurosawa, Hajime Koyanagi, Ken Murayama, Tsuneo Terasawa, "AFM measurement of linewidth with sub-nanometer scale precision," Proc. SPIE 5752(2005):156. Ken Murayama, Satoshi Gonda, K. Kinoshita, Hajime Koyanagi, Tsuneo Terasawa, Sumio Hosaka, "Height Measurement Using High-Precision Atomic Force Microscope Scanner Combined with Laser Interferometers," Jpn. J. Appl. Phys. 45(2006):8832-8838. Satoshi Gonda, "Metrology AFM and Nanometrology," Hyomen Kagaku 27(2006):662-668; http://www.jstage.jst.go.jp/article/jsssj/27/11/27_662/_article.

[1223] S. Gonda, T. Doi, T. Kurosawa, Y. Tanimura, N. Hisata, T. Yamagishi, H. Fujimoto, H. Yukawa, "Real-time, interferometrically measuring atomic force microscope for direct calibration of standards," Rev. Sci. Instr. 70(1999):3362-3368. S. Gonda, T. Doi, T. Kurosawa, Y. Tanimura, N. Hisata, T. Yamagishi, H. Fujimoto, H. Yukawa, "Accurate topographic images using a measuring atomic force microscope," Applied Surface Science, 144(April 1999):505-509. I. Misumi, S. Gonda, T. Kurosawa, K. Takamasu, "Uncertainty in pitch measurements of onedimensional grating standards using a nanometrological atomic force microscope," Meas. Sci. Technol. 14(7 March 2003):463-471. I. Misumi, S. Gonda, T. Kurosawa, Y. Tanimura, N. Ochiai, J. Kitta, F. Kubota, M. Yamada, Y. Fujiwara, Y. Nakayama, K. Takamasu, "Submicrometre-pitch intercomparison between optical diffraction, scanning electron microscope and atomic force microscope," Meas. Sci. Technol. 14(6 October 2003):2065-2074; http://www.nano.pe.u-tokyo.ac.jp/pdffiles/mst3_12_004.pdf. I. Misumi, S. Gonda, T. Kurosawa, Y. Azuma, T. Fujimoto, I. Kojima, T. Sakurai, T. Ohmi, K. Takamasu, "Reliability of parameters of associated base straight line in step height samples: Uncertainty evaluation in step height measurements using nanometrological AFM," Prec. Eng. 30(2006):13-22. http://www.nmij.jp/dms-std/Paper/2005/Paper4.pdf.

[1224] I. Misumi, S. Gonda, T. Kurosawa, K. Takamasu, "Uncertainty in pitch measurements of onedimensional grating standards using a nanometrological atomic force microscope," Meas. Sci. Technol. 14(7 March 2003):463-471.

[1225] Satoshi Gonda, Kazuto Kinoshita, Hironori Noguchi, Hajime Koyanagi, Tsuneo Terasawa, "Compact high-resolution homodyne interferometer for nanometer-scale multidimensional AFM metrology," in Wolfgang Osten, Erik Novak, eds., Interferometry XII: Applications, Proc. SPIE 5532(2004):229-236. Satoshi Gonda, Kazuto Kinoshita, Hironori Noguchi, Tomizo Kurosawa, Hajime Koyanagi, Ken Murayama, Tsuneo Terasawa, "AFM measurement of linewidth with sub-nanometer scale precision," Proc.

The nanometrological AFM shown in Figure 4-67. To summarize:[1226] The nanometrological AFM is a stage scanning-type system, and is operated in the contact AFM mode. It consists of a stage unit, an AFM probe unit, and interferometer units. The stage unit comprises a piezo-driven leaf spring stage, which is used as an XY-axis scanner, and a tube-type piezoactuator which is used as a Z-axis scanner. The scanning area of this stage unit is approximately **17.5 μm x 17.5 μm x 2.5 μm**. A three-sided moving mirror as the target of the interferometer units is set on top of the Z-axis scanner. Each interferometer unit has four optical paths on each axis and its resultant resolution is approximately **40 pm**. The laser sources of the interferometer unit are frequency-stabilized He-Ne lasers with a wavelength of 633 nm (model 117A, Spectra-Physics, Ltd.). The laser frequency is calibrated using an I_2-stabilized He-Ne laser, prior to the step height measurement. The atomic force between a cantilever and a sample surface is detected from the bending of the cantilever using a conventional optical lever method. The Z-axis scanner position is servo-controlled so that the atomic force is kept constant during the XY scan. The resultant displacement of the Z-axis scanner, therefore, corresponds to the displacement of the top of the cantilever at the contact point with the surface. The XY scan is servo-controlled using interferometer signals so that the cantilever is positioned to the desired picture element of an AFM image. The Z-axis displacement is monitored by the interferometer during the step height measurement. Since the AFM profiles of step height standards are identical to the displacement of the top of the cantilever, the calibration of step height standards is directly traceable to the unit of length.

Figure 4-68 shows a cross-sectional view of the AFM main unit with a three-axis laser interferometer and a 3D scanner. Scanning in the three axial directions is performed by a 3D scanner comprising a combination of a commercial type monolithic fine-motion XY stage (P-730, Physik Instrumente) and a Z scanning piezo tube translator. In order to avoid angular deviation, the gain of the voltage applied to the four electrodes on the Z tube is adjusted so that the bending motion of the tube is minimized. A three-sided mirror (TSM) block serves as both a moving mirror of the three-axis laser interferometer and a sample holder. The TSM block is made of fused quartz and the reflection sides are carefully polished at right angles to each other with an error of less than 1 arcsec. The mirror is placed on top of the Z scanner. The good perpendicularity of the TSM and careful optical alignment to the TSM enable the realization of an excellent rectangular coordinate system for 3D position measurement. A frame mount is inserted between the TSM and the Z scanner in order to secure the optical path of the Z interferometer unit.

SPIE 5752(2005):156. Ken Murayama, Satoshi Gonda, K. Kinoshita, Hajime Koyanagi, Tsuneo Terasawa, Sumio Hosaka, "Height Measurement Using High-Precision Atomic Force Microscope Scanner Combined with Laser Interferometers," Jpn. J. Appl. Phys. 45(2006):8832-8838.

[1226] I. Misumi, S. Gonda, T. Kurosawa, Y. Azuma, T. Fujimoto, I. Kojima, T. Sakurai, T. Ohmi, K. Takamasu, "Reliability of parameters of associated base straight line in step height samples: Uncertainty evaluation in step height measurements using nanometrological AFM," Prec. Eng. 30(2006):13-22. http://www.nmij.jp/dms-std/Paper/2005/Paper 4.pdf.

Figure 4-67. Atomic force microscope with three-axis laser interferometer (nanometrological AFM), which consists of a stage unit, an AFM probe unit (not mounted in this photograph), and interferometer units.[1227]

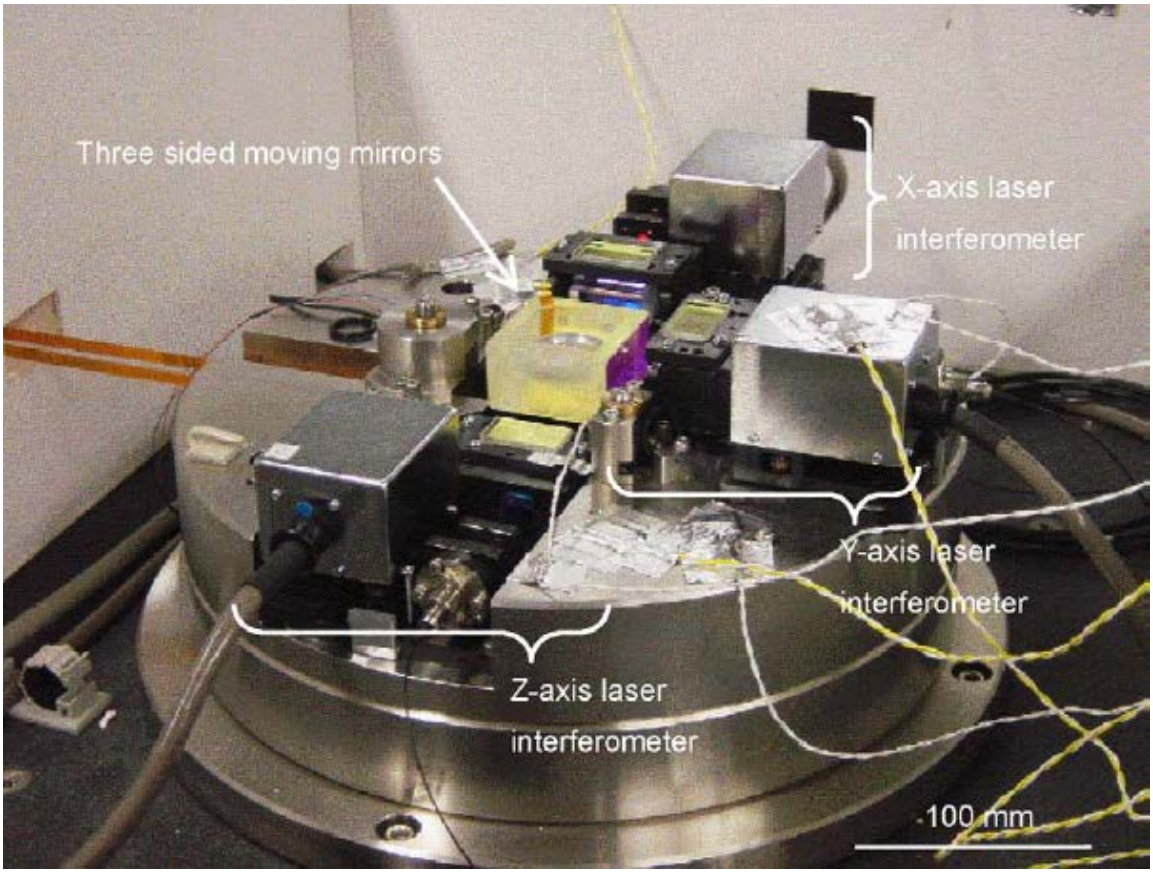

[1227] I. Misumi, S. Gonda, T. Kurosawa, Y. Azuma, T. Fujimoto, I. Kojima, T. Sakurai, T. Ohmi, K. Takamasu, "Reliability of parameters of associated base straight line in step height samples: Uncertainty evaluation in step height measurements using nanometrological AFM," Prec. Eng. 30(2006):13-22. http://www.nmij.jp/dms-std/Paper/2005/Paper 4.pdf.

Figure 4-68. Schematic cross section of the main unit of the measuring AFM. PU: probe unit, LD: laser diode, SPD: segmented photodiode, TSM: three-sided mirror, IU: interferometer unit, BM: bending mirror (for IU of Z axis), BD: belt drive, XYS:XY fine motion stage, ZT: Z translator.[1228]

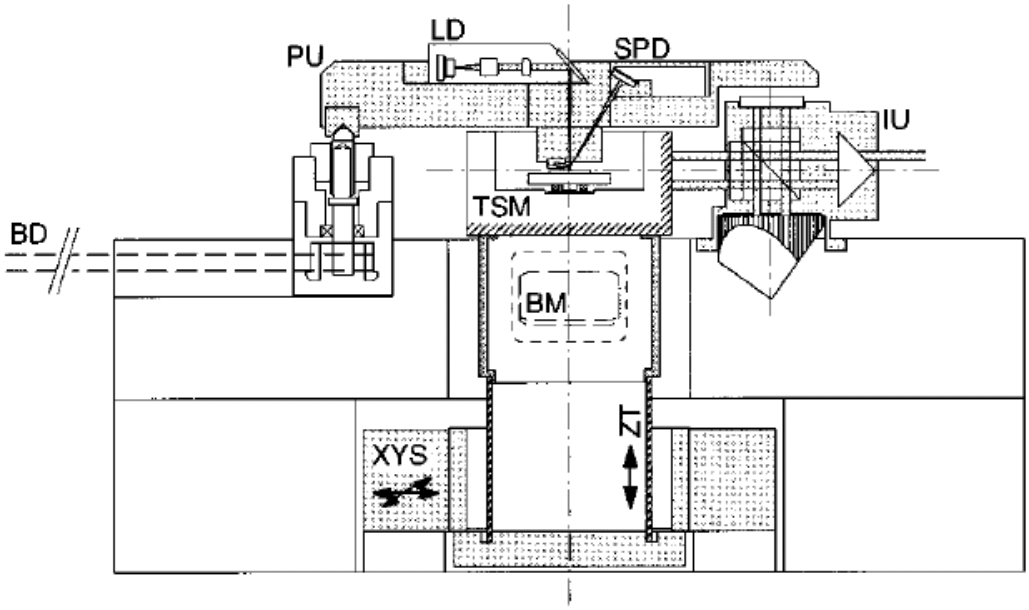

The atomic force probing unit is set on the 3D scanner by a kinematic mount that enables reproducible positioning of the probe-point at the center of the TSM. The atomic force detecting method is the same as that used conventionally, using a fixed-position cantilever, a laser diode, and a quadruplet photodiode for the optical lever method. Samples are set on permalloy disks of appropriate thickness so that the vertical position of the sample surface meets the optical axes of the laser interferometers, after which they are fixed on the TSM by an electromagnetic chuck. The coarse XY positioning is conducted by the impact drive method. There is no tilting and rotating mechanism at present. The maximum area for the interferometric measurement of 17.5 x 17.5 x 2.5 μm^3 is not limited by the maximum scan range of the scanner but by the maximum allowable servo error due to the angular deviation of the 3D scanner. (The typical scan speed in this experiment[1229] was set to as low as 2.5 μm/sec to minimize the Z-axis servo error of the probe-surface contact.) The main unit of the apparatus except for the lasers is built on a vibration-isolated table and covered by a sound and thermal isolation shield. The temperature and humidity of the laboratory are controlled within ±0.1 K and ±1%, respectively.

[1228] S. Gonda, T. Doi, T. Kurosawa, Y. Tanimura, N. Hisata, T. Yamagishi, H. Fujimoto, H. Yukawa, "Real-time, interferometrically measuring atomic force microscope for direct calibration of standards," Rev. Sci. Instr. 70(1999):3362-3368.

[1229] S. Gonda, T. Doi, T. Kurosawa, Y. Tanimura, N. Hisata, T. Yamagishi, H. Fujimoto, H. Yukawa, "Real-time, interferometrically measuring atomic force microscope for direct calibration of standards," Rev. Sci. Instr. 70(1999):3362-3368.

The three-axis laser interferometer designed for this system has three interferometer units. Each unit is assembled and adjusted to each reflection surface of the TSM as a reference. A beam of a frequency-stabilized He-Ne laser is supplied to each unit of the interferometer through a polarization-maintaining single-mode fiber. Figure 4-69 (top) shows a bird's-eye view of the optical path arrangement of the interferometer unit and a summary diagram is shown in Figure 4-70. The incident beam is divided into two beams, one directed toward the reference mirror and the other toward the TSM. Both beams travel back and forth four times between the interferometer unit and the TSM through a polarizing beam splitter, a corner reflector, and a roof mirror, resulting in a displacement sensitivity improvement by a factor of 4. The mean optical axes of XYZ interferometer units are set perpendicular to each mirror plane of the TSM and aligned so as to intersect at the force-probing point at the sample surface.

Figure 4-69. <u>Top:</u> Bird's-eye view of the optical path arrangement of the interferometer unit. TSM: three-sided mirror, CCP: corner cube prism, RM: reference mirror, RP: roof prism, P: polarizer, FC: fiber connector, PBS: polarizing beam splitter, NPBS: nonpolarizing beam splitter, HWP: half-wave plate, QWP: quarter-wave plate, PD: photodiode. <u>Bottom:</u> Interferometric signal processing diagram for error reduction and resolution improvement.[1230]

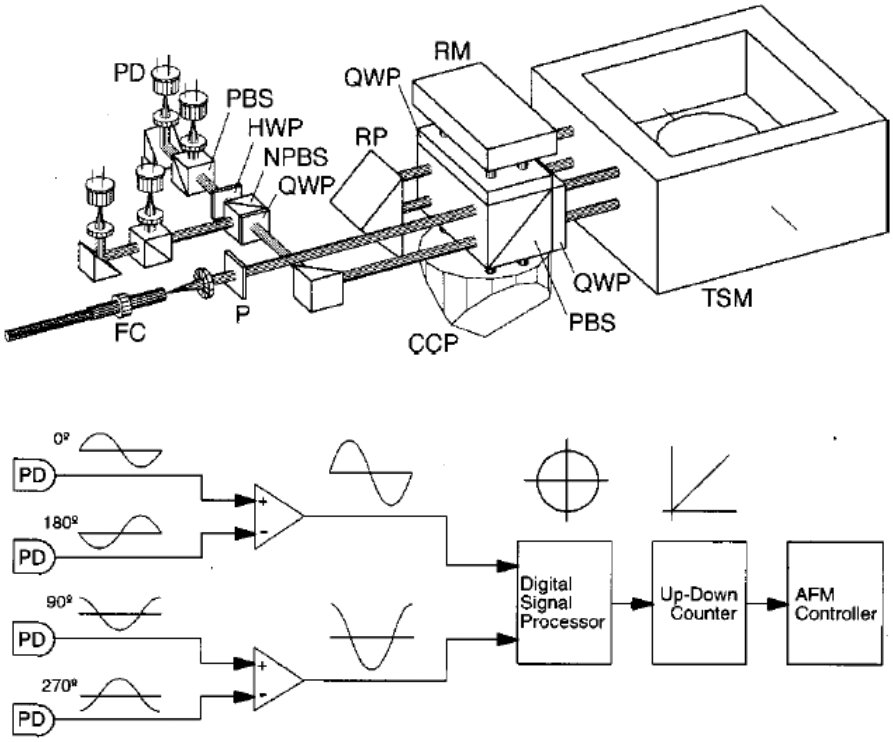

[1230] S. Gonda, T. Doi, T. Kurosawa, Y. Tanimura, N. Hisata, T. Yamagishi, H. Fujimoto, H. Yukawa, "Real-time, interferometrically measuring atomic force microscope for direct calibration of standards," Rev. Sci. Instr. 70(1999):3362-3368.

Figure 4-70. <u>Left:</u> Cross-sectional drawing of the main unit of the nanometrological AFM, which consists of a stage unit, an AFM probe unit and interferometer units. <u>Right:</u> Block diagram of the nanometrological AFM system; the stage position is servo-controlled using the interferometer signals in real time.[1231]

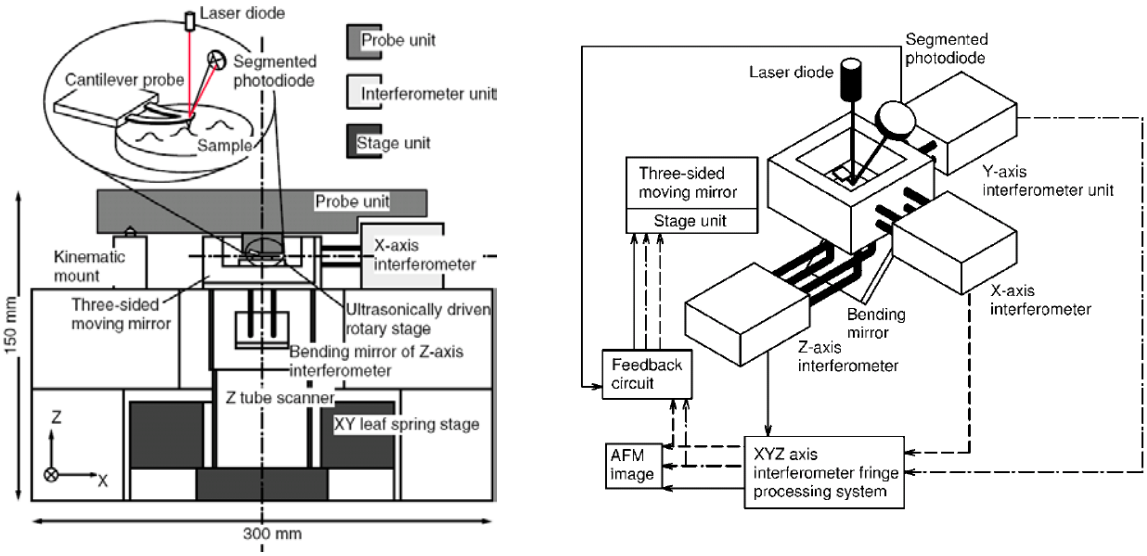

The four signals from the interference beam, phase shifted by 90° with respect to each other by a series of polarizing beam splitters, half- and quarter-wave plates, are detected by four photodiodes. A diagram of the signal processing procedure is illustrated in Figure 4-69 (bottom). Two of the four signals with a phase difference of 180° are electrically subtracted so that the output signal has a twofold amplitude and no dc component. Then the two signals are introduced into an A/D converter and the phase angle is calculated by real-time digital processing. In this step, offset correction and gain adjustment for the two signals are accomplished prior to the phase angle calculation. Lissajous figures plotted with one of the two signals as abscissa against the other signal as ordinate after an offset correction and gain adjustment by digital processing appear to be almost perfect circles and therefore can assist in making accurate phase calculations. The phase angle corresponding to the displacement position is calculated with the resolution of $2\pi/2048$ by RISC processors and ROM tables of arc tangent. (Each complete Lissajous circle corresponds to a displacement of $\lambda/8$, and the circle is electronically subdivided into 2048 segments, or approximately 633 nm / (8 x 2048) ~ 40 pm.) The calculated phase is then compared with the former phase and the phase difference is outputted to an up/down counter in a pulse format, achieiving a total resolution (equivalent to the least square bit) for each interferometer unit of **40 pm** ($\lambda/16384$) and a maximum sampling rate of 15 kHz. However, the

[1231] I. Misumi, S. Gonda, T. Kurosawa, K. Takamasu, "Uncertainty in pitch measurements of onedimensional grating standards using a nanometrological atomic force microscope," Meas. Sci. Technol. 14(7 March 2003):463-471.

average drift rates for the outputs of the interferometers are 30-350 pm/minute which is a bit too high for DMS work.

The primary source of uncertainty in the measurements was derived from interferometer nonlinearity of ~115 pm (Figure 4-71). Noise amplitude of 90-160 pm (rms) is mainly caused by the mechanical vibration of the 3D scanner. The XY servo control yields a small noise of 220-270 pm and there is additional hysteretic variation between the X and Y axes of ~10 nm over an entire 20 micron scan length.[1232] The combined standard uncertainty is ~150 pm and an estimated expanded uncertainty (k = 2) of less than 300 pm was obtained across the scanning range.[1233]

Figure 4-71. Evaluation of cyclic error in the interferometer: response of a laser interferometer in the single axis scan.[1234] Note that the raw variation is approximately ±100 pm.

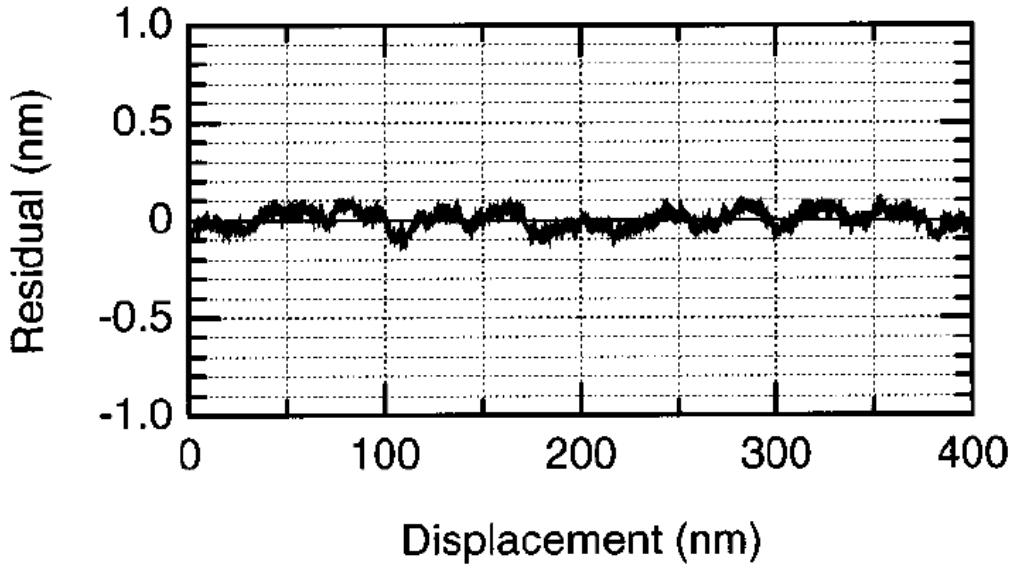

[1232] S. Gonda, T. Doi, T. Kurosawa, Y. Tanimura, N. Hisata, T. Yamagishi, H. Fujimoto, H. Yukawa, "Real-time, interferometrically measuring atomic force microscope for direct calibration of standards," Rev. Sci. Instr. 70(1999):3362-3368.

[1233] I. Misumi, S. Gonda, T. Kurosawa, K. Takamasu, "Uncertainty in pitch measurements of onedimensional grating standards using a nanometrological atomic force microscope," Meas. Sci. Technol. 14(7 March 2003):463-471. I. Misumi, S. Gonda, T. Kurosawa, Y. Azuma, T. Fujimoto, I. Kojima, T. Sakurai, T. Ohmi, K. Takamasu, "Reliability of parameters of associated base straight line in step height samples: Uncertainty evaluation in step height measurements using nanometrological AFM," Prec. Eng. 30(2006):13-22. http://www.nmij.jp/dms-std/Paper/2005/Paper 4.pdf.

[1234] S. Gonda, T. Doi, T. Kurosawa, Y. Tanimura, N. Hisata, T. Yamagishi, H. Fujimoto, H. Yukawa, "Real-time, interferometrically measuring atomic force microscope for direct calibration of standards," Rev. Sci. Instr. 70(1999):3362-3368.

A redesigned optical path layout in this high-resolution homodyne interferometer, when installed in a prototype CD-AFM (critical-dimension atomic force microscope), as part of the MIRAI (Millennium Research for Advanced Information Technology) project,[1235] allowed displacement of the scanner to be resolved and calibrated at better than 50 pm and 200 pm, respectively, using a DSP-based (digital signal processing) electronic interpolation technique.[1236] A wide linearity range from 0.1 nm to 1 micron was demonstrated for the CD-AFM and a one-sigma repeatability of 250 pm was obtained by measuring reference samples of 50 nm and 1000 nm step heights.[1237]

4.6.3.7 Crystal Reference Interferometry with SPM (Japan)

In 1990, Kawakatsu and Higuchi[1238] proposed that a regular crystalline lattice had the potential of being used as a well-defined, universal reference scale in the metrological application of scanning tunneling microscopes (STMs). A dual tunneling-unit (DTU) STM, incorporating one XY scanner and two Z scanners with tips, was developed to check the feasibility of the "crystal-reference" STM. Promising simulation results were obtained as to the noise tolerance of the controls. In 1999, Aketagawa et al.[1239] performed a feasibility evaluation of long atomic imaging over a 5-µm long region for the comparative length measurement using a crystalline lattice as the reference scale and a dual-tunneling-unit scanning tunneling microscope (DTU-STM) as a detector. For suppression of the thermal deformation error, an ultralow thermally drifted DTU-STM was developed with the body of the DTU-STM fabricated from ultralow linear expansion glass and Super-Invar. A thermostabilized cell reduced the temperature fluctuation to less than 0.05 K around the DTU-STM, achieving a minimum lateral element of thermal drift rate of less than 200 pm/hour at room temperature. By 2001, the same research group proposed that sub-nanometer resolution and a measuring range of a few millimeters could be attained by combining a "crystalline lattice scale" and laser interferometry as fine and coarse reference scales, using a regular crystalline surface as a reference and a scanning tunneling microscope (STM) as a

---

[1235] Satoshi Gonda, Kazuto Kinoshita, Hironori Noguchi, Tomizo Kurosawa, Hajime Koyanagi, Ken Murayama, Tsuneo Terasawa, "AFM measurement of linewidth with sub-nanometer scale precision," Proc. SPIE 5752(2005):156.

[1236] Satoshi Gonda, Kazuto Kinoshita, Hironori Noguchi, Hajime Koyanagi, Tsuneo Terasawa, "Compact high-resolution homodyne interferometer for nanometer-scale multidimensional AFM metrology," in Wolfgang Osten, Erik Novak, eds., Interferometry XII: Applications, Proc. SPIE 5532(2004):229-236.

[1237] Ken Murayama, Satoshi Gonda, K. Kinoshita, Hajime Koyanagi, Tsuneo Terasawa, Sumio Hosaka, "Height Measurement Using High-Precision Atomic Force Microscope Scanner Combined with Laser Interferometers," Jpn. J. Appl. Phys. 45(2006):8832-8838.

[1238] H. Kawakatsu, T. Higuchi, "A dual tunneling unit scanning tunneling microscope," J. Vac. Sci. Technol. 8(January 1990):319-323.

[1239] M. Aketagawa, K. Takada, N. Takeshina, K. Yamada, J.D. Lee, "Long atomic imaging over a 5-µm-long region using an ultralow thermally drifted dual-tunneling-unit scanning tunneling microscope in a thermostabilized cell," Rev. Sci. Instr. 70(1999):133-136.

detector.[1240] Aketagawa and Takada[1241] obtained a 5-μm-long atomic image of a highly oriented pyrolytic graphite (HOPG) crystal along the fast scanning axis using the DTU-STM in the temperature control cell, and a stabilization technique for atomic tracking control was developed.[1242] In 2003, following an earlier proposal by IMGC (former Italian Standard Institute),[1243] an instrument for direct measurement of the lattice spacing on regular crystalline surfaces, incorporating a scanning tunneling microscope (STM) and a phase modulation homodyne interferometer (PMHI), was developed[1244] that allowed measurement of the relative displacement of the X-axis sample stage between optical interference dark fringes (= null points) of the PMHI with a resolution of **10 pm** or less using the phase modulation technique. The lattice spacing on a highly oriented pyrolytic graphite (HOPG) crystalline surface was measured by comparing the number of atoms in the atomic STM image of 100 nm length with the optical fringes of the PMHI. The mean and expanded uncertainty (k = 2) of the lattice spacing between alpha sites of the HOPG surface were 246 pm and 7 pm, respectively.

In 2004, the group proposed a technique for highly stabilized atom-tracking control of a scanning tunneling microscope (STM) tip by referring to an atomic point on a regular crystalline surface.[1245] The aim was to prevent jumping of the STM tip to neighboring atoms even in a noisy environment, using graphite crystal, whose lattice spacing is approximately 250 pm, as the reference. By 2005, Aketagawa et al.[1246] had demonstrated this technique for highly stable atom-tracking control of a scanning tunnelling microscope (STM) tip by referring to an atomic point on

---

[1240] P. Rerkkumsup, M. Aketagawa, K. Takada, T. Takagi, T. Watanabe, S. Sadakata, "Proposal of Absolute Length Measuring Machine by Combining Crystalline Lattice Scale and Laser Interferometry," Initiatives of Precision Engineering at the Beginning of a Millennium, 10th International Conference on Precision Engineering (ICPE) 18-20 July 2001, Yokohama, Japan, Springer USA, 2002.

[1241] Masato Aketagawa, Koji Takada, "Length and angle measurements using regular crystalline lattice as reference," International Journal of Machine Tools and Manufacture 41(October 2001):2079-2085.

[1242] P. Rerkkumsup, N.T. Thinh, Y. Kozuma, M. Aketagawa, K. Takada, "Stabilization technique for atomic tracking control of scanning tunneling microscope tip by referring regular crystalline surface," Seimitsu Kogakkai Taikai Gakujutsu Koenkai Koen Ronbunshu 2002(2002):596.

[1243] G. Basile, A. Bergamin, G. Cavagnero, G. Mana, "Phase modulation in high resolution optical interferometry," Metrologia 28(1992):455-461.

[1244] Pongpun Rerkkumsup, Masato Aketagawa, Koji Takada, Tomonori Watanabe, Shin Sadakata, "Direct measurement instrument for lattice spacing on regular crystalline surfaces using a scanning tunneling microscope and laser interferometry," Rev. Sci. Instrum. 74(March 2003):1205.

[1245] Pongpun Rerkkumsup, Masato Aketagawa, Koji Takada, Yoichi Togawa, Nguyen Tien Thinh, Yosuke Kozuma, "Highly stable atom-tracking scanning tunneling microscopy," Rev. Sci. Instrum. 75(16 March 2004):1061; http://link.aip.org/link/?RSINAK/75/1061/1. Yoichi Togawa, Pongpun Rerkkumsup, Hiroshi Honda, Masato Aketagawa, Koji Takada, "Highly stable atom-tacking control of using regular crystalline lattice and scanning tunneling microscope-Validation of Atomic Encoder," Journal of the Japan Society for Precision Engineering 70(2004):1433-1438. In Japanese.

[1246] M. Aketagawa, K. Takada, P. Rerkkumsup, Y. Togawa, H. Honda, "Real-time atomic encoder using scanning tunnelling microscope and regular crystalline surface," Meas. Sci. Technol. 16(2005):1-6.

a regular crystalline surface, including an atomic encoder using "atom-by-atom" step control along a graphite crystalline axis. The method was also applied to atom-step control of the STM tip by referring to a specific crystalline axis. Atom-stepping control along a crystalline axis over a range of 200 atoms and at a rate of 10 atoms/sec was performed and demonstrated without missing the atomic array.

The lattice spacing of approximately 246 pm for graphite regular crystalline lattices is uniform and stable over a long range when the crystals are stress free, allowing these crystals to be used as a reference scale with sub-nanometer resolution. In 2007, Aketagawa et al.[1247] developed an instrument for calibrating optical encoders by combining a graphite crystalline lattice as a fine scale and the optical fringe of the PMHI[1248] as a coarse scale. The instrument (Figure 4-72) consists of a precise linear X-axis sample stage on which the reference graphite crystal and the optical encoder scale are set (Figure 4-73).

Figure 4-72. Outline photograph of the calibration instrument.[1249]

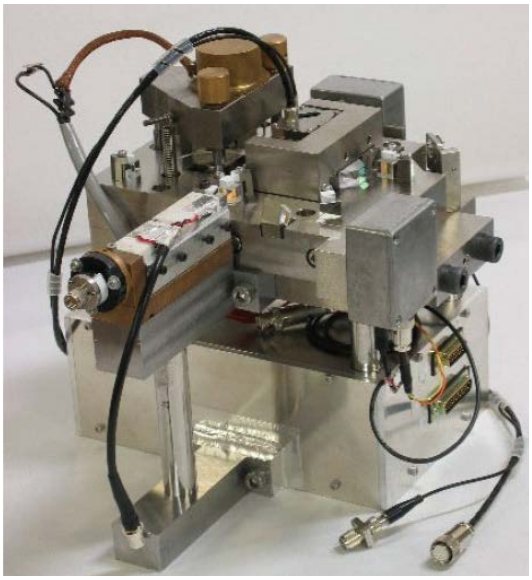

[1247] Masato Aketagawa, Yosuke Ikeda, Nuttapong Tanyarat, Masashi Ishige, "Optical encoder calibration using lattice spacing and optical fringe derived from a scanning tunnelling microscope and optical interferometer," Meas. Sci. Technol. 18(February 2007):503-509.

[1248] Masashi Ishige, Fumio Matsuura, Masaaki Kawasugi, Masato Aketagawa, "Phase Modulation Homodyne Interferometer with a 10-pm Resolution Using a Tunable Laser Diode," International Journal of Precision Engineering and Manufacturing 8(2007):80-84; http://www.ijpem.org/journal/files/issues/E06-31.pdf.

[1249] Masato Aketagawa, Yosuke Ikeda, Nuttapong Tanyarat, Masashi Ishige, "Optical encoder calibration using lattice spacing and optical fringe derived from a scanning tunnelling microscope and optical interferometer," Meas. Sci. Technol. 18(February 2007):503-509.

Figure 4-73. Schematic side view of a calibration instrument for optical encoders realized by combining regular crystalline surface, STM and PMHI.[1250]

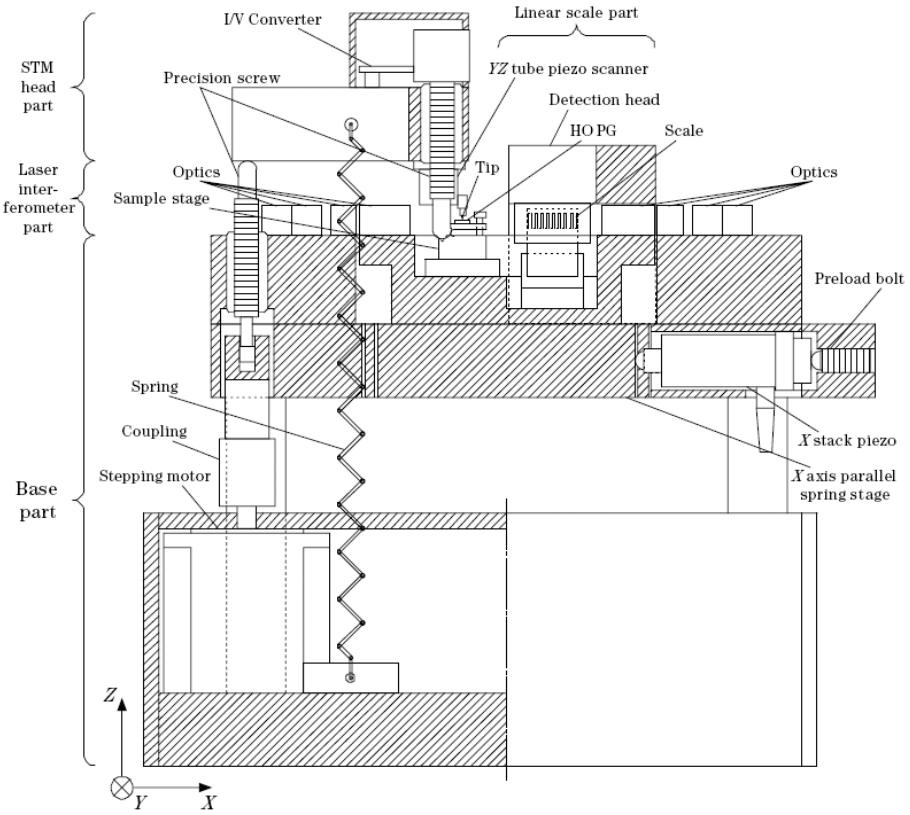

Figure 4-74 shows the experimental system and optical layout of the PMHI. The X-axis displacement of the sample stage is measured with the PMHI and the optical encoder. At the same time, a three-dimensional scan of the STM tip over the graphite crystalline surface is performed using the X-axis sample stage and the YZ tip scanner; therefore, the atomic image of the graphite is obtained using the STM. Z-servo control and raster signals input to the YZ tip scanner are obtained from a STM controller. A driving signal to the X-axis sample stage is generated by a 16-bit digital-to-analogue converter (D/A) with a digital signal processor (DSP). A high-voltage amplifier is employed for driving the stacked-type piezo actuator. The 16-bit analog-to-digital converter (A/D) and 32-bit digital input–output (DIO) board are used for collecting the three signals.

[1250] Masato Aketagawa, Yosuke Ikeda, Nuttapong Tanyarat, Masashi Ishige, "Optical encoder calibration using lattice spacing and optical fringe derived from a scanning tunnelling microscope and optical interferometer," Meas. Sci. Technol. 18(February 2007):503-509.

Figure 4-74. Experimental system and optical path layout for the calibration instrument. PBS: polarizing beam splitter, NPBS: nonpolarizing beam splitter, P(45◦): 45◦ polarizer, PD: photodetector, RP: right-angle prism, TP: trapezoid prism, MP: movable prism, AM: adjustment mirror and LIA: lock-in amplifier.[1251]

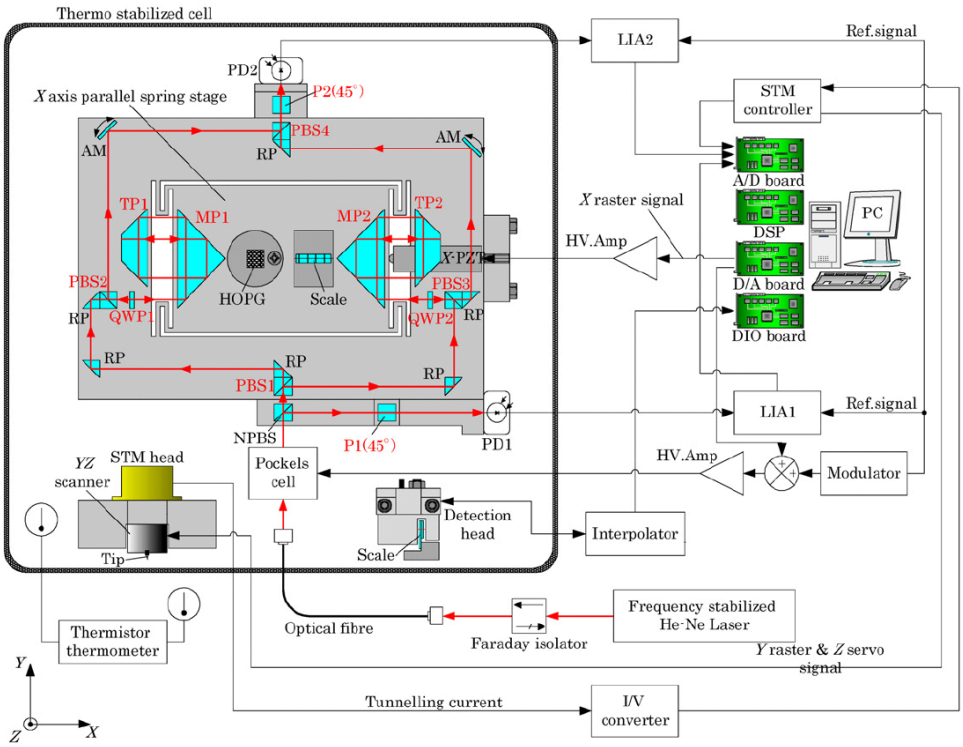

The relative displacement of the X-axis sample stage between optical interference dark fringes (= null points) of the PMHI, which is λ/16 times the integer value in the design, can be measured with picometer resolution using the phase modulation technique. A lattice spacing of 246 pm on the graphite crystalline surface is derived as the fine scale from the STM image and the optical fringes of the PMHI. In the experiment, the periodical error of the optical encoder, whose minimum resolution is less than a nanometer, is measured using both the lattice spacing of graphite and the optical fringes of the PMHI. The results show that the proposed instrument has the feasibility to calibrate optical encoders with an uncertainty on the order of 10 pm. The instrument has a scanning range of 500 nm in X and 2.5 nm in Y, but it runs in air, not UHV. The paper is unclear because its Figs. 5 and 6 appear to show a nonlinear periodic error of ±125 pm, but its Table 3 lists for the optical encoded calibration a combined standard uncertainty of

---

[1251] Masato Aketagawa, Yosuke Ikeda, Nuttapong Tanyarat, Masashi Ishige, "Optical encoder calibration using lattice spacing and optical fringe derived from a scanning tunnelling microscope and optical interferometer," Meas. Sci. Technol. 18(February 2007):503-509.

25.5 pm and an expanded uncertainty (k=2) of 51 pm, which would seem to be (just barely) adequate for DMS work.

In other papers published in 2007-2008,[1252] the Aketagawa group proposed a two-dimensional (2D) encoder with picometer resolution using multi-tunnelling-probes scanning tunnelling microscope (MTP-STM) as detector units and a regular crystalline lattice as a reference. In experiments to demonstrate the method using a highly oriented pyrolytic graphite (HOPG) crystal as the reference, the proposed method is compared with a capacitance sensor whose resolution is improved to approximately 100 pm by limiting the sensor's bandwidth to 300 Hz. The results showed that the proposed method has the capability to measure 2D lateral displacements with a resolution on the order of 10 pm with a maximum measurement speed of 100 nm/sec or more. This proposed instrument could scan at 0.1 micron/sec while achieving a resolution of 10 pm. The group has continued refining their system, e.g., adding a spherical closed surface capsule for temperature control[1253] reminiscent of the one employed in the M^3 system described in Section 4.6.1.1.

The group reports an improved proposal in their most recent (2009) paper,[1254] as follows:

"In our previous research,[1255] a 2D displacement atom encoder technique with 10 pm resolution using a combination of a scanning tunneling microscope (STM) and HOPG crystal was proposed. The STM, which is popular in surface engineering, is capable of observing an atomic image of the crystalline surface. A lattice spacing of approximately 246 pm[1256] is observable when the HOPG crystalline surface is uniform and stable over a long range when the crystals are

---

[1252] Masato Aketagawa, Hiroshi Honda, Masashi Ishige, Chaikool Patamaporn, "Two-dimensional encoder with picometre resolution using lattice spacing on regular crystalline surface as standard," Meas. Sci. Technol. 18(February 2007):342-349. P. Chaikool, M. Aketagawa, E. Okuyama, "Two-dimensional Displacement Measurement Using the Six-point Atomic Encoder Technique," Abstract 2674, 2008 Annual Meeting, American Society for Precision Engineering, 2008; http://www.aspe.net/meetings/2008_Annual/Oral_Presentations_2008.html.

[1253] P. Rerkkumsup, P. Prachprayoon, "The proposal of novel design of temperature control system for scanning tunneling microscope: The closed surface capsule," 3rd IEEE International Conference on Nano/Micro Engineered and Molecular Systems (NEMS 2008), 6-9 January 2008, pp. 432-435. P. Yimsamerjit, P. Rerkkumsup, "The proposal of novel design of temperature control system for scanning tunneling microscope: The high stability temperature control," 3rd IEEE International Conference on Nano/Micro Engineered and Molecular Systems (NEMS 2008), 6-9 January 2008, pp. 436-439.

[1254] Patamaporn Chaikool, Masato Aketagawa, Eiki Okuyama, "A two-dimensional atom encoder using one lateral-dithered scanning tunneling microscope (STM) tip and a regular crystalline lattice," Meas. Sci. Technol. 20(2009):084006.

[1255] Masato Aketagawa, Hiroshi Honda, Masashi Ishige, Chaikool Patamaporn, "Two-dimensional encoder with picometre resolution using lattice spacing on regular crystalline surface as standard," Meas. Sci. Technol. 18(February 2007):342-349.

[1256] Pongpun Rerkkumsup, Masato Aketagawa, Koji Takada, Tomonori Watanabe, Shin Sadakata, "Direct measurement instrument for lattice spacing on regular crystalline surfaces using a scanning tunneling microscope and laser interferometry," Rev. Sci. Instrum. 74(March 2003):1205.

stress free. In the previous paper,[1257] one or two mono-crystalline areas of the HOPG surface are utilized as 2D references, and observed by one or two lateral-dithered STM tip(s). But the three-point and eight-point methods proposed in our previous research have some disadvantages. The three-point method can be easily performed, since only one lateral-dithered STM tip is required. In this method, the displacement is derived from the cosine function of lattice spacing and it can't perform the interpolation method, so measurement of displacements smaller than the lattice spacing is impossible. The eight-point method can solve the interpolation problem but is complicated for practical application and design due to the need for two STM tips. To overcome these disadvantages of the previous proposal, a new method is proposed that allows the interpolation and use of only one STM tip: a new 2D displacement atom encoder technique using only one lateral-dithered STM tip and one mono-crystalline area of HOPG. Multi-tunneling-current signals from six specific points on the HOPG crystalline surface, which is observed by the one STM tip, are used to determine the displacement of the XY-stage."

The single-tip "atom encoder" method[1258] makes use of the non-isotropic 2D pattern of carbon atoms on the HOPG surface to measure the orientation angle of the lattice pattern. The tip-dithering method, confirmed using an STM experimental setup, allows interpolation of the displacement to a resolution of 5%-10% of the ~246 pm HOPG lattice spacing, or ~**20 pm**. The displacement of a second (e.g., DMS) tip rigidly linked to the first one would presumably be measured to the same resolution. The method gives a measurement repeatability (or noise level) of approximately 20 pm – the measurement speed is ~100 nm/sec and the repeatability (or noise level) of the atom encoder in terms of standard deviation σ (at measurement time = 100 ms) is calculated to be 24 pm, vs. ~120 pm for the comparison capacitive displacement sensors, with the method successfully used without crashing the tip and sample for a period of about 1 month. The thermal drift velocities were measured as 147 pm/min and 587 pm/min along the X- and Y-axes, respectively, in the experimental apparatus.

4.6.3.8 Dual-Wavelength Vernier Zooming Interferometer (China)

In 1996, Matsumoto and Minoshima[1259] (National Research Laboratory of Metrology, Japan) developed a "self-zooming" interferometer in which errors including cyclic error (typical in conventional laser interferometry)[1260] could be reduced. This first-generation device incorporated an optical-frequency doubling crystal. In this zooming interferometer, the displacement of the one stage is scaled down K times (where K is the zooming ratio) in the displacement of the second stage by feeding back the phase variation caused by the displacement of the stages. Thus

---

[1257] Masato Aketagawa, Hiroshi Honda, Masashi Ishige, Chaikool Patamaporn, "Two-dimensional encoder with picometre resolution using lattice spacing on regular crystalline surface as standard," Meas. Sci. Technol. 18(February 2007):342-349.

[1258] Patamaporn Chaikool, Masato Aketagawa, Eiki Okuyama, "A two-dimensional atom encoder using one lateral-dithered scanning tunneling microscope (STM) tip and a regular crystalline lattice," Meas. Sci. Technol. 20(2009):084006.

[1259] H. Matsumoto, K. Minoshima, "High-accuracy ultrastable moving stage using a novel self-zooming optical scale," Opt. Commun. 132(1996):417-420.

[1260] N. Bobroff, "Recent advances in displacement measuring interferometry," Meas. Sci. Technol. 4(1993):907-926. C.-M. Wu, R.D. Deslattes, "Analytical modeling of the periodic nonlinearity in heterodyne interferometry," Appl. Opt. 37(1998):6696-6700.

the motion of one stage is slaved to the motion of the other stage (but "down-geared" by K-fold) using control electronics. Noise in the interferometer, which is induced in the optical system and includes cyclic errors, is also scaled down K times in the second stage. From rough measurements on the first stage, the displacement of the second stage can be measured with a K-times higher resolution and accuracy. However, the accuracy could not be determined precisely because the original device was operated in air, and the zooming ratio K is determined by the ratio of the wavelength of the optical source to the difference in refractive indices of the air between the original wavelength and that at the doubled wavelength. (Their continuing work appears in Section 4.6.3.9.)

In 2002, Chen et al.[1261] in the Department of Precision Instruments at Tsinghua University (Beijing, China) improved on this interferometer with their dual-wavelength vernier zooming interferometer, which demonstrates a fringe subdivision method that uses a synthetic wavelength to subdivide the interference fringes formed by a single wavelength. Synthetic wavelengths have been widely used to measure the absolute distance and to extend the nonambiguity range of the measurement,[1262] with an even smaller synthetic wavelength used to measure a longer absolute distance, but in this setup a larger synthetic wavelength is employed to subdivide an interference fringe to determine a smaller nanometer displacement (unlike the conventional two-wavelength heterodyne interferometer[1263] which is based on a beat frequency and the Doppler shift). While the heterodyne interferometer cannot eliminate the nonlinear effect caused by the division of phases of sinusoidal interference signals with an equal time interval,[1264] the dual-wavelength interferometer does not have this nonlinear effect because it is required to maintain a constant phase difference between two interference signals. The dual-wavelength interferometer also has a simple optical configuration that minimizes external disturbance, eliminates the need for sophisticated electronic signal processing, and provides a high measurement resolution due to its high subdivision factor (up to 1/440,000).

[1261] Benyong Chen, Xiaohui Cheng, Dacheng Li, "Dual-wavelength interferometric technique with subnanometric resolution," Appl Opt. 41(1 October 2002):5933-5937. Yang Zhao, Xiaohui Cheng, Dacheng Li, "Dual-wavelength parallel interferometer with superhigh resolution," Opt. Lett. 27(1 April 2002):503-505.

[1262] R. Dandliker, Y. Salvade, E. Zimmermann, "Distance measurement by multiple-wavelength interferometry," J. Opt. 29(1998):105-114. V. Mahal, A. Arie, "Distance measurements using two frequency-stabilized Nd:YAG lasers," Appl. Opt. 35(1996):3010-3015. E. Gelmini, U. Minoni, F. Docchio, "Tunable, doublewavelength heterodyne detection interferometer for absolutedistance measurements," Opt. Lett. 19(1994):213-215.

[1263] R.S. Sirohi, M.P. Kothiyal, Optical Components, Systems, and Measurement Techniques, Marcel Dekker, New York, 1991, Section 4.3.4, pp. 167-170. R.C. Quenelle, L.J. Wuerz, "A new microcomputercontrolled laser dimensional measurement and analysis system," Hewlett-Packard J. 34(1983):3-13.

[1264] R.C. Quenelle, "Nonlinearity in interferometric measurements," Hewlett-Packard J. 34(1983):10. 1129. N.M. Oldham, J.A. Kramar, P.S. Hetrick, T.C. Teague, "Electronic limitations in phase meters for heterodyne interferometry," Precis. Eng. 15(1993):173-179.

In the optical configuration of the interferometer (Figure 4-75A), there are two Michelson interferometers: one is the measurement interferometer that consists of a beam splitter (BS), a reference corner cube (RCC), and a measurement corner cube (MCC); the other is the reference interferometer that consists of a BS, a RCC and a polarizing beam splitter (PBS). Beams λ_1 and λ_2 are two orthogonal linearly polarized beams emitted by a He-Ne laser. Beam λ_1 produces interference only in the reference interferometer, and beam λ_2 produces interference only in the measurement interferometer. The interference signal of the reference interferometer is detected by photodetector PD_1, giving a phase difference φ_1 for an optical path difference of length L in the reference interferometer. The interference signal of the measurement interferometer is detected by photodetector PD_2, giving a phase difference φ_2 for L_2 which is the optical path between the PBS and the MCC in the measurement interferometer.

Figure 4-75. (A) Left: Schematic of the dual-wavelength interferometer based on the fringe subdivision method: P, polarizers; PD, photodetectors; PBS, polarized beam-splitter; other abbreviations are defined in the text. (B) Right: Second displacement experiment with a step-voltage value of approximately 0.1 V (~500 pm steps) in the PZT: (a) deviations of the measurement results and (b) measurement results and their linear fit.[1265]

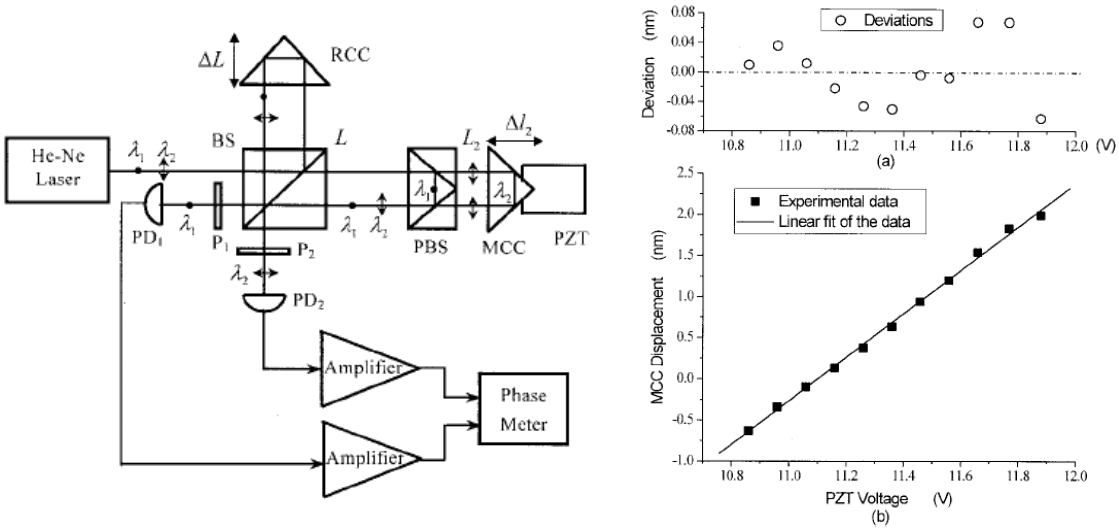

The phase difference $\Delta\varphi$ between φ_1 and φ_2 is given by $\Delta\varphi = 2\pi\,(\,(L/\lambda_S) - (L_2/\lambda_2))$, where $\lambda_S = \lambda_1\lambda_2 / |\lambda_1 - \lambda_2|$ is a synthetic wavelength. The phase difference $\Delta\varphi$ is tested by a phasemeter that uses a time interval analyzer to determine the number of clock pulses between zero crossings of the two interference signals. When the MCC is moved a nanometer displacement of Δl_2 (optical path length), the phase difference $\Delta\varphi$ becomes $\Delta\varphi'$. To keep the phase difference $\Delta\varphi$ constant (e.g., $\Delta\varphi = 0$) we can make the RCC move a displacement ΔL, that is, $L \rightarrow L + \Delta L$, whereupon $\Delta\varphi' \rightarrow \Delta\varphi$, and so $\Delta l_2 = (\lambda_2 / \lambda_S)\,\Delta L$ – and we can obtain the measured nanometer-displacement

---

[1265] Benyong Chen, Xiaohui Cheng, Dacheng Li, "Dual-wavelength interferometric technique with subnanometric resolution," Appl Opt. 41(1 October 2002):5933-5937.

Δl_2 by measurement of RCC millimeter-displacement ΔL. Because λ_2 is a nanometer-scale parameter but λ_S is a millimeter-scale parameter, the MCC-measured nanometer displacement is amplified to the scale of the RCC millimeter displacement which is much easier to determine by conventional means. The interference fringe is subdivided by the synthetic wavelength, i.e., the fringe subdivision factor is $K_{div} = \lambda_2 / \lambda_S$.

The experimental setup[1266] used an iodine absorption line-stabilizing (Zeeman-stabilized) dual-longitudinal-mode He-Ne laser with a wavelength of λ_2 = 632.8 nm, a stability of 2.5 x 10^{-8}, and a frequency difference between the two modes of $\Delta\nu$ = 1078.462255 MHz, giving a synthetic wavelength $\lambda_S = c/\Delta\nu$ = 278.17 mm with a subdivision factor of K_{div} = 1 / 439,585.97. (E.g., a 500 pm displacement of MCC would produce an easily-measured 0.21979 mm displacement of RCC.) In one experimental run, a piezoelectric transducer (PZT) with a 5 nm/volt response over a 1000 volt range was used to step the MCC through a series of linear ~500 pm (0.1 volt) displacements (Figure 4-75B); after each step, RCC was moved to restore $\Delta\varphi = 0$, and the displacement of RCC was determined by simple fringe counting in the reference interferometer circuit. The standard deviation of these measurements of the position of MCC during a 2 nm translation was a resolution of **50 pm**. Note that if, as seems likely, a compensating RCC displacement as small as $\lambda_2/2$ could be measured (equivalent to a fringe count of 1), then the resulting minimum measurable MCC displacement would be ~0.72 pm, close to the theoretical measurement uncertainty of 0.57 pm as defined by the quadrature-summed laser amplitude noise and classical detector noise limits for Michelson laser interferometry (Section 4.6.3.1).

4.6.3.9 Super-Heterodyne Zooming Interferometer (Japan)

As previously noted, in 1996 Matsumoto and Minoshima[1267] developed a "self-zooming" interferometer in which errors including cyclic error (typical in conventional laser interferometry)[1268] could be reduced. Later on, Chen et al.[1269] improved on this interferometer in their wavelength-vernier zooming interferometer, using two modes of a Zeeman-stabilized He-Ne laser as the optical source, taking advantage of the possibility of precise determination of the wavelength of the light (Section 4.6.3.8). However, the zooming ratio of this interferometer was so large that it limited the range of lengths that could be measured. A suitable zooming ratio for

---

[1266] Benyong Chen, Xiaohui Cheng, Dacheng Li, "Dual-wavelength interferometric technique with subnanometric resolution," Appl Opt. 41(1 October 2002):5933-5937.

[1267] H. Matsumoto, K. Minoshima, "High-accuracy ultrastable moving stage using a novel self-zooming optical scale," Opt. Commun. 132(1996):417-420.

[1268] N. Bobroff, "Recent advances in displacement measuring interferometry," Meas. Sci. Technol. 4(1993):907-926. C.-M. Wu, R.D. Deslattes, "Analytical modeling of the periodic nonlinearity in heterodyne interferometry," Appl. Opt. 37(1998):6696-6700.

[1269] Benyong Chen, Xiaohui Cheng, Dacheng Li, "Dual-wavelength interferometric technique with subnanometric resolution," Appl Opt. 41(1 October 2002):5933-5937. Yang Zhao, Xiaohui Cheng, Dacheng Li, "Dual-wavelength parallel interferometer with superhigh resolution," Opt. Lett. 27(1 April 2002):503-505.

practical picometer-length measurements is about 500 to 1000, if the higher resolution and smaller size of the system are taken into consideration.

In 2007-2008, Kajima and Matsumoto[1270] developed a new "super-heterodyne" zooming interferometer in which K is again based on the wavelength ratio. In their new two-color system, one wavelength is λ_1 = 633 nm which is produced by a He-Ne laser. The second wavelength is λ_2 = 400 μm, a value about 600 times larger than that of the He-Ne laser. The wavelength of 400 μm is a synthetic wavelength, λ_s, that is generated by the center wavelength (inverse beat frequency) of two external-cavity diode lasers (ECDLs) with wavelengths of, for example, $\lambda_{ECDL1} \approx 781$ nm and $\lambda_{ECDL2} \approx 780$ nm, respectively; λ_s is then equal to $1/(1/\lambda_{ECDL1} - 1/\lambda_{ECDL2})$. By using a synthetic wavelength produced by two ECDLs, the zooming ratio can be tuned between 300 and 9000 by a suitable choice of the center wavelengths of the two ECDLs. A femtosecond optical-frequency comb was used as an optical-frequency reference to control and stabilize the center wavelength of the two ECDLs. Because it is possible to choose the modes to which the ECDLs are stabilized, the synthetic wavelength can be tuned arbitrarily, and thereby the zooming ratio can be changed arbitrarily.

In the Kajima-Matsumoto device, two interferometers with different operating wavelengths were combined into one optical zooming interferometer in this experiment. Figure 4-76A is a schematic showing the design of the optical zooming interferometer. One interferometer, which operates at a wavelength λ_1, is sensitive only to the displacement of a first moveable reflector CC1. The second interferometer, which operates at a wavelength of λ_2, is sensitive only to the displacement of the second moveable reflector CC2. During zooming control, the displacement of CC1 was controlled by means of the phase difference between two interference signals. The first interferometer with wavelength λ_1 has a fixed reflector and a movable reflector CC1. When CC1 moves by distance x_1, the phase of the interference signal, as it passes through air having refractive index n_1 at wavelength λ_1 and is detected by photodiode PD_1, will change by $\delta\varphi_1 = 4\pi\, n_1 x_1/\lambda_1$. Similarly, the second interferometer with wavelength λ_2 has a fixed reflector and a movable reflector CC2. When CC2 moves a distance x_2, the phase of the interference signal that passes through air having refractive index n_2 at wavelength λ_2 and is detected by photodiode PD_2, will change by $\delta\varphi_2 = 4\pi\, n_2 x_2/\lambda_2$. These two interferometers are combined to form one super-heterodyne zooming interferometer using a zooming control system. To control the zooming interferometer, the phase difference $\Delta\varphi = \delta\varphi_1 - \delta\varphi_2$ is maintained at a value of zero by feeding back a control signal to the stage that displaces CC1. In this case, the relation between the displacement of the two movable corner reflectors, CC1 and CC2, can be expressed as $x_1 = (n_2/n_1)(\lambda_1/\lambda_2)\, x_2 = (1/K)\, x_2$, where $K\ (= n_1\lambda_2/n_2\lambda_1)$ is called the zooming ratio. The zooming ratio K depends only on the wavelengths of the optical sources (λ_1 and λ_2) and the refractive indices of air at these wavelengths (n_1 and n_2). (In a vacuum version of this device, $n_1 = n_2 = 1$ and the precision of K would then be determined by the precision with which λ_1 and λ_2 are known.) When λ_2 is much larger than λ_1, the zooming ratio become large. The movement of

---

[1270] Mariko Kajima, Hirokazu Matsumoto, "Super-heterodyne laser interferometer using femtosecond frequency comb for linear encoder calibration system," Proc. SPIE 6616(2007):66160G. M. Kajima, H. Matsumoto, "Self-zooming stable stage with sub-nm resolution using femtosecond frequency comb," 2007 Conference on Lasers and Electro-Optics (CLEO 2007), 6-11 May 2007, pp. 1-2. Mariko Kajima, Hirokazu Matsumoto, "Picometer positioning system based on a zooming interferometer using a femtosecond optical comb," Optics Express 16(4 February 2008):1497-1506.

CC1 can thus be controlled precisely by positionally manipulating CC2 in the zooming interferometer. For example, when K is 1000 and CC2 can be positioned with resolution of 10 nm, it should be possible to position CC1 with resolution of 10 pm. Since positioning a stage at a resolution of 10 nm is much easier than positioning one at a resolution of 10 pm, the zooming interferometer can realize very high resolutions much more easily than can be achieved by direct positioning.

Figure 4-76. (A) Left: Schematic of zooming interferometer – BS: beam splitter, PD: photo detector, CC: corner reflector; two interferometers with different operating wavelengths were combined into one optical zooming interferometer. (B) Right: Optical system of the zooming control system – ECDL: external-cavity diode lasers, AOM: acousto-optic modulators, CC: corner reflectors, PD: photodetectors, DS: displacement sensors used for sensing the displacement of the corner reflectors. The 100-kHz heterodyned interference signal of the He-Ne laser is detected by PD1; the 100-kHz heterodyned beat signal of the interference signals of ECDL1 and ECDL2 is detected by PD2; the phase difference between the signals detected by PD1 and PD2 is measured by a lock-in amplifier and fed back to Stage 1 to control the position of CC1 through the PID controller.[1271]

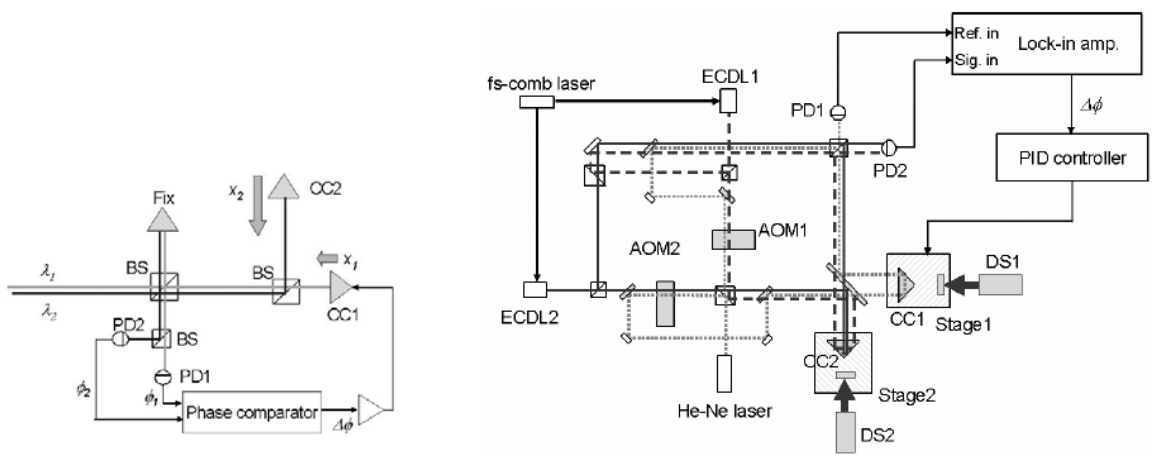

Because the difference in wavelengths between the two ECDLs was large ($\lambda_{ECDL1} - \lambda_{ECDL2} \sim 1$ nm), a special system was required for detecting the interference signal of the synthetic wavelength. Two acousto-optical modulators (AOMs) with modulation frequencies of 79.8 MHz and 79.9 MHz, respectively, were used to generate a heterodyned signal of 100 kHz on the interference signal of the synthetic wavelength (Figure 4-76B). The beam from the He-Ne laser was divided by a beam splitter into a reference path and a measurement path with a corner reflector, CC1. The reference-path beam was shifted by 79.8 MHz by AOM1, the measurement-path beam was shifted by 79.9 MHz by AOM2, and the interference signal was detected by a

---

[1271] Mariko Kajima, Hirokazu Matsumoto, "Picometer positioning system based on a zooming interferometer using a femtosecond optical comb," Optics Express 16(4 February 2008):1497-1506.

photodetector PD_1. The interference signal detected by PD_1 was a 100-kHz-heterodyned signal with a cycle of 633 nm. Laser beams from ECDL1 and ECDL2 passed through almost identical light paths. The beam of the measurement arm from ECDL1 passed through AOM1 and a corner reflector, CC2. The interference signal generated by the beam from ECDL1 had a wavelength of 781 nm, shifted by 79.8 MHz with AOM1, and was detected by photodetector PD_2. Similarly, the interference signal generated by the beam from ECDL2 had a wavelength of 780 nm, shifted by 79.9 MHz with AOM2, and was detected by photodetector PD_2. Photodetector PD_2 detected the phase change in the 100-kHz beat signal between the two interference signals of ECDL1 and ECDL2. The phase change of the beat signal between the two interference signals was equivalent to the 100-kHz heterodyned interference signal of the synthetic wavelength produced by ECDL1 and ECDL2, which had a wavelength of about 400 μm, and was related to the displacement of CC2.

The phase difference between the 100 kHz-heterodyned 633-nm-cycle interference signal from the He-Ne laser and the 100-kHz-heterodyned 400-μm-cycle beat signal produced by the synthetic wavelength between ECDL1 and ECDL2 was measured by a lock-in amplifier. The 100-kHz-heterodyned interference signal of the He-Ne laser, measured by PD_1, was used as a reference signal for the lock-in amplifier, and the interference signal of the synthetic wavelength, as measured by PD_2, was used as the input signal for the lock-in amplifier. The phase-difference signal was fed back to Stage 1 by means of a proportional-integral-derivative (PID) controller having sufficiently low electronic noise to control the zooming system by displacing CC1. A piezo-electric actuator stage (**16 μm movable range** without built-in position control) was used to displace CC1. A linear motor stage (50-mm movable range at 20-nm resolution, with position control) was used to displace CC2.

The zooming principle was first verified by showing that CC1 was displaced following a displacement of CC2 during zooming control. The displacement of CC1 was measured by means of a separate laser-interferometric displacement sensor, and the displacement of CC2 was measured by using an external laser displacement sensor. Results for a single forward-and-backward control cycle are shown in Figure 4-77A which shows that movements of CC1 followed closely those of CC2. In ten forward-and-backward control cycles, the averaged amplitude of displacement of CC2 was 400.0 μm and that of CC1 was 562.0 nm, giving a measured zooming ratio in this experiment of K = (400.0 μm) / (562.0 nm) = 711.7. As measured by a wavelength meter, the wavelengths of the He-Ne laser, ECDL1, and ECDL2 were 632.991 nm, 781.164 nm and 779.816 nm, respectively, implying a synthetic wavelength from the two ECDLs of 451.9 μm, thus giving a theoretical zooming ratio in this experiment of 713.9 which agrees with the measured zooming ratio to within 0.3%.

To verify that the zooming control system has the ability to control the position of CC1 with a sub-nm resolution, the phase difference error was measured during zooming stabilization with CC2 stopped. Figure 4-77B shows the fluctuations in phase difference during zooming control. The standard deviation of the fluctuation in phase difference was 0.030°. The displacement fluctuation of CC1 (Δx) was estimated from the phase difference $\Delta\varphi$, measured by means of the lock-in amplifier, as $\Delta x = (\Delta\varphi / 2\pi)$ (633.0 nm / 2). The standard deviation of the position control error of CC1 was calculated to be 26.3 pm, which implies that this system has a resolution of about **30 pm**.

Figure 4-77. (A) Left: Control of corner cube displacement by zooming control. Black line: displacement of CC1 in nm. Gray line: displacement of CC2 in µm. (B) Right: Position control error in CC1. left axis: Left axis: the fluctuations in phase difference during zooming control, right axis: corresponding position control error.[1272]

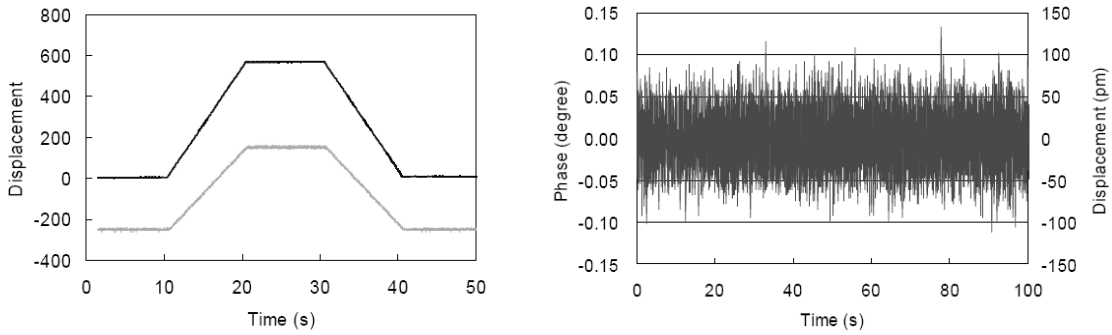

In these early experiments by Kajima and Matsumoto,[1273] the accuracy of the determination of the zooming ratio obtained by averaging ten measurements was only 0.3%. This value corresponds to a 1-nm displacement error in CC1 and is of the same level as the measurement accuracy of the external displacement sensors. In terms of linearity and accuracy, the laser-interferometric displacement sensor, which was used to measure the displacement of CC1, and the laser-displacement sensor, which was used to measure the displacement of CC2, are thought to be among the significant sources of the errors in the zooming ratio. By using more-accurate displacement sensors than those used in this experiment (for example, high-precision linear encoders*), the zooming ratio could be determined more accurately (and thus the displacement error significantly reduced). Fluctuations in the phase in the interferometer are thought to be another major source of error in the zooming ratio, along with cosine errors in the external displacement sensors and in the stages of CC1 and CC2.

Also in this experiment, because the optical system is not perfectly common-path, the zooming principle cannot completely compensate for some kinds of disturbance in the interferometer such as refractive-index variations in the air (as a result of environmental changes), thermal expansion or contraction of the optical base, or vibration of optical components. In particular, the different optical paths in the reference arms decrease the stability of the interferometer. For this reason, the stability of positioning of CC1 was not as high as the stability estimated from the zooming principle. The lack of commonality of the optical paths is also affected on the correlation in the

---

[1272] Mariko Kajima, Hirokazu Matsumoto, "Picometer positioning system based on a zooming interferometer using a femtosecond optical comb," Optics Express 16(4 February 2008):1497-1506.

[1273] Mariko Kajima, Hirokazu Matsumoto, "Super-heterodyne laser interferometer using femtosecond frequency comb for linear encoder calibration system," Proc. SPIE 6616(2007):66160G. M. Kajima, H. Matsumoto, "Self-zooming stable stage with sub-nm resolution using femtosecond frequency comb," 2007 Conference on Lasers and Electro-Optics (CLEO 2007), 6-11 May 2007, pp. 1-2. Mariko Kajima, Hirokazu Matsumoto, "Picometer positioning system based on a zooming interferometer using a femtosecond optical comb," Optics Express 16(4 February 2008):1497-1506.

behavior of phase change between two interferometers during free-run of zooming control. To produce a 5° phase fluctuation in this experiment, the temperature variation is estimated to be about 0.01 K. Since stabilizing the temperature of the interferometer as a whole to within 0.01 K is rather difficult even if active temperature control is adopted, installing the interferometer in a vacuum (as would be intended for our molecular workstation) may be an effective method for stabilizing the interferometers. The addition of a position-control system for the 400-μm wavelength interferometer might also help stabilize the interferometer.

The stability of the interferometer could be improved more than tenfold (i.e., to ~100 pm) using all of these improvements. Despite realizing 30-pm resolution by the zooming control system, the total accuracy of the current zooming system was not sufficient for calibration of high-precision linear encoders[1274]* because of insufficient stability of the interferometer during the experiments. Implementing all improvements mentioned above would be necessary to reduce noise in the interferometer sufficiently to allow it to be used as a calibration system; in that case, the resolution of the lock-in amplifier, the electrical noise in the PZT amplifier, and the shot noise of the optical sources would be the remaining obstacles to reaching the full potential of resolution and positional accuracy of this system.

4.6.3.10 Positioning Control Method (Chassagne Group, France)

Chassagne's group in France has led the design of a positioning control system with repeatable 53 pm accuracy over 1 micron of travel,[1275] a similar control system with repeatable 500 pm accuracy over 5 mm of travel,[1276] and another positioning system with repeatable nanometer accuracy over 1 mm of travel.[1277]

In a homodyne interferometer, though it is difficult to prevent periodic errors, it is theoretically possible to reduce the noise or nonlinearity of electronics to nearly zero by the precise treatment and measurement of polarization.[1278] In early work on homodyne interferometers by Chassagne's

---

[1274] A linear encoder is a sensor, transducer or readhead paired with a scale that encodes position. The sensor reads the scale in order to convert the encoded position into an analog or digital signal, which can then be decoded into position by a digital readout.

[1275] Luc Chassagne, Suat Topcu, Yasser Alayli, Patrick Juncar, "Highly accurate positioning control method for piezoelectric actuators based on phase-shifting optoelectronics," Meas. Sci. Technol. 16(2005):1771-1777.

[1276] L. Chassagne, M. Wakim, S. Xu, S. Topcu, P. Ruaux, P. Juncar, Y. Alayli, "A 2D nano-positioning system with sub-nanometric repeatability over the millimetre displacement range," Meas. Sci. Technol. 18(2007):3267-3272.

[1277] A. Sinno, P. Ruaux, L. Chassagne, S. Topçu, Y. Alayli, G. Lerondel, S. Blaize, A. Bruyant, P. Royer, "Enlarged atomic force microscopy scanning scope: Novel sample-holder device with millimeter range," Rev. Sci. Instrum. 78(2007):095107.

[1278] C.-M. Wu, C.-S. Su, "Nonlinearity in measurements of length by optical interferometry," Meas. Sci. Technol. 7(1996):62-68. S. Topcu, L. Chassagne, Y. Alayli, P. Juncar, "Improving the accuracy of

group[1279] the periodic error was not actually reduced to sub-nanometer levels experimentally, though the abstract noted that it could be:

"We demonstrate a simple homodyne Michelson interferometer design capable of fringe interpolation accuracy of one part in 36,000 leading to **a potential accuracy of 10 pm**. This improvement becomes possible thanks to the significant advances in polarimetry that permit measurement of the ellipsometric parameters ψ and Δ with an accuracy of 0.01° with readily available commercial equipment. The proposed method has been set up and we make a direct comparison with a commercial heterodyne interferometer by measuring the displacement of the same target mirror. This latter has been displaced by steps of 20 nm using a high accuracy position control method."

In heterodyne interferometry several groups achieved sub-nanometer accuracies in displacement measurement by using analyzing electronics,[1280] most notably the Chassagne group.[1281] Following their proposal in 2003,[1282] the group later in 2005[1283] developed a highly accurate positioning control method for piezoelectric actuators based on phase-shifting optoelectronics:

---

homodyne Michelson interferometers using polarization state measurement techniques," Opt. Commun. 247(March 2005):133-139.

[1279] S. Topcu, L. Chassagne, Y. Alayli, P. Juncar, "Improving the accuracy of homodyne Michelson interferometers using polarization state measurement techniques," Opt. Commun. 247(March 2005):133-139.

[1280] John Lawall, Ernest Kessler, "Michelson interferometer with 10 pm accuracy," Rev. Scient. Instrum. 71(2000):2669-2676. http://link.aip.org/link/?RSINAK/71/2669/1. Luc Chassagne, Suat Topcu, Yasser Alayli, Patrick Juncar, "Highly accurate positioning control method for piezoelectric actuators based on phase-shifting optoelectronics," Meas. Sci. Technol. 16(2005):1771-1777. L. Chassagne, M. Wakim, S. Xu, S. Topcu, P. Ruaux, P. Juncar, Y. Alayli, "A 2D nano-positioning system with sub-nanometric repeatability over the millimetre displacement range," Meas. Sci. Technol. 18(2007):3267-3272. S. Topcu, L. Chassagne, D. Haddad, Y. Alayli, P. Juncar, "Heterodyne interferometric technique for displacement control at the nanometric scale," Rev. Sci. Instrum. 74(2003):4876-4880. A. Sinno, P. Ruaux, L. Chassagne, S. Topçu, Y. Alayli, G. Lerondel, S. Blaize, A. Bruyant, P. Royer, "Enlarged atomic force microscopy scanning scope: Novel sample-holder device with millimeter range," Rev. Sci. Instrum. 78(2007):095107.

[1281] Luc Chassagne, Suat Topcu, Yasser Alayli, Patrick Juncar, "Highly accurate positioning control method for piezoelectric actuators based on phase-shifting optoelectronics," Meas. Sci. Technol. 16(2005):1771-1777. L. Chassagne, M. Wakim, S. Xu, S. Topcu, P. Ruaux, P. Juncar, Y. Alayli, "A 2D nano-positioning system with sub-nanometric repeatability over the millimetre displacement range," Meas. Sci. Technol. 18(2007):3267-3272. S. Topcu, L. Chassagne, D. Haddad, Y. Alayli, P. Juncar, "Heterodyne interferometric technique for displacement control at the nanometric scale," Rev. Sci. Instrum. 74(2003):4876-4880. A. Sinno, P. Ruaux, L. Chassagne, S. Topçu, Y. Alayli, G. Lerondel, S. Blaize, A. Bruyant, P. Royer, "Enlarged atomic force microscopy scanning scope: Novel sample-holder device with millimeter range," Rev. Sci. Instrum. 78(2007):095107.

[1282] S. Topcu, L. Chassagne, D. Haddad, Y. Alayli, P. Juncar, "Heterodyne interferometric technique for displacement control at the nanometric scale," Rev. Sci. Instrum. 74(2003):4876-4880.

[1283] Luc Chassagne, Suat Topcu, Yasser Alayli, Patrick Juncar, "Highly accurate positioning control method for piezoelectric actuators based on phase-shifting optoelectronics," Meas. Sci. Technol. 16(2005):1771-1777.

"We propose a sub-nanometric positioning control method for piezoelectric actuators based on a home-made high frequency phase shifting electronic circuit and a heterodyne interferometer. The method has been set up. Using a readily available piezoelectric actuator, we demonstrate that our method allows back and forth displacement without nonlinearities. **Repeatability of 53 pm** has been obtained over 1 µm displacement range. **Displacement steps as low as 260 pm** are presented. Such a method could be very useful for the nanotechnology and nanometrology communities for nano-scale manipulations or nano-assembly applications."

The Chassagne group developed an optoelectronic system board which controls the position of a moving mirror with sub-nanometric accuracy (Figure 4-78). The heterodyne interferometer has a heterodyne frequency of 20 MHz. The information on the position of the moving mirror is deduced by comparing the phases of the optical beams incoming and outcoming from the interferometer. A high-frequency electronic board produces two signals at the heterodyne frequency of 20 MHz. One of these signals, S_1, is sent to the laser head to combine the two synchronous signals at the heterodyne frequency. The second one, S_2, is used as a reference and is phase-compared with the phase of the signal S_3 coming from the output of the interferometer. Phase shifts can be imposed either on the S_1 signal or on the S_2 signal via computer control. The phase of the signal S_3 at the output of the heterodyne interferometer is locked-in on the phase of the signal S_2 via an analogue servo-loop. If a phase shift is imposed on the signal S_2, the servo-loop moves the mirror to compensate this phase shift using the Doppler effect. If the phase shift is made on the signal S_1, the mirror moves the other way. The hysteresis, creep, and nonlinearity phenomena of the piezoelectric actuator are irrelevant because the lock-in servo-loop extracts positional information from the phase of the interferometer. Hence it is possible to control the position of the target mirror by controlling the phase shift applied on the signals S_1 or S_2. The laser is a calibrated frequency stabilized red line helium-neon laser with a vacuum wavelength λ_0 = 632.991 528 nm with a relative uncertainty of 1.6 x 10^{-9} (1σ).

Figure 4-78. Principle of the positioning control method.[1284] A homemade electronic circuit puts out two synchronous signals both at a frequency of 20 MHz. A voltage controlled oscillator (VCO) in the laser head generates the heterodyne components of the laser source. This VCO is synchronized with the signal S_2 using the phase-locked loop (PLL) system. The other signal (S_1) is sent to a mixer to be phase-compared with the signal S_3 coming from the output of the interferometer.

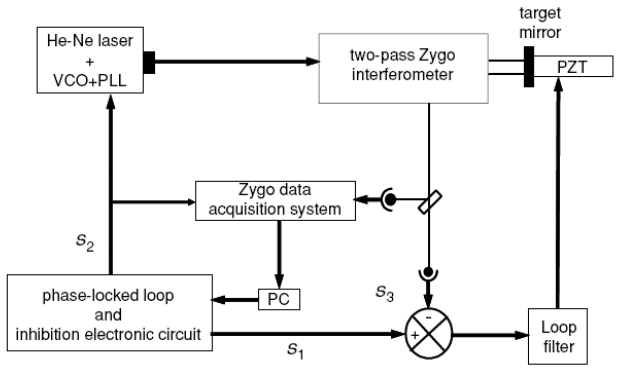

[1284] Luc Chassagne, Suat Topcu, Yasser Alayli, Patrick Juncar, "Highly accurate positioning control method for piezoelectric actuators based on phase-shifting optoelectronics," Meas. Sci. Technol. 16(2005):1771-1777.

In classical AFM controllers, intrinsic nonlinearity defects of the PZT-driven scanner are software controlled, usually using the inverse hysteresis model according to the equation $\mathbf{V(x) = x^{-1} (V_0, x_0)}$ in order to calculate the desired control voltage V to apply to the PZT actuators to attain a position x as a function of the actual state (voltage V_0 and position x_0) of the actuator. This method presents two major drawbacks. First, this equation uses linearization coefficients that were defined under specific environmental conditions and then implemented on the AFM controller board. These coefficients and model will cease to be valid if conditions change, causing the the PZT behavior to change. PZT actuators also age with time and behave differently at each stable operating temperature, making the AFM displacements inaccurate unless real time calibration is used. In the positioning control method, the PZT tries to keep track of the desired trajectory by locking the phase of the measured signal on the phase of the reference signal. This means that the PZT will contract/retract by the necessary distance until the phase difference nulls, whatever the actual state of the PZT is and whatever the operating temperature at which the system has stabilized. Hysteresis, creep, and temporal instabilities of the PZT are thus eliminated, greatly enhancing the repeatability of the displacement measurements. Second, the hyteresis equation is usually software implemented in the AFM controller and usually incorporates a lot of coefficients and thus needs complex computation, especially when complex algorithms are used to better track the linear model and reducing the bandwidth of the control loop. In the positioning control method, nonlinearity rectification is hardware implemented based on the phase locking principle and depends on the robustness of the analog servo loop controller that is implemented.

The phase locked electronic board is composed of an ultrahigh stability oscillator at a frequency of 10 MHz. A phase locked loop (PLL) generates the two signals at the frequency of 20 MHz. A phase shifting electronic (PSE) circuit can impose some phase shift of $\Delta\varphi_1 = 2\pi/p$ or $\Delta\varphi_2 = 2\pi/q$ on these signals. The factors p or q are digitally programmable with the PC (computer) link. For a two-pass interferometer, a phase change of 2π corresponds to a movement of $\lambda_0/4n$ where λ_0 is the wavelength under vacuum of the laser source and n the refractive index of the air. The displacement corresponding to a phase shift of $\Delta\varphi$ is $\mathbf{\Delta d = \lambda_0\, \Delta\varphi\, /\, 8\, \pi\, n}$. Phase shifts are controlled with command pulses via a digital pulse generator. As the phase shift is generated numerically, the uncertainty in the position steps is mainly limited by the uncertainty in the laser wavelength. Experimental results (see below) have demonstrated a position **step size as small as 259 pm** and repeatability below 1 nm for **micron-range displacements**.

Choosing the values of p and q judiciously, the resulting phase-shift can be very small. For example, with p = 36 and q = 34, $\Delta\varphi = 2\pi/612 = 10.3$ mrad resulting in a minimal step value equal to 258 pm hence giving the possibility for quasi-continuous displacements. (It is important to remember that such a level of accuracy can be reached only if the surrounding environment is controlled, since temperature changes and vibrations will cause changes in position at the nanometre level.)

During the experiment, phase-shifts $\Delta\varphi_1$ and $\Delta\varphi_2$ are generated respectively in S_1 and S_2. As the servo-loop is closed, the target mirror moves until the difference of the phase between S_1 and S_3 becomes null thanks to the Doppler shift as seen previously. The corresponding displacement of the mirror is calculated as: $\mathbf{\Delta x = (\lambda_0/4n)\, (q - p)\, /\, (q\, p)}$. Several values for p and q have been tested. In each case, the phase-shifts are generated at a frequency of 2 Hz (one step every 0.5 sec), producing the experimental results shown in Figure 4-79. In the first case (Figure 4-79a),

the phase-shifts are made only in S_1 and p = 32 which leads to $\Delta\varphi_1 = 2\pi/32$ and $\Delta\varphi_2 = 0$. Taking n = 1, the corresponding theoretical step size is equal to $\Delta x_1 = 4.945$ nm. In the second case (Figure 4-79b), p = 32 and q = 36 which leads to $\Delta\varphi = 2\pi/288$. The corresponding theoretical displacement of the target mirror is then equal to $\Delta x_2 = 549$ pm.

Figure 4-79. Experimental results.[1285] According to the values of p and q, different steps of the piezoelectric actuator are realized: (a) p = 32, q = 0, Δx_1 = 4.945 nm; (b) p = 32, q = 36, Δx_2 = 549 pm; (c) p = 34, q = 36, Δx_3 = 259 pm.

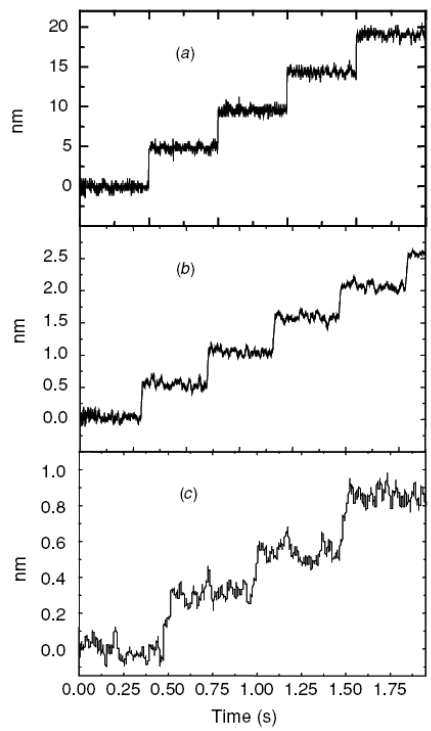

In the last case (Figure 4-79c), p = 34 and q = 36 leading to $\Delta\varphi = 2\pi/612$ and $\Delta x_3 = 259$ pm, with the parameters of the loop filter adjusted to minimize overshooting. The rise time for each step is ~5 ms, but this could be reduced to <1 ms by changing the parameters of the proportional integral derivative (PID) filter in principle allowing up to a ~1 kHz stepping rate.[1286] The sampling

---

[1285] Luc Chassagne, Suat Topcu, Yasser Alayli, Patrick Juncar, "Highly accurate positioning control method for piezoelectric actuators based on phase-shifting optoelectronics," Meas. Sci. Technol. 16(2005):1771-1777.

[1286] Higher velocity displacements are feasible with this method. The velocity of the target mirror is linked to the frequency of the phase-shifts f_c by $V = f_c\,\Delta x$. For a velocity higher than V = 1 mm/sec, one needs an inhibition rate up to tens of kilohertz. The authors verified that only one phase-shift occurs for each pulse of the command inhibition signal using a specific test bench that was developed. The phase-shifts are generated at a frequency f_c on the S_1 signal. This is measured over few hours with a frequency counter. All

frequency is equal to 10 kHz (limited by the data acquisition rate of the measurement software) and each point of the results depicted in Figure 2 has been averaged over 1 ms. Furthermore, as the step levels Δx_2 and Δx_3 are near to the residual noise level of our system (σ = 220 pm), a first order Savitsky-Golay filter was used to obtain Figure 4-79b and Figure 4-79c.

Note that this servo-control system does not allow direct measurement of absolute displacement in meters – all distances are measured in shift-counts (= K). To assess the repeatability of this method, the inhibition control was programmed to generate exactly K phase-shifts generating a precise displacement of the target mirror from zero to x_B. The repeatability is given by the standard deviation of the set of values of $x_B = K\ \Delta x$ (= the theoretical displacement). Figure 4-80 shows the results of 13 independent runs of K = 4896 steps (using p = 34, q = 36). The theoretical displacement in air is equal to 1265.666 nm (taking $n - 1 = 2.50 \times 10^{-4}$). (In UHV, n = 1 exactly and the experimental displacement should then exactly match the theoretical.) The experimental mean value of x_B = 1265.660 nm over 13 measurements with a standard deviation of 53 pm. This shows that the theoretical and experimental mean values of the displacement are in good agreement, and that this positioning control method provides a repeatability at the sub-nanometric level over a micrometric travel range.

Figure 4-80. Repeatability of the method:[1287] 4896 (=K) -step phase-shifts were programmed to generate thirteen independent displacements of the target mirror from zero to x_B. The repeatability is given by the standard deviation of the set of values of x_B, which is ~53 pm. The straight line represents the mean value.

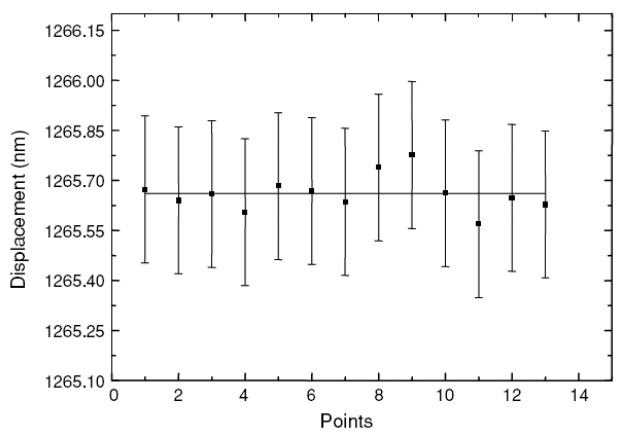

---

the systems are synchronized using the ultrastable frequency quartz oscillator of the counter ($\sigma_y < 5 \times 10^{-10}$ for 1-1000 sec). The signal S_1 is phase-shifted with steps of $2\pi/32$ so its frequency is equal to f_{S1} = 20 MHz $- f_c/32$. For example, if f_c = 32 000 Hz, the frequency of S_1 is exactly equal to 19.999 000 MHz (the frequency counter can be configured with ten significant digits), and the authors have verified for a large range of f_c (up to 10 MHz) that there are strictly no missing or additional phase-shifts. The same verification has been done for the signal S_2.

[1287] Luc Chassagne, Suat Topcu, Yasser Alayli, Patrick Juncar, "Highly accurate positioning control method for piezoelectric actuators based on phase-shifting optoelectronics," Meas. Sci. Technol. 16(2005):1771-1777.

Repeatability of the motions could be limited by the hysteresis of the actuator. The authors measured the hysteresis level of the piezoelectric actuator in the open mode (Figure 4-81A) and in the closed mode (Figure 4-81B). In the open mode, the applied voltage is changed and the response of the actuator is measured by the Michelson interferometer, which produces an observed 8% of nonlinearity over a displacement of 2 μm. In the closed mode, the displacement is controlled by to the electronic servo-loop (p = 32, q = 0, f_c = 1800 Hz*)* and back and forth displacements are imposed on the actuator, verifying that actually hysteresis becomes negligible in the closed mode.

Figure 4-81. (A) Hysteresis is observed when the piezoelectric actuator is used in the open mode. (B) Hysteresis is not observed when the piezoelectric actuator is used in the closed mode; the center of the curve has been zoomed over 200 nm.[1288]

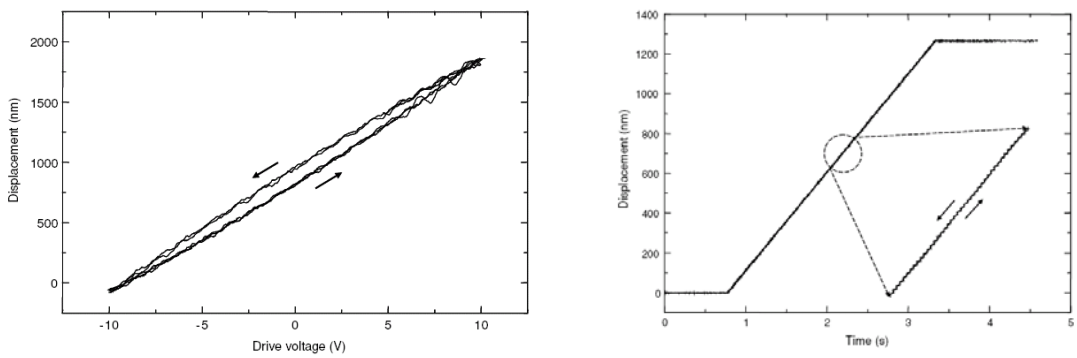

(A) **(B)**

In their second 2007 work,[1289] the Chassagne group extended their positioning control method to two dimensions and extended the range of displacement at the cost of a modest reduction in repeatable accuracy:

"We propose a 2D displacement control system (Figure 4-82) with sub-nanometric repeatability on position over the millimetre travel range on both axes. It could be useful for nanofabrication processes or other applications related to the nanotechnology community. In our case, the apparatus is planned to be used in atomic force microscopes and lithography systems as a sample-holding device. The method is based on a heterodyne interferometric sensor and a home-made high frequency phase-shifting electronic board. This paper presents the complete mechanical system and gives experimental results showing a **repeatability of 500 pm over a moving range of 5 mm**."

[1288] Luc Chassagne, Suat Topcu, Yasser Alayli, Patrick Juncar, "Highly accurate positioning control method for piezoelectric actuators based on phase-shifting optoelectronics," Meas. Sci. Technol. 16(2005):1771-1777.

[1289] L. Chassagne, M. Wakim, S. Xu, S. Topcu, P. Ruaux, P. Juncar, Y. Alayli, "A 2D nano-positioning system with sub-nanometric repeatability over the millimetre displacement range," Meas. Sci. Technol. 18(2007):3267-3272.

As illustrated in Figure 4-82A, the group developed a two-axis XY moving system associated with dual servo-control. The first stage is composed of two linear motors $ST1_X$ and $ST1_Y$ which can move over 50 mm with their own lock-in system based on a proportional integral derivative (PID) unit. Their resolutions are 10 nm, limited by the encoder used in the servo loop. The flatness and the straightness are below 1 µm over a range of 50 mm and below 500 nm over a 5 mm range; pitch, yaw and roll are negligible regarding straightness over the 5 mm range. The second level stage ST2 is composed of 2D piezoelectric actuators PZT_{XY} with displacement range of 15 µm and sub-nanometric resolution, chosen for its high cut-off frequency (2.5 kHz on both axes).

Figure 4-82. (A) 3D overview of the system. (X_m; Y_m) are the displacement axes of the long-range stages; (X_p; Y_p) are the axes of the piezoelectric actuators; (X_o; Y_o) are the axes of the mirror cube. The angles α and β are respectively the misalignment angles between (X_m; Y_m) and (X_o; Y_o) and between (X_m; Y_m) and (X_p; Y_p). (B) Repeatability for long-range displacements. A sequence of 20 back and forth displacements of 5 mm is launched. The straight line represents the mean value and the dotted lines the standard deviation which is equal to ~500 pm.[1290]

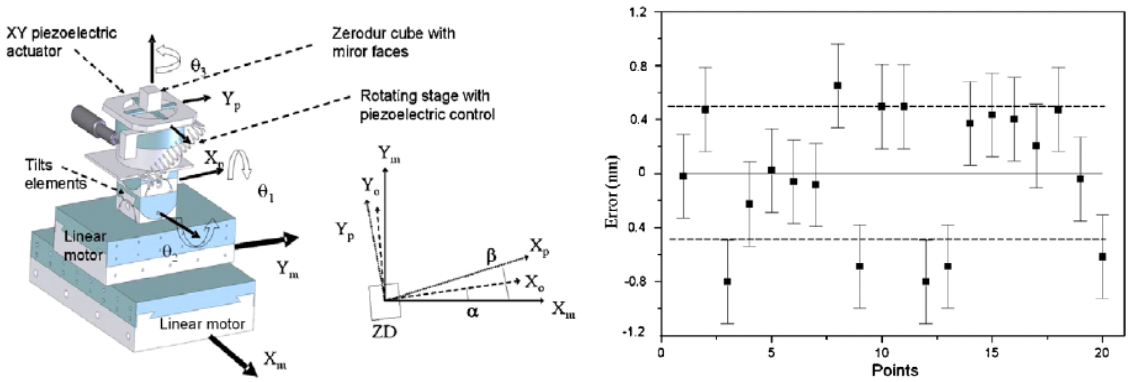

(A) **(B)**

The target mirrors are two orthogonal faces of a Zerodur cube with a 20 mm edge. The defect of orthogonality between both faces is less than 1 arcsec. This cube is adjusted with respect to the piezoelectric actuators using a rotating element and the whole system is assembled onto the ST1 unit. The orthogonality between the two translation axes of the motors is controlled by an interferometric technique with an accuracy of 5 arcsec. The two heterodyne interferometers measure the position of the mirrors with a resolution of 310 pm. The repeatability was measured over long-range motions, with the control system programmed to make 5 mm back-and-forth

---

[1290] L. Chassagne, M. Wakim, S. Xu, S. Topcu, P. Ruaux, P. Juncar, Y. Alayli, "A 2D nano-positioning system with sub-nanometric repeatability over the millimetre displacement range," Meas. Sci. Technol. 18(2007):3267-3272.

displacements along the X axis at a 1 mm/sec velocity using ST2 step positions with 250 pm resolution. For 20 independent displacements, the repeatability of these displacements (the standard deviation of the positioning error $x_A - x_A'$, where x_A is the starting position and xA' is the position after the back-and-forth displacement) was ~500 pm (Figure 4-82B).

4.6.3.11 Laser Doppler Displacement Meter (Argonne Natl. Lab)

Since 1998 a prototype laser Doppler linear encoder (LDLE) with multiple reflections has been under development at Argonne.[1291] With a customized commercial Laser Doppler Displacement Meter (LDDM),[1292] this novel linear encoder has achieved sub-Angstrom sensitivity in a 300 mm measuring range. The LDDM is based on the principles of radar, the Doppler effect, and optical heterodyning. A commercial Laser Doppler Displacement Meter (LDDM) system includes four components: a laser head, a processor module, a display module, and a target reflector. The laser head houses a frequency-stabilized He-Ne laser, an electro-optic assembly, and a photodetector, which functions as a receiver. The laser light reflected by the target is frequency shifted by the motion of the target. The photodetector measures the phase variation caused by the frequency shift, which corresponds to the displacement of the target.[1293]

[1291] D. Shu, E.E. Alp, J. Barraza, T.M. Kuzay, T. Mooney, "A Novel Laser Doppler Linear Encoder Using Multiple-Reflection Optical Design for High Resolution Linear Actuator," Proc. SPIE 3429(1998):284-292. D. Shu, "Optical design for laser encoder resolution extension and angular measurement," U.S. Patent No. 5,896,200 (1999). D. Shu, J. Maser, B. Lai, Y. Han, S. Vogt, T.S. Toellner, E.E. Alp, "Linear Stage System with Subnanometer Resolution and Centimeters Travel Range," ASPE Spring 2004 meeting; http://www.aspe.net/publications/Spring_2004/04SP%20Extended%20Abstracts/1402-Shu.PDF. D. Shu, J. Maser, B. Lai, S. Vogt, M. Holt, C. Preissner, A. Smolyanitskiy, R. Winarski, G.B. Stephenson, "High Precision Positioning Mechanisms for a Hard X-ray Nanoprobe Instrument," MEDSI Spring 2006 Conference; http://medsi2006.spring8.or.jp/program/021.Shu.a.pdf. D. Shu, J. Maser, "Design and Test of a 2-D Precision Weak-link Stage System with Sub-centimeter Travel Range and Sub-nanometer Resolution," Abstract 2712, 2008 Annual Meeting, American Society for Precision Engineering (http://www.aspe.net/meetings/2008_Annual/Oral_Presentations_2008.html), http://www.aspe.net/aspe_member/php/abstracts/absdisplay.php?Abstract_ID=2712. Deming Shu, "Nanopositioning Systems for X-ray Optical Instrumentation," MEDSI/SRI-2008 Workshop for Challenges in Beamline Optics, 10 June 2008; http://www.google.com/url?sa=t&source=web&ct=res&cd=4&url=http%3A%2F%2Fwww.lightsource.ca%2Fmedsi-sri2008%2Fpdf%2FPPT-Nanopositioning_systems_for_X-ray_optical_instrumentation.pdf&ei=Z-23ScqQNYnOtQOC5uDmAQ&usg=AFQjCNGPm27WUtHOd5prHqH8KNeB5ZKGFw&sig2=-84jq7gj1o8Idxt8r55VSQ. "Optomechanical structure for a multifunctional hard x-ray nanoprobe instrument," U.S. Patent No. 7331714, 19 February 2008; http://www.patents.com/Optomechanical-structure-a-multifunctional-hard-x-ray-nanoprobe-instrument/US7331714/en-US/. Curt Preissner, Soon Hong Lee, "Research and Development for a New Paradigm in Nanopositioning and Focusing Mechanics," APS Strategic Planning Proposal, 28 March 2008; http://www.aps.anl.gov/Renewal/RD/APS_1270057.pdf.

[1292] LDDM is a trademark of the Optodyne Inc., 1180 Mahalo Place, Compton, CA 90220, U.S.A.

[1293] Deming Shu, "Nanopositioning Systems for X-ray Optical Instrumentation," MEDSI/SRI-2008 Workshop for Challenges in Beamline Optics, 10 June 2008; http://www.google.com/url?sa=t&source=web&ct=res&cd=4&url=http%3A%2F%2Fwww.lightsource.ca

In the self-aligning multiple-reflection optical design for the LDDM system, the heterodyning detector is housed coaxially inside the frequency-stabilized laser source. Instead of a typical single reflection on the moving target, the laser beam is reflected back and forth twelve times between the fixed base and the moving target as shown in Figure 4-83A. The laser beam, which is reflected back to the heterodyning detector, is frequency-shifted by the movement of the moving target relative to the fixed base. With the same LDDM laser source and detector electronics, this optical path provides twelve times greater resolution for the linear displacement measurement and encoding. Figure 4-83B shows a photograph of the one-dimensional laser Doppler linear actuator (LDLA) system for an atomic force microscope. In this coarse/fine closed-loop control setup, a PZT (piezo-actuator)-driven motion-reduction mechanism was mounted on the top of a DC-motor-driven stage to drive the motion object (for this example, a sample holder for atomic force microscope). A laser Doppler displacement meter with an optical resolution extension assembly is used to measure the sample holder motion in a 25 mm range with sub-Angstrom resolution. The LDDM position signal is fed back through a system-control computer to control the PZT. The PZT drives the motion-reduction mechanism with sub-Angstrom resolution to stabilize the motion. The system control computer also synchronizes the stage position and PZT feedback lock-in point with the LDDM position signal.

Figure 4-83. (A) Left: Schematic of the the self-aligning multiple-reflection optical design; with same LDDM laser source and detector electronics, this optical path provides twelve times greater resolution for the linear displacement measurement and encoding. (B) Right: Photograph of the one-dimensional laser Doppler linear actuator system for an atomic force microscope.[1294]

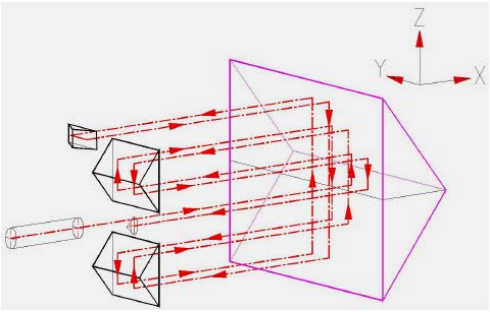

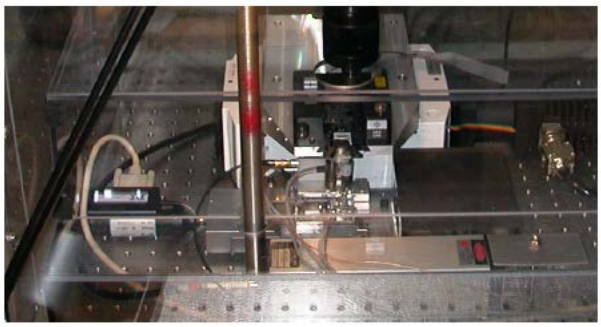

%2Fmedsi-sri2008%2Fpdf%2FPPT-Nanopositioning_systems_for_X-ray_optical_instrumentation.pdf&ei=Z-23ScqQNYnOtQOC5uDmAQ&usg=AFQjCNGPm27WUtHOd5prHqH8KNeB5ZKGFw&sig2=-84jq7gj1o8Idxt8r55VSQ.

[1294] D. Shu, J. Maser, B. Lai, Y. Han, S. Vogt, T.S. Toellner, E.E. Alp, "Linear Stage System with Subnanometer Resolution and Centimeters Travel Range," ASPE Spring 2004 meeting; http://www.aspe.net/publications/Spring_2004/04SP%20Extended%20Abstracts/1402-Shu.PDF.

Shu et al.[1295] have measured the closed-loop control resolution for a one-dimensional laser Doppler linear actuator system, demonstrating a series of 300 pm steps (Figure 4-84A) in 2004,[1296] 100 pm steps (Figure 4-84A, Figure 4-84B) in 2004[1297] and 2008,[1298] and 80 pm steps (Figure 4-84B) in 2008[1299] over a 25 mm travel range in one dimension of travel. Figure 4-84C shows a test of the closed-loop feedback system (closed loop at left and right, open loop in center), revealing a motion stage driving sensitivity better than 30 pm (see insert) using a weak-link linear-motion-reduction mechanism over a 1-micron travel range.[1300]

[1295] D. Shu, J. Maser, B. Lai, Y. Han, S. Vogt, T.S. Toellner, E.E. Alp, "Linear Stage System with Subnanometer Resolution and Centimeters Travel Range," ASPE Spring 2004 meeting; http://www.aspe.net/publications/Spring_2004/04SP%20Extended%20Abstracts/1402-Shu.PDF. Deming Shu, "Nanopositioning Systems for X-ray Optical Instrumentation," MEDSI/SRI-2008 Workshop for Challenges in Beamline Optics, 10 June 2008; http://www.google.com/url?sa=t&source=web&ct=res&cd=4&url=http%3A%2F%2Fwww.lightsource.ca%2Fmedsi-sri2008%2Fpdf%2FPPT-Nanopositioning_systems_for_X-ray_optical_instrumentation.pdf&ei=Z-23ScqQNYnOtQOC5uDmAQ&usg=AFQjCNGPm27WUtHOd5prHqH8KNeB5ZKGFw&sig2=-84jq7gj1o8Idxt8r55VSQ.

[1296] D. Shu, J. Maser, B. Lai, Y. Han, S. Vogt, T.S. Toellner, E.E. Alp, "Linear Stage System with Subnanometer Resolution and Centimeters Travel Range," ASPE Spring 2004 meeting; http://www.aspe.net/publications/Spring_2004/04SP%20Extended%20Abstracts/1402-Shu.PDF.

[1297] D. Shu, J. Maser, B. Lai, Y. Han, S. Vogt, T.S. Toellner, E.E. Alp, "Linear Stage System with Subnanometer Resolution and Centimeters Travel Range," ASPE Spring 2004 meeting; http://www.aspe.net/publications/Spring_2004/04SP%20Extended%20Abstracts/1402-Shu.PDF.

[1298] Deming Shu, "Nanopositioning Systems for X-ray Optical Instrumentation," MEDSI/SRI-2008 Workshop for Challenges in Beamline Optics, 10 June 2008; http://www.google.com/url?sa=t&source=web&ct=res&cd=4&url=http%3A%2F%2Fwww.lightsource.ca%2Fmedsi-sri2008%2Fpdf%2FPPT-Nanopositioning_systems_for_X-ray_optical_instrumentation.pdf&ei=Z-23ScqQNYnOtQOC5uDmAQ&usg=AFQjCNGPm27WUtHOd5prHqH8KNeB5ZKGFw&sig2=-84jq7gj1o8Idxt8r55VSQ.

[1299] Deming Shu, "Nanopositioning Systems for X-ray Optical Instrumentation," MEDSI/SRI-2008 Workshop for Challenges in Beamline Optics, 10 June 2008; http://www.google.com/url?sa=t&source=web&ct=res&cd=4&url=http%3A%2F%2Fwww.lightsource.ca%2Fmedsi-sri2008%2Fpdf%2FPPT-Nanopositioning_systems_for_X-ray_optical_instrumentation.pdf&ei=Z-23ScqQNYnOtQOC5uDmAQ&usg=AFQjCNGPm27WUtHOd5prHqH8KNeB5ZKGFw&sig2=-84jq7gj1o8Idxt8r55VSQ.

[1300] Deming Shu, "Nanopositioning Systems for X-ray Optical Instrumentation," MEDSI/SRI-2008 Workshop for Challenges in Beamline Optics, 10 June 2008; http://www.google.com/url?sa=t&source=web&ct=res&cd=4&url=http%3A%2F%2Fwww.lightsource.ca%2Fmedsi-sri2008%2Fpdf%2FPPT-Nanopositioning_systems_for_X-ray_optical_instrumentation.pdf&ei=Z-23ScqQNYnOtQOC5uDmAQ&usg=AFQjCNGPm27WUtHOd5prHqH8KNeB5ZKGFw&sig2=-84jq7gj1o8Idxt8r55VSQ.

Figure 4-84. (A) Top: 2004 resolution test of the one-dimensional laser Doppler linear actuator closed-loop control system, showing a series of 300 pm (left side) and 100 pm (right side) steps. (B) Middle: 2008 resolution test of the one-dimensional laser Doppler linear actuator closed-loop control system, showing a series of 100 pm (left side) and 80 pm (right side) steps. (C) Bottom: Test of closed-loop feedback system (closed loop at left and right, open loop in center), showing motion stage driving sensitivity better than 30 pm (see insert).

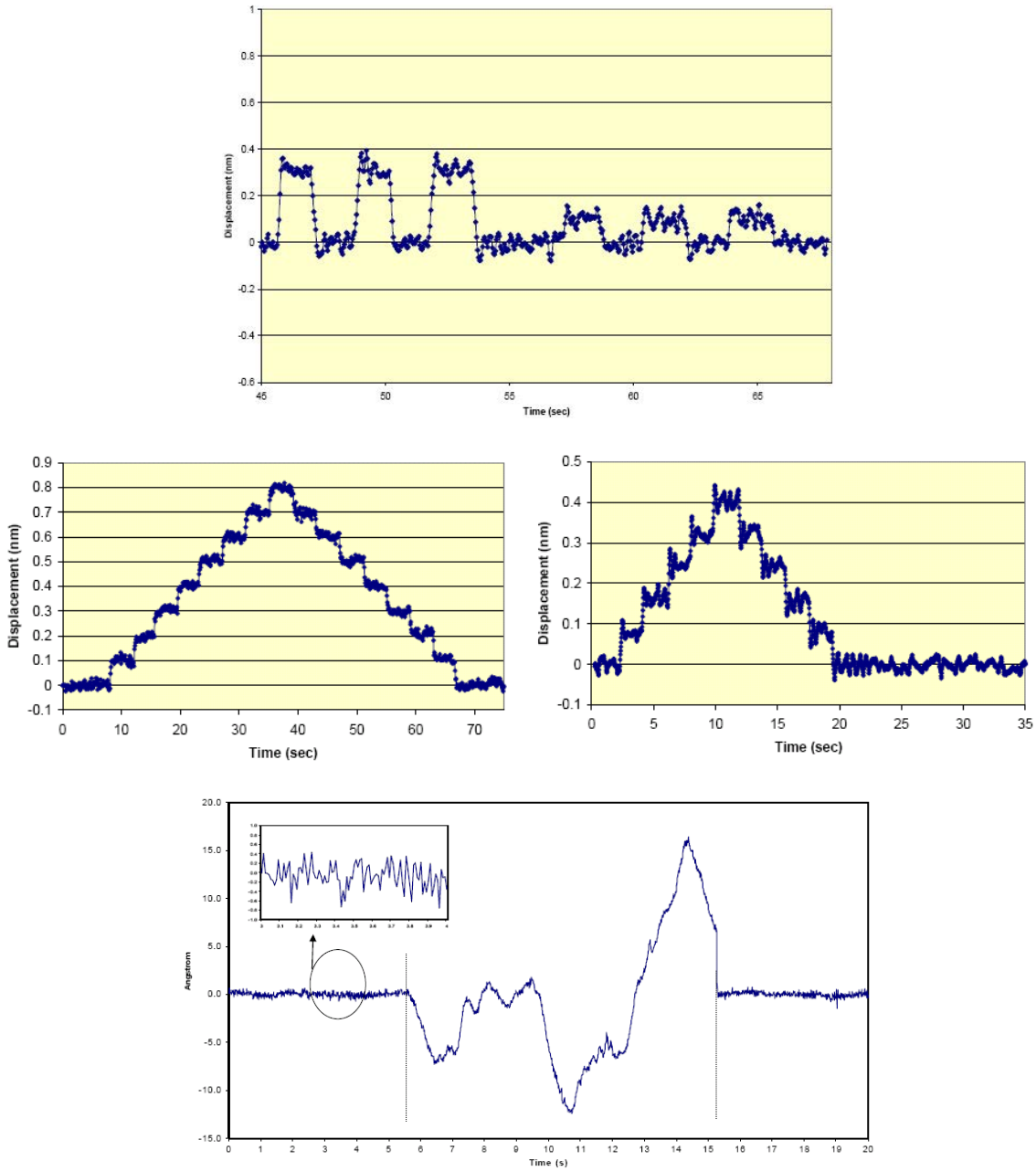

According to researchers,[1301] while the Laser Doppler Displacement Meter (LDDM) is the state-of-the-art for x-ray nanopositioning, the Polytec Laser Doppler Vibrometer (LDV) may offer lower noise and a simpler optic path as compared to the LDDM. "We see the potential for improvement through the use of a LDV to replace the LDDM. The LDV has sub-picometer resolution and according to the manufacturer, the LDV doesn't require multiple passes or multiple prisms to achieve this result. The single path and simple retroreflector free up space and mass on the target stage. We are also considering the use of the LDV for a relatively long range measurement and capacitive sensors for measurement over a small range and then employing a relay sensing mechanism."

4.6.3.12 Heterodyne Displacement Measuring Interferometer (Univ. Florida)

During 2000-2009, Schmitz, Beckwith and Kim[1302] in the Machine Tool Research Center (MTRC) at the University of Florida have constructed, tested, verified and patented a new heterodyne Michelson-type displacement measuring interferometer that minimizes periodic error and thus virtually eliminates the current accuracy limitation imposed by periodic error, which appears as a cyclical oscillation of the measured displacement about the true value during motion. In the new design, the two (heterodyne) frequencies are generated and spatially separated using acousto-optic modulators (AOMs) as a beamsplitter/recombiner and is generally polarization independent. The periodic error is eliminated by removing the potential for overlap and frequency mixing within the interferometer. The new concept replaces the traditional method of "polarization coding" wherein the two optical frequencies are initially coincident with orthogonal polarization states and then separated using polarization-dependent optics.[1303]

In the new setup (Figure 4-85), a single frequency, stabilized He-Ne laser is used as the light source rather than the two frequency source used in polarization dependent configurations. The

---

[1301] Curt Preissner, Soon Hong Lee, "Research and Development for a New Paradigm in Nanopositioning and Focusing Mechanics," APS Strategic Planning Proposal, 28 March 2008; http://www.aps.anl.gov/Renewal/RD/APS_1270057.pdf.

[1302] H.S. Kim, T. Schmitz, "A New Heterodyne Interferometer with Zero Periodic Error and Tunable Beat Frequency," Abstract 2576, Proceedings of American Society for Precision Engineering Annual Meeting, 19-24 October 2008, Portland, OR; http://www.aspe.net/aspe_member/php/abstracts/absdisplay.php?Abstract_ID=2576. H.S. Kim, T. Schmitz, J. Beckwith, "Chapter 20: Periodic Error in Heterodyne Interferometry: Examination and Elimination," in D. Halsey, W. Raynor, eds., Interferometers: Research, Technology and Applications, Vol. 1, Nova Science Publishers, Inc., Hauppauge, NY, 2009. Tony L. Schmitz, John F. Beckwith, "Heterodyne interferometer with angstrom-level periodic nonlinearity," U.S. Patent No. 6847455, 25 January 2005; http://www.patentstorm.us/patents/6847455/description.html.

[1303] H.S. Kim, T. Schmitz, "A New Heterodyne Interferometer with Zero Periodic Error and Tunable Beat Frequency," Abstract 2576, Proceedings of American Society for Precision Engineering Annual Meeting, 19-24 October 2008, Portland, OR; http://www.aspe.net/aspe_member/php/abstracts/absdisplay.php?Abstract_ID=2576.

collimated He-Ne beam passes through the first acousto-optic modulator (AOM1), oriented at the Bragg angle. This yields two beams at the AOM1 exit: 0th order and 1st order (diffracted). The 1st order beam is directed toward the fixed retroreflector for the measurement signal and one of the two (fixed) retroreflectors for the reference signal, while the 0th order beam continues toward the second acousto-optic modulator (AOM2), again oriented at the Bragg angle but with a different driving frequency than AOM1. The 1st order (diffracted) beam from AOM2 is directed toward the moving target retroreflector and the second retroreflector for the reference signal. Both the 1st order beams from AOM1 and AOM2 are retroreflected and recombined at AOM1 (i.e., it functions as a beamsplitter). The reference and measurement signal beat frequencies are detected using two photodetectors with fiber optic pickups. Because the frequency difference between AOM1 and AOM2 is user selected, the beat frequency is adjustable.[1304]

Figure 4-85. Heterodyne Displacement Measuring Interferometry. Two frequency laser heads and accompanying phase measurement boards are available; various beam splitters, retroreflectors, multimode fiber optics, and prisms are also available for use.[1305]

Displacement data (determined from traditional phase measurement hardware) and spectral content (collected using an analog spectrum analyzer) were analyzed to verify zero periodic error, and compared to data collected using a traditional polarization-coded heterodyne interferometer with small variations in the optical alignment to demonstrate different levels of first and second

---

[1304] H.S. Kim, T. Schmitz, "A New Heterodyne Interferometer with Zero Periodic Error and Tunable Beat Frequency," Abstract 2576, Proceedings of American Society for Precision Engineering Annual Meeting, 19-24 October 2008, Portland, OR; http://www.aspe.net/aspe_member/php/abstracts/absdisplay.php?Abstract_ID=2576.

[1305] http://mtrc.mae.ufl.edu/facilities.php.

order periodic error.[1306] Assuming standard uncertainties of 6 x 10^{-6} nm in laser wavelength (0.01 ppm) and 0.5 dB in amplitude, the combined standard uncertainty in the periodic error measurement result would be **10 pm**.[1307] This value reflects the uncertainty in the periodic error computed from the spectrum analyzer signal alone; additional signal corruption, which can be imposed by the phase-measuring electronics, for example, may still occur and is generally highly system dependent.

A proof-of-concept device[1308] verified the possibility of using an AOM as a polarization-independent interferometer. An interference signal demonstrated 48.8 dB attenuation between the measurement signal and first-order periodic error on a bench-top setup (Figure 4-85) with no external technique for reducing the system nonlinearity and a mechanical slide for motion generation (i.e., typical experimental setups use a vacuum cell, for example). The AOM DMI, however, did exhibit a first-order phase error, attributed to bi-directional acoustic interactions within the AOM, with a resulting periodic error of **180 pm**.

The patent filing[1309] recites several benefits, aside from the decreased periodic error. First, with respect to the required equipment, a single frequency laser light source is used rather than a more complex and expensive two-frequency laser head, fewer optical components are required, and only one photoreceiver per multiple axis system is necessary. The latter can be accomplished utilizing different AOM driving frequencies in each axis. Second, single mode fiber feed to each axis allows easy setup and alignment of a miniaturized package. Third, fiber launching of the light is generally simplified because polarization-maintaining fiber is not necessary for the polarization-independent interferometer.

[1306] H.S. Kim, T. Schmitz, "A New Heterodyne Interferometer with Zero Periodic Error and Tunable Beat Frequency," Abstract 2576, Proceedings of American Society for Precision Engineering Annual Meeting, 19-24 October 2008, Portland, OR; http://www.aspe.net/aspe_member/php/abstracts/absdisplay.php?Abstract_ID=2576.

[1307] Tony L. Schmitz, John F. Beckwith, "Heterodyne interferometer with angstrom-level periodic nonlinearity," U.S. Patent No. 6847455, 25 January 2005; http://www.patentstorm.us/patents/6847455/description.html.

[1308] Tony L. Schmitz, John F. Beckwith, "Heterodyne interferometer with angstrom-level periodic nonlinearity," U.S. Patent No. 6847455, 25 January 2005; http://www.patentstorm.us/patents/6847455/description.html.

[1309] Tony L. Schmitz, John F. Beckwith, "Heterodyne interferometer with angstrom-level periodic nonlinearity," U.S. Patent No. 6847455, 25 January 2005; http://www.patentstorm.us/patents/6847455/description.html.

4.6.3.13 Heterodyne Interferometer with Subatomic Periodic Nonlinearity (Wu et al. 1999)

In 1999 Wu et al.[1310] demonstrated one of the first heterodyne interferometers for differential displacement measurements that was, in principle,[1311] free of periodic nonlinearity (Figure 4-86). In this set-up, a pair of spatially separated light beams with different frequencies was produced by two acousto-optic modulators, thus avoiding the main source of periodic nonlinearity in traditional heterodyne interferometers that are based on a Zeeman split laser. Laser beams of the same frequency were used in the measurement and the reference arms, giving the interferometer theoretically perfect immunity from common-mode displacement. A residual level of periodic nonlinearity of less than **20 pm** in amplitude was demonstrated experimentally, with the remaining periodic error attributed to unbalanced ghost reflections that drift slowly with time. More information is needed on this approach.

Figure 4-86. <u>Left:</u> Typical setup for heterodyne interferometry. BS, beam splitter; E_s, reference beam at frequency f_1; E_p, measurement beam at frequency f_2; E_p', Doppler-shifted measurement beam at frequency f_2'; I_m, measurement signal; I_r, reference signal. <u>Right:</u> Equivalent topology of the differential heterodyne interferometer designed to measure an actual displacement. PM SM-fiber, polarization maintaining single-mode fiber; BS, beam splitter; RAP, right-angle prism; BC, beam combiner.

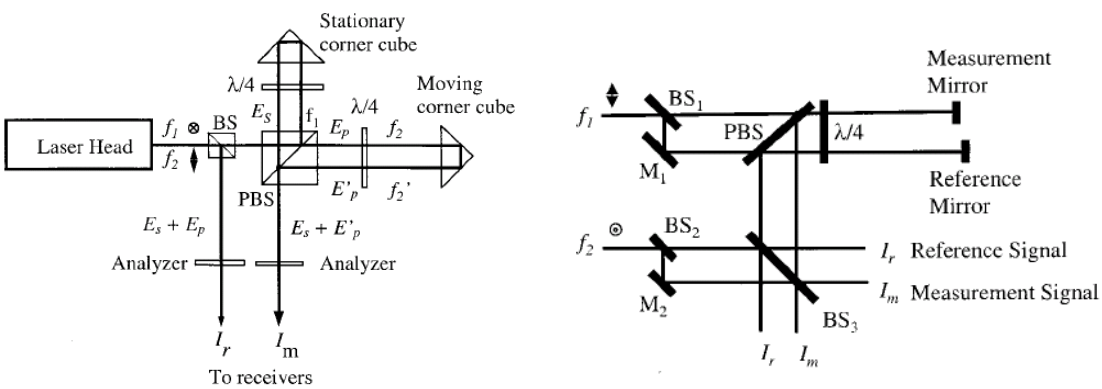

[1310] C.M. Wu, J. Lawall, R.D. Deslattes, "Heterodyne interferometer with subatomic periodic nonlinearity," Appl. Opt. 38(1999):4089-4094.

[1311] C.M. Wu, R.D. Deslattes, "Analytical modeling of the periodic nonlinearity in heterodyne interferometry," Appl. Opt. 37(1 October 1998):6696-6700.

4.6.3.14 Heidenhain Interferometer (Germany)

By the early 2000s, according to Peggs and Yacoot,[1312] Heidenhain,[1313] a specialty German company best known for manufacturing angular, rotary and linear encoders (along with digital readouts and numerical controls delivered to manufacturers of machine tools and automated facilities/machines), had "developed a new homodyne type of optical interferometer (see Spanner and Thiel[1314]) with an inherent resolution of **19 pm** and residuals of **100 pm**. An innovative design of beam-splitter and fibre coupling of the light source makes the design well-suited to many applications requiring sub-nanometre resolution." The paper by Spanner and Thiel[1315] "introduces a homodyne laser interferometer with a new optical design for the beamsplitter and featuring the generation of phase-shifted signals by polarisation optical means. It describes measurements of the frequency stability of the laser, as well as a method of measuring the interpolation error in the **subnanometer range** by means of a piezo flexure stage."

4.6.3.15 Phase Shifting Interferometry (PSI)

Phase-shifting interferometery (PSI),[1316] which typically uses either a single-wavelength laser or "white" (i.e., polychromatic) light, has several well-known advantages:[1317] (1) fast measurement

---

[1312] G.N. Peggs, A. Yacoot, "A review of recent work in sub-nanometre displacement measurement using optical and X-ray interferometry," Philos Transact A Math Phys Eng Sci. 360(15 May 2002):953-968; http://journals.royalsociety.org/content/nj5d8xydfdy8b85d/fulltext.pdf.

[1313] e.g., Dr. Johannes Heidenhain GmbH, Traunreut, Germany, http://www.heidenhain.de; Heidenhain (company), http://www.heidenhain.com/..

[1314] E. Spanner, J. Thiel, "Homodyne laser interferometer with new interferometer optics and fibre-coupled measuring head for ultra precision measurement below 1 nm," in: A. Balsamo et al., eds. Proc. 2nd EUSPEN Int. Conf., Turin, 2001, pp. 222-225.

[1315] E. Spanner, J. Thiel, "Homodyne laser interferometer with new interferometer optics and fibre-coupled measuring head for ultra precision measurement below 1 nm," in: A. Balsamo et al., eds. Proc. 2nd EUSPEN Int. Conf., Turin, 2001, pp. 222-225.

[1316] P. Hariharan, B. F. Oreb, T. Eiju, "Digital phase-shifting interferometry: a simple error-compensating phase calculation algorithm," Appl. Opt. 26(1987):2504-2505. K. Creath, "Phase measurement interferometry techniques" in: E. Wolf, ed., Progress in Optics XXVI, North-Holland, Amsterdam, 1988, pp. 349-393. C. Ai, J.C. Wyant, "Effect of spurious reflection on phase shift interferometry," Appl. Opt. 27(1988):3039-3045. C.P. Brophy, "Effect of intensity error correlation on the computed phase of phase-shifting interferometry," J. Opt. Soc. Am. A 7(1990):537-541. J.E. Greivenkamp, J.H. Bruning, "Phase shifting interferometry" in: D. Malacara, ed., Optical Shop Testing, 2nd edition, Wiley, New York, 1992, pp. 501-598. B. Ovryn, E.M. Haacke, "Temporal averaging of phase measurements in the presence of spurious phase drift: application to phase-stepped, real-time holographic interferometry," Appl. Opt. 32(1993):147-154. B. Ovryn, "Two camera phase measurements using phase stepped, real-time holographic interferometry," in: H. Podbielska, ed., Holography, Interferometry and Optical Pattern Recognition in Biomedicine III, Proc. SPIE 1889(1993):120-131. P.J. de Groot, "Vibration in phase-shifting interferometry," J. Opt. SOC. Am. A 12(1995):354-365. Patrick Sandoz, "An algorithm for profilometry by white-light phase-shifting interferometry," Journal of Modern Optics 43(August

speed, (2) high phase-measurement accuracy, (3) good results even when the fringe contrast is poor, (4) phase measurements independent of spatial intensity variation across the wave front, (5) phase obtained at a fixed grid of data points, and (6) polarity of wave front can be determined. The basic idea of PSI is that, if the phase difference between the two interfering beams is made to vary in some known manner, such as changing in discrete steps or changing linearly with time, three or more measurements of the intensity distribution across the pupil for different phase differences between the interfering beams can be used to determine the phase distribution across the pupil. In the situation of testing surface roughness when no tilt fringes are present, PSI can be a very high precision measurement technique with a precision of measurement in the range from $\lambda/100$ to $\lambda/1000$, peak-valley.

In a phase shifting interferometer (Figure 4-87C), piezo-electric transducers actually move the reference surface (Figure 4-87A) in a number of predetermined steps (often in 1/4 wave steps) towards the test piece (Figure 4-87B), via PZT actuation (or other means) under software control.[1318] At each position, the interferometer's "frame grabber" captures an interferogram and stores it for analysis by the software. As shown in Figure 4-87A, with each step of the phase shifter the fringes move 1/4 wave to the right. The frame data are then processed by the computer to calculate optical wavefront errors. The software finds aberrations and computes both peak-to-valley (PV) and root-mean-square (rms) values, with the operator having the option to subtract tilt, power, astigmatism, coma, and spherical aberrations from the data, allowing interpretation of the output and numerical quantitative results.

1996):1545-1554. Feng Zhao, Jennifer E. Logan, Stuart Shaklan, Michael Shao, "A common-path, multi-channel heterodyne laser interferometer for sub-nanometer surface metrology," Jet Propulsion Laboratory, California Institute of Technology, 4800 Oak Grove Drive, Pasadena, California 91109, U.S.A., SPIE Proceedings 3740(1999):642-645; http://trs-new.jpl.nasa.gov/dspace/bitstream/2014/17017/1/99-0434.pdf. Michael B. North-Morris, James E. Millerd, Neal J. Brock, John B. Hayes, "Phase-Shifting Multi-Wavelength Dynamic Interferometer," 2004 SPIE, Denver, 2004 MWL Manuscript v4.doc; http://www.4dtechnology.com/reflib/Phase-shifting%20multi-wavelength%20dynamic%20interferometer%2004%20SP.pdf. Wei Zhu, Wencai Jing, Hongxia Zhang, Dagong Jia, Yimo Zhang, Yan Li, Feng Tang, "Design and implementation of a nanometer phase-shifting interferometer for micro-surface profile measurement," Proc. SPIE 6027(2006):60270M. Hyuck Choo, Rishi Kant, David Garmire, James Demmel, Richard S. Muller, "Fast, MEMS-Based, Phase-Shifting Interferometer," Technical Digest, 2006 Solid-State Sensors, Actuators, and Microsystems Workshop, Transducers Research Foundation, Hilton Head Island, SC, 4-8 June 2006, pp. 94-95.

[1317] Yeou-Yen Cheng, James C. Wyant, "Two-wavelength phase shifting interferometry," Applied Optics 23(15 December 1984):4539-4543.

[1318] "How Phase Shifting Works," http://www.grahamoptical.com/phase.html.

Figure 4-87. (A) Left: Conceptual schematic of phase-shifting interferometer (PSI) function. (B) Center: Mechanism for imposing phase-shift on scanned signal, in this case a PZT actuator. (C) Right: Michelson-type PSI layout.[1319]

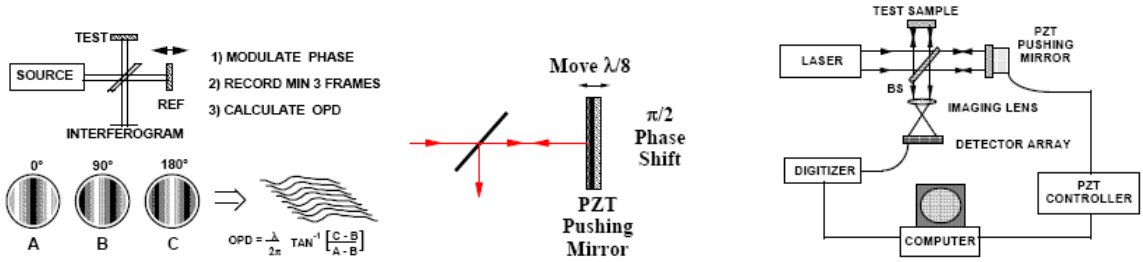

A good example of the PSI approach is the work of Ovryn's group during 1996-2001[1320] which combined PSI with laser feedback interferometry (LFI) to obtain sub-nanometer accuracy in measuring oscillatory and dc changes in the optical path length (OPL). In this configuration, interference arises by reflecting the light from a sample back into the cavity of a continuous-wave He-Ne laser (an apparatus that can be modeled as a three-mirror Fabry-Pérot etalon). Changes in phase and fringe visibility are calculated from an overdetermined set of phase-shifted intensity measurements, with the phase shifts being introduced with an electro-optic modulator that is used to introduce discrete known changes in OPL. The interferometer was applied to the determination of cantilever bending of a piezoelectric bimorph and could measure displacements below 1 Hz with sub-nanometer rms error from a sample that reflects only 3% of the 28 mW that is incident upon its surface. The phase-shifting laser feedback interferometer was assembled from a He-Ne laser. The beam emitted from the front of the laser was sent through an electro-optic modulator, a linear polarizer with a fixed orientation parallel to the polarization of the laser, and then focused onto a sample using a long working distance microscope objective. Fluctuations in the laser's steady-state power were determined by monitoring the light transmitted through the laser's rear mirror using a photodetector. The voltage signal from the photodetector was digitized with a 100-kHz, 16-bit analog-to-digital board on a PC bus; this board was also used to send voltage steps to a high-voltage operational amplifier and then to the EOM. The entire apparatus was mounted on a vibration isolation table and enclosed in a double Plexiglas

---

[1319] "How Phase Shifting Works," http://www.grahamoptical.com/phase.html.

[1320] B. Ovryn, J.H. Andrews, S.J. Eppell, J.D. Khaydarov, "Phase shifted real time laser feedback interferometry," in: M. Kujawinska, R.J. Pryputniewicz, M. Takada, eds., Laser Interferometry VIII: Techniques and Analysis, Proc. SPIE 2860(1996):263-274. Ben Ovryn, James H. Andrews, "Phase-shifted laser feedback interferometry," Opt. Lett. 23(1998):1078-1080. See also: Phase-Shifted Laser Feedback Interferometry, 1998; http://www.grc.nasa.gov/WWW/RT/RT1998/6000/6712ovryn.html. Ben Ovryn, James H. Andrews, "Measurement of changes in optical path length and reflectivity with phase-shifting laser feedback interferometry," Appl. Optics 38(1 April 1999):1959-1967; http://ovrynlab.org/reprints/ovryn_andrews.pdf. D.G. Fischer, B. Ovryn, "Phase shifting optical coherence tomography (OCT)," in: Valery V. Tuchin, Joseph A. Izatt, James G. Fujimoto, eds., Coherence Domain Optical Methods in Biomedical Science and Clinical Applications V, Proceedings SPIE 4251(2001):97-101; http://ovrynlab.org/reprints/fischer_ovryn.pdf.

box. The single-period rms OPL measurement error of **140 pm** was obtained (Figure 4-88).[1321] Response times are limited by photon lifetime, detector electronics, and modulator rise time rather than lock-in detection and feedback loop parameters.

Figure 4-88. Phase-shifted laser feedback interferometry (Ovryn group):[1322] Measured optical path length (OPL) and visibility for a 5-nm ramp applied to the electro-optic modulator (EOM); the rms OPL error, obtained from a linear fit to a single period, is 140 pm.

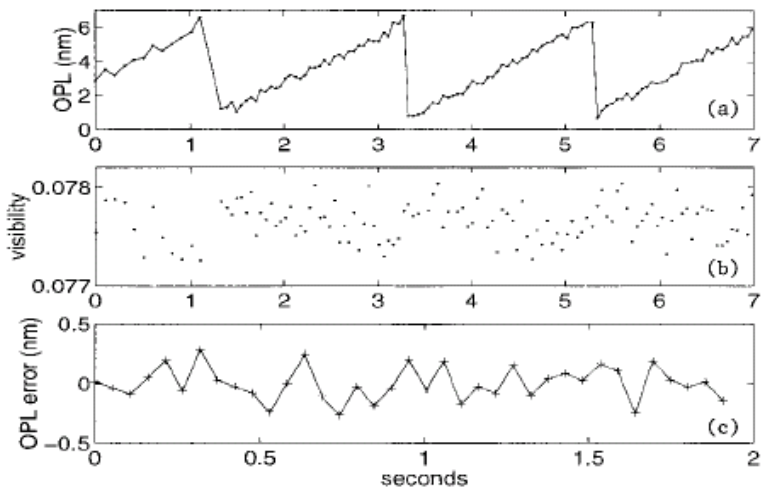

Probably the most serious impediment to the wider use of PSI is its sensitivity to external vibration[1323] which causes incorrect phase shifts between data frames. The magnitude of this error depends on the frequency of the vibrations that are present and on the phase of vibration relative to the phase shifting, and can be reduced by (1) reducing the ambient vibrations, (2) take data fast, (3) take all frames at once, or (4) measure the vibration and introduce additional

---

[1321] Ben Ovryn, James H. Andrews, "Measurement of changes in optical path length and reflectivity with phase-shifting laser feedback interferometry," Appl. Optics 38(1 April 1999):1959-1967; http://ovrynlab.org/reprints/ovryn_andrews.pdf.

[1322] Ben Ovryn, James H. Andrews, "Measurement of changes in optical path length and reflectivity with phase-shifting laser feedback interferometry," Appl. Optics 38(1 April 1999):1959-1967; http://ovrynlab.org/reprints/ovryn_andrews.pdf.

[1323] P.J. de Groot, "Vibration in phase-shifting interferometry," J. Opt. SOC. Am. A 12(1995):354-365. James C. Wyant, "Optics 505," course notes, University of Arizona, 2000; http://www.optics.arizona.edu/jcwyant/Optics505(2000)/ChapterNotes/Chapter09/phaseshiftinginterferometry.pdf.

vibrations that are 180° out of phase to cancel the ambient vibrations.[1324] Major sources of measurement error include:[1325] (1) incorrect phase shift between data frames,[1326] (2) vibrations,[1327] (3) detector nonlinearity,[1328] (4) stray reflections,[1329] (5) quantization errors, (6) frequency stability, and (7) intensity fluctuations.

In the case of white-light interferometry, the usual phase shifting methods cannot be used because the modulation in the interference intensity is due to both the phase variation and to the coherence envelope. Sandoz[1330] has proposed a practical approach in which the coherence envelope is considered as locally linear. The classical four-point calculation algorithm is adapted to a set of seven intensities which are weighted with adapted coefficients in order to compensate for the effect of the coherence envelope.

4.6.3.16 Other Michelson-Based Systems

A number of systems based on Michelson interferometry have been developed (and continue to be pursued) in the last decade, but many or most probably provide insufficient (picometric) precision for use in a molecular workstation for DMS. These include:

(1) **KAIST** (Korea), 2007 – an AFM system for length measurement over several tens of microns, designed to reduce Abbe error of the XY scanning stage; expanded uncertainty is estimated as ~**2000 pm**.[1331]

[1324] James C. Wyant, "Optics 505," course notes, University of Arizona, 2000; http://www.optics.arizona.edu/jcwyant/Optics505(2000)/ChapterNotes/Chapter09/phaseshiftinginterferometry.pdf.

[1325] James C. Wyant, "Optics 505," course notes, University of Arizona, 2000; http://www.optics.arizona.edu/jcwyant/Optics505(2000)/ChapterNotes/Chapter09/phaseshiftinginterferometry.pdf.

[1326] Yeou-Yen Cheng, James C. Wyant, "Two-wavelength phase shifting interferometry," Applied Optics 23(15 December 1984):4539-4543.

[1327] P.J. de Groot, "Vibration in phase-shifting interferometry," J. Opt. SOC. Am. A 12(1995):354-365.

[1328] James C. Wyant, "Optics 505," course notes, University of Arizona, 2000; http://www.optics.arizona.edu/jcwyant/Optics505(2000)/ChapterNotes/Chapter09/phaseshiftinginterferometry.pdf.

[1329] C. Ai, J.C. Wyant, "Effect of spurious reflection on phase shift interferometry," Appl. Opt. 27(1988):3039-3045.

[1330] Patrick Sandoz, "An algorithm for profilometry by white-light phase-shifting interferometry," Journal of Modern Optics 43(August 1996):1545-1554.

[1331] D. Kim, D.Y. Lee, D.G. Gweon, "A new nano-accuracy AFM system for minimizing Abbe errors and the evaluation of its measuring uncertainty," Ultramicroscopy 107(April-May 2007):322-328.

(2) **KRISS** (Korea), 2008 – a metrological AFM system (MAFM) with expanded uncertainties (k = 2) of measured pitch values less than 200 pm and 400 pm for each specimen; the displacement of the XY nanoscanners was measured using a two-axis laser interferometer with a resolution of **1240 pm**.[1332]

(3) **KAIST** (Korea), 2009 – a simple heterodyne laser interferometer that has subnanometer periodic errors uses two spatially separated beams that can reduce the periodic errors, and the use of a right-angle prism makes the optical configuration much simpler than previous interferometers; experiments demonstrated the periodic errors are less than **150 pm** owing to the frequency mixing of the optical source.[1333]

(4) **National Metrology Institute of Japan**, 2005 – a novel phase-shifting interferometric microscope achieved a typical expanded uncertainty of **600 pm**, when a sample with a 100-nm step height is measured.[1334]

(5) **CMS/ITRI** (Taiwan) – Danzebrink[1335] reports the construction of a purpose-built system with **500 pm** uncertainty on pitch measurements for a homodyne laser interferometer set-up with three axes, with a travel range of 100 μm x 100 μm x 10 μm. No other literature reference to this work has been located, other than an oblique 1994 reference to a Taiwan-proposed course of work "to **use picometer metrology and AFM** to continuously scan with atomic resolution a surface strip of about 2 nm x 10 mm area on a single silicon crystal in a 2 x 10^{-11} torr vacuum chamber to measure silicon lattice spacings to 0.1-1 ppb".[1336]

[1332] J.A. Kim, J.W. Kim, B.C. Park, T.B. Eom, J.W. Hong, "Development of a metrological atomic force microscope for the length measurements of nanometer range," Journal of the Korean Society for Precision Engineering 21(November 2004):75-82. R. Glöß, P. Pertsch, "Systeme der Nanopositionierung," Feinwerk & Messtechnik, 107(1999):64-68. Jong-Ahn Kim, Jae Wan Kim, Chu-Shik Kang, Tae Bong Eom, "Measurements of Two-dimensional Gratings Using a Metrological Atomic Force Microscope with Uncertainty Evaluation," Intl. J. Precision Eng. and Manufacturing 9(April 2008):18-22; http://www.ijpem.org/journal/files/issues/E07-02-82.pdf.

[1333] K.N. Joo, J.D. Ellis, J.W. Spronck, P.J. van Kan, R.H. Schmidt, "Simple heterodyne laser interferometer with subnanometer periodic errors," Opt Lett. 34(1 February 2009):386-388.

[1334] Takuma Doi, Tomizo Kurosawa, "Absolute calibration of step height by a novel interferometric microscope," Proc. SPIE 5776(2005):121.

[1335] H.-U. Danzebrink, L. Koenders, G. Wilkening, A. Yacoot, H. Kunzmann, "Advances in Scanning Force Microscopy for Dimensional Metrology," CIRP Annals - Manufacturing Technology 55(2006):841-878.

[1336] Wei-Tou Ni, Jia-Ruey Duann, Gwo-Sheng Peng, Hsien-Fen Hsieh, Chung-Ping Lai, King-Hung Lee, Yeou-Song Lee, Fu-Jeng Lin, Huay-Chung Liou, Sheau-Shi Pan, Chien-Ming Wu, Hsien-Chi Yeh, Mei-yun Yeh, "A new method to measure silicon lattice spacings and possible newdefinition of the kilogram: scheme and progress," 1994 Conference on Precision Electromagnetic Measurements, 27 Jun - 1 Jul 1994, pp. 341-342, DOI 10.1109/CPEM.1994.333369.

(6) **DFM** (Danish Fundamental Metrology) (Lyngby, Denmark) – Danzebrink[1337] reports a scanning tip for grating and step height metrology with a travel range of 70 μm x 70 μm x 6 μm and a lateral distance uncertainty of **150 pm over only 1 micron of travel**. No other literature reference to this work has been located.

(7) **METAS** (Switzerland) – This is a homodyne laser interferometer profiler[1338] using a commercial metrology AFM and a linear long-range stage with a travel range of 70 μm x 70 μm x 5 μm and a mean pitch uncertainty of **500 pm** for a 10 micron pitch and a lateral distance uncertainty of **1225 pm** for a 10 micron displacement.[1339] There is also a description of a Coordinate Measuring Machine (CMM) built by METAS called the "ultra-precision coordinate measuring machine for small parts" which is described[1340] as follows:

In order to fulfil the expectations for quality and precision of future microtechnology, METAS has developed a new ultra-precise 3D measuring machine for small mechanical objects. Its success is mainly based on two key components: A new probe head was developed in a research project launched by METAS in collaboration with the EPF Lausanne and the industrial partner Mecartex SA, Losone. Based on flexure hinges, the probe exhibits very week contact forces, but maintains a high rigidity to reach a precision of a few nanometers. The translation stage was developed at Philips CFT. It incorporates in a clever way all metrological principles to cancel or correct to its best all remaining motion errors. Characterised in its finest details, our μCMM thus exhibits an unprecedented precision for 3D measurements: a repeatability in one point <5 nm and an uncertainty (U95) <80 nm within its whole working volume. Its user interface integrates all functionality for point-to-point measurement and scanning.

(8) **MIKES** (Finland) – Mittatekniikan Keskus, Centre for Metrology and Accreditation, TKK Mittaustekniikka, Metrology Research Institute at Helsinki University of Technology – or MIKES[1341] – has modified a commercial scanning force microscope (an AFM) using position

---

[1337] H.-U. Danzebrink, L. Koenders, G. Wilkening, A. Yacoot, H. Kunzmann, "Advances in Scanning Force Microscopy for Dimensional Metrology," CIRP Annals - Manufacturing Technology 55(2006):841-878.

[1338] F. Meli, R. Thalmann, "Long range AFM profiler used for accurate pitch measurements," Meas. Sci. Technol. 9(1998):1087-1092.

[1339] H.-U. Danzebrink, L. Koenders, G. Wilkening, A. Yacoot, H. Kunzmann, "Advances in Scanning Force Microscopy for Dimensional Metrology," CIRP Annals - Manufacturing Technology 55(2006):841-878. F. Meli, R. Thalmann, "Long range AFM profiler used for accurate pitch measurements," Meas. Sci. Technol. 9(1998):1087-1092. F. Meli, et al., "Z-calibration of a metrology AFM scanner using an interferometer and a tilting device with linear stage," Proc. of the Third Seminar on Quantitative Microscopy, Lyngby, Denmark, PTB-F-34(1998):61-67. F. Meli, "International comparison in the field of nanometrology: Pitch of 1D gratings," Proc. of 2nd Intl. EUSPEN Conference (Nano4), Italy, 1(2001):358-361. F. Meli, "Lateral and vertical diameter measurements on polymer particles with a metrology AFM," in: G. Wilkening, L. Koenders, eds., Nanoscale Calibration Standards and Methods, Wiley-VCH, Weinheim, Germany, 2005, pp. 361-374. F. Meli, "Design of a new 3D-metrology AFM at METAS using differential Jamin type interferometers," Nanoscale 2008 poster, METAS, Bern-Wabern, Switzerland, 2008.

[1340] F. Meli, A. Küng, R. Thalmann, "Ultrapräzises Koordinatenmessgerät für Mikroteile metINFO," Vol. 12, No. 3 , S.4-10, 2005 (1.9 MB) In German. http://www.metas.ch/root_legnet/Web/Dokumentation/Publikationen/METinfo/PDF/METinfo2005_3.pdf.

[1341] http://www.mikes.fi/.

sensors calibrated by interferometry and 1-dimensional grids (calibrated by laser diffractometer). The system has a nominal 150 pm resolution in XY and 50 pm resolution in Z, and even lower 20 pm and 10 pm resolutions are claimed in "low-voltage mode",[1342] or 9 pm for 2 μm grating,[1343] but over the total travel range of 100 μm x 100 μm x 16 μm gives a step height uncertainty of **1500 pm** for a 10 micron vertical displacement and a lateral distance uncertainty of **4359 pm** for a 10 micron lateral displacement.[1344] The design goal for the MIKES system appears to be a repeatable 3-D interferometric measurement accuracy of 1 nm[1345] and a repeatable step height measurement uncertainty of 2 nm.[1346] Unfortunately, the group's publications are all conference presentations[1347] and apparently all in Finnish, not English.

(9) **NPL** (UK) – In the mid-2000s, Haycocks and Jackson[1348] constructed a Metrological Atomic Force Microscope (MAFM) for the traceable calibration of transfer standards using scanning probe microscopy (a modified commercial instrument). The MAFM uses optical interferometry to generate image scales with direct traceability to the national standard of length. Three homodyne optical interferometers monitor the relative displacements of the AFM tip and sample in the X, Y and Z directions, with perhaps **100-200 pm** minimal uncertainty but with

---

[1342] "Microscopy – Atomic force microscope"; http://www.mikes.fi/documents/upload/afm_engl_04032008.pdf.

[1343] V. Korpelainen, A. Iho, J. Seppa, A. Lassila, "High accuracy laser diffractometer: angle-scale traceability by the error separation method with a grating," Meas. Sci. Technol. 20(2009):084020. See also: V. Korpelainen, A. Lassila, "Calibration of a commercial AFM: traceability for a coordinate system," Meas. Sci. Technol 18(2007):395-403.

[1344] H.-U. Danzebrink, L. Koenders, G. Wilkening, A. Yacoot, H. Kunzmann, "Advances in Scanning Force Microscopy for Dimensional Metrology," CIRP Annals - Manufacturing Technology 55(2006):841-878.

[1345] NanoScale2004 poster, http://www.mikes.fi/documents/upload/nanoscale2004_afm.pdf.

[1346] http://www.mikes.fi/documents/upload/calibration_of_microscopes_05032008.pdf.

[1347] A. Lassila, V. Korpelainen, B. Hemming, I. Palosuo, "Recent developments at nanometre scale metrology at MIKES," Nanotechnology in Northern Europe, Helsinki, Finland, 26-28 April 2005; V.-P. Esala, B. Hemming, K. Nyholm, A. Lassila, "MIKES' facility for calibration of commercial laser interferometers," in Proc. of EUSPEN 2005 Conference, Montpellier 8.- 12.5.2005, 4 pp; V. Korpelainen, A. Lassila, "Quantitative microscopy at MIKES - traceability of AFM measurements," in Northern Europe, Helsinki, Finland, 26-28 April 2005; V. Korpelainen, A. Lassila, "Calibration and traceability of a commercial AFM at MIKES," in Nanotechnology in Northern Europe 2006, 16-18 May 2006, Helsinki, Finland; A. Manninen, O. Hahtela, P. Hakonen, J. Hassel, P. Helistö, A. Kemppinen, M. Möttönen, M. Paalanen, J. Pekola, A. Satrapinski, H. Seppä, "Towards direct closure of the quantum metrological triangle," Conference Digest, CPEM 2008 (Broomfield, Colorado, USA, 8 - 13 June, 2008), pp. 630-631.

[1348] J. Haycocks, K. Jackson, "Traceable calibration of transfer standards for scanning probe microscopy," Prec. Eng. 29(2005):168-175. J. Haycocks, K. Jackson, "Detecting and addressing the surface following errors in the calibration of step heights by atomic force microscopy," Meas. Sci. Technol. 18(February 2007):469-475.

additional uncertainty as a function of displacement distance and sample length or height.[1349] The interferometer data is used directly to construct 3D images of sample surfaces. As of 2007, Haycocks[1350] seemed primarily interested in metrological step height standards.

(10) **PTB** (Germany) – During the early 2000s, PTB put together a series of nanometrology systems aimed primarily at achieving traceable measurements of step height. One system was a metrological scanning force microscope (M-SFM), a modified commercial instrument called the "Veritekt C" as shown in Figure 4-89 below.[1351] The version "C" is a modified version of the "Veritekt B", an SPM described in connection with the NANO2 project.[1352] It is a scanning sample system with a stationary fixed cantilever probe. The 3D monolithic flexure-hinge stage with a scanning range of 70 µm x 15 µm x 15 µm along X-, Y- and Z-axes, respectively, is driven by piezoelectric translators (PZTs) equipped with capacitive sensors. The sample holder is fixed on the flexure-hinge stage. Its position is measured by three homodyne planar interferometers, which were designed in co-operation with SIOS Messtechnik GmbH and the Technical University of Ilmenau.[1353] When the sample is mounted, its measurement point lies at the point of intersection of the three interferometer measurement beams so that the Abbe error can be minimized. The resolution of the interferometers is **100 pm**, but over the XYZ measuring range of 70 µm x 15 µm x 15 µm the resolution is only about **1000 pm, 250 pm, and 250 pm**.

[1349] H.-U. Danzebrink, L. Koenders, G. Wilkening, A. Yacoot, H. Kunzmann, "Advances in Scanning Force Microscopy for Dimensional Metrology," CIRP Annals - Manufacturing Technology 55(2006):841-878.

[1350] J. Haycocks, K. Jackson, "Detecting and addressing the surface following errors in the calibration of step heights by atomic force microscopy," Meas. Sci. Technol. 18(February 2007):469-475.

[1351] L. Koenders, R. Bergmans, J. Garnaes, J. Haycocks, N. Korol, T. Kurosawa, F. Meli, B.C. Park, G.S. Peng, G.B. Picot, E. Prieto, S. Gao, B. Smereczynska, T. Vorburger, G. Wilkening, "WGDM-7: Preliminary comparison on nanometrology according to the rules of CCL key comparisons. Nano 2 Step height standards," Metrologia Technical Report, 40(2003):04001.

[1352] M. Bienias, S. Gao, K. Hasche, R. Seemann, K. Thiele, "A metrological scanning force microscope used for coating thickness and other topographical measurements," J. Appl. Phys. A 66(1998):837-842. K. Thiele, K. Hasche, K. Herrmann, R. Seemann, "Determination of the geometry of micro hardness indenters using a calibrated scanning force microscope," Proc. 3rd Seminar on Quantitative Microscopy, Lyngby, Denmark, PTB-F-34, Braunschweig, December 1998, ISBN 3-89701-280-4, pp. 115-122. L. Koenders, R. Bergmans, J. Garnaes, J. Haycocks, N. Korol, T. Kurosawa, F. Meli, B.C. Park, G.S. Peng, G.B. Picot, E. Prieto, S. Gao, B. Smereczynska, T. Vorburger, G. Wilkening, "Comparison on Nanometrology: Nano 2-Step height," Metrologia 40(2003):04001 (Tech. Suppl.).

[1353] G. Jäger et al., VDI Berichte 1530, VDI Verlag Düsseldorf 2000, pp. 271-278.

Figure 4-89. <u>Left:</u> Sketch of the Veritekt C. <u>Right:</u> View of the metrological SFM with tip sensor unit removed.[1354]

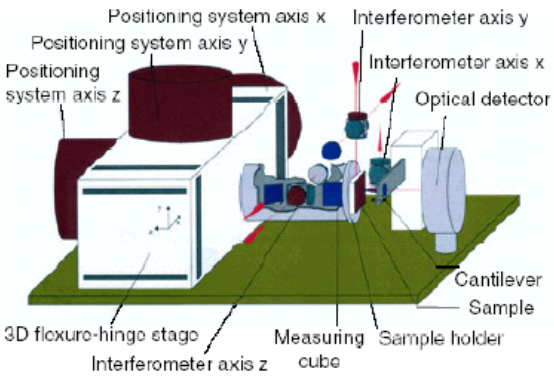

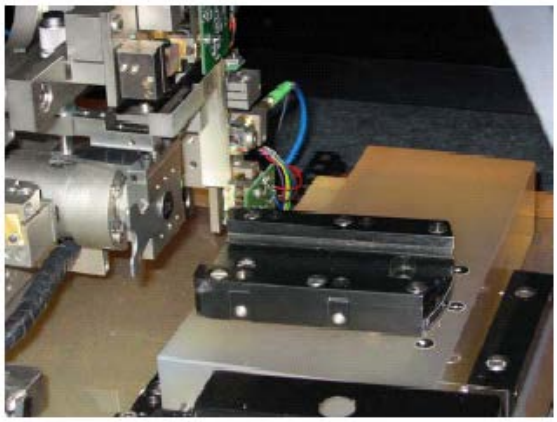

(11) **IMGC** (Italy) – In 2001, Picotto and Pisani described[1355] "a sample scanning device operating in a working volume of **30 µm x 30 µm x 18 µm** with interferometer and capacitance-based controls of displacements. The XY-stage uses plane mirror linear interferometers and fast phase-meters for control of displacements of precise ball-bearing stages driven by piezo flexure actuators. The stage operates with a full range bandwidth of 200 Hz, and an estimated accuracy (k = 2) of 3 nm + 1 x 10^{-3} L, where L is the lateral displacement. A novel Z-stage uses a kinematic coupling between two plates, the upper one being moved by three bimorph plates and the distance being measured by three capacitive sensor. The tilt of the Z-stage was kept within fractions of a microrad, leading to a full range estimated accuracy of 2 nm + 2 × 10^{-3} h, where h is the vertical displacement," giving positional accuracy of **a few nanometers** with a control bandwidth of about 1 kHz.

(12) In 2003, Haitjema et al.[1356] adapted a commercially available heterodyne laser interferometer by feeding the measurement signal into a fast lock-in amplifier and use the laser interferometer reference signal as a reference, then measuring both the in-phase and quadrature component which allows an uncorrected phase to be directly measured. By recording both components while the phase changes between 0 and 2π a typical ellipse is recorded from which the first and second harmonics of periodic deviations can be derived, and these can be corrected

---

[1354] L. Koenders, R. Bergmans, J. Garnaes, J. Haycocks, N. Korol, T. Kurosawa, F. Meli, B.C. Park, G.S. Peng, G.B. Picot, E. Prieto, S. Gao, B. Smereczynska, T. Vorburger, G. Wilkening, "WGDM-7: Preliminary comparison on nanometrology according to the rules of CCL key comparisons. Nano 2 Step height standards," Metrologia Technical Report, 40(2003):04001.

[1355] G.B. Picotto, M. Pisani, "A sample scanning system with nanometric accuracy for quantitative SPM measurements," Ultramicroscopy, 86(2001):247-254.

[1356] Han Haitjema, Suzanne J.A.G. Cosijns, N.J.J. Roset, Maarten J. Jansen, "Improving a commercially available heterodyne laser interferometer to sub-nm uncertainty," Proc. SPIE 5190(2003):347-354.

independent of their origin, decreasing measured uncertainty to about **±1500 pm**. (Sacconi[1357] and Picotto[1358] used a similar setup, but they employed a phase detector rather than a lock-in amplifier.)

(13) **Nanyang Technological University** (Singapore) – In 2005, Yeh et al.[1359] described "a two-dimensional interferometric nanopositioning system consisting of rectilinear flexure stage, calibrated laser interferometer, and digital feedback control system. We implement a correlation matrix, determined by the piezoelectric constant and the crosstalk between two axes, into the closed-loop control algorithm to compensate the nonlinearity and the crosstalk of the PZT-driven stage. In the tests on nanopositioning, the **1000-pm-step motion** and the tracking along a 1-nm-radius circular target path are accomplished to verify the short-term repeatability and the subnanometer-level precision. Additionally, a scanning tunneling microscope equipped with the interferometric nanopositioning system is built up to demonstrate the metrological functions of scanning probe microscopy."

(14) **Czech Metrology Institute** (2009) – Lazar et al.[1360] have designed a three-axis stage with **200 µm x 200 µm x 10 µm** of XYZ travel that allows positioning with **300 pm** resolution in all three axes under a closed loop control with position detection via capacitive sensors and an interferometric system (dc homodyne detection) monitoring all six degrees of freedom of the stage to ensure full metrological traceability and to improve resolution and overall precision of the displacement monitoring. The interferometers are in a double-pass configuration designed to operate with plane-mirror reflectors with a fixed corner-cube reflector in both the reference arm and the measuring arm. The principal resolution of the system in a simple fringe-counting regime is $\lambda/4$; the resolution of the interferometric detection and data processing system is 10 bit with 1 LSB (least significant bit) being 1/1024 of one cycle of the interferometric signal. Here the $\lambda/4$ resolution of the interferometric system itself results in a final value of $\lambda/4096$ which means that for the 532 nm wavelength (solid-state Nd:YAG laser, which is brighter than a He-Ne laser) the best possible resolution would be 130 pm.

(15) **Yoshida Nano Mechanism Projec**t (JRDC, Tsukuba Research Consortium, Japan) – In 1989, Akira Ishida[1361] developed a two-wavelength displacement-measuring interferometer, using second-harmonic light to eliminate air-turbulence-induced errors in the measurement of linear displacement. An interferometer was developed with two different laser

---

[1357] G.P.A. Sacconi, W. Pasin, "Interferometric calibration of piezo-capacitive displacement actuators," Proc. 4th IMEKO Symposium on Laser Metrology, 1996.

[1358] G.B. Picotto, M. Pisani, "A sample scanning system with nanometric accuracy for quantitative SPM measurements," Ultramicroscopy, 86(2001):247-254.

[1359] H.-C. Yeh, W.-T. Ni, S.-S. Pan, "Digital closed-loop nanopositioning using rectilinear flexure stage and laser interferometry," Control Eng. Pract. 13(2005):559-566.

[1360] J. Lazar, P. Klapetek, O. Cip, M. Cizek, M. Sery, "Local probe microscopy with interferometric monitoring of the stage nanopositioning," Meas. Sci. Technol. 20(2009):084007.

[1361] Akira Ishida, "Two-Wavelength Displacement-Measuring Interferometer Using Second-Harmonic Light to Eliminate Air-Turbulence-Induced Errors," Jpn. J. Appl. Phys. 28(1989):L473-L475.

beams (wavelengths of 488 nm, emitted from an Ar+ laser, and 244 nm, the second harmonic generated by a nonlinear crystal β-BaB_2O_4 inserted in the Ar+ laser cavity) using second harmonic generation (SHG) was developed.

(16) **Zetetic Institute** (U.S.) – In 2000, Henry A. Hill, President of Zetetic Institute, a nonprofit organization located in Tucson AZ, gave a conference presentation[1362] on "A New Interferometer Family for Sub-nanometer Stage Metrology." The Institute claims on its website to be doing research in the area of "precision stage metrology" and to possess facilities including "13,000 square feet and consist of offices, laboratories and shops." However, we have been unable to find any more recent information on these efforts.

4.6.3.17 Summary of Michelson-Based Systems

The leading Michelson-based metrology systems include the Lawall-Kessler differential optical interferometry at NIST, achieving **10 pm** resolution for mirror positioning over a 1 mm range (Section 4.6.3.1); the common path two-wavelength homodyne counting interferometer at the Czech Metrology Institute providing **10 pm** resolution over 100 μm displacements, albeit with high drift rate (Section 4.6.3.5); the multireflection approach at INRIM-Italy providing **20-50 pm** repeatable resolution (Section 4.6.3.4); the "zooming" interferometer approaches of Matsumoto at the National Research Laboratory of Metrology of Japan achieving **30 pm** resolution (Section 4.6.3.9) and Chen et al. at Tsinghua University of China achieving **50 pm** resolution (Section 4.6.3.8); and the positioning control system of Chassagne's group in France, which demonstrates repeatable **53 pm** accuracy over 1 micron of travel and repeatable 500 pm accuracy over 5 mm of travel (Section 4.6.3.10).

Michelson-based systems that have been employed in SPM metrology include the crystal lattice ruler approach of the Aketagawa group in Japan, using a dual tunneling-unit (DTU) STM incorporating one XY scanner and two Z scanners with tips showing a resolution of **10 pm** over 500 nm (Section 4.6.3.7); Silver's tunable-laser interferometer at NIST, achieving **20 pm** accuracy over a range of ~165 nm for a UHV STM tip (Section 4.6.3.2); the laser Doppler displacement meter for AFM at Argonne, performing 80 pm steps over a 25 mm travel range in one dimension of travel with a motion stage driving sensitivity better than **30 pm** (Section 4.6.3.11); the AFM with a 3-axis laser interferometer by the Gonda group in Japan, achieving **40 pm** total resolution over 2-20 micron displacements (Section 4.6.3.6), and the related CD-AFM project in Japan providing **50-200 pm** resolution over a wide linearity range from 0.1 nm to 1 micron (Section 4.6.3.6).

It appears that Michelson-based interferometers can provide positional detection of sufficient precision to enable dead-reckoning pick-and-place DMS operations (without continuous sensory

---

[1362] Henry A. Hill (Zetetic Institute, http://www.zetetic.org/), "2. A New Interferometer Family for Sub-nanometer Stage Metrology," Session IV: High-accuracy Displacement Interferometry, Precision Interferometric Metrology, ASPE2000, 2000 Spring Topical Meeting, 10-12 May 2000; http://pem.kaist.ac.kr/bupe/conferences/aspe-tucson.PDF.

feedback, though likely requiring periodic re-registration), in a molecular workstation to be used for atomically precise DMS-based molecular manufacturing.

4.6.4 Fabry-Pérot (FP) Interferometry Systems

This Section describes methods for measuring displacements using conventional Fabry-Pérot interferometry that have been proposed or demonstrated that are capable of picometer resolution.

4.6.4.1 Atomic Displacement Metrology (ADM) Project at NIST (U.S.)

The Atomic Displacement Metrology (ADM) project at NIST was in full swing at the turn of the century, as already mentioned in Section 4.6.2.5. For instance, university grants were being let to students in 1998],[1363] with John Lawall as advisor: "Scanning Fabry-Pérot interferometry requires the input laser beam to match the mode of the cavity as the length of the cavity changes. We propose doing this with an adaptive optic consisting of two independent moveable lenses. We present calculations appropriate to the NIST Atomic Displacement Metrology project for a Fabry-Pérot cavity with length scanning from 18 to 23 cm."

According to the Technical Activities 2000 report from NIST,[1364] the Atomic Displacement Metrology (ADM) project "seeks to measure and control motion at the atomic scale over distances of many centimeters. It exploits Michelson, Fabry-Pérot, and X-ray interferometry so as to make fundamentally independent measurements of displacement and to rigorously probe the systematic errors associated with each method. Figure 4-90 shows the concept, with the Michelson interferometer and its fringes in red and the Fabry-Pérot interferometer with its fringes in blue. We have demonstrated accuracy in interpolation of sinusoidal fringes from a Michelson interferometer to one part in 30,000, corresponding to a resolution of 10 picometers. As the figure suggests, even higher resolution is possible by starting with the intrinsically narrower Airy line shape characteristic of a Fabry-Pérot interferometer. One of the challenges arising in Fabry-Pérot displacement interferometry is maintaining a 'mode-matched' condition in a cavity of variable length. At the top and bottom are shown two of the lovely but ultimately undesired patterns of transmitted light realized when such a cavity is not correctly mode-matched, and in the center is the Gaussian intensity distribution characteristic of the desired fundamental cavity mode. Combining the optical techniques with simultaneous X-ray interferometry will allow us to perform a measurement of the lattice constant of silicon over a longer range than has ever been attempted. The program will address the metrology requirements of the semiconductor industry in the coming decade and have impacts to science in areas as diverse as gamma-ray spectroscopy and the realization of a non-artifact kilogram."

[1363] "Dynamic Mode-Matching into a Scanning Fabry-Perot Cavity," Grant Number: 8T8004, 1998; http://www.msel.nist.gov/surf1998abstracts.html.

[1364] "Technical Activities 2000," Atomic Physics Division, 2000; http://physics.nist.gov/TechAct.2000/Div842/div842.html (online April 2001).

Figure 4-90. Summary of the NIST Atomic Displacement Metrology Project[1365]

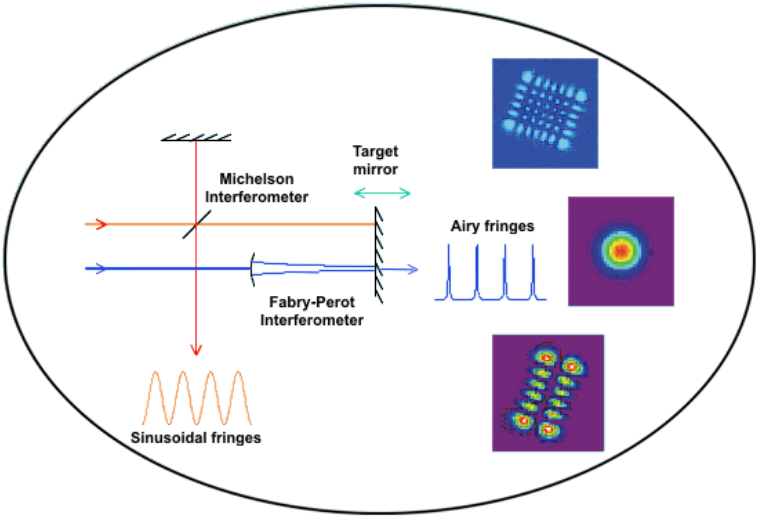

Another NIST document published in 2000[1366] provides additional details of the project: "**Sub-Atomic Displacement Metrology.** Linear displacement is a primitive component of many fundamental physical and technical measurements, yet its realization with atomic scale refinement and accuracy is difficult. Displacements are related to primary wavelength standards by interferometry, and at the moment the accuracy of interferometric measurements is at least two orders of magnitude below that of commercially available reference lasers. This project, which is a collaboration with the Manufacturing Engineering Laboratory and supported by competence funding, is aimed at improving the understanding and application of interferometry. The one-dimensional displacement of a specially fabricated translation stage will be simultaneously measured by means of heterodyne Michelson interferometry, scanning Fabry-Pérot interferometry, and X-ray interferometry. This approach will reveal and provide a means of correcting for systematic errors that currently limit the accuracy of displacement measurements. The translation stage will be controlled in real time by closing a servo loop incorporating multiple Michelson interferometers. We are currently working towards measuring a displacement of up to 5 cm with 50 pm resolution in a high-vacuum, vibration-controlled environment."

A 1 January 2001 summary[1367] of NIST metrology efforts noted that the focus of the Atomic-Scale Displacement Metrology effort was "to **develop the laboratory capability to precisely**

[1365] "Technical Activities 2000," Atomic Physics Division, 2000; http://physics.nist.gov/TechAct.2000/Div842/div842.html (online April 2001).

[1366] "Current Directions in 2000," NIST Physics Laboratory, http://physics.nist.gov/TechAct.2000/Div842/div842c.html.

[1367] Dennis A. Swyt, "Length and dimensional measurements at NIST (National Institute of Standards and Technology)," 1 January 2001; http://nvl.nist.gov/pub/nistpubs/jres/106/1/j61swy.pdf or http://www.encyclopedia.com/doc/1G1-82777385.html.

generate and accurately measure displacements in increments of 50 pm over distances of tens of centimeters. The intended result is improvement by an order of magnitude upon the approximate relative uncertainty of 5 X 10^{-8} that forms the practical lower limit in long length measurements done using displacement interferometry in air. Such capability is to be based in part on advancing the state-of-the-art of displacement interferometry by a direct intercomparison of x-ray, Fabry-Pérot, and optical-heterodyne interferometry. In addition, it is to be based on long-range high-precision stages. These stages are to incorporate laser-based metrology; control of translation, pitch, and yaw, and positional capability commensurate with pm-level displacements. The resulting system of interferometry and stage will form the prototype for production and metrology stages of the future."

A list[1368] of projects and deliverables for 2001 by Michael T. Postek, Program Manager of Nanometer-Scale Metrology at NIST, included the ADM Project, then headed by Thomas LeBrun,[1369] listed the following:

2001 Deliverables

Complete the necessary research and develop a vacuum chamber and fine stage to compensate for errors for the Atomic Displacement Metrology (ADM) testbed including a control system for the 6 DOF stage and to install an X-ray interferometer in the 50 mm test bed chamber.

FY 2000 Accomplishments

• Vacuum Isolation system delivered and under construction.
• XRI alignment system built and ready for test.
• Phasemeter array attains 15 pm errors.
• Six-degree-of-freedom Fine stage delivered and tested.
• Next Generation LSI being built next to current LSI.
• X-ray interferometer is tested to ensure flatness.
• Testing the six-degree-of freedom fine stage and the phasemeter array.

Interestingly, we get a glimpse at how much all of this is costing. There are 11 separate projects going on within MEL, of which ADM is just one, all funded in FY2000 by a total of $3.3M, or a crude average of $0.3M/yr per project. The resources are listed as follows:

• Funding – approximately $3.2-3.3 M
– About $2.61 M devoted to salaries (and $200 K devoted to MELSA)
• Personnel - 11 FTE technical staff + secretary + 10 Guest Researchers
• Loss of Lowell Howard – Industry Position
• Loss of Fred Scire – Retirement (Guest Researcher Contract)

[1368] http://www.mel.nist.gov/div821/webdocs-14/nanoscale-metrology_2001.pdf.

[1369] By October 2001, LeBrun was apparently off the project, and Lawall was then running it. As of 2008, Tom LeBrun was still at NIST (http://www.mel.nist.gov/div821/staff/TLeBrun.htm, Email: thomas.lebrun@nist.gov) and is still a Research Physicist in the Nanoscale Metrology Group (821.14). Judging from his publications list, he never got a paper out of his ADM work and has spent much of his time since 2001 working on optical tweezer-based nanoassembly.

• Loss of Steven Fox – Post Doc - Industry Position
• Gain – Vincent Scheuerman
• Gain – Satoshi Gonda – NRLM Guest Researcher
• Gain – Forest Chen – Taiwan
• Gain – Yann Bednarek - France
• Needed Resources
– Technicians
• SEM Metrology
• M3/Atom-based
• New LSI development
– Equipment
• METROLOGY CD-SEM – SEMATECH Collaboration on RMS

In 2004-5, the ADM group, now led by John Lawall,[1370] reported operating a UHV-based tunable-laser-based Fabry-Pérot interferometer able to measure 25-50 mm distances to 0.1 Å (10 pm) accuracy – see Section 4.6.4.2, below, for a further description. Unfortunately there were no further major publications on this system after 2005 and the last update to the NIST website on "Atomic Displacement Metrology" was in late 2007. It now appears that Lawall's Fabry-Pérot instrument has either been cannibalized or been diverted to another project, based on the following passage that appears in a FY2008 Small Business Innovation Research Program Solicitation:[1371] "NIST is determined to maintain the leadership position in capacitance metrology and is currently conducting research to develop an automated calculable capacitor employing a **tunable-laser-based Fabry-Pérot interferometer**[1372] that was **previously used in the NIST Atomic Displacement Metrology project**. The absolute uncertainty of this best-in-the-world interferometer for 1D linear translation measurements is **below 10 pm**, allowing it to potentially reduce the size of the calculable capacitor by two orders of magnitude, in addition to automation enabled by the tunable laser." Lawall is now measuring mirror curvature radii very accurately using Fabry-Pérot interferometry.[1373]

[1370] J. Lawall, "Interferometry for accurate displacement metrology," Opt. Photonics News 15(2004):40-45. J.R. Lawall, "Fabry-Perot metrology for displacements up to 50 mm," J. Optical Soc. Amer. A 22(December 2005):2786-2798; http://www.opticsinfobase.org/abstract.cfm?URI=josaa-22-12-2786 . See also: "Physicists measure 'long' distances with picometer accuracy," 2 December 2005; http://www.physorg.com/news8668.html.

[1371] "9.07.1-1.R 3D Laser Interferometer for Nanometrology," Small Business Innovation Research, PROGRAM SOLICITATION, FY 2008, NIST - 08 - SBIR – R; http://tsapps.nist.gov/ts_sbir//fy08%20sbir%20r.doc.

[1372] J.R. Lawall, "Fabry-Perot metrology for displacements up to 50 mm," J. Optical Soc. Amer. A 22(December 2005):2786-2798; http://www.opticsinfobase.org/abstract.cfm?URI=josaa-22-12-2786 . See also: "Physicists measure 'long' distances with picometer accuracy," 2 December 2005; http://www.physorg.com/news8668.html.

[1373] John R. Lawall, "High resolution determination of radii of curvature using Fabry-Perot interferometry," Meas. Sci. Technol. 20(2009):045302.

Nanometrology work is still continuing at NIST, e.g., as reported for their "Atom-based Dimensional Metrology" effort which is part of their Next-Generation Nanometrology (NGN) Program within the Precision Engineering Division's program in NIST's Manufacturing Engineering Laboratory. Some relevant extracts from the pdf document[1374] of the NGN Program at NIST are as follows:

(p. 40): The ultimate future for nanoscale dimensional metrology is to develop intrinsic standards based on **integral numbers of atom spacings** within an ordered, crystalline lattice. Single-atom step height standards have been fabricated and calibrated; ...

(p. 41): Two complex multi chamber vacuum STM imaging facilities are used in this effort. The first system is a **five chamber ultra high vacuum (UHV) facility** regularly capable of producing 133 x 10^{-10} Pa (1 x 10^{-10} torr) base pressures, along with **vibration isolation that yields a subangstrom noise floor**. The other system has a FIFEM (Field-Ion/Field-Electron Microscope), which is used to image scanned probe tips on the atomic scale; this has become an essential tool for atomic resolution work as well as more recent linewidth metrology work. This system also has an STM equipped with UHV interferometry in the first application of a direct atomic imaging system with interferometry.

(p. 41): Develop atom-based fabrication techniques for the sub-5 nm to atomic scale critical dimension domain.

(p. 42): Accomplishments: Recent collaborations with leading university and nanotechnology manufacturing concerns have recently evolved to a long term funded structure aimed at commercialization of advanced single and **multi probe metrology and fabrication techniques**. Planned Future Accomplishments: Demonstrate new methods for nanofabrication of silicon based structures on the nanometer scale. This includes the investigation of Si(100) for enhanced and repeatable nanomanufacturing of features with sub-10 nm dimensions. (Completed by 4th Quarter 2010) Customers and Collaborators: **Zyvex** and University of Illinois.

As of 2007-9, Michael Postek was head of the Precision Engineering Division (PED), John Kramar was the head of the Nanoscale Metrology Group within PED, and John Lawall was still active at NIST – but one or more of them might already have contractual relations with Zyvex.

4.6.4.2 Tunable-Laser FP Interferometer at NIST (Lawall, U.S.)

As noted earlier (Section 4.6.4.1), in 2005 John Lawall's group at NIST reported[1375] operating a UHV-based tunable-laser-based Fabry-Pérot interferometer able to measure **25-50 mm**

[1374] "Next-Generation Nanometrology (NGN) Program," NIST, 2008; http://www.mel.nist.gov/programs/ngn.pdf.

[1375] J.R. Lawall, "Fabry-Perot metrology for displacements up to 50 mm," J. Optical Soc. Amer. A 22(December 2005):2786-2798; http://www.opticsinfobase.org/abstract.cfm?URI=josaa-22-12-2786 . See also: "Physicists measure 'long' distances with picometer accuracy," 2 December 2005; http://www.physorg.com/news8668.html.

displacements to within 0.1 Å (**10 pm**) accuracy. The following are some details on this important work.

Typically in a Michelson interferometer, optical laser light is used to measure distances by counting the number of wavelengths (the distance between successive peaks of the wave pattern, or fringes) of light between two points. This basic method is intrinsically accurate to distances on the order of the wavelength, typically 633 nm for the red light most often used. A more precise method employed by the Lawall group[1376] uses Fabry-Pérot interferometry and measures the frequency of the laser light rather than the wavelength. In Lawall's apparatus (Figure 4-91), the laser light is introduced into the chamber through an optical fiber where it is stored between two highly reflective mirrors which form an optical cavity – creating the optical analog of an organ pipe. The length of an organ pipe can be measured by driving the pipe with sound waves of a known frequency (pitch). The sound emitted by the organ pipe is loudest when it is driven at one of its "natural" or resonance frequencies, commonly called harmonics – when one or more of these frequencies is identified, the pipe length can be determined. Similarly in the NIST work, light is transmitted through both mirrors only when the frequency of the light matches a specific harmonic frequency that can be used to determine the distance between the mirrors. While this approach has been used previously[1377] for the measurement of short distances (i.e., ~1 micron), the new work extends this capability 25,000-fold by demonstrating a range of 25 millimeters. (Ultimately, the design should accommodate a range of up to 50 mm.) Also, Lawall's method excites two harmonics of the optical system, rather than one, a redundancy that increases the range while achieving picometer accuracy.

More technical details are below, but first we note the abstract:[1378] "A system designed to apply Fabry-Pérot interferometry to the measurement of displacements is described. Two adjacent modes of a Fabry-Pérot cavity are probed, and both the absolute optical frequencies and their difference are used to determine displacements via changes in cavity length. Light is coupled to the cavity via an optical fiber, making the system ideal for remote sensing applications. Continuous interrogation is not necessary, as the cavity length is encoded in the Free Spectral Range (FSR). (Recall from Section 2.3.1.3.1 that the FSR is defined as the frequency difference per mode, as measured between two longitudinal frequency modes of the FP cavity, and is typically a few GHz in optical FP setups.) The absolute uncertainty is determined to be below 10 pm, which for the largest displacement measured corresponds to a relative uncertainty of 4×10^{-10}, the smallest relative uncertainty in a displacement measurement ever demonstrated."

[1376] J.R. Lawall, "Fabry-Perot metrology for displacements up to 50 mm," J. Optical Soc. Amer. A 22(December 2005):2786-2798; http://www.opticsinfobase.org/abstract.cfm?URI=josaa-22-12-2786 . See also: "Physicists measure 'long' distances with picometer accuracy," 2 December 2005; http://www.physorg.com/news8668.html.

[1377] "Technical Activities 2000," Atomic Physics Division, 2000; http://physics.nist.gov/TechAct.2000/Div842/div842.html (online April 2001).

[1378] J.R. Lawall, "Fabry-Perot metrology for displacements up to 50 mm," J. Optical Soc. Amer. A 22(December 2005):2786-2798; http://www.opticsinfobase.org/abstract.cfm?URI=josaa-22-12-2786 . See also: "Physicists measure 'long' distances with picometer accuracy," 2 December 2005; http://www.physorg.com/news8668.html.

Figure 4-91. Fabry-Pérot interferometer in vacuum chamber at NIST is used to measure millimeter distances to picometer accuracy. Laser light is sent into the chamber through an optical fiber and stored between two highly reflective mirrors (left and bottom arrows), which form an optical cavity. By measuring the frequency of the light, which is tuned to match specific properties of the cavity, changes can be detected in the lower mirror's position with picometer accuracy. Image from J. Lawall/NIST.[1379]

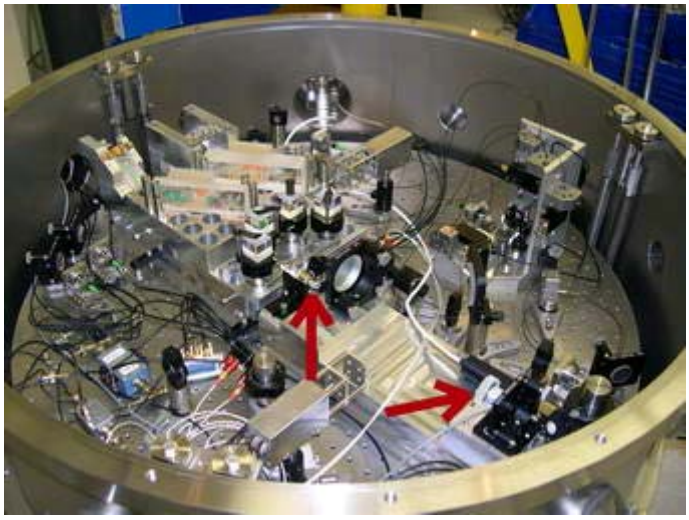

This system should be adaptable to a molecular workstation design because: (1) the system imports metrological light through a single flexible optical fiber, (2) the Fabry-Pérot cavity is geometrically open (i.e., no physical side walls are needed to form the "cavity"), and (3) one of the two mirrors that forms the cavity could be affixed to a moving AFM tip-positioner mechanism.

Lawall notes several additional benefits of the Fabry-Pérot approach:[1380] "The Fabry-Pérot interferometer is particularly attractive because of its intrinsic high resolution and the fact that the displacement measured is precisely defined by the distance between two parallel mirrors, independent of an external reference interferometer arm and not involving a beam splitter in the optical path." Fabry-Pérot interferometers have already been applied to SPMs, traditionally to

---

[1379] J.R. Lawall, "Fabry-Perot metrology for displacements up to 50 mm," J. Optical Soc. Amer. A 22(December 2005):2786-2798; http://www.opticsinfobase.org/abstract.cfm?URI=josaa-22-12-2786 . See also: "Physicists measure 'long' distances with picometer accuracy," 2 December 2005; http://www.physorg.com/news8668.html.

[1380] J.R. Lawall, "Fabry-Perot metrology for displacements up to 50 mm," J. Optical Soc. Amer. A 22(December 2005):2786-2798; http://www.opticsinfobase.org/abstract.cfm?URI=josaa-22-12-2786 . See also: "Physicists measure 'long' distances with picometer accuracy," 2 December 2005; http://www.physorg.com/news8668.html

measure very small displacements, e.g., inside tunneling microscopes.[1381] The Fabry-Pérot approach presents additional opportunities not available in a more traditional two-beam interferometer. Lawall's system measures displacements using both the shift in the frequency of an individual Fabry-Pérot resonance and the shift in the difference frequency between two adjacent resonances, with the inherent measurement redundancy providing an important check on systematic errors. From the standpoint of ultimate accuracy, use of a Fabry-Pérot cavity offers exquisite control of the spatial mode of the light, and thus allows for better control of diffraction than in the two-beam case.

Perhaps most important for molecular workstation design, in Lawall's system the frequency difference between resonances encodes absolute distance information – so this approach is uniquely suited to applications where the light might be blocked or extinguished during the motion of a cavity mirror (which could give the workstation designers more flexibility), or in which the target undergoes temporary rapid accelerations (as is likely for workstation components during tool changeout and related operations). This is in stark contrast to a two-beam interferometer in which the measured displacement is proportional to the number of fringes counted, and so even a momentary lapse in optical signal cannot be tolerated.

Lawall[1382] explains the technical principle of operation of the tunable-laser Fabry-Pérot interferometer as follows. The transmission spectrum of a Fabry-Pérot cavity of length L is a set of Airy peaks separated by the cavity free spectral range, approximately equal to c/(2L). The finesse F of the cavity is defined as the ratio of the free spectral range to the width (FWHM) of the peaks (see prior definition of finesse in Section 2.3.1.3.1; Figure 2-31C). Alternatively, if the length of the cavity is swept, transmission of light with fixed wavelength λ will occur every time the cavity length becomes an integral multiple of $\lambda/2$, and the FWHM of the transmission as a function of the length will be $\lambda/(2F)$. Recalling that every fringe in a two-beam interferometer corresponds to a displacement of $\lambda/2$, it is apparent that the resolution of a Fabry-Pérot instrument is intrinsically higher by a factor of F, which may exceed 100,000. This resolution comes at the price of speed, of course, since it depends on the interference of light that has made many round trips within the cavity. More significant for applications, however, is the fact that over most of the scan of the cavity length no light is transmitted and thus no information is furnished. The cavity provides highly accurate markers of $\lambda/2$ but nothing more.

More versatility can be achieved by coupling light from a tunable laser into the cavity. In this formulation, a tunable laser is locked to a cavity resonance via a feedback control circuit. When the cavity length changes, the laser frequency automatically follows the cavity mode frequency, and the displacement is inferred from the change in laser frequency (Figure 4-92). The range over which the cavity length can be changed, however, is limited by the tuning range of the tunable laser, and is in general quite small. To extend the measurement range, the system

---

[1381] L. Howard, J. Stone, J. Fu, "Real-time displacement measurements with a Fabry-Perot cavity and a diode laser," Precis. Eng. 25(October 2001):321-335.

[1382] J.R. Lawall, "Fabry-Perot metrology for displacements up to 50 mm," J. Optical Soc. Amer. A 22(December 2005):2786-2798; http://www.opticsinfobase.org/abstract.cfm?URI=josaa-22-12-2786 . See also: "Physicists measure 'long' distances with picometer accuracy," 2 December 2005; http://www.physorg.com/news8668.html

employs simultaneous interrogation of two adjacent cavity modes (neighboring cavity resonance frequencies along the optical spectrum).

Figure 4-92. <u>Left</u>: Layout of laser system: B.E., beam expander; OI, (Faraday) optical isolator; VCO, voltage controlled oscillator; AOM, acousto-optic modulator; EOM, electro-optic modulator; BS, beam splitter; PBS, polarizing beam splitter; SMPM, single-mode polarization maintaining. <u>Right</u>: Scanning Fabry-Pérot cavity, optical elements for mode matching light into the cavity, and detectors; all equipment is built on a vibration-isolated platform in vacuum.[1383]

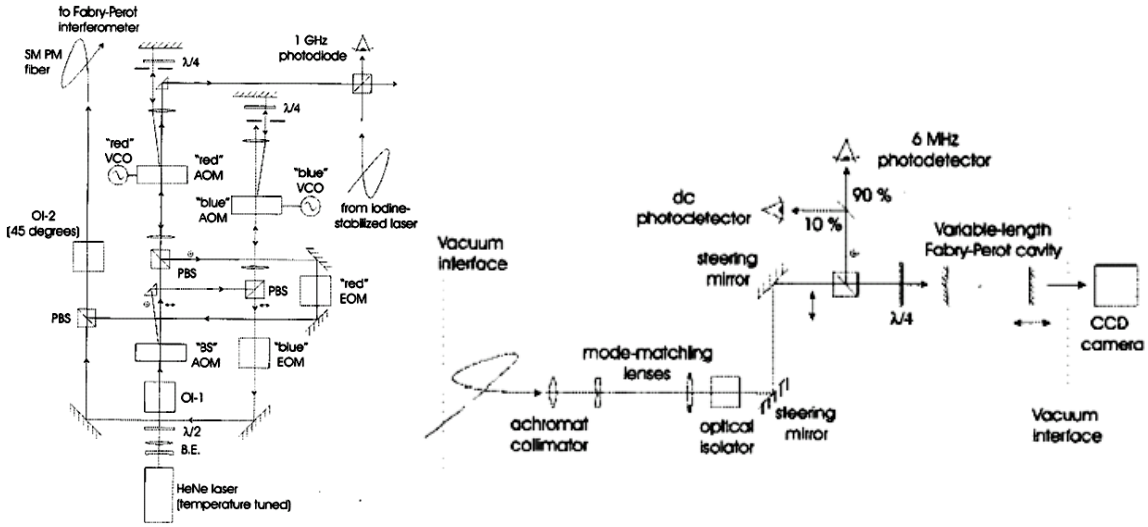

Early work along these lines was proposed in 1971 by Bay[1384] and carried out in 1996 by Dunn and co-workers.[1385] As the cavity length changes, not only do the optical frequencies of both of the resonances change, but the difference between the two resonances changes as well. Keeping track of the frequency difference alone is sufficient in this work to measure displacement with an uncertainty of the order of 20 nm without being limited by the tuning range of the tunable laser. When the information contained in the frequency difference is combined with that of the optical displacement of an individual mode, the mechanical change in the cavity length can be monitored over a very long range while maintaining the full resolution of the Fabry-Pérot technique. Lawall's particular system is designed to interrogate a scanning cavity (Figure 4-92) whose

---

[1383] J.R. Lawall, "Fabry-Perot metrology for displacements up to 50 mm," J. Optical Soc. Amer. A 22(December 2005):2786-2798; http://www.opticsinfobase.org/abstract.cfm?URI=josaa-22-12-2786 . See also: "Physicists measure 'long' distances with picometer accuracy," 2 December 2005; http://www.physorg.com/news8668.html.

[1384] Z. Bay, "The use of microwave modulation of lasers for length measurements," Natl. Bur. Stand. (U.S.) Spec. Publ. 343(1971):59-62.

[1385] T.J. Dunn, T.-M. Lee, K. Jain, "Absolute distance measurement interferometry for alignment systems for advanced lithography tools," J. Vac. Sci. Technol. B 14(1996):3960-3963.

length changes over the range of 180 mm to 230 mm (total **50 mm span**) and provides an absolute uncertainty of below **10 pm**, limited largely by the iodine-stabilized reference laser that provides an absolute frequency reference with a fractional uncertainty of 2.5×10^{-11}. If data can be taken fast enough to permit a 20 Hz stepping speed,[1386] then at 10 pm/step the system could be continuously stepped at ~0.2 nm/sec – though continuous stepping is not required to establish the absolute distance traveled. However, to use this system in a molecular workstation the typical cavity resonance frequency drift rate of 39 kHz/sec, corresponding to about 17 pm/sec, must be significantly reduced. For comparison, the COXI system described in Section 4.6.2.1 had a far lower typical drift rate of ±13 pm in 400 sec.

To measure displacement with a Fabry-Pérot cavity, one of the mirrors must be flat to have a unique normal, which defines the measurement direction. The other mirror must then be curved, so that the cavity supports stable modes. For the NIST device, light is injected into the fixed Fabry-Pérot mirror which has a nominal radius of curvature of R = 1.0 m, a reflectivity R_1 = 99.7% at 633 nm, and an incident surface that is antireflection coated. The output mirror is flat, with a high reflector (R_2 = 99.993%) coating. (The transmission of the first mirror will dominate the cavity losses and thus largely determine the finesse.) The exit surface of the output mirror is antireflection coated and the substrate incorporates a slight wedge to minimize parasitic optical resonances. It is mounted to a piezoelectrically activated fine positioning stage providing translational control over a range of 6 microns as well as control of pitch and yaw (though the angular degrees of freedom are not used in this work). The fine-positioning stage is itself mounted atop a one-dimensional positioning stage employing an inchworm motor with a range of 25 mm.

In collaboration with the private company Hytec,[1387] Lawall also designed and built a vibration-isolated UHV platform for the entire tunable-laser Fabry-Pérot interferometer system. According to the abstract:[1388] "The system provides isolation from both seismic and acoustic disturbances with a residual acceleration of 2.9×10^{-6} m/s^2 rms (root-mean-square) in the vertical direction and 6.3×10^{-6} m/s^2 rms in the horizontal in the bandwidth from 5 to 400 Hz. The environmental decoupling provided by the spring suspension, air-spring table legs, and vacuum are evaluated sequentially to illustrate the effects of each. The vibration contributed by the turbomolecular pump is measured and shown to fall into a low-frequency zone from 26 to 76 Hz as well as peaks at the pump rotation frequency of 820 Hz and its harmonic at 1.64 kHz. The low-frequency noise arising from the pump is less than 2% of the total residual acceleration in the bandwidth from 0.25 to 400 Hz. The platform is used to construct a high-finesse open-cavity Fabry-Pérot interferometer, using standard commercial mounts, with relative motion below 2 pm rms in a 3 kHz bandwidth. Of this motion, the contribution due to the pump at 820 Hz is only 0.3 pm. The

---

[1386] J.R. Lawall, "Fabry-Perot metrology for displacements up to 50 mm," J. Optical Soc. Amer. A 22(December 2005):2786-2798; http://www.opticsinfobase.org/abstract.cfm?URI=josaa-22-12-2786 . See also: "Physicists measure 'long' distances with picometer accuracy," 2 December 2005; http://www.physorg.com/news8668.html. 645.

[1387] Hytec Inc. http://hytecinc.com/hei/adm.html.

[1388] J. Lawall, E. Kessler, "Design and Evaluation of a Simple Ultra Low Vibration Vacuum Environment," Rev. Sci. Instrum. 73(January 2002):209-215.

acoustic decoupling provided by the vacuum environment allows experiments that are prohibitive at atmospheric pressure even in a tightly sealed enclosure."

4.6.4.3 Tunable-Laser FP Interferometer at NIST (Howard, U.S.)

The laser-frequency-based displacement measurement method has no periodic errors and it can measure displacements with picometer resolution and accuracy. In this method, the optical frequency of a tunable laser is locked to one of the resonances of a Fabry-Pérot (FP) cavity with one of its mirrors connected to the element whose displacement is to be measured. The displacement is then converted into an optical frequency change, and this frequency change is measured using a reference laser. This method has been used in displacement sensor calibration systems[1389] and STMs (a Michelson setup)[1390] (Section 4.6.3.2). However, the dynamic ranges of these systems are limited to the measurement range of the optical frequency change. Traditionally, the measurement range of the optical frequency change was limited to several GHz around the reference laser, which limits the displacement measurement range to typically less than 1 μm. To expand the displacement measurement range, the mode change scheme of the FP cavity was utilized by Brand and Herrmann[1391] and Haitjema et al.,[1392] while Howard et al.[1393] (see below) used an external cavity diode laser with a tuning range sufficiently wide (20 GHz) to avoid mode-jumping behavior of the laser-locking system.

In 2001, Howard et al.[1394] at NIST described a system in which a tunable external cavity diode laser system is servo-locked to a Fabry-Pérot interferometer cavity. Their system had a measurement bandwidth of 100 Hz and a resolution of **tens of picometers**. It was used to measure the nonlinearity in a heterodyne optical interferometer and for measurement of Z-axis displacements of an atomic force microscope with a 60 pm noise level for the combined AFM/interferometer system.

[1389] L. Howard, J. Stone, J. Fu, "Real-time displacement measurements with a Fabry-Perot cavity and a diode laser," Precis. Eng. 25(October 2001):321-335. 663. 664. 665.

[1390] R.M. Silver, H. Zhou, S. Gonda, B. Damazo, J. Jun, C. Jensen, L. Howard, "Atomic-resolution measurements with a new tunable diode laser-based interferometer," Opt. Eng. 43(2004):79-86.

[1391] U. Brand, K. Herrmann, "A laser measurement system for the high-precision calibration of displacement transducers," Meas. Sci. Technol. 7(1996):911-917.

[1392] H. Haitjema, P.H.J. Schellekens, S.F.C.L. Wetzels, "Calibration of displacement sensors up to 300 μm with nanometer accuracy and direct traceability to a primary standard of length," Metrologia 37(2000):25-33.

[1393] L. Howard, J. Stone, J. Fu, "Real-time displacement measurements with a Fabry-Perot cavity and a diode laser," Precis. Eng. 25(October 2001):321-335.

[1394] L. Howard, J. Stone, J. Fu, "Real-time displacement measurements with a Fabry-Perot cavity and a diode laser," Precis. Eng. 25(October 2001):321-335.

Note the authors:[1395] "We present the basic operating principles of a traceable measurement system suitable for use with atomic force microscopes (AFMs) and nanometer-resolution displacement sensors. Our method is based upon a tunable external-cavity diode laser system which is servo-locked via a phase-modulated heterodyne locking technique to a Fabry-Pérot interferometer cavity. We discuss mechanical considerations for the use of this cavity as a displacement metrology system and we describe methods for making real-time (<10 ms sampling period) measurements of the optical heterodyne signals. Our interferometer system produces a root-mean-squared (RMS) displacement measurement resolution of **20 pm**. Two applications of the system are described. First, the system was used to examine known optical mixing errors in a heterodyne Michelson interferometer. Second, the Fabry-Pérot interferometer was integrated into the Z-axis of a commercial AFM scanning stage and used to produce interferometer-based images of a 17 nm step height specimen. We also demonstrate atomic resolution interferometer-based images of a 0.3 nm silicon single atomic step-terrace specimen."

Figure 4-93 illustrates the basic components necessary to implement a Fabry-Pérot interferometer for measuring small displacements on the order of picometers using a laser locked to a Fabry-Pérot cavity. This cavity is the heart of the system – "a specially constructed Fabry-Pérot interferometer that allows easy access to the moving mirror which is constrained to move in a linear fashion along the Z direction defined by the metrology block flexure stage. A tracking laser illuminates the Fabry-Pérot cavity. The tracking laser is tunable over a frequency range which must be broader than the free spectral range (FSR) of the Fabry-Pérot cavity. An optical tuning discriminator generates an error signal that is used to tune the tracking laser so as to maintain a resonance condition in the Fabry-Pérot cavity. Part of the light from the tracking laser is optically heterodyned with light from a fixed frequency local oscillator laser. The difference, or beat frequency, between the two lasers is produced by light impinging on a high-speed photodetector and is sent to the frequency counter for measurement. The beat frequency is a measurand that can represent the displacement of the moving mirror and thus calibrate a device under test, such as a scanned probe microscope or a high-resolution transducer."[1396]

The uncertainty budget is given in Table 4-7. The authors claim a displacement measurement uncertainty of 20 pm, and it is true that the interferometric errors alone are down around 20 pm. However, in the actual working system there are several additional errors that must be dealt with, including thermomechanical error (120 pm), cosine error (60-600 pm), FSR measurement (50-500 pm), and Abbe error (100-1000 pm). (If applied to the molecular workstation, the reported refractive index errors disappear because we're operating our system in vacuum, unlike Howard et al. whose system is operating in air.) For their diode laser Fabry-Pérot interferometer, Howard et al.[1397] estimated the standard measurement uncertainty components as shown in Table 4-7. For a total tip displacement of Δl = 100 nm, these 11 error sources total up to 403 pm, or 352 pm in

---

[1395] L. Howard, J. Stone, J. Fu, "Real-time displacement measurements with a Fabry-Perot cavity and a diode laser," Precis. Eng. 25(October 2001):321-335.

[1396] L. Howard, J. Stone, J. Fu, "Real-time displacement measurements with a Fabry-Perot cavity and a diode laser," Precis. Eng. 25(October 2001):321-335.

[1397] L. Howard, J. Stone, J. Fu, "Real-time displacement measurements with a Fabry-Perot cavity and a diode laser," Precis. Eng. 25(October 2001):321-335.

vacuum – e.g., about twice as large as the total 158.59 pm estimated for the Silver group's interferometer described in Section 4.6.3.2 (Table 4-6). These total uncertainties are about an order of magnitude too large and would have to be reduced before these systems could be considered for use in a successful DMS molecular workstation. In a personal correspondence in late 2008, Howard noted that "those papers represent old work that is no longer representative of the current art. **In general, 1 pm interferometric sensing and control can be performed using almost totally off-the-shelf equipment now.**"

Figure 4-93. Simplified block diagram of the diode laser nanometrology system showing major components necessary for operation.[1398]

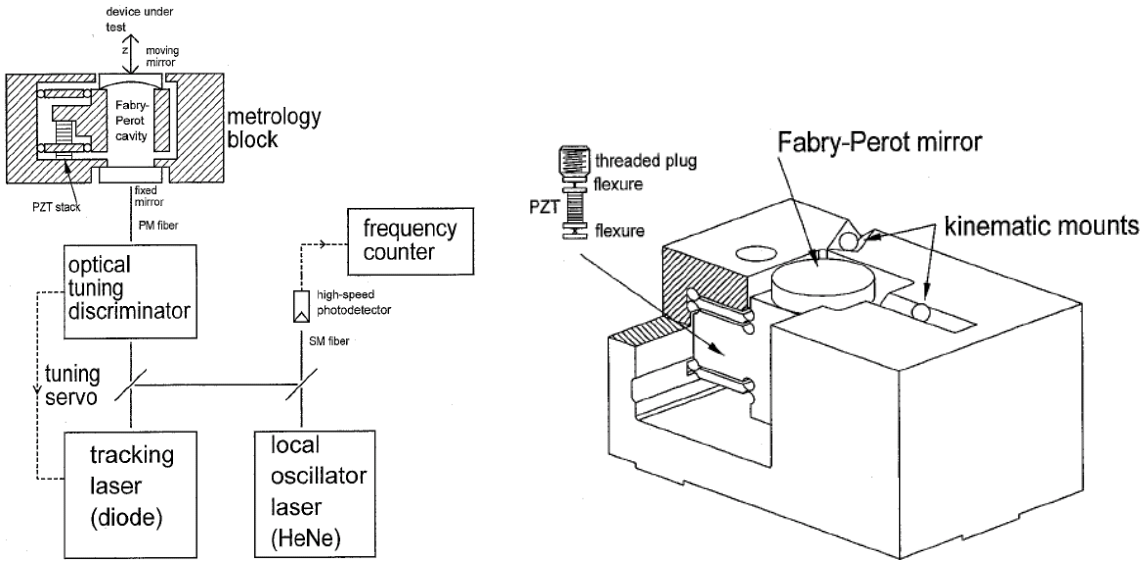

[1398] L. Howard, J. Stone, J. Fu, "Real-time displacement measurements with a Fabry-Perot cavity and a diode laser," Precis. Eng. 25(October 2001):321-335.

Table 4-7. Uncertainty budget for the diode laser Fabry-Pérot interferometer system when used for two displacement ranges; all entries except last row are estimated standard uncertainties.[1399]

Source of standard uncertainty	Displacement of 1 μm	Displacement of 100 nm
Frequency measurement	<0.001 nm	<0.001 nm
Reference laser noise	0.016 nm	0.016 nm
Cavity locking servo noise	0.005 nm	0.005 nm
Thermomechanical	0.12 nm	0.12 nm
Cosine error	0.6 nm	0.06 nm
Abbe error	1 nm	0.1 nm
FSR measurement	0.5 nm	0.05 nm
Refractive index (n)	<0.001 nm	<0.001 nm
Refractive index measurement noise and hysteresis (Δn)	0.05 nm	0.05 nm
Quadrature summation	1.3 nm	0.18 nm
Expanded uncertainty (k = 2)	2.5 nm	0.36 nm

The molecular workstation also will require applying the positioning system to AFMs having multiple DOFs. Howard and LeBrun (Section 4.5.1) have worked together on the design and performance evaluation of a six-degree-of-freedom piezoelectrically actuated fine motion stage intended to be used for three dimensional error compensation of a long-range translation mechanism.[1400]

4.6.4.4 Tunable-Laser FP using Optical Frequency Combs (Japan)

In 2006, Bitou et al.[1401] developed a new laser-frequency-based displacement measurement system with sub-nanometer uncertainty using an optical frequency comb[1402] generator, consisting of an electro-optic modulator (EOM) placed inside an optical resonator. In this method, the optical frequency of a tunable laser is locked to the resonance of a Fabry-Pérot cavity. One of the

---

[1399] L. Howard, J. Stone, J. Fu, "Real-time displacement measurements with a Fabry-Perot cavity and a diode laser," Precis. Eng. 25(October 2001):321-335.

[1400] Richard M. Seugling, Thomas LeBrun, Stuart T. Smith, Lowell P. Howard, "A six-degree-of-freedom precision motion stage," Rev. Sci. Instrum. 73(2002):2462-2468.

[1401] Youichi Bitou, Thomas R. Schibli, Kaoru Minoshima, "Accurate wide-range displacement measurement using tunable diode laser and optical frequency comb generator," Opt. Express 14(2006):644-654; http://www.opticsinfobase.org/oe/abstract.cfm?URI=oe-14-2-644.

[1402] Mode-locked lasers produce a series of optical pulses separated in time by the round-trip time of the laser cavity. The spectrum of such a pulse train is a series of Dirac delta functions separated by the repetition rate (the inverse of the round trip time) of the laser. The series of sharp spectral lines that are thus formed is called a "frequency comb".

two mirrors of this Fabry-Pérot cavity is connected to the element whose displacement is to be measured. The optical frequency measurement range can be expanded to several hundreds of GHz using such an optical frequency comb generator,[1403] allowing the authors to measure displacements of more than **10 µm range** with **220 pm uncertainty** without changing the mode of the FP cavity by combining the optical frequency comb and a widely tunable CW laser. A theoretical analysis showed that the first-order effects of the dispersion due to the wide-range-optical-frequency-tuning could be neglected, hence the displacement measurement range could in principle be extended without compromising the measurement accuracy.

Two-beam amplitude splitting interferometers (homodyne or heterodyne interferometers) provide the capability to measure large displacements with resolutions reaching sub-nanometer level. However, substantial efforts have to be undertaken to avoid an intrinsic problem of all two-beam interferometers: nonlinear errors (cyclic errors) in the detection system. These non-linear errors are naturally caused by optical crosstalk or imperfections in the quadrature detection system commonly used in two beam interferometers.[1404] Fabry-Pérot (FP) cavity based displacement measurements are an interesting alternative to the homodyne and heterodyne two-beam interferometers because they can overcome some of the limitations of two-beam interferometers, namely, the aforementioned non-linear errors and the limited sensitivity or resolution of most two-beam interferometers. Avoidance of non-linear errors is achieved by tracking the center of the FP resonance rather than the sinusoidal fringe pattern of a two-beam interferometer; the limited resolution of two-beam interferometers is achieved by employing a higher finesse of the FP cavity. Increasing the finesse of the FP cavity not only increases the resolution of the system, but it also reduces the effect of unwanted optical crosstalk by increasing the frequency selectivity of the cavity without increasing the unwanted crosstalk. Fabry-Pérot type displacement measurements do pose several technical difficulties, among them limitations in the displacement ranges and the requirement for widely and precisely tunable lasers. The limitation on range in FP systems can be addressed by using the method pioneered by Lawall[1405] (Section 4.6.4.2), which requires a vacuum system to achieve the required stability. The requirement for very wide tuning ranges was addressed by Bitou et al.[1406] who developed a frequency measurement system based

---

[1403] M. Kourogi, K. Nakagawa, M. Ohtsu, "Wide-span optical frequency comb generator for accurate optical frequency difference measurement," IEEE J. Quantum Electron. 29(1993):2693-2701. Y. Zhang, J. Ishikawa, F.-L. Hong, "Accurate frequency atlas of molecular iodine near 532 nm measured by an optical frequency comb generator," Opt. Commum. 200(2001):209-215.

[1404] C.-M. Wu, R.D. Deslattes, "Analytical modeling of the periodic nonlinearity in heterodyne interferometry," Appl. Opt. 37(1998):6696-6700. T. Keem, S. Gonda, I. Misumi, Q. Huang, and T. Kurosawa, "Removing nonlinearity of a homodyne interferometer by adjusting the gains of its quadrature detector systems," Appl. Opt. 43(2004):2443-2448.

[1405] J.R. Lawall, "Fabry-Perot metrology for displacements up to 50 mm," J. Optical Soc. Amer. A 22(December 2005):2786-2798; http://www.opticsinfobase.org/abstract.cfm?URI=josaa-22-12-2786 . See also: "Physicists measure 'long' distances with picometer accuracy," 2 December 2005; http://www.physorg.com/news8668.html.

[1406] Youichi Bitou, Thomas R. Schibli, Kaoru Minoshima, "Accurate wide-range displacement measurement using tunable diode laser and optical frequency comb generator," Opt. Express 14(2006):644-654; http://www.opticsinfobase.org/oe/abstract.cfm?URI=oe-14-2-644.

on an optical frequency comb that allowed them to achieve up to ~100 pm resolution under stable atmospheric conditions.

Figure 4-94 shows a schematic layout of the first-generation laser-frequency-based displacement measurement system using the optical frequency comb.[1407] The optical frequency of a tunable laser diode (ECLD: external cavity laser diode) tracks the resonance frequency of a FP cavity using EOM_1 (electro-optic modulator) and a lock-in amplifier. If one of the mirrors of the FP cavity is displaced, the resulting optical frequency change of the ECLD is measured by the optical frequency measurement system using a Rb-stabilized diode laser and the optical frequency comb generator.

Figure 4-94. Schematic layout of the laser-frequency-based displacement measurement system: ECLD, external cavity laser diode; PBS, polarizing beam splitter; BE, beam expander.[1408]

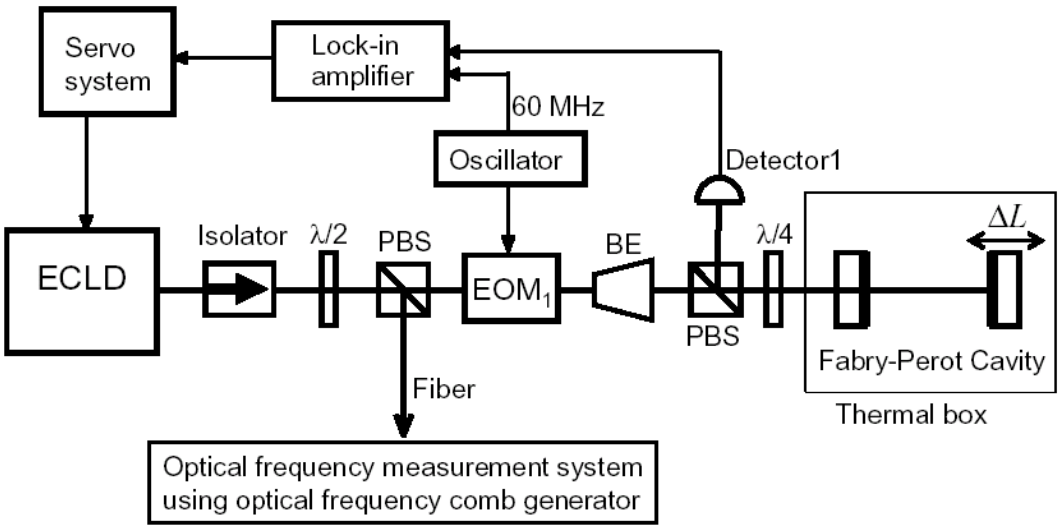

In the conventional laser-frequency-based displacement measurement method, the dispersion effect due to the optical frequency tuning was ignored because the frequency tuning range was small and the displacement ΔL was given as:[1409] $\Delta L = -(\Delta f / nf) L$, where f is the optical

---

[1407] Youichi Bitou, Thomas R. Schibli, Kaoru Minoshima, "Accurate wide-range displacement measurement using tunable diode laser and optical frequency comb generator," Opt. Express 14(2006):644-654; http://www.opticsinfobase.org/oe/abstract.cfm?URI=oe-14-2-644.

[1408] Youichi Bitou, Thomas R. Schibli, Kaoru Minoshima, "Accurate wide-range displacement measurement using tunable diode laser and optical frequency comb generator," Opt. Express 14(2006):644-654; http://www.opticsinfobase.org/oe/abstract.cfm?URI=oe-14-2-644.

[1409] L. Howard, J. Stone, J. Fu, "Real-time displacement measurements with a Fabry-Perot cavity and a diode laser," Precis. Eng. 25(October 2001):321-335.

frequency of a given longitudinal mode of the FP cavity, Δf is the optical frequency change of this mode caused by a change ΔL of the length L of the FP cavity, and n is the refractive index of the air at f (= 1 in vacuum). Knowing the optical frequency f and its change Δf, the refractive index, and the initial optical length of the cavity, we can determine the displacement ΔL. To obtain all values in the equation, the measurement procedure of the laser-frequency-based displacement measurement method consists of two steps. In the first step, we determine the initial optical length L of the FP cavity by measuring the free spectral range (FSR) of the cavity; in the second step, we measure the optical frequency and its change caused by the displacement.

During the measurement, f and Δf are obtained by measuring the optical frequencies of the tunable laser diode, which is locked to one of the longitudinal modes of the FP cavity, before and after the displacement using a reference laser. The refractive index n is determined from environmental data. The initial optical length L of the cavity is determined from L = c / (2 FSR), where c is the velocity of light. The FSR is obtained from an independent measurement (the first step in the measurement procedure) by measuring the optical frequency difference ΔF between different longitudinal mode numbers m_i and m_j of the FP cavity while maintaining the initial cavity length. The FSR can then be determined from FSR = $\Delta F/\Delta m$, with $\Delta m = m_j - m_i$. Usually, the relative measurement uncertainty of f and n is better than 10^{-6} and negligibly small in the determination of displacement ΔL. The measurement uncertainty of ΔF is similar to that of Δf and does not depend on the value of Δm. Therefore, the relative measurement uncertainty of FSR becomes small as Δm becomes large. In conventional optical frequency measurement systems, the measurable mode number change Δm is typically very limited. But by using the optical frequency comb system, the measurable optical frequency changes Δf and ΔF (Δm) can be expanded, and consequently the measurement range of the displacement ΔL can be extended and the measurement uncertainty of the FSR can be reduced – though in that case the dispersion effect must be properly accounted for.

In 2006 a related second-generation displacement measurement system was developed by the same research group,[1410] as illustrated schematically in Figure 4-95. This displacement measurement setup is based on two Fabry-Pérot cavities (to suppress the influence of atmospheric fluctuations) and a widely tunable wavelength generator based on a wavelength-stabilized optical fs-comb that provides wide tuning ranges with sub-10 attometer wavelength resolution. Using a wavelength stabilized laser instead of a frequency stabilized laser provides a powerful means to suppress environmental perturbations such as air-pressure or air-temperature induced changes of the refractive index of air and can achieve sub-pm resolution (ignoring, e.g., Abbe error) for displacements as large as 12 μm. The setup, when operated in air, provides <1 pm stability over 1 minute and <10 pm stability over 30 minutes without airtight enclosure of the Fabry-Pérot

---

[1410] T.R. Schibli, K. Minoshima, Y. Bitou, F. Hong, H. Inaba, A. Onae, H. Matsumoto, "Displacement Metrology Setup with Sub-pm Stability in Air Utilizing a Fs-Comb Based Wavelength Synthesizer," Paper CMY4, Conference on Lasers and Electro-Optics/Quantum Electronics and Laser Science Conference and Photonic Applications Systems Technologies, Technical Digest (CD), Optical Society of America, 2006; http://www.opticsinfobase.org/abstract.cfm?URI=CLEO-2006-CMY4. T.R. Schibli, K. Minoshima, Y. Bitou, F.-L. Hong, H. Inaba, A. Onae, H. Matsumoto, "Displacement metrology with sub-pm resolution in air based on a fs-comb wavelength synthesizer," Opt. Express 14(2006):5984-5993; http://www.opticsinfobase.org/abstract.cfm?URI=oe-14-13-5984.

cavities.[1411] (The standard deviation of all stability data over 50 hours of measurements was 47 pm.)

Figure 4-95. Experimental setup: solid and dashed lines represent optical and electrical signals, respectively. AOM: acousto-optic modulator; EOM: electro-optic modulator; PBS: polarizing beamsplitter; PZT: piezo-electric transducer; FP1/2: Fabry-Pérot cavities with a finesse ~156 on common CLEARCERAM-Z base; MISER: monolithic isolated single-mode end-pumped ring oscillator; PDH: Pound-Drever-Hall error-signal; Enclosure is not airtight but reduces airflow and rapid temperature changes; mode-matching optics for coupling to the FP cavities are not shown.[1412]

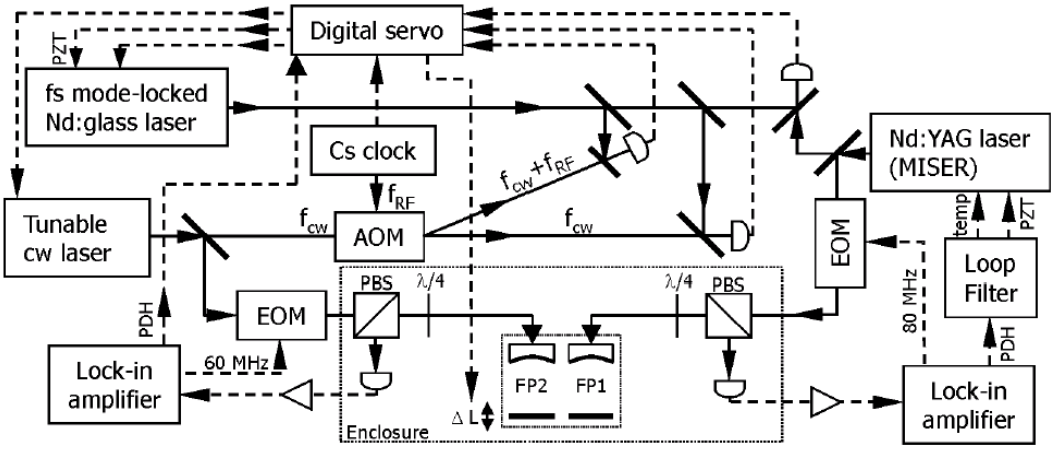

In 2009, Bitou[1413] reported an updated displacement metrology and control system using an optical frequency comb generator and a dual Fabry-Pérot cavity in which the optical frequency comb generator has expanded the displacement measurement range and the dual cavity system has suppressed the environmental fluctuation. The absolute uncertainty of the displacement measurement system was estimated as ~**190 pm** for a displacement of **14 µm**, while accurate displacement control using a phase-locked loop was demonstrated with a resolution of approximately **24 pm**.

[1411] T.R. Schibli, K. Minoshima, Y. Bitou, F.-L. Hong, H. Inaba, A. Onae, H. Matsumoto, "Displacement metrology with sub-pm resolution in air based on a fs-comb wavelength synthesizer," Opt. Express 14(2006):5984-5993; http://www.opticsinfobase.org/abstract.cfm?URI=oe-14-13-5984.

[1412] T.R. Schibli, K. Minoshima, Y. Bitou, F.-L. Hong, H. Inaba, A. Onae, H. Matsumoto, "Displacement metrology with sub-pm resolution in air based on a fs-comb wavelength synthesizer," Opt. Express 14(2006):5984-5993; http://www.opticsinfobase.org/abstract.cfm?URI=oe-14-13-5984.

[1413] Youichi Bitou, "High-accuracy displacement metrology and control using a dual Fabry-Perot cavity with an optical frequency comb generator," Precision Engineering 33(April 2009):187-193.

4.6.4.5 Fabry-Pérot 1D Metrology Platform (Haitjema group)

As of 2004, Han Haitjema was director of Mitutoyo Research Center Europe, a Japanese company located in the Netherlands. Starting in the mid-1990s when he was at PTB (Germany), then in the late 1990s while at NMi (Netherlands),[1414] he built a 1D displacement generator for nanometrology work to allow calibration of a wide variety of displacement-measuring probes such as probes of roundness testers, roughness testers, and stand-alone type scanning probe microscopes (SPMs), with a standard uncertainty below 1 nm. In his earliest set-up (Figure 4-96), a digital piezo translator (DPT) drives a flat mirror which serves as the calibration platform. This mirror is locked to an elastic, hysteresis-free, monolithic parallel guide. Calibration of the platform displacement was carried out by various methods including tunable and stabilized lasers, Fabry-Pérot interferometry and laser interferometry. The system was calibrated with a standard uncertainty of about **100 pm** using three independent methods.[1415]

Figure 4-96. <u>Left:</u> Sketch of the 1D calibration system with Fabry-Pérot set-up. <u>Right:</u> Residuals from the calibration curve for the Digital Piezo Translator.[1416]

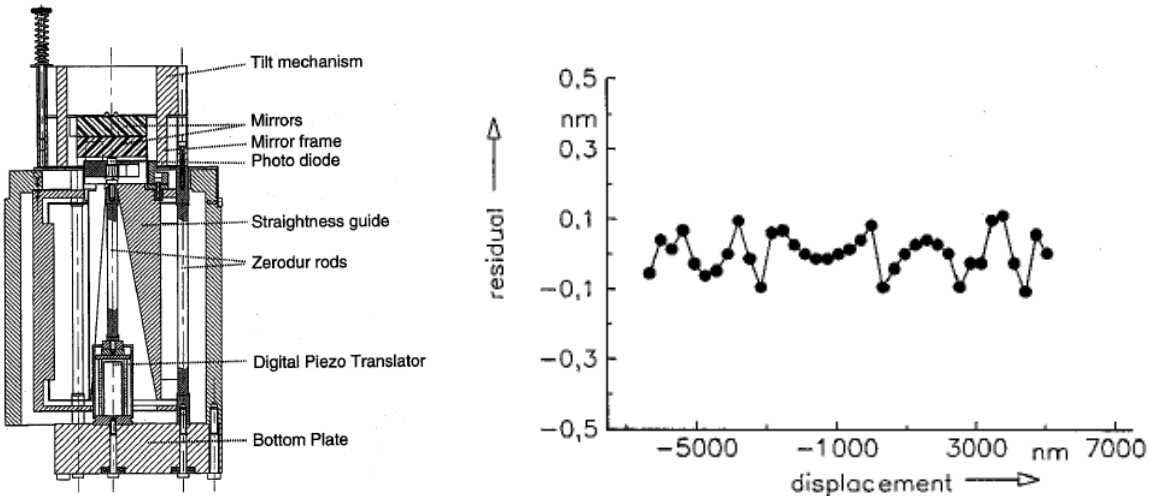

[1414] H. Haitjema, N. Rosielle, G. Kotte, Hans Steijaert, "A universal parallel-moving platform for nano-metrology," PTB-Mitteilungen 6(1997):417-419. Han Haitjema, Nick Rosielle, Gerard Kotte, Hans Steijaert, "Design and calibration of a parallel-moving displacement generator for nano-metrology," Measurement Science and Technology 9(July 1998):1098-1104.

[1415] Han Haitjema, Nick Rosielle, Gerard Kotte, Hans Steijaert, "Design and calibration of a parallel-moving displacement generator for nano-metrology," Measurement Science and Technology 9(July 1998):1098-1104.

[1416] H. Haitjema, N. Rosielle, G. Kotte, Hans Steijaert, "A universal parallel-moving platform for nano-metrology," PTB-Mitteilungen 6(1997):417-419.

In 2000 Haitjema et al.[1417] created an instrument to calibrate nanometer displacement sensors using a Fabry-Pérot cavity. One mirror of this cavity generates the required displacement. A so-called slave laser is stabilized to the cavity length. The frequency of this slave laser is compared with the frequency of a primary length standard. In this way the displacement is measured with a resolution of a few picometers, a range of 300 µm and an uncertainty of about **1 nm**. In 2008 Haitjema was still publishing on the topic of sub-nanometer uncertainty using interferometry-based nanometrology,[1418] but it was unknown if further progress had been made on his 1-D FP metrology platform.

4.6.4.6 Combined Optical Interferometer (BUPE Project, S. Korea)

During 1999-2003, the South Korean scientific organization KAIST (Korean Advanced Institute of Science and Technology) sponsored the Billionth Uncertainty Precision Engineering (BUPE) Project,[1419] with the specific goal of achieving the systematized ability of ultra-precision positioning with an accuracy of **1 nm** over large working volumes of up to 1 meter on a side.[1420] The "billionth uncertainty" represents the ratio of one nanometer accuracy to a one meter working range, whereas in the late 1990s the best level achievable around the world was ~10^{-6} relative uncertainty in nanoscale measurement technologies (Figure 4-97).

BUPE had three working groups, and their ultimate goal of one billionth uncertainty precision engineering was scheduled to be accomplished within a total period of nine years – measuring from the earliest publication/meeting date of 1999, the completion of the project was envisioned by 2007. (The program may have been terminated early because no publications or other records pertaining to BUPE could be found online more recent than 2003.) BUPE was led by Professor Seung-Woo Kim, and included 19 researchers (3 PhD, 8 MA, 8 BS) with a total budget of 900 million won ($0.75M) for 2003. If the program lasted 5 years before it was cancelled, the total expenditure on BUPE was probably around $3.75M.

[1417] H. Haitjema, P.H.J. Schellekens, S.F.C.L. Wetzels, "Calibration of displacement sensors up to 300 µm with nanometer accuracy and direct traceability to a primary standard of length," Metrologia 37(2000):25-33.

[1418] Han Haitjema, "Achieving traceability and sub-nanometer uncertainty using interferometric techniques," Meas. Sci. Technol. 19(2008):084002.

[1419] "Annual Report 2003," KAIST, http://pem.kaist.ac.kr/bupe/Annual%20Accomplishments%20for%20FY%202003.htm.

[1420] Seung-Woo Kim, ¡°New design of precision CMM based on phase-measuring volumetric interferometry," Annals of CIRP 51/1(2001):357-360; http://pem.kaist.ac.kr/bupe/publications/New%20design%20of%20precision_CF.pdf. Min-Seok Kim, Seung-Woo Kim, "Two-Longitudinal mode He-Ne laser for heterodyne interferometry of displacement measurement," Applied Optics 41(1 October 2002):5938-5942; http://pem.kaist.ac.kr/bupe/publications/Two-Longitudinal_Min Suk_IJ.pdf. Seung-Woo Kim, Hyug-Gyo Rhee, Ji-Young Chu, "Volumetric phase-measuring interferometer for three-dimensional coordinate metrology," Precision Engineering 27(2003):205-215.

Figure 4-97. Seven major categories of measuring principles that are considered within the scope of the billionth uncertainty precision engineering (BUPE) project, whose global objectives are to improve the currently available measuring principles and also to invent new scientific and engineering principles to achieve the ultimate goal of one-billionth uncertainty in three-dimensional metrology.[1421]

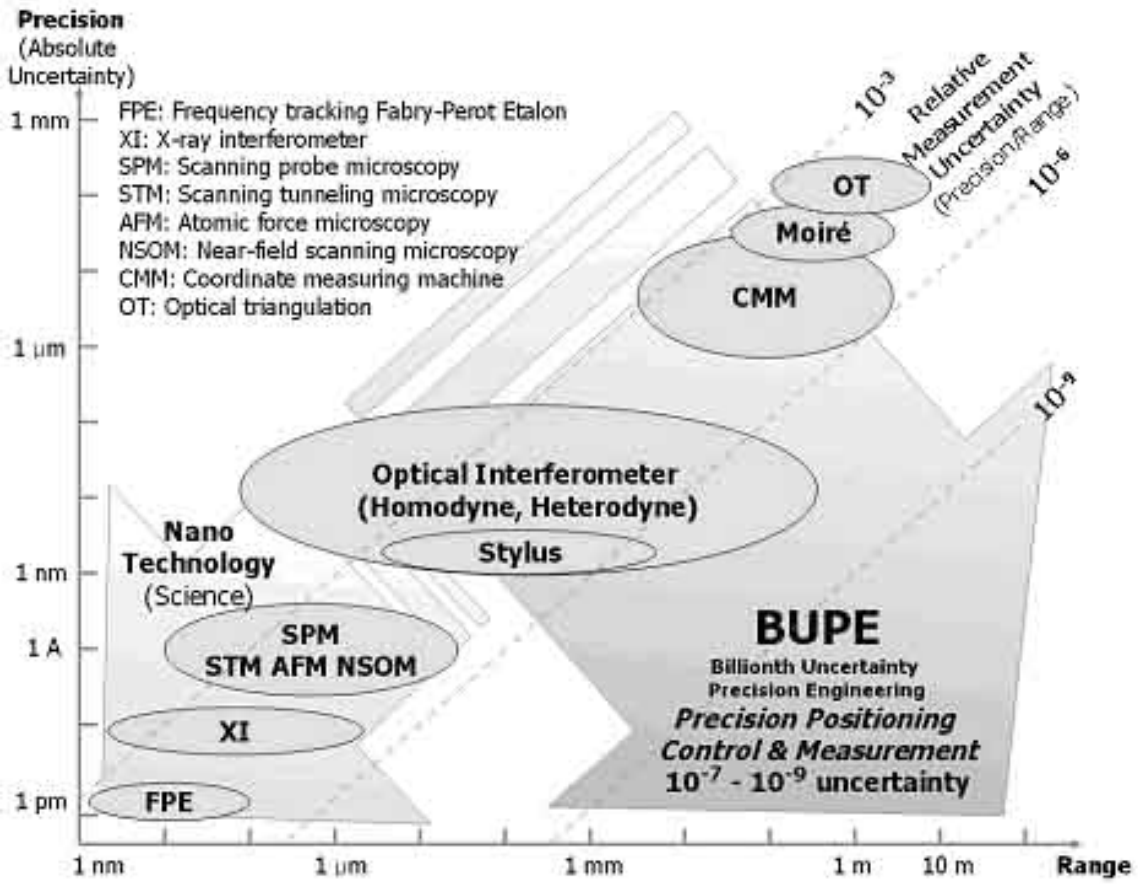

The final output of BUPE was intended to be the Ultra-Precision Coordinates Measuring Machine (UP-CMM), with objectives of the three phases of work (~3 years per phase) as outlined in Table 4-8. Note that although the UP-CMM measuring resolution was planned to reach 10 pm, the overall accuracy of the system over its entire range of motion was originally only intended to reach 1000 pm, fully 20-50 times poorer than would be needed for our molecular workstation.

[1421] "Annual Report 2003," KAIST, http://pem.kaist.ac.kr/bupe/Annual%20Accomplishments%20for%20FY%202003.htm.

Table 4-8. Objectives for realization of systems integrated technology via UP-CMM[1422]			
Performance Metric	**Phase 1 (1999-2001)**	**Phase 2 (2002-2004)**	**Phase 3 (2005-2007)**
Size/dimensions (X, Y, Z)	300 x 300 x 100 mm	600 x 600 x 200 mm	1000 x 1000 x 300 mm
Measuring resolution	100 pm	10 pm	10 pm
Accuracy	30 nm	6 nm	1 nm
Relative uncertainty	10^{-7}	10^{-8}	10^{-9}

The heterodyne laser interferometers developed in Phase 1 (FY1999-FY2001) provided an extremely fine measuring resolution less than 100 pm. However, the measuring accuracy suffered a relatively high non-linearity error that was cyclic with a peak-to-valley fluctuation of more than 3 nm within a wavelength. In FY2002, to improve the measuring accuracy, a new concept of a combined optical interferometer (COI) was proposed and tested. Figure 4-98 shows the basic optical configuration, whose key idea was to integrate the heterodyne interferometer with a **Fabry-Pérot (FP) cavity** for two purposes. One purpose was for frequency stabilization by locking the output frequency of He-Ne tube lasers to the resonance frequency of the FP cavity. The other purpose was to use the FP cavity as a displacement sensor to compensate for the non-linear error of the heterodyne interferometer.[1423]

The upper main part of the COI comprises two identical sets of a He-Ne laser tube and a FP cavity for frequency locking. The stability of the output frequency is assessed with measurement of beat frequency between the two sets of frequency stabilization. The FP cavity in the bottom of the figure is the one used for displacement measurement by translating one end mirror of the cavity with a piezoelectric actuator. The measuring range of the FP cavity is limited to several wavelengths of light (**~2 μm range**), but its accuracy is free from non-linear errors with a fine resolution in the range of **picometers**. The heterodyne laser placed on the left is connected to the machine axis to be controlled, while one of the reflecting mirrors is attached to the left mirror of the FP cavity for displacement measurement. The combined scheme of two different optical interferometers allows compensating for the non-linear error of the heterodyne interferometer by use of the reading of the FP cavity, while its operation can be extended up to a few meters.

[1422] "Annual Report 2003," KAIST, http://pem.kaist.ac.kr/bupe/Annual%20Accomplishments%20for%20FY%202003.htm.

[1423] "Annual Report 2003," KAIST, http://pem.kaist.ac.kr/bupe/Annual%20Accomplishments%20for%20FY%202003.htm.

Figure 4-98. Optical configuration of the combined optical interferometer (COI).[1424]

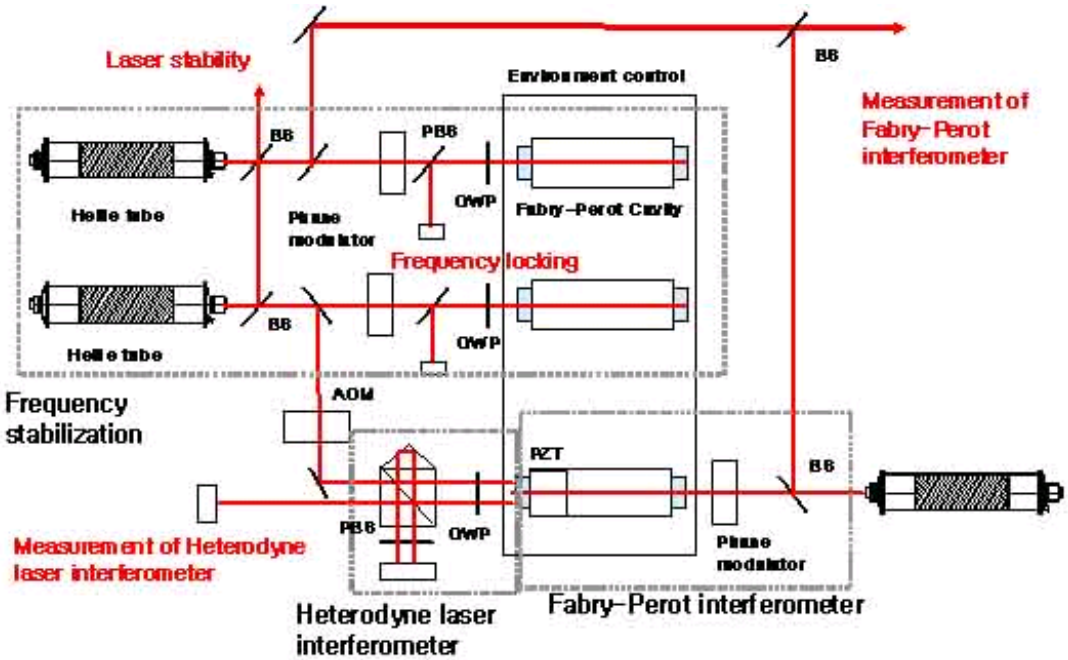

By FY 2002, a prototype had been designed and its feasibility was tested to verify the concept of the combined optical interferometer. A refined method of phase modulation with electro-optical modulators was being investigated to achieve more effective operation of frequency locking to the FP cavity.[1425]

4.6.4.7 White-Light Interferometry (WLI)

White-light[1426] interferometry (aka. low-coherence interferometry) allows for making accurate optical surface measurements (nanometer level) over a relatively long range (millimeters).[1427]

[1424] "Annual Report 2003," KAIST, http://pem.kaist.ac.kr/bupe/Annual%20Accomplishments%20for%20FY%202003.htm.

[1425] "Annual Report 2003," KAIST, http://pem.kaist.ac.kr/bupe/Annual%20Accomplishments%20for%20FY%202003.htm.

[1426] Note that "white light" in this context generally does not refer to thermal blackbody-type optically-white light spanning the entire 400-700 nm range, but rather to more limited non-laser "broadband" light sources. For instance, one WLI apparatus* uses an erbium-doped fiber amplifier (EDFA) with a wavelength bandwidth of 40 nm (1540-1580 nm) as the broadband light source.
* A. Majumdar, H. Huang, "Development of an in-fiber white-light interferometric distance sensor for absolute measurement of arbitrary small distances," Appl Opt. 47(20 May 2008):2821-2828; http://astl.uta.edu/Presentations/Majumdar-development%20of%20an%20in-

For distance measurements, white-light extrinsic Fabry-Pérot interferometric (EFPI) fiber-optic sensors have received a great deal of interest in past years because of their many advantages compared with (monochromatic) laser-based EFPI sensors, including high accuracy, high resolution, absolute measurements with a large dynamic measurement range, and immunity to optical power fluctuations.[1428] (Laser-based extrinsic Fabry-Pérot interferometric (EFPI) fiber-optic sensors, as briefly mentioned in Section 2.3.1.3.5, are Fabry-Pérot sensors typically based on air-glass reflection.) Optical fiber-based white-light interferometric (WLI) distance sensors have attracted attention because they can overcome the shortcomings of coherent (laser-based) interferometric distance sensors such as directional ambiguity and the need of a reference measurement.[1429] Since an incoherent light source with a broadband light spectrum, i.e., a white light, is utilized as the illumination source for the WLI distance sensors, the resulting interference fringes can be presented in the wavelength domain, from which the absolute distance measurement can be demodulated without requiring any reference signal. The optical fiber-based extrinsic Fabry-Pérot interferometric distance sensor is probably one of the most popular WLI distance sensors, as compared to other sensor configurations such as Michelson, Mach-Zehnder,

---

fiber%20WLI%20distance%20sensor%20for%20absolute%20measurement%20of%20arbitrary%20small%20distances.pdf.

[1427] M. Shaalan, V. Little, "The application of multiple-beam, white-light fringes to the study of surfaces," Applied Physics 8(1975):1003-1007. M. Krieg, R. Klaver, J. Braat, "Absolute optical path difference measurement with angstrom accuracy over ranges of millimeters," in: W. Osten, W. Juptner, M. Kujawinska, eds., Optical Measurement Systems for Industrial Inspection II: Application in Industrial Design, Proceedings SPIE 4398 (2001). J. Schwider Pförner, "3-λ Metrology," in: K. Creath, J. Schmidt, eds., Interferometry XI: Techniques and Analysis, Proceedings SPIE 4777 (2002).

[1428] Ming Han, Yan Zhang, Fabin Shen, Gary R. Pickrell, Anbo Wang, "Signal-processing algorithm for white-light optical fiber extrinsic Fabry-Perot interferometric sensors," Optics Lett. 29(1 August 2004):1736-1738. H.C. Lefevre, "White light interferometry in optical fiber sensors," in Proc. 7th Intl. Conf. Optical Fiber Sensors, Sydney, U.K., 1990, pp. 345-351. B.T. Meggitt, "Fiber optic white-light interferometric sensors," in: K.T.V. Grattan, B.T. Meggit, eds., Optical Sensor Technology, Chapman and Hall, London, U.K., 1995, pp. 269-310, and Chapman and Hall, London, U.K., 2000, pp. 193-238. Y.J. Rao, D.A. Jackson, "Recent progress in fiber optic low-coherence interferometry," Meas. Sci. Technol. 7(1996):981-999. T. Li, R.G. May, A. Wang, R.O. Claus, "Optical scanning extrinsic Fabry-Perot interferometer for absolute microdisplacement measurement," Appl. Opt. 36(1997):8858-8861. L.B. Yuan, L.M. Zhou, W. Jin, C.C. Chan, "Recent progress of white light interferometric fiberoptic strain sensing techniques," Rev. Sci. Instrum. 71(December 2000):4648-4654. K.A. Murphy, M.E. Gunther, A. Wang, R.O. Claus, A.M. Vengsarkar, "Extrinsic Fabry-Perot optical fiber sensor," in Proceeding of the 8th Optical Fiber Sensor Conference (IEEE, 1992), pp. 193-196.. N. Furstenau, M. Schmidt, H. Horack, W. Goetze, W. Schmidt, "Extrinsic Fabry-Perot interferometer vibration and acoustic systems for airport ground traffic monitoring," Proc. Inst. Elect. Eng. Optoelectron. 144(June 1997):134-144. A. Wang, H. Xiao, J. Wang, Z. Wang, W. Zhao, R.G. May, "Self-calibrated interferometric-intensity-based optical fiber sensors," J. Lightwave Technology 19(October 2001):1495-1501.

[1429] B.T. Meggitt, "Fiber optic white-light interferometric sensors," in: K.T.V. Grattan, B.T. Meggit, eds., Optical Sensor Technology, Chapman and Hall, London, U.K., 1995, pp. 269-310, and Chapman and Hall, London, U.K., 2000, pp. 193-238.

and Sagnac interferometers, because of its simple construction (ease in fabrication), low cost, lightness and compactness, high reliability, and ultrahigh distance resolution.[1430]

Scanning WLI (S-WLI) and spectral-domain WLI (SD-WLI) are two major kinds of WLI:[1431]

(1) A conventional S-WLI system is generally composed of a sensing interferometer and a local receiving interferometer.[1432] The sensing interferometer is used to convert the measurand's perturbation into phase modulation of the light waves through variation of the optical path difference (OPD) between its sensing and reference arms. It usually has an OPD larger than the coherence length of the light source such that interference fringes cannot be observed. Recovering the OPD of the sensing interferometer requires that the OPD of the local receiving interferometer be scanned, creating a fringe pattern. When the OPDs of the two interferometers are the same, the system has the maximum fringe peak, which is termed the central fringe, or centroid. A great number of algorithms to locate the centroid are available. In general, S-WLI has a large dynamic range but also a large system size, low mechanical stability, and relatively low resolution. A variation of S-WLI is widely used in time-domain optical coherence tomography,[1433] surface metrology,[1434] and some Mach-Zehnder or Michelson sensors, in which the optical length of the reference arm is directly scanned. The major advantage of this configuration is that only one interferometer is required. However, it is hard, if not impossible, to apply S-WLI to Fabry-Pérot and Sagnac interferometers because of difficulty of access to the reference beam. Another issue is that the two arms may experience different environmental fluctuations.

(2) The other major alternative, SD-WLI, is based on detection of the output spectrum of a sensing interferometer with a spectrometer.[1435] Once the output spectrum is obtained, fringe tracking or a Fourier transform may be used to recover the OPD of the interferometer. SD-WLI

[1430] K.A. Murphy, M.E. Gunther, A. Wang, R.O. Claus, A.M. Vengsarkar, "Extrinsic Fabry-Perot optical fiber sensor," in Proceeding of the 8th Optical Fiber Sensor Conference (IEEE, 1992), pp. 193-196. Ki Dong Oh, "Chapter 2 – Extrinsic Fabry-Perot Interferometer Measuring Magnetic Field," in Optical Fiber Fabry-Perot Interferometer based Sensor Instrumentation System for Low Magnetic Field Measurement, PhD dissertation, Dept. of Electrical and Computer Engineering, Virginia Polytechnic Institute, 18 December 1997; http://scholar.lib.vt.edu/theses/available/etd-11198-54532/unrestricted/ch2.pdf.

[1431] Bing Yu, Anbo Wang, Gary Pickrell, Juncheng Xu, "Tunable-optical-filter-based white-light interferometry for sensing," Optical Lett. 30(15 June 2005):1452-1454.

[1432] Y.J. Rao, D.A. Jackson, "Recent progress in fiber optic low-coherence interferometry," Meas. Sci. Technol. 7(1996):981-999.

[1433] J.M. Schmitt, "Optical coherence tomography (OCT): A review," IEEE J. Quantum Electron. 5(1999):1205-1215.

[1434] L. Deck, P.D. Groot, "High-speed noncontact profiler based on scanning white-light interferometry," Appl. Opt. 33(1994):7334-7338.

[1435] S.H. Yun, G.J. Tearney, B.E. Bouma, B.H. Park, J.F. de Boer, "High-speed spectral-domain optical coherence tomography at 1.3 μm wavelength," Opt. Express 11(2003):3598-3604.

is applicable to all types of interferometer, is insensitive to source fluctuations, is accurate and reliable, and requires no mechanical scanning. (Speed and price are two significant issues with SD-WLI, since commercial spectrometers in general are slow and expensive, especially in the 1.0-1.7 μm band.) In the spectral detection approach, a spectrometer with a charge-coupled device (CCD) array is usually employed to record the optical spectrum of EFPI's output and a computer is used for signal processing.[1436] The four experimental set-ups described in this Section are all examples of the spectral detection approach.

The price which is paid for all of the advantages of WLI is the need to perform relatively complicated output signal processing, as compared to conventional intensity-based fiber-optic sensors. Even though WLI distance sensors can achieve absolute measurement from its interference spectrum, they require a data interrogation process to demodulate the distance. Data interrogation algorithms such as fringe counting,[1437] Fourier transform spectroscopy,[1438] improved fringe matching technique,[1439] and least-square fitting[1440] (see below) have been published. In general, the more the fringes are presented in the interference fringe spectrum, the higher the accuracy a data demodulation algorithm can achieve. More importantly, in order for the data demodulation algorithm to be applicable, a minimum number of interference fringes must be presented in a given spectral bandwidth. The narrow spectral bandwidth of a white-light source, therefore, imposes a limit on how small a distance a WLI distance sensor can measure.

Many of these sensors use a single-mode fiber connected to a Fabry-Pérot (FP) cavity that can be formed when a reflector is placed at some distance to the cleaved fiber end. When broadband "white" light is launched into the sensor, the two reflections from the two end faces in the FP cavity interfere and form a fringe pattern in the spectral domain (i.e., "rainbow" fringes). The fringe pattern can be modulated by the measurand-induced variations in either (1) the refractive index of the medium that separates the reflecting surfaces, or (2) the distance separating the two end faces of the FP cavity. The phase delay between the two reflections will be proportional to the product of the refractive index of the medium between the two reflecting surfaces and the distance between the surfaces. This product is the actual "measurand" and can be referred to as the optical path difference (OPD); if the medium separating the two reflecting surfaces is

---

[1436] Bing Yu, Anbo Wang, Gary Pickrell, "Analysis of Fiber Fabry-Perot Interferometric Sensors Using Low-Coherence Light Sources," J. Lightwave Technology 24(April 2006):1758-1767.

[1437] V. Arya, K.A. Murphy, A. Wang, R.O. Claus, "Microbend losses in single-mode optical fibers: theoretical and experimental experimental investigation," J. Lightwave Technol. 13(1995):1998-2002.

[1438] G. Schrofer, W. Elflein, M. de Labachelerie, H. Porte, S. Ballandras, "Lateral optical accelerometer micromachined in (100) silicon with remote readout based on coherence modulation," Sens. Actuators A 68(1998):344-349.

[1439] H. Huang, "Data Interrogation for Fabry-Perot white-light interferometry," Proc. SPIE 6174(2006):617319.

[1440] Ming Han, Yan Zhang, Fabin Shen, Gary R. Pickrell, Anbo Wang, "Signal-processing algorithm for white-light optical fiber extrinsic Fabry-Perot interferometric sensors," Optics Lett. 29(1 August 2004):1736-1738.

vacuum or air, then refractive index is constant and any phase delay is due only to the gap distance between the two reflecting surfaces, thus the measurand becomes almost purely distance.

Several signal demodulation methods in the spectral domain have been proposed to achieve high measurement resolution using single-mode fiber (SMF) EFPI sensors, the validity of which depends on the fact that the phase and period of the interferogram are solely determined by the OPD of the FP cavity in SMF-EFPI sensors. These demodulation methods include the wavelength-tracking method,[1441] in which the wavelength shift of one fringe peak is employed to detect the small OPD variations induced by the measured parameters, and the curve-fitting method,[1442] in which the absolute OPD is obtained by curve fitting the measured interferogram to theoretical results.

A good example of the latter (curve-fitting) approach is provided by Han et al.[1443] who describe a signal-processing method for a single-mode fiber (SMF-EFPI) sensor that can produce both high sensitivity and absolute measurement of the FP cavity thickness over a large dynamic measurement range. As shown in Figure 4-99A, the step-index weakly guiding lead-in SMF has a core diameter of 2a and refractive indices n_1 in the core and n_2 in the cladding. The FP cavity with air gap d is formed between end face R_1 of the lead-in SMF and another reflector, R_2. The multireflections in the FP cavity can be ignored because the reflections at the air-glass interface are small, so the total field reflected back to the lead-in fiber may be expressed as the summation of E_1, the field that is due to the first reflection at R_1, and E_2, the field contributed by the reflection at R_2. The normalized spectrum fringe $I_{norm}(\lambda, d)$, which is the spectrometer-measured reflected fringe spectrum $I(\lambda, d)$ normalized by the light source's power spectrum, $I_0(\lambda)$, may then be expressed as $I_{norm}(\lambda, d) = A + B \cos(4\pi d/\lambda + \pi + \theta)$, where A and B are two constants, λ is optical wavelength, and the fringe phase comprising three terms: (1) the air-gap related phase shift, (2) the π phase shift that arises from the reflection at R_2, and (3) the coupling-induced phase shift θ. (The coupling phase shift θ can be calculated as a function of air gap d at wavelength λ.) The above formula for $I_{norm}(\lambda, d)$ can then be fitted to the fringe spectrum measured by a calibrated spectrometer after a test displacement, allowing calculation of the new air gap d using using fitting parameters A, B, and d. Additional parameters are added as a linear function of wave number to account for fiber bending losses and for the predicted slight departure of the coupling phase shift θ from its true value due to imperfections of the sensor head and calculation errors, using a least-squares fitting approach on the linear function to adjust the phase of the fitted curve to its theoretical result in the fitting process when the theoretical phase shift is close to its true value.

[1441] V. Bhatia, M.B. Sen, K.A. Murphy, R.O. Claus, "Wavelength-tracked white light interferometry for highly sensitive strain and temperature measurements," Electron. Lett. 32(1996):247-249.

[1442] Ming Han, Yan Zhang, Fabin Shen, Gary R. Pickrell, Anbo Wang, "Signal-processing algorithm for white-light optical fiber extrinsic Fabry-Perot interferometric sensors," Optics Lett. 29(1 August 2004):1736-1738.

[1443] Ming Han, Yan Zhang, Fabin Shen, Gary R. Pickrell, Anbo Wang, "Signal-processing algorithm for white-light optical fiber extrinsic Fabry-Perot interferometric sensors," Optics Lett. 29(1 August 2004):1736-1738.

Figure 4-99. (A) At left: Schematic of a SMF-EFPI sensor system (inset, schematic of a SMF-EFPI sensor head); (B) At right: Construction of the SMF-EFPI sensor used in the test.[1444]

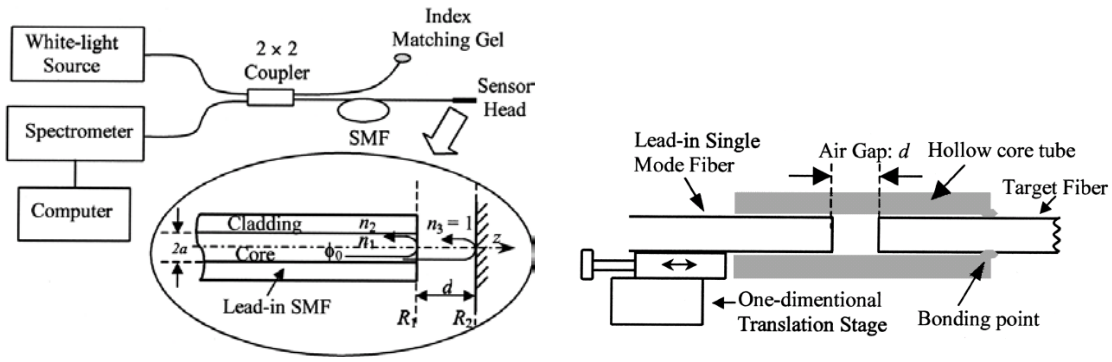

This signal-processing algorithm for SMF-EFPI sensors was experimentally investigated with the help of the FP cavity optical setup (~100 μm displacement range) and optical sensor (two cleaved-end 125-μm-diameter fibers inside a 132-μm inner-diameter hollow tube) shown in Figure 4-99B. A high-resolution swept laser interrogator functioned both as a white-light source and as a spectrometer, with spectral intensity sampled from 1520-1570 nm for N = 2000 samples at equal wavelength intervals of 25 pm. During measurement the air gap was increased from 55.0 μm to 62.3 μm in ten steps (total air-gap change 7.3 μm) by adjusting the translation stage, and at each step the spectrum was sampled for roughly 2 min at a sample rate of 0.5 Hz. Using an SMF-EFPI sensor, the positioning stage can be swept as rapidly as desired through its range with no need for continuous tracking; the primary limit is the time required for the spectrometer to accumulated data at the travel endpoint, to determine the final resting position of the stage.

The measured air gap (Figure 4-100A) increased slightly at each level owing to the mechanical drift of the translation stage after the air gap was adjusted. This effect is magnified in Figure 4-100B, where the air gap that corresponds to measurement numbers 103-156 is displayed, corresponding to the third step shown in Figure 4-100A. The drift of the mechanical translation stage is clearly evident in Figure 4-100B as a diagonal solid trendline representing the least-squares linear fit of the measurement of the air gap as a function of the measurement number. The fluctuation of measured points about the best-fit line through the data can be taken as a measure of the standard deviation of the fitting error of the algorithm – obviously sub-nanometer from the chart (Figure 4-100B), and calculated to be **288 pm** – represents the variation due to all sources of error including the algorithm and can be taken as a worst-case estimate of the resolution of the algorithm. It is possible that some of the variation about the line is due to the mechanical translation stage as well, and other errors might be introduced by various

---

[1444] Ming Han, Yan Zhang, Fabin Shen, Gary R. Pickrell, Anbo Wang, "Signal-processing algorithm for white-light optical fiber extrinsic Fabry-Perot interferometric sensors," Optics Lett. 29(1 August 2004):1736-1738.

imperfections of the sensor such as nonparallelism of the two fiber ends. The model assumes that the spectrum fringe is a cosine function with a linear amplitude modulation as a function of the wave number; however, more-complex modulations of the fringe envelope owing to bending losses of the single-mode fiber may cause the fitting process to converge to an erroneous air-gap value, though this error could be compensated for by using a higher-order polynomial to fit the envelope modulations.[1445] Additional corrections are necessary when a multi-mode fiber (MMF) is used in place of the SMF in an EFPI sensor.[1446]

Figure 4-100. (A) At left: Result of evaluation of the sensor's air gap at 10 air-gap levels, taking ~0.8 μm steps. (B) At right: Enlarged view of the evaluation result for the third air-gap level measurement and its linear fitting as the measurement number; the standard deviation of the data points around the fitted trendline is 288 pm.[1447]

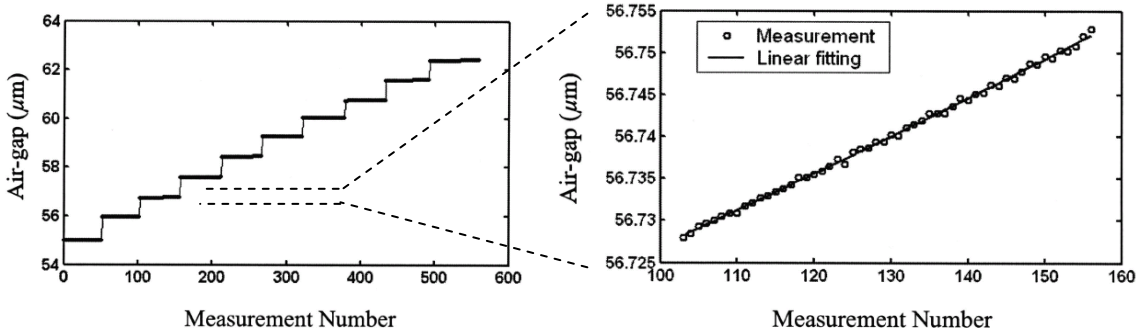

Yu et al.[1448] describe an alternative to SD-WLI, termed tunable-optical-filter-based WLI (TOF-WLI). By introducing a tunable optical filter into a WLI system, one can interrogate an interferometer with either quadrature demodulation or spectral-domain detection at low cost. Figure 4-101 shows a general configuration of a TOF-WLI interferometric measurement sensor system. It consists of a broadband light source, a circulator, a sensing interferometer, a tunable optical filter, receiving electronics, a computer, and optical fibers to connect all the optical parts. The output spectrum of the sensing interferometer is readily obtained by scanning the tunable

---

[1445] Ming Han, Yan Zhang, Fabin Shen, Gary R. Pickrell, Anbo Wang, "Signal-processing algorithm for white-light optical fiber extrinsic Fabry-Perot interferometric sensors," Optics Lett. 29(1 August 2004):1736-1738.

[1446] Ming Han, Anbo Wang, "Mode power distribution effect in white-light multimode fiber extrinsic Fabry-Perot interferometric sensor systems," Optics Lett. 31(1 May 2006):1202-1204.

[1447] Ming Han, Yan Zhang, Fabin Shen, Gary R. Pickrell, Anbo Wang, "Signal-processing algorithm for white-light optical fiber extrinsic Fabry-Perot interferometric sensors," Optics Lett. 29(1 August 2004):1736-1738.

[1448] Bing Yu, Anbo Wang, Gary Pickrell, Juncheng Xu, "Tunable-optical-filter-based white-light interferometry for sensing," Optical Lett. 30(15 June 2005):1452-1454.

optical filter (TOF). The system can work similarly to SD-WLI and most of the developed signal-processing algorithms (e.g., fringe peak tracking and Fourier transformation) can be directly applied. In a scan mode, a scan range of 50-100 nm and a filter bandwidth of **500-2000 pm** are preferred for high resolution and a high signal-to-noise ratio.

Figure 4-101. TOF-WLI measurement system; SMF = single-mode fiber.[1449]

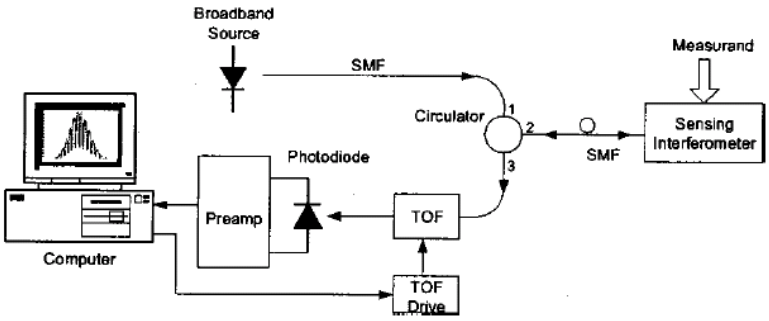

Another interesting WLI displacement sensor that could in principle be adapted as a workstation displacement measurement system was demonstrated in 2008 by Majumdar and Huang[1450] who introduced a Long-Period Fiber Grating (LPFG) (aka. Bragg grating) into the FPI (Fabry-Pérot Interferometer) optical fiber at a distance from the fiber end. (An LPFG can be either permanently engraved in a single-mode fiber (SMF) using a high power UV laser or mechanically induced by introducing periodic microbending.) The in-fiber LPFG-based WLI distance sensing system (Figure 4-102A) consists of a broadband light source, an optical circulator, a distance sensor, and an optical spectrum analyzer (OSA). The light generated by the broadband light source propagates along the optical fiber and is routed toward the distance sensor by an optical circulator. The distance sensor probe (Figure 4-102B) is simply a cladding-coated single mode fiber (SMF) with a LPFG located at a distance from its cleaved end. The LPFG serves as a beam splitter that separates the core propagating light into a core mode and a cladding mode. Passing the LPFG, the core mode continues to travel along the fiber core toward the sample under test, as indicated by the solid arrow in Figure 4-102B. At the end of the optical fiber, it exits the probe, propagates in the air, then is reflected by the sample, and finally is coupled back to the fiber core and propagates toward the LPFG. The light that is coupled into the cladding by the LPFG propagates along the cladding (dashed arrows in Figure 4-102B) until it reaches the mirrored end of the probe. Reflecting from the mirror, this cladding mode will trace its path back to the LPFG. Based on the reciprocity principle of light propagation, the reflected cladding mode will be

---

[1449] Bing Yu, Anbo Wang, Gary Pickrell, Juncheng Xu, "Tunable-optical-filter-based white-light interferometry for sensing," Optical Lett. 30(15 June 2005):1452-1454.

[1450] A. Majumdar, H. Huang, "Development of an in-fiber white-light interferometric distance sensor for absolute measurement of arbitrary small distances," Appl Opt. 47(20 May 2008):2821-2828; http://astl.uta.edu/Presentations/Majumdar-development%20of%20an%20in-fiber%20WLI%20distance%20sensor%20for%20absolute%20measurement%20of%20arbitrary%20small%20distances.pdf.

coupled back to the core mode. When the cladding mode is recombined with the core mode, the two light waves interfere constructively and destructively because of the different optical paths they have traveled. By routing these two reflected lights to the OSA using the optical circulator, the interference fringe spectrum can be measured.

Figure 4-102. (A) At left: In-fiber LPFG-based WLI distance sensing system. (B) At right: White-light interference generated by LPFG and cladding-coated sensor probe.[1451]

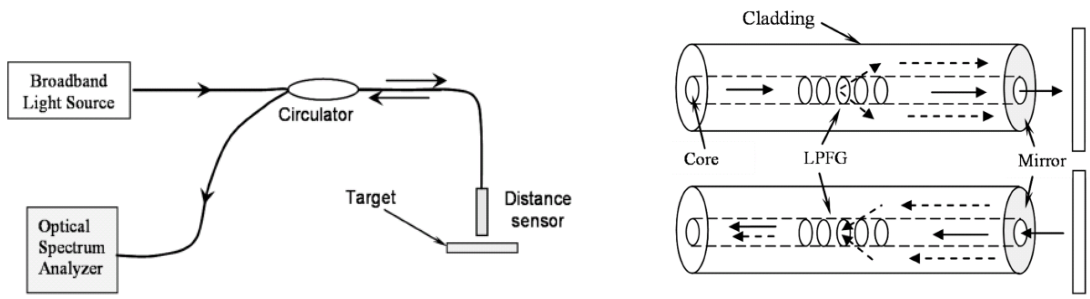

In the experimental apparatus, a mirror served as the target and was placed on a horizontal translation stage whose movement was controlled by a motorized actuator; the the LPFG-based distance sensor and its mirror target were illuminated by a broadband light source having a wavelength bandwidth of 40 nm (1540-1580 nm). The fringe spectra of the distance sensor, acquired at different cavity distances, were first normalized with the spectrum of the laser source. Fast Fourier transform (FFT) was then applied to the normalized fringe spectra in order to obtain their frequency components, after converting the wavelength to wave number. The frequency position f_p of the FFT peak is directly correlated to the OPD, i.e., f_p = OPD. Therefore, for a LPFG-based WLI distance sensor, the free-space cavity distance d (between the fiber end and the target mirror) can be calculated from the FFT peak frequency directly if ΔnL is known, assuming $n_m = 1$ (i.e., the refractive index of the medium in the free-space, here, in air), where $\Delta n = n_{clad} - n_{core}$ is the difference between the refractive indices of the fiber core and cladding, and L is the distance between the LPFG and the fiber end.

When the sensor probe is placed in front of a mirror, the reflectance spectra are contributed to by the following three interferences:

I. The interference between the reflected cladding mode and the core mode reflected by the fiber/air interface, i.e., the LPFG effect.

[1451] A. Majumdar, H. Huang, "Development of an in-fiber white-light interferometric distance sensor for absolute measurement of arbitrary small distances," Appl Opt. 47(20 May 2008):2821-2828; http://astl.uta.edu/Presentations/Majumdar-development%20of%20an%20in-fiber%20WLI%20distance%20sensor%20for%20absolute%20measurement%20of%20arbitrary%20small%20distances.pdf.

II. The interference between the core mode reflected at the fiber/air interface and the core mode reflected by the mirror, i.e., the FPI effect.

III. The interference between the reflected cladding mode and the core mode reflected by the mirror, i.e., the combined LPFG and FPI effect (LPFG+FPI interference).

The LPFG fringe spectrum, i.e., from interference I, is independent of the FPI cavity distance d and is identical to the fringe spectrum obtained when the mirror is not presented. The other two interferences, however, are directly controlled by the cavity distance d. The resulting interference fringes from these three interferences are shown in Figure 4-103A. The FFT of the interference fringes clearly demonstrates the existence of these three interferences, as shown in Figure 4-103B. The locations of the three frequency peaks in the FFT spectrum correspond to the OPD of the three interferences – the OPD of the LPFG+FPI interference is equal to the OPD of the LPFG interference plus that of the FPI interference.

Figure 4-103. (A) At left: Typical fringe spectrum from all three interferences. (B) At right: the Fast Fourier Transform (FFT) of the same fringe spectrum.[1452]

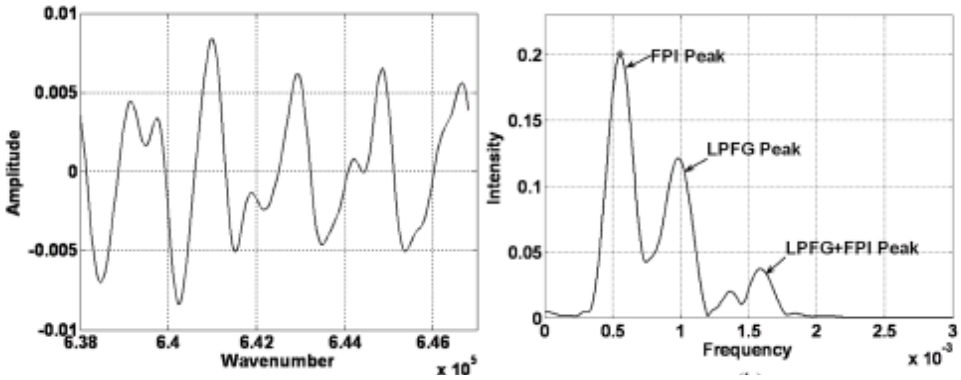

Figure 4-104A compares the cavity distances measured from the FPI interference with those measured from the LPFG+FPI interference. The distance between the sensor probe and the mirror was adjusted by traversing the mirror using the motorized translation stage in steps of 20 μm. At each position, the reflectance spectrum of the LPFG-based WLI distance sensor was recorded, from which the cavity distance was calculated from the positions of the FPI peak and the LPFG+FPI peak independently. Figure 4-104A shows that the distances measured from both interferences demonstrated a linear relationship with the traversed distances, as calculated from the motor position feedback. Figure 4-104B shows the relationship between the distance traversed by the translation stage as well as the distance measured from the LPFG+FPI peak. A

[1452] A. Majumdar, H. Huang, "Development of an in-fiber white-light interferometric distance sensor for absolute measurement of arbitrary small distances," Appl Opt. 47(20 May 2008):2821-2828; http://astl.uta.edu/Presentations/Majumdar-development%20of%20an%20in-fiber%20WLI%20distance%20sensor%20for%20absolute%20measurement%20of%20arbitrary%20small%20distances.pdf.

linear relationship is demonstrated over the cavity distances ranging from 350 to 4.5 µm, a much smaller distance than that which can be measured by a conventional white-light FPI distance sensor alone. The minimum positional resolution achieved in this experiment was not explicitly reported in the paper (though sig figs in formulas in Figure 4-104 would be consistent with **0.1-10 nm** resolution).

Figure 4-104. (A) At left: Distances estimated from the FPI (upper) and the LPFG+FPI (lower) interference fringes. (B) At right: Linear relationship between the distances moved by the target and the distances measured by the LPFG-based WLI distance sensor.[1453]

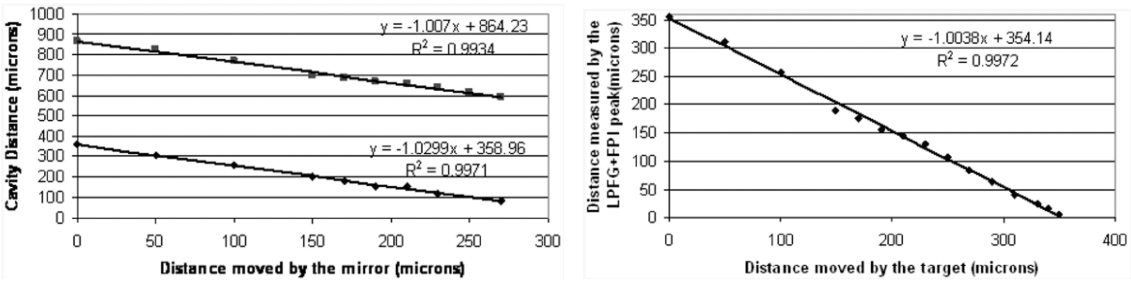

For further comparison, it's probably worth mentioning another good example of the performance of a non-Fabry-Pérot *intrinsic* white-light interferometric sensor[1454] that was reported by Tapia-Mercado et al.[1455] in 2001. Their spectral domain technique could be used to optimize any sensor based on different types of interferometers but in this case was demonstrated exerimentally on a Sagnac interferometer having a twisted high-birefringence fiber (HBF) of length L. In this interferometric sensor, the optical path difference (OPD) generated in the interferometer varies as a function of the measurand (i.e., temperature, in this experiment). To obtain the value of ΔL by the spectral domain technique, a spectral analyzer (spectrograph) is used to record the modulated output power spectrum, which has the form $I(\lambda) = I_0(\lambda)[1 + m_0\cos(2\pi\Delta L/\lambda)]$ where $I_0(\lambda)$ is the output power spectrum when $\Delta L = 0$ and m_0 is the output spectrum modulation index. Figure 4-

---

[1453] A. Majumdar, H. Huang, "Development of an in-fiber white-light interferometric distance sensor for absolute measurement of arbitrary small distances," Appl Opt. 47(20 May 2008):2821-2828; http://astl.uta.edu/Presentations/Majumdar-development%20of%20an%20in-fiber%20WLI%20distance%20sensor%20for%20absolute%20measurement%20of%20arbitrary%20small%20distances.pdf.

[1454] C.E. Lee, W.N. Gibler, R.A. Atkins, H.F. Taylor, "In-line fiber Fabry-Perot interferometer with high-reflectivity internal mirrors," J. Lightwave Technology 10(October 1992):1376-1379.

[1455] J. Tapia-Mercado, A.V. Khomenko, A. García-Weidner, "Precision and Sensitivity Optimization for White-Light Interferometric Fiber-Optic Sensors," J. Lightwave Technology 19(January 2001):70-74; http://optica.cicese.mx/includes/investigadores/akhom/JLT19-70.pdf.

105 shows a typical output spectrum recorded in their experiments.[1456] To extract the cosine term from the output spectrum I(λ) and calculate the path difference ΔL, we need to eliminate the wavelength dependent factor $I_0(\lambda)$. This can be done when a pre-recorded (during sensor calibration) spectrum $I_0(\lambda)$ is used to normalize I(λ), as done by Han et al.[1457] But Tapia-Mercado et al. tried another method for signal processing[1458] that they thought might be more accurate and more independent of intensity variations, in which the output spectrum is first smoothed by a convolution with a Hanning window to eliminate false maxima and minima caused by noise, then two auxiliary spectra are calculated, $I_{max}(\lambda)$ and $I_{min}(\lambda)$, by interpolating the maxima and minima of the smoothed spectrum I(λ), respectively (Figure 4-105a), thus allowing the cosine term from the above equation to be calculated.

Figure 4-105. <u>At left:</u> <u>(a)</u> Output signal of CCD spectrograph I(λ) with interpolated maxima $I_{max}(\lambda)$ and minima $I_{min}(\lambda)$, and L = 20 cm. <u>(b)</u> The same signal after processing. <u>(c)</u> Interpolated signal near λ_1. <u>At right:</u> Experimental setup, with oil-based controlled-temperature bath.[1459]

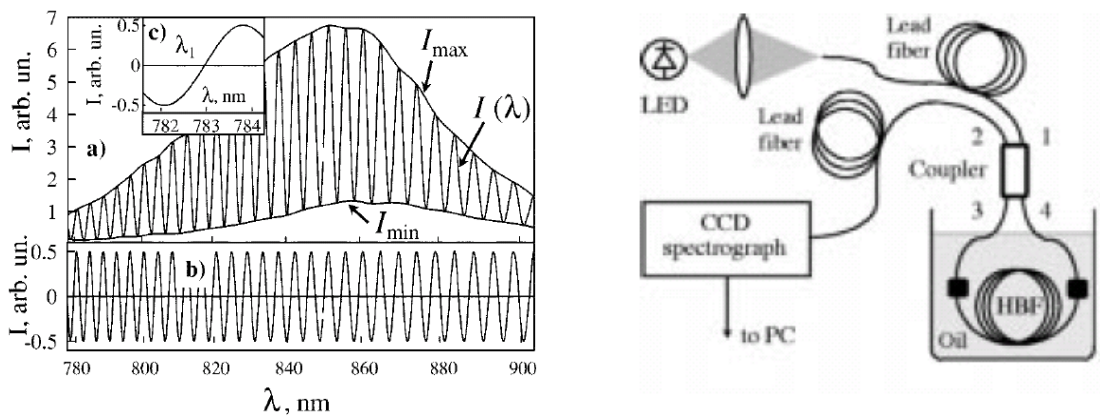

[1456] J. Tapia-Mercado, A.V. Khomenko, A. García-Weidner, "Precision and Sensitivity Optimization for White-Light Interferometric Fiber-Optic Sensors," J. Lightwave Technology 19(January 2001):70-74; http://optica.cicese.mx/includes/investigadores/akhom/JLT19-70.pdf.

[1457] Ming Han, Yan Zhang, Fabin Shen, Gary R. Pickrell, Anbo Wang, "Signal-processing algorithm for white-light optical fiber extrinsic Fabry-Perot interferometric sensors," Optics Lett. 29(1 August 2004):1736-1738.

[1458] R. Cortés, A.V. Khomenko, A.N. Starodumov, N. Arzate, L.A. Zenteno, "Interferometric fiber-optic temperature sensor with spiral polarization couplers," Opt. Commun. 154(1998):268-272.

[1459] J. Tapia-Mercado, A.V. Khomenko, A. García-Weidner, "Precision and Sensitivity Optimization for White-Light Interferometric Fiber-Optic Sensors," J. Lightwave Technology 19(January 2001):70-74; http://optica.cicese.mx/includes/investigadores/akhom/JLT19-70.pdf.

The final goal of the signal processing is the unambiguous determination of the optical path difference ΔL. To accomplish this task one needs to know only three values: the spectral position of two zeros for the aforementioned cosine term and the number of the cycles between them. Measurement precision increases with increasing spectral distance between zeros. The number of cycles between two spectral zeros is an integer and should be determinable without uncertainty when the signal-to-noise ratio (SNR) is adequate. Thus the uncertainty in the calculated phase results only from the uncertainty in the signal zero locations, which in turn is determined by the noise. For a noise-free signal, zeros could be located with unlimited accuracy by an interpolation of the signal between data points, but for any practical signal some noise is unavoidable which sets a limit on measurement accuracy for ΔL. There is also an optimal path difference L_{opt} ~ 25 cm that produces the absolute minimum of the wavelength uncertainty, $d\lambda_{min}$ = 1.2 pm, at λ = 840 nm and SNR ~ 250 (Figure 4-106).

Figure 4-106. Wavelength uncertainty of zero location as a function of the birefringent fiber length; the curve was calculated using a theoretical relation and the filled circles are the experimentally obtained data.[1460]

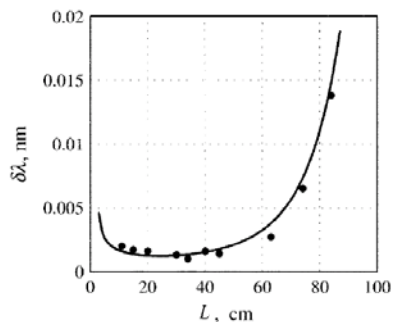

The experimental setup is designed to measure temperature change as the optical fiber heats and expands, increasing slightly in length. Taking the coefficient of expansion for optical fiber as $\alpha = 5.5 \times 10^{-7}\ K^{-1}$ and the estimated minimum detectable temperature difference as ΔT = 0.002 K for this apparatus, the smallest detectable optical path difference is $OPD_{min} \sim \alpha\ L_{opt}\ \Delta T \sim$ **275 pm**.

In yet another approach, near-field surface profiling using a near-field scanning optical microscope (NSOM) is a very useful technique for the optical investigation of materials in the subwavelength range, in which the NSOM positions a tapered optical fiber probe in the near-field surface of the sample and thus overcomes the diffraction limit of conventional optical microscopes. An interferometric optical feedback mechanism has been explored[1461] for NSOM

[1460] J. Tapia-Mercado, A.V. Khomenko, A. García-Weidner, "Precision and Sensitivity Optimization for White-Light Interferometric Fiber-Optic Sensors," J. Lightwave Technology 19(January 2001):70-74; http://optica.cicese.mx/includes/investigadores/akhom/JLT19-70.pdf.

[1461] Hitoshi Shiku, Jeffrey R. Krogmeier, Robert C. Dunn, "Noncontact Near-Field Scanning Optical Microscopy Imaging Using an Interferometric Optical Feedback Mechanism," Langmuir 15(17 February 1999):2162-2168.

tip-sample distance control, wherein an optical signal, based on the interference between the light exiting the tip aperture and that reflecting off the sample surface, is used to implement a feedback scheme to regulate tip-sample displacements. This method allows nanometric height changes to be detected with millisecond time resolution. NSOM's capability for ultraprecise absolute distance measurement can be exploited for position feedback but its basic image construction technique relies solely on measuring the intensity of the sample light using a photomultiplier tube, so the NSOM signal is susceptible to noises induced by laser power fluctuation and optical fiber bending.

4.6.4.8 Other Fabry-Pérot Interferometry Systems

A number of systems based on Fabry-Pérot interferometry have been developed (and continue to be pursued) in the last decade, but most probably provide insufficient (picometric) precision or may not provide measurement capability that is strictly required in a molecular workstation for DMS. These include:

(1) **Brand-Herrmann FP Interferometer** (1996) – Brand and Herrmann[1462] at PTB (Germany) reported a laser-frequency-based displacement measurement system whose resolution is known to picometer precision, using a mode change scheme for a Fabry-Pérot cavity to expand displacement measurement from a typical range of less than 1 μm to a range potentially on the order of millimeters. To accomplish this, they built a laser system for displacement measurements based on the iodine-stabilized He-Ne laser wavelength standard at 633 nm. Two resonator mirror moving systems with displacement ranges of 3 μm (nonlinear deviations ±2000 pm, noise fluctuations ±500 pm) and 13 μm (nonlinear deviations ±2500 pm, noise fluctuations ±1500 pm) respectively were investigated and the guidance deviations of the latter were corrected. An inductive displacement transducer was calibrated using the measuring laser, with the overall measurement uncertainty of **2470 pm** (260 pm systematic uncertainty + 2210 pm random uncertainty) estimated for a single-measurement calibration of the inductive transducer over a total displacement length of 13 μm.

(2) **Dual FP Interferometer** (Tsinghua University, China, 2001) – On the basis of analyzing sinusoidal phase-modulating Fabry-Pérot interferometry, a method, believed to be novel, is proposed[1463] for achieving nanometer measurement accuracy by measuring the time interval between equal amplitudes of the two elementary frequency signals of the transmitted intensities of a dual Fabry-Pérot interferometer. A nanometer measurement system based on the method was designed and tested. The experimental results show that the displacement resolution of the system is **320 pm** at a 1-kHz modulating signal.

[1462] U. Brand, K. Herrmann, "A laser measurement system for the high-precision calibration of displacement transducers," Meas. Sci. Technol. 7(1996):911-917.

[1463] B. Chen, R. Zhu, Z. Wu, D. Li, S. Guo, "Nanometer Measurement with a Dual Fabry-Perot Interferometer," Appl. Opt. 40(2001):5632-5637; http://www.opticsinfobase.org/abstract.cfm?URI=ao-40-31-5632.

(3) **FP Displacement Interferometer** (Nederlands Meetinstituut, Netherlands, 2005) – At the Nederlands Meetinstituut in Delft, Netherlands, van den Berg et al.[1464] report building a Fabry-Pérot interferometer capable of measuring nanometer-scale absolute displacements. From the abstract: "Fabry-Pérot interferometry is a powerful technique for the measurement of extremely small displacements. We have developed a Fabry-Pérot interferometer for the calibration of displacement sensors with **nanometer accuracy**, in order to provide direct traceability of such sensors to the primary standard of length. In conclusion, the Fabry-Pérot interferometer provides the possibility to calibrate nanosensors, like capacitive and inductive sensors, with nm accuracy."

(4) **FP Thickness Profilometer** (CSIRO, Australia, 2007) – From the abstract of Farrant et al.:[1465] "The resolution of an angle-scanning technique for measuring transparent optical wafers is analyzed, and it is shown both theoretically and experimentally that **subnanometer resolution** can be readily achieved. Data are acquired simultaneously over the whole area of the wafer, producing two-dimensional thickness variation maps in as little as 10 sec. Repeatabilities of **70 pm** have been demonstrated, and wafers of up to 100 mm diameter have been measured, with 1 mm or better spatial resolution. A technique for compensating wafer and system aberrations is incorporated and analyzed."

(5) **FB Angle Sensor** (China University of Geosciences, 2008) – From the abstract of Lu et al.:[1466] "An optical fiber angle sensor that consists of a cam, linear displacement attenuators, and a sensitive Fabry-Pérot cavity (FPC), is demonstrated to simultaneously measure small angle and infinite angle with high resolution. When the cam is driven to rotate by a fixed rotary shaft, a linear displacement transformed from an angle will be further attenuated by linear displacement attenuators and will subsequently modulate the FPC, which causes the reflected interference intensity of FPC to vary. By using the method of interferometric fringe counting, we can measure an infinite angle accurately and continuously. Moreover, a small angle measurement can be performed in a locally linear region. Experimental results show that two resolutions of 0.5 arcsec and 1.5 arcsec in the angle ranges of 0.1944 degrees and 3.5496 degrees are achieved, respectively."

[1464] S.A. van den Berg, P.J.M. van Kan, R.H. Bergmans, "Absolute measurement of nanometer displacement with Fabry-Perot interferometry," in: Conference on Lasers and Electro-Optics Europe, 2005 (CLEO/Europe 2005), 12-17 June 2005, p. 438, ISBN: 0-7803-8974-3, INSPEC Accession Number: 8803603, Digital Object Identifier: 10.1109/CLEOE.2005.1568216, Current Version Published: 2006-01-23.

[1465] D.I. Farrant, J.W. Arkwright, P.S. Fairman, R.P. Netterfield, "Measuring the thickness profiles of wafers to subnanometer resolution using Fabry-Perot interferometry," Appl Opt. 46(20 May 2007):2863-2869.

[1466] T. Lü, X. Lang, Y. Han, "Optical fiber sensor for small angle and infinite angle detection," Rev Sci Instrum. 79(May 2008):053105.

4.6.4.9 Summary of Fabry-Pérot Interferometry Systems

The leading Fabry-Pérot based metrology systems are the tunable laser Fabry-Pérot interferometers, including the one built by Lawall's group at NIST that reported measuring 25-50 mm displacements to within **10 pm** accuracy (Section 4.6.4.2); the one built by Howard's group at NIST that reported **20 pm** RMS displacement measurement resolution (Section 4.6.4.3); and the one built by Bitou's group in Japan that demonstrated accurate displacement control using a phase-locked loop with **24 pm** resolution, although the absolute uncertainty of the displacement measurement system over a total displacement of 14 μm was only **190 pm** (Section 4.6.4.4). The South Korean BUPE Project, apparently defunded in 2004, built an FP-based combined optical interferometer having a ~2 μm range and a nonlinear-error-free resolution in the range of "**picometers**" (Section 4.6.4.6). Two other FP setups involving white-light interferometry yielded systems with minimum detectable optical path difference of **275-288 pm** (Section 4.6.4.7), probably too poor to be useful for a molecular workstation unless significant improvements are possible.

The most notable Fabry-Pérot interferometer system employed in SPM metrology is the tunable laser Fabry-Pérot interferometer built by Howard's group at NIST with a resolution of **tens of picometers** that was used to measure Z-axis displacements of an AFM with a **60 pm** noise level for the combined AFM/interferometer system (Section 4.6.4.3).

It appears that Fabry-Pérot interferometers can probably provide positional detection of sufficient precision to enable dead-reckoning pick-and-place DMS operations (without continuous sensory feedback, though likely requiring periodic re-registration), in a molecular workstation to be used for atomically precise DMS-based molecular manufacturing.

4.6.5 Digitally Enhanced Heterodyne Interferometry (Shaddock, Australia)

Heterodyne interferometry (Section 2.3.1.5) is a widely used technique for sub-nanometer displacement metrology. Digitally enhanced heterodyne interferometry (DI), as pioneered by Daniel Shaddock,[1467] is a new technique that augments conventional heterodyne interferometry with digital modulation-demodulation to provide robust, high-sensitivity displacement measurements. DI employs pseudorandom noise (PRN) phase modulation to isolate interferometric signals based on their delay, with interferometric signals effectively time-tagged by phase modulating the laser source with the binary PRN code. Digitally enhanced interferometry improves measurement sensitivity by exploiting the autocorrelation properties of the PRN to isolate only the signal of interest and reject spurious signals (e.g., from scattered light). The properties of the PRN code determine the degree of isolation. In contrast to standard PRN-based measurements, digitally enhanced interferometry retains the full interferometric sensitivity determined by the optical wavelength. Another benefit of delay-based signal isolation is the ability to measure multiple optical components (i.e., multiplexing capability) with a single

---

[1467] D.A. Shaddock, "Digitally enhanced heterodyne interferometry," Opt. Lett. 32(15 November 2007):3355-3357.

metrology system. This multiplexing capability significantly simplifies measurements of multiple components, such as displacement monitoring of a train of optics or segments of a multimirror telescope. The primary goal of Shaddock's research has been to provide an improved method for detecting minute changes in distance among components of a space-based gravity wave detector.[1468] However, in private correspondence with Freitas in March 2009,[1469] Shaddock confirmed that "for scanning probe microscopy", the idea underlying DI "could be adapted to work quite well [and] we are looking into this application in collaboration with the National Measurement Institute in Sydney." This is confirmed by the Australian NMI's "Nanometrology" division in early 2009:[1470] "Within the next few years we aim to...acquire, develop and operate a metrological atomic force microscope to provide traceability for dimensional nanoscale measurements in Australia." See update.[1471]

Figure 4-107 shows a digitally enhanced heterodyne interferometer used to measure changes in the separation of three partially reflective mirrors. (These mirrors were intended to be mounted on components of a gravity wave detector, but the multiple mirrors could equally well be affixed to X, Y and Z fiducial members of an AFM positioning system.) A beam splitter divides the laser output into a local oscillator and probe beam. The local oscillator is frequency shifted by an acousto-optic modulator (AOM) to provide a heterodyne signal at the photodetector with a frequency f_h. A PRN code generator drives an electro-optic modulator (EOM) to produce a zero or π phase shift on the probe beam before it is directed toward the three mirrors. (Low reflectivity mirrors ensure that each reflection is of comparable amplitude and reduce ambiguity arising from multiple reflections associated with optical cavity effects; reflections from multiple round trips will have a different delay and reduced amplitude and thus are easily excluded.) The reflected light is recombined with the local oscillator and the interference signal is measured by the photodetector. The optical system differs from a conventional heterodyne interferometer

---

[1468] B.J.J. Slagmolen, G. de Vine, D.S. Rabeling, K. McKenzie, A.J. Mullavey, D.A. Shaddock, D.E. McClelland, M. Evans, Y. Aso, "Advanced LIGO arm cavity pre-lock acquisition system," http://www.ligo.caltech.edu/docs/T/T080139-00.pdf (2008).

[1469] Personal communication; email from Daniel Shaddock to Robert A. Freitas Jr., 26 March 2009.

[1470] National Measurement Institute, Sydney, Australia; "Nanometrology" division http://www.measurement.gov.au/index.cfm?event=object.showContent&objectID=F47BBE50-FE60-E6AE-137DEC3A3CF731B8 (last updated 11 February 2009); see also a 2006 paper at http://www.measurement.gov.au/assets/documents/nmiinternet/NMI_TR_1220061130091501.pdf.

[1471] Malcolm Lawn; Jan Herrmann; Christopher H. Freund; John R. Miles; Malcolm Gray; Daniel Shaddock; Victoria A. Coleman; Asa K. Jämting, "Traceable nanoscale length metrology using a metrological Scanning Probe Microscope (Proceedings Paper)," Proceedings Vol. 7729 Scanning Microscopy 2010, Michael T. Postek; Dale E. Newbury; S. Frank Platek; David C. Joy, Editors, 77290L, Date: 3 June 2010. Abstract: "We give an overview of the design and planned operation of the metrological Scanning Probe Microscope (mSPM) currently under development at the National Measurement Institute Australia (NMIA) and highlight the metrological principles guiding the design of the instrument. The mSPM facility is being established as part of the nanometrology program at NMIA and will provide the link in the traceability chain between dimensional measurements made at the nanometer scale and the realization of the SI meter at NMIA. The instrument will provide a measurement volume of 100 μm × 100 μm × 25 μm with a target uncertainty of 1 nm for the position measurement."

primarily by the PRN phase modulation. With no PRN modulation the phase of the heterodyne signal at the photodetector would be determined by the vector sum of the reflections from all three mirrors, and information about individual mirror positions is lost. When the PRN modulation is present, each signal possesses a time-varying phase shift unique to its time of flight from the EOM. Digitally enhanced interferometry reassigns the rejection of spurious interference from a hardware responsibility to a signal processing function. This relaxes requirements on mirror loss or polarizer extinction ratio compared to conventional heterodyne measurements. Isolation through digital signal processing is deterministic with no degradation over time, and provides scalability as processing power continues to improve.

Figure 4-107. Digitally enhanced heterodyne interferometer for monitoring the separation of mirrors M1, M2, and M3; reflections from the different mirrors are isolated by matching the decoding delays to the optical delays; EOM, electro-optic modulator; AOM, acousto-optic modulator; PRN, pseudorandom noise.[1472]

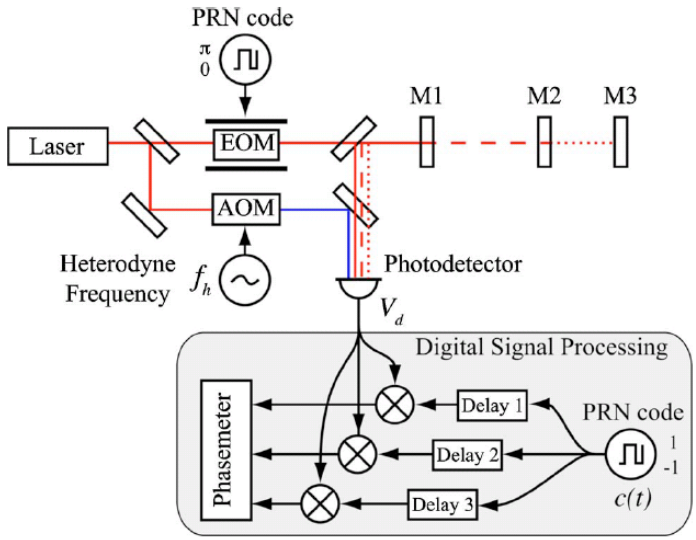

The PRN phase modulation randomly inverts the amplitude of the heterodyne signal measured by the photodetector. To recover the heterodyne signal the photodetector output is multiplied by the same code delayed by an amount equal to the total optical-electronic delay of the reflection of interest. With matched delays this multiplication reverses the inversion of, say, the M1 signal and recovers a standard heterodyne signal, whereupon M1 information is said to be despread into a pure sinusoid at the heterodyne frequency. The phase of this heterodyne signal contains the mirror displacement information. For reflections where the modulation and demodulation delays differ by more than one code length these signals are not despread but instead are randomly reinverted and appear as a broadband noise background to the measurement. This broadband noise can be strongly rejected by appropriate averaging in the phasemeter. Mirror separation

---

[1472] D.A. Shaddock, "Digitally enhanced heterodyne interferometry," Opt. Lett. 32(15 November 2007):3355-3357.

information is obtained by differencing the phase of the decoded signals. The binary noise generator outputs a random bit at each "chip" (tick of the clock). Chip frequency f_{chip} determines the minimum delay difference needed for optimal isolation between reflections, requiring a minimum mirror separation of $\Delta L \geq c / 2f_{chip} \sim 60$ cm for $f_{chip} = 250$ MHz, the frequency used in the first experimental work[1473] involving a Michelson-type configuration to perform "range-gated metrology". This work demonstrated a positional cyclic error of **1100 pm** with a displacement measurement update rate of 2.5 KHz, but claimed that resolution would be improved by a factor of 2 for every factor of 4 decrease in the update rate.[1474] Shaddock's DI technique shares the same sensitivity to shot noise and laser frequency noise as conventional interferometry – but this noise can be mitigated in the usual ways, for example, by stabilizing the laser frequency or by measuring the difference between two equal length arms. Like other broadband noise (e.g. electronic noise), the shot noise level is unaffected by the digital decoding due to the random nature of shot noise and its lack of correlation with the PRN code.

In 2009, the DI technique was used to measure the displacement of a Fabry-Pérot cavity by detecting the light transmitted through the cavity.[1475] Cavity displacement can be inferred from the phase difference between the single-pass and the first round-trip beams. Previous experimental work[1476] employed reflection-based DI measurements where minimizing cross-talk between the respective signals requires the use of low reflectivity mirrors to approximately match the electric field amplitudes. For highly reflective optical components, such as those used in optical cavities, the reflection from the first mirror will dominate the signals at the photodetector. The transmitted signals, however, will have approximately equal amplitudes and thus transmission-based DI measurements are preferred for highly reflective optical components.

In this experiment (Figure 4-108A), two partially reflecting mirrors, M1 and M2, form an optical cavity. A beamsplitter divides the laser output field into a local oscillator beam and a probe beam. The local oscillator is frequency-shifted by an acousto-optic modulator (AOM), providing a heterodyne signal with frequency f_h at the photodetector. A PRN code generator drives an electro-optic modulator (EOM) to produce either a zero or π phase shift on the probe beam before it is directed toward mirrors M1 and M2. The transmitted light is recombined with the local oscillator and the interference signal is measured by the photodetector. The optical cavity under test was 3.75 m long (chosen to equal the wavelength of the PRN code) with a finesse $F \approx 30$ mounted on an optical bench in air. Both cavity mirrors had a power reflectivity of 90%, with a flat input coupler and a 6 m radius of curvature output coupler.

[1473] O.P. Lay, S. Dubovitsky, D.A. Shaddock, B. Ware, "Coherent range-gated laser displacement metrology with compact optical head," Optics Letters 32(15 October 2007):2933-2935.

[1474] O.P. Lay, S. Dubovitsky, D.A. Shaddock, B. Ware, "Coherent range-gated laser displacement metrology with compact optical head," Optics Letters 32(15 October 2007):2933-2935.

[1475] Glenn de Vine, David S. Rabeling, Bram J.J. Slagmolen, Timothy T-Y. Lam, Sheon Chua, Danielle M. Wuchenich, David E. McClelland, Daniel A. Shaddock, "Picometer level displacement metrology with digitally enhanced heterodyne interferometry," Opt. Express 17(19 January 2009):828-837; http://www.phys.ufl.edu/~bernard/IREU2007/Publications/OE17_828.pdf.

[1476] O.P. Lay, S. Dubovitsky, D.A. Shaddock, B. Ware, "Coherent range-gated laser displacement metrology with compact optical head," Optics Letters 32(15 October 2007):2933-2935.

Figure 4-108. (A) Left: Digital Interferometer for monitoring displacements of two mirrors, M1 and M2; signals are isolated by matching the decoding delays to the optical delays. (B) Right: Spectral density of the DI measurement of cavity displacement when the cavity is locked using PDH (Pound-Drever-Hall) locking; spectral density averaged for clarity (3x for 0.1 > f > 1 Hz, and 10x for f > 1 Hz); roll-off above 100 Hz is due to the transfer function of the phasemeter.[1477]

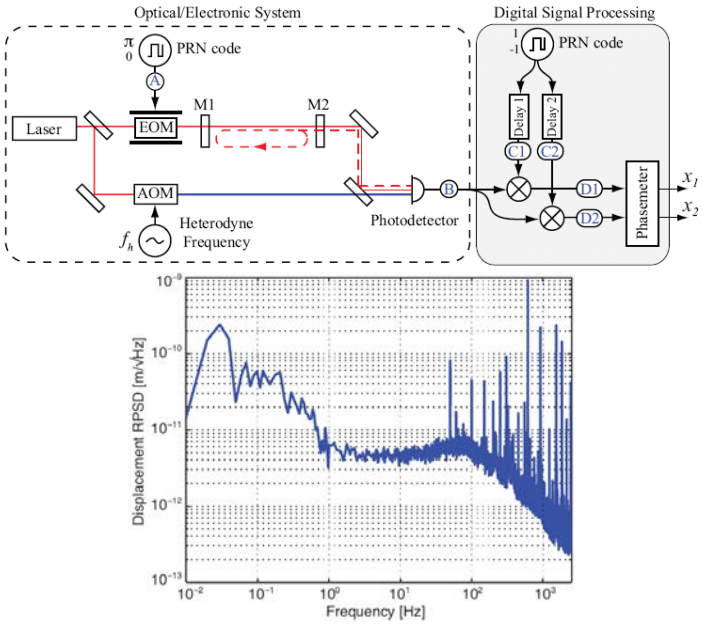

A displacement sensitivity of approximately **5 pm/√Hz** was achieved at frequencies above 1 Hz (Figure 4-108B). The roll-off above 100 Hz is due to the transfer function of the phasemeter and does not signify improved displacement noise – the phasemeter's digital phase locked loop unity gain frequency was ~100 Hz, therefore it did not faithfully reproduce phase fluctuations above this frequency.

[1477] Glenn de Vine, David S. Rabeling, Bram J.J. Slagmolen, Timothy T-Y. Lam, Sheon Chua, Danielle M. Wuchenich, David E. McClelland, Daniel A. Shaddock, "Picometer level displacement metrology with digitally enhanced heterodyne interferometry," Opt. Express 17(19 January 2009):828-837; http://www.phys.ufl.edu/~bernard/IREU2007/Publications/OE17_828.pdf.

4.6.6 Astronomical Metrological Interferometer Systems

In astronomy, state-of-the-art interferometry systems are currently employed in two major applications: astrometry and extrasolar planet detection (Section 4.6.6.1) and gravitational wave detection (Section 4.6.6.2).

4.6.6.1 Astrometry and Extrasolar Planet Detection

Astrometry is the science of determining the positions and motion of celestial objects. The SIM (Section 4.6.6.1.1) mission will employ interferometers to track stellar locations to extreme accuracy, allowing the measured stellar wobble to reveal the presence of otherwise unseen planets orbiting the star; the Keck Interferometer (Section 4.6.6.1.2) is a ground-based telescope with one future mission to observe extrasolar planets by measuring interferometric phase differences between parent star and planet. The GAIA mission (Section 4.6.6.1.3) is planned to compile a highly-accurate billion-star astrometric map of the galaxy using a Fizeau interferometer, and there are a few other interferometric astrometry projects that are mentioned for completeness (Section 4.6.6.1.4).

4.6.6.1.1 JPL/SIM Lite Astrometric Observatory

The Space Interferometry Mission (SIM), also known as SIM Lite and formerly known as SIM PlanetQuest, is a planned space telescope (Figure 4-109) being developed by the U.S. National Aeronautics and Space Administration (NASA), in conjunction with contractor Northrop Grumman.[1478] One of the main goals of the mission is to hunt for Earth-sized planets orbiting stars other than the Sun. The project is being managed by NASA's Jet Propulsion Laboratory (JPL) in Pasadena, California.

After initial approval in 1996, in 1997 three separate teams were awarded $200K each to perform competing four-month preliminary architecture studies.[1479] After that was completed, the major initial contracts for SIM Lite were awarded in 1998, totaling US$200 million. The project's scientific team was selected in November 2000 and consisted of 10 principal investigators and five mission specialists, included notable names from the world of extrasolar planet research. Work on the SIM project required scientists and engineers to move through eight specific new

---

[1478] "Space Interferometry Mission," 22 October 2009; http://en.wikipedia.org/wiki/Space_Interferometry_Mission.

[1479] "NASA picks three teams to study space interferometry," Academic Universe, Aerospace Daily, 14 January 1997, Vol. 181, No. 9, p. 62; http://www.ulib.niu.edu:2453/universe/document?_m=4e9e19bf8d6f46ae0ab0eda2744ec796&_docnum=8&wchp=dGLzVzz-zSkVA&_md5=bbcf4b5cbe531342ce8b691473c63895. R.L. Baron, M.H. Milman, K.M. Aaron, "SIM vs. SOS: A Space Interferometry Trade Study," Astronomical Telescopes and Instrumentation, Kona, Hawaii, USA, 19 March 1998; http://trs-new.jpl.nasa.gov/dspace/bitstream/2014/19389/1/98-0739.pdf.

technology milestones, all of which had been completed by November 2006. SIM Lite was originally scheduled for a 2005 launch aboard an Evolved Expendable Launch Vehicle (EELV), but as a result of continued budget cuts the launch date has been pushed back at least five times. NASA has set a preliminary launch date for 2015 and U.S. federal budget documents confirm that a launch date is expected "no earlier" than 2015. By February 2007 the budget cuts outlined in the FY 2007 budget had already forced SIM engineers at JPL to find other areas to work in, and the program's fate remained uncertain.[1480]

Figure 4-109. A 2006 artist's impression of SIM PlanetQuest.[1481]

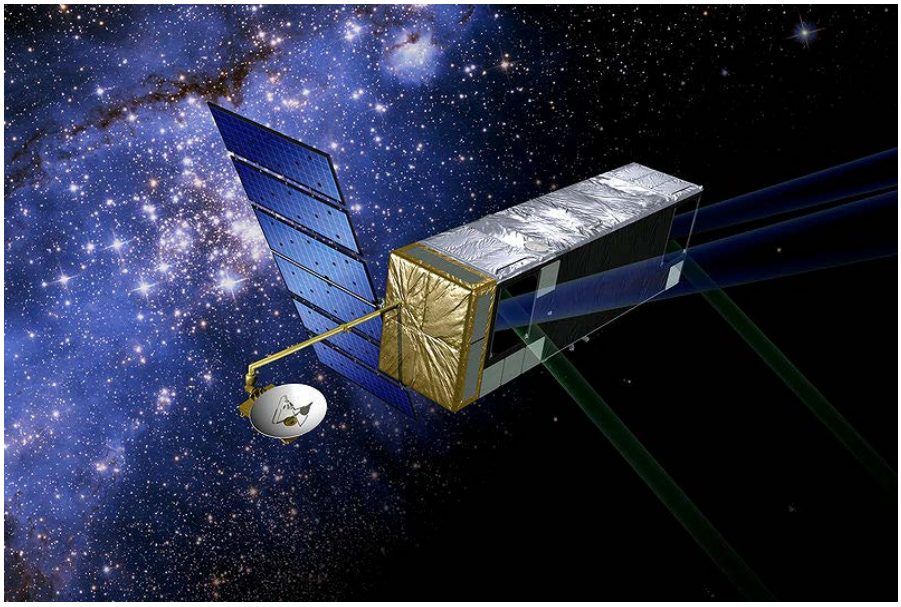

SIM Lite will be the first space-based long baseline Michelson interferometer designed for precision astrometry. It will operate in an Earth-trailing heliocentric orbit, 95 million km from Earth. SIM will perform a search for nearby terrestrial planets (such as Earth or Mars) around approximately 250 nearby stars by looking for the "wobble" in the parent star's apparent motion as the planet orbits.[1482] The spacecraft will accomplish this task, titled the Deep Search, to an accuracy of one millionth of an arcsecond (1 micro-arcsec ~ 5 picoradians). This requires measurement of differential changes in optical path (optical path difference, OPD) between the

---

[1480] "Space Interferometry Mission," 22 October 2009; http://en.wikipedia.org/wiki/Space_Interferometry_Mission.

[1481] http://en.wikipedia.org/wiki/File:SIM_Concept2006_lr.jpg.

[1482] "Space Interferometry Mission (SIM)," JPL, 22 October 2009; http://nexsci.caltech.edu/missions/SIMPQ/ and see also: http://planetquest.jpl.nasa.gov/SIM/index.cfm.

left and right arm of a 10-meter baseline interferometer to be known to within **50 pm** RMS,[1483] so the error budgeted to each metrology interferometer is **10 pm** RMS for motions (of fiducials separated by 1-7 meters) of less than 1 mm, over a period of ~1000 sec.[1484]

The SIM Lite instrument (mounted on a 3-axis stabilized spacecraft) consists of two visible-wavelength Michelson (pupil plane) stellar interferometer sensors, one 30 cm Guide telescope, and one external metrology sensor, all supported by a Precision Structure subsystem (PSS) and controlled by the Real-Time Control (RTC) subsystem (Figure 4-110A).[1485] The instrument is comprised of three interferometers having two telescopes each. The angle of the science interferometer baseline to the target star is measured with respect to distant "fixed" reference stars. The accuracy of this relative measurement is dependent on knowledge of the position of each fiducial in the instrument truss as these fiducials define the various interferometer baselines. The legs of the truss are external to the starlight path within each interferometer, and therefore the measurement of the lengths of these legs are referred to as External Metrology. In contrast, Internal Metrology refers to the measurement of the optical path difference between the lengths of the starlight paths originating from each collector bay.[1486]

The External Metrology sensor is a laser truss that measures the baseline length and relative orientation of the interferometers. The truss consists of ten laser beams launched by 10 metrology gauges that are each capable of measuring the direct distance between pairs of optical corner cube fiducials (rather than the path difference between the left and right arms of the interferometers) to an accuracy of **a few picometers** using heterodyne metrology beam launchers. This truss is used in non-real-time to reconstruct on the ground where the optical elements were located relative to each other as a function of time, correlated to science measurements.[1487] The brassboard External Metrology beam launcher (Figure 4-110B) has met nearly all design requirements – the driving requirement is a narrow-angle performance of 3.0 pm and the

---

[1483] http://instrumentsystems.jpl.nasa.gov/active/picometer/index.cfm.

[1484] P.G. Halverson, L.S. Azevedo, R.T. Diaz, R.E. Spero, "Characterization of Picometer repeatability displacement metrology gauges," Optoelectronic Distance/Displacement Measurements and Applications, Pavia, Italy, 20 September 2001; http://trs-new.jpl.nasa.gov/dspace/bitstream/2014/13060/1/01-1565.pdf.

[1485] Bijan Nemati, "Chapter 16. Astrometric Interferometers," in: JPL, SIM Lite Astrometric Observatory, January 2009, pp. 165-172; http://planetquest.jpl.nasa.gov/SIM/keyPubPapers/SIMLiteBook/Chapter-16-LR.pdf. Frank G. Dekens, Bijan Nemati, Rolf Danner, Fabien Nicaise, "Chapter 20. SIM Lite Flight System Design," Theme VI: Project Technology Readiness, in: JPL, SIM Lite Astrometric Observatory, January 2009, pp. 219-238; http://planetquest.jpl.nasa.gov/SIM/files/Chapter-20-LR.pdf.

[1486] Gary M. Kuan, Frank G. Dekens, "Picometer level modeling of a shared vertex double corner cube in the Space Interferometry Mission Kite Testbed," Astonomical Telescopes and Instrumentation, Probing the Universe from Ground and Space, Orlando, Florida, May 24-31, 2006. Pasadena, CA : Jet Propulsion Laboratory, National Aeronautics and Space Administration, 2006; http://trs-new.jpl.nasa.gov/dspace/bitstream/2014/40134/1/06-1402.pdf.

[1487] "Space Interferometry Mission (SIM)," JPL, 22 October 2009; http://nexsci.caltech.edu/missions/SIMPQ/ and see also: http://planetquest.jpl.nasa.gov/SIM/index.cfm.

brassboard performance was measured to be **3.5 pm**.[1488] The Internal Metrology launcher design (Figure 4-110C) has been driven by the narrow-angle scenario performance requirement of 3.5 pm of error; the brassboard model has achieved **3.1 pm**.[1489] The fiducials needed for SIM Lite are challenging to build because they must satisfy many tight optical tolerances. Two of the fiducials require two corner cubes, and two require three corner cubes to be fashioned in such a way that their vertices coincide to <6 μm. The wavefront error of the base plate is required to be 3 nm and that of the wedges 6 nm.[1490]

A laser heterodyne interferometer system with better than **10 picometer (pm) accuracy** in displacement measurement and 1-3 microns in absolute distance ranging accuracy are required for SIM.[1491] Commercially available displacement measuring interferometers (DMIs) that are based on traditional polarization-type configurations are limited to 1-2 nm in periodic non-linear error. To make a DMI with ~10 pm accuracy and absolute distance measurement accuracy of 1-3 microns for SIM, by 2001 JPL engineers first built a laser heterodyne interferometer that employs a "switched heterodyne laser source" and a "common-path heterodyne interferometer (COPHI)".[1492] The switched heterodyne laser source consists of two single frequency lasers that are frequency-offset-locked to each other by 15 GHz. Two acousto-optic modulators (AOM) are used as high contrast optical switches to switch between the two lasers. The 15 GHz frequency difference resulting from this "two color laser" produces a synthetic wavelength of about 2 cm that is used to do absolute distance measurement. The alternating input (1 KHz switching) from the lasers is then sent to the third and fourth AOMs which are used as frequency shifters.

[1488] Frank G. Dekens, Bijan Nemati, Rolf Danner, Fabien Nicaise, "Chapter 20. SIM Lite Flight System Design," Theme VI: Project Technology Readiness, in: JPL, SIM Lite Astrometric Observatory, January 2009, pp. 219-238; http://planetquest.jpl.nasa.gov/SIM/files/Chapter-20-LR.pdf.

[1489] Frank G. Dekens, Bijan Nemati, Rolf Danner, Fabien Nicaise, "Chapter 20. SIM Lite Flight System Design," Theme VI: Project Technology Readiness, in: JPL, SIM Lite Astrometric Observatory, January 2009, pp. 219-238; http://planetquest.jpl.nasa.gov/SIM/files/Chapter-20-LR.pdf.

[1490] Frank G. Dekens, Bijan Nemati, Rolf Danner, Fabien Nicaise, "Chapter 20. SIM Lite Flight System Design," Theme VI: Project Technology Readiness, in: JPL, SIM Lite Astrometric Observatory, January 2009, pp. 219-238; http://planetquest.jpl.nasa.gov/SIM/files/Chapter-20-LR.pdf.

[1491] Feng Zhao, "Development of high-precision laser heterodyne metrology gauges," Proc. SPIE 5634(2005):247. Peter G. Halverson, Robert E. Spero, "Signal processing and testing of displacement metrology gauges with picometre-scale cyclic nonlinearity," J. Opt. A: Pure Appl. Opt. 4(2002):S304-S310.

[1492] Feng Zhao, Jennifer E.. Logan, Stuart Shaklan, Michael Shao, "A common-path, multi-channel heterodyne laser interferometer for subnanometer surface metrology", DSpace at JPL, 1999; http://trs-new.jpl.nasa.gov/dspace/bitstream/2014/17017/1/99-0434.pdf. Feng Zhao, Jennifer E. Logan, Stuart Shaklan, Michael Shao, "A common-path, multi-channel heterodyne laser interferometer for sub-nanometer surface metrology," Jet Propulsion Laboratory, California Institute of Technology, 4800 Oak Grove Drive, Pasadena, California 91109, U.S.A., SPIE Proceedings 3740(1999):642-645; http://trs-new.jpl.nasa.gov/dspace/bitstream/2014/17017/1/99-0434.pdf. Feng Zhao, "Picometer laser metrology for the Space Interferometery Mission," Conference on Lasers and Electro-Optics (CLEO) 2004, San Francisco, CA, 16-21 May 2004; http://trs-new.jpl.nasa.gov/dspace/bitstream/2014/38602/1/03-3442.pdf.

Figure 4-110. (A) SIM Lite instrument optical configuration. (B) The brassboard external metrology beam launcher, shown with its interfaces, monitors the distance between SIM Lite's fiducials. (C) Brassboard internal metrology beam launcher; both launchers successfully passed vibration tests, thermal tests, and metrology stability and cyclic error requirements at the 3 pm level.[1493] (D) Original bench prototype for the external metrology beam launcher shown in (B).[1494]

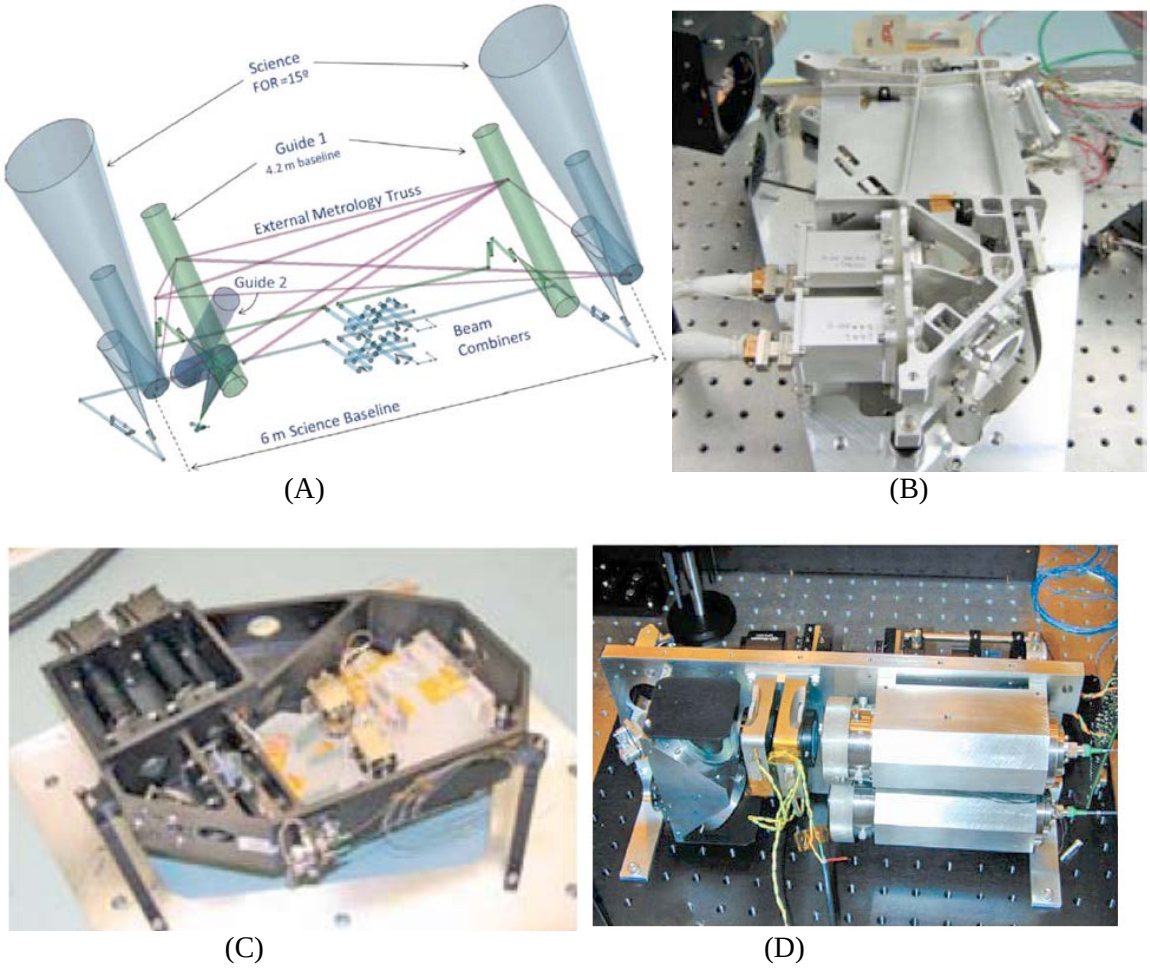

[1493] Frank G. Dekens, Bijan Nemati, Rolf Danner, Fabien Nicaise, "Chapter 20. SIM Lite Flight System Design," Theme VI: Project Technology Readiness, in: JPL, SIM Lite Astrometric Observatory, January 2009, pp. 219-238; http://planetquest.jpl.nasa.gov/SIM/files/Chapter-20-LR.pdf.

[1494] Bijan Nemati, Inseob Hahn, Oscar S. Alvarez-Salazar, "Chapter 19. Technology Program Accomplishments," in: JPL, SIM Lite Astrometric Observatory, January 2009, pp. 195-217; http://planetquest.jpl.nasa.gov/SIM/keyPubPapers/SIMLiteBook/Chapter-19-LR.pdf.

In this Michelson-type interferometer,[1495] both the measurement and reference beams are collimated from a pair of polarization-maintaining fibers with two Zerodur off-axis parabolic mirrors. The displacement measurement configuration uses a flat mirror with a center hole as fiducial A and a second flat mirror as fiducial B (Figure 4-111). (In a molecular workstation design, fiducial B would represent the moving AFM.) The center hole in fiducial A allows the center portion of the beam at frequency f_0 to reach fiducial B. This way the measurement beam f_0 is split into two symmetric sections. Both mirrors are aligned to retro-reflect the beams back to the interferometer to combine with the reference beam at $f_0+\Delta f$, which serves as a local oscillator. At this point, two interference fringes are formed, the annular fringe formed by fiducial A and the center fringe formed by fiducial B. Then the heterodyne fringes are spatially separated with a truncated mirror and focused into separate photodetectors. The phase difference between the reference and measurement signals is then used to calculate the displacement between the fiducials.

Figure 4-111. Schematic of a common-path heterodyne interferometer, configured for displacement measurement.[1496]

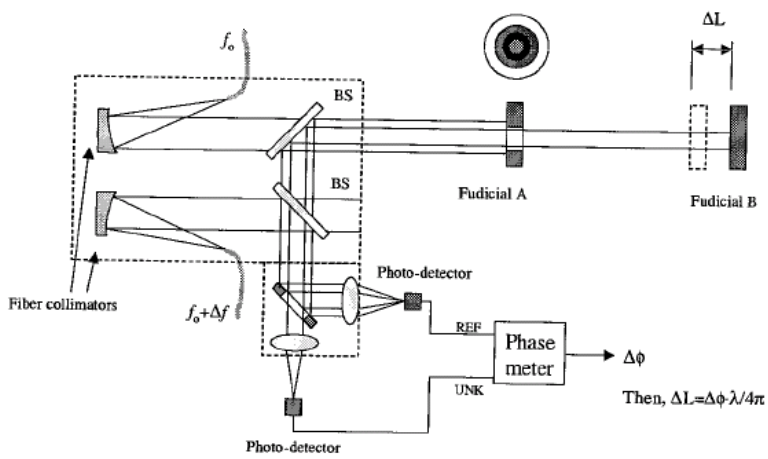

[1495] Feng Zhao, Jennifer E. Logan, Stuart Shaklan, Michael Shao, "A common-path, multi-channel heterodyne laser interferometer for sub-nanometer surface metrology," Jet Propulsion Laboratory, California Institute of Technology, 4800 Oak Grove Drive, Pasadena, California 91109, U.S.A., SPIE Proceedings 3740(1999):642-645; http://trs-new.jpl.nasa.gov/dspace/bitstream/2014/17017/1/99-0434.pdf. Feng Zhao, "Picometer laser metrology for the Space Interferometery Mission," Conference on Lasers and Electro-Optics (CLEO) 2004, San Francisco, CA, 16-21 May 2004; http://trs-new.jpl.nasa.gov/dspace/bitstream/2014/38602/1/03-3442.pdf.

[1496] Feng Zhao, Jennifer E. Logan, Stuart Shaklan, Michael Shao, "A common-path, multi-channel heterodyne laser interferometer for sub-nanometer surface metrology," Jet Propulsion Laboratory, California Institute of Technology, 4800 Oak Grove Drive, Pasadena, California 91109, U.S.A., SPIE Proceedings 3740(1999):642-645; http://trs-new.jpl.nasa.gov/dspace/bitstream/2014/17017/1/99-0434.pdf.

To measure the residual periodic nonlinear error, a PZT is used to translate fiducial B "linearly" over a distance of many laser wavelengths.[1497] The distance is then measured with a phase meter. A periodic error in this "linear" translation can be estimated by looking at the power spectral density of the displacement data. Here, λ = 532 nm and the PZT has a total stroke of 5 microns with a triangle wave modulation of 0.05 Hz (~1 sawtooth ever 20 sec) so cyclical error with $\lambda/2$ periodicity can be found at ~2 Hz in the spectral domain (Figure 4-112A). As the PZT is moving "linearly" in one direction for ~9 seconds, the periodic error distinguishes itself from the noise background in the spectral domain – in this case, the cyclic error is about 27 pm RMS (see arrow). Background noise measurement with the PZT driver off indicated that peaks above 10 Hz are attributable to mechanical vibrations in this prototype experimental setup. To measure thermal stability, fiducials A and B are replaced with a single Zerodur mirror to ensure that there is no change in the fiducials during the measurement – therefore any changes in the phase between the annular and central fringes are due to the drift of the interferometer itself. Figure 4-112B shows a measurement of the drift over 10 hours, indicating stability to better than 100 pm/hour. Lay et al.[1498] provide more details on a similar interferometer configuration, called MSTAR (Modulation Sideband Technology for Absolute Ranging), that was demonstrated in the lab in 2003 by a group led from JPL.

SIM has a Wide- and Narrow-Angle observing mode, the latter of which is designed for individual stars to which ~20X more time will be dedicated. In this mode, the specified performance goal is 8 pm of displacement error per star per gauge. In 2004,[1499] using the "KITE" testbed[1500] for the prototype SIM interferometers in which the target was observed for 15 sec followed by 15 sec on a reference star (constituting one "chop"), a series of runs of 40 chops per run in various directions in the field of view produced the displacement error per star per gauge as shown in Figure 4-113A; a histogram of the same data in Figure 4-113B shows a displacement error of 5.6 pm RMS per star per gauge.[1501]

[1497] Feng Zhao, Jennifer E. Logan, Stuart Shaklan, Michael Shao, "A common-path, multi-channel heterodyne laser interferometer for sub-nanometer surface metrology," Jet Propulsion Laboratory, California Institute of Technology, 4800 Oak Grove Drive, Pasadena, California 91109, U.S.A., SPIE Proceedings 3740(1999):642-645; http://trs-new.jpl.nasa.gov/dspace/bitstream/2014/17017/1/99-0434.pdf.

[1498] Oliver P. Lay, Serge Dubovitsky, Robert Peters, Johan Burger, Seh-Won Ahn, William H. Steier, Harrold R. Fetterman, Yian Chang, "Absolute distance measurement with the MSTAR sensor," The International Society for Optical Engineering (SPIE), International Symposium on Optical Science and Technology, San Diego, California, 3-8 August 2003; http://trs-new.jpl.nasa.gov/dspace/bitstream/2014/40465/1/03-1892.pdf.

[1499] Frank G. Dekens, Oscar Alvarez-Salazar, Alireza Azizi, Steven Moser, Bijan Nemati, John Negron, Timothy Neville, Daniel Ryan, "Kite : status of the External Metrology Testbed for SIM," SPIE Astronomical Telescopes and Instrumentation, Glasgow, Scotland, 21-25 June 2004; http://trs-new.jpl.nasa.gov/dspace/bitstream/2014/40739/1/04-1692.pdf.

[1500] Bijan Nemati, "External Metrology Truss Technology Demonstration (KITE)," Proc. SPIE 4852(2003):90; http://trs-new.jpl.nasa.gov/dspace/bitstream/2014/10469/1/02-2465.pdf.

[1501] Frank G. Dekens, Oscar Alvarez-Salazar, Alireza Azizi, Steven Moser, Bijan Nemati, John Negron, Timothy Neville, Daniel Ryan, "Kite : status of the External Metrology Testbed for SIM," SPIE

Figure 4-112. (A) Left: Power spectral density of the displacement data. (B) Right: Stability measurement of the interferometer showing drift of less than 100 pm/hour.[1502]

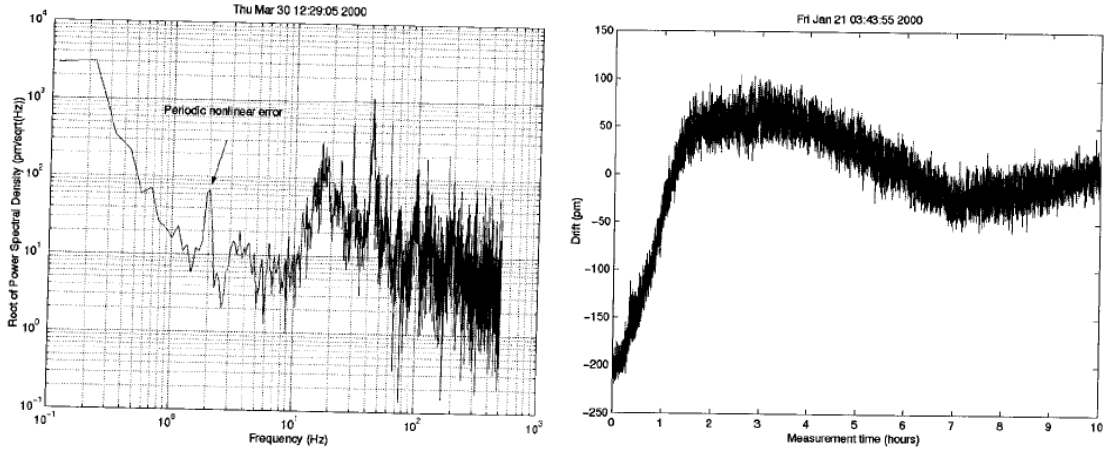

Figure 4-113. (A) Left: Comparison of Narrow-Angle mode chops in different directions in field of view. (B) Right: Histogram of 8 chop error averages.[1503]

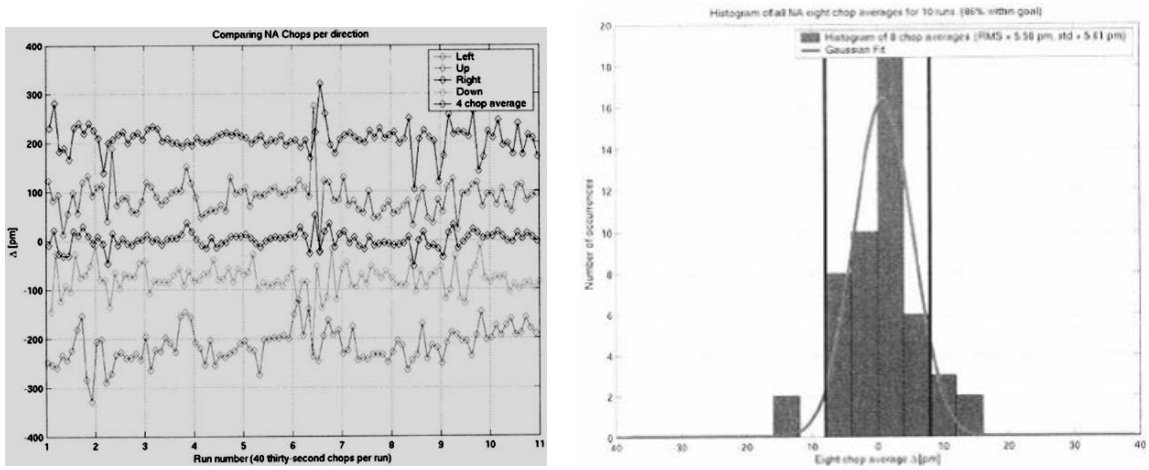

Astronomical Telescopes and Instrumentation, Glasgow, Scotland, 21-25 June 2004; http://trs-new.jpl.nasa.gov/dspace/bitstream/2014/40739/1/04-1692.pdf.

[1502] Feng Zhao, Jennifer E. Logan, Stuart Shaklan, Michael Shao, "A common-path, multi-channel heterodyne laser interferometer for sub-nanometer surface metrology," Jet Propulsion Laboratory, California Institute of Technology, 4800 Oak Grove Drive, Pasadena, California 91109, U.S.A., SPIE Proceedings 3740(1999):642-645; http://trs-new.jpl.nasa.gov/dspace/bitstream/2014/17017/1/99-0434.pdf.

[1503] Frank G. Dekens, Oscar Alvarez-Salazar, Alireza Azizi, Steven Moser, Bijan Nemati, John Negron, Timothy Neville, Daniel Ryan, "Kite : status of the External Metrology Testbed for SIM," SPIE Astronomical Telescopes and Instrumentation, Glasgow, Scotland, 21-25 June 2004; http://trs-new.jpl.nasa.gov/dspace/bitstream/2014/40739/1/04-1692.pdf.

According to a more recent 2004 technical update,[1504] the prototype gauges for SIM had been refined to <20 pm linearity, <10 micron absolute accuracy, and stability to <200 pm over the typical SIM observation period of ~1 hour. The mission requirements for relative accuracy had been loosened to ~10 pm RMS over a 90 sec timescale and ~57 pm over a 1-hour timescale, and the equipment now employed active alignment of metrology beams. The COPHI configuration was apparently further refined to a more compact configuration as shown in Figure 4-114A. Leakage between the outer beam, which measures distance between corner cube fiducials, and the inner beam, which acts as a reference, can still cause cyclic error but is partly removed by masking. Testbed (Figure 4-114B) results indicated that all technical goals for the SIM Lite mission had been accomplished (Figure 4-114C).[1505]

Random errors, also called white noise, will average down with integration time. Aside from noise considerations, the SIM technology program has demonstrated the mitigation of systematic instrument errors down to the level of $\lambda/60000$ (e.g., ~10 pm at ~600 nm optical wavelength).[1506] One question remaining to be resolved is whether the SIM/MSTAR system can be cycled fast enough, while maintaining continuous picometer positional accuracy, to be useful in the context of an AFM-based molecular workstation.

[1504] Peter G. Halverson, Oscar Alvarez-Salazar, Alireza Azizi, Frank Dekens, Bijan Nemati, Feng Zhao, "Progress towards picometer accuracy laser metrology for the Space Interferometry mission - update for ICSO 2004," International Conference on Space Optics, Toulouse, France, 30 March 2004; http://trs-new.jpl.nasa.gov/dspace/bitstream/2014/38265/1/04-0594.pdf.

[1505] Bijan Nemati, Inseob Hahn, Oscar S. Alvarez-Salazar, "Chapter 19. Technology Program Accomplishments," in: JPL, SIM Lite Astrometric Observatory, January 2009, pp. 195-217; http://planetquest.jpl.nasa.gov/SIM/keyPubPapers/SIMLiteBook/Chapter-19-LR.pdf.

[1506] Bijan Nemati, "Chapter 16. Astrometric Interferometers," in: JPL, SIM Lite Astrometric Observatory, January 2009, pp. 165-172; http://planetquest.jpl.nasa.gov/SIM/keyPubPapers/SIMLiteBook/Chapter-16-LR.pdf.

Figure 4-114. (A) Left: Block diagram of updated SIM metrology interferometer.[1507] (B) Right: MAM (MicroArcsec Metrology) testbed for SIM Lite, shown here in a 4-meter-diameter vacuum chamber. (C) Below: SIM Lite's chopping scheme is seen in this quasi-static test to be highly effective in bringing errors down to the required picometer class.[1508]

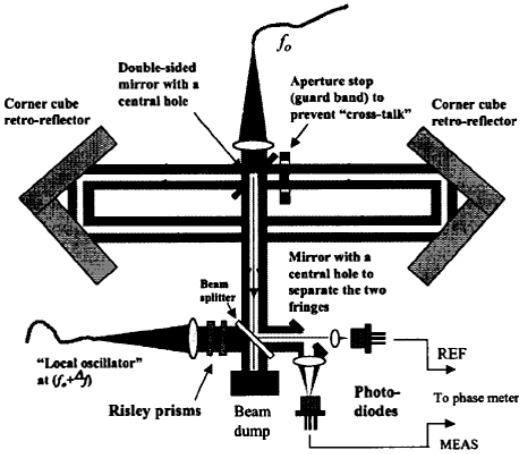

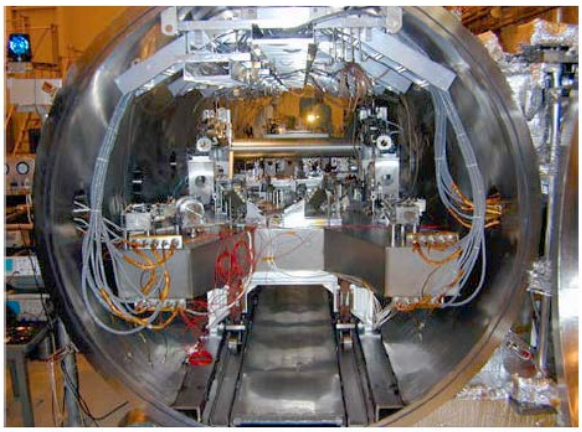

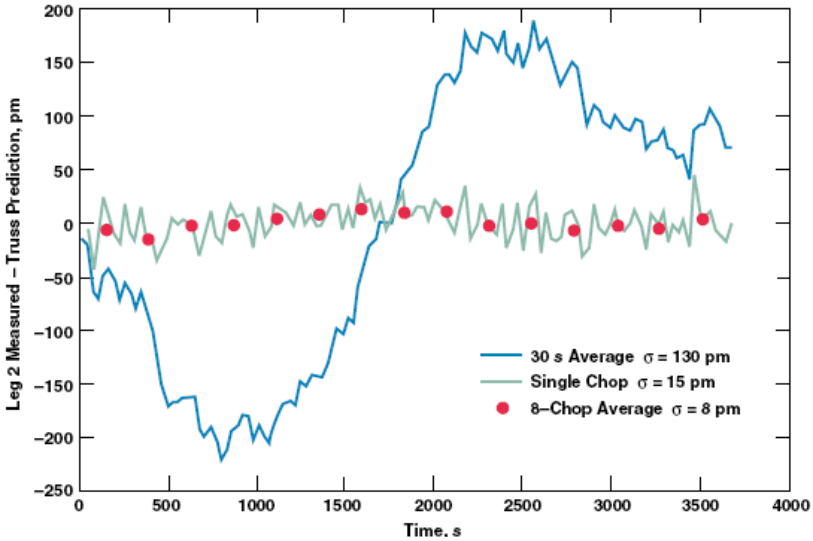

[1507] Peter G. Halverson, Oscar Alvarez-Salazar, Alireza Azizi, Frank Dekens, Bijan Nemati, Feng Zhao, "Progress towards picometer accuracy laser metrology for the Space Interferometry mission - update for ICSO 2004," International Conference on Space Optics, Toulouse, France, 30 March 2004; http://trs-new.jpl.nasa.gov/dspace/bitstream/2014/38265/1/04-0594.pdf.

[1508] Bijan Nemati, Inseob Hahn, Oscar S. Alvarez-Salazar, "Chapter 19. Technology Program Accomplishments," in: JPL, SIM Lite Astrometric Observatory, January 2009, pp. 195-217; http://planetquest.jpl.nasa.gov/SIM/keyPubPapers/SIMLiteBook/Chapter-19-LR.pdf.

4.6.6.1.2 The Keck Interferometer

The Keck Observatory[1509] is a two-telescope astronomical observatory at an elevation of 4,145 meters (13,600 ft) near the summit of Mauna Kea in Hawaii. The primary mirrors of each of the two telescopes (Keck I and Keck II) are 10 meters (33 ft) in diameter, and they can operate together to form a single Michelson-type astronomical interferometer called the Keck Interferometer (KI). The 85-meter (280 ft) separation between the two telescopes gives them the effective angular resolution in one direction of an 85-meter (280 ft) mirror. The KI uses a technique called nulling to distinguish starlight from the reflected light of a nearby exoplanet that is orbiting the star (Figure 4-115).

Figure 4-115. Keck Interferometer. Top: Cut-away view of the Keck Telescopes, showing the 100 foot domes as well as the workshops and basement laboratory. Bottom: Starlight bounces off mirrors on left of screen, goes to long delay lines in the middle, and to fast delay lines on the right.[1510]

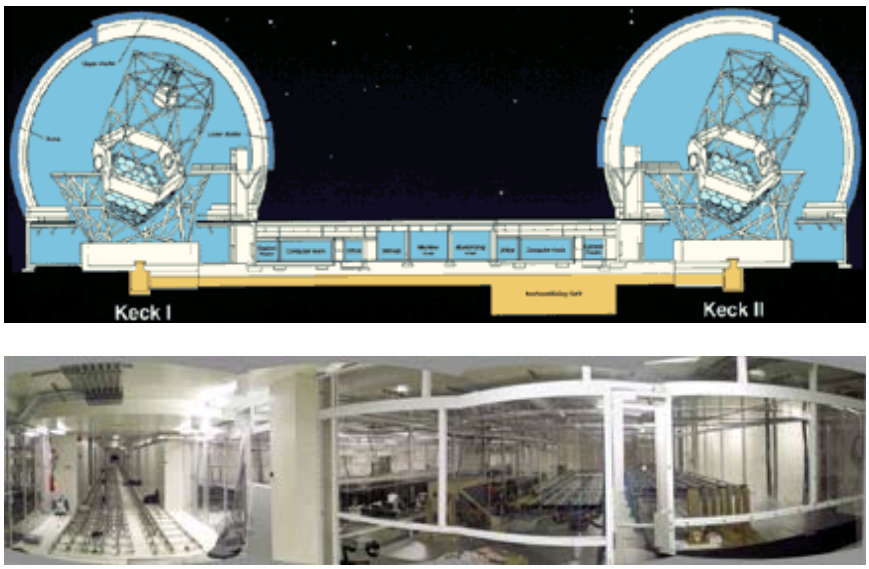

According to the technical page at the Keck website:[1511] "The light from the beam transport system is directed to the beam injection and switching optics, which feed the light into the long

---

[1509] W.M. Keck Observatory, http://en.wikipedia.org/wiki/Keck_Interferometer and http://planetquest.jpl.nasa.gov/Keck/keck_index.cfm.

[1510] Keck Subsystems, Delay Lines and Metrology, http://planetquest.jpl.nasa.gov/Keck/keck_subsystems.cfm.

[1511] Keck Subsystems, Delay Lines and Metrology, http://planetquest.jpl.nasa.gov/Keck/keck_subsystems.cfm.

delay line system. The long delay line system employs flat mirrors mounted on sleds which move along the coude tunnel in the basement. Each sled delays both the primary and secondary beams from a telescope by up to 170 m; the longer delays use a double pass through the delay line system. These are "move and clamp" delay lines, which are stationary during an observation and are only repositioned between targets. The delay lines employ a four-stage servo design with a PZT, two voice coils, and a microstepped tractor motor, and provide full position and rate commanding. The delay lines employ local laser metrology for real-time control of the servo systems. This is similar to that used at PTI, except that the laser sources are fiber remoted to the control room to minimize heat dissipated in the beam combining lab. In addition, separate end-to-end laser metrology which monitors the entire optical system is implemented as required for narrow-angle astrometry and cophasing." The total astrometric noise budget for the KI was initially estimated (in 1998) as **12.12 nm** from all sources,[1512] but the final working system (in 2005) showed an RMS optical path difference variation of **30-42 nm** while tracking.[1513] This is consistent with the stated Keck angular resolution of 5-24 milliarcsec, about 1000-fold poorer than SIM (which requires ~10 pm accuracy).

However, in 2003 Yekta Gursel at NASA-JPL noted that the future Keck Interferometer differential-phase planet-detection system will require a large (2-4 μm) amplitude optical path-length modulator that can be linearly translated with picometer accuracy, and then built and tested a Michelson-type prototype metrological interferometry system or "gauge" that can do this.[1514] To detect extra-solar planets orbiting distant stars, one method is to interferometrically track the star-planet system while making observations of the interferometric phase at several wavelengths at once. Since the light from the planet has a spectral distribution different from that of the parent star, the difference in the detected interferometric phase between different wavelengths is a function of the apparent star-planet separation.[1515] The intensity of the light from the planet is many orders of magnitude smaller than the intensity of the light emitted by the parent star. As a result, the interferometric differential phase measurements have to be very accurate to distinguish the star-planet signal from the instrument noise.

[1512] G.T. van Belle, A.F. Boden, M.M. Colavita, M. Shao, G. Vasisht, J.K. Wallace, "Astrometry with the Keck Interferometer," Proc. SPIE 3350(1998):362-372, http://www.eso.org/~gvanbell/publications/spie_astrometry.pdf.

[1513] S.L. Crawford, M.M. Colavita, J.I. Garcia, E.R. Ligon, B. Mennesson, C.G. Paine, E. Serabyn, R.F. Smythe, M.R. Swain, G. Vasisht, "Final Laboratory Integration and Test of the Keck Interferometer Nuller," JPL-NASA, 2005, http://trs-new.jpl.nasa.gov/dspace/bitstream/2014/37736/1/05-2536.pdf.

[1514] Yekta Gursel, "Picometer-accuracy laser-metrology gauge for the Keck Interferometer Differential Phase Subsystem," SPIE 4838(2003):995; http://trs-new.jpl.nasa.gov/dspace/bitstream/2014/10164/1/02-2224.pdf.

[1515] R.L. Akeson, M.R. Swain, M.M. Colavita, "Differential phase technique with the Keck Interferometer," in: P.J. Lena, A. Quirrenbach, eds., Interferometry in Optical Astronomy, Proceedings of SPIE 4006(2000):321.

A common way to measure interferometric phase is to change the interferometric path-length difference by precise amounts while recording the interferometric fringe intensity.[1516] The phase can then be de-convolved from this series of intensity measurements. This method is known as phase-shifting interferometry (Section 4.6.3.15) as the interferometric phase changes linearly with the changing optical path-length. The device that changes the optical path-length in an interferometer is the path-length modulator. The path-length modulator serves two different purposes. One is to change the path-length by precisely known amounts, and the other is to modulate the path-length rapidly so that a synchronous detection of the interferometric phase can be made to avoid the effects of atmospheric turbulence and ground-induced vibrations. The path-length modulator is constructed by placing a retro-reflector on a linear magnetic drive. The starlight bounces off the retro-reflector as it moves back and forth, modulating the phase of the light that reflects from it proportional to the wavelength of the light and the amplitude of the retro-reflector motion. The motion of the retro-reflector has to be monitored very precisely in order to be able to de-convolve the interferometric phase with sufficient accuracy to detect the differential phase signal created by the star-planet system.

Gursel's gauge is a polarization-insensitive heterodyne gauge which consists of matched collimators, photo-diode receivers, and beam separators. It is fed by a heterodyne plate that uses a stabilized He-Ne laser to supply four, fiber-coupled laser beams which are pairwise 80 kHz apart in frequency to feed two heterodyne gauges. The modulator-driver is a one-dimensional, voice-coil motion element, with dual stainless-steel membranes with pre-load that supplies the linear restoring force, which confine the motion to a single degree of freedom. The driver has two such independent units at opposing ends moving simultaneously in opposite directions. One end of the modulator holds the retro-reflector cube, while the other end carries a precisely matched counter-weight to cancel any linear momentum during the operation resulting in no-vibration transfer to the rest of the instrument. The gauge can monitor the amplitude of the motion of a path-length modulator and is claimed to be capable of reaching a sensitivity of at least 3 pm/√Hz within a bandwidth of 1 Hz at 250-1250 Hz. Testing two Keck gauges against each other (Figure 4-116A) while monitoring a common optical path-length modulator to determine their accuracy yielded a systematic error per gauge of about **25 pm** RMS; Figure 4-116B shows that the two gauge readings agree to within 25 pm or better for frequencies above ~8 Hz. Since the gauge differential appears to rise to ~1000 pm for DC operation, it is unclear if this method would be useful in the context of an AFM-based molecular workstation. The Keck Interferometer (another of NASA's Exoplanet Exploration programs along with SIM) also suffered budget cuts in 2007.

[1516] R.L. Akeson, M.R. Swain, M.M. Colavita, "Differential phase technique with the Keck Interferometer," in: P.J. Lena, A. Quirrenbach, eds., Interferometry in Optical Astronomy, Proceedings of SPIE 4006(2000):321.

Figure 4-116. (A) Left: Experimental setup, with both Keck gauges aligned to the retro-reflector pick-off mirror. (B) Right: The magnitude of fourier transform of the difference between the two gauge readings of the one-way path-length change as they monitor the slowly moving retro-reflector.[1517]

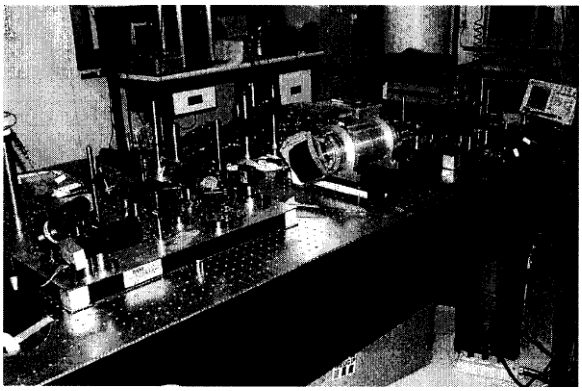

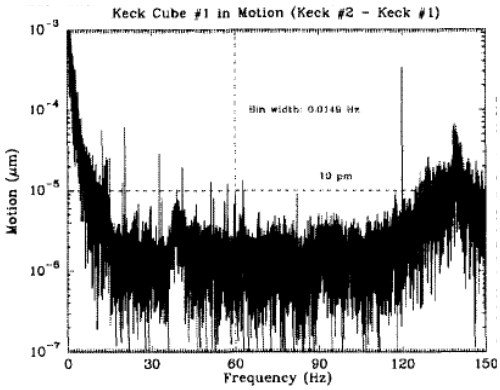

4.6.6.1.3 GAIA Astrometric Metrology Mission

GAIA (Global Astrometric Interferometer for Astrophysics) is a European Space Agency (ESA) astrometry space mission, and a successor to the ESA Hipparcos mission.[1518] It was included within the context of the ESA Horizon 2000 Plus long-term scientific programme in 2000. The 2030 kg spacecraft is expected to be launched by the ESA in the Spring of 2012, and will be operated in a Lissajous orbit around the Sun-Earth L2 Lagrangian point. The GAIA mission will create an ultra-precise three-dimensional map of about one billion stars in our Galaxy. SIM and GAIA are largely complementary missions. SIM has been designed and optimized for pointed observations – SIM's longer baseline, its ability to point at a single source for an extended period of time, and the real-time monitoring of the position of the SIM baseline allow higher accuracy on targets so faint that they cannot even be detected by GAIA. GAIA will not be able to increase the measurement accuracy for a specific target by observing it for a longer time: the duration of each observation is fixed a priori by the spin of the spacecraft. Note that the required measurement accuracy quoted for GAIA is "per mission" and will only be achieved by combining the full five years' worth of observations; SIM can reach similar accuracies in a single observation. As a survey mission, GAIA makes up for its limitations in single-target observations by virtue of the number of targets; GAIA's ability to determine positions and velocities for a very

---

[1517] Yekta Gursel, "Picometer-accuracy laser-metrology gauge for the Keck Interferometer Differential Phase Subsystem," SPIE 4838(2003):995; http://trs-new.jpl.nasa.gov/dspace/bitstream/2014/10164/1/02-2224.pdf.

[1518] GAIA websites: http://en.wikipedia.org/wiki/Gaia_mission and http://sci.esa.int/science-e/www/area/index.cfm?fareaid=26.

large number of stars within the Galaxy will make it extremely valuable for broad galactic structure problems.

The metrology design was originally envisioned as a Fizeau interferometer,[1519] even though a 2004 paper[1520] claimed that only actively stabilized Fabry-Pérot (FP) laser interferometry could meet the mission requirements. Such active stabilization, operating in closed-loop, would need appropriate instruments to measure the basic angle variations (e.g., one-meter length FP interferometers locked to a frequency-stabilized laser beam and capable of picometer precision) and actuators to force them to zero (e.g., piezo-electric translators),[1521] with distances to be controlled defined by mirrors faced to form Fabry-Pérot cavities. As of September 2009,[1522] the Basic Angle Monitoring (BAM) system reportedly consists of a Fizeau interferometer, measuring fluctuations in the basic angle between the two telescopes. Rather than using active control, a five-degrees-of-freedom static mechanism is implemented behind the secondary mirrors of the two telescopes (based on the three-mirror anastigmat design) for securing the optical performance in orbit and cancelling static residual errors due to mirror micro-settings and gravity release.[1523]

TNO Science and Industry (Netherlands)[1524] is developing the picometer metrology system[1525] – the Basic Angle Monitoring Opto-Mechanical Assembly – for this mission. The angle between the lines of sight of the two telescopes is 106.5°, called the Basic Angle. A Basic Angle Monitoring system[1526] continuously measures the angle between the line of sight of the two telescopes, to be able to make corrections for small thermal deformations. Maximum fluctuation of the Basic Angle in flight is assumed to be lower than <7 µarcsec RMS for the random contri-

---

[1519] M. Gai, M.G. Lattanzi, G. Mana, "A Fizeau interferometer for astrometry in space: the metrology point of view," Meas. Sci. Technol. 10(1999):1254-1260.

[1520] E.S. Canuto, F. Musso, "Distributed metrology and active control for according stabilization of space telescopes," Proceedings of the 2004 IEEE International Symposium on Intelligent Control, 2-4 September 2004, pp. 316-321.

[1521] E.S. Canuto, F. Musso, "Distributed metrology and active control for according stabilization of space telescopes," Proceedings of the 2004 IEEE International Symposium on Intelligent Control, 2-4 September 2004, pp. 316-321.

[1522] GAIA Payload Module Metrology, 23 September 2009; http://sci.esa.int/science-e/www/object/index.cfm?fobjectid=40129&fbodylongid=1913.

[1523] GAIA Payload Module Metrology, 23 September 2009; http://sci.esa.int/science-e/www/object/index.cfm?fobjectid=40129&fbodylongid=1913.

[1524] Consultancy for TNO (http://www.tno.nl/gaiabam).

[1525] E.A. Meijer, J.N. Nijenhuis, R.J.P. Vink, F. Kamphues, "Picometer metrology for the GAIA mission," Space Telescopes and Instrumentation 2008: Optical, Infrared, and Millimeter, Marseille, France, 23 June 2008, Proc. SPIE 7010(2008):70102O. See also: Ellart Meijer, Fred Kamphues, "Picometer metrology in space," Mikroniek, Nr. 3, 2008, pp. 5-9.

[1526] Marielle van Veggel, "The Basic Angle Monitoring system: picometer stability with Silicon Carbide optics," Thesis, 2007, 235 pp; http://alexandria.tue.nl/extra2/200710084.pdf.

bution and <4 μarcsec for the systematic contribution during the nominal spin period of six hours. The Basic Angle will be monitored in flight with accuracy better than 0.5 μarcsec RMS for every five-minute interval of scientific operation. The system consists of two laser interferometers. Two pairs of parallel laser bundles are sent to the two telescopes, which create two interference patterns on a detector. If the basic angle varies, the interference patterns will shift. Considering a telescope base length of 0.6 m, this variation corresponds to an optical path difference of **1.5 picometer** RMS.[1527] Of course, a measurement interval fixed at 5 minutes/cycle would be much too slow for use in a practical molecular workstation.

The GAIA payload module is completely built of sintered silicon carbide (SSiC) because of its low thermal expansion, a high thermal conductivity, high specific stiffness, and excellent dimensional stability, although the material is very brittle and requires care to work with.[1528]

4.6.6.1.4 Other Interferometric Astrometry Projects

Other spaceborne interferometric systems for detecting extrasolar planets have been proposed. For example, the planned ESA Darwin 2020[1529] would require positional accuracy (among multiple independent spacecraft) of only 70 microns over a distance of up to 250 meters.[1530] The related Terrestrial Planet Finder (TPF) mission[1531] proposed by JPL (Figure 4-117) (and postponed indefinitely by Congress in 2007) would require RMS interferometric path length control to within ~**1.5 nm**.[1532] Both Darwin and TPF employ IR frequencies, reducing their potential utility in an AFM context. Pierce et al.[1533] describe an interferometer designed to provide 1-10 nm/√Hz displacement measurement resolution at 0.01-1 Hz while in low Earth orbit

---

[1527] Consultancy for TNO (http://www.tno.nl/gaiabam).

[1528] http://www.precisieportaal.nl/files/2008-3%20GAIA.pdf.

[1529] Wikipedia http://en.wikipedia.org/wiki/Darwin_%28ESA%29 and ESA Darwin website, http://www.esa.int/esaSC/120382_index_0_m.html . See also: Charles S. Cockell et al, "Darwin − A Mission to Detect, and Search for Life on, Extrasolar Planets," 2008; http://arxiv.org/abs/0805.1873.

[1530] Bastiaan Lucas Swinkels, "High-accuracy absolute distance metrology," PhD Thesis, 2006; http://www.optica.tn.tudelft.nl/publications/Thesis/Thesis%20Swinkels.pdf.

[1531] http://en.wikipedia.org/wiki/Terrestrial_Planet_Finder. See also: "Terrestrial Planet Finder," JPL; http://planetquest.jpl.nasa.gov/TPF/tpf_index.cfm.

[1532] "Terrestrial Planet Finder Interferometer," JPL; http://planetquest.jpl.nasa.gov/TPF-I/tpf-I_index.cfm. See also: "Interferometer Architecture: Instability noise and the X-array," JPL, http://planetquest.jpl.nasa.gov/TPF-I/instabilityNoise.cfm ; and Charles Beichman, Peter Lawson, Oliver Lay, Asif Ahmed, Steve Unwin, K. Johnston, "Status of the Terrestrial Planet Finder Interferometer (TPF-I)," 2006, http://trs-new.jpl.nasa.gov/dspace/bitstream/2014/39781/1/06-1881.pdf.

[1533] R. Pierce, J. Leitch, M. Stephens, P. Bender, R. Nerem, "Intersatellite range monitoring using optical interferometry," Applied Optics 47(September 2008):5007-5019; http://www.opticsinfobase.org/abstract.cfm?uri=ao-47-27-5007.

– the interferometer comprises two units, each with its own laser and in separate satellites, which would be in the same orbit separated by ~50 km.

Figure 4-117. Terrestrial Planet Finder mission proposed by JPL.[1534]

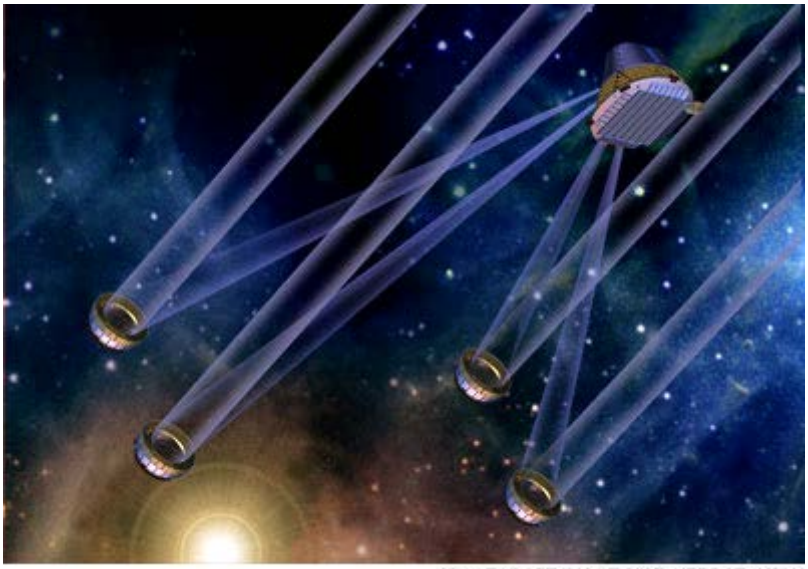

4.6.6.2 Gravitational Wave Detection

Interferometry is also being used in an attempt to detect the passage of gravitational waves that are predicted to exist by General Relativity. The leading efforts include the ground-based LIGO observatory (Section 4.6.6.2.1) and the space-based LISA observatory (Section 4.6.6.2.2).

4.6.6.2.1 Laser Interferometer Gravitational-Wave Observatory (LIGO)

Founded in 1992, LIGO (Laser Interferometer Gravitational-Wave Observatory) is a joint project between scientists at MIT and Caltech, sponsored by the National Science Foundation (NSF) at a cost of $365 million (in 2002 USD).[1535] The LIGO interferometers located in Hanford, Washington and Livingston, Louisiana consist of mirrors suspended at each of the corners of an L (Figure 4-118). They are **Michelson** laser interferometers enhanced by multiple coupled optical resonators that are 4-kilometer long **Fabry-Pérot** cavities placed in each arm of the

---

[1534] http://en.wikipedia.org/wiki/Terrestrial_Planet_Finder. See also: "Terrestrial Planet Finder," JPL; http://planetquest.jpl.nasa.gov/TPF/tpf_index.cfm.

[1535] LIGO (Laser Interferometer Gravitational-Wave Observatory); http://en.wikipedia.org/wiki/LIGO.

interferometer. The mirrors that form the cavities are suspended from a single loop of wire mounted inside suspension cages that are mounted on seismically isolated optical platforms within the LIGO vacuum system (10^{-8} torr). A pre-stabilized laser emits a 10 watt beam that passes through an optical mode cleaner before reaching a beam splitter at the vertex of the L. There the beam splits into two paths, one for each arm of the L; each arm contains Fabry-Pérot cavities that store the beams and increase the effective path length. Passage of a gravitational wave through the interferometer is expected to produce an effective change in the length of one or both of the cavities, bringing the cavity very slightly out of resonance and causing the light currently in the cavity to become very slightly out of phase with the incoming light.

Figure 4-118. LIGO Hanford Observatory (LHO) in aerial view; the 4-km interferometer arms are shown with the 5 main buildings along the orthogonal arm layout.[1536]

After an equivalent of approximately 75 trips down the 4 km length to the far mirrors and back again, the two separate beams leave the arms and recombine at the beam splitter. The beams returning from two arms are kept out of phase so that when the arms are both in resonance (as when there is no gravitational wave passing through), their light waves subtract, and no light should arrive at the photodiode. When a gravitational wave passes through the interferometer, the distances along the arms of the interferometer are shortened and lengthened, causing the beams to become slightly less out of phase, so some light arrives at the photodiode, indicating a signal. Light that does not contain a signal is returned to the interferometer using a power recycling mirror, thus increasing the power of the light in the arms. In actual operation, noise sources can cause movement in the optics which produces similar effects to real gravitational wave signals; a great deal of the art and complexity in the instrument is in finding ways to reduce these spurious motions of the mirrors. The detector is so sensitive that there is a 30 foot no-walk zone around the mirrors reportedly because the system can pick up the gravity created by a human body, though this precaution would also serve to reduce footfall-induced vibrations.

The Advanced LIGO suspension system uses sensors with 100 pm sensitivity at 1 Hz and a 700 micron working range; the micro-roughness target for the 40 kg test-mass mirrors is <200 pm RMS across a 340 mm x 200 mm surface; the main differential control requirement for

---

[1536] LIGO (Laser Interferometer Gravitational-Wave Observatory); http://en.wikipedia.org/wiki/LIGO.

differential arm length and near-mirror Michelson differential length is 0.001 pm RMS.[1537] Frequency-doubled light at 532 nm is to be injected through the end mirrors of the 4 km cavities, and the resulting cavity length detected using Pound-Drever-Hall sensing;[1538] the original LIGO required arm length control "with high accuracy, ranging from nm to less than 0.1 pm".[1539] LIGO uses PDH (Pound-Drever-Hall) locking of the FP cavity length, which has a noise limit of **~1 pm** at 1 Hz.[1540]

The German-British GEO600 Gravity Wave detector is a competing system to be built in the lowlands near Hannover, with arms of 600 m in length.[1541] Other competing ground-based gravity wave detectors include VIRGO, a European gravitational interferometric detector, and TAMA 300, a Japanese gravitational interferometric detector.

4.6.6.2.2 Laser Interferometry Space Antenna (LISA)

The Laser Interferometry Space Antenna (LISA) is the first dedicated space-based gravitational wave observatory.[1542] LISA will use an advanced system of laser interferometry and the most delicate measuring instruments ever made to directly detect gravitational waves. To accomplish its science objectives, the LISA mission depends on three core technologies: gravitational reference sensors, micronewton thrusters, and laser interferometry.[1543]

[1537] "Advanced LIGO Reference Design," LIGO M060056-v1, 24 March 2009; https://dcc.ligo.org/cgi-bin/DocDB/RetrieveFile?docid=1507.

[1538] "Advanced LIGO Reference Design," LIGO M060056-v1, 24 March 2009; https://dcc.ligo.org/cgi-bin/DocDB/RetrieveFile?docid=1507.

[1539] R. Bork, R. Abbott, D. Barker, J. Heefner, "LIGO Laboratory: An Overview of the LIGO Control and Data Acquisition System," 2001; http://www.slac.stanford.edu/econf/C011127/TUBI001.pdf.

[1540] Bram Slagmolen, Adam Mullavey, David Rabeling, Daniel Shaddock, David McClelland, Matt Evans, Peter Fritschel, Rana Adhikari, Yoichi Aso, "Adv. LIGO Arm Length Stabilisation," G08xxxx-Z – Slagmolen, LVC Amsterdam, 23 September 2008; http://www.ligo.caltech.edu/docs/G/G080551-00/G080551-00.ppt.

[1541] German-British Gravitational Wave Detector (http://geo600.aei.mpg.de). H. Grote, G. Heinzel, A. Freise, S. Gossler, B. Willke, H. Lück, H. Ward, M. Casey, K.A. Strain, D. Robertson, J. Hough, K. Danzmann, "The automatic alignment system of GEO 600," Class. Quantum Grav. 19(2002):1849-1855.

[1542] Shane L. Larson, "LISA: A modern astrophysical observatory," 2005; http://gravity.psu.edu/~shane/papers/slac_LISA.pdf.

[1543] http://lisa.nasa.gov/TECHNOLOGY/challenges.html. Thilo Schuldt, Martin Gohlke, Dennis Weise, Achim Peters, Ulrich Johann, and Claus Braxmaier, "Sub-nanometer interferometry for industrial high-precision metrology," 13 November 2007, SPIE Newsroom. DOI: 10.1117/2.1200710.0896; http://spie.org/x17505.xml?ArticleID=x17505.

LISA uses a technique known as interferometry to detect gravitational waves. LISA consists of three spacecraft, shaped like hockey pucks or pillboxes, freely flying (not connected to each other) five million kilometers (a little more than three million miles) apart, in an equilateral triangle (Figure 4-119A). The spacecraft are arranged in an approximately equilateral triangle to form a giant **Michelson** interferometer. Light from the central spacecraft is sent out to the other two spacecraft. Each spacecraft contains freely floating 2-kg Au-Pt cubical test masses (Figure 4-119B) that act as mirrors and reflect the light back to the source spacecraft where it hits a detector causing an interference pattern of alternating bright and dark lines. If the light from the two arms is in phase then there will be a bright spot at the center of the detector. When two beams of light with the same wavelength are in phase then the peaks of the waves will arrive at the same time. If they are out of phase the peaks arrive at different times, causing the bright spot to move away from the center of the detector. If the arms are the same length then the light waves will be in phase. The passage of a gravitational wave will lengthen one arm relative to the other one, and so the light waves will be out of phase.[1544]

Figure 4-119. (A) Arrangement of the LISA spacecraft in orbit.[1545] (B) The 4-cm mirror-cube test masses.[1546]

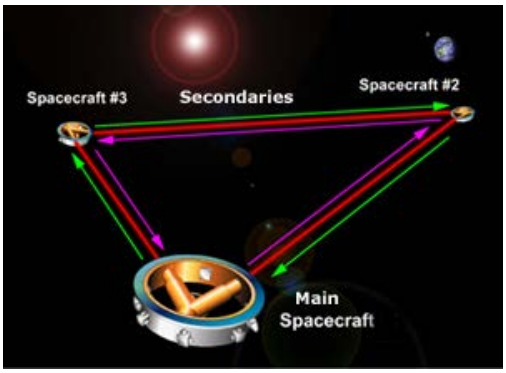

(A)

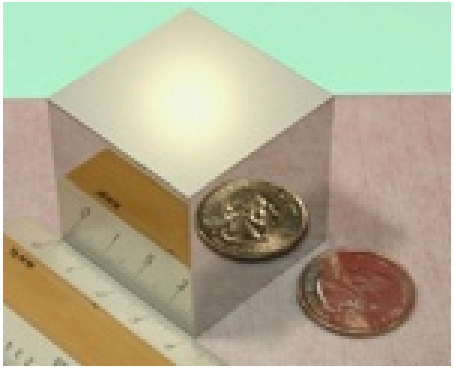

(B)

Positional measurement is optical heterodyne: The received laser beam (about 10^{-10} W) is mixed with about 1 mW of local laser light on a quadrant photodiode. Measurements from all three pairs of spacecraft are combined using time-delay interferometry to synthesize two independent Michelson interferometers and a third independent Sagnac interferometer. Optical-path errors caused by detector shot noise, pointing jitter, etc., in total are not to exceed 2×10^{-11} m/$\sqrt{}$(Hz) (the position noise budget) over the LISA bandwidth of 0.0001-0.1 Hz,[1547] implying a positional measurement resolution in the range of **63-2000 pm**. Danzmann[1548] gives the detectable

---

[1544] http://lisa.nasa.gov/TECHNOLOGY/LISA_interfer.html.
[1545] http://lisa.nasa.gov/TECHNOLOGY/LISA_interfer2.html.
[1546] http://lisa.nasa.gov/WHATIS/mission.html.
[1547] http://lisa.nasa.gov/facts.html.

[1548] K. Danzmann, "The LISA cornerstone: an ESA/NASA collaborative mission," in: Proc. 4th Intl. Conf. Space Optics, Centre National D' Etudes Spatiales, Toulouse, 5-7 December 2000, pp. 343-348.

spacecraft separation difference as **20 pm**, and the Interferometry Measurement System measurement sensitivity derived from the science requirements is **40 pm/√Hz**.[1549]

4.6.7 Multimode Waveguide Interferometry (MWI)

Multimode waveguide interferometry is a radically new approach to laser interferometer displacement measurement based on the revivals[1550] and oscillations of the momentum of light, as first described in the context of metrological displacement sensing by Ovchinnikov and Pfau in 2001,[1551] and by Ovchinnikov[1552] and others[1553] in subsequent work.

As explained in the key paper,[1554] when a monochromatic light beam enters a planar metal multimode waveguide at some large angle, the light experiences not only full and fractional revivals[1555] of its initial phase distribution along the waveguide, but also additional oscillations of the transverse momentum. This is related to the beatings between the adjacent populated transverse modes of the waveguide. Based on this effect, a new type of interferometer with a fringe spacing much smaller than the wavelength of light has been demonstrated. The basic setup

---

[1549] B. Cramer et al., "LISA Technology Readiness and Implementation Plan," 2003; http://www.srl.caltech.edu/lisa/documents/LISA_TRIP.pdf.

[1550] R.W. Robinett, "Quantum wave packet revivals," Physics Reports, 2008, 149 pp; http://arxiv.org/abs/quant-ph/0401031.

[1551] Yu.B. Ovchinnikov, T. Pfau, "Revivals and oscillations of the momentum of light in a planar multimode waveguide," Phys. Rev. Lett. 87(2001):12390-1 - 12390-4; http://www.pi5.uni-stuttgart.de/publications/prl-87-2001-ovchinnikov.pdf.

[1552] Yu. B. Ovchinnikov, "Revivals of light in a planar metal waveguide," Opt. Comm. 182(2000):35-43. Yuri B. Ovchinnikov, "Chapter 6. A multimode waveguide interferometer," in William T. Arkin, ed., Focus on Lasers and Electro-Optics Research, Nova Science Publishers, Inc., 2004, pp. 169-185; http://books.google.com/books?hl=en&lr=&id=EiUfHHOB6FcC&oi=fnd&pg=PA169&ots=AitC5Li1Fl&sig=a2UZDykA68A_D2r0KVjywWW0EE8. Y.B. Ovchinnikov, T. Pfau, "Multimode waveguide-interferometer," 19th Congress of the International Commission for Optics: Optics for the Quality of Life, 12 January 2004, Proc. SPIE 4829(2003):491, http://dx.doi.org/10.1117/12.525521.

[1553] R.M. Jenkins, A.F. Blockley, J. Banerji, A.R. Davies, "Multimode waveguide interferometer with λ/200 displacement sensitivity," 2005 Conference on Lasers and Electro-Optics Europe (CLEO/Europe), 12-17 June 2005, p. 455. R.M. Jenkins, A.F. Blockley, J. Banerji, A.R. Davies, "Fiber-coupled dual-mode waveguide interferometer with lambda/130 fringe spacing," Phys. Rev. Lett. 100(25 April 2008):163901. H.G. de Chatellus, J.P. Pique, "Lambda/2 fringe-spacing interferometer," Opt. Lett. 34(15 March 2009):755-757.

[1554] Yu.B. Ovchinnikov, T. Pfau, "Revivals and oscillations of the momentum of light in a planar multimode waveguide," Phys. Rev. Lett. 87(2001):12390-1 - 12390-4; http://www.pi5.uni-stuttgart.de/publications/prl-87-2001-ovchinnikov.pdf.

[1555] Yu. B. Ovchinnikov, "Revivals of light in a planar metal waveguide," Opt. Comm. 182(2000):35-43.

is shown in Figure 4-120. The waveguide is realized by two metal mirrors placed parallel to each other at distance d. The plane monochromatic light wave enters the waveguide at an angle β. The initial distribution has a constant amplitude and its phase changes linearly in the x direction. The numerical calculations of the light momentum distribution at the output of the waveguide show quasiperiodic oscillations between the two main directions +β and -β as a function of the length L of the waveguide. The tuning of the waveguide from one transmission fringe to the next can be done by changing either the length L or the width d of the waveguide, or the light wavelength λ. One way to change the relative length s of the waveguide is to vary the width d, while the length of the waveguide L is fixed. Since $s = L\lambda / 8d^2$ is nonlinear in d, the fringe spacing δd also changes nonlinearly in d, as $\delta d = d^2 / L \sin(\beta)$. Compared to all other types of interferometers, where the minimal fringe spacing is equal to λ/2, the distance δd can be much smaller than the light wavelength. This can be explained by the fact that in a waveguide the interfering modes experience multiple reflections between the mirrors before their phase difference is observed.[1556]

Figure 4-120. Experimental setup of the planar metal waveguide for observing the oscillations and revivals of the transverse momentum of light.[1557]

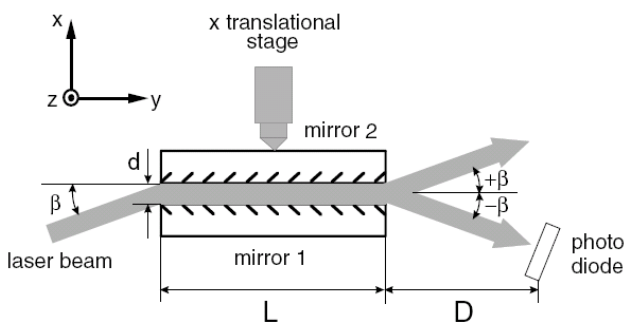

"Experimentally the waveguide was formed by two parallel flat mirrors of equal length (L = 5 cm), coated with bare gold. The substrates were made of fused silica and polished to a surface figure ~λ/20. All degrees of freedom of one of the mirrors were adjustable. This mirror was attached to a precise mechanical translational stage driven by a "COHERENT" Encoder Driver System 37-0486 which provided a resolution in translation of ~10 nm and a total range of 13 mm in the x direction. Using a He-Ne laser with wavelength λ = 633 nm, divergence about 1 mrad, linear polarization, directed parallel to the mirrors, and a beam diameter of ~2 mm, in the first experiment the entrance edge of the waveguide was illuminated at an angle of β = 0.253 rad. A

[1556] Yu.B. Ovchinnikov, T. Pfau, "Revivals and oscillations of the momentum of light in a planar multimode waveguide," Phys. Rev. Lett. 87(2001):12390-1 - 12390-4; http://www.pi5.uni-stuttgart.de/publications/prl-87-2001-ovchinnikov.pdf.

[1557] Yu.B. Ovchinnikov, T. Pfau, "Revivals and oscillations of the momentum of light in a planar multimode waveguide," Phys. Rev. Lett. 87(2001):12390-1 - 12390-4; http://www.pi5.uni-stuttgart.de/publications/prl-87-2001-ovchinnikov.pdf.

photodiode, used to detect the oscillations, was placed in the reflected output light beam at a distance D = 10 cm behind the waveguide. Each measurement of the light intensity in the reflected beam as a function of the waveguide width d was done in a single sweep of the driven mirror. The corresponding dependencies are shown in Figure 4-121. The period of fringes decreases with the reduction of width d of the waveguide. For m = 9 (d ~ 30 μm) fringes are observed with a period δd ~ 70 nm. These fringes are shown in the inset of Figure 4-121. For such a small fringe spacing the single steps of the Encoder Driver, which are of the order of 10 nm, were resolved.

Figure 4-121. Light intensity in the reflected beam of the light past the waveguide as a function of the waveguide width d.[1558]

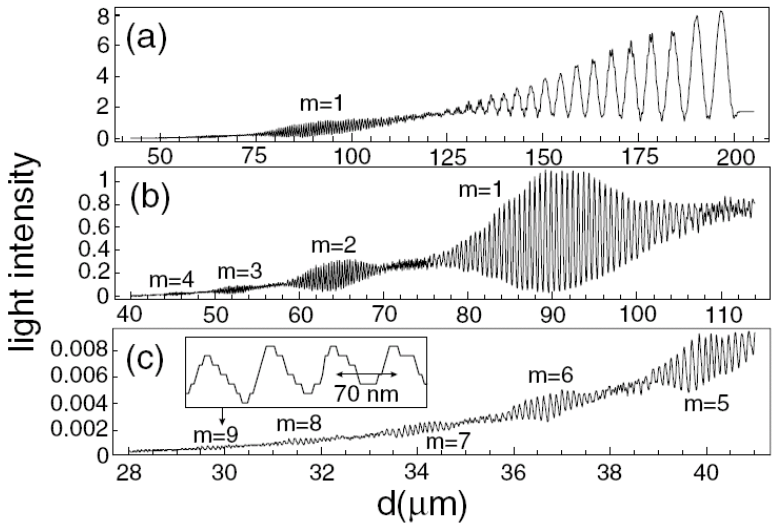

Notes Ovchinnikov and Pfau:[1559] "From all these observations we come to the conclusion that the multimode waveguide at large incidence angles of the input light beam can be considered as a new type of interferometer. The definite advantage of such an interferometer, compared to other known types, such as Fabry-Pérot or Michelson interferometers, is that its fringe spacing can be much smaller than λ/2. The observed period of λ/9 was solely limited by technical factors in our first experiment. For a very narrow waveguide (d ~ λ) the period of revivals and mode beatings becomes smaller than in the multimode waveguide considered above (d >> λ). Especially interesting is the limit when the waveguide contains only two propagating modes, wherein the

---

[1558] Yu.B. Ovchinnikov, T. Pfau, "Revivals and oscillations of the momentum of light in a planar multimode waveguide," Phys. Rev. Lett. 87(2001):12390-1 - 12390-4; http://www.pi5.uni-stuttgart.de/publications/prl-87-2001-ovchinnikov.pdf.

[1559] Yu.B. Ovchinnikov, T. Pfau, "Revivals and oscillations of the momentum of light in a planar multimode waveguide," Phys. Rev. Lett. 87(2001):12390-1 - 12390-4; http://www.pi5.uni-stuttgart.de/publications/prl-87-2001-ovchinnikov.pdf.

fringes of such a waveguide become uniform and periodic. The fringe spacing of such an interferometer is expected to be very small. For example, in a case of a waveguide with d = 0.7 μm, L = 100 μm, λ = 633 nm, and β = 33°, the fringe spacing is expected to be δd = **560 pm**."

Even more explicitly, Ovchinnikov adds:[1560] "The most prominent feature of the interferometer is certainly its small fringe spacing. This interferometer provides the possibility of very precise measurement of the relative displacement of two mirrors and can be used for an accurate positioning of objects. The individual structure of the interference fringes of the MWI makes it possible to use it also for precise measurement of the absolute distance between the two mirrors. The fringe spacing of the interferometer can be substantially smaller than the wavelength of light. Theoretically, it is limited only by the physical size of the interferometer, although practically, the minimum fringe spacing is limited by the quality of the mirrors and their reflectivity. A new type of an interferometer based on this effect with fringe spacing of λ/9 has been demonstrated experimentally, and periods as small as λ/1000 seem to be feasible. The possibility to get the fringe spacing as small as 2 pm is discussed."

At least two other research groups are pursuing this approach. In 2005, Jenkins et al.[1561] at QinetiQ in the U.K. described a multimode waveguide interferometer based on a planar mirror configuration (created from a pair of fully reflecting gold coated copper mirrors), demonstrating an order of magnitude improvement in displacement sensitivity. By 2008, the same group reported[1562] an improved multimode waveguide interferometer operating in a fiber-coupled, "dual-mode" regime. With a 1.32 μm light source, a complete switching cycle of the output beam was produced by a 10.0 nm incremental change in the 8.0 μm width of the hollow planar mirror waveguide. This equates to a fringe spacing of approximately λ/130, again an order of magnitude smaller than previously reported results for this form of interferometer. In 2009, Chatellus and Pique,[1563] a second group at CNRS-Université Joseph Fourier in France, presented some early work along similar lines: "The precision of interferometry is directly linked to the fringe spacing of the recorded interferogram. Whereas all interferometric devices show a fringe spacing equal to a wavelength of the laser light we present a novel scheme of a two-beam interferometer exhibiting a fringe spacing reduced by a factor of 2; the direct detection of the beat signal is replaced with the monitoring of the fluorescence of a twofold degenerate atomic system resonant with the laser. The λ/2 fringe spacing in the fluorescence signal is demonstrated with a hot sodium vapor excited by a broadband laser tuned to the D1 line. In the saturation

---

[1560] Yu.B. Ovchinnikov, T. Pfau, "Revivals and oscillations of the momentum of light in a planar multimode waveguide," Phys. Rev. Lett. 87(2001):12390-1 - 12390-4; http://www.pi5.uni-stuttgart.de/publications/prl-87-2001-ovchinnikov.pdf. 916.

[1561] R.M. Jenkins, A.F. Blockley, J. Banerji, A.R. Davies, "Multimode waveguide interferometer with λ/200 displacement sensitivity," 2005 Conference on Lasers and Electro-Optics Europe (CLEO/Europe), 12-17 June 2005, p. 455.

[1562] R.M. Jenkins, A.F. Blockley, J. Banerji, A.R. Davies, "Fiber-coupled dual-mode waveguide interferometer with lambda/130 fringe spacing," Phys. Rev. Lett. 100(25 April 2008):163901.

[1563] H.G. de Chatellus, J.P. Pique, "Lambda/2 fringe-spacing interferometer," Opt. Lett. 34(15 March 2009):755-757.

regime, the dark fringes are expected to be extremely narrow, leading to the possibility of **nanoscale displacement measurements or atom localization**."

4.6.8 Electron Interferometry

The de Broglie wavelength of an electron ($\lambda = h/p$, momentum $p = m_e v$) is about 12.3 pm at 10 kilovolts of energy and only 2.5 pm at 200 KV, far smaller than the 400-700 nm wavelength for optical photons, so in principle it should be possible to create an SPM-tracking electron interferometer that exhibits a measurement precision as good as, or even superior to, that which is possible for optical systems.

Although electron interferometers have existed since at least the early 1950s,[1564] by 2009 the field was still in its relative infancy.[1565] The first Mach-Zehnder electron interferometer (Figure 4-122A) was demonstrated in 2006 by Gronniger et al.[1566] Interference fringes were observed at low energies ranging from 6 to 10 keV, with contrasts of up to 25% for an electron count rate of 200/sec. However, because of the design the fringe periodicity was only 50 nm (Figure 4-122B), ten times better than conventional Michelson optical interferometers but still far larger than what should be possible, at least theoretically. Miniaturized electron interferometers[1567] and electron interferometers using scanning probe tips[1568] have been demonstrated experimentally. Future developments in this field will be watched with interest.

[1564] L. Marton, "Electron Interferometer," Phys. Rev. 85(1952):1057-1058.

[1565] G. Gronniger, B. Barwick, H. Batelaan, "A three-grating electron interferometer," New J. Phys. 8(2006):224; http://www.iop.org/EJ/article/1367-2630/8/10/224/njp6_10_224.html. G.F. Missiroli, G. Pozzi, U. Valdre, "Electron interferometry and interference electron microscopy," J. Phys. E: Sci. Instrum. 14(1981):649-671. A.N. Cleland, J.S. Aldridge, D.C. Driscoll, A.C. Gossard, "Nanomechanical displacement sensing using a quantum point contact," Appl. Phys. Lett. 81(26 August 2002):1699-1701.. Franz Hasselbach, "Biprism interferometry with electrons and ions, a valuable tool to study the fundamentals of quantum mechanics and quantum statistics," paper B1.00003 (18 May 2005), 36th Meeting of the Division of Atomic, Molecular and Optical Physics, 17-21 May 2005, Lincoln, Nebraska; http://meetings.aps.org/Meeting/DAMOP05/Event/30128. M.P. Jura, M.A. Topinka, M. Grobis, L.N. Pfeiffer, K.W. West, D. Goldhaber-Gordon, "Electron interferometer formed with a scanning probe tip and quantum point contact," Phys. Rev. B 80(7 July 2009):041303(R). J.C. Spence, U. Weierstall, M. Howells, "Phase recovery and lensless imaging by iterative methods in optical, X-ray and electron diffraction," Philos Transact A Math Phys Eng Sci. 360(15 May 2002):875-895; http://rsta.royalsocietypublishing.org/content/360/1794/875.long.

[1566] G. Gronniger, B. Barwick, H. Batelaan, "A three-grating electron interferometer," New J. Phys. 8(2006):224; http://www.iop.org/EJ/article/1367-2630/8/10/224/njp6_10_224.html.

[1567] Franz Hasselbach, "Biprism interferometry with electrons and ions, a valuable tool to study the fundamentals of quantum mechanics and quantum statistics," paper B1.00003 (18 May 2005), 36th Meeting of the Division of Atomic, Molecular and Optical Physics, 17-21 May 2005, Lincoln, Nebraska; http://meetings.aps.org/Meeting/DAMOP05/Event/30128.

[1568] M.P. Jura, M.A. Topinka, M. Grobis, L.N. Pfeiffer, K.W. West, D. Goldhaber-Gordon, "Electron interferometer formed with a scanning probe tip and quantum point contact," Phys. Rev. B 80(7 July 2009):041303(R).

Figure 4-122. **(A) At left: Sketch showing the experimental setup including the light interferometer used to measure the grating position (not to scale): Two slits are used to collimate the electron beam before it reaches the three-grating (100 nm periodicity) interferometer and an additional slit is used to select the interferometer output port (output ports 1 and 2 are indicated and 1 is selected in this example). (B) At right: Experimental data comparison to theory. The result of the classical straight line path calculation is represented by the solid line. The result of the full path integral calculation is represented by the dashed line. Experimental data are represented by square dots. The contrast of our device exceeds the classical contrast by about three times, showing the quantum mechanical nature of the data.**[1569]

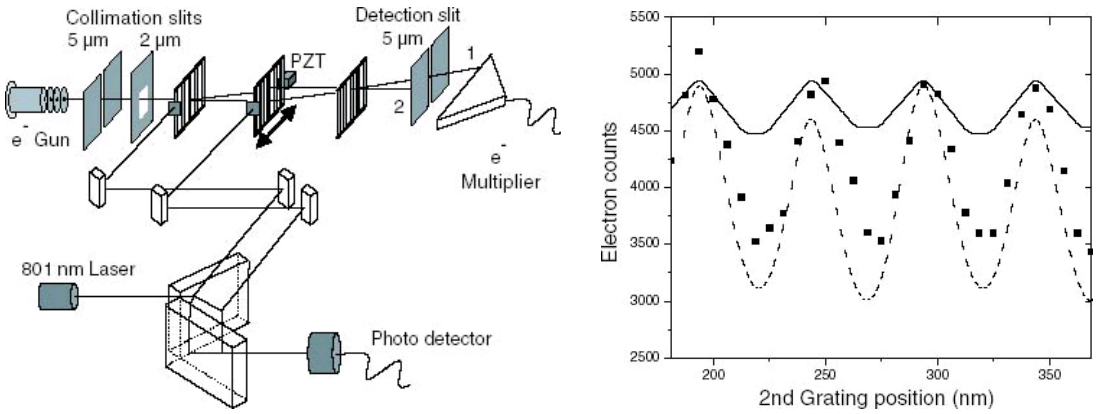

4.6.9 Non-Interferometric Backscatter Detection (Univ. of Colorado)

In some circumstances, it appears possible to dramatically stabilize an AFM tip without the use of metrological interferometry. An excellent example is the approach demonstrated experimentally by the Perkins group at the University of Colorado during 2004-2009[1570] that uses a local, high-

---

[1569] G. Gronniger, B. Barwick, H. Batelaan, "A three-grating electron interferometer," New J. Phys. 8(2006):224; http://www.iop.org/EJ/article/1367-2630/8/10/224/njp6_10_224.html.

[1570] Lora Nugent-Glandorf, Thomas T. Perkins, "Measuring 0.1-nm motion in 1 ms in an optical microscope with differential back-focal-plane detection," Optics Lett. 29(15 November 2004):2611-2613; http://jilawww.colorado.edu/perkinsgroup/GlandorfPerkins2004Measuring0.1nmin1ms.pdf. A.R. Carter, G.M. King, T.A. Ulrich, W. Halsey, D. Alchenberger, T.T. Perkins, "Stabilization of an optical microscope to 0.1 nm in three dimensions," Appl. Opt. 46(2007):421-427; http://jilawww.colorado.edu/perkinsgroup/Carter%20et%20al%203D%20stabilization%20of%20an%20optical%20microscope.pdf. A.R. Carter, G.M. King, T.T. Perkins, "Back-scattered detection provides atomic-scale localization precision, stability, and registration in 3D," Optics Express 15(28 September 2007):13434; http://jilawww.colorado.edu/perkinsgroup/Carter%20et%20al%202007%20Back-scattered%20detection%20in%203D.pdf. Allison B. Churnside, Gavin M. King, Ashley R. Carter, Thomas T. Perkins, "Improved performance of an ultrastable measurement platform using a field-programmable

bandwidth measurement of both the tip and sample position to form the foundation for a robust stabilization technique using only conventional laser tracking with quadrant photodiodes (QPDs) and commercial AFM tips. (Perkins is a staff member of NIST's Quantum Physics Division[1571] but is in the Department of Molecular, Cellular, and Developmental Biology and Univ. Colorado.) Perkins et al. hypothesized that laser light backscattered off the apex of the AFM tip (not its back side) could be used to locally measure the tip's position (Figure 4-123a) via back-scattered detection (BSD) using a single lens to focus and collect the light. Because the motivation of work was to create an ultrastable AFM for use in air and liquid (for biological applications, the apparatus (Figure 4-123b) involves beams of laser light passing through a transparent glass slide of the kind commonly used in optical microscopy when examining biological specimens. In this scheme, focused laser light in two co-linear beams of different frequencies (traveling along optical fibers to increase the pointing stability) passes through the glass plate and separately scatters off an AFM tip and a fiducial marker (silicon disk, r = 300 nm and h = 60 nm) fabricated on the upper surface of a glass cover slip (via physical vapor deposition of silicon through a silicon-nitride shadow mask) in an epoxy-stabilized flow cell filled with water. Three layers of environmental isolation were used: (i) optics external to the microscope were enclosed in a box; (ii) the whole assembly was enclosed by a custom-built, acoustically isolated box; and (iii) the experiment was mounted on a research grade optical table.

Back-scattered signals were collected and used to deduce the position of the tip and the sample relative to each laser beam, with atomic-scale sensitivity in all three coordinate dimensions. Specifically: Movement of the fiducial mark in X and Y relative to the detector beam causes a corresponding change in the distribution of light on the QPD. The difference between the left and right halves measures the X signal, and the difference between the top and bottom halves yields the Y signal. The Z signal is deduced from the sum of the power falling on all QPD quadrants. With such 3D detection, the pair of lasers creates a local, differential reference frame that enables an ultrastable AFM. The stability of the reference frame arises from the excellent differential pointing stability between the lasers (e.g., Figure 4-123a, δy_{lasers} = 20 pm). Sample position was controlled with a 3D, direct-drive, closed-loop PZT translation stage (Physik Instrumente, P-733.3DD, E-710).

---

gate array for real-time, deterministic control," in: Michael T. Postek, John A. Allgair, eds., Instrumentation, Metrology, and Standards for Nanomanufacturing II, Proc. SPIE 7042(2008):704205. Gavin M. King, Ashley R. Carter, Allison B. Churnside, Louisa S. Eberle, Thomas T. Perkins, "Ultrastable Atomic Force Microscopy: Atomic-Scale Stability and Registration in Ambient Conditions," Nano Lett. 9(March 2009): 1451-1456.

[1571] Gavin M. King, Ashley R. Carter, Allison B. Churnside, Louisa S. Eberle, Thomas T. Perkins, "Ultrastable Atomic Force Microscopy: Atomic-Scale Stability and Registration in Ambient Conditions," Nano Lett. 9(March 2009): 1451-1456.

Figure 4-123. Schematic of the experimental layout. (a) Detailed view of the tip and sample shows focused lasers scattering off an AFM tip and a fiducial mark (silicon disk) on the sample. Back-scattered signals were collected and used to deduce the position of the tip and the sample relative to each laser beam. (b) Two stabilized diode lasers (SDL) at different wavelengths [λ = 810 nm (green), λ = 845 nm (red)] were sent into the microscope and focused by a high numerical-aperture objective (Obj). Back-scattered light was separated from the incoming light by an optical isolator formed by a polarizing beam splitter (PBS) and a quarter-wave plate (λ/4). At different wavelengths, the signals were separated by dichroic mirrors and detected by independent QPDs. A third laser [λ = 785 nm (blue)] was reflected off the backside of the cantilever for force control during AFM imaging. Tip and sample control were achieved via feedback loops to two PZT stages. Blue-shaded components are in optically conjugate planes. The long axis of the cantilever was along the Y-axis.[1572]

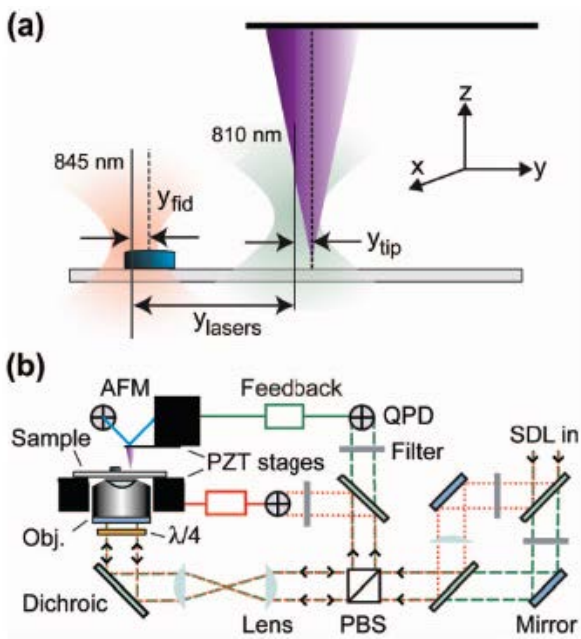

Implementation of a faster (500 Hz) FPGA-based (Field Programmable Gate Array) feedback control[1573] significantly improved lateral stability performance (Figure 4-124a, color) compared

---

[1572] Gavin M. King, Ashley R. Carter, Allison B. Churnside, Louisa S. Eberle, Thomas T. Perkins, "Ultrastable Atomic Force Microscopy: Atomic-Scale Stability and Registration in Ambient Conditions," Nano Lett. 9(March 2009): 1451-1456.

[1573] Allison B. Churnside, Gavin M. King, Ashley R. Carter, Thomas T. Perkins, "Improved performance of an ultrastable measurement platform using a field-programmable gate array for real-time, deterministic control," in: Michael T. Postek, John A. Allgair, eds., Instrumentation, Metrology, and Standards for Nanomanufacturing II, Proc. SPIE 7042(2008):704205.

to initial results using slower (<100 Hz) software-based feedback in earlier work[1574] (Figure 4-124a, grey). To quantify stability (the ability to accurately hover over one location), Perkins et al. monitored the position of the fiducial mark for 100 sec. After boxcar-averaging the data within a 50 ms window (preserving a 10 Hz frequency component) and decimating the data to 20 points per second, the analysis yielded a standard deviation of **10 pm** in both X and Y,[1575] compared to the software-based feedback standard deviation of 33 pm, shown as histograms in Figure 4-124b. This degree of lateral localization stability (10 pm) represents an order-of-magnitude enhancement over the manufacturer's nominal (100 pm) resolution of the stage.

Figure 4-124. Demonstration of improved performance provided by FPGA-based feedback control.[1576] (a) Lateral stabilization records (X, dark green; Y, dark red) achieved with 500-Hz FPGA control in comparison to control achieved with 100 Hz software-based feedback (light grey). Both data sets are filtered to 10 Hz and offset for clarity. (b) Histograms of the X signal corresponding to the FPGA-based feedback and the software-based feedback are well fit by histograms with standard deviations of 10 and 33 pm, respectively.

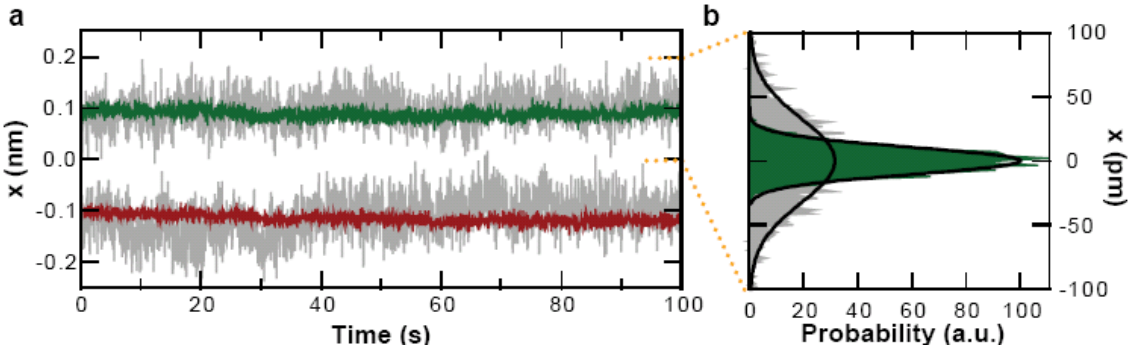

Ultrastable scanning of a sample requires precise steps. The Perkins group also demonstrated simultaneous precise scanning (with stabilization) using BSD to locally measure and thereby control sample location during a series of uniform steps. A staircase of 500 pm steps sequentially

---

[1574] A.R. Carter, G.M. King, T.T. Perkins, "Back-scattered detection provides atomic-scale localization precision, stability, and registration in 3D," Optics Express 15(28 September 2007):13434; http://jilawww.colorado.edu/perkinsgroup/Carter%20et%20al%202007%20Back-scattered%20detection%20in%203D.pdf.

[1575] Allison B. Churnside, Gavin M. King, Ashley R. Carter, Thomas T. Perkins, "Improved performance of an ultrastable measurement platform using a field-programmable gate array for real-time, deterministic control," in: Michael T. Postek, John A. Allgair, eds., Instrumentation, Metrology, and Standards for Nanomanufacturing II, Proc. SPIE 7042(2008):704205.

[1576] Allison B. Churnside, Gavin M. King, Ashley R. Carter, Thomas T. Perkins, "Improved performance of an ultrastable measurement platform using a field-programmable gate array for real-time, deterministic control," in: Michael T. Postek, John A. Allgair, eds., Instrumentation, Metrology, and Standards for Nanomanufacturing II, Proc. SPIE 7042(2008):704205.

in all three axes demonstrates uniformity in the step size (Figure 4-125A), with sample position actively controlled in 3D at all times. Precision is also fundamental to registration – the ability to repeatedly return to a particular sample position. Sample drift limits registration – in conventional scanning applications, excellent registration improves the repeatability of image acquisition and enables returning to a particular location in that image for subsequent detailed study. To demonstrate registration, the Perkins group repeatedly moved the sample back and forth in 100-nm steps individually on all three axes for a total of fifteen 6-sec long cycles (Figure 4-125B). The average step position for each step back to the starting location was compared to the initial step value and plotted versus the step number to show the spread in the relative registration (Figure 4-125C). The standard deviations of the relative position of these steps were **25 pm**, **21 pm**, and **58 pm** in X, Y, and Z, respectively. The experiment was repeated with a staircase of 1-nm steps (Figure 4-125D) and yielded essentially identical results. Thus, the registration was deemed to be near to and limited by the long-term low-frequency stability (standard deviations σ_x = 11 pm, σ_y = 16 pm, σ_z = 40 pm, in 100 sec of data filtered to 0.3 Hz). The nominal rise time (10% to 90%) per step was ~2 ms (Figure 4-125D, inset), which approaches the fastest step their stage (resonance frequency ~1000 Hz) could be expected to achieve, so the overall delay between requesting and completing a step was 3 ms. Optimization of the control code of the FPGA, faster stage controllers, and better feedback parameters were expected to improve this delay by a factor of two; further improvements will likely require stiffer stages with higher resonant frequencies.

Optical crosstalk can lead to inaccurate positional control – e.g., motion in X leads to voltage changes in all three detection axes. More significantly, crosstalk increases as the reference mark is moved further out of the laser focus. Using a previously published control algorithm[1577] designed for an FPGA, crosstalk compensation significantly improved control of the stage position, particularly near the edges of the calibrated region where discrepancies were more pronounced (Figure 4-126a).[1578] The stage was moved in a grid of points with 10 nm spacing over the entire 200 x 200 nm^2 calibrated range. Near the center of the calibrated range (Figure 4-126b, blue region), this test yielded an average residual error of 144 pm using a linear calibration versus **8 pm** using full cross-talk compensation, an 18-fold improvement. Near the corner of the calibrated range (Figure 4-126c, red region), a similar analysis yielded residual errors of 730 pm with the linear calibration versus **24 pm** with compensation, a 30-fold improvement. Thus, the crosstalk compensation software allows for precise and accurate scanning over a much larger area while maintaining excellent sample stability.

[1577] M.J. Lang, C.L. Asbury, J.W. Shaevitz, S.M. Block, "An automated two-dimensional optical force clamp for single molecule studies," Biophys. J. 83(2002):491-501.

[1578] Allison B. Churnside, Gavin M. King, Ashley R. Carter, Thomas T. Perkins, "Improved performance of an ultrastable measurement platform using a field-programmable gate array for real-time, deterministic control," in: Michael T. Postek, John A. Allgair, eds., Instrumentation, Metrology, and Standards for Nanomanufacturing II, Proc. SPIE 7042(2008):704205.

Figure 4-125. Ultrastable scanning and uniform stepping.[1579] (A) At top left, the sample was moved in 500-pm steps sequentially along each axis (X: green, Y: red, Z: blue) under active stabilization. (B) At top center, the sample was moved in a series of fifteen back-and-for th100-nm steps sequentially on each axis. (C) At top right, mean values of step position around the starting location as a function of step number demonstrates excellent registration to within ±70 pm over 14 cycles. (D) At bottom, a record of sample position from a series of 1-nm steps filtered to 2 kHz; rise time for the requested motion was ~2 ms (inset) with the total step completed ~3 ms after the request.

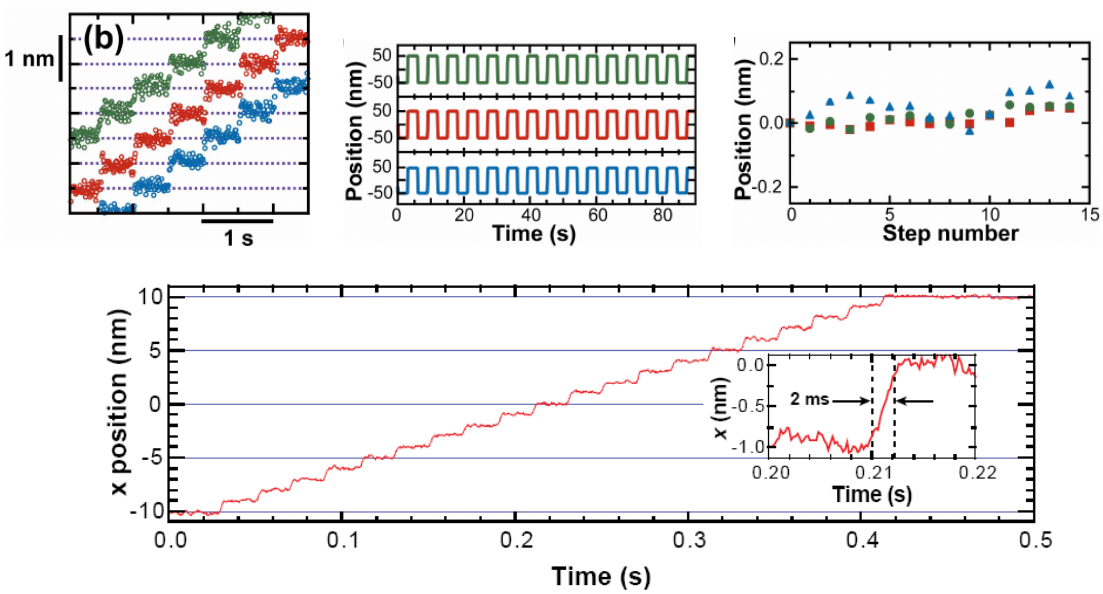

[1579] A.R. Carter, G.M. King, T.T. Perkins, "Back-scattered detection provides atomic-scale localization precision, stability, and registration in 3D," Optics Express 15(28 September 2007):13434; http://jilawww.colorado.edu/perkinsgroup/Carter%20et%20al%202007%20Back-scattered%20detection%20in%203D.pdf. Allison B. Churnside, Gavin M. King, Ashley R. Carter, Thomas T. Perkins, "Improved performance of an ultrastable measurement platform using a field-programmable gate array for real-time, deterministic control," in: Michael T. Postek, John A. Allgair, eds., Instrumentation, Metrology, and Standards for Nanomanufacturing II, Proc. SPIE 7042(2008):704205.

Figure 4-126. (a) Two-dimensional scanning with (open green circles) and without (closed red circles) cross-talk compensation. (b & c) Enlarged plots of the center (blue; 8 pm residual error) and corner (red; 24 pm residual error) regions, respectively.[1580]

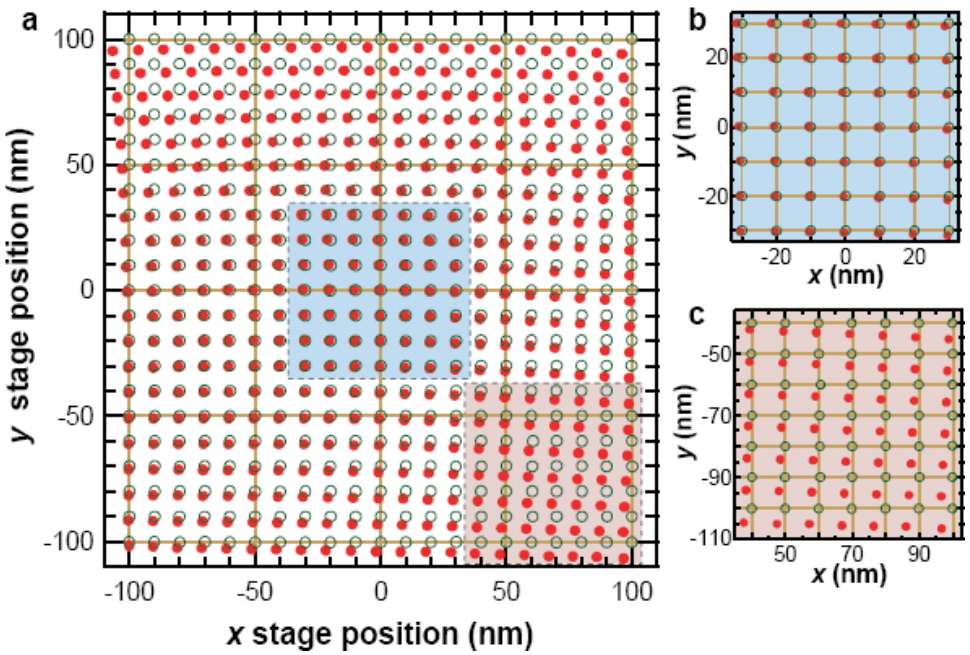

Implementation of this scheme for the molecular workstation would present numerous potential problems that would have to be addressed and overcome:

(1) The current method depends upon laser light being transmitted through a transparent workspace surface. As noted by King et al.:[1581] "In the current implementation, we used transparent substrates in air, but we have also achieved tip-based BSD signals in liquid and through thin metal films (2 nm Ti + 6 nm Au) on glass. Since the detection beams pass through the sample, degradation of the signal due to scattering from the sample could lead to erroneous tip positioning." If the workspace presentation or fabrication surface could be made of single-crystal transparent diamond (or thin-film diamond deposited over clear glass via CVD or related techniques) might allow this method to be used in the moecular workstation. Nanocrystalline diamond and some DLC surfaces prepared by conventional means are not transparent and would

---

[1580] Allison B. Churnside, Gavin M. King, Ashley R. Carter, Thomas T. Perkins, "Improved performance of an ultrastable measurement platform using a field-programmable gate array for real-time, deterministic control," in: Michael T. Postek, John A. Allgair, eds., Instrumentation, Metrology, and Standards for Nanomanufacturing II, Proc. SPIE 7042(2008):704205.

[1581] Gavin M. King, Ashley R. Carter, Allison B. Churnside, Louisa S. Eberle, Thomas T. Perkins, "Ultrastable Atomic Force Microscopy: Atomic-Scale Stability and Registration in Ambient Conditions," Nano Lett. 9(March 2009): 1451-1456.

not work, and proposed germanium, tin, lead, graphite (e.g., HOPG), or bulk metal surfaces are opaque. A thin several-nm film of Ge or metallic Pb on glass might be workable for DMS, but not pure glass which is an amorphous – atomically imprecise – material. Perkins suggests[1582] that "silicon wafers, in lieu of cover glass, can be accommodated by shifting to longer wavelength lasers where silicon is transparent," a strategy that might also work for germanium. For instance, silicon is nominally transparent above the band edge ($\lambda > 1.2$ mm, e.g., at 1.55 microns), and germanium is apparently transparent at IR wavelengths in the ranges of 3-5 μm and 8-14 μm. More investigation of this point is clearly required.

(2) The method may not be workable if the laser beams are introduced from the side or above, rather than straight up from below, because significant effort is already being made to get the backscattered signal intensity up high enough to detect (~5%) compared to normal (~0.1%), and side-illuminated structures might reflect light more poorly than bottom-illuminated structures. Notwithstanding, the authors claim[1583] that "a fiducial mark could be engineered into the cantilever that spatially separates the tip from its fiducial mark, analogous to the silicon disk currently used to deduce sample motion. Such separation would enable strongly scattering or optically opaque samples to be studied with a similar degree of stability and registration." The ability to employ this scheme using only top- or side-illumination in the case of an opaque sample or workspace surface needs clarification.

(3) It is not clear what the drift rate is, using this method. The data (Figure 4-125C) appear consistent with a drift rate of ~100 pm per 30 steps; assuming 3 steps per 20 seconds for this data (Figure 4-125B) suggests a drift rate of ~20 pm/min, thus requiring re-registration of the moving tip every 1-2 minutes to remain within the 20-50 pm accuracy requirement, which suggests that the registration site must lie within 2-4 microns of the worksite. King et al.[1584] claim a lateral (XY) drift rate during scans of 4-5 pm/min at 300 K in ambient air. These residual rates, achieved in air at room temperature, are close to the best found in cryogenic UHV conditions: Stipe et al.[1585] used UHV-STM and a sharp tungsten tip to measure acetylene molecules on copper surface at **8 K** to a lateral resolution of better than **10 pm** and vertical resolution (the "corrugation" of the acetylene molecules lying on the surface) of better than **1 pm**, with measured drift rates of **1 pm/min** in the horizontal direction and **0.1 pm/min** in the vertical

---

[1582] Gavin M. King, Ashley R. Carter, Allison B. Churnside, Louisa S. Eberle, Thomas T. Perkins, "Ultrastable Atomic Force Microscopy: Atomic-Scale Stability and Registration in Ambient Conditions," Nano Lett. 9(March 2009): 1451-1456.

[1583] Gavin M. King, Ashley R. Carter, Allison B. Churnside, Louisa S. Eberle, Thomas T. Perkins, "Ultrastable Atomic Force Microscopy: Atomic-Scale Stability and Registration in Ambient Conditions," Nano Lett. 9(March 2009): 1451-1456.

[1584] Gavin M. King, Ashley R. Carter, Allison B. Churnside, Louisa S. Eberle, Thomas T. Perkins, "Ultrastable Atomic Force Microscopy: Atomic-Scale Stability and Registration in Ambient Conditions," Nano Lett. 9(March 2009): 1451-1456. "Making a point: Picoscale stability in a room-temperature AFM," eScience news, published Wednesday, 25 March 2009 - 08:51; http://esciencenews.com/articles/2009/03/25/making.a.point.picoscale.stability.a.room.temperature.afm.

[1585] B.C. Stipe, M.A. Rezaei, W. Ho, "Single-molecule vibrational spectroscopy and microscopy," Science 280(1998):1732-1735.

direction – thermal stability of the UHV-STM and the sample to within 0.01 K was reached 4 hours after initial cooling from room temperature. Subfemtometer displacement sensing has also been reported.[1586]

(4) The registration tests checked only 100-nm single-step excursions from a start point, followed by an immediate 100-nm single-step return to the start point. It is unknown the degree to which multi-step excursions to more distant targets from the start point, or the use of larger or smaller step sizes, or the taking of many more sequential steps, would degrade the claimed resolution. To operate efficiently, the molecular workstation will need to take at least many thousands, if not many millions, of steps between re-registrations. Assuming cycling at the 2 ms rise time with 1 nm steps at 500 Hz, the maximum tip displacement speed is ~0.5 μm/sec.

(5) In this scheme the DMS tip is directly and continuously illuminated by laser light, so there is the possibility of thermally-induced geometry changes. For example, when measuring the position of a metal-coated AFM cantilever in vacuum, the deflection due to laser heating can be substantial (~1 nm/μW),[1587] even for the relatively low laser power (800 μW at the laser focus)[1588] employed here. (King et al.[1589] admitted that increasing laser power from 400 μW to 800 μW introduced a slight Z offset (<1 nm) of the tip.) The continuous illumination might also affect the mechanochemical reactions that are taking place at the tip.

(6) As 3-D product objects are fabricated on the upper surface of the workspace, they present increasing material thickness in the vertical direction which can progressively reduce the transmission of the impinging laser light. To the extent that growing product objects cast a deepening shadow onto the moving tip, the tip may lose visibility to the light beam arriving from below, possibly degrading measurement accuracy or the continuity of displacement data using this scheme. King et al.[1590] searched for scattering effects by interposing gold nanospheres on the

---

[1586] A. Naik, O. Buu1, M.D. LaHaye, A.D. Armour, A.A. Clerk, M.P. Blencowe, K.C. Schwab, "Cooling a nanomechanical resonator with quantum back-action," Nature 443(14 September 2006):193-196.

[1587] J.R. Barnes, R.J. Stephenson, C.N. Woodburn, S.J. Oshea, M.E. Welland, T.Rayment, J.K. Gimzewski, C. Gerber, "A Femtojoule Calorimeter Using Micromechanical Sensors," Rev. Sci. Instrum. 65(1994):3793-3798. J.M. Antonietti, J. Gong, V. Habibpour, M.A. Rottgen, S. Abbet, C.J. Harding, M. Arenz, U. Heiz, C. Gerber, "Micromechanical sensor for studying heats of surface reactions, adsorption, and cluster deposition processes," Rev. Sci. Instrum. 78(2007):054101.

[1588] A.R. Carter, G.M. King, T.T. Perkins, "Back-scattered detection provides atomic-scale localization precision, stability, and registration in 3D," Optics Express 15(28 September 2007):13434; http://jilawww.colorado.edu/perkinsgroup/Carter%20et%20al%202007%20Back-scattered%20detection%20in%203D.pdf.

[1589] Gavin M. King, Ashley R. Carter, Allison B. Churnside, Louisa S. Eberle, Thomas T. Perkins, "Ultrastable Atomic Force Microscopy: Atomic-Scale Stability and Registration in Ambient Conditions," Nano Lett. 9(March 2009): 1451-1456.

[1590] Gavin M. King, Ashley R. Carter, Allison B. Churnside, Louisa S. Eberle, Thomas T. Perkins, "Ultrastable Atomic Force Microscopy: Atomic-Scale Stability and Registration in Ambient Conditions," Nano Lett. 9(March 2009): 1451-1456.

sample stage, analyzed the results, then proposed: "In principle, the optical-scattering signal of the tip detection laser due to the sample could be recorded at each pixel with the tip retracted and then subtracted from the total tip signal during imaging. The high degree of sample stability and registration ensure that no significant drift will occur and that such background subtraction would remain valid for long durations."

(7) The tip will be moving around the workspace, at least several microns and perhaps much more, in normal operations. It is unclear how much separation can be tolerated between the tip and the fiducial marker before the accuracy of this method begins to degrade. Churnside et al.[1591] note that their 3D control is only calibrated over a 200 nm x 200 nm x 100 nm operating volume, but Carter et al.[1592] suggest that "the scanning range can be easily extended to several microns by sequential moves of the detector beam with a PZT mirror." Extension to several hundreds of microns while retaining repeatable high accuracy might prove more difficult to arrange, though here again Churnside et al.[1593] appear optimistic: "as newer generations of FPGA-PCI cards become available, they will likely provide higher feedback bandwidths coupled with more reconfigurable logic blocks that will allow for **high-precision displacements over a larger dynamic range**."

(8) It is unknown to what extent this method can accommodate the presence of two or more tips simultaneously present in the same workspace. Note Churnside et al.:[1594] "Looking forward, we expect that the intrinsically parallel and deterministic control provided by FPGA architecture will become increasingly valuable for future precision nanoscience applications, such as optically stabilized AFM, that demand **real time control of many (>3) independent axes**."

(9) It is unclear how this method would handle the problem of re-entrant tips (e.g., tips that leave the workspace and later return, tips that are replaced during changeout, etc.).

[1591] Allison B. Churnside, Gavin M. King, Ashley R. Carter, Thomas T. Perkins, "Improved performance of an ultrastable measurement platform using a field-programmable gate array for real-time, deterministic control," in: Michael T. Postek, John A. Allgair, eds., Instrumentation, Metrology, and Standards for Nanomanufacturing II, Proc. SPIE 7042(2008):704205.

[1592] A.R. Carter, G.M. King, T.T. Perkins, "Back-scattered detection provides atomic-scale localization precision, stability, and registration in 3D," Optics Express 15(28 September 2007):13434; http://jilawww.colorado.edu/perkinsgroup/Carter%20et%20al%202007%20Back-scattered%20detection%20in%203D.pdf.

[1593] Allison B. Churnside, Gavin M. King, Ashley R. Carter, Thomas T. Perkins, "Improved performance of an ultrastable measurement platform using a field-programmable gate array for real-time, deterministic control," in: Michael T. Postek, John A. Allgair, eds., Instrumentation, Metrology, and Standards for Nanomanufacturing II, Proc. SPIE 7042(2008):704205.

[1594] Allison B. Churnside, Gavin M. King, Ashley R. Carter, Thomas T. Perkins, "Improved performance of an ultrastable measurement platform using a field-programmable gate array for real-time, deterministic control," in: Michael T. Postek, John A. Allgair, eds., Instrumentation, Metrology, and Standards for Nanomanufacturing II, Proc. SPIE 7042(2008):704205.

(10) It is unclear how well this method will work to accurate track the positions of pre-tilted tips, or of vertically positioned tips that become (perhaps reversibly) tilted during normal operations.

4.6.10 Other Metrology Approaches

Several other unusual nanometrology approaches (of uncertain value to our project) have appeared in the literature, including:

(1) **Electromechanical Resonator.** Cleland et al.:[1595] "We describe a radio frequency mechanical resonator that includes a quantum point contact, defined using electrostatic top gates. We can mechanically actuate the resonator using either electrostatic or magnetomotive forces. We demonstrate the use of the quantum point contact as a displacement sensor, operating as a radio frequency mixer at the mechanical resonance frequency of 1.5 MHz. We calculate a displacement sensitivity of about **3 pm** / $Hz^{1/2}$. This device will potentially permit quantum-limited displacement sensing of nanometer-scale resonators, allowing the quantum entanglement of the electronic and mechanical degrees of freedom of a nanoscale system."

(2) **Optical DVD Head.** Hwu et al.,[1596] in 2009: "The development of a highly sensitive (sub-nanometer) and multi-platform scanning probe microscope (SPM) module is presented. The module is based on an optical DVD pick-up head and uses its astigmatic detection scheme to detect the vertical displacement of the SPM cantilevers. The complete hybrid SPM module is capable of scanning in SPM intermittent contact, SPM contact and optical profilometry modes. The module can be used in a modified optical microscope or be implemented in a stand-alone system. Measurement results prove that the mechanical stability of this SPM module is high enough for atomic resolution imaging. Both scanning-sample and scanning-probe-type SPM setups have been tested based on this SPM module. The noise level and drift rate in the Z-direction of the stand-alone system are **10 pm** (rms) and **200 pm/min**, respectively.

(3) **Non-Piezo Actuation.** Otsuka et al.:[1597] In 2005, four researchers at Shizuoka Institute of Science and Technology, Sigma-Tech Ltd., and Enomoto Industries Ltd., in Japan, reported "the development of an ultraprecision positioning device with positioning resolution of 5 nm. The device uses a stepping motor and ball screw **without a piezoelectric actuator** for fine positioning. Here, the stepping motor is driven at high speed with an open loop control, at medium speed with a closed loop control and a low-speed drive with a closed loop control using the feedback-loop displacement sensor of 5 nm resolution. With the step responses repeated we achieved a positioning accuracy equal to or less than **5 nm**. Since this ultraprecision positioning

---

[1595] A.N. Cleland, J.S. Aldridge, D.C. Driscoll, A.C. Gossard, "Nanomechanical displacement sensing using a quantum point contact," Appl. Phys. Lett. 81(26 August 2002):1699-1701.

[1596] E.-T. Hwu, H. Illers, L. Jusko, H.-U. Danzebrink, "A hybrid scanning probe microscope (SPM) module based on a DVD optical head," Meas. Sci. Technol. 20(2009):084005.

[1597] Jiro Otsuka, Soji Ichikawa, Tomio Masuda, Kazuhiro Suzuki, "Development of a small ultraprecision positioning device with 5 nm resolution," Meas. Sci. Technol. 16(2005):2186-2192.

device is very small, the stage has a high resonance frequency of 670 Hz for external forces, and we made sure that the positioning device was very resilient to vibrations from the outside."

(4) **Graduated Scales.** Graduated scales, such as holographic-grating-based systems, have been used to achieve **sub-nanometer** displacement accuracies (as described by Kunzmann et al.[1598]) and have the potential for ultra-precise metrology. Both scales and laser interferometers are linear displacement measuring systems (LBS). It is the performance of the LBS that limits the accuracy of servo-positioning machine tools and/or measuring instruments, and the traditional systems for this purpose (besides lead-screws) have been graduated scales.

(5) **Other Picometer Measurements.** In the 1990s it was shown that laser-based measurements could achieve subpicometer localization of micrometer-sized beads (though instrumental drift, particularly at low frequencies, limited such measurements).[1599] Less well known are the requirements in the medical world for ultra-high-accuracy (picometer-range) displacement measurements such as are required for research into the workings of the inner ear[1600] and investigations into the converse piezo-electric effect in bones.[1601]

4.6.11 Summary of Possible Workstation Metrology Systems

Considering all available existing or proposed metrology systems that could be applied to the design and construction of a molecular workstation (having the required capabilities; Section 1.5), the big picture is as follows:

(1) High-Precision Large-Range SPM-Based Systems (Section 4.6.1). Many national metrology institutes worldwide (plus a few university and commercial groups) have initiated ongoing efforts in the development of high-quality SPM-based metrology instruments. We have reviewed more than a dozen complete SPM-based metrology systems that have been designed, constructed and operated during the last 2 decades. Most of the instruments surveyed operate over sub-millimeter ranges, but there are a few large-range (≥25 mm) interferometer-based SPM metrology instruments and stages that have also been developed. None of these complete systems provides all of the positional precision needed for the molecular workstation – the best achieve only ~1000 pm repeatable accuracy over long travels, about 20-50x poorer than the 20-50 pm we require – but they are nonetheless good examples of what a complete system might look

---

[1598] H. Kunzmann, T. Pfeifer, J. Flugge, "Scales versus laser interferometers: performance and comparison of two measuring systems," CIRP Ann. 42(1993):753-767.

[1599] W. Denk, W.W. Webb, "Optical measurement of picometer displacements of transparent microscopic objects," Appl. Opt. 29(1990):2382-2391.

[1600] F. Mammano, J.F. Ashmore, "A laser interferometer for sub-nanometer measurements in the cochlea," J. Neurosci. Meth. 60(1995):89-94.

[1601] P. Gizdulich, G. Aschero, F. Mango, "An optical dilatometer for picometer displacements," Meas. Sci. Technol. 10(1995):232-238.

like. It seems likely that our molecular workstation will have many elements in common with these setups, at least at the systems level of organization.

(2) COXI-Based Systems (Section 4.6.2.8). COXI-based systems have demonstrated 35 pm measurement uncertainty over 100 micron round-trip displacement paths in 1 dimension (1 DOF) at the 95% confidence level with a drift rate of ~2 pm/min (European NPL/PTB/IMGC group, Sections 4.6.2.1, 4.6.2.2, and 4.6.2.3; European Nanotrace Project, Section 4.6.2.4), and 2-dimensional COXI (2 DOFs) has also been demonstrated experimentally, albeit with somewhat poorer precision, by two groups (the South Korean KRISS/KAIST group, Section 4.6.2.6; Yacoot's group at NPL/PTB, Section 4.6.2.2). COXI-based detection has also been demonstrated on AFM systems (the NPL/PTB group, Section 4.6.2.2). It appears that COXI-based systems could likely provide positional detection of sufficient precision to enable dead-reckoning pick-and-place DMS operations (without continuous sensory feedback, though likely requiring periodic re-registration), in a molecular workstation to be used for atomically precise DMS-based molecular manufacturing.

(3) Michelson-Based Systems (Section 4.6.3.17). Michelson-based systems that have been employed in SPM metrology include the crystal-lattice ruler approach of the Aketagawa group in Japan, using a dual tunneling-unit (DTU) STM incorporating one XY scanner and two Z scanners with tips showing a resolution of **10 pm** over 500 nm (Section 4.6.3.7); Silver's tunable-laser interferometer at NIST, achieving **20 pm** accuracy over a range of ~165 nm for a UHV STM tip (Section 4.6.3.2); the laser Doppler displacement meter for AFM at Argonne, performing 80 pm steps over a 25 mm travel range in one dimension of travel with a motion stage driving sensitivity better than **30 pm** (Section 4.6.3.11); the AFM with a 3-axis laser interferometer by the Gonda group in Japan, achieving **40 pm** total resolution over 2-20 micron displacements (Section 4.6.3.6), and the related CD-AFM project providing **50-200 pm** resolution over a wider linearity range from 0.1 nm to 1 micron (Section 4.6.3.6). Michelson-based systems apparently can provide positional detection of sufficient precision to enable dead-reckoning pick-and-place DMS operations (without continuous sensory feedback, though likely requiring periodic re-registration), in a molecular workstation to be used for atomically precise DMS-based molecular manufacturing.

(4) Fabry-Pérot-Based Systems (Section 4.6.4.9). The most notable Fabry-Pérot system employed for SPM metrology is the tunable laser Fabry-Pérot interferometer built by Howard's group at NIST with a resolution of **tens of picometers** that was used to measure Z-axis displacements of an AFM with a **60 pm** noise level for the combined AFM/interferometer system (Section 4.6.4.3). Fabry-Pérot-based systems can probably provide positional detection of sufficient precision to enable dead-reckoning pick-and-place DMS operations (without continuous sensory feedback, though likely requiring periodic re-registration), in a molecular workstation to be used for atomically precise DMS-based molecular manufacturing.

(5) Digitally Enhanced Heterodyne Interferometry (Section 4.6.5). Shaddock's digitally enhanced heterodyne interferometry (DI) has been used for displacement measurement in both Michelson and Fabry-Pérot configurations; e.g., using an FP cavity, the method has demonstrated a displacement sensitivity of approximately **5 pm/√Hz** above 1 Hz. As of 2009, Shaddock's group was collaborating with the Australian NMI's Nanometrology division to "acquire, develop and operate a metrological atomic force microscope to provide traceability for dimensional nanoscale measurements in Australia" using the DI technique.

(6) Multimode Waveguide Interferometry (Section 4.6.7). Multimode waveguide interferometry, which involves measuring "the oscillations and revivals of the transverse

momentum of light" as light enters a planar metal multimode waveguide at some large angle and then traverses the length of the waveguide, was first proposed by Ovchinnikov in 2001. Although a totally novel interferometric technique completely distinct from both Michelson and Fabry-Pérot interferometry, the method has already been demonstrated experimentally by three groups, including Ovchinnikov who resolved single displacement steps as small as **10 nm** (for an observed period of $\lambda/9$ in the first experiment, which "was solely limited by technical factors"). Ovchinnikov asserts that "periods as small as $\lambda/1000$ seem to be feasible" – e.g., for a smaller waveguide with d = 0.7 μm, L = 100 μm, λ = 633 nm, and $\beta = 33^o$, the fringe spacing would be expected to be δd = **560 pm** (~ $\lambda/1130$) – and offers the further possibility of getting the fringe spacing as small as **2 pm**.

(7) Non-Interferometric Backscatter Detection (Section 4.6.9). The Perkins group at the University of Colorado can positionally stabilize an AFM tip without the use of metrological interferometry, using light shined through the workpiece surface that illuminates the AFM tip from below the workpiece. Movement of a tip in X and Y can be monitored to **10 pm** RMS, a degree of lateral localization stability that represents an order-of-magnitude enhancement over the manufacturer's specified nominal resolution (100 pm) for the stage. A series of 500 pm steps produced XYZ resolutions of **25 pm**, **21 pm**, and **58 pm** RMS, respectively. Use of this method in an AFM-based molecular workstation performing DMS operations would be problematic for a large number of reasons, but at least some of these problems appear to have possible solutions and so the method is believed to be worthy of further investigation.

(8) Astronomical Metrological Interferometer Systems (Section 4.6.6). These systems have been built to accomplish one of two missions – Astrometry and Extrasolar Planet Detection (Section 4.6.6.1) and Gravitational Wave Detection (Section 4.6.6.2), each include two exemplar systems:

(A) SIM Lite (Section 4.6.6.1.1). Hardware for the space-based SIM mission has demonstrated 3-10 pm accuracy for displacement measurements using a common-path heterodyne Michelson interferometer consisting of two parallel flat mirrors (one with a hole in it), with excellent drift stability of better than 100 pm/hour, in some benchmarking tests. In 2004-5 the mission requirements for relative accuracy were relaxed to ~10 pm RMS over a 90 sec timescale and ~57 pm over a 1-hour timescale. The SIM approach appears applicable to SPM-based picoscale metrology but further investigation and analysis will be required to confirm this expectation.

(B) Keck Interferometer (Section 4.6.6.1.2). In 2003 Yekta Gursel at NASA-JPL designed an improved metrology gauge that could be used to upgrade the ground-based Keck Interferometer, then built a prototype polarization-insensitive heterodyne gauge that yielded a systematic error per gauge of about **25 pm** RMS. However, the gauge differential appears to rise to ~1000 pm for DC operation so further investigation is required to determine if this method might be useful for an AFM-based molecular workstation.

(C) LIGO (Section 4.6.6.2.1). LIGO is a ground-based gravity wave detector that employs Michelson laser interferometers enhanced by multiple coupled optical resonators that are 4-kilometer-long Fabry-Pérot cavities placed in each arm of the interferometer, using Pound-Drever-Hall locking of the FP cavity length with a noise limit of **~1 pm** at 1 Hz.

(D) LISA (Section 4.6.6.2.2). LISA is a space-based gravity wave detector using an optical heterodyne Michelson interferometer configuration with a total optical path error budget not to exceed **63 pm** for 0.1 Hz gravity waves. One author gives the detectable spacecraft

separation difference as **20 pm**, and the Interferometry Measurement System measurement sensitivity derived from the science requirements is **40 pm/√Hz**. It is not clear if either of the approaches used in LIGO or LISA are applicable to SPM-based picoscale metrology because of the extremely long baselines involved in gravity wave detection interferometry.

4.7 Environmental Isolation

Atomic-scale sensing lies at the heart of a variety of high-resolution microscopies, but environmental perturbations (e.g. temperature, acoustic, liquid) can lead to unmeasured drift – typically, the position of a microscope stage may drift ~2 nm/min without active stabilization.[1602] Extreme stability can be achieved passively in highly controlled environments. For example, the pinnacle of picoscale control for scanning probe microscopy (SPM) is achieved using instruments that are secluded from the perturbative environment by multiple layers of isolation and that operate at very low (LHe) temperature and ultrahigh vacuum – these impressive levels of isolation can achieve drift rates as low as ~1 pm/min.[1603]

The molecular workstation must be isolated from the ambient environment to minimize metrology errors and maintain adequate DMS tooltip positioning accuracy to within 20-50 pm over multiple cycles of operation without re-registration. This will require incorporating three specific environmental isolation subsystems into the workstation design: (1) an ultra-high vacuum (UHV) system (Section 4.7.1), (2) a temperature regulation system (Section 4.7.2), and (3) a vibration islation system (Section 4.7.3).

4.7.1 Ultra-High Vacuum System

We need to establish and maintain ultra-high vacuum (UHV) throughout the entire operating volume of the molecular workstation. Besides the DMS workspace (which includes workpiece, tooltips, toolracks, tool manipulators and all metrology appurtenances such as beams, fiducials, PZT actuators, etc.) this volume must also include: (1) any heaters required for high-temperature bakeout, (2) cold-traps and wall-freezers to condense out free contaminants, (3) chemical- or binding-site-based getters to absorb targeted contaminant molecules, and (4) other supporting facilities that will help to establish and maintain a good vacuum.

UHV is generally defined as an ambient gas pressure lower than about 10^{-7} Pa (i.e., 100 nanopascals; aka. ~10^{-9} torr, 10^{-12} atm, 10^{-12} bar or 10^{-9} mbar) which is 2.45 x 10^{13} molecules/m^3 at 300 K or 9.17 x 10^{13} molecules/m^3 at 80 K for an ideal gas). At this threshold pressure, about the same as in low-Earth orbit at ~300 km or ~185 miles altitude, the mean free path for a gas

---

[1602] Allison B. Churnside, Gavin M. King, Ashley R. Carter, Thomas T. Perkins, "Improved performance of an ultrastable measurement platform using a field-programmable gate array for real-time, deterministic control," in: Michael T. Postek, John A. Allgair, eds., Instrumentation, Metrology, and Standards for Nanomanufacturing II, Proc. SPIE 7042(2008):704205.

[1603] B.C. Stipe, M.A. Rezaei, W. Ho, "Single-molecule vibrational spectroscopy and microscopy," Science 280(1998):1732-1735.

molecule at 300 K is ~230 km and the molecules are colliding with the chamber walls many times before colliding with each other. A 34.4 micron cubic box (40,800 micron^3) containing gas at 10^{-9} torr (10^{-12} atm) and 300 K contains, on average, a single gas molecule. UHV is considered to range from 10^{-9}-10^{-12} torr (~10^{-12}-10^{-15} atm). The minimum lifetime of a radical site ($t_{radical}$) on a diamondoid mechanosynthesis (DMS) tooltip that is exposed to a 10^{-9} torr (10^{-12} atm) threshold-UHV environment may be estimated as the time required for a binding event to occur (as a function of the molecular impingement rate), which is given, analogously for binding sites,[1604] by:

$$t_{radical} \sim (N_{encounters} / A_{radical}\, n_{gas})\, (\pi\, MW_{kg} / 2\, k_B T\, N_A)^{1/2} = 19{,}325 \text{ sec } (\textbf{~5 hr}) \qquad (4.1)$$

where $A_{radical}$ = active receptor cross-sectional area ~ 0.0237 nm^2 for a carbon radical site in a diamond matrix, $n_{gas} = 2.45 \times 10^{13}$ molecules/m^3 for ideal gas molecules at 10^{-9} torr (10^{-12} atm) and T = 300 K, $N_{encounters}$ ~ 10 random molecule-radical encounters required for a binding event, MW_{kg} = 0.002 kg/mole for H_2 to give the most conservative result, $k_B = 1.381 \times 10^{-23}$ J/K (Boltzmann constant), and $N_A = 6.023 \times 10^{23}$ molecules/mole (Avogadro's number).

Radical site lifetime can be increased to **~2.2 days** by dropping ambient UHV operating pressure from 10^{-9} torr (10^{-12} atm) to 10^{-10} torr (10^{-13} atm) – the same pressure to which vacuum tubes are typically pumped (i.e., 10^{-7}-10^{-10} torr; 10^{-10}-10^{-13} atm). Operation on the lunar surface (10^{-11} torr; ~10^{-14} atm) would increase $t_{radical}$ to **~22 days**. Operating at the lowest pressures currently achievable in the laboratory 10^{-13} torr (~10^{-16} atm),[1605] 10^{-14} torr (~10^{-17} atm),[1606] or 10^{-15} torr (~10^{-18} atm)),[1607] $t_{radical}$ would increase to 6-600 years.

[1604] Robert A. Freitas Jr., Nanomedicine, Volume I: Basic Capabilities, Landes Bioscience, Georgetown, TX, 1999; Section 4.2.1, p. 94; http://www.nanomedicine.com/NMI/4.2.1.htm.

[1605] H. Ishimaru, "Ultimate Pressure of the Order of 10^{-13} Torr in an Aluminum Alloy Vacuum Chamber," J. Vac. Sci. Technol. **7(**1989**):**2439-2442. H. Akimichi, M. Hirata, "Generation and pressure measurement of extremely high vacuum (XHV) using a TiN coated chamber," Metrologia 42(2005):S184-S186, http://www.iop.org/EJ/abstract/0026-1394/42/6/S08; "Non-Evaporable Getter (NEG) Thin Film Coatings," CERN Technology Transfer DSU-TT, 2008, http://technologytransfer.web.cern.ch/TechnologyTransfer/en/Technology/NEG.html; Marcy Stutzman, Philip Adderley, "Vacuum at CEBAF: Seminar for Accelerator Operators," 17 January 2006, http://www.jlab.org/accel/inj_group/docs/2006/Operator_Vacuum_Talk.ppt; Marcy Stutzman, Philip Adderley, Matt Poelker, "Extreme High Vacuum: The Need, Production, and Measurement," Thomas Jefferson National Accelerator Facility, 14 November 2006, http://www.jlab.org/accel/inj_group/docs/2006/XHV.ppt.. P. Chiggiato, "Production of extreme high vacuum with non evaporable getters," Phys. Scr. T71(1997):9-13; http://www.iop.org/EJ/abstract/1402-4896/1997/T71/002/.

[1606] P. Chiggiato, "Production of extreme high vacuum with non evaporable getters," Phys. Scr. T71(1997):9-13; http://www.iop.org/EJ/abstract/1402-4896/1997/T71/002/. Dr.-Ing. K. Busch GmbH, "What is vacuum?" Busch Vacuum Pumps and Systems, 2002; http://www.busch.com.au/whatisvacuum.htm. (~10^{-14} torr was achieved during a test by IBM Thomas J. Watson Research Center, New York, USA, October 1976, in a cryogene system using cryopumping at ~4 K with an outer guard vacuum; also reported in 1994 Guinness Book of Records.)

[1607] "Vacuum Pumps," in: McGraw Hill Encyclopedia of Science and Technology, 7th Edition, 1992, Vol. 19, p. 128. Also mentioned in http://hypertextbook.com/facts/1998/RobertSaronson.shtml.

The pressure range of 10^{-13} torr (~10^{-16} atm) and below is often called the XHV (Extremely High Vacuum) region.[1608] For comparison, interplanetary space is ~10^{-15} torr (10^{-18} atm) and interstellar space is ~10^{-16} torr (10^{-19} atm).

Note that the M^3 nanometrology system (Section 4.6.1.1) uses a vacuum system that typically achieves a base pressure of only ~10^{-7} torr (~100-fold above UHV levels), apparently because "several of the machine components will not withstand the bake-out temperatures needed to achieve ultra-high vacuum levels".[1609] However, this does not appear to be a fundamental limit for large-scale nanometrology systems that are designed to operate at UHV.

For example, as part of its "Atom-based Dimensional Metrology" effort in its Next-Generation Nanometrology (NGN) Program (Section 4.6.4.1), NIST is building a five-chamber ultra high vacuum (UHV) facility that will be regularly capable of producing 133 x 10^{-10} Pa (1 x 10^{-10} torr) base pressures.[1610] Large laboratory UHV vacuum chambers typically range from 2 m^3 to 10 m^3 in volume,[1611] laboratory STM work often uses 10^{-11} torr UHV;[1612] 10^{-10} torr is typical for large nuclear beamline facilities[1613] and much larger systems such as the 1080 m^3 internal UHV

[1608] H. Akimichi, M. Hirata, "Generation and pressure measurement of extremely high vacuum (XHV) using a TiN coated chamber," Metrologia 42(2005):S184-S186, http://www.iop.org/EJ/abstract/0026-1394/42/6/S08; "Non-Evaporable Getter (NEG) Thin Film Coatings," CERN Technology Transfer DSU-TT, 2008, http://technologytransfer.web.cern.ch/TechnologyTransfer/en/Technology/NEG.html; Marcy Stutzman, Philip Adderley, "Vacuum at CEBAF: Seminar for Accelerator Operators," 17 January 2006, http://www.jlab.org/accel/inj_group/docs/2006/Operator_Vacuum_Talk.ppt; Marcy Stutzman, Philip Adderley, Matt Poelker, "Extreme High Vacuum: The Need, Production, and Measurement," Thomas Jefferson National Accelerator Facility, 14 November 2006, http://www.jlab.org/accel/inj_group/docs/2006/XHV.ppt.

[1609] E. Clayton Teague, "The National Institute of Standards and Technology Molecular Measuring Machine Project: Metrology and precision engineering design," J. Vac. Sci. & Technol. A 8(September 1990):3876-3877; J. Kramar, J. Jun, W. Penzes, F. Scire, C. Teague, J. Villarrubia, E. Amatucci, D. Gilsinn, "The Molecular Measuring Machine," Proceedings of the 1998 International Conference on Mechatronic Technology, 30 November – 2 December 1998, Hsinchu, Taiwan (ICMT'98), pp. 477-487, http://www.isd.mel.nist.gov/documents/amatucci/ICMTreal.pdf; John A. Kramar, "Nanometre resolution metrology with the Molecular Measuring Machine," Meas. Sci. Technol. 16(2005):2121-2128.

[1610] "Next-Generation Nanometrology (NGN) Program," NIST, 2008; http://www.mel.nist.gov/programs/ngn.pdf.

[1611] "Ultrahigh Vacuum Chambers – a New Service from ITL," J. Synchrotron Rad. 2(1995):75; http://journals.iucr.org/s/issues/1995/01/00/a28079/a28079.pdf. P. Sonato, W.R. Baker, P. Fiorentin, G. Marchiori, P. Zaccaria, G. Zollino, V. Antoni, M. Bagatin, D. Desideri, G. Serianni, L. Tramontin, R. Bertoncello, "The wall conditioning techniques in RFX," Vacuum 47(June-August 1996):977-980.

[1612] Y.-W. Mo, D.E. Savage, B.S. Swartzentruber, M.G. Lagally, "Kinetic Pathway in Stranski-Krastanov Growth of Ge on Si(001)," Phys. Rev. Lett. 65(20 August 1990):1020-1023.

[1613] "Preliminary Design Report for the VESPERS Beamline at the Canadian Light Source Inc.," 22 November 2005; http://www.uwo.ca/ssw/research/vespers/resources/vespers_pdr_rev0.pdf.

vacuum volume of the proposed ITER fusion reactor[1614] are well-known. ITER requires a base pressure no higher than ~10^{-8} torr during operation but ~10^{-10} torr for non-fuel components,[1615] and there is also ~80 km of cabling inside the ITER vacuum volume.[1616] The world's largest vacuum chamber belongs to NASA: the Space Power Facility (originally built in 1969 and since refurbished several times) that resides at NASA Glenn Research Center's Plum Brook Station in Sandusky, Ohio. The SPF measures 100 feet (~30.5 m) in diameter and 122 feet (~37.2 m) tall giving a total enclosed high-vacuum chamber volume of ~27,000 m^3 (Figure 4-127).[1617] The SPF pumping system includes sixteen 48-inch diameter LN_2-baffled electrically heated oil diffusion pumps (pumping speed ~700,000 liters/s) and ten 48-inch diameter cryopumps with vacuum isolation gate valves (pumping speed ~600,000 liters/s), giving a pumpdown time of 2 hours from atmospheric pressure down to 20 torr, 4 hours from 20 torr down to 10^{-3} torr, and another 2-6 hours from 10^{-3} torr down to 10^{-6} torr.[1618] Adding more cryopumps or using longer pumpdown times presumably would allow the NASA system to reach UHV conditions even inside this extremely large volume.

[1614] R.J.H. Pearce, M.E.P. Wykes, C. Lowry, C. Day, V. Hauer, "Requirements and progress in vacuum conductance modeling on ITER," Paper 051, 51st IUVSTA Workshop, 9-12 July 2007, Djuronaset, Varmdo, Sweden; http://www.vgd07.dl.ac.uk/Presentaions/Program%20and%20Abstracts.pdf.

[1615] Nick Balshaw, "Vacuum for Fusion – ITER," Vacuum KTN Meeting, London, March 2007, N.H. Balshaw, UKAEA; http://www.scitech.ac.uk/Resources/PDF/Balshaw.pdf.

[1616] Nick Balshaw, "Vacuum for Fusion – ITER," Vacuum KTN Meeting, London, March 2007, N.H. Balshaw, UKAEA; http://www.scitech.ac.uk/Resources/PDF/Balshaw.pdf.

[1617] "World's Largest Vacuum Chamber to Test Orion," 19 June 2007, http://www.nasa.gov/mission_pages/constellation/orion/vacuum_chamber.html; "NASA Space Power Facility – Quick Facts," 24 January 2007; http://facilities.grc.nasa.gov/spf/quick.html.

[1618] "NASA Space Power Facility – Facility Capabilities," 24 January 2007; http://facilities.grc.nasa.gov/spf/capabilities.html.

Figure 4-127. Worlds largest vacuum chamber, the Space Power Facility at NASA Glenn Research Center's Plum Brook Station in Sandusky, Ohio, has a ~27,200 m^3 volume of vacuum.[1619]

External view of facility

Inside the vacuum chamber

Cooling the external system to ~54 K will cause all major atmospheric constituents to freeze out on the chamber walls (Table 4-9), reducing the ambient concentration of likely contaminant gases by up to four additional orders of magnitude. Ignoring He, which is inert, this leaves molecular hydrogen (H_2) as the principal remaining potentially reactive contaminant. Molecular hydrogen getters are often made with hydrogen-absorbing platinum or palladium metals or oxides like PdO; the PdO type, like STAYDRY™ H2-3000 (CSPM), is highly effective since hydrogen is converted to water that is then removed by a moisture getter in the same material.[1620] Other molecular hydrogen getter systems such as ZrCo,[1621] strained SiGe,[1622] and dehydrogenated diamond surface are well-known.

[1619] "World's Largest Vacuum Chamber to Test Orion," 19 June 2007, http://www.nasa.gov/mission_pages/constellation/orion/vacuum_chamber.html; "NASA Space Power Facility – Quick Facts," 24 January 2007; http://facilities.grc.nasa.gov/spf/quick.html.

[1620] "Hydrogen Effects of GaAs Microwave Semiconductors," Report #SMC97-0701, prepared for JPL, July 1997. Cited by: Ken Gilleo, Steve Corbett, "Getters – Molecular Scavengers for Packaging," Advances in Microelectronics (2000); HDI(January 2001):26-29; http://www.et-trends.com/files/GETTERS_HDI2001.pdf.

[1621] R.D. Penzhorn, M. Devillers, M. Sirch, "R-D Evaluation of ZrCo and Other Getters for Tritium Handling and Storage," J. Nucl. Mater. 170(March 1990):217-231.

Table 4-9. Pressure Reduction Achieved by Freezing Out Normal Atmospheric Constituent Gases[1623] at Progressively Lower Temperatures (excluding the highly variable H_2O content which is also frozen out; typical air concentration ~7.75 x 10^{-2} atm)

Atmos-pheric Gas	Freeze Temp (K)	Partial Pressure (atm)	Cumulative P_{atm} (atm)	Atmos-pheric Gas	Freeze Temp (K)	Partial Pressure (atm)	Cumulative P_{atm} (atm)
HCO_2H	281.55	1 x 10^{-14}	1	CH_3Cl	176.15	7 x 10^{-10}	0.999639676
H_2O_2	272.74	2 x 10^{-10}	1	COF_2	159.15	1 x 10^{-14}	0.999639676
NO_2	261.95	2.3 x 10^{-11}	1	HCl	158.35	1 x 10^{-9}	0.999639675
HCN	259.15	1.7 x 10^{-10}	1	PH_3	139.65	1 x 10^{-20}	0.999639675
HNO_3	231.15	5 x 10^{-11}	1	OCS	135.15	6 x 10^{-10}	0.999639674
SF_6	222.65	1 x 10^{-14}	1	NO	109.55	3 x 10^{-10}	0.999639674
HI	222.35	3 x 10^{-12}	1	CH_4	90.67	1.7 x 10^{-6}	0.999637974
CO_2	216.55	3.6 x 10^{-4}	0.99964	C_2H_6	90.35	2 x 10^{-9}	0.999637972
SO_2	200.45	3 x 10^{-10}	0.999639999	Ar	83.95	9.3 x 10^{-3}	0.990337972
NH_3	195.45	5 x 10^{-11}	0.999639999	O_3	80.45	2.66 x 10^{-8}	0.990337945
C_2H_2	191.35	3 x 10^{-10}	0.999639999	CO	74.15	1.5 x 10^{-7}	0.990337795
HF	190.05	1 x 10^{-14}	0.999639999	N_2	63.29	7.81 x 10^{-1}	0.209337795
H_2S	187.65	1 x 10^{-14}	0.999639999	O_2	54.75	2.09 x 10^{-1}	0.000337795
HBr	184.65	1.7 x 10^{-12}	0.999639999				
N_2O	182.35	3.2 x 10^{-7}	0.999639679	*and:*			
H_2CO	181.15	2.4 x 10^{-9}	0.999639677	H_2O	273.15	*(variable)*	< 0.0001

Combining cryogenics with hydrogen getters should put UHV vacuum levels of 10^{-12} torr (and perhaps XHV levels) well within reach for the molecular workstation.

4.7.2 Temperature Regulation System

We also need to establish and maintain good thermal isolation from the outside environment with internal temperature maintained constant to within perhaps ±1-10 millikelvins (mK). For example, the nickel-iron alloy Invar is widely used in metrology systems because of its unique proptery of low and linear thermal expansion (typically $\alpha = 1.3 \times 10^{-6}\ K^{-1}$)[1624] over a wide

---

[1622] Arthur J. Pitera, E.A. Fitzgerald, "Hydrogen gettering and strain-induced platelet nucleation in tensilely strained $Si_{0.4}Ge_{0.6}$/Ge for layer exfoliation applications," J. Appl. Phys. 97(2005):104511; http://sauvignon.mit.edu/papers/2005/pitera.pdf.

[1623] "Major Concentration of Gases in the Atmosphere," NOAA S/T 76-1562, 1976; "AFGL Atmospheric Constituent Profiles (0-120 km)," AFGL-TR-86-0110, 1986; U.S. Standard Atmosphere, 1962 and 1976, Supplement 1966, U.S. Govt. Printing Office, Washington DC, 1976.

[1624] http://www.azom.com/details.asp?ArticleID=515.

temperature range, with a few alloys having even lower coefficients of linear thermal expansion, such as Invar 36, with $\alpha = 0.6 \times 10^{-6}\ K^{-1}$, the same as quartz.[1625] Thus Invar 36 components of a molecular workstation that are fabricated to ~100 micron mechanical accuracy will exhibit a differential expansion of 60 pm/K, or a negligible 0.06 pm to 0.6 pm variation for temperature excursions of 1 mK to 10 mK, respectively. (Control of interferometry apparatus temperature to ±10 mK has been commonplace for decades.[1626]) Invar generally retains good mechanical characteristics and ductility at cryogenic temperatures.

The M^3 nanometrology system (Section 4.6.1.1) was operated at room temperature with the machine core assembly enclosed in a temperature control shell (Figure 4-28) – a gold-coated copper sphere about 50 mm larger in diameter than the machine core, spiral-wrapped with polyimide-insulated copper wire at a 6 mm spacing, the shell penetrated by three doors on rails to allow the removal and replacement of the coarse motion carriages.[1627] A stable temperature at 20 °C was maintained by holding the room at 17 °C ± 0.01 °C and regulating current flow through the heater shell wire. The control scheme is to maintain stability through thermal inertia and by keeping a constant heat load, using several thermocouples distributed about the temperature control shell and the machine core to monitor the temperature, as well as platinum resistance thermometers on the probe mounting plate and near the sample. Between the large thermal mass of the copper core and the weak coupling between it and the temperature control shell, the temperature rise time for the system was on the order of one day and ~1 mK temperature stability was demonstrated.[1628]

The molecular workstation will normally be operating at cryogenic temperatures, where a control requirement of ±1-10 mK seems readily attainable with current technology. For example, one manufacturer of cryogenic temperature sensors and control systems offers equipment[1629] that

---

[1625] http://en.wikipedia.org/wiki/Coefficient_of_thermal_expansion.

[1626] U. Brand, K. Herrmann, "A laser measurement system for the high-precision calibration of displacement transducers," Meas. Sci. Technol. 7(1996):911-917.

[1627] E. Clayton Teague, "The National Institute of Standards and Technology Molecular Measuring Machine Project: Metrology and precision engineering design," J. Vac. Sci. & Technol. A 8(September 1990):3876-3877; J. Kramar, J. Jun, W. Penzes, F. Scire, C. Teague, J. Villarrubia, E. Amatucci, D. Gilsinn, "The Molecular Measuring Machine," Proceedings of the 1998 International Conference on Mechatronic Technology, 30 November – 2 December 1998, Hsinchu, Taiwan (ICMT'98), pp. 477-487, http://www.isd.mel.nist.gov/documents/amatucci/ICMTreal.pdf; John A. Kramar, "Nanometre resolution metrology with the Molecular Measuring Machine," Meas. Sci. Technol. 16(2005):2121-2128.

[1628] E. Clayton Teague, "The National Institute of Standards and Technology Molecular Measuring Machine Project: Metrology and precision engineering design," J. Vac. Sci. & Technol. A 8(September 1990):3876-3877; J. Kramar, J. Jun, W. Penzes, F. Scire, C. Teague, J. Villarrubia, E. Amatucci, D. Gilsinn, "The Molecular Measuring Machine," Proceedings of the 1998 International Conference on Mechatronic Technology, 30 November – 2 December 1998, Hsinchu, Taiwan (ICMT'98), pp. 477-487, http://www.isd.mel.nist.gov/documents/amatucci/ICMTreal.pdf; John A. Kramar, "Nanometre resolution metrology with the Molecular Measuring Machine," Meas. Sci. Technol. 16(2005):2121-2128.

[1629] 1094. "Sensor Performance Data," CryoCon Model 22 Temperature Controller, Cryogenic Control Systems, Inc., 2003; http://www.cryocon.com/Model22/mod22brochure.pdf.

provides temperature measurement accuracy of 0.07-1.6 mK at 4 K and 1.1-12 mK at 77 K, with thermal control stability of 0.08-0.5 mK at 4 K and 0.5-3.8 mK at 77 K.

4.7.3 Vibration Isolation System

The molecular workstation also needs to be vibrationally isolated over specific ranges of vibrational and acoustic frequencies that could introduce positional uncertainty into the positioning or metrology systems. The specific vibrational frequencies most likely to pose problems for reliable workstation operation need to be identified and eliminated from the workspace, using a variety of dampeners, filters, and isolation techniques.

Here again the example of the M^3 nanometrology system at NIST (Section 4.6.1.1) is instructive.[1630] M^3 employs an active vibration isolation system in which the entire workspace is suspended inside an outer shell, kinematically constrained by means of six actuator rods in the Mallock[1631] suspension configuration, with each actuator having an accompanying accelerometer mounted as nearly as possible coaxially on the suspended inner mass. Different vibration compensation control algorithms are implemented using a digital signal processor (DSP)[1632] which are effective when the vibration environment is noisy, e.g., when the turbomolecular pump is operating, but are less useful in the normally more quiet operating environment in which the performance of the active system is limited by sensor noise. The entire instrument is contained in a vacuum system equipped with a turbo pump for roughing the vacuum and eight symmetrically placed ion pumps for quiet operation. The vacuum system containment is itself contained within an environmental control chamber that can be hermetically sealed to provide further acoustic isolation. This chamber is supported by pneumatic isolators having level control and a damped natural resonance of about 1 Hz.

The entire instrument was later moved to a new Advanced Metrology Laboratory[1633] (Figure 4-31) in a building that is completely underground,[1634] providing an acoustically quiet class-100

[1630] E. Clayton Teague, "The National Institute of Standards and Technology Molecular Measuring Machine Project: Metrology and precision engineering design," J. Vac. Sci. & Technol. A 8(September 1990):3876-3877; J. Kramar, J. Jun, W. Penzes, F. Scire, C. Teague, J. Villarrubia, E. Amatucci, D. Gilsinn, "The Molecular Measuring Machine," Proceedings of the 1998 International Conference on Mechatronic Technology, 30 November – 2 December 1998, Hsinchu, Taiwan (ICMT'98), pp. 477-487, http://www.isd.mel.nist.gov/documents/amatucci/ICMTreal.pdf; John A. Kramar, "Nanometre resolution metrology with the Molecular Measuring Machine," Meas. Sci. Technol. 16(2005):2121-2128.

[1631] R.S. Whipple, "The design and construction of scientific instruments," Trans. Opt. Soc. Lond. 22(1921):35-52.

[1632] K.-J. Lan, J.-Y. Yen, J.A. Kramar, "Active vibration isolation for a long range scanning tunneling microscope," Asian J. Control 6(2004):179-186; K.-J. Lan, J.-Y. Yen, J.A. Kramar, "Sliding mode control for active vibration isolation of a long range scanning tunneling microscope," Rev. Sci. Instrum. 75(2004):4367-4373.

[1633] Advanced Measurement Laboratory 2004; http://www.nist.gov/public affairs/amlbrochure.htm; The National Institute of Standards and Technology Advanced Measurement Laboratory, Gaithersburg, MD; http://www.nanobuildings.com/projects/nist/.

clean room with ±0.01 °C temperature control. The instrument rests on a pneumatically supported concrete slab that is in a pit under the walk-on floor, with most of the electronics and power supplies that drive the instrument located in an adjacent control room.

As an example of a fairly simple vibration isolation system used at NIST in the early 2000s, Lawall and Kessler[1635] describe a vibration-isolated platform that they employed for prototyping optical interferometers that were intended to be used in a high-vacuum (~10^{-4} Pa, ~10^{-6} torr) environment. The system provides isolation from both seismic and acoustic disturbances with a residual acceleration of 2.9 x 10^{-6} m/s^2 RMS in the vertical direction and 6.3 x 10^{-6} m/s^2 RMS in the horizontal direction, in the bandwidth from 5 to 400 Hz, a frequency region that includes seismic and acoustic noise, as well as low-frequency noise contributed by the turbomolecular pump. The environmental decoupling provided by the spring suspension, air-spring table legs, and vacuum were evaluated sequentially to illustrate the effects of each. The vibration contributed by the turbomolecular pump was measured and found to fall in a low-frequency zone from 26-76 Hz as well as peaks at the pump rotation frequency of 820 Hz and its first harmonic at 1.64 kHz. The low-frequency noise arising from the pump is less than 2% of the total residual acceleration in the bandwidth from 0.25 to 400 Hz. The platform was also used to construct a high-finesse open-cavity Fabry-Pérot interferometer, using standard commercial mounts, having relative motion below 2 pm RMS in a 3 kHz bandwidth. Of this motion, the contribution due to the pump at 820 Hz was only 0.3 pm. The acoustic decoupling provided by the vacuum environment allows researchers to do experiments that would be prohibitive at atmospheric pressure even in a tightly sealed enclosure.[1636] NIST is also building a facility for its "Atom-based Dimensional Metrology" effort in its Next-Generation Nanometrology (NGN) Program (Section 4.6.4.1) with vibration isolation that yields a sub-Angstrom noise floor.[1637]

[1634] The Advanced Metrology Laboratory (AML)[*] was completed in 2003 and is a suite of 5 large buildings, including two that are 40 feet underground. According to the AML brochure: "27 specialized AML laboratories offer the ultimate in vibration isolation. These modules are located about 12 meters (40 feet) below ground level in structurally isolated building wings, a first line of defense against vibration. Instruments sit atop specially designed, heavy mass isolation slabs supported on pneumatic "air springs." An isolated, raised floor system spans over the pit containing each isolation slab so that researchers can run their experiments without affecting the isolation systems." According to NANObuildings.com, the AML cost $235M and had 536,500 SF of floor space, implying a rough cost per square foot of $438/SF. By this measure (which naively assumes a constant cost per SF as a function of size), a future proprietary 5000 SF facility in the Bay Area foothills might cost $2.2M plus land cost (probably another $800K), or a ~$3M total, to build.

[*] Advanced Measurement Laboratory 2004; http://www.nist.gov/public affairs/amlbrochure.htm; The National Institute of Standards and Technology Advanced Measurement Laboratory, Gaithersburg, MD; http://www.nanobuildings.com/projects/nist/.

[1635] J. Lawall, E. Kessler, "Design and Evaluation of a Simple Ultra Low Vibration Vacuum Environment," Rev. Sci. Instrum. 73(January 2002):209-215.

[1636] J. Lawall, E. Kessler, "Design and Evaluation of a Simple Ultra Low Vibration Vacuum Environment," Rev. Sci. Instrum. 73(January 2002):209-215.

[1637] "Next-Generation Nanometrology (NGN) Program," NIST, 2008; http://www.mel.nist.gov/programs/ngn.pdf.

Active vibration isolation is an active area of study.[1638] Several companies also specialize in designing vibration-isolation structures and systems. For example, Colin Gordon & Associates[1639] provided design analysis for state-of-the-art AML buildings for NIST in the early 2000s. Northrop Grumman's Space Technology Division has the development contract with JPL for the SIM Lite mission (Section 4.6.6.1.1) and is described as having "special expertise in thermal control, vibration isolation, damping, and high precision structures".[1640]

4.8 Ancillary Facilities

Provision must be made for any ancillary facilities that are required to support the workstation, especially those that must communicate directly with the workspace volume. Most likely in this category would be a bake-out annex, in which surfaces, tools or nanoparts can be heated, the gases driven off without poisoning the vacuum, and then the baked-out objects transferred into the main workspace volume without breaking vacuum.

The system must also include a means for inserting and removing possibly up to four workpiece or feedstock "chips" up to 1 cm in linear dimension through an airlock mechanism without breaking internal vacuum. The system must also include a means for orienting, aligning and co-leveling the "chips" inside the workspace chamber.

4.9 Control Software

We need to obtain software that can drive the positioning and metrology systems, and then coordinate this with our DMS reaction sequence trajectory database so that arbitrary sequences of DMS operations can be strung together and executed in series. The repetition rate for tip re-registration, the methods to be used (e.g., turn on qPlus for registration, turn off for DMS), and the scheduling and execution of those maneuvers, requires further analysis of thermal drift effects. We also need to integrate control of tool pickup and storage at the toolrack, tip registration procedures, and all necessary environmental controls. Much of this development activity must wait until a systems design exists for the molecular workstation.

[1638] "Buildings for Advanced Technology Workshop," NanoBuildings.com, NIST, Gaithersburg MD, 14-16 January 2003; http://www.nanobuildings.com/bat/presentations/Isolation.htm. Jia-Yush Yena, Kuo-Jung Lan, John A. Kramar "Active vibration isolation of a large stroke scanning probe microscope by using discrete sliding mode control," Sensors and Actuators A: Physical 121(31 May 2005):243-250; http://www.sciencedirect.com/science?_ob=ArticleURL&_udi=B6THG-4FW7R2W-1&_user=10&_rdoc=1&_fmt=&_orig=search&_sort=d&view=c&_acct=C000050221&_version=1&_urlVersion=0&_userid=10&md5=b844958b646d203519fa9b2156278337.

[1639] Colin Gordon & Associates ; http://www.colingordon.com.

[1640] http://www.st.northropgrumman.com/capabilities/space/science/sim.html.

Control systems design for nanoscale positioning of SPM systems is an area of active research interest.[1641] A number of industrial companies also have relevant products in traditional applications. For example, Precitech[1642] makes high-precision machining equipment. They offer the Nanoform 700 Ultra[1643] and the Nanoform 700 Ultra,[1644] both of which include the "QNx real time Operating System with industry leading 0.01 nanometer (**10 pm**) programming resolution, and Linear holographic glass scales with **16 pm** feedback resolution." (Apparently their controller can be programmed to 10 pm accuracy, even when the SPM hardware can't come anywhere close to this level of repeatable accuracy.)

Automation of atomic scale positioning motions has also been demonstrated by the "Autonomous Atom Assembly" project at NIST,[1645] by Hla's group,[1646] and by others.

[1641] K.K. Leang, A.J. Fleming, "High-speed serial-kinematic AFM scanner: design and drive considerations," Asian Journal of Control 11(2009):144-153 (special issue on Advanced Control Methods for Scanning Probe Microscopy); http://www.leang.com/academics/pubs/LeangKK_2009d.pdf. G.M. Clayton, S. Tien, K.K. Leang, Q. Zou, S. Devasia, "A review of feedforward control approaches for nano precision positioning in high speed SPM operation," ASME Journal of Dynamic Systems, Measurement, and Control (2009), in press. U. Aridogan, Y. Shan, K.K. Leang, "Design and analysis of discrete-time repetitive control for scanning probe microscopes," ASME Journal of Dynamic Systems, Measurement, and Control (2009), in press.

[1642] Precitech; http://www.precitech.com/.

[1643] Nanoform 700 Ultra; http://www.precitech.com/Precitech_nano700_features.html.

[1644] Nanoform 250 Ultra; http://www.precitech.com/Precitech_nano250features.html.

[1645] "Autonomous Atom Assembly," NIST, July 2004; http://cnst.nist.gov/epg/Projects/STM/aaa_proj.html.

[1646] T. Skeini, J.F. Steiner, S.W. Hla, "Automated Atomicscale Construction," Sixth IEEE Conference on Nanotechnology, 2006 (IEEE-NANO 2006), 17-20 June 2006, Vol. 2, pp. 610-612.

5. Conclusions

This document has provided detailed background information and a comprehensive review of all major technical components that are required to build and operate a molecular workstation capable of serving as a diamondoid mechanosynthesis-based molecular manufacturing system.

Although some minor uncertainties exist and a few minor issues remain unresolved, we conclude that as of this writing in late 2009, the current state-of-the-art of the nine categories of key enabling technologies is probably sufficient to permit a successful dedicated effort to design, build, and operate a molecular workstation as defined in Chapter 1 of this report.

Waiting longer to initiate this effort will lower total implementation costs but should not significantly reduce technical risk, and will raise the opportunity cost and the risk of increased competition in the years ahead.